Roberto Tenchini
Claudio Verzegnassi

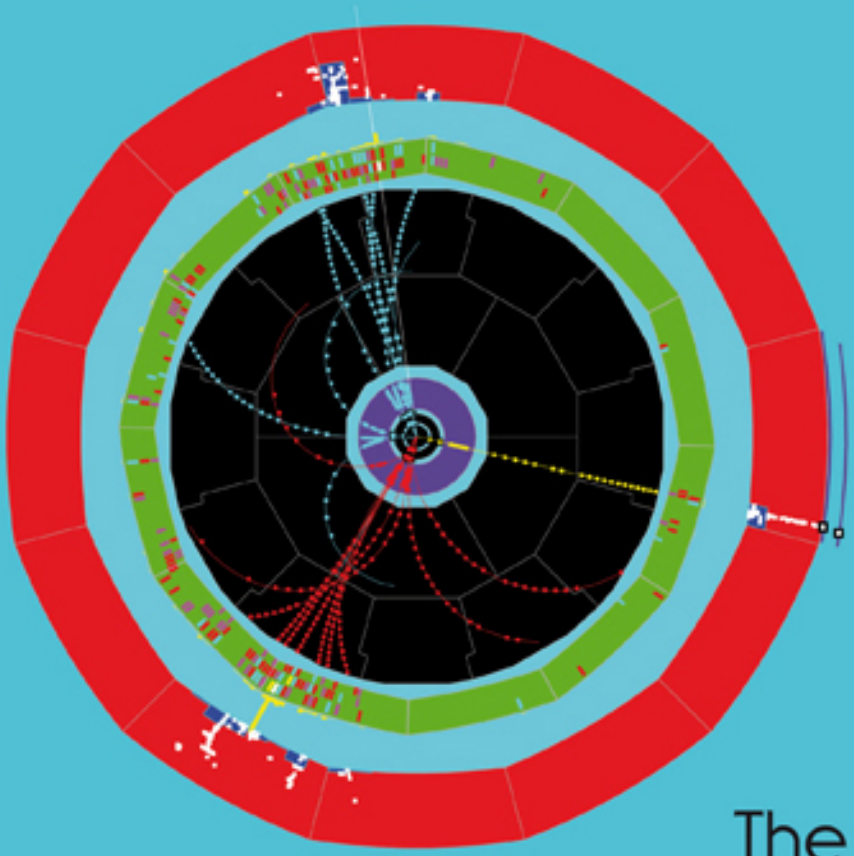

The Physics of the Z and W Bosons

World Scientific

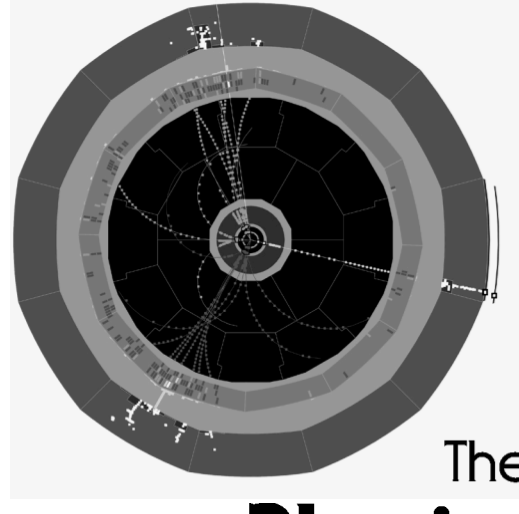

The Physics of the Z and W Bosons

This page intentionally left blank

Roberto Tenchini (INFN Pisa, Italy)
Claudio Verzegnassi (University of Trieste, Italy)

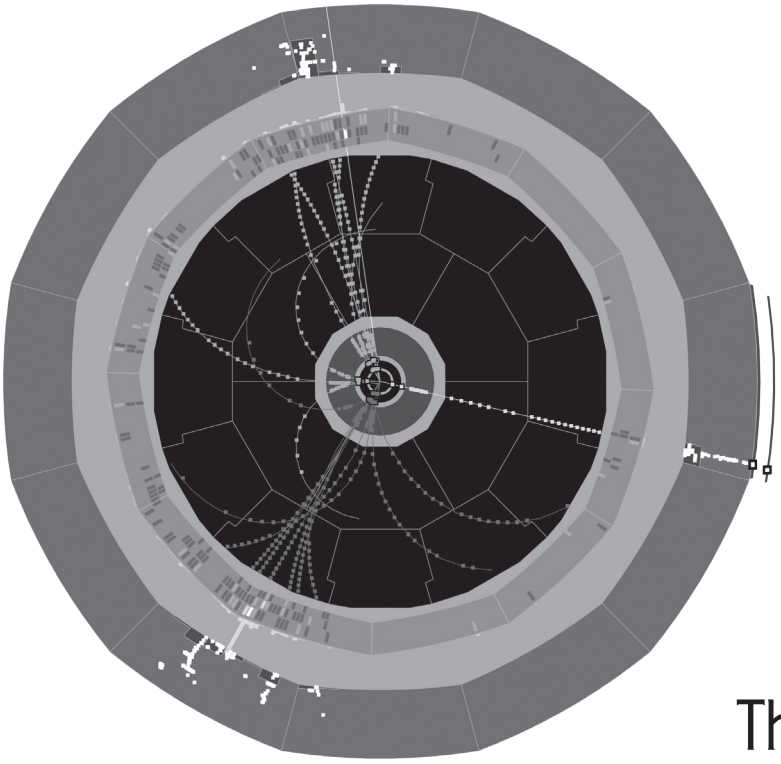

The Physics of the Z and W Bosons

World Scientific
NEW JERSEY • LONDON • SINGAPORE • BEIJING • SHANGHAI • HONG KONG • TAIPEI • CHENNAI

Published by

World Scientific Publishing Co. Pte. Ltd.

5 Toh Tuck Link, Singapore 596224

USA office: 27 Warren Street, Suite 401-402, Hackensack, NJ 07601

UK office: 57 Shelton Street, Covent Garden, London WC2H 9HE

British Library Cataloguing-in-Publication Data
A catalogue record for this book is available from the British Library.

THE PHYSICS OF THE Z AND W BOSONS

ISBN-13 978-981-270-702-4
ISBN-10 981-270-702-6

Printed in Singapore.

To Marina, Ludovica, Rodolfo and Federico.

To Nicoletta, Francesco, Lavinia and Sara.

This page intentionally left blank

Preface

It would be hard to persuade a new student beginning particle physics in 2007 that there once was a time when there was *not yet* a Standard Model. How else, would he object, could one explain all known features of strong, electro-magnetic and weak interactions? The absence of Flavour Changing Neutral Currents (FCNC), the universality of weak charged current interactions, the smallness of the $K^0 - \bar{K^0}$ mixing, the existence of the Δ^{++} resonance, the apparently infinitely rising neutrino cross-section, the $\Delta I = \frac{1}{2}$ rule in weak decays, the hadron spectroscopy respecting the eightfold way, CP violation... How could you live for such a long time with all these problems without inventing the Standard Model which solves them all?

Of course, shall we older people answer, it took more than ten years from the original idea of the existence of the W boson [1] to the realization that an experimentally successful model with weak isospin symmetry [2] would imply the existence, not only of Neutral Weak Currents but also of charmed particles [3, 4], and a few more years for 't Hooft [5] to demonstrate that such a model would constitute a mathematical consistent theory. This we believe is the main answer to our student's surprise: the solution of the puzzle required i) two new experimental discoveries, that of Neutral Currents and that of Charm; and ii) a theoretical breakthrough, the renormalization of the Gauge Theory.

The dam broke in 1973 with the observation of Neutral Currents. The sequence of events that followed this discovery is really breathtaking: charm in 1974, tau lepton in 1975, beauty in 1977, direct observation of the W and Z bosons in 1983. The model was soon universally accepted, especially when more precise verifications of its quantitative predictions were made in atoms [6] and in electron nucleon scattering [7]. For the last 25 years the

Model has met a long series of experimental verifications, proving itself an unbelievably successful scheme.

So successful the model is, that it would be perhaps even harder to persuade the aforementioned beginner physicist that a time could well come when there will be *no more* a Standard Model. Why should one abandon such a successful scheme, after all?

As a matter of fact, it has been argued by many respectable physicists that, although the Standard Model is in contradiction with no known experimental result in particle physics today, it certainly leaves several fundamental questions unanswered; among these, the fact that it requires as arbitrary input so many different particle masses. Also, the observed baryon-anti-baryon asymmetry in the Universe is very hard to explain within its framework. Furthermore, the role and the nature of the Higgs particle or even its existence are far from being clarified. Without entering now the details of these deep questions, we feel that, in analogy with the pre-Standard Model situation, a solution to these problems would require a new extraordinary combination of i) experimental discoveries, and ii) theoretical breakthroughs.

The aim of this book is to illustrate, in a pedagogical way, the most precise experimental verifications of the Standard Model to date. These were obtained by the thorough study of the two massive resonances, whose role in the model turns out to be crucial : the Z and the W bosons.

As we shall see, the results of campaigns of experiments at LEP and SLC, as well as at $p\bar{p}$ colliders, have established in a definitive way many features of the Model, and probed it with an unprecedented accuracy. The main results of these investigations will be discussed in detail in this book, with special emphasis on precise measurements of several quantities sensitive to electroweak radiative corrections.

This last point, on one hand, provided beautiful confirmation of the validity of the theoretical scheme. On the other hand, the sensitivity of Electroweak radiative corrections to virtual particles, albeit too massive to be directly accessible to experimental observation, has led to the prediction of the top quark mass, well before this particle was observed directly in $p\bar{p}$ collisions. One must honestly say that a major building block of the Standard Model is still missing, since the Higgs boson has not yet been discovered in direct searches. However, once the top quark mass was experimentally known, the interest of radiative corrections as indirect probes of unknown effects was considerably enhanced, since the only remaining open question, at least in the framework of the Standard Model, would be that

of the Symmetry Breaking mechanism. In fact, from a combined analysis of several independent measurements, it has become possible to reach two fundamental conclusions. The first one is that, if the unknown mechanism of symmetry breaking were different from that advocated by the Standard Model, its visible manifestations would be practically indistinguishable at the available level of precision. The second conclusion is that, if the Standard Model is correct, the Higgs boson must be relatively light, i.e. well accessible to the next generation of colliders.

This book begins with a short introduction to weak interactions. The main virtues of Fermi theory are reviewed, together with its main deficiencies that led to the introduction of the intermediate massive vector bosons. The essential features of the Standard Model, in particular the Higgs mechanism, are subsequently quickly summarized. The discussion of specific processes is organized in the book in the following way: in the first part, we discuss the physics of the Z boson, starting with the tree level calculation of electron-positron annihilation into fermion pairs, $e^+e^- \to f\bar{f}$, given in Chapter 2. This contains the expressions of total cross-sections, angular distributions, Z partial decay widths. Particles polarization effects, especially longitudinal polarization, are given.

Since this is one of the main motivations of precision electroweak measurements, it is natural to continue in Chapter 3 with a pedagogical description of the virtual electroweak radiative effects. A one-loop treatment is given here, working in the approximation of massless final fermions, with goal to provide understanding of the structure of these virtual effects, and of why and how they are sensitive to heavy physics, symmetry breaking and possibly new particles. A particular attention is given to the running of α_{QED}, as this constitutes an important source of uncertainty. The specially relevant case of massive final fermions is treated in detail in Chapter 4, with emphasis on $b\bar{b}$ production. The main results of Chapters 3 and 4 are summarized in a table that concludes the description of the one-loop treatment.

After a short description of the main experimental tools for Z and W physics, i.e. high energy colliders and detectors, the detailed discussion of the high-precision tests of the electroweak theory starts in Chapter 6. This Chapter describes what constitutes arguably the most unique achievement of LEP: the measurement of the Z lineshape. A discussion of the global strategy, including the estimate of real radiation of photons, that plays a very important rôle in this particular set of measurements, is followed by a

detailed account of the measurements of cross-sections, including luminosity monitoring and Z decay event selection. The first historical result of LEP and SLC, the determination of the number of light neutrino species, is described and commented. From the lineshape one obtains precise determinations of the Z mass and width, that will probably remain unchallenged for some time, and a complete set of Z leptonic and inclusive hadronic partial widths. In Chapter 7 the main experimental issues involving Z decays to heavy quarks are discussed. The necessary tools related to beauty and charm quark tagging are introduced. These sophisticated methods allow, for instance, the precise determination of the partial Z decay into $b\bar{b}$ and of the b and c quark asymmetries, whose rôle for the high precision tests turns out to be particularly relevant. In Chapter 8 we come to some of the observables that are most sensitive to Electroweak Radiative Corrections involving the Higgs boson, in particular we shall consider the longitudinal polarization asymmetry, measured at the SLC, the τ lepton polarization and the unpolarized forward-backward asymmetries of leptons and quarks. Chapter 8 ends with a summary of all measurements of the leptons and quarks couplings.

In the following Chapter (Chapter 9), the focus moves from the Z boson to the W boson. After a description of W production processes at colliders, a discussion is given of one of the most important parameters measurable at these machines, the W mass. In fact, the production of W bosons opens the possibility of performing direct tests of the sector of the electroweak interactions related to gauge boson-gauge boson couplings. The precision measurements of the triple gauge couplings required by the model are here discussed in some detail.

In the final Chapters of the book, the direct production of the top quark and of the Higgs boson are discussed; results are compared to bounds from electroweak precision tests. After a brief review of top physics, mostly devoted to its discovery and to the measurement of its mass at the Tevatron (Chapter 10), a detailed description of the searches for the Higgs boson at LEP is given in Chapter 11. This is followed by a discussion about the indirect bounds on the Higgs boson mass, and by the results of a model-independent analysis of electroweak data. A short conclusive Chapter 12 discusses the outlook for further improvements in the domain of high precision tests at future colliders.

R. Tenchini
C. Verzegnassi

Contents

This page intentionally left blank

Chapter 1

The Standard Model of Electroweak Interactions

1.1 Weak interactions in the original Fermi approach

For a long period of time, weak interactions were described by the so called Fermi theory, that was essentially based on the use of an effective four-fermion interaction Lagrangian $\mathcal{L}$, with a weak coupling constant to be conventionally called G_F. This Lagrangian was able to incorporate and explain in a remarkably satisfactory way the major part of the experimental features of weak interactions for several years after its proposal. In particular, it was possible to give an operative meaning to the coupling constant G_F by relating it *rigorously* to the experimentally measured muon weak decay. Given this operative definition of G_F, and following the Galilean "provando e riprovando" philosophy, an impressive number of theoretical successful predictions were given for processes describable by *charged* weak fermion *currents*. The latter quantities had two special features, a) their formal expression was similar to that of the electromagnetic current, i.e. terms transforming like Lorentz four-vectors were involved, and b) a special combination of vector and axial vector terms was required to meet the experimental existing evidence. This was officially called the V-A form, and corresponded to the typical expression, e.g. for a lepton component ℓ,

$$J^{(W)}_{\alpha,\ell} = \bar{\psi}_{\nu_\ell}\gamma_\alpha(1-\gamma_5)\psi_\ell \tag{1.1}$$

where ν_ℓ is the ℓ-type neutrino [1]. Analogous expressions for quarks were eventually introduced and successfully developed. As one notices immediately, the effective fermion currents, that generalize Eq. (1.1), can be identically re-expressed in terms of *left*-handed fermion fields defined as

[1] The conventions of Ref. [8] are followed in this book. The representations of the γ and Pauli matrices can be found in Section 2.1.

$$\psi_{fL} = \frac{1}{2}(1-\gamma_5)\psi_f \tag{1.2}$$

since

$$J^{(W)}_{\alpha,\ell} = 2\bar{\psi}_{\nu_\ell}\gamma_\alpha\psi_{\ell L} \equiv 2J^{(+)}_{\alpha,\ell} \tag{1.3}$$

where we have used the definition

$$J^{(+)}_{\alpha,\ell} \equiv \bar{\psi}_{\nu_\ell L}\gamma_\alpha\psi_{\ell L}$$

and the identity $\gamma_\alpha(1-\gamma_5) = \frac{1}{2}(1+\gamma_5)\gamma_\alpha(1-\gamma_5)$. One defines also right-handed fields as

$$\psi_{fR} = \frac{1}{2}(1+\gamma_5)\psi_f\,. \tag{1.4}$$

For massless fermions, the definitions of Eqs. (1.2),(1.4) also correspond to the two different spin orientations. This point will be discussed in Section 2.2.

What we can say at this stage is that a large amount of weak interaction processes can be satisfactorily described assuming that *charged* weak currents exist that are exclusively made of *left-handed* fermion fields. In terms of these currents, the effective Fermi Lagrangian is conventionally written in the form:

$$\mathcal{L}_W(x) = -\frac{G_F}{\sqrt{2}}\sum_{i,j} J^{(W)}_{\alpha,i}(x)J^{(W)\alpha\dagger}_{j}(x) + \text{ h.c. }. \tag{1.5}$$

Clearly, the possible existence of weak interaction processes, related to *neutral* weak currents, is not taken into account by the Fermi Lagrangian. Low energy charged current processes, however, are satisfactorily described by Eq. (1.5). As already mentioned the muon decay is a particularly relevant example. The matrix element of the process $\mu^-(p) \to e^-(k)\bar{\nu}_e(q_1)\nu_\mu(q_2)$, where p is the four momentum of the decaying muon and k, q_1, q_2 the four momenta of the electron and two neutrinos, respectively, can be computed from Eq. (1.5) as

$$M = \sqrt{\frac{1}{2}}G_F J^{(W)}_{\alpha,\mu}J^{(W)\alpha\dagger}_{e}\,. \tag{1.6}$$

The matrix element squared, gives (the detailed calculation can be found in [9])

$$\Sigma|M|^2 = 64G_F^2(p_\alpha q_1^\alpha)(k_\beta q_2^\beta) \tag{1.7}$$

leading to the muon decay width

$$d\Gamma = \frac{\Sigma|M|^2}{4m_\mu} d\Phi^{(3)} \tag{1.8}$$

where the last term is the three-body phase space. Integrating over the neutrino four momenta yields the energy (E) spectrum of the electron

$$d\Gamma(y)dy = \frac{G_F^2 m_\mu^5}{96\pi^3}(3-2y)y^2 dy \tag{1.9}$$

where $y = E/E_{max} = 2\frac{E}{m_\mu}$ is the fractional electron energy. Equation (1.9) is experimentally verified with high precision. Indeed the most general form that can be computed assuming Lorentz invariance is [10]

$$d\Gamma(y)dy = \frac{G_F^2 m_\mu^5}{16\pi^3}[(1-y) - \frac{2}{9}\rho(3-4y)]y^2 dy \tag{1.10}$$

that is reduced to Eq. (1.9) if ρ, usually called Michel parameter, equals 0.75. The experimental measurements give $\rho = 0.7518 \pm 0.0028$ [11] in agreement with the Fermi Lagrangian. The decay of polarized muons has been also studied by accurate experiments. The electron angular distribution can be studied as a function of the direction of the emitted electron $\vec{n}$ with respect to the muon polarization $\vec{\eta}$ (both vectors are unit vectors). Defining $cos\theta = \vec{n} \cdot \vec{\eta}$ the electron angular distribution, integrated over the electron energy can be written as

$$\frac{d\Gamma(cos\theta)}{\Gamma} = \frac{1}{2}(1 - \frac{1}{3}\xi cos\theta)d\theta \tag{1.11}$$

with the asymmetry parameter $\xi = 1$ for the Fermi Lagrangian. The measurement gives [12] $\xi = 1.005 \pm 0.009$ in agreement with the expectation. Finally the total decay width can be computed by integrating Eq. (1.9) yielding

$$\Gamma = \frac{G_F^2 m_\mu^5}{192\pi^3} \tag{1.12}$$

that gives the operative definition of G_F, measured by the muon lifetime: the muon decays through $\mu \to e^- \bar{\nu}_e \nu_\mu$ with $\approx 100\%$ branching ratio and

$\tau_\mu = \frac{1}{\Gamma}$. The experimental result for the muon lifetime is actually very precise [13]

$$\tau_\mu = (2197.03 \pm 0.04)\,\text{ns}$$

and a meaningful definition of G_F requires Quantum-ElectroDynamic radiative corrections to be computed. These are due to the emission of real photons and to damping effects (*vertex corrections*) associated with virtual photons [14] and modify Eq. (1.12) by a factor $\approx (1 + \frac{\alpha}{2\pi}[\frac{25}{4} - \pi^2])$, where $\alpha \equiv e^2/4\pi$ is the fine-structure constant. The QED correction to the muon decay rate is relevant (about 0.4%) and has been accurately computed to the second order in Feynman diagrams (*two-loop corrections*) in the framework of the Fermi Lagrangian [15]. Equation (1.12) is modified as

$$\Gamma = \frac{G_F^2 m_\mu^5}{192\pi^3}\; F\left(\frac{m_e^2}{m_\mu^2}\right)[1 + \Delta Q]\;, \tag{1.13}$$

where $F(x)$ is a phase-space term taking into account the finite electron mass

$$F(x) = 1 - 8x + 8x^3 - x^4 - 12x^2 \ln x \tag{1.14}$$

and ΔQ represents the radiative corrections. Equation(1.13) gives

$$G_F = 1.16637(1) \times 10^{-5}\,\text{GeV}^{-2}\,. \tag{1.15}$$

The 9×10^{-6} relative error on G_F from the input quantities is dominated by the experimental uncertainty on τ_μ.

In spite of its success in describing the muon decay and other low energy phenomena as the β decay, the Fermi Lagrangian fails at high energy. Taking, as an example, $\nu_e(k_1) + e(p_1) \to \nu_e(k_2) + e(p_2)$ scattering (k_1, p_1, k_2, p_2 indicate the four momenta of the initial and final state neutrinos and electrons) from crossing symmetry the matrix element of the process can be readily computed from Eq. (1.6), giving

$$\Sigma|M|^2 = 64 G_F^2 (p_{1\alpha} k_1^\alpha)(p_{2\beta} k_2^\beta) \tag{1.16}$$

and the related cross section is computed from

$$d\sigma = \frac{\Sigma|M|^2}{4(k_1 p_1)} d\Phi^{(2)} \tag{1.17}$$

where $\Phi^{(2)}$ represent the two-body phase space.

In the centre-of-mass frame Eq. (1.17) yields

$$\frac{d\sigma}{d\Omega} = \frac{G_F^2}{4\pi^2}\frac{(s-m_e^2)^2}{s} \tag{1.18}$$

where s is the squared centre-of-mass energy. The integration over the angles, neglecting the electron mass, yields

$$\sigma = \frac{G_F^2}{\pi}s\,. \tag{1.19}$$

In the laboratory frame, assuming the target electron at rest, $s = 2m_eE_\nu$, showing that the cross section grows linearly with the neutrino energy, as experimentally verified. Equation (1.19), however, is bound to violate unitarity constraints, as can be seen by relating it to the maximal cross section expected by the optical theorem. Since, as shown by Eq. (1.18), the reaction occurs in s-wave, the optical theorem gives

$$\sigma_{tot} = \frac{4\pi}{k}Imf_{l=0}\,. \tag{1.20}$$

where $k = \frac{\sqrt{s}}{2}$ and $f_{l=0}$ is the s-wave scattering amplitude, usually parametrized as $\frac{1}{2ik}(\eta e^{2i\epsilon} - 1)$, with ϵ as a real phase and the inelasticity η bounded by $0 \leq \eta \leq 1$. On gets

$$\sigma_{tot} \leq \frac{2\pi}{k^2}(\eta + 1) \leq \frac{4\pi}{k^2} \tag{1.21}$$

which compared to Eq. (1.19) yields

$$\frac{G_F^2}{\pi}s \leq \frac{4\pi}{k^2} = \frac{16\pi}{s} \tag{1.22}$$

showing that unitary is violated at $s = \frac{4\pi}{G_F}$, corresponding to a centre-of-mass energy of the neutrino of about 500 GeV and a very large neutrino energy (500 TeV) in the laboratory frame.

In conclusion the Fermi Lagrangian satisfactorily describes charged-current processes at low energy, but violates unitarity, which is intimately related to the fact that Fermi theory is not renormalizable. The description of weak interactions at high energies requires therefore a new theoretical scheme, that should also be able to incorporate neutral current processes. A picture that will satisfy these two mandatory requirements will be that with intermediate vector bosons, discussed in the following Section.

1.2 Weak interactions and the intermediate vector bosons

From a purely formal point of view, the possibility of describing charged weak interactions as if they were *mediated* by the exchange of charged spin one bosons appears as a natural consequence of the validity of the assumed parameterization Eq. (1.5). The latter can be actually considered as the effective parameterization, valid in the limit of negligible momentum transfer, of the lowest order corresponding *charged vector boson* (CVB) formulation derivable from the Lagrangian:

$$\mathcal{L}_{CVB}(x) = -\frac{g}{\sqrt{2}} \sum_i \left[J^{(+)}_{\alpha,i}(x) W^{+\alpha}(x) + \text{h.c.} \right] \tag{1.23}$$

where W^+_α is the field operator describing a charged spin one boson and g is its weak coupling to left-handed fermions. The condition that fixes the aforementioned equivalence is that the original "normalization" of the Fermi description is reproduced by the intermediate vector boson formulation Eq. (1.23). In particular, the value of the muon lifetime calculated in the latter formalism at lowest order via W exchange (formally, at zero momentum transfer) must be numerically equal to the experimental value. This is, in turn, related to the definition (i.e. to the *numerical* value) of G_F given by Eq. (1.15). In terms of this precisely defined quantity, the normalization condition that makes the intermediate vector boson description acceptable is, as one can easily verify [9, 16], that:

$$\frac{G_F}{\sqrt{2}} = \frac{g^2}{8 m_W^2} \, . \tag{1.24}$$

Equation (1.24) will be of paramount importance for the remaining part of this book, and we shall make this point evident, very frequently, in the next Sections. At this preliminary stage we shall only stress the fact that, for the moment, the equality that is written only implies the parameters of a certain Lagrangian $\mathcal{L}(g, m_W)$ and a quantity derived from $\mathcal{L}$ at lowest order. In other words, all quantities in Eq. (1.24) should be considered for the moment as *bare* ones, and we shall return to this point later on. Independently of this feature, the fundamental consequence that is derived from Eq. (1.24) is that, if one wants to adopt an equivalent formulation to the description of weak charged interactions that postulates the exchange of charged vector bosons, these particles *must be massive*, $m_W \neq 0$, if the (reasonable) phenomenological requirement of reproducing the finite value of the muon lifetime (with a non trivially vanishing g) is satisfied.

Keeping in mind this very strong phenomenological constraint, one can now return to the expression of the Lagrangian Eq. (1.23) and simply realize the fact that it looks like an almost obvious generalization of the QED interaction Lagrangian, with the electric charge e replaced by g, the fermion fields replaced by their left-handed counterparts and the photon replaced by the $W^{\pm}$ bosons. It appears in a sense almost natural and aesthetically motivated to postulate that the Lagrangian of the weak interactions has gauge invariance [16], like QED, with (at least) two W_α gauge bosons, electrically charged, whose presence guarantees the invariance of the Lagrangian under transformations of a certain gauge group to be identified. Since each gauge boson is associated to one of the group generators, the candidate group should have two generators at this stage, a requirement that has no realistic known solution. The nearest possibility is provided by a local $SU(2)$ group, which has *three* generators, T_1, T_2, T_3 two of which can be combined to produce two *charged* generators $T^{\pm} = (T_1 \pm iT_2)$ which might be associated with $W^{\pm}$. From the commutation relations obeyed by $SU(2)$ generators, $[T_i, T_j] = i\epsilon^{ijk}T_k$ the third generator T_3 can be expressed as the commutator of the *charged* generators, T^+, T^- :

$$[T^+,\, T^-] = T^+T^- - T^-T^+ = 2T_3\,. \tag{1.25}$$

If this picture turned out to be correct, a first candidate symmetry group of weak interactions would therefore be a local $SU(2)$ group, whose non Abelian nature is summarized by the commutation relation Eq. (1.25). From the expression of charged currents given in Eq. (1.3) one can derive the expressions of the corresponding charges (supposedly, SU(2) generators) finding

$$T^+ = \frac{1}{2}\int J^{(W)}_{0,\ell}(x)d^3x = \frac{1}{2}\int 2\bar{\psi}_{\nu_\ell}\gamma_0(1-\gamma_5)\psi_\ell d^3x\,, \tag{1.26}$$

$$T^- = (T^+)^\dagger \tag{1.27}$$

and from Eq. (1.25) one has

$$T_3 = \frac{1}{4}\int \bar{\psi}_{\nu_\ell}\gamma_0(1-\gamma_5)\psi_{\nu_\ell} - \bar{\psi}_\ell\gamma_0(1-\gamma_5)\psi_\ell d^3x\,, \tag{1.28}$$

This shows that T_3 will not change the electric charge and will be consequently associated with an electrically neutral vector boson, to be coupled in an extended Lagrangian with neutral fermion currents. In order to generalize in a consistent way the phenomenology of the charged component

of the interaction, the involved fermions, supposedly transforming as suitable irreducible representations of the symmetry group, should be of pure left-handed type. For this reason, the candidate symmetry group should be called $SU(2)_L$, and the corresponding generators T_L^+, T_L^- and T_{3L}.

A very important statement, to be made at this precise point, is that the postulated electrically neutral gauge boson to be associated with T_{3L} *cannot* be the photon if the assumed scenario only contains the fields of Eq. (1.3). Actually a different scheme existed in which additional heavy leptons were postulated, so that the commutator of the overall T^+ and T^- reproduced the electric charge [17]. Without neutral currents, that model was abandoned after the discovery of the latter ones in 1973, also because suitable heavy leptons were not observed. The fact that the new neutral gauge boson is not the photon is an immediate consequence of the commutation relation Eq. (1.25) since, as one can easily verify, the commutator of the charges (generators) associated with the fermion currents $J_\alpha^{(+)}, J_\alpha^{(-)}$ is *not* the electric charge but some different, electrically neutral, quantity. At this stage, this unknown gauge boson will be called W_3, and considered as a technical requirement of the theoretical proposal.

From a purely aesthetical point of view, it appears certainly attractive to endow weak interactions with gauge invariance e.g. of the previous type. In a sense, this would lead in a natural way to the beautiful idea that there should exist a kind of unification between weak and electromagnetic interactions, the latter ones being invariant with respect to a $U(1)$ gauge group. Leaving the discussion of electro-weak unification to the next Subsections, we now concentrate our attention on this possibility and accept the idea of a $SU(2)_L$ (non Abelian) gauge symmetry. One obvious and unavoidable problem is that such a symmetry *cannot* be exact , unlike the similar case of QED, since its candidate gauge bosons must be *massive*. Therefore, one must necessarily assume that $SU(2)_L$ is, from the beginning, a broken symmetry.

The simplest possibility of an explicit symmetry breaking, that would correspond to the addition "by hand" of an extra non invariant mass term to the Lagrangian $\sim m_W^2 W_\alpha W^\alpha$, is immediately ruled out since it would lead to a tough theoretical difficulty, given the fact that the associated field theory would become non renormalizable, and the canonical perturbative calculations would loose any sense. Technically speaking, this would be an immediate consequence of the expression of the W propagator, that would

become:

$$i\, P_{\mu\nu}(q) = -i\frac{(g_{\mu\nu} - q_\mu q_\nu / m_W^2)}{q^2 - m_W^2 + i\epsilon} \tag{1.29}$$

and would approach a constant, rather than vanishing, in the limit $q \to \infty$. This means that one must find a way of giving a mass to the $SU(2)_L$ gauge bosons without breaking *explicitly* the symmetry. One appealing solution mechanism that achieves this goal is the combination of *spontaneous* symmetry breaking with the Higgs mechanism.

In the next Section we shall choose a particularly simple and relevant example to show very briefly the main, interesting features of this deservedly famous topics.

1.3 The Higgs mechanism in the local $SU(2)$ gauge symmetry case

We consider the example (that will be very useful to understand the main features of the Standard Model, to be discussed in the next Section) of a system of complex *scalar* fields, invariant with respect to a certain local $SU(2)$ group. The simplest case is provided by a system consisting of a couple of such fields, transforming under $SU(2)$ as a doublet. In a conventional notation, the scalar doublet will be associated to a column:

$$S \equiv \begin{vmatrix} S_u \\ S_d \end{vmatrix} \tag{1.30}$$

where S_u, S_d are complex scalar fields. By hypothesis, S will transform under a general local $SU(2)$ transformation as a $SU(2)$ doublet i.e.

$$S' = e^{-i\left[\alpha_\kappa(x)\frac{\tau_\kappa}{2}\right]} S \tag{1.31}$$

where τ_κ are the three Pauli matrices, that express the effect of the $SU(2)$ generators T_κ in the irreducible doublet representation.

Although this is not in principle necessary, let us consider the simplest case of infinitesimal transformations and let us replace $\alpha_\kappa(x)$ by $\epsilon_\kappa(x)$ in this limiting situation. Then, neglecting $\mathcal{O}(\epsilon^2)$ effects, Eq. (1.31) can be read as:

$$S' \equiv \begin{vmatrix} S'_u \\ S'_d \end{vmatrix} = \left[1 - i\epsilon_\kappa(x)\frac{\tau_\kappa}{2}\right] S = \begin{vmatrix} S_u \\ S_d \end{vmatrix} - i\epsilon_\kappa(x)\frac{\tau_\kappa}{2} \begin{vmatrix} S_u \\ S_d \end{vmatrix} . \tag{1.32}$$

From the known expressions of the Pauli matrices one then easily derives:

$$\begin{vmatrix} S'_u \\ S'_d \end{vmatrix} = \begin{vmatrix} S_u \\ S_d \end{vmatrix} - \frac{i}{2}\left\{ \epsilon_1(x) \begin{vmatrix} S_d \\ S_u \end{vmatrix} + \epsilon_2(x) \begin{vmatrix} -iS_d \\ iS_u \end{vmatrix} + \epsilon_3(x) \begin{vmatrix} S_u \\ -S_d \end{vmatrix} \right\} . \tag{1.33}$$

Equation (1.33) shows how the scalar doublet changes under the most general infinitesimal transformation belonging to the local $SU(2)$ group. In particular, one can see the effect of each single independent transformation $\epsilon_\kappa(x)$ related to the corresponding generator T_κ of the group.

In a quantum field theory, where the fields are local operators, the effect of an infinitesimal (κ) transformation of the group on a given field can also be identically represented as the action of the associated generator T_κ in the form

$$S' \equiv e^{i\epsilon_\kappa(x)T_\kappa} S e^{-i\epsilon_\kappa(x)T_\kappa} \tag{1.34}$$

that can also be written as:

$$S' - S \simeq i\epsilon_\kappa(x)[T_\kappa, S] \equiv \delta S_{(\kappa)} \tag{1.35}$$

(no summation on the index κ). Equating this expression to Eq. (1.33) one formally gets:

$$[T_1, S] \equiv \begin{vmatrix} [T_1,\ S_u] \\ [T_1,\ S_d] \end{vmatrix} = -\frac{1}{2} \begin{vmatrix} S_d \\ S_u \end{vmatrix} \tag{1.36}$$

$$[T_2, S] = -\frac{1}{2} \begin{vmatrix} -iS_d \\ iS_u \end{vmatrix} \tag{1.37}$$

$$[T_3, S] = -\frac{1}{2} \begin{vmatrix} S_u \\ -S_d \end{vmatrix} . \tag{1.38}$$

Equations (1.33)–(1.38) remain valid when one "sandwiches" their left- and right-hand members into the vacuum state and considers the scalar fields expectation values in the vacuum (vev). When such an operation is performed, on realizes that, provided that *at least one* of the "basic" vevs $\langle S_u \rangle_0$, $\langle S_d \rangle_0$ is different from zero, *all* the three commutators of Eqs. (1.36)–(1.38), that express the change of $\langle S \rangle_0$ under the three independent infinitesimal transformations, are non vanishing. This means that, under the condition that either $\langle S_u \rangle_0$ or $\langle S_d \rangle_0$ is not vanishing, none of the three generators $T_{1,2,3}$ can annihilate the vacuum:

$$T_\kappa |0\rangle \neq 0 , \qquad \kappa = 1,\, 2,\, 3 . \tag{1.39}$$

In particular, since the fields are supposedly complex, it will be sufficient to require that one of the components of either S_u or S_d has non vanishing vev. Defining conventionally:

$$S_u \equiv s_2 + is_1 \tag{1.40}$$

$$S_d \equiv s_0 + is_3 \tag{1.41}$$

one usually assumes that $\langle s_0 \rangle_0 \neq 0$ and defines the *real* quantity:

$$\langle s_0 \rangle_0 \equiv \frac{1}{\sqrt{2}} v \tag{1.42}$$

so that

$$\langle S \rangle_0 = \frac{1}{\sqrt{2}} \begin{vmatrix} O \\ v \end{vmatrix} . \tag{1.43}$$

Starting from Eqs. (1.40)–(1.43), one can now return to Eqs. (1.36)–(1.38) and derive the following equalities (as a consequence of the reality of v), just by taking the expectation values in the vacuum of all involved members:

$$\langle [T_1,\, s_1] \rangle_0 = -\frac{i}{2} \langle s_0 \rangle_0 \tag{1.44}$$

$$\langle [T_2,\, s_2] \rangle_0 = \frac{i}{2} \langle s_0 \rangle_0 \tag{1.45}$$

$$\langle [T_3,\, s_3] \rangle_0 = -\frac{i}{2} \langle s_0 \rangle_0 \, . \tag{1.46}$$

Until now, no assumption has been made concerning the invariance of the system with respect to the chosen group, and only the formal property of transforming like a doublet has been imposed on S. If one now wishes to postulate a symmetry of the system with respect to the $SU(2)$ local group transformations, and wants at the same time to retain a non vanishing vev like in Eq. (1.42), one sees that the immediate consequence will be that the realization of the symmetry will be of a rather particular kind. Actually, it will still be possible to impose the invariance of the Lagrangian under the group transformations; but for the vacuum this will not be possible, since owing to Eq. (1.39) all the three independent local SU(2) transformations will change it. This situation is conventionally defined as that of a *spontaneously broken* symmetry. More precisely, this definition is used when at least one of the generators has this property. In our case, all three generators have it. One should stress at this point the fact that this is not a general feature of the chosen group, but indeed of the assumed doublet representation, and would not remain valid in other situations (like for instance one in which the scalar fields are supposed to transform like a real triplet).

Having seen that a possible local $SU(2)$ symmetry of the considered system must be spontaneously broken if the vacuum "hosts" a scalar field,

we now reconsider the three Eqs. (1.44)–(1.46). If the symmetry had been a *global* one (corresponding to the case of constant $\epsilon_{1,2,3}$), these equations would have been the starting point for the rigorous derivation of a theorem, due to Goldstone, whose conclusion would have been the predicted existence of three massless Goldstone bosons corresponding to the three fields s_1, s_2, s_3 . This can be seen e.g. by inserting a complete set of physical states into the left-hand members of Eqs. (1.44)–(1.46) and associating a conserved current to each generator; we defer to Ref. [18] for a rigorous proof. This conclusion would not be correct in the case of a local symmetry that we are considering.

Let us therefore and finally consider the requirement of local symmetry in more detail. If the SU(2) symmetry were of global type the traditional choice for the Lagrangian would be

$$\mathcal{L}_G = (\partial_\mu S)^\dagger (\partial^\mu S) - V(S) \tag{1.47}$$

where

$$V(S) = -\mu^2 (S^\dagger S) + \lambda (S^\dagger S)^2 \ . \tag{1.48}$$

The Lagrangian Eq. (1.47) is manifestly invariant under a global $SU(2)$ group, but also manifestly non invariant under the gauge generalization. To achieve an invariant Lagrangian, the known prescription is that of adding to the system three spin one gauge bosons A^1_μ, A^2_μ, A^3_μ with prescribed transformation properties under the group, and to replace systematically the ordinary derivative ∂_μ by the covariant derivative D_μ, the latter being defined in the chosen system as:

$$D_\mu S = \left(\partial_\mu - ig\frac{\tau_\kappa}{2} A^\kappa_\mu\right) S \tag{1.49}$$

where g is by definition the local $SU(2)$ coupling constant. The same coupling will also appear in the transformation law obeyed by the gauge bosons A^i_μ in order to make the term $(D_\mu S)^\dagger (D^\mu S)$ gauge invariant. The full local $SU(2)$ invariant Lagrangian will be finally written as:

$$\mathcal{L}_L = (D_\mu S)^\dagger (D^\mu S) - V(S) - \frac{1}{4} F^\kappa_{\mu\nu} F^{\mu\nu}_\kappa \tag{1.50}$$

with

$$F^\kappa_{\mu\nu} = \partial_\mu A^\kappa_\nu - \partial_\nu A^\kappa_\mu + g\epsilon^{\kappa\ell m} A^l_\mu A^m_\nu \ . \tag{1.51}$$

Until now, no special requirement has been imposed upon the scalar field S. As one sees immediately, this situation would correspond, in the

classical analogue, to a minimum of the potential for conventional negative values of μ^2 in Eq. (1.48). But for positive μ^2 values, the picture is quite different, and the classical minimum would correspond to

$$\langle S^\dagger S\rangle_0 = \frac{1}{2}\frac{\mu^2}{\lambda} \; . \tag{1.52}$$

The simplest way of meeting Eq. (1.52) is to take

$$\langle S\rangle_0 = \frac{1}{\sqrt{2}}\begin{vmatrix} 0 \\ v \end{vmatrix} \tag{1.53}$$

where

$$v = \sqrt{\frac{\mu^2}{\lambda}} \tag{1.54}$$

that corresponds to the assumed configuration Eq. (1.43), and generates consequently spontaneous symmetry breaking.

The canonical way of treating the system proceeds now by replacing the original field S by a "shifted" field $\tilde{S}$ that will be by definition more convenient for perturbative expansions:

$$\tilde{S} \equiv S - \langle S\rangle_0 \; . \tag{1.55}$$

In terms of this shifted field, the product of covariant derivatives in Eq. (1.50) becomes then:

$$\begin{aligned}(D_\mu S)^\dagger (D^\mu S) = (\partial_\mu \tilde{S})^\dagger(\partial^\mu \tilde{S}) + \frac{g^2}{4}A_{\mu\kappa}A^\mu_\kappa \langle S^\dagger S\rangle_0 - gIm\left[\langle S^\dagger\rangle_0 \tau_\kappa A_{\mu\kappa}\partial^\mu \tilde{S}\right] \\ -gIm\left[\tilde{S}^\dagger \tau_\kappa A_{\mu\kappa}\partial^\mu \tilde{S}\right] + \frac{g^2}{4}A_{\mu\kappa}A^\mu_\kappa\left[\tilde{S}^\dagger\tilde{S} + 2Re(\tilde{S}^\dagger\langle S\rangle_0)\right] \\ = \frac{1}{2}\left(\frac{gv}{2}\right)^2 \quad A_{\mu\kappa}A^\mu_\kappa + O(\tilde{S}^2,\, A_\mu\tilde{S},\, A_\mu\tilde{S}^2,\, A^2_\mu\tilde{S},\, A^2_\mu\tilde{S}^2)\end{aligned} \tag{1.56}$$

(the properties of the Pauli matrices have been used). One realizes immediately that the three gauge bosons have acquired a (*equal*) mass, as a direct consequence of the assumed existence of a non vanishing scalar field vev, and that

$$M_A = \frac{1}{2}gv \; . \tag{1.57}$$

Independently of this rather surprising fact, one would still expect to find three massless scalars in the overall Lagrangian. With this aim, one looks for all possible quadratic terms in the shifted fields, rewriting the potential $V(S)$ Eq. (1.48), and finds:

$$V(S) = -\mu^2\left[(\tilde{S} + \langle S\rangle_0)^\dagger(\tilde{S} + \langle S\rangle_0)\right] + \lambda\left[(\tilde{S} + \langle S\rangle_0)^\dagger(\tilde{S} + \langle S\rangle_0)\right]^2$$

$$= -\mu^2 \tilde{S}^\dagger \tilde{S} + \lambda \left[2\tilde{S}^\dagger \tilde{S} \langle S^\dagger S \rangle_0 + 4(Re\tilde{S}^\dagger \langle S \rangle_0)^2 \right]$$

$$+\text{non quadratic terms} \, . \tag{1.58}$$

Using the assumed Eq. (1.52) one sees that the first two terms in the quadratic expression cancel exactly, leaving the residual term:

$$V_{\text{Quad}} = 4\lambda (Re\tilde{S}^\dagger \langle S \rangle_0)^2 = 4\lambda \left[Re \left(\tilde{S}_u^\dagger \langle S_u \rangle_0 + \tilde{S}_d^\dagger \langle S_d \rangle_0 \right) \right]^2$$

$$= 4\lambda \left[\tilde{s}_0 \langle s_0 \rangle_0 + \tilde{s}_1 \langle s_1 \rangle_0 + \tilde{s}_2 \langle s_2 \rangle_0 + \tilde{s}_3 \langle s_3 \rangle_0 \right]^2 \, . \tag{1.59}$$

A glance to Eq. (1.59) shows that, provided that *at least one* of the four vev of the original fields is non vanishing, as assumed, there will always be *one and only one* massive shifted field, by definition the linear combination that appears in Eq. (1.59). In the simplest case that is normally adopted, only $\langle s_0 \rangle$ is different from zero and the associated shifted field $\tilde{s}_0$ will remain massive:

$$V_{\text{Quad}} = 4\lambda \tilde{s}_0^2 \langle s_0 \rangle^2 = \mu^2 2 \tilde{s}_0^2 \tag{1.60}$$

whilst the remaining three field $\tilde{s}_{1,2,3}$, being associated to vanishing $s_{1,2,3}$ vevs, will be massless. The residual massive field $\sqrt{2}\tilde{s}_0 \equiv (1/\sqrt{2})(\tilde{S}_d + \tilde{S}_d^\dagger)$ is called the Higgs boson field. For what concerns the three remaining fields, the impression at this stage, as announced, is that the standard Goldstone theorem prediction is verified.

The fact that invalidates this conclusion is provided by the existence of the third term in Eq. (1.56). Assuming for simplicity the existence of one single non vanishing $vev = \langle s_0 \rangle_0$ like in Eqs. (1.42), (1.43) one derives that this term becomes:

$$-gIm \left[\langle S^\dagger \rangle_0 \tau_\kappa A_{\mu\kappa} \partial^\mu \tilde{S} \right] = -g \langle s_0 \rangle_0 \left[A_{\mu 1} \partial^\mu \tilde{s}_1 + A_{\mu 2} \partial^\mu \tilde{s}_2 - A_{\mu 3} \partial^\mu \tilde{s}_3 \right] \, . \tag{1.61}$$

This mixing between the gauge bosons and the *candidate* Golstone bosons introduces an unwanted complication in the Lagrangian, that would make the physical interpretation of the associated masses far from being clean. Since the origin of the mixing terms is deeply related with the introduction (in the covariant derivative) of the gauge bosons, typical features of the local gauge theory that is being considered, one would think that the gauge freedom that is available should be able, somehow, to cure this intrinsic disease, which is in fact exactly the case. The procedure in this

direction consists of rewriting the scalar doublet in the so called polar form:

$$S(x) \equiv e^{\frac{i}{v}[\tau_\kappa \tilde{s}'_\kappa(x)]} \begin{vmatrix} O \\ \frac{v+\tilde{s}'_0(x)}{\sqrt{2}} \end{vmatrix} \tag{1.62}$$

retaining the spontaneous symmetry breaking scheme of Eq. (1.43), so that $\langle \tilde{s}_{0,1,2,3} \rangle_0 = 0$. Once the polar representation Eq. (1.62) is adopted, one removes completely the three fields $\tilde{s}'_{1,2,3}$ by means of a special gauge transformation:

$$S_u(x) = e^{-\frac{i}{v}[\tau_\kappa \tilde{s}'_\kappa(x)]} S(x) = \frac{1}{\sqrt{2}} \begin{vmatrix} O \\ v + \tilde{s}'_0(x) \end{vmatrix} . \tag{1.63}$$

This remarkable gauge, in which the scalar doublet is represented by one residual real scalar field, is called the unitary gauge. When one moves to it, it becomes necessary to transform also the original gauge fields A_μ in a way that is fixed by known prescriptions, $A_\mu \to A^{(u)}_\mu$. At the end of this canonical game, one is left with a Lagrangian of the following form:

$$\begin{aligned} \mathcal{L} &= (D_\mu S_u)^\dagger (D^\mu S_u) - 2\mu^2 \frac{\tilde{s}'^2_0}{2} - \lambda v \tilde{s}'^3_0 - \frac{\lambda}{4} \tilde{s}'^4_0 + \frac{1}{4}\mu^2 v^2 \\ &= \partial_\mu \frac{\tilde{s}'_0}{\sqrt{2}} \partial^\mu \frac{\tilde{s}'_0}{\sqrt{2}} + \frac{1}{2}\left(\frac{gv}{2}\right)^2 A^\kappa_{\mu u} A^{\mu\kappa}_u + \frac{vg^2}{2\sqrt{2}} A^\kappa_{\mu u} A^{\mu\kappa}_u \frac{\tilde{s}'_0}{\sqrt{2}} \\ &\quad + \frac{g^2}{4} A^\kappa_{\mu u} A^{\mu\kappa}_u \frac{\tilde{s}'^2_0}{2} - 2\mu^2 \frac{\tilde{s}'^2_0}{2} - \lambda v \tilde{s}'^3_0 - \frac{\lambda}{4} \tilde{s}'^4_0 + \frac{1}{4}\mu^2 v^2 . \end{aligned} \tag{1.64}$$

This transformed Lagrangian, that is by assumption perfectly equivalent to the starting one Eq. (1.50), describes now a physical system consisting of three massive gauge boson of common equal mass $M_{Au} = (1/2)gv$ and of *one* massive scalar field $\tilde{s}'_0/\sqrt{2}$ of mass

$$m = \sqrt{2}\mu . \tag{1.65}$$

As expected, no ambiguous bilinear mixing with the gauge bosons survives (naively, the transformed quantity Eq. (1.61) is now zero given the intrinsic reality of S_u). All the three *candidate* Goldstone bosons scalars have totally disappeared. As one says, they have been "eaten" by the corresponding gauge bosons, and for this reason they are usually called *would-be* Goldstone bosons. This remarkable mechanism is generally called the Higgs mechanism, and the surviving massive scalar field $\tilde{s}'_0/\sqrt{2}$, that corresponds to the "cartesian coordinate" $\tilde{s}_0$ of the original doublet S, is called the Higgs scalar field, with a Higgs scalar as its associated *elementary* particle.

This rather long discussion has been performed as a useful introduction to the following presentation of the main features of the Standard Model.

Before entering this next topics, we want to stress two points that deserve, at this stage, special attention. The first one is the fact that, in the considered example, the generation of mass for the gauge bosons was so to say, a "private business" between the latter ones and the scalar doublet. No fermions were present in the system, and one guesses that their addition, necessary to describe a realistic physical situation, will not add extra features or modify the previously discussed mechanism. The second point is the fact that, although the physically meaningful situation is only achieved in the unitary gauge, each other gauge is, by definition, able to reach the same results for observable quantities. In other words, one expects to find the same predictions for physical observables both in the unitary gauge and in other gauges where, however, the unphysical *would be Goldstone bosons* will be surviving. This point will be particularly important, and discussed in great detail, in the Section that will be devoted to the practical calculations within the Standard Model at the so called one-loop level.

After this statement, we are now ready to begin a short review of the Standard Model of electroweak interactions.

1.4 Unification of weak and electromagnetic interactions in the Standard Model

1.4.1 *The $SU(2) \times U(1)$ description of electroweak interactions*

We have summarized in the previous Sections the motivations that led to believe that a promising symmetry group for weak interactions should be a spontaneously broken local $SU(2)_L$. We have seen in the previous Section that for a symmetry of this type, a doublet of complex scalar fields guarantees an equal mass generation for all the three gauge bosons, without any internal theoretical difficulty, via the Higgs mechanism. The main theoretical ingredients for a tentative description of weak interactions would be therefore, at this point, ready and only an addition of suitable fermion fields to the Lagrangian Eq. (1.50) would seem necessary. The new, extra feature that makes the theoretical construction more ambitious and appealing is the realization that, with a modest and almost unavoidable effort, one can enlarge the symmetry group of the weak interactions so that electromagnetic interactions are also incorporated. In such a way a beautiful unification of the two phenomena would be achieved, since both kinds of forces would be the result of exchange of gauge bosons, carriers of their

interaction and manifestation of two local gauge groups under which the physical system would be symmetric.

Clearly, from the very beginning, if such an ambitious program were successful, the realization of the two symmetries related to the two interactions should be quite different, for the simple reason that photons must evidently remain massless. Therefore, the associated symmetry will be allowed to remain realized without the introduction of any spontaneous breaking mechanism. Keeping this in mind, the construction of the enlarged symmetry group is, so to say, relatively simple to understand.

First of all, the simplest candidate symmetry group must accommodate only one extra gauge boson, precisely the photon. Therefore only one more symmetry generator should be added to the three previously defined ones T_L^+, T_L^+, T_{3L}. There is no simple group available with four generators. But one can form the so called direct product of the already accepted $SU(2)_L$ with another local group having the mathematical property of a $U(1)$ (one generator). The resulting candidate symmetry group should thus be of the form $SU(2)_L \times U(1)$.

To learn something more on the nature of this extra $U(1)$, one can start from the mathematical requirement that the associated generator must commute with those of $SU(2)_L$, in order to build a proper direct product. The simplest possibility is then to start from the lightest couple of left-handed neutrino and electron that must appear in the weak current Eq. (1.1). In a picture that has a $SU(2)_L$ symmetry, the immediate choice is that of grouping them into a $SU(2)_L$ doublet, to be conventionally denoted as ℓ_{1L}:

$$\ell_{1L} = \left| \begin{array}{c} \psi_{\nu_\ell L} \\ \psi_{\ell L} \end{array} \right| \ . \tag{1.66}$$

The ordering in the doublet corresponds to values of $T_{3L}(\equiv I_{3L}) = +(1/2)$ (neutrino) and $-(1/2)$ (electron). This is motivated by the requirement that e.g. T_+ raises at the some time by one unity both the value of T_{3L} (mathematical requirement) and that of Q (by its definition).

It is now straightforward to realize that, for both members of the ℓ_{1L} doublet, the value of $(Q - T_{3L})$ is the same. In a group theoretical language, this corresponds to the fact that the quantity $(Q - T_{3L})$ *commutes* with the generators of $SU(2)_L$. It appear thus reasonable to define the desired $U(1)$ generator as:

$$Y_L \equiv 2(Q - T_{3L}) \tag{1.67}$$

where the subscript L is dictated by the presence of T_{3L} in the r.h.s of Eq. (1.67). Note the presence of the (arbitrary) factor 2. This is due to the

fact that in this way the relationship between the local gauge group generators Y_L and T_{3L} is formally identical with that relating the corresponding strong interaction quantities Y (hypercharge) and T_3 (third component of the isospin).

We can now investigate in more detail the main features of the candidate symmetry group $G_{e.w.}$ of electroweak interactions, by definition chosen as:

$$G_{e.w.} \equiv SU(2)_L \times U(1)_{Y_L} \ . \tag{1.68}$$

The first relevant question to be answered is that of which elementary particles will have to be accommodated from the beginning in the proper invariant Lagrangian, and with which transformation properties under the group. Two main classification criteria occur at this point, dictated by rather different motivations.

The first requirement in that the elementary fermion fields involved in the generalized electroweak interactions description have definite chirality, i.e. either left-handed or right-handed fields will appear in the irreducible representations. Since one wants to generate the charged weak current, phenomenologically forced to be of purely left-handed type, from a covariant derivative of the type of Eq. (1.49) acting on fermions, it is reasonably clear that left-handed leptons and quarks, transforming as $SU(2)_L$ doublets, will have to be inserted in a proper way in the Lagrangian as a generalization of the example given by Eq. (1.66). On the other hand one knows from the starting assumption that a proper description of the conventional electromagnetic interactions must be provided. Since the related force does not differentiate left-handed from right-handed fermions, it is evident that the latter ones will have to be included in the Lagrangian as well. In order not to interfere with the desired structure of the charged weak interactions, they will have to be "neutral" under $SU(2)_L$ i.e. they will transform with respect to this group as singlets. For what concerns the other group $U(1)_{Y_L}$, the transformation properties of both left- and right-handed fermions will be dictated by the values of their *weak hypercharge* Y_L, as fixed from Eq. (1.67).

Note that, in the conventional approach, the assignment of Y_L for fermions (both left- and right-handed ones) is done to ensure the correct phenomenological electric charges. The value of Y_L is taken to be be equal to one for the Higgs doublet, and follows from Eq. (1.67) for any other field of the model. In fact, without giving details of this statement, we can say that a self-consistent description requires the appearance in the Lagrangian of a number of fermion *families*, differing essentially because of the different

masses of the components, and such that, within each family, the sum of the electric charges of *all* the basic leptons and quarks components is exactly vanishing (this guarantees the absence of unwanted *anomalies* [22]). By assumption, the behavior of an elementary fermion in the presence of electroweak interactions is completely determined by its $SU(2)_L \times U(1)_{Y_L}$ quantum number (I_{3L}, Y_L) and not by its mass, therefore it is sufficient to consider the features of that component of the full Lagrangian that corresponds to a single family to derive the main properties of the model. In particular, we shall now consider the first, lightest family. This will consist of the following basic fermions (Tab. 1.1):

a) A doublet of left-handed neutrino and electron (ν_{eL}, e_L) transforming under $SU(2)_L$ as a doublet (overall electric charge $= -1$).
b) A doublet of left-handed *up* and *down* (u_L, d_L) quarks with analogous $SU(2)_L$ behavior, each quark appearing in three different *color* states (the quarks' color will determine their properties under strong interactions, but not that under electroweak interactions). This makes a total of six left-handed quark states, with overall electric charge $= +1$.
c) One right-handed electron e_R, by definition a $SU(2)_L$ singlet, required by the properties of the electromagnetic interactions (overall electric charge $= -1$).
d) Two right-handed *up* and *down* u_R, d_R quarks, $SU(2)_L$ singlets and in three color states each (overall electric charge $= +1$), which makes six more states.

Table 1.1 Values of I_{3L} and Y_L for the charged fermion fields (first family).

	I_{3L}	Y_L
$\psi_{\nu_e L}$	$+1/2$	-1
ψ_{eL}	$-1/2$	-1
ψ_{eR}	0	-2
ψ_{uL}	$+1/2$	$+1/3$
ψ_{dL}	$-1/2$	$+1/3$
ψ_{uR}	0	$+4/3$
ψ_{dR}	0	$-2/3$

These *fifteen* fermion fields are sufficient to generate a model with all

the desired properties, as we shall immediately show. Clearly, the so called *family replication* will involve the muon family and the τ family with their neutrinos and quarks. This will be discussed later. We want to stress at this point the fact that there is no right-handed neutrino (in each family). This will lead to fundamental theoretical consequences (massless neutrinos), as we will see. From a theoretical point of view, there is no motivation to exclude such an elementary component from the beginning, only a "minimality" requirement of the theoretical picture. In fact, the commonly accepted version of the model without right-handed neutrinos in also called *minimal* Standard Model.

We are now ready to begin the illustration of the main features of the model that has been proposed. This will be done in the forthcoming pages.

1.4.2 *Gauge boson masses in the $SU(2)_L \times U(1)_{Y_L}$ scheme*

From all our previous considerations, we are now ready to accept the idea that, given a family like that discussed in the last Subsection, a promising candidate to describe its electroweak interactions appears to be a Lagrangian $\mathcal{L}$ with local $SU(2)_L \times U(1)_{Y_L}$ gauge invariance spontaneously broken in the Higgs mode by a doublet of complex scalars, whose only physical residual particle will be that associated with the real Higgs scalar fields. Given this prescription, it is relatively simple to derive the formal expression of $\mathcal{L}$. In the commonly accepted version, this consists of four separate pieces, whose discussion can be separately performed. We shall use the convention denomination

$$-\mathcal{L} = \mathcal{L}_{\mathcal{SG}} + \mathcal{L}_{\mathcal{FG}} + \mathcal{L}_{\mathcal{GG}} + \mathcal{L}_{\mathcal{FS}} \tag{1.69}$$

(S,G,F denote here the Higgs, the gauge bosons, the fermions respectively) and begin to investigate the properties of the first term. This is essentially the modification of the Lagrangian of Eqs. (1.47), (1.48), with the requirement of $SU(2)_L$ and of additional $U(1)_{Y_L}$ invariance. In practice, this means that the normal derivative Eq. (1.47) have to be modified and becomes the so called *covariant derivative*

$$D_\mu S = \left(\partial_\mu - ig\frac{\tau_\kappa}{2}A_\mu^\kappa - ig'\frac{1}{2}B_\mu\right) S \tag{1.70}$$

where the new gauge field B_μ is associated with the $U(1)_{Y_L}$ group, A_μ^κ, $\kappa = 1, 2, 3$, are the three gauge bosons associated with $SU(2)_L$ and g, g' are by definition the coupling constants of the two groups.

The transformation properties of A^κ_μ, B_μ under the corresponding groups are orthogonal. Under infinitesimal transformations of $SU(2)_L$, A^κ_μ changes ($\kappa = 1, 2, 3$), while B_μ is unchanged. Under infinitesimal $U(1)_{Y_L}$ transformations $\sim e^{i\eta(x)Y_L/2}$, A_μ is unaffected while B_μ becomes

$$B'_\mu = B_\mu - \frac{1}{g'}\partial_\mu \eta(x) \; . \tag{1.71}$$

The factor $1/2$ that follows g' is the value of the weak hypercharge $Y_L/2$ of the scalar doublet, fixed by Eq. (1.67) and by the requirement that $S_{u,d}$ [Eq. (1.30)] have electric charge $+1$ and zero respectively.

The gauge bosons mass generation will be produced by the term $(D_\mu S)^\dagger (D^\mu S)$, belonging to the scalar-gauge component of the Lagrangian $= \mathcal{L}_{SG}$. We can repeat essentially the derivation of Section 1.3 and compute the product in the unitary gauge, obtaining:

$$\begin{aligned}(D_\mu S)^\dagger_u (D^\mu S)_u = \partial_\mu \frac{\tilde{s}'_0}{\sqrt{2}} \partial^\mu \frac{\tilde{s}'_0}{\sqrt{2}} + \frac{1}{2}\left[v^2 + 2\sqrt{2}v\frac{\tilde{s}'_0}{\sqrt{2}} + 2\frac{\tilde{s}'^2_0}{2}\right] \\ \times \left[\frac{g^2}{4}\left(A^1_{\mu,u}A^{\mu 1}_u + A^2_{\mu,u}A^{\mu 2}_u\right)\right. \\ \left. + \frac{1}{4}\left(gA^3_{\mu,u} - g'B_\mu\right)^2\right]\end{aligned} \tag{1.72}$$

where $A^\kappa_{\mu,u}$ are the gauge fields in the unitary gauge (B_μ is not affected by the $SU(2)_L$ transformation).

A glance to Eq. (1.72) immediately shows that, for what concerns the (1,2) indexes, the situation has remained the same as in the pure $SU(2)_L$ invariant case represented by Eq. (1.64). One defines in a conventional way the charged gauge bosons $W^{+,-}_\mu$ as:

$$W^\pm_\mu = \frac{1}{\sqrt{2}}\left[A^1_{\mu,u} \mp iA^2_{\mu,u}\right] \; . \tag{1.73}$$

The residual neutral scalar field $\tilde{s}'_0/\sqrt{2}$ is the conventionally defined Higgs field and will be denoted by a corresponding symbol $= H$ from now on. For what concerns the charged gauge boson component, Eq. (1.72) can be consequently written in the form:

$$(D_\mu S)^\dagger_u (D^\mu S)_u = m^2_W W^+_\mu W^{-\mu} + W^+_\mu W^{-\mu}\left[\sqrt{2}m_W gH + \frac{g^2}{2}H^2\right] \tag{1.74}$$

that corresponds to a charged gauge boson W, of a mass

$$m_W = \frac{gv}{2} \tag{1.75}$$

interacting with the Higgs scalar in a way that corresponds to the two terms in the square bracket in the r.h.s. of Eq. (1.74).

For what concerns the neutral gauge boson sector, the situation is now quite different from that corresponding to the pure $SU(2)_L$ invariance, Eq. (1.64). One notices that, as a consequence of the presence of the extra $U(1)_{Y_L}$ symmetry, corresponding to a not vanishing g' coupling, the original symmetry between A^1_μ, A^2_μ and A^3_μ has disappeared. Moreover, neither A^3_μ nor B_μ can be thought of as mass eigenstates, owing to the bilinear mixing term that contains them in Eq. (1.72). In fact, at first sight one can already conclude that there will only be *one* massive state, corresponding to the linear combination of $A^3_{\mu,u}$, B_μ whose square appears in that equation.

The situation can be better understood introducing a (non diagonal) 2×2 mass matrix in the so called $(A^3_\mu,\, B_\mu)$ base and writing the corresponding bilinear term as:

$$\frac{v^2 g^2}{8}\left(A^3_{\mu,u} - \frac{g'}{g}B_\mu\right)^2 = \frac{v^2}{8}|A^3_{\mu,u}B_\mu| \begin{vmatrix} g^2 & -gg' \\ -gg' & g'^2 \end{vmatrix} \begin{vmatrix} A^3_{\mu,u} \\ B_\mu \end{vmatrix}$$
$$\equiv \frac{1}{2}|A^3_{\mu,u}B_\mu|[\mathcal{M}^2_{3,B}] \begin{vmatrix} A^3_{\mu,vu} \\ B_\mu \end{vmatrix} \qquad (1.76)$$

where $\mathcal{M}^2_{3,B}$ is a non diagonal mass matrix, by definition given by the expression:

$$\mathcal{M}^2_{3,B} = \frac{v^2}{4}\begin{vmatrix} g^2 & -gg' \\ -gg' & g'^2 \end{vmatrix} \equiv \begin{vmatrix} m_3^2 & -m_3 m_B \\ -m_3 m_B & m_B^2 \end{vmatrix} \qquad (1.77)$$

where $m_{3,B} = gv/2$, $g'v/2$ are *not* to be interpreted as rigorous mass terms, but only as parameters of the Lagrangian.

The situation summarised by Eq. (1.76) can be re-expressed by saying that on one hand A^3_μ, B_μ are intrinsically associated with the two independent symmetry groups $SU(2)_L$, $U(1)_{Y_L}$, i.e. they are transforming *independently* and with definite prescriptions under the two groups [in particular, A^3_μ belongs to a $SU(2)_L$ *triplet*, together with $A^{1,2}_\mu$, while B_μ is transformed like in Eq. (1.71)]. But on the other hand A^3_μ, B_μ are not the proper *mass eigenstates*: the latter ones should appear in the Lagrangian quadratically, and without mixing terms.

To determine the proper mass eigenstates is straightforward. One knows from elementary matrix theory that, given a non diagonal matrix $\mathcal{M}^2_{3,B}$ like that of Eq. (1.77), there always exists a unitary matrix D that diagonalises $\mathcal{M}^2_{3,B}$ via a similarity transformation

$$D\mathcal{M}^2_{3,B}D^\dagger \equiv \mathcal{M}^2 = \begin{vmatrix} m_Z^2 & O \\ O & m_A^2 \end{vmatrix}. \qquad (1.78)$$

By definition, the transformation Eq. (1.78) conserves both the determinant and the trace of $\mathcal{M}^2_{3,B}$. Since the determinant of $\mathcal{M}^2_{3,B}$ is vanishing, this leads to the (expected) conclusion that either m_Z or m_A must be zero. Setting e.g. $m_A = O$, m_Z^2 is then given by the trace of $\mathcal{M}^2_{3,b}$ i.e.

$$m_Z^2 = \frac{v^2}{4}(g^2 + g'^2) \; . \tag{1.79}$$

The formal expression of the D matrix is fixed by the requirement of being unitary (and real), which leaves only one free parameter, an angle to be called θ_W (the *Weinberg* angle)

$$D = \begin{vmatrix} \cos\theta_W & -\sin\theta_W \\ \sin\theta_W & \cos\theta_W \end{vmatrix}, \qquad DD^\dagger = D^\dagger D = 1 \tag{1.80}$$

with θ_W being related to g, g' by the property:

$$tg\theta_W = \frac{m_B}{m_3} = \frac{g'}{g} \tag{1.81}$$

that can be re-expressed by saying that:

$$\cos^2\theta_W = \frac{1}{1 + g'^2/g^2} = \frac{g^2}{g^2 + g'^2} \equiv 1 - \sin^2\theta_W \; . \tag{1.82}$$

The final step is now to rewrite Eq. (1.76) in the perfectly identical form:

$$\begin{aligned} |A^3_{\mu,u} B_\mu|[\mathcal{M}^2_{3,B}] \begin{vmatrix} A^3_{\mu,u} \\ B_\mu \end{vmatrix} &\equiv \left[|A^3_{\mu,u}, B_\mu| D^\dagger\right] \left[D\mathcal{M}^2_{3,B} D^\dagger\right] \left[D \begin{vmatrix} A^3_{\mu,u} \\ B_\mu \end{vmatrix} \right] \\ &\equiv |Z_\mu A_\mu| \left[\mathcal{M}^2\right] \begin{vmatrix} Z_\mu \\ A_\mu \end{vmatrix} \\ \begin{vmatrix} Z_\mu \\ A_\mu \end{vmatrix} &\equiv \left[D \begin{vmatrix} A^3_{\mu,u} \\ B_\mu \end{vmatrix} \right] \; . \end{aligned} \tag{1.83}$$

Evidently, the states Z_μ, A_μ are the desired mass eigenstates, the first one belonging to the eigenvalue given by Eq. (1.79), the second one belonging to the vanishing value $M_A = 0$. In terms of $A^3_{\mu,u}, B_\mu$ their expression is given by Eq. (1.83). We can write it in terms of the parameter θ_W Eqs. (1.80), (1.81) as:

$$\begin{aligned} Z_\mu &= \cos\theta_W A^3_{\mu,u} - \sin\theta_W B_\mu \\ \\ A_\mu &= \sin\theta_W A^3_{\mu,u} + \cos\theta_W B_\mu \; . \end{aligned} \tag{1.84}$$

The massive spin one boson, linear combination of the $SU(2)_L$ and of the $U(1)_{Y_L}$ gauge bosons, is conventionally called the Z boson. As one sees, its field is proportional to the combination $(A^3_{\mu,u} - (g'/g)B_\mu)$ as instinctively expected from the previous discussion. The value of its mass Eq. (1.79) is different from the that of the W mass Eq. (1.75), but the two quantities are strictly connected by a relationship that will be particularly relevant in the model. This will be discussed in the forthcoming Subsection.

1.4.3 *The (W, Z) mass relationship and the ρ_0 parameter*

The values of the (W, Z) masses Eqs. (1.75), (1.78) have been obtained by assuming that the local $SU(2)_L \times U(1)_{Y_L}$ gauge symmetry is spontaneously broken by a set S of complex scalar fields *transforming under $SU(2)_L$ as a doublet* Eq. (1.31). Keeping this last feature in mind, we can consequently write the following identity, valid under the previously assumed circumstances:

$$\frac{m_W^2}{m_Z^2 \cos^2 \theta_W} = 1 \tag{1.85}$$

where Eq. (1.82) has been used. Using the definition of the parameters m_3, m_B Eq. (1.77), Eq. (1.85) can be rewritten as:

$$\begin{aligned} \frac{m_W^2}{m_Z^2 \cos^2 \theta_W} = \frac{m_W^2(1 + tg^2\theta_W)}{m_Z^2} = \frac{1}{m_Z^2}\left[m_W^2 + \frac{m_W^2 m_B^2}{m_3^2}\right] \\ = \frac{m_W^2}{m_3^2}\left[\frac{m_3^2 + m_B^2}{m_Z^2}\right] = \frac{m_W^2}{m_3^2} = 1 \end{aligned} \tag{1.86}$$

where the invariance of the matrix trace $m_3^2 + m_B^2 = m_Z^2$ has been used.

In the conventional notation one *defines* the ρ_0 parameter of a spontaneously broken $SU(2)_L \times U(1)_{Y_L}$ gauge as

$$\frac{m_W^2}{m_Z^2 \cos^2 \theta_W} = \frac{m_W^2}{m_3^2} \equiv \rho_0 \tag{1.87}$$

even when the spontaneous breakdown is *not* due to the a not vanishing vev produced by a scalar $SU(2)_L$ doublet. In this case, in principle, ρ_0 *could be different from one.*

One can re-express the fact that $\rho_0 = 1$ when the spontaneous breakdown in generated by a $SU(2)_L$ doublet in the following way. Imagine that in the covariant derivative Eq. (1.70) the $SU(2)_L$ interaction $\sim g$ is turned on at a preliminary stage, with the Y_L interaction $\sim g'$ still switched off. Then the mass generation proceeds as in the pure $SU(2)_L$ case illustrated in Section 1.3, leading to Eq. (1.64) and to an *equal* quadratic term $\sim (A_\mu^1 A^{\mu^1} + A_\mu^2 A^{\mu^2} + A_\mu^3 A^{\mu^3})$. The introduction of Y_L adds extra terms $\sim B_\mu B^\mu$ *and* $A_\mu^3 B^\mu$, without modifying the $\sim v^2 A_\mu^3 A^{\mu^3}$ coefficient. This means that the value of the parameter defined as m_3^2 in Eq. (1.77) is totally fixed by the $SU(2)_L$ component of the covariant derivative Eq. (1.70), and for a discussion of this quantity one can safely assume that $g' = 0$. A consequence of Eq. (1.64) then is the fact that, under this condition, the manifest symmetry of the scalar-gauge component of the Lagrangian with

respect to "rotations" in the 3d-space of the vectors A^1_μ, A^2_μ, A^3_μ [a $O(3)$ group, mathematically equivalent to a $SU(2)$ group], is translated into the fact that, even after switching on the hypercharge interaction, one will still have the same m_3^2, and in particular one will be left with

$$m_3^2 = m_W^2 \Rightarrow \rho_0 = 1 \; . \tag{1.88}$$

The previous result can be actually derived from a property of the Higgs sector of the model. In the case of a single scalar field, the scalar potential of Eq. (1.47) has a O(4) global symmetry. The presence of a vacuum expectation value of the scalar field reduces this symmetry to O(3), which is mathematically equivalent to SU(2). This residual global symmetry of the Higgs sector, that automatically implies Eq. (1.88) (see e.g. [18]) is called *custodial SU(2) symmetry*. Note that this residual symmetry is a *global* one, not necessarily related to any of the usually encountered $SU(2)$ groups and, in general, not necessarily surviving in the model in case of different mechanisms of spontaneous symmetry breaking. In particular, one can easily list a number of situations where the custodial symmetry is valid, or not. We shall illustrate the simplest case of non validity, when the spontaneous breaking is generated by three real scalar fields, transforming under $SU(2)_L$ as a *triplet*. This set can be represented by a three dimensional vector column

$$\vec{\chi} \equiv \begin{vmatrix} \chi^1 \\ \chi^2 \\ \chi^3 \end{vmatrix} \tag{1.89}$$

whose transformation under $SU(2)_L$ is fixed by formulae, analogous to Eq. (1.31). To maintain the group invariance, the covariant derivative acting on χ in the part of Lagrangian that contains it (that would be formally identical to Eqs. (1.47), (1.48)) should be modified in the following way:

$$\partial_\mu \vec{\chi} \to D_\mu \vec{\chi} = \left[\partial_\mu \vec{\chi} - ig(\vec{\chi} \wedge \vec{A_\mu}) \right] \; . \tag{1.90}$$

Spontaneous symmetry breaking can be generated allowing one component of χ to be "hosted" by the vacuum. Taking for instance $\langle \chi_3 \rangle_0 \equiv (v_3/\sqrt{2}) \neq 0$, one has

$$\langle \vec{\chi} \rangle_0 \equiv \frac{1}{\sqrt{2}} \begin{vmatrix} 0 \\ 0 \\ v_3 \end{vmatrix} \; . \tag{1.91}$$

This generates a vector boson mass term of the form:

$$(D_\mu \vec{\chi})^\dagger (D^\mu \vec{\chi}) \Rightarrow g^2 \frac{v_3^2}{2} (A^1_\mu A^{\mu^1} + A^2_\mu A^{\mu^2}) = (g v_3)^2 W^+_\mu W^{\mu -} \qquad (1.92)$$

where *only* the charged boson W has acquired a mass. For this type of spontaneous symmetry breaking mechanism one would have therefore, formally, no meaningful definition of the ρ_0 parameter if the breaking were *only* due to the scalar triplet. If the triplet were *added* to the conventional scalar, a value of ρ_0 different from (and clearly larger than) one would be obtained, numerically dependent on the values of v_3 and v.

The considered example can be generalised to other situations. From the previous discussion, it is relatively simple to conclude that, whenever the spontaneous breaking is generated by any combination of scalar fields transforming under $SU(2)_L$ either as a *doublet* or as a *singlet* (the latter being unaffected by the transformations), the value of ρ_0 will be equal to one: this property is generally lost when scalars with different transformation properties are added to the scenario.

This short discussion has been concentrated, and we shall return on it later on, on some properties of the *massive* (W, Z) boson sector. We still have to understand the physical meaning of the residual massless gauge boson A_μ that appears in Eqs. (1.83), (1.84). In the forthcoming Subsection we shall show that it can be identified with the *photon*. This will have a fundamental consequence, since the Z couplings e.g. to the fermions will be fixed in a way that will be experimentally testable.

1.4.4 *Electroweak unification and weak neutral currents*

From the previous discussion we have learned that, in the Minimal Standard Model, the proposed mechanism of spontaneous symmetry breaking automatically generates a *massless* neutral gauge boson associated with the field operator A_μ given by Eq. (1.84). Since one obviously wants to identify this massless particle with the photon, some extra condition must be imposed. The most obvious requirement is that the couplings of A_μ to the fermions are those of a photon, fixed by the fermions' electric charge according to the conventional QED prescriptions. To meet this requirement, one must consider the interaction of fermions with the neutral gauge bosons Z_μ, A_μ. This is provided by the component $\mathcal{L}_{FG}$ of the Lagrangian, that describes the full interaction of fermions and gauge bosons, considering only the neutral gauge bosons contribution. The latter is obtained by replacing in the fermion field derivative terms of the Lagrangian $\sim i\bar{\psi}_j \gamma^\mu \partial_\mu \psi_j$ (with

j as the general fermion field index) the normal derivative by the covariant derivative D_μ. For purposes of illustration, it will be sufficient to consider e.g. the first fermion family and to be limited in the discussion to the lepton contribution to the Lagrangian. This will originally contain two terms: one is generated by the $SU(2)_L$ doublet represented as a vector column ℓ_{1L} defined by Eq. (1.66),

$$\ell_{1L} = \left| \begin{array}{c} \psi_{\nu_e L} \\ \psi_{eL} \end{array} \right| ,$$

with weak hypercharge $Y_L = -1$ (in order to produce the correct electric charges according to Eq. (1.67)); the second is generated by ψ_{eR}, the right-handed electron, $SU(2)_L$ singlet ($I_{3L} = 0$) with $Y_L = -2$. The corresponding interaction with the neutral gauge bosons will be contained in the quantities

$$\bar{\ell}_{1L}\gamma^\mu D_\mu \ell_{1L} \equiv \bar{\ell}_{1L}\gamma^\mu(\partial_\mu - ig\frac{\tau_\kappa}{2}A^\kappa_{\mu,u} + ig'\frac{1}{2}B_\mu)\ell_{1L} \tag{1.93}$$

and

$$\bar{\psi}_{eR}\gamma^\mu D_\mu \psi_{eR} \equiv \bar{\psi}_{eR}\gamma^\mu(\partial_\mu + ig' B_\mu)\psi_{eR} \, . \tag{1.94}$$

The *charged* component of the interaction entirely comes from the $SU(2)_L$ doublet part of Eq. (1.93); it can be formally written as:

$$\overset{(\text{charged})}{\mathcal{L}_{FG}} \equiv \frac{g}{\sqrt{2}}(J^{(+)}_{\mu,1L}W^{+\mu} + J^{(-)}_{\mu,1L}W^{-\mu}) \tag{1.95}$$

where

$$J^{(+)}_{\mu,1L} \equiv (J^{(-)}_{\mu,1L})^\dagger = \bar{\psi}_{\nu_e L}\gamma_\mu \psi_{eL} \, . \tag{1.96}$$

This is, as discussed previously, the expected reformulation of the Fermi interaction in the $SU(2)_L$ language that can be easily generalized to the first family quarks, and must satisfy the normalization condition Eq. (1.24) to reproduce satisfactorily the known phenomenology of the charged weak interaction sector. Its generalization to more than one family will be discussed at the end of the Chapter. The lepton-neutral gauge bosons interaction component will be written as:

$$\begin{aligned} \overset{(\text{neutral})}{\mathcal{L}_{FG}} &= i\left[\bar{\ell}_{1L}\gamma^\mu\left(-ig\frac{\tau_3}{2}A^3_{\mu,u} + i\frac{g'}{2}B_\mu\right)\ell_{1L} + \bar{\psi}_{eR}\gamma^\mu ig' B_\mu \psi_{eR}\right] \\ &= g\left(\bar{\ell}_{1L}\gamma^\mu\frac{\tau_3}{2}\ell_{1L}\right)A^3_{\mu,u} \end{aligned}$$

$$+g'\left(-\frac{1}{2}\bar{\ell}_{1L}\gamma^{\mu}\ell_{1L}-\bar{\psi}_{eR}\gamma^{\mu}\psi_{eR}\right)B_{\mu}\ . \tag{1.97}$$

Defining the lepton *weak isospin* and *weak hypercharge currents* as:

$$J^{(3)}_{\mu,e}=\bar{\ell}_{1L}\gamma_{\mu}(I_3\ell_{1L})\equiv\bar{\ell}_{1L}\gamma_{\mu}\frac{\tau_3}{2}\ell_{1L} \tag{1.98}$$

and

$$J^{(Y_L/2)}_{\mu,e}=\bar{\ell}_{1L}\gamma_{\mu}\left(\frac{Y_L}{2}\ell_{1L}\right)+\bar{\psi}_{eR}\gamma_{\mu}\left(\frac{Y_L}{2}\psi_{eR}\right)\equiv-\frac{1}{2}\bar{\ell}_{1L}\gamma_{\mu}\ell_{1L}-\bar{\psi}_{eR}\gamma_{\mu}\psi_{eR} \tag{1.99}$$

Eq. (1.97) can be rewritten as:

$$\begin{aligned}\mathcal{L}^{(\text{neutral})}_{FG}&=gJ^{(3)\mu}_{e}A^{3}_{\mu,u}+g'J^{(Y_L/2)\mu}_{e}B_{\mu}\\&\equiv gJ^{(3)\mu}_{e}\left[\cos\theta_W Z_{\mu}+\sin\theta_W A_{\mu}\right]\\&+g'J^{(Y_L/2)\mu}_{e}\left[-\sin\theta_W Z_{\mu}+\cos\theta_W A_{\mu}\right]\ .\end{aligned} \tag{1.100}$$

The contribution to Eq. (1.100) coming from A_{μ} can be written as

$$\mathcal{L}^{(A_{\mu})}_{FG}=g\sin\theta_W A_{\mu}\left[J^{(3)\mu}_{e}+J^{(Y_L/2)\mu}_{e}\right] \tag{1.101}$$

since $g'\cos\theta_W=g\sin\theta_W$ from Eq. (1.81). The quantity in the square bracket in Eq. (1.101) becomes, as one easily sees:

$$J^{(3)\mu}_{e}+J^{(Y_L/2)\mu}_{e}=-\left[\bar{\psi}_{eL}\gamma^{\mu}\psi_{eL}+\bar{\psi}_{eR}\gamma^{\mu}\psi_{eR}\right]=-\bar{\psi}_{e}\gamma^{\mu}\psi_{e}\equiv J^{(Q)\mu}_{e} \tag{1.102}$$

where $J^{(Q)\mu}$ is the (conventionally defined) electromagnetic current, that associates to each j-fermion with electric charge Q_j (in unities of $|e|$, the positron charge) the term

$$J^{(Q)\mu}_{j}\equiv Q_j\bar{\psi}_j\gamma^{\mu}\psi_j\equiv Q_j\left[\bar{\psi}_{jL}\gamma^{\mu}\psi_{jL}+\bar{\psi}_{jR}\gamma^{\mu}\psi_{jR}\right] \tag{1.103}$$

and Eq. (1.102) is a natural consequence of the initial choice $Q=I_{3L}+1/2Y_L$, Eq. (1.67). Therefore we can write at this stage

$$\mathcal{L}^{(A_{\mu})}_{FG}=\left(g\sin\theta_W\ J^{\mu Q}_{\ell}\right)A_{\mu}\ . \tag{1.104}$$

This term coincides with the conventional electromagnetic current – photon interaction $\equiv|e|J^{\mu Q}_{1\ell}A_{\mu}$ provided that one fixes the condition:

$$|e|\equiv g\sin\theta_W=g'\cos\theta_W\ . \tag{1.105}$$

In this way, one achieves a *unification* of weak and electromagnetic interactions, in the sense that the same mechanism that is advocated to generate the first type of forces Eq. (1.93) automatically produces (when Eq. (1.94)

is added) also the second one, with the correct value of the electric charge ensured by the constraint Eq. (1.105). One easily sees that the same formal proof can be extended to the *quarks* of the first family (and also to each remaining family), with a proper choice of the quarks weak hypercharges fixed by Eq. (1.67). The conclusion is that one can write, in full generality, for each j-family:

$$\mathcal{L}_{FG,j}^{(\text{neutral})} = |e| J^{(Q)\mu,j} A_\mu + \mathcal{L}_{FG,j}^{(Z)} \tag{1.106}$$

where $J^{(Q)\mu,j}$ is the conventional electromagnetic current, whose expression e.g. for the first family is

$$J^{(Q)\mu,1} = -\bar{\psi}_e \gamma^\mu \psi_e + \frac{2}{3} \sum_i \bar{\psi}_u^{(c_i)} \gamma^\mu \psi_u^{(c_i)} - \frac{1}{3} \sum_i \bar{\psi}_d^{(c_i)} \gamma^\mu \psi_d^{(c_i)} \tag{1.107}$$

(a sum over the color index c_i, $i = 1, 2, 3$ is understood) while analogous expressions describe the corresponding current for the second and third family, with the replacement of 'e' by 'μ, τ' and of 'u, d' by 'c, s' and 't, b' respectively. Note that this component of the *neutral* Lagrangian is perfectly known, and no extra arbitrary parameters must be included into the construction.

The genuinely weak new component of the neutral Lagrangian is in fact that containing the Z_μ field. This can be rewritten (always considering the first family for simplicity) in the following way, from the definition Eq. (1.100):

$$\mathcal{L}_{FG,1}^{(Z)} = Z_\mu \left[g \cos\theta_W J_1^{(3)\mu} - g' \sin\theta_W (J_1^{(Q)\mu} - J_1^{(3)\mu}) \right] \tag{1.108}$$

where $J_1^{(3)\mu}$ is the weak isospin current of the first family, that generalizes Eq. (1.98):

$$J_1^{(3)\mu} = \bar{\ell}_{1L} \gamma^\mu \frac{\tau_3}{2} \ell_{1L} + \sum_i \bar{q}_{1L}^{(c_i)} \gamma^\mu \frac{\tau_3}{2} q_{1L}^{(c_i)} \ , \tag{1.109}$$

$q_{1L}^{(c_i)}$ is a $SU(2)_L(u, d)$ quark doublet, i.e.:

$$q_{1L}^{(c_i)} \equiv \begin{vmatrix} \psi_{uL}^{(c_i)} \\ \\ \psi_{dL}^{(c_i)} \end{vmatrix} \tag{1.110}$$

and a sum over the color index $c_i, i = 1, 2, 3$ is understood. Using Eq. (1.81), Eq. (1.108) acquires the conventional expression:

$$\mathcal{L}_{FG,1}^{(Z)} = \frac{|e|}{\sin\theta_W \cos\theta_W} [J_1^{\mu(Z)} Z_\mu] \tag{1.111}$$

where

$$J_1^{\mu(Z)} = J_1^{\mu 3} - \sin^2\theta_W J_1^{\mu Q} \tag{1.112}$$

is the weak neutral current, associated to the massive gauge boson Z_μ, and representing a completely new theoretical input of the Standard Model with respect to the previous Fermi theory.

To better appreciate the genuinely new features of the Z current Eq. (1.112) with respect to those of the electromagnetic one, it is useful to write its expression in terms of the left- and right-handed fermion fields. For the first family this gives:

$$\begin{aligned} J_1^{\mu(Z)} = & \frac{1}{2}\bar{\psi}_{\nu L}\gamma^\mu\psi_{\nu L} + \bar{\psi}_{eL}\gamma^\mu\psi_{eL}\left(-\frac{1}{2} + \sin^2\theta_W\right) \\ & + \bar{\psi}_{uL}\gamma^\mu\psi_{uL}\left(\frac{1}{2} - \frac{2}{3}\sin^2\theta_W\right) \\ & + \bar{\psi}_{dL}\gamma^\mu\psi_{dL}\left(-\frac{1}{2} + \frac{1}{3}\sin^2\theta_W\right) \\ & + \bar{\psi}_{eR}\gamma^\mu\psi_{eR}\left(\sin^2\theta_W\right) \\ & + \bar{\psi}_{uR}\gamma^\mu\psi_{uR}\left(-\frac{2}{3}\sin^2\theta_W\right) \\ & + \bar{\psi}_{dR}\gamma^\mu\psi_{dR}\left(\frac{1}{3}\sin^2\theta_W\right) \end{aligned} \tag{1.113}$$

(a summation over the color index for u, d quarks is not explicitly indicated but understood). Denoting by a conventional fermions index $j = \nu, e, u, d$ the four fermion fields of the first family, Eq. (1.113) can be rewritten as:

$$J_1^{\mu(Z)} = \sum_j \left(g_{Lj}\bar{\psi}_{jL}\gamma^\mu\psi_{jL} + g_{Rj}\bar{\psi}_{jR}\gamma^\mu\psi_{jR}\right) \ . \tag{1.114}$$

In particular, one has:

$$g_{L\nu} = \frac{1}{2} \ ; \quad g_{R\nu} = 0 \tag{1.115}$$

$$g_{Le} = -\frac{1}{2} + \sin^2\theta_W \ ; \quad g_{Re} = \sin^2\theta_W \tag{1.116}$$

$$g_{Lu} = \frac{1}{2} - \frac{2}{3}\sin^2\theta_W \ ; \quad g_{Ru} = -\frac{2}{3}\sin^2\theta_W \tag{1.117}$$

$$g_{Ld} = -\frac{1}{2} + \frac{1}{3}\sin^2\theta_W \ ; \quad g_{Rd} = \frac{1}{3}\sin^2\theta_W \tag{1.118}$$

that corresponds, for a general fermion f of given chirality, left-isospin and charge, to the rule for its coupling g_f with the Z boson:

$$g_f \equiv I_{3L,f} - \sin^2\theta_W Q_f \ . \tag{1.119}$$

It is convenient to write here the expressions of the vector (g_V) and axial (g_A) couplings defined as $g_V = g_L + g_R$ and $g_A = g_L - g_R$, respectively, as they will be often used in this book. One has

$$g_V \equiv I_{3L} - 2\sin^2\theta_W Q_f \ , \tag{1.120}$$

$$g_A \equiv I_{3L} \tag{1.121}$$

corresponding to

$$g_{V\nu} = \frac{1}{2} \ ; \quad g_{A\nu} = \frac{1}{2} \tag{1.122}$$

$$g_{Ve} = -\frac{1}{2} + 2\sin^2\theta_W \ ; \quad g_{Ae} = -\frac{1}{2} \tag{1.123}$$

$$g_{Vu} = \frac{1}{2} - \frac{4}{3}\sin^2\theta_W \ ; \quad g_{Au} = \frac{1}{2} \tag{1.124}$$

$$g_{Vd} = -\frac{1}{2} + \frac{2}{3}\sin^2\theta_W \ ; \quad g_{Ad} = \frac{1}{2} \ . \tag{1.125}$$

Equations (1.115)–(1.118) can be generalized to the fermions of the second and third family with the obvious replacements that were already mentioned as we shall show in more detail in the final part of this Subsection. From their expressions several fundamental conclusions can be drawn, a couple of which appear to us specially relevant. More precisely:

a) showing a completely different attitude with respect to the photon, the Z couples in a different way with fermions of opposite chirality. This intrinsic *asymmetry* will lead to several experimentally testable predictions related to the processes of production and/or decay of a Z from/into couples of equal fermions with *opposite* chirality. In particular, the existence of longitudinal polarisation asymmetries, to be exhaustively investigated in the forthcoming Sections, will be predicted and shown to play a specially relevant theoretical rôle.

b) one sees from Eqs. (1.111), (1.113) that all the Z interactions with different fermions are described by only one new theoretical parameter, the Weinberg angle θ_W. A variety of theoretical predictions concerning production and decay of a Z into *different* fermion

couples will be strongly correlated in the model, without apparent room for theoretical explanations of possible experimental disagreements.

An almost unavoidable consequence of the two previous points is that a process in which the Z boson were very copiously produced, so that an exhaustive series of measurements of all its various couplings with the existing fermions could be performed with the highest possible accuracy, would represent a stringent test of the model, at least for what concerns the fermions neutral weak interaction sector. The most immediate possibility of achieving these conditions is provided by the annihilation of an electron–positron couple at the resonant energy, that corresponds to m_Z, the Z mass. To carry on this program, a preliminary knowledge of this parameter m_Z is required. As a matter of fact in the Standard Model the value of m_Z (and also, that of m_W) is, at least in first approximation, predicted. This will be discussed in the next Subsection.

1.4.5 *Numerical prediction for the gauge boson masses in the Minimal Standard Model*

In the Minimal Standard Model (MSM), the quantities m_W, m_Z (*mass* parameters of $W^{\pm}$ and Z in the proposed electroweak Lagrangian) are given by Eqs. (1.75), (1.79) in terms of three different electroweak parameters (g, g' and v). However, the *ratio* m_W^2/m_Z^2 can be expressed in terms of the Weinberg angle only, since one has from Eq. (1.85)

$$\frac{m_W^2}{m_Z^2} = \cos^2\theta_W \ . \tag{1.126}$$

Even at this preliminary stage, where no discussion has been given on the experimental determination of $\sin^2\theta_W/\cos^2\theta_W$, it is clear that the ratio of Eq. (1.126) will be in principle fixed e.g. by measuring the couplings of the Z boson to fermions, as shown by Eqs. (1.115)–(1.118). A possibility of this type would be available by identifying e.g. an experimental process that could *only* proceed via Z exchange. Twenty-five years ago, a realistic proposal was that of looking for the reaction

$$\nu_\mu e^- \Rightarrow \nu_\mu e^- \tag{1.127}$$

that would be allowed, to lowest order in the Feynman diagrams corresponding to the MSM Lagrangian, thanks to a t-channel Z exchange depicted in Fig. 1.1.

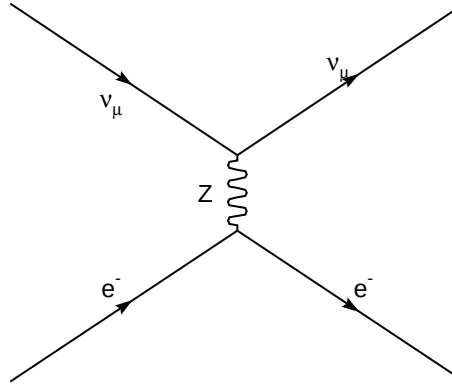

Fig. 1.1 Elastic electron- muonic neutrino scattering via t-channel Z exchange.

Also, neutrino–nucleon scattering experiments would be explained to lowest order by W *and* Z exchange. In fact, the fundamental experimental discovery that led the community of physicists to consider the MSM with special attention was that of the existence of (weak) neutral currents in processes of the kind neutrino-fermion scattering. From those glorious experiments [23], a preliminary value of $\sin^2\theta_W$ was derived, such that, in the early eighties, one could write [24]:

$$\sin^2\theta_W \simeq 0.22 \tag{1.128}$$

and thus one would predict the numerical result

$$m_W^2 \simeq (0.78) m_Z^2 \ . \tag{1.129}$$

The final piece of information still needed to produce a next and testable prediction is provided, in the MSM, by the (fundamental) equation (1.24) that can be rewritten, for our purposes, in the more convenient form:

$$m_W^2 = \frac{\sqrt{2}}{8\,G_F} g^2 = \frac{\sqrt{2}}{8\,G_F}\,\frac{e^2}{\sin^2\theta_W} \ . \tag{1.130}$$

Using the experimental values of e^2, G_F and the neutral current result Eq. (1.128) a value of m_W can be derived, that is:

$$m_W \simeq 79\,\mathrm{GeV} \tag{1.131}$$

with m_Z consequently fixed by Eq. (1.129)

$$m_Z \simeq 90\,\mathrm{GeV} \ . \tag{1.132}$$

Clearly, Eqs. (1.131), (1.132) are a clear, and brave, theoretical prediction that represents a "necessary" condition for the survival of the model. In

this spirit, it is undeniable that the discovery of W and Z by the $UA(1)$ and $UA(2)$ experiments in 1983 [25, 26] gave the next, enormous experimental support to the theoretical belief in the validity of the MSM. It should be reminded that the result of combinations of those memorable measurements was:

$$m_W = 80.8 \pm 2.7 \tag{1.133}$$

$$m_Z = 92.9 \pm 1.6 \tag{1.134}$$

that agrees, within the experimental errors of the time, with the corresponding theoretical predictions. Thus, after 1983, it was clear that, in order to perform an extremely rigorous test of the model, electron–positron collisions at a c.m. energy of approximately 90 GeV were the first choice, and that the next possibility was to produce in electron–positron annihilation a pair of W bosons at c.m. energy of approximately 160 GeV, almost twice as large. The first part of this book will be completely devoted to an illustration, and to a discussion, of the large research program that is commonly classified as that of "Physics of the Z resonance", based on the study of electron–positron annihilations at the c.m. resonant energy that corresponds to the physical Z boson mass. The production of W pairs in e^+e^- collisions will be illustrated in Chapter 9. But before entering these dedicated Chapters, we feel that a few general remarks about the kind of test that these collisions represent for the MSM would be appropriate. These will be presented in the next Section for what concerns the Z resonance production.

1.5 Z physics as a test of the MSM

Strictly speaking, accepting the validity of the MSM leads to postulating that the *electroweak* component of the Lagrangian which describes the strong and electroweak interactions of the known elementary particles has the form given by Eq. (1.69), where F, G, S denote respectively the fermion, gauge and scalar field operators. For the purposes of the following discussion, it will be convenient to indicate the electroweak Lagrangian of the MSM with a corresponding apex, writing:

$$\mathcal{L}_{E.W.}^{(MSM)} = \mathcal{L}_{SG}^{(MSM)} + \mathcal{L}_{FG}^{(MSM)} + \mathcal{L}_{GG}^{(MSM)} + \mathcal{L}_{FS}^{(MSM)} \ . \tag{1.135}$$

It is reasonable to assume that, to a very good approximation, electron–positron collisions at the resonant energy $\sqrt{(p_e + p'_e)^2} = m_Z$ can be described by Feynman diagrams where one Z is exchanged in the s chan-

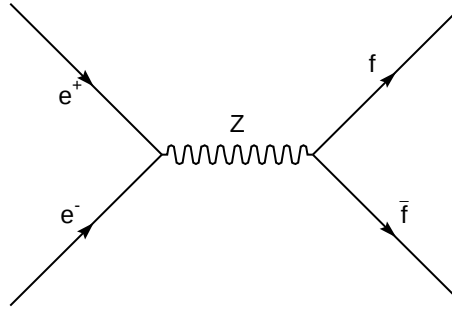

Fig. 1.2 Electron-positron annihilation into a fermion (f) antifermion pair via s-channel Z exchange.

nel. The simplest final state to be considered corresponds to a fermion–antifermion couple (two leptons or two quarks), represented as in Fig. 1.2

In this approximate treatment, evidently any measurement of this process for arbitrary f would represent a test, not of the full structure of the Lagrangian Eq. (1.135), but rather of the pure *neutral* component of the fermion-gauge boson component $\mathcal{L}_{FG}^{(MSM)}$. Clearly, any theoretical model of different nature, but of identical fermion-gauge boson component, would give in first approximation the same predictions on the Z peak for electron–positron annihilation. This would not be automatically true at the level of a more refined theoretical treatment where also higher order effects, corresponding to less elementary Feynman diagrams, would be included. It is at this precise point that the renormalizability of the model plays a fundamental rôle, making a systematic calculation performable. In particular, as a first consequence of t'Hooft's memorable effort [5], the complete set of the so called *one-loop* electroweak effects has been computed, making a tentative test of the remaining components of the MSM Lagrangian, in principle, realizable.

Without entering the details of this statement, that will be fully illustrated in the next Chapters, let us give a few illustrative examples. At the simplest level of Feynman diagrams involving corrections to the Z propagator, one can understand that parameters (the ZWW couplings) provided by $\mathcal{L}_{GG}^{(\mathrm{MSM})}$ will affect the Feynman diagram represented in Fig. 1.3.

Similarly,parameters provided by the $\mathcal{L}_{SG}^{(\mathrm{MSM})}$ component (the ZZH coupling) will in principle enter e.g. Fig. 1.4 while a possible influence of the

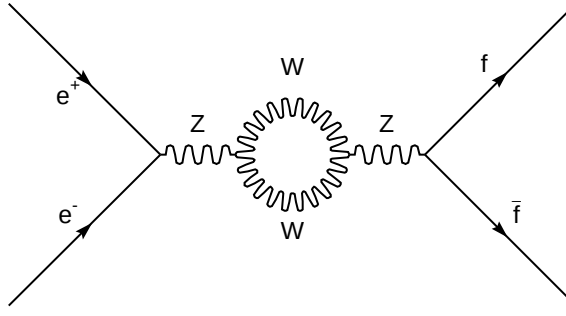

Fig. 1.3 Example of a Feynman diagram, involving the ZWW couplings, that contributes the process $e^+e^- \to f\bar{f}$.

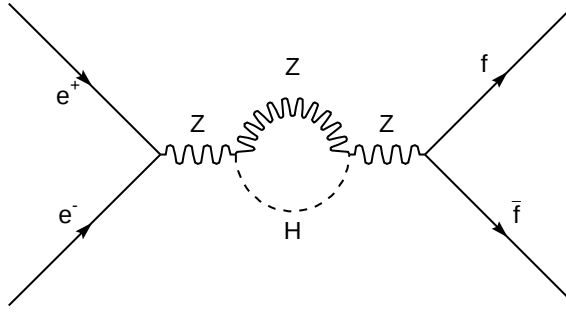

Fig. 1.4 Example of a Feynman diagram, involving the ZZH couplings, that contributes the process $e^+e^- \to f\bar{f}$.

$\mathcal{L}_{FS}^{(\mathrm{MSM})}$ component is depicted in Fig. 1.5.

All the effects represented in Figs. 1.3–1.5 are classified as *one-loop corrections* to the leading effect of Fig. 1.2, and one expects (and verifies) that their relative size should be small (typically, of the percent order). The effectiveness of very high precision measurements becomes now clear: in principle, theoretical models with identical $\mathcal{L}_{FG}$ but different remaining components might be accepted or discarded, depending on the small predicted one-loop effect. As we shall see in the Chapter 11, in some special cases it will be indeed possible to draw *negative* indications on alternative

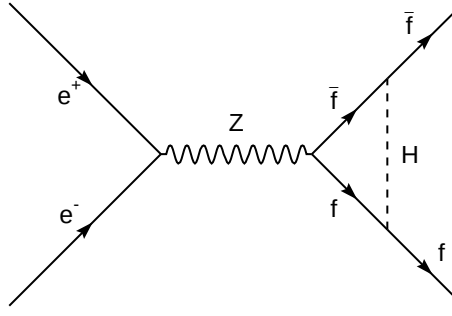

Fig. 1.5 Example of a Feynman diagram, involving the $Hf\bar{f}$ couplings, that contributes the process $e + e- \rightarrow f\bar{f}$.

models from a special subset of very high precision measurements. This will be particularly relevant for a class of models that propose an alternative solution to the mass generation problem that does *not* require the existence of the Higgs scalar. For the moment, we can anticipate that their validity is still an open problem, whose final answer would be obviously provided by the discovery of the Higgs scalar. This is, in fact, the main still open experimental question to be understood, to which we shall devote the brief discussion of the forthcoming Subsection.

1.5.1 *The Higgs scalar mass in the MSM*

In the MSM there is no theoretical prediction concerning the mass m_H of the Higgs scalar. Contrary to the case of the weak gauge bosons W, Z whose experimental discovery represented a first spectacular confirmation of the model, m_H remains a free parameter in the scheme. The prediction in the scalar sector would rather be given, once the Higgs were discovered with a certain value for its mass, for the quartic scalar interactions whose coupling λ is fixed by m_H and v by Eq. (1.54), (1.55). Clearly, this lack of theoretical indications on m_H represents a not small experimental problem.

As a matter of fact, at a more delicate theoretical level, a number of reasonable arguments exists that sets, at least, limits , in the form of upper bounds. Without entering a detailed discussion, it seems fair to say that

the reasonable expectation exists that the Higgs scalar should be relatively light, i.e. of a mass below the $\simeq 1$ TeV limit. A particularly simple example is the following. From Eqs. (1.75) and (1.130) one derives $v = 2^{-\frac{1}{4}} G_F^{-\frac{1}{2}} \simeq 250\,\text{GeV}$. From Eqs. (1.65) and (1.54) $m_H = \sqrt{2\lambda} v$ is obtained. Imposing $\lambda \leq 1$ (that would correspond, roughly, to reliability of the perturbative expansion) fixes the limit $m_H \leq 350$ GeV.

Keeping in mind the fact that alternative solutions are still, in principle, allowed, it is undeniable that the enormous success of the MSM for what concerns the predictions that were testable on Z resonance provides a strong support to the belief that the Higgs should indeed exist. Let us therefore conclude this Section by reviewing the features of the MSM that were testable (and tested) at CERN and SLAC. This will require a brief preliminary discussion, that takes into account several important facts that have until now not been considered.

1.5.2 *A more complete formulation of the MSM*

In the short presentation of the MSM that has been given in this Chapter, we have omitted a number of points that should be now mentioned, in order to understand the main features of some of the forthcoming discussions.

To be more precise, we have neglected:

1) the inclusion of strong interactions when the final state is a couple of quarks;
2) the masses of leptons and quarks;
3) the generalization of the treatment to the next fermion families (family *replication*).

For the purposes of the remaining part of this book, the brief following summary should be sufficient, although necessarily qualitative.

1.5.2.1 *Inclusion of strong interactions*

The accepted description of the strong interactions of quarks has an exact $SU(3)_c$ gauge symmetry and eight massless gluons, carriers of the interaction between the colored quarks [29]. It seems attractive and natural to propose a description of electroweak and strong interactions in which all these forces are generated by the same mechanism of emission of gauge bosons. The complete Lagrangian is supposed to have an enlarged $SU(3)_c \otimes SU(2)_L \otimes SU(1)Y_L$ local gauge symmetry, where by assumption all

the generators of the $SU(3)_c$ group commute with those of $SU(2)_L \otimes U(1)_{Y_L}$. It can be obtained by adding to the already defined electroweak component Eq. (1.135) the genuinely strong term. The latter is given by the following expression:

$$\mathcal{L}_s = \sum_{c_{i=1}}^{3} \sum_{j=1}^{N} \bar{q}_j^{(ci)} i\gamma^\mu D_\mu q_j^{(ci)} - \frac{1}{2} Tr G_{\mu\nu,G} G_G^{\mu\nu} \tag{1.136}$$

where N is the number of different quark flavours (two in the first family, where the two lightest u, d quarks appear), c_i is the color index and the eight $SU(3)$ generators are each one in correspondence with one gluon field (spin one) operator, to be denoted as $A^a_{\mu G}$. These fields enter the covariant derivative D_μ as:

$$D_\mu = \partial_\mu - i g_s \sum_{a=1}^{8} A^a_{\mu G} \frac{\lambda^a}{2} \tag{1.137}$$

where g_s is the $SU(3)_c$ (strong) coupling and λ^a are the Gell-Mann 3×3 matrices that satisfy the commutation relations of the $SU(3)$ algebra:

$$\left[\frac{\lambda^a}{2} \, , \, \frac{\lambda^b}{2} \right] = i \sum_{c=1}^{8} f^{abc} \frac{\lambda^c}{2} \, . \tag{1.138}$$

The 3×3 matrix $G_{\mu\nu,G}$ is formally defined as:

$$\begin{aligned} G_{\mu\nu,G} = & \sum_{a=1}^{8} \left(\partial_\mu A^a_{\nu,G} - \partial_\nu A^a_{\mu,G} \right) \frac{\lambda^a}{2} \\ & - i g_s \sum_{a,b=1}^{8} \left[A^a_{\mu,G} \frac{\lambda^a}{2}, \; A^b_{\nu,G} \frac{\lambda^b}{2} \right] \end{aligned} \tag{1.139}$$

and to compute the trace in Eq. (1.136) one needs the condition:

$$Tr(\lambda^a \lambda^b) = 2\delta^{ab} \, . \tag{1.140}$$

Two comments are relevant at this point. The first one is that the first term of $\mathcal{L}_s$, describing the quark-gluon interaction, can be identically rewritten in terms of the conventional chiral fields as:

$$\sum_{c_i} \sum_{j=1}^{N} \bar{q}_j^{(c_i)} i\gamma^\mu D_\mu q_j^{(c_i)} \equiv \sum_{c_i} \sum_{j=1}^{N} \left[\bar{q}_{jL}^{(c_i)} i\gamma^\mu D_\mu q_{jL}^{(c_i)} + \bar{q}_{jR}^{(c_i)} i\gamma^\mu D_\mu q_{jR}^{(c_i)} \right] \, . \tag{1.141}$$

Considering for the moment the first family u, d quarks, Eq. (1.141) can be rewritten using the notation of Eq. (1.110) i.e.:

$$\mathcal{L}_s = \sum_{c_i=1}^{3} \left[\bar{q}_{1,L}^{(c_i)} i\gamma^\mu D_\mu q_{1,L}^{(c_i)} + \sum_j \bar{q}_{jR}^{(c_i)} i\gamma^\mu D_\mu q_{jR}^{(c_i)} \right] - \frac{1}{2} Tr G_{\mu\nu,G} G_G^{\mu\nu} \tag{1.142}$$

where $q_{1,L}$ is the $SU(2)_L$ left-handed quark doublet defined in Eq. (1.110) and $q_{jR} \equiv u_R, d_R$ are the $SU(2)_L$ right-handed quark singlets. One sees that the term Eq. (1.142) that describes the strong interactions of the quarks of the first family, and is by construction $SU(3)_c$ symmetric, has also automatically the same $SU(2)_L \otimes U(1)_Y$ local symmetry of the corresponding electroweak interactions, being built by quark terms that are all singlets under the electroweak symmetry group (the gluons too are by definition meeting this requirement). This means that the delicate mechanisms that are ensured by $SU(2)_L \otimes U(1)_{Y_L}$ gauge invariance will not be altered by the inclusion of strong interactions.

1.5.2.2 *Masses of leptons and quarks*

Quite generally, any j-th fermion *mass* term in the Lagrangian is by definition proportional to the product $\bar{q}_j q_j \equiv \bar{q}_{jL} q_{jR} + \bar{q}_{jR} q_{jL}$, where q_j is the field operator associated to the j-th fermion. The constant that multiplies $\bar{q}_j q_j$ is conventionally called the *bare* (or Lagrangian, or *current*) mass $\equiv m_j$. In a formulation that starts from a Lagrangian that is supposedly $SU(2)_L$ invariant, terms of the form $m_j \bar{q}_j q_j$ cannot appear since, as discussed in this Subsection, they would explicitly break the symmetry. The problem is therefore that of generating fermion mass terms without explicitly breaking $SU(2)_L$.

One natural and elegant possibility in the MSM is provided by the observation that, in the original Lagrangian, there would be room for a symmetric term that is formally written as a Yukawa type interaction between the fermions and the scalars of the model. In fact, given the nature of the scalar fields, that transform like an $SU(2)_L$ doublet (S in the notation of Eq. (1.30)), we see that the assumed local $SU(2)_L \otimes U(1)_{Y_L}$ gauge invariance allows the presence in the electroweak Lagrangian (for the moment, within the first family) of the following fermion-scalar component ($\mathcal{L}_{FS}$ in the notation of Eq. (1.69)):

$$\mathcal{L}_{FS} = \left[f_e \bar{\ell}_{1L} S \psi_{eR} + f_d \bar{q}_{1L} S \psi_{dR} + f_u \bar{q}_{1L} \hat{S} \psi_{uR} \right] + \text{'hermitian conjugate'} \tag{1.143}$$

where ℓ_{1L}, q_{1L} are given by Eqs. (1.66), (1.110) and

$$\hat{S} \equiv i\tau_2 S^+ = \begin{vmatrix} S_d^+ \\ -S_u^+ \end{vmatrix} = \begin{vmatrix} s_0 - is_3 \\ -s_2 + is_1 \end{vmatrix} \tag{1.144}$$

has the same transformation properties under $SU(2)_L$ as S (a doublet), but an opposite value $Y_L = -1$ (for $S, Y_L = +1$).

The introduction of $\hat{S}$ is motivated by the requirement that the additional Lagrangian of Eq. (1.143) has $Y_L = 0$, which is automatic for the first two terms is the r.h.s. of that equation where S appears. On the contrary, a term $\sim \bar{q}_{1L} S \psi_{uR}$ would have overall weak hypercharge $Y_L = +2$, as one can derive from inspection of Table 1.1 (Subsection 1.4.1, the values of Y_L for the $\bar{\psi}_s$ operators are opposite to those of the associated ψ_s). We see therefore that $\bar{q}_{1L}\hat{S}\psi_{uR}$ has the correct value $Y_L = 0$. Note that, a priori, this would have been also true for a term of the kind $f_\nu \bar{\ell}_{1L}\hat{S}\psi_{\nu R}$ if a right-handed neutrino field had been introduced, with does *not* happen in the *minimal* version of the model.

The mechanism for generating fermion masses is now evident. The spontaneous breakdown of the symmetry generates a not vanishing v.e.v. of the scalar field. Assuming as we did in the previous discussions that $\langle s_0 \rangle_0 \equiv (1/\sqrt{2})v$, we obtain immediately after moving to the shifted fields $\tilde{S} = S - \langle S \rangle_0$, Eq. (1.55), that *mass terms* will remain in the Lagrangian. Denoting by $\mathcal{L}_{\tilde{S}F}$ an expression identical to that of $\mathcal{L}_{SF}$ with the formal replacement $S \to \tilde{S}$, we have in fact that;

$$\mathcal{L}_{SF} = \mathcal{L}_{\tilde{S}F} + \frac{v}{\sqrt{2}}[f_e(\bar{\psi}_{eL}\psi_{eR} + \bar{\psi}_{eR}\psi_{eL}) + f_u(\bar{\psi}_{uL}\psi_{uR} + \bar{\psi}_{uR}\psi_{uL}) + f_d(\bar{\psi}_{dL}\psi_{dR} + \bar{\psi}_{dR}\psi_{dL})] \tag{1.145}$$

which means a generation of charged fermion masses:

$$m_e = \frac{v}{\sqrt{2}} f_e \; ; \quad m_{u,d} = \frac{v}{\sqrt{2}} f_{u,d} \tag{1.146}$$

while, as a consequence of the *assumed* absence of a right-handed neutrino field, the neutrino remains massless in the model.

The previous formal derivation has only shown that in the MSM it is possible to generate fermion masses in a "natural" way, i.e. by exploiting the same mechanism that was able to provide masses to the W and Z bosons. The big difference is that in the fermion case the various masses are arbitrary parameters of the model, whose addition is not forbidden, but certainly not theoretically motivated. The precise values of the fermion masses (forgetting for the moment the extra complication of a meaningful definition of a "quark mass") have to be put in by hand.

Leaving aside this undeniably not fully satisfactory fermion mass generation, a short remark might be worthwhile. The final physically acceptable panel with massive W, Z *and* fermions is the result of a series of theoretical assumptions that include: 1) the assumed mechanism of spontaneous $SU(2)_L \otimes U(1)_{Y_L}$ symmetry breaking; 2) the existence of a scalar doublet "hosted" by the vacuum and 3) the introduction in the complete Lagrangian (including in this definition also that of the strong interaction component $\mathcal{L}_s$, Eq. (1.142)) of a specific, Yukawa type, interaction Eq. (1.143). We wish to conclude this Subsection with a discussion of the third point.

1.5.2.3 *Family replication*

Until now we have only considered *one* family of fermions i.e. 15 chiral particles corresponding to the lightest leptons (the electron and its associated *electron neutrino* ν_e) and quarks (u, d with three colors each). Experimentally, one knows nowadays that *at least* two more sets of fermions exist that can be formally grouped assigning them to a second and third *family* whose behavior under the electroweak symmetry group is identical to that of the first family, the only difference being represented by their masses, that seem to increase regularly leading to a second family (with the muon, the muonic neutrino, the quarks c and s) "heavier" than the first and to a third family (with the tau, the tau neutrino, the t and b quarks) "heavier" than the second one. In principle, this does not represent a problem since we have seen in the last Subsection that masses are put in by hand. There is, though, a more subtle theoretical disease that we try to summarize, again for self-consistency purposes, ignoring a more rigorous and historical discussion of experimental and theoretical glorious issues (Cabibbo angle, flavour changing neutral currents) that were already known before the final assessment of the MSM and that we shall exhibit as a byproduct of the following presentation.

Let us first assume the existence of N fermion families grouped, for what concerns $SU(2)_L \otimes U(1)$, as an exact replication of the first. Let us introduce an index i for family, variable from 1 to N. For each i-th family, we shall define the left-handed lepton doublet as $\ell_L^{(i)}$ and the right-handed leptons are $\psi_{\ell R}^{(i)}$:

$$\ell_L^{(i)(W)} \equiv \left| \begin{array}{c} \psi_{\nu L}^{(i)(W)} \\ \\ \psi_{\ell_L}^{(i)(W)} \end{array} \right| \quad \psi_{eR}^{(i)(W)} \tag{1.147}$$

with the convention that $i = 1, 2, 3$ correspond to electron, muon and tau

families (so that e.g. $\psi^{(2)}_{\nu L} \equiv \psi_{\nu\mu L}$, $\psi^{(2)}_{\ell L} \equiv \psi_{\mu L}$, $\psi^{(3)}_{\ell R} = \psi_{\tau R}$...). Analogously, we shall define the quark doublets and singlets of each family as follows:

$$q^{(i)(W)}_L \equiv \begin{vmatrix} \psi^{(i)(W)}_{u_L} \\ \\ \psi^{(i)(W)}_{d_L} \end{vmatrix} \qquad \psi^{(i)(W)}_{uR},\ \psi^{(i)(W)}_{dR} \tag{1.148}$$

(color indexes are omitted now) with the convention that $u^{(1),(2),(3)}$ correspond to the usual up (1), charm (2) and top (3) and $d^{(1),(2),(3)}$ to the usual down (1), strange (2) and bottom (3) flavour indexes.

The lepton and quark particle fields that appear in Eqs. (1.147) and (1.148) are by definition those that have *definite transformation properties* under the electroweak gauge group $SU(2)_L \otimes U(1)_{Y_L}$, i.e. definite I^2_L, I_{3L}, Y_L quantum numbers. They are usually called the *gauge fields*. This mathematical property is enclosed into the upper index $W(\equiv$ weak), that refers to the fact that the $SU(2)_L$ structure (doublets and singlets) of the considered fields is fixed. In the construction of any quantity that is supposedly a *scalar* under $SU(2)_L \otimes U(1)_{Y_L}$, these gauge fields will be necessarily used as starting objects to be combined with other different *gauge eigenstates* (like the scalar doublet S) to obtain the desired scalar, in the some spirit that led to the construction of the Yukawa term Eq. (1.143) for the first family.

To better understand the extra complication that arises when more than one family of fermions is supposed to get masses in the model, let us first consider the pure quark sector of the Lagrangian. For N families, the most immediate and allowed generalization of Eq. (1.143) has then the following form:

$$\mathcal{L}^{(N)}_{FS} \equiv \mathcal{L}^{(N)}_{QS} + \mathcal{L}^{(N)}_{\ell S} \tag{1.149}$$

where the quark component can be written as:

$$\mathcal{L}^{(N)}_{QS} = \sum_{i,i'=1}^{N} \left[G_{ii'} \bar{q}^{(i)(W)}_L S \psi^{(i')(W)}_{dR} + \hat{G}_{ii'} \bar{q}^{(i)(W)}_L \hat{S} \psi^{(i')(W)}_{uR} \right] \tag{1.150}$$

$$+\text{'hermitian conjugate'} \ (\equiv \text{h.c.})$$

where we have introduced the most general $N \times N$ matrices G, $\hat{G}$ on which no stringent particular constraint is set by the requirement that Eq. (1.150) is $SU(2)_L \otimes U(1)_{Y_L}$ invariant. After spontaneous symmetry breaking, the

following *quark mass* Lagrangian will be generated from the usual mechanism:

$$\mathcal{L}^{(N)}_{QS,M} \equiv \frac{v}{\sqrt{2}} \sum_{i,i'} \left[G_{ii'} \bar{\psi}^{(i)(W)}_{dL} \psi^{(i\prime)(W)}_{dR} + \hat{G}_{ii'} \bar{\psi}^{(i)(W)}_{uL} \psi^{i')(W)}_{uR} + \text{h.c.} \right] . \tag{1.151}$$

Defining

$$M^{(d)}_{ii'} = \frac{v}{\sqrt{2}} G_{ii'} \; ; \quad M^{(u)}_{ii'} = \frac{v}{\sqrt{2}} \hat{G}_{ii'} \tag{1.152}$$

and introducing the N-dimensional column vectors $\phi^{(W)}$:

$$\phi^{(W)}_{uL,R} \equiv \left| \begin{array}{c} \psi^{(1)(W)}_{uL,R} \\ \vdots \\ \psi^{(N)(W)}_{uL,R} \end{array} \right| \; ; \quad \psi^{(W)}_{dL,R} = \left| \begin{array}{c} \psi^{(1)(W)}_{dL,R} \\ \vdots \\ \psi^{(N)(W)}_{dL,R} \end{array} \right| \tag{1.153}$$

we can rewrite Eq. (1.151) as:

$$\mathcal{L}^{(N)}_{QS,M} = \bar{\phi}^{(W)}_{uL} M^{(u)} \phi^{(W)}_{uR} + \bar{\phi}^{(W)}_{dL} M^{(d)(W)} \phi_{dR} + \text{h.c.}$$

$$= \bar{\psi}^{(1)(W)}_{uL} \left[M_{11} \psi^{(1)(W)}_{uR} + M_{12} \psi^{(2)(W)}_{uR} + M_{13} \psi^{(3)(W)}_{uR} \right] + ... \tag{1.154}$$

showing that, a priori, the presence of not diagonal terms $\sim \bar{\psi}^{(i)(W)}_{L} \psi^{(i')(W)}_{R}$, $i \neq i'$, cannot be excluded by the mechanism. In other words, the quark *gauge eigenstates*, that appear necessarily as the building block of the electroweak interactions, are *not* physical *mass eigenstates* and, as such, loose meaning from the point of view of observational properties.

This situation in the MSM is not actually new. We have already met the case of the gauge eigenstates W_3, B that were not mass eigenstates. We expect therefore to be able also in this new case to replace the *gauge* quarks with the *massive* ones by means of a suitable matrix transformation. This can actually be done, in full generality.

The mathematical ingredients that must be involved are relatively simple. It is known that, given a general and non diagonal $N \times N$ matrix $= M$, it is always possible to find *two* unitary matrices U_1, U_2 such that

$$U_1 M U_2 \equiv \mathcal{M} \tag{1.155}$$

is *both* diagonal *and* real.

Defining the four matrices required to diagonalize $M^{(u)}, M^{(d)}$ as:

$$\begin{aligned} U^{(u)}_1 &\equiv U_L \; ; \; U^{(u)}_2 \equiv U^{+}_R \; , \\ U^{(d)}_1 &\equiv V_L \; ; \; U^{(d)}_2 \equiv V^{+}_R \end{aligned} \tag{1.156}$$

we shall have that

$$U_L M^{(u)} U_R^+ \equiv \mathcal{M}^{(p)} \tag{1.157}$$

$$V_L M^{(d)} V_R^+ \equiv \mathcal{M}^{(n)} \tag{1.158}$$

with $\mathcal{M}^{(p),(n)}$ diagonal and real. Then, we see that the *physical* quarks will be obtained from the *gauge* eigenstates by rewriting Eq. (1.154) using the unitarity property $U_L U_L^+ = U_L^+ U_L = 1$ (similarly for U_R, V_L and V_R):

$$\begin{aligned} \bar{\phi}_{dL}^{(W)} M^{(d)} \phi_{dR}^{(W)} &+ \bar{\phi}_{uL}^{(W)} M^{(u)} \phi_{UR}^{(W)} + \text{h.c.} \\ &\equiv \bar{\phi}_{uL}^{(W)} U_L^+ (U_L M^{(u)} U_R^+) U_R \phi_{uR} + \text{h.c.} \\ &\equiv \bar{\psi}_{nL} \mathcal{M}^{(n)} \psi_{nR} + \bar{\psi}_{pL} \mathcal{M}^{(p)} \psi_{pR} + \text{h.c.} \\ &\equiv \bar{\psi}_n \mathcal{M}^{(n)} \psi_n + \bar{\psi}_p \mathcal{M}^{(p)} \psi_p \end{aligned} \tag{1.159}$$

($\mathcal{M}^{(n,p)}$ are now real diagonal matrices) where $\psi_{n,p}$ are N-dimensional column vectors whose elements are by definition the *physical* (mass eigenstates) quarks. These will be denoted in the following way:

$$\psi_{pL,R} \equiv \begin{vmatrix} \psi_{uL,R}^{(1)} \\ \vdots \\ \psi_{uL,R}^{(N)} \end{vmatrix} \tag{1.160}$$

$$\psi_{nL,R} \equiv \begin{vmatrix} \psi_{dL,R}^{(1)} \\ \vdots \\ \psi_{dL,R}^{(N)} \end{vmatrix} \tag{1.161}$$

where the *physical* quark fields are indicated by the same symbols $\psi_{L,R}^{(i)}$ as in Eqs. (1.148), (1.153) but *without* the upper W index that specifies the *gauge* eigenstates. Thus, $\psi_u^{(1),(2),(3)}$ will now correspond to the *physical* up, charm, top flavour quarks, and analogously for the down type (1,2,3) indexes (down, strange and bottom). In matrix form, the relationship between the physical and the gauge quarks will be expressed as follows:

$$\psi_{pL,R} = U_{L,R} \phi_{uL,R}^{(W)} \tag{1.162}$$

$$\psi_{nL,R} = V_{L,R} \phi_{dL,R}^{(W)} \, . \tag{1.163}$$

Having defined the physical quarks, it is now useful to express the various terms of the electroweak Lagrangian in terms of these quantities. For

what concerns the residual interaction with the scalar doublet $\tilde{S}$, generalization of what was called $\mathcal{L}_{\tilde{S}F}$ in Eq. (1.145), it is straightforward to verify that in the unitary gauge one has:

$$\mathcal{L}_{\tilde{S}F} = \frac{1}{v} H \left[\bar{\psi}_n \mathcal{M}^{(n)} \psi_n + \bar{\psi}_p \mathcal{M}^{(p)} \psi_p \right] \tag{1.164}$$

where H is the physical Higgs scalar. Thus, the Higgs scalar automatically *interacts with the physical quarks*.

Let us consider now the gauge-fermion interaction in the quark sector that is originally expressed in terms of the gauge fields. We want to express it in terms of the physical fields in the general case.

Consider the charged current interaction first. From Eqs. (1.95), (1.96) one can generalize the definition of $J^{(+)}_{\mu,1L}$:

$$\mathcal{L}^{(\text{charged})}_{FG} = \mathcal{L}^{(\text{charged})}_{\ell G} + \mathcal{L}^{(\text{charged})}_{qG} = \frac{g}{\sqrt{2}} \left[\left(J^{(+)}_{\mu,\ell} + J^{(+)}_{\mu,q} \right) W^{+\mu} + \text{h.c.} \right] \tag{1.165}$$

where

$$J^{(+)}_{\mu,q} = \sum_{i=1}^{3} \bar{\psi}^{(i)(W)}_{uL} \gamma_\mu \psi^{(i)(W)}_{dL} \equiv \bar{\psi}^{(W)}_{uL} \gamma_\mu \psi^{(W)}_{dL} \ . \tag{1.166}$$

Equation (1.166) can also be rewritten in terms of the physical quarks as:

$$J^{(+)}_{\mu,q} \equiv \bar{\psi}_{pL} \gamma_\mu [U_L V_L^+] \psi_{nL} = \bar{\psi}_{pL} \gamma_\mu U \psi_{nL} \tag{1.167}$$

(color indexes are omitted now) where

$$U = U_L V_L^+ \tag{1.168}$$

is a *unitary* $N \times N$ matrix, in principle complex and determined by $(N-1)^2$ real independent parameters. In fact, the unitarity condition

$$U_{\alpha\beta} U^+_{\beta\gamma} \equiv U_{\alpha\beta} U^*_{\gamma\beta} = \delta_{\alpha\beta} (\alpha, \beta, \gamma = 1, ., ., N) \tag{1.169}$$

imposes N^2 conditions, reducing the number of parameters from $2N^2$ to N^2, in particular leaving $N(N-1)/2$ *moduli* and $N(N+1)/2$ *phases*. One can then change $(2N-1)$ *relative* phases of the $2N$ fields that appear in Eq. (1.167) absorbing a corresponding number of U phases, remaining therefore with $N(N-1)/2$ moduli and $(N-1)(N-2)/2$ phases (total= $(N-1)^2$) in U (for a detailed explanation see [18])

If N were equal to 2, the only possible form for U would then be:

$$U_{(N=2)} \equiv \begin{vmatrix} \cos\theta_c & \sin\theta_c \\ -\sin\theta_c & \cos\theta_c \end{vmatrix} \tag{1.170}$$

that reproduces the Cabibbo parameterization [27], with θ_c to be experimentally determined.

Consider next the case $N = 3$. The U matrix then depends on 4 parameters, that can be classified as 3 (real) moduli and one phase.

Actually, any unitary 3×3 matrix can be cast in the form:

$$U \equiv U_1 U^{KM} U_2 \tag{1.171}$$

where

$$U_1 = \begin{vmatrix} 1 & 0 & 0 \\ 0 & e^{i\gamma} & 0 \\ 0 & 0 & e^{i\epsilon} \end{vmatrix} \; ; \quad U_2 = \begin{vmatrix} e^{i\alpha} & 0 & 0 \\ 0 & e^{i\beta} & 0 \\ 0 & 0 & e^{i\eta} \end{vmatrix} \tag{1.172}$$

and U^{kM} is the so called *Cabibbo–Kobayashi–Maskawa matrix* [28], that can be written in the form:

$$U^{KM} = \begin{vmatrix} c_1 & s_1 c_3 & s_1 s_3 \\ -s_1 c_2 & [c_1 c_2 c_3 - e^{i\delta} s_2 s_3] & [c_1 c_2 s_3 + e^{i\delta} s_2 c_3] \\ -s_1 s_2 & [c_1 s_2 c_3 - e^{i\delta} c_2 s_3] & [c_1 s_2 s_3 + e^{i\delta} c_2 c_3] \end{vmatrix} \tag{1.173}$$

where s_i, $c_i \equiv \sin\theta_i, \cos\theta_i$ and δ is a certain phase. Then $U_{1,2}$ are *reabsorbed* by a redefinition of the field relative phases, and in the final expression U^{KM} remains as a generalization of the Cabibbo matrix in the case $N = 3$, with the four parameters θ_1, θ_2, θ_3, δ to be determined experimentally.

The existence of a phase $\delta \neq 0$ is of paramount theoretical relevance since it can be shown that, in connection with this fact, there will be in the electroweak Lagrangian the presence of *CP violation*. This will be caused by those terms in the CKM matrix where δ appears.

To understand this statement, one must recall the transformation properties of a general fermion field under C (charge conjugation) and P (parity), that can be found for instance in Ref. [30]. Given the latter ones, one can compute the transformation of the Lagrangian (Eq. (1.165)) and verify that for $N \geq 3$ the presence of phases makes CP invariance fail. With these conventions and notations, we can consequently expect CP violation in those processes where the matrix elements $U^{KM}_{22,23,32,33}$ are involved provided that δ, the *CP violating* phase, is different from zero. In practice, anticipating an experimental determination that will be exploited in the following part of the book, one finds that the CKM matrix is "essentially" diagonal, in the sense that

$$|U_{11}| \approx |U_{22}| \approx |U_{33}| >> |U_{ik}|, i \neq k. \tag{1.174}$$

We now come to the neutral current sector of the weak interaction. Repeating exactly the some procedure as in the charged case, one easily sees that all the *current* components can be written in the form:

$$\bar{\psi}_{pL}\gamma_\mu[U_L U_L^+]\psi_{pL}\ ;\ \bar{\psi}_{pR}\gamma_\mu[U_R U_R^+]\psi_{pR}\ ;$$
$$\bar{\psi}_{nL}\gamma_\mu[V_L V_L^+]\psi_{nL}\ ;\ \bar{\psi}_{nR}\gamma_\mu[V_R V_R^+]\psi_{nR} \tag{1.175}$$

and thus, from the unitarity of $(U,V)_{L,R}$ these currents are automatically *diagonal (i.e. not flavour changing)* in the physical fields.

Similar results are obtained in the lepton sector. Without repeating again the full procedure, one can treat it as a special case of Eq. (1.150) with $\hat{G}_{ij} \equiv 0$, *(since no* $\psi_{\nu R}^{(i)(W)}$ *are included,* $m_\nu \equiv 0$*).*

This means that the diagonalization of $\hat{G} \equiv 0$ can be achieved with *any* couple of matrices U_1, U_2 in particular with $U^{(\nu)} \equiv V^{(e)}$. Then both the charged current ($U^{KM,\ell} \equiv 1$) and the neutral one *are automatically diagonal in the physical fields* denoted without the upper W index (i.e. $\bar{\psi}_{\nu eL}\gamma_\mu\psi_{eL}, \bar{\psi}_{\nu\mu L}\gamma_\mu\psi_{\mu L}, \bar{\psi}_{\nu\tau L}\gamma_\mu\psi_{\tau L}$ etc.), *and the various lepton numbers are separately conserved.*

A final point concerns the strong interaction component of the MSM represented by Eq. (1.136). As one sees immediately, the quark gluon interaction is automatically diagonal also in the physical quarks, and can simply be rewritten in terms of the mass eigenstates with no formal change of the interaction. The mass eigenstates are also, therefore, the quarks that are involved in the strong sector of the model.

After this remarks we are now in a position to discuss in a realistic way the tests of the MSM that can be provided at the Z resonance.

1.5.3 *Tests of the MSM at LEP1/SLC*

We can now return to the investigation of the kind of tests of the MSM that can be provided by accurate measurements of the observable properties of the process of electron-positron annihilation *on top* of Z resonance. For this purpose it will be useful to write again the overall expression of the complete Lagrangian that describes strong and electroweak interactions in the MSM. This will read:

$$\mathcal{L}^{(\mathrm{MSM})} = \mathcal{L}_s^{(\mathrm{MSM})} + \mathcal{L}_{\mathrm{E.W.}}^{(\mathrm{MSM})} \tag{1.176}$$

where the strong component $\mathcal{L}_s^{(\mathrm{MSM})}$ is given by Eq. (1.136) and the electroweak component $\mathcal{L}_{\mathrm{E.W.}}$ can be written in the form of Eq. (1.135) as the

sum of four terms

$$\mathcal{L}_{\text{E.W.}}^{(\text{MSM})} = \mathcal{L}_{SG}^{(\text{MSM})} + \mathcal{L}_{FG}^{(\text{MSM})} + \mathcal{L}_{GG}^{(\text{MSM})} + \mathcal{L}_{\text{FS}}^{(\text{MSM})} \tag{1.177}$$

corresponding to the interactions between scalars and gauge boson (SG), fermions and gauge bosons (FG), gauge bosons-gauge bosons (GG) and fermions with scalars (FS). The first quantity coincides with the first terms written in the r.h.s. of Eq. (1.50):

$$\mathcal{L}_{SG}^{(\text{MSM})} = (D_\mu S)^\dagger (D^\mu S) - V(S) \tag{1.178}$$

and in fact it contains also the self-interaction of the scalar fields (for conventional reasons). The fermion-gauge boson terms will be expressed as from Eqs. (1.95), (1.97) i.e.:

$$\mathcal{L}_{FG}^{(\text{charged})(\text{MSM})} = \frac{g}{\sqrt{2}} \left[(J_{\mu,\ell}^{(+)} + J_{\mu,Q}^{(+)}) W^{+\mu} + \text{h.c.} \right] \tag{1.179}$$

$$\mathcal{L}_{FG}^{(\text{neutral})(\text{MSM})} = |e| (J_{\rho,\ell}^{(Q)} + J_{\rho,q}^{(Q)}) A^\rho + \frac{|e|}{\sin\theta_W \cos\theta_W} (J_{\rho,\ell}^{(Z)} + J_{\rho,q}^{(Z)}) Z^\rho \tag{1.180}$$

with the understanding that

$$\mathcal{L}_{FG}^{(\text{MSM})} = \mathcal{L}_{FG}^{(\text{charged})(\text{MSM})} + \mathcal{L}_{FG}^{(\text{neutral})(\text{MSM})} \,. \tag{1.181}$$

In Eqs. (1.179), (1.180) we have used the definitions:

$$J_{\mu,\ell}^{(+)} = \bar{\psi}_{\nu_e L} \gamma_\mu \psi_{eL} + \bar{\psi}_{\nu_\mu L} \gamma_\mu \psi_{\mu L} + \bar{\psi}_{\nu_\tau L} \gamma_\mu \psi_{\tau L} + \cdots \tag{1.182}$$

$$J_{\mu,q}^{(+)} = \sum_{c_i=1}^{3} \sum_{i,j=1}^{N} \bar{\psi}_{pL,i}^{(c_i)} \gamma_\mu U_{ij} \psi_{nL,j}^{(c_i)} \tag{1.183}$$

$$J_{\rho,\ell}^{(Q)} = -\left[\bar{\psi}_e \gamma_\rho \psi_e + \bar{\psi}_\mu \gamma_\rho \psi_\mu + \bar{\psi}_\tau \gamma_\rho \psi_\tau + \cdots \right] \tag{1.184}$$

$$J_{\rho,q}^{(Q)} = \sum_{c_i=1}^{3} \left[\frac{2}{3} \bar{\psi}_p^{(c_i)} \gamma_\rho \psi_p^{(c_i)} - \frac{1}{3} \bar{\psi}_n^{(c_i)} \gamma_\rho \psi_n^{(c_i)} \right] \tag{1.185}$$

$$J_{\rho,\ell}^{(Z)} = \left[\frac{1}{2} \bar{\psi}_{\nu_e L} \gamma_\rho \psi_{\nu_e L} + \left(-\frac{1}{2} + \sin^2\theta_W \right) \cdot \bar{\psi}_{eL} \gamma_\rho \psi_{eL} + \sin^2\theta_W \bar{\psi}_{eR} \gamma_\rho \psi_{eR} \right] + (\mu, \tau \cdots) \tag{1.186}$$

$$J_{\rho,q}^{(Z)} = \left[\bar{\psi}_{uL} \gamma_\rho \psi_{uL} \left(\frac{1}{2} - \frac{2}{3} \sin^2\theta_W \right) + \bar{\psi}_{dL} \gamma_\rho \psi_{dL} \left(-\frac{1}{2} + \frac{1}{3} \sin^2\theta_W \right) \right.$$

$$+\bar{\psi}_{uR}\gamma_\rho\psi_{uR}\left(-\frac{2}{3}\sin^2\theta_W\right)+\bar{\psi}_{dR}\gamma_\rho\psi_{dR}\left(\frac{1}{3}\sin^2\theta_W\right)\Big]$$
$$+(c,s,t,b\cdots)\,. \tag{1.187}$$

Here $\psi_p \equiv \psi_{pL}+\psi_{pR}$ and $\psi_n=\psi_{nL}+\psi_{nR}$, the chiral quantities being defined by Eqs. (1.160), (1.161). A (diagonal) sum over the color index c_i is explicitly written (the Lagrangian must be a $SU(3)_c$ scalar); the number of families N is left free for the moment.

The gauge boson-gauge boson term contains the $SU(2)_L$ component already appearing in Eq. (1.50), with the addition of the $U(1)_{Y_L}$ contribution;

$$\mathcal{L}_{GG}^{(\mathrm{MSM})}=-\frac{1}{4}\sum_{\kappa=1}^{3}F_{\mu\nu}^{\kappa}F^{\mu\nu,\kappa}-\frac{1}{4}B_{\mu\nu}B^{\mu\nu} \tag{1.188}$$

where $F_{\mu\nu}^{\kappa}$ is defined by Eq. (1.51) (κ denotes the $SU(2)_L$ spin one vector $W_\mu^{(1),(2),(3)}$) and

$$B_{\mu\nu}=\partial_\mu B_\nu-\partial_\nu B_\mu \tag{1.189}$$

where B_μ is the $U(1)_{Y_L}$ gauge boson. The expression of $\mathcal{L}_{GG}^{(\mathrm{MSM})}$ in terms of the mass eigenstates Z_μ, A_μ is straightforward and will not be explicitly shown.

The fermion-scalar term $\mathcal{L}_{FS}^{(\mathrm{MSM})}$ has been exhaustively discussed in the previous Subsection. It can be taken from Eq. (1.149), the leptonic part being defined with the pure $\sim S$ term (no right-handed neutrinos) and the physical charged lepton field operators in the formal expression, the diagonal mass matrix being an obvious modification of Eq. (1.161), with the 'd' index replaced by a 'ℓ' = charged lepton one, and

$$m_{\ell,\mu,\tau}=\frac{v}{\sqrt{2}}\left[G_{11}^{(\ell)},G_{22}^{(\ell)},G_{33}^{(\ell)}\right]$$

where $G^{(\ell)}$ corresponds to G, Eq. (1.150).

Given the overall expression of the Lagrangian, let us consider the process of electron-positron annihilation at the Z mass energy (*on top* of Z resonance). To the lowest order in a perturbation expansion, this is described by the Feynman diagram of Fig. (1.2). In this approximation, any measurement on Z resonance represents a test of the assumed form *of the pure Z component* of the neutral part of the Lagrangian $\mathcal{L}_{FG}^{(\mathrm{MSM})}$, second term in the r.h.s. of Eq. (1.180). Let us assume for the moment that such an approximate lowest order description is "satisfactory", and let us see what general theoretical assumptions can be tested in this way.

1.5.4 *Universality of weak interactions and number of fermion families*

A first fundamental consequence of the assumed theoretical framework is the property of *universality* of the fermion-gauge boson interactions. This corresponds to the fact that the couplings to W^+, W^- and Z of fermions belonging to different families only depend on their weak isospin and charge, but not on the *flavour* or on other typical features of the families. Strictly speaking, for what concerns the $W^{+,-}$ couplings, the previous statement ignores the fermion family mixing, discussed in Subsection 1.5.2. In first approximation we shall here assume that the CKM matrix is essentially diagonal, as anticipated in that Subsection, since our main interest in concentrated on the Z couplings.

In particular, the Z interacts with the fermions in a way that is specified by Eqs. (1.111), (1.114), (1.119) and one predicts the same couplings with e.g. electrons, muons and taus (analogously, with the three kinds of neutrinos and with the different flavour kinds of *up-type* and *down-type* quarks). Modulo small and calculable kinematical effects due to different masses, the decays of Z into e.g. different charged leptons (or neutrinos, or quarks) should be identical for the same $(I_{3L},\, Q_f)$ quantum numbers.

If should be stressed that this universality prediction is indeed a consequence of the assumed theoretical scheme and, more precisely, of the non Abelian nature of the $SU(2)_L$ component of the symmetry group. To be more specific, let us suppose that a second doublet of left-handed fermions is added to a first one in the original Lagrangian. The form of the covariant derivative that acts on this doublet is then forced to contain *the same* $SU(2)_L$ *coupling* g that appeared in the first doublet, if one wishes to realize the symmetry with the same set of gauge bosons, that transform under the group in the same way. In other words, assuming that the second doublet is coupled to the $SU(2)_L$ gauge bosons with strength $= hg$ (g is the strength of the first doublet), one finds that necessarily $h = 1$ as a consequence of the non Abelian nature of $SU(2)_L$. Note that this fact would not be true for an Abelian group like e.g. the QED $U(1)$. In this case, if one charged fermion couples with the photon with a strength e, any other charged fermion can couple to the (same) photon with strength he and arbitrary h.

Given the relevance of this universality property, we shall now try to sketch a qualitative proof. Consider first the case of two charged fermions f_1, f_2 of electric charge 'e' and 'he' respectively. The generator of the $U(1)$ QED symmetry group is Q, the electric charge. Under a transformation of

the group, $f_{1,2}$ become:

$$f_1' = e^{-i\epsilon(x)} f_1 \left(\bar{f}_1' = \bar{f}_1 e^{i\epsilon(x)}\right) \tag{1.190}$$

$$f_2' = e^{-ih\epsilon(x)} f_2 \left(\bar{f}_2' = \bar{f}_2 e^{ih\epsilon(x)}\right) \tag{1.191}$$

where $\epsilon(x)$ is a real space-time dependent phase.

The covariant derivatives on $f_{1,2}$ will be:

$$D_\mu f_1 = (\partial_\mu + ieA_\mu) f_1 \tag{1.192}$$

$$D_\mu f_2 = (\partial_\mu + iheA_\mu) f_2 \, . \tag{1.193}$$

From the requirement of $U(1)$ invariance of the terms $\bar{f}_1 \gamma^\mu D_\mu f_1$ and $\bar{f}_2 \gamma^\mu D_\mu f_2$ one derives the $U(1)$ transformation properties of A_μ, that must be by definition the same in the two cases. Actually, one has that imposing

$$\bar{f}_1'(D_\mu f_1)' = \bar{f}_1 D_\mu f_1 \tag{1.194}$$

gives for the $U(1)$ transformed field

$$A_\mu'(x) = A_\mu(x) + \frac{1}{e}\partial_\mu \epsilon(x) \tag{1.195}$$

and the *same* condition is derived by imposing that

$$\bar{f}_2'(D_\mu f_2)' = \bar{f}_2 D_\mu f_2 \tag{1.196}$$

independently of h. Let us show this in the particularly simple case of an infinitesimal transformation, for which $e^{-ih\epsilon(x)} \simeq (1 - ih\epsilon(x))$.

We find then:

$$\begin{aligned}
\bar{f}_2'(D_\mu f_2)' &\simeq \bar{f}_2(1 + ih\epsilon(x)) \left(\partial_\mu + iheA_\mu'(x)\right) (1 - ih\epsilon(x)) f_2 \\
&= \bar{f}_2 \left[\partial_\mu + iheA_\mu'(x) - ih(\partial_\mu \epsilon(x))\right] f_2 \\
&\quad + \bar{f}_2 h^2 e \left[A_\mu'(x)\epsilon(x) - \epsilon(x)A_\mu'(x)\right] + O(\epsilon^2) \\
&\equiv \bar{f}_2 \left[\partial_\mu + iheA_\mu(x)\right] f_2
\end{aligned} \tag{1.197}$$

(the last equality follows by the requirement that $\bar{f}_2(D_\mu f_2)' = \bar{f}_2 D_\mu f_2$). Equation (1.197) leads to the condition (1.195) $A_\mu' = A_\mu + (1/e)\partial_\mu \epsilon(x)$ that does not depend on h, since all the residual terms of the equality are linear in h, that can be consequently factorized and eliminated. This is a consequence of an exact cancellation of the two terms that are quadratic

in h in Eq. (1.197), which in term is due to the Abelian nature of the $U(1)$ group.

Let us repeat the treatment for two $SU(2)_L$ doublets, denoted by the symbols ψ_1 and ψ_2. Assuming a $SU(2)_L$ *coupling* of strength g, hg respectively one will have in this case

$$\psi_1' = e^{-i\frac{\vec{\tau}}{2}\cdot\vec{\epsilon}(x)}\psi_1 \tag{1.198}$$

$$\psi_2' = e^{-ih\frac{\vec{\tau}}{2}\cdot\vec{\epsilon}(x)}\psi_2 \tag{1.199}$$

where the Pauli τ_i matrices satisfy the commutation relations of the associated $SU(2)_L$ generators:

$$\left[\frac{\tau_i}{2}\ ,\ \frac{\tau_j}{2}\right] = i\ \epsilon_{ij\kappa}\frac{\tau_\kappa}{2} \tag{1.200}$$

that exhibits the non Abelian nature of the $SU(2)_L$ group. For the covariant derivatives, we shall have now

$$D_\mu\psi_1 = \left(\partial_\mu - ig\frac{\vec{\tau_i}\vec{A}_\mu}{2}\right)\psi_1 \tag{1.201}$$

$$D_\mu\psi_2 = \left(\partial_\mu - ihg\frac{\vec{\tau_i}\vec{A}_\mu}{2}\right)\psi_2\ . \tag{1.202}$$

Considering again infinitesimal transformations, one finds by imposing the invariance of the term $\bar{\psi}_1 D_\mu\psi_1$ that the $SU(2)_L$ transformed gauge bosons fields must be ($i = 1, 2, 3$):

$$A_\mu'^i = A_\mu^i - \frac{1}{g}\partial_\mu\epsilon_i(x) + \epsilon_{ij\kappa}\epsilon_j(x)A_\mu^\kappa\ . \tag{1.203}$$

In the case of Eq. (1.202), one is led to the following equality from the requirement of $SU(2)_L$ invariance of the quantity $\bar{\psi}_2 D_\mu\psi_2$:

$$\begin{aligned}\bar{\psi}_2\left(\partial_\mu - ihg\frac{\tau_i}{2}A_\mu^i\right)\psi_2 = \bar{\psi}_2\left[\partial_\mu - ihg\frac{\tau_i}{2}A_\mu'^i - ih\frac{\tau_i}{2}(\partial_\mu\epsilon_i(x))\right]\psi_2 \\ -\bar{\psi}_2 h^2 g\left[\frac{\tau_\kappa}{2}A_\mu^\kappa\frac{\tau_j}{2}\epsilon_j(x) - \frac{\tau_j}{2}\epsilon_j(x)\frac{\tau_\kappa}{2}A_\mu^\kappa\right]\psi_2 \\ +O(\epsilon^2)\ .\end{aligned} \tag{1.204}$$

As one sees, the residual quadratic term in h is now *not* vanishing because of the $SU(2)_L$ commutation relation Eq. (1.200), contrary to the $U(1)$ case Eq. (1.197). Taking Eq. (1.200) into account gives in fact:

$$A_\mu'^i(x) = A_\mu^i(x) - \frac{1}{g}\partial_\mu(\epsilon_i(x) + h\epsilon_{ij}\epsilon_j(x)A_\mu^\kappa \tag{1.205}$$

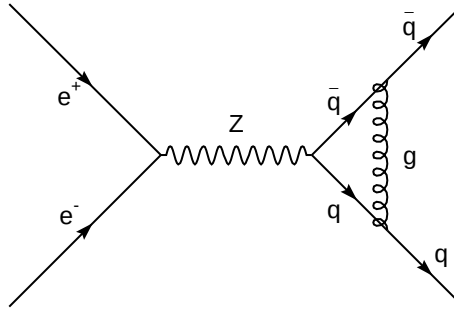

Fig. 1.6 Example of gluon (A^a) exchange in $q\bar{q}$ production.

from which, to guarantee $SU(2)_L$ invariance with the same triplet of gauge bosons, one must necessarily set $h = 1$.

In conclusion, the couplings of Z to the fermions will be fixed by only one unknown parameter : the Weinberg quantity $\sin^2\theta_W$, with fermions of each family *universally* coupled as from Eqs. (1.186), (1.187). This prediction (*and* the value of $\sin^2\theta_W$) can be at first sight checked (and derived) by e^+e^- measurements on Z resonance.

Another very important issue concerns the (a priori free) number of families N. Clearly only those fermions that are sufficient light to be produced in couples by an e^+e^- energy equal to m_Z would be "seen" on Z resonance. Therefore, "heavy" families would escape observation, with the exception of their neutrinos, if the assumed pattern of massless neutrinos is maintained.

Qualitatively, one can imagine that measuring the properties of the Z decays the number of *invisible* decays into neutrinos can be counted. This is undoubtedly another very important feature of the model that can directly measured.

The previous discussion was assuming the validity of a lowest order description of e^+e^- annihilation on top of Z resonance, corresponding to the *tree* diagram represented in Fig. 1.2. But the fundamental property of being renormalisable allows to perform in the MSM calculations of higher order effects, in particular of Feynman diagram at the next *one-loop* level like e.g. those of electroweak type represented in Figs. 1.3–1.5. Also, for a final quark-antiquark states, higher order diagrams involving strong gluon

exchange will have to be retained, like e.g. that represented in Fig. 1.6.

Clearly, these higher order effects will allow to provide tests of the remaining parts of the Lagrangian, as already discussed . These tests will be necessarily less stringent than those related to the lowest order Z exchange, given the fact that the extra effects to be predicted will be necessarily relatively smaller than the leading one.

Nevertheless, in some particular cases they will be not only not negligible, but also in a specific sense very predictive. We shall return on this point in great detail in the forthcoming Chapters.

This final discussion concludes Chapter 1 that was devoted to a brief, self-contained summary of some of the main features of the MSM. In the next Chapter, we shall begin to illustrate which experimental quantities can be actually measured on Z resonance, and what are the related theoretical predictions at the one loop level to be compared with the various experimental results.

This page intentionally left blank

Chapter 2

Z Physics at Tree Level

This Chapter introduces a number of measurable quantities in e^+e^- annihilation and the basic technique that is necessary to calculate them. Since parity violation plays a crucial rôle in electroweak interactions, we derive chirality amplitudes directly without using trace theorems. Although the latter ones provide a general framework for performing calculations, the decomposition that we shall describe here highlights suitably the Standard Model separation into left-handed and right-handed fermions. The property of asymmetries and of polarization observables at the Z pole to offer informations from parity violation effects rather than from $Z\gamma$ interference is also easier to understand in this way. This Chapter is organized as follows. In Section 2.1, the basic expressions for spinors are recalled. The differential cross section for the process $e^+e^- \to \mu^+\mu^-$ via photon exchange, for the four possible combinations of initial and final state helicities is given in Section 2.2. This allows the general expression of polarized and of unpolarized cross sections to be derived. The Z propagator is then introduced in Section 2.3 in an *effective* way, leading to the general expression for the Z-mediated cross sections. The magnitudes of the photon and of the Z cross sections are compared. The important calculation of the $Z \to f\bar{f}$ process is then described, for massless fermions, in Section 2.4. The massless-fermion hypothesis will allow a simplification of the cross section formula previously derived. The different couplings of the Z to left and right-handed fermions lead to a large number of parity violating effects. The angular asymmetries and the polarization asymmetries are described in Section 2.5 where it is also shown that these observables, that are related to parity violation can be expressed in terms of one single parameter, the electroweak mixing angle. Moving away from the Z peak, general expressions including $Z\gamma$ interference will be given in Section 2.6.

2.1 Conventions, spinors and basic cross sections

The e^-e^+ initial state is defined by the electron-positron four-momenta ℓ^μ and ℓ'^μ:

$$\ell^\mu = (\ell^0, \ell) = (\ell^0, 0, 0, \ell) \tag{2.1}$$
$$\ell'^\mu = (\ell^0, -\ell) = (\ell^0, 0, 0, -\ell) \tag{2.2}$$
$$\ell^0 = \sqrt{\ell^2 + m_e^2}\,. \tag{2.3}$$

This corresponds to the experimental situation at LEP and SLC, with head-on collisions in the centre of mass frame, although, due to energy spread or slight momentum asymmetries, small boosts might have to be considered occasionally. The centre-of-mass squared energy is

$$s = (\ell^\mu + \ell'^\mu)^2 = 4(\ell^0)^2. \tag{2.4}$$

The aim of the following discussion is mostly that of arriving in a simple way to the definition of those quantities that will be relevant for our description of the physics at the Z pole. In this spirit, we shall assume the preliminary knowledge of some basic ingredients of the mathematical features of relativistic fermions. There exist excellent review books on the topics, in particular we shall adopt the notations and conventions of Renard [31] and proceed in a very quick way to the aimed results.

The spin state of a fermion can be described by the polarization four-vector ξ^μ as follows. In the fermion rest frame, r, choosing as usual the system $\hbar = c = 1$, so that $\ell^r_\mu = (m_e, 0, 0, 0)$, the polarization four-vector ξ_μ has the form $\xi^r_\mu = (0, \vec{\xi_r})$, where $\vec{\xi_r}$ is a unit 3-vector aligned with the electron spin. By definition, ξ_μ always satisfies the two constraints:

$$\xi \cdot \ell = 0;\ \xi^2 = -1. \tag{2.5}$$

The spinor $u(\ell, \xi)$ is related to the free-electron wave function $\psi_{l\xi}(x)$, solution of the Dirac equation, by the usual expression

$$\psi_{\ell\xi}(x) = \frac{1}{(2\pi)^{\frac{3}{2}}} \frac{1}{\sqrt{2\ell_0}} \exp\left(-i\ell \cdot x\right)\, u(\ell, \xi)\,. \tag{2.6}$$

In the rest frame r, choosing the Z axis as the quantization one for the electron spin and calling $(\chi\pm)$ the 2-component spinors eigenstates of $\sigma_z = \begin{vmatrix} 1 & 0 \\ 0 & -1 \end{vmatrix}$

$$\sigma_z \chi^{\pm} = \pm \chi^{\pm} \tag{2.7}$$

$$\chi^{+} = \begin{vmatrix} 1 \\ 0 \end{vmatrix}, \ \chi^{-} = \begin{vmatrix} 0 \\ 1 \end{vmatrix} \tag{2.8}$$

the electron states with spin along the positive and the negative Z axis are described by

$$u_I = \sqrt{2m_e} \begin{vmatrix} \chi^{+} \\ 0 \end{vmatrix} = \sqrt{2m_e} \begin{vmatrix} 1 \\ 0 \\ 0 \\ 0 \end{vmatrix} \equiv u(\ell^r, \hat{\xi}_Z) \tag{2.9}$$

$$u_{II} = \sqrt{2m_e} \begin{vmatrix} \chi^{-} \\ 0 \end{vmatrix} = \sqrt{2m_e} \begin{vmatrix} 0 \\ 1 \\ 0 \\ 0 \end{vmatrix} \equiv u(\ell^r, -\hat{\xi}_Z) \tag{2.10}$$

where

$$\hat{\xi_z} = (0, 0, 0, 1) \tag{2.11}$$

and the normalization is such that

$$\bar{u}u = u^{\dagger}\gamma_0 u = 2m_e \tag{2.12}$$

where

$$\gamma_0 = \begin{pmatrix} I & 0 \\ 0 & -I \end{pmatrix}. \tag{2.13}$$

In a general frame, the four-vector $\ell_\mu = (\ell_o, \vec{\ell})$ can be obtained from the rest frame vector ℓ^r_μ via a Lorentz transformation with coefficients a^ν_μ

$$\ell_\mu = a^\nu_\mu \ell^r_\nu \tag{2.14}$$

and the corresponding value of the polarization vector will be, similarly,

$$\xi_\mu = a^\nu_\mu \xi^r_\nu \ . \tag{2.15}$$

From the canonical transformation properties of spinors under a Lorentz transformation one derives the expression of the general spinors with polarization ξ_μ

$$u(\ell, \xi) = \frac{\not{\ell} + m_e}{\sqrt{2m_e(\ell_0 + m_e)}} u_I \tag{2.16}$$

$$u(\ell, -\xi) = \frac{\not{\ell} + m_e}{\sqrt{2m_e(\ell_0 + m_e)}} u_{II} \tag{2.17}$$

where $\not{\ell} = \gamma^\mu \ell_\mu \equiv \gamma^0 \ell^0 - \vec{\gamma} \cdot \vec{\ell}$. The three $\vec{\gamma}$ matrices can be represented by

$$\gamma^i = \begin{vmatrix} 0 & \sigma_i \\ -\sigma_i & 0 \end{vmatrix} \tag{2.18}$$

indicating with σ_i, $i = 1, 2, 3$, the Pauli matrices,

$$\sigma_1 = \begin{vmatrix} 0 & 1 \\ 1 & 0 \end{vmatrix}, \sigma_2 = \begin{vmatrix} 0 & -i \\ i & 0 \end{vmatrix}, \sigma_3 = \begin{vmatrix} 1 & 0 \\ 0 & -1 \end{vmatrix} \equiv \sigma_z. \tag{2.19}$$

Equations (2.16) and (2.17) are a direct consequence of Dirac equation $(\not{\ell} - m_e)u(\ell, \xi) = 0$. Expressing $u(\ell, \xi)$ with 2-component spinors,

$$u(\ell, \xi) = \begin{pmatrix} \chi \\ \phi \end{pmatrix}, \tag{2.20}$$

a relationship between ϕ and χ is obtained: $\phi = \frac{\vec{\sigma} \cdot \vec{\ell}}{\ell_0 + m_e} \chi$.

A more convenient classification of the spin states of the fermions at high energies is given in terms of their helicity λ. This is defined as the spin ($\vec{s}$) component along the direction of the 3-momentum, and for spin $\frac{1}{2}$ fermions has the expression

$$\lambda = \frac{\vec{s} \cdot \vec{\ell}}{|\vec{\ell}|} = \frac{1}{2} \frac{\ell_i}{|\vec{\ell}|} \begin{vmatrix} \sigma_i & 0 \\ 0 & \sigma_i \end{vmatrix}. \tag{2.21}$$

The helicity takes discrete values and $\lambda = \pm\frac{1}{2}$ for spin $\frac{1}{2}$ particles. It is not Lorentz invariant if the particle mass is different from zero: a Lorentz transformation can reverse the direction of $\vec{\ell}$, hence the sign of helicity. Assuming, however, that the direction of $\vec{\ell}$ is not changed by the Lorentz boost, the helicity corresponds to the eigenvalues of σ_z in the rest frame of the particle (Eq. (2.7)).

The expressions of the Dirac spinors with four-momentum ℓ and helicity $\lambda = \pm\frac{1}{2}$ are then the following ones (choosing the direction of $\vec{\ell}$ as the Z axis):

$$u(\ell, \lambda = +\frac{1}{2}) = \sqrt{\ell_0 + m_e} \begin{vmatrix} \chi+ \\ \frac{\ell}{\ell_0 + m_e} \chi+ \end{vmatrix} = \sqrt{\ell_0 + m_e} \begin{vmatrix} 1 \\ 0 \\ \frac{\ell}{\ell_0 + m_e} \\ 0 \end{vmatrix} \tag{2.22}$$

$$u(\ell,\lambda=-\frac{1}{2})=\sqrt{\ell_0+m_e}\left|\begin{array}{c}\chi-\\ -\frac{\ell}{\ell_0+m_e}\chi-\end{array}\right|=\sqrt{\ell_0+m_e}\left|\begin{array}{r}0\\1\\0\\-\frac{\ell}{\ell_0+m_e}\end{array}\right|. \quad (2.23)$$

U-spinors are related in the conventional scheme to the annihilation of the incoming fermions, while the creation of fermions will be described by the barred spinors $\bar{u}=u^{\dagger}\gamma_0$. For anti-fermions, the analogous operation are described by the $\bar{v}$ (annihilation) and v (creation) spinors. For the latter ones, one can repeat the previous analysis and obtain the expressions of the two states with four-momentum ℓ' and helicity $\lambda'=\pm\frac{1}{2}$, having chosen the three-momentum $\vec{\ell'}$ in the negative -Z direction and $|\vec{\ell'}|=|\vec{\ell}|$, $\ell'_0=\ell_0$:

$$v(\ell',\lambda'=+\frac{1}{2})=\sqrt{\ell_0+m_e}\left|\begin{array}{c}-\frac{\ell}{\ell_0+m_e}\chi+\\ \chi+\end{array}\right|=\sqrt{\ell_0+m_e}\left|\begin{array}{r}-\frac{\ell}{\ell_0+m_e}\\0\\1\\0\end{array}\right| \quad (2.24)$$

$$v(\ell',\lambda'=-\frac{1}{2})=-\sqrt{\ell_0+m_e}\left|\begin{array}{c}\frac{\ell}{\ell_0+m_e}\chi-\\ \chi-\end{array}\right|=\sqrt{\ell_0+m_e}\left|\begin{array}{r}0\\-\frac{\ell}{\ell_0+m_e}\\0\\-1\end{array}\right|. \quad (2.25)$$

The previous short summary has been mostly given for self-consistency reasons, since we shall need the various equations that have been written to derive several relevant features of electron-positron annihilation in the quickest and simplest way. A detailed illustration of the considered properties can be found in Ref. [31].

2.2 Chiral fermions and polarized cross sections in the one-photon exchange

The previously defined helicity is affected by a problem: it is not a fully Lorentz invariant quantity. Roughly, one defines then a new, Lorentz invariant quantity that coincides with helicity in the limit of very high energy when masses can be neglected. This quantity is called chirality and we will briefly summarize its main properties.

The chirality operators are

$$\frac{1}{2}(1+\gamma_5) \equiv \mathcal{P}_R \tag{2.26}$$

$$\frac{1}{2}(1-\gamma_5) \equiv \mathcal{P}_L \ . \tag{2.27}$$

One easily sees that they satisfy projector conditions, since ${\mathcal{P}_R}^2 = \mathcal{P}_R$, ${\mathcal{P}_L}^2 = \mathcal{P}_L$, $\mathcal{P}_R\mathcal{P}_L = \mathcal{P}_L\mathcal{P}_R = 0$.

One defines, then, the following chiral spinors:

$$u_R(\ell) = \sqrt{\ell_0}\begin{vmatrix}1\\0\\1\\0\end{vmatrix}, u_L(\ell) = \sqrt{\ell_0}\begin{vmatrix}0\\1\\0\\-1\end{vmatrix}, \tag{2.28}$$

$$v_R(\ell') = \sqrt{\ell'_0}\begin{vmatrix}0\\-1\\0\\-1\end{vmatrix}, v_L(\ell') = \sqrt{\ell'_0}\begin{vmatrix}-1\\0\\1\\0\end{vmatrix}, \tag{2.29}$$

with ($\ell'_0 = \ell_0, \vec{\ell} + \vec{\ell'} = 0, \vec{\ell}$ along Z). The previous spinors are eigenstates of the chirality projectors, since :

$$\mathcal{P}_R u_R(\ell) = u_R(\ell)\ ;\ \mathcal{P}_R u_L(\ell) = 0 \tag{2.30}$$

$$\mathcal{P}_L u_R(\ell) = 0\ ;\ \mathcal{P}_L u_L(\ell) = u_L(\ell) \tag{2.31}$$

$$\mathcal{P}_R v_R(\ell') = v_R(\ell')\ ;\ \mathcal{P}_R v_L(\ell') = 0 \tag{2.32}$$

$$\mathcal{P}_L v_R(\ell') = 0\ ;\ \mathcal{P}_L v_L(\ell') = u_L(\ell'). \tag{2.33}$$

In the common language, u_L, v_L are called "left-handed" spinors and u_R, v_R "right-handed" spinors. To better understand their physical meaning, we shall use the formal high energy identities

$$\lim_{\frac{\ell_0}{m_e}\to\infty} u(\ell, \pm\frac{1}{2}) = u_{R(L)}(\ell) \tag{2.34}$$

$$\lim_{\frac{\ell_0}{m_e}\to\infty} v(\ell', \pm\frac{1}{2}) = v_{L(R)}(\ell') \tag{2.35}$$

which are derived from Eqs. (2.22)–(2.25). Thus, in the high energy limit, the chiral spinors are essentially identical with the helicity spinors. One

can quantify the difference between the corresponding states by making a power expansion in the small $\frac{m}{\ell_0}$ parameter. This gives, formally :

$$u(\ell, +\frac{1}{2}) = u_R(\ell) + O(\frac{m}{\ell_0}) \tag{2.36}$$

and similarly for three remaining helicity eigenstates, with the various $O(\frac{m}{\ell_0})$ that can be easily computed. Given the value of the electron mass, for the electron energies of several GeV size that occur at LEP1 the difference between the helicity eigenstates and the corresponding chirality partners is indeed miserable and one can, in practice, neglect it. The same approximation will be normally used for the final fermion/anti-fermion states. A word of caution must at this point be spent concerning the adopted convention, to avoid a possible source of confusion. In our notation, $u_{R,L}$ describes electrons with spin components along the positive (R) or negative (L) Z axis and $v_{R,L}$ describes positrons which follow the identical spin convention. (In the original definition, Eqs. (2.24)–(2.25), the quantization was given along the negative Z axis.)

We are now ready to derive a first important property of e^+e^- annihilation in the Standard Model framework. With this aim, we need the expression of the all the barred spinors $\bar{u}_{L,R}, \bar{v}_{L,R}$. With our choice of γ_0 they read

$$\bar{u}_R \equiv u_R^+\gamma_0 = \sqrt{\ell_0}\,\big|\,1\ 0\ -1\ 0\,\big| \tag{2.37}$$

$$\bar{u}_L = \sqrt{\ell_0}\,\big|\,0\ 1\ 0\ 1\,\big| \tag{2.38}$$

$$\bar{v}_R = \sqrt{\ell_0}\,\big|\,0\ -1\ 0\ 1\,\big| \tag{2.39}$$

$$\bar{v}_L = \sqrt{\ell_0}\,\big|\,-1\ 0\ -1\ 0\,\big|\ . \tag{2.40}$$

Let us consider now the case of $e^+e^- \to \mu^+\mu^-$ via a photon exchange. From the conventional Feynman rules we have in the initial state four terms that correspond to the four possible initial (i) helicity configurations, i.e.,

$$e^-_{\Rightarrow}e^+_{\Leftarrow} \Rightarrow J^{\mu,i}_{RL} = \bar{v}_L\gamma^\mu u_R \tag{2.41}$$

$$e^-_{\Rightarrow}e^+_{\Rightarrow} \Rightarrow J^{\mu,i}_{RR} = \bar{v}_R\gamma^\mu u_R \tag{2.42}$$

$$e^-_{\Leftarrow}e^+_{\Leftarrow} \Rightarrow J^{\mu,i}_{LL} = \bar{v}_L\gamma^\mu u_L \tag{2.43}$$

$$e^-_{\Leftarrow}e^+_{\Rightarrow} \Rightarrow J^{\mu,i}_{LR} = \bar{v}_R\gamma^\mu u_L\ . \tag{2.44}$$

Using our chosen γ^μ representation (Eq. (2.18)) one easily obtains that

$$J^{\mu,i}_{RL} = J^{\mu,i}_{LR} = 0\ . \tag{2.45}$$

In other words, the initial currents vanishes in the case of total spin 0, leaving only the two configurations with total spin 1. For the latter ones one obtains infact :

$$J^{\mu,i}_{RR} \equiv \bar{v}_R \gamma^\mu u_R = (0, -2\ell_0, -2i\ell_0, 0) \tag{2.46}$$

$$J^{\mu,i}_{LL} \equiv \bar{v}_L \gamma^\mu u_L = (0, 2\ell_0, -2i\ell_0, 0)\ . \tag{2.47}$$

If one considers now the final state $\mu^+\mu^-$ one realizes that they also can only appear in the two configurations

$$J^{\mu,f}_{RR} \equiv \bar{u}_R \gamma^\mu v_R \tag{2.48}$$

$$J^{\mu,f}_{LL} \equiv \bar{u}_L \gamma^\mu v_L\ . \tag{2.49}$$

Actually, for final state fermions, whose centre-of-mass 3-momentum $\vec{p'}$ makes in general a certain non-zero angle θ with respect the electron 3-momentum $\vec{p}$, the previous statement can be simply derived from the general expression of the electromagnetic current

$$J^{\text{e.m.}}_\mu = \bar{\psi}(x)\gamma_\mu\psi(x) = \bar{\psi}(x)[\mathcal{P}_R + \mathcal{P}_L]\gamma_\mu[\mathcal{P}_L + \mathcal{P}_R]\psi(x) \tag{2.50}$$

where $\mathcal{P}_{R,L}$ are defined in Eq (2.26),(2.27). From the anti-commutation property $\gamma_5\gamma_\mu = -\gamma_\mu\gamma_5$ on then recovers the known result

$$J^{\text{e.m.}}_\mu = \bar{\psi}(x)_L\gamma_\mu\psi(x)_L + \bar{\psi}(x)_R\gamma_\mu\psi(x)_R \tag{2.51}$$

where $\psi_{R,L} = \mathcal{P}_{R,L}\psi$.

Moving to the u, v spinors leaves then the chirality initial and final eigenstates in the combinations of Eqs. (2.46),(2.47),(2.48),(2.49) for any value of the final muon angle θ. In general the expression of Eqs. (2.48),(2.49) will not be as simple as that of the initial electron current, that remain fixed by Eqs. (2.46),(2.47).

A useful situation to be considered at this point is that of forward scattering, $\theta = 0$. In this case the expression of the final currents can be computed using the same spinors representation that we have so patiently derived, and whose utility will soon become evident. It is then simple to see that

$$J^{\mu,f}_{RR} = (0, -2\ell_0, 2i\ell_0, 0) \tag{2.52}$$

$$J^{\mu,f}_{LL} = (0, 2\ell_0, 2i\ell_0, 0)\ . \tag{2.53}$$

From the conventional Feynman rules, the expression of the invariant scattering amplitude for a certain transition is given, at the lowest Born level by the formula

$$M_{fi} = (-ie)^2 \frac{J^{\mu,f} g_{\mu\nu} J^{\nu,i}}{s} \tag{2.54}$$

where $s = 4\ell_0^2$ is the squared centre-of-mass energy. We can therefore define, in full generality, four different scattering amplitudes, i.e.,

$$M_{LL}, M_{RR}, M_{LR}, M_{RL} \tag{2.55}$$

that correspond to the four combinations ${J^{\mu,i}}_{LL}{J_\mu}^f{}_{LL}$, ${J^{\mu,i}}_{RR}{J_\mu}^f{}_{RR}$, ${J^{\mu,i}}_{LL}{J_\mu}^f{}_{RR}$, ${J^{\mu,i}}_{RR}{J_\mu}^f{}_{LL}$.

The corresponding differential cross section, proportional to the square of the scattering amplitude and to known phase space factors, will be called

$$\frac{d\sigma_{LL}}{d\Omega}, \frac{d\sigma_{RR}}{d\Omega}, \frac{d\sigma_{LR}}{d\Omega}, \frac{d\sigma_{RL}}{d\Omega} \approx |M_{LL}|^2, ... \tag{2.56}$$

Collecting Eqs. (2.46),(2.47),(2.52),(2.53) and (2.54) one easily sees that, at $\theta = 0$

$$M_{LR}(\theta = 0) = M_{RL}(\theta = 0) = 0 \tag{2.57}$$

while

$$M_{LL}(\theta = 0) = M_{RR}(\theta = 0) = 2e^2 \, . \tag{2.58}$$

The correct proportionality factor between $\frac{d\sigma}{d\Omega}$ and $|M|^2$ can be derived in a straightforward way, following, e.g., Ref. [31]. For our purposes, we shall be limited to quote the relevant final formula

$$\frac{d\sigma}{d\Omega} = \frac{|M|^2}{16s(2\pi)^2} \, . \tag{2.59}$$

Combining Eq. (2.59) with Eq. (2.58) we obtain the desired information:

$$\frac{d\sigma_{LL}}{d\Omega}(\theta = 0) = \frac{d\sigma_{RR}}{d\Omega}(\theta = 0) = \frac{\alpha^2}{s} \;\; (\text{where}\, \alpha \equiv \frac{e^2}{4\pi}) \, . \tag{2.60}$$

It is now straightforward to derive correspondingly simple expressions for the backward configuration, $\theta = \pi$. Here one simply and intuitively exchanges the final indexes with respect to the forward situation and finds:

$$\frac{d\sigma_{LL}}{d\Omega}(\theta = \pi) = \frac{d\sigma_{RR}}{d\Omega}(\theta = \pi) = 0 \, , \tag{2.61}$$

$$\frac{d\sigma_{LR}}{d\Omega}(\theta = \pi) = \frac{d\sigma_{RL}}{d\Omega}(\theta = \pi) = \frac{\alpha^2}{s} \, . \tag{2.62}$$

The previous Eqs. (2.60),(2.62) give the expressions of the differential cross sections for an initial state with spin one and a final state with 3-momentum parallel and antiparallel. To derive the expressions for a general

angle θ, one can follow the procedure of projecting onto an axis situated at that angle. We shall not perform here the explicit derivation, but will give the final result, which appears to be a natural extension of the two cases $\theta = 0, \theta = \pi$, i.e.:

$$\frac{d\sigma_{LL}}{d\Omega}(\theta) = \frac{d\sigma_{RR}}{d\Omega}(\theta) = \frac{\alpha^2}{s}\left(\frac{1+\cos\theta}{2}\right)^2, \tag{2.63}$$

$$\frac{d\sigma_{LR}}{d\Omega}(\theta) = \frac{d\sigma_{RL}}{d\Omega}(\theta) = \frac{\alpha^2}{s}\left(\frac{1-\cos\theta}{2}\right)^2. \tag{2.64}$$

In all those cases where the polarization of the final state are not measured, one gives the expression for the averaged unpolarized differential cross section, i.e.:

$$\frac{d\sigma}{d\Omega} = \frac{1}{4}\left[\frac{d\sigma_{LL}}{d\Omega} + \frac{d\sigma_{RR}}{d\Omega} + \frac{d\sigma_{LR}}{d\Omega} + \frac{d\sigma_{RL}}{d\Omega}\right] = \frac{1}{4}\frac{\alpha^2}{s}\left(1+\cos^2\theta\right). \tag{2.65}$$

Integrating over θ and ϕ one then obtains the well known expression ($\gamma \equiv$ photon exchange)

$$\sigma_{\gamma}^{e^+e^-\to\mu^+\mu^-}(s) = \frac{4}{3}\pi\frac{\alpha^2}{s}. \tag{2.66}$$

Our brief summary of the main features of e^+e^- scattering in the one-photon-exchange description is now completed. In the same spirit of relaxed technicalities we shall now move, in next Section, to the extension of the previous formulae to the description of the scattering via a single Z boson exchange.

2.3 Interaction involving a Z boson

We consider now the process $e^+e^- \to \mu^+\mu^-$ via exchange of a Z boson, retaining the reasonable approximation of treating electrons and muons as massless. In fact, in all processes that we shall describe, the final states will be always of the type "light-fermion light-antifermion", and considered as essentially massless, with the possible unique exception of $b\bar{b}$ production, that will be separately treated in Chapter 4. One immediate problem that we have to face is that, strictly speaking, at this stage of the book the Z boson properties have not been yet well defined, which might introduce some confusion to the reader. To proceed in a reasonably consistent was,

we shall follow an heuristic approach where the Z boson is only defined, for the moment, as a massive particle of spin one, with different couplings to left-handed and right-handed fermions that are described by $\approx \gamma_\mu$ vector currents (similarly to the photon ones). Calling $g^i{}_\lambda$ the coupling constants to the i-th fermion of chirality $\lambda = L, R$ (that remains related to the helicity in our high energy configuration), the derivation of the matrix elements for the process is completely analogous to that presented for the photon exchange, since the possible allowed initial chiralities are obviously not changed, and for the final pair the pseudovector current allows the same chiral combination of the vector one. In fact, the main difference between the photon and the Z exchange is represented by the form of the respective propagators. Here, a clarifying discussion is requested. Rigorously, we are at this step illustrating the process of electron-positron at the lowest order. At this Born level, we should therefore simply replace the bare photon propagator with the bare Z propagator, inserting in particular a $\approx (s - m_Z^2)$ term in the denominator. As well known, this is not the final and meaningful replacement, and we shall discuss thoroughfully in the next Section the correct procedure. As a tolerable compromise, we shall therefore introduce here an *effective* denominator D_Z defined as

$$D_Z = (s - m_Z^2)^2 + m_Z^2 \Gamma_Z^2(s) \tag{2.67}$$

calling, for the moment, $\Gamma_Z(M^2)$ the Z *width*. We hope that the inaccurate treatment will be tolerated by the reader, since it will be completely explained, as we anticipated, in next Section, and since, for a qualitative understanding of the features that we want to derive now, it seems to us an acceptable and unavoidable "ansatz".

After these premises, the derivation of the chiral cross sections can now proceed reasonably clearly, following the steps illustrated in the previous Section. In particular one finds:

$$\frac{d\sigma_{LL}}{d\Omega}(\theta) = g_{Le}^2 g_{L\mu}^2 \frac{s}{D_Z(s)} \left(\frac{1+\cos\theta}{2}\right)^2 \frac{e^4}{s_W^4 c_W^4}, \tag{2.68}$$

$$\frac{d\sigma_{RR}}{d\Omega}(\theta) = g_{Re}^2 g_{R\mu}^2 \frac{s}{D_Z(s)} \left(\frac{1+\cos\theta}{2}\right)^2 \frac{e^4}{s_W^4 c_W^4}, \tag{2.69}$$

$$\frac{d\sigma_{LR}}{d\Omega}(\theta) = g_{Le}^2 g_{R\mu}^2 \frac{s}{D_Z(s)} \left(\frac{1-\cos\theta}{2}\right)^2 \frac{e^4}{s_W^4 c_W^4}, \tag{2.70}$$

$$\frac{d\sigma_{RL}}{d\Omega}(\theta) = g_{Re}^2 g_{L\mu}^2 \frac{s}{D_Z(s)} \left(\frac{1-\cos\theta}{2}\right)^2 \frac{e^4}{s_W^4 c_W^4}\ , \tag{2.71}$$

where $s_W \equiv \sin\theta_W$ and $c_W \equiv \cos\theta_W$ are the sinus and cosinus of the Weinberg angle, respectively, defined by Eq.(1.82). From the previous expressions one can derive by integration the cross sections for all the allowed configurations of initial and final polarizations. In particular, in the case of unpolarized initial and final states, one finds the average value

$$\begin{aligned}\frac{d\sigma}{d\Omega} &= \frac{1}{4}\left[\frac{d\sigma_{LL}}{d\Omega} + \frac{d\sigma_{RR}}{d\Omega} + \frac{d\sigma_{LR}}{d\Omega} + \frac{d\sigma_{RL}}{d\Omega}\right] \\ &= \frac{1}{16}\frac{s}{D_Z(s)}\frac{e^4}{s_W^4 c_W^4} \\ &\times \left\{\left[1+\cos^2\theta\right]\left[(g_{Le}^2+g_{Re}^2)(g_{L\mu}^2+g_{R\mu}^2)\right]\right. \\ &+ \left. 2\cos\theta\left[(g_{Le}^2-g_{Re}^2)(g_{L\mu}^2-g_{R\mu}^2)\right]\right\}\end{aligned} \tag{2.72}$$

and integrating over the angles gives

$$\sigma_Z^{e^+e^-\to\mu^+\mu^-}(s) = \frac{1}{4}\frac{s}{D_Z}\frac{4\pi}{3}\left[(g_{Le}^2+g_{Re}^2)(g_{L\mu}^2+g_{R\mu}^2)\right]. \tag{2.73}$$

Note that, differently from the (parity conserving) one-photon exchange, in the differential cross section a term proportional to $\cos\theta$ appears. This will have fundamental experimental consequences, in particular related to the measurement of the forward-backward asymmetry discussed in Chapter 8. At the Z resonance centre-of-mass energy, $s = M_Z^2$, one has

$$\sigma_Z^{e^+e^-\to\mu^+\mu^-}(s) = \frac{1}{4}\frac{4\pi}{3}\left[(g_{Le}^2+g_{Re}^2)(g_{L\mu}^2+g_{R\mu}^2)\right]\frac{1}{\Gamma_Z^2}\frac{e^4}{s_W^4 c_W^4}. \tag{2.74}$$

to be compared with the corresponding photon-mediated expression, Eq. (2.66)

$$\sigma_\gamma^{e^+e^-\to\mu^+\mu^-}(s) = \frac{4}{3}\pi\frac{\alpha^2}{M_Z^2}. \tag{2.75}$$

At this point of the book, we cannot yet quote numerical values for $\Gamma_Z, g_{(L,R)(e,\mu)}$. This will be done later in the book; we can anticipate, though, that at the Z resonance the Z mediated cross section (to be correctly computed, i.e. beyond the simple Born level) will be approximately 50 times larger than the photon-mediated one, for final muon states (and even larger for final hadronic ones). Note that we did not consider, in this Section, possible $Z\gamma$ interference cross sections. The reason will become transparent in next Section, where we shall define, and compute at Born level, those very important quantities that are called *Z partial widths*.

2.4 Computation of Z partial widths

For the purpose of testing the Standard Model with high precision, a specially relevant rôle is played by the various decay rates of the produced Z boson. We proceed now to calculate the rate of decay into a pair of muons, $Z \to \mu^+\mu^-$, following the same methods that were employed in the previous Subsections. The theoretical expression for the partial width will be assumed to be known and we limit ourselves to writing it, for a general fermion-antifermion pair, as

$$\Gamma_f = \frac{(2\pi)^4}{2\sqrt{s}} \int d\rho_f |M_f|^2 = \frac{1}{16s} \int d\Omega |M_f|^2 \,. \tag{2.76}$$

The matrix element is obtained from the Interaction Lagrangian defined in Chapter 1, i.e.,

$$\mathcal{L}_{If} = \frac{e}{\sin^2\theta_W \cos^2\theta_W} Z^\mu \left[g_L^f \bar{\psi}_L^f \gamma_\mu \psi_L^f + g_R^f \bar{\psi}_R^f \gamma_\mu \psi_R^f \right] \,. \tag{2.77}$$

The transition amplitude will be written as

$$M_f = \frac{e}{\sin^2\theta_W \cos^2\theta_W} \epsilon^\mu \left[g_L^f J_\mu{}^f{}_{LL} + g_R^f J_\mu{}^f{}_{RR} \right] \tag{2.78}$$

where $J_{\mu RR,LL}$ are defined similarly to Eqs. (2.42),(2.43), and ϵ^μ is the Z polarization vector. The latter is defined as to meet the properties $\epsilon^\mu p_\mu = 0$, $\epsilon^\mu \epsilon_\mu^* = 1$, where p_μ is the Z four-momentum.

The next steps that allow to derive the expression of the decay width are technical details that can be easily worked out from existing literature [8]. Briefly, one arrives at the following fundamental formula:

$$\Gamma_{Z\to\mu^+\mu^-} = \frac{1}{24\pi} \frac{e^2}{s_W^2 c_W^2} [g_{L\mu}^2 + g_{R\mu}^2] m_Z = \frac{\sqrt{2} G_F m_Z^3}{6\pi} [g_{L\mu}^2 + g_{R\mu}^2] \,. \tag{2.79}$$

This formula can be easily extended to any producible final lepton-antilepton or quark-antiquark pair, remembering that in the latter case a multiplication by the number of colours must be performed. Its numerical value is fixed by those of the electric charge, of the Z mass, of the left and right fermion couplings and of $\sin^2\theta_W$. Although we did not describe yet the complete determination of all these parameters, we anticipate for the reader's convenience the different results, still assuming that all the produced fermions are massless, and show them in Table 2.1.

Table 2.1 Partial decay widths of the Z boson for various fermion species at tree level. QCD corrections are not included. A value of $\sin^2\theta_W = 0.23$ has been used.

Fermion	$\Gamma_{Z\to f\bar{f}}$ (MeV)
ν	166
ℓ	83
u quark	288
d quark	367
Total= 3ν+3e+2u+3d	2424

The previous Table allows to understand, at least qualitatively, the statement given in the previous Section concerning the fact that the Z-mediated cross section is so much bigger than the photon-mediated one, at the Z resonance energy $s = m_Z^2$. A word of caution is still necessary since the Table contains the results at the tree level, in particular without enclosing the important one-loop QCD effects, that will increase the hadronic widths by approximately 4 percent, and the total width by about 70 MeV.

Starting from Eq. (2.79) one can now return to the expression of the unpolarized Z-mediated cross section and rewrite it in the more frequently used way:

$$\sigma_{Z\to\mu^+\mu^-}(s) = \frac{s}{M_Z^2}\frac{12\pi\Gamma_e\Gamma_\mu}{(s-M_Z^2)^2 + M_Z^2\Gamma_Z^2(s)} \ . \tag{2.80}$$

An important point must now be stressed before closing this Section. From our previous formulae we can conclude that, at the Z peak ($s = m_Z^2$), the Z-mediated cross section Eq. (2.74) dominates the photon-mediated one Eq. (2.66). In principle, the cross section might also contain a γ Z interference term, which does not appear in our formulae. Actually, in this preliminary qualitative discussion, we defined an *effective* Z denominator $D_Z(s)$ in Eq. (2.67). A rigori, we should have started from an *effective* Z propagator and from an *effective* tree level expression of the neutral current matrix element. The latter would have been written in the form:

$$M_{\lambda e\lambda\nu} = -J_e^\mu g_{\mu\nu}\left[\frac{e^2}{s} + \frac{e^2}{s_W^2 c_W^2}\frac{g_{\lambda e}g_{\lambda\mu}}{(s-M_Z^2) + im_Z\Gamma_Z(s)}\right] J_f^\nu \ . \tag{2.81}$$

At the Z peak, the second term is purely imaginary. Thus the cross section, proportional to the squared modulus of Eq. 2.81, only contains the squared photon and the the squared Z contributions, and the γ Z interference term vanishes. This fact is no longer true when one moves

away from the the Z peak, in which case the γ Z interference term must be retained in the expression of the complete cross section. Although one expects that, in the vicinity of the Z peak, the single Z term is by far the dominant one, the rigorous calculation will have to take into account the extra small *not single Z* terms. This point will be discussed in detail in the final Section of this Chapter. Before doing that, a description of those other extremely important quantities that are the angular and the polarization asymmetries of the process, based on the formalism developed in this Section and in the previous ones, will be given.

2.5 Angular and polarization asymmetries

The various formulae that we have derived in the previous Sections in case of Z exchange for the differential and total cross sections are characterized by a fundamental feature, the parity violation of the intrinsic interaction. Contrary to the case of the parity conserving photon exchange, one sees that the expression of the unpolarized differential cross section, Eq. (2.72), as already stressed, contains a term proportional to the cosine of the scattering angle θ. One notices that the coefficient of the cosine would vanish if the lepton left and right couplings were identical, as in the electromagnetic case. But the parity violation makes the two couplings different, therefore producing three essential consequences that we are now going to list.

The first consequence is the possibility of defining another not vanishing measurable quantity, called longitudinal polarization asymmetry, A_{LR}, and defined as :

$$A_{LR} = \frac{\sigma_{e_L^-} - \sigma_{e_R^-}}{\sigma_{e_L^-} + \sigma_{e_R^-}} \tag{2.82}$$

where $\sigma_{e_L^-}$, $\sigma_{e_R^-}$ are the total cross section for production of a final muon-antimuons pair from a left(right)handed electron, obtained with a sum over the possible positron polarizations. In other terms:

$$\sigma_{e_L^-} = \sigma_{LL} + \sigma_{LR} = \frac{s}{D_Z(s)} \frac{e^4}{s_W^4 c_W^4} \frac{4}{3} \pi g_{Le}^2 (g_{L\mu}^2 + g_{R\mu}^2) \tag{2.83}$$

$$\sigma_{e_R^-} = \sigma_{RR} + \sigma_{RL} = \frac{s}{D_Z(s)} \frac{e^4}{s_W^4 c_W^4} \frac{4}{3} \pi g_{Re}^2 (g_{L\mu}^2 + g_{R\mu}^2) \,. \tag{2.84}$$

Using the expressions of the chiral couplings, one is led to the final "canonical" expression:

$$A_{LR} = \frac{g_{Le}^2 - g_{Re}^2}{g_{Le}^2 + g_{Re}^2} \,. \tag{2.85}$$

The second consequence is the possibility of defining a not vanishing measurable quantity, called (unpolarized) forward-backward asymmetry A_{FB}. Technically, this is defined as :

$$A_{FB} = \frac{\int_{\theta=0}^{\theta=\pi/2} \frac{d\sigma}{d\cos\theta} - \int_{\theta=\pi/2}^{\theta=\pi} \frac{d\sigma}{d\cos\theta}}{\int_{\theta=0}^{\theta=\pi/2} \frac{d\sigma}{d\cos\theta} + \int_{\theta=\pi/2}^{\theta=\pi} \frac{d\sigma}{d\cos\theta}} \,. \tag{2.86}$$

To introduce the third consequence of the parity-violating nature of the Z boson, we must make a general premise. The reader might have the impression, at this point, that a certain lack of democracy exists at the Z pole between the initial state couplings and the final state ones, for which until now no experimental quantity has been proposed that provides their separate measurement. Actually, this impression is false. At the Z peak two quantities can be defined that do fill this democratic ambition. Denoting by f the final fermion of the produced pair, one can first consider a quantity originally called [32] polarized forward-backward asymmetry and defined as:

$$A_{FB}^{f,pol} = \frac{(\sigma_{e_L^- f_F} - \sigma_{e_R^- f_F}) - (\sigma_{e_L^- f_B} - \sigma_{e_R^- f_B})}{\sigma_{e_L^- f_F} + \sigma_{e_R^- f_F} + \sigma_{e_L^- f_B} + \sigma_{e_R^- f_B}} \tag{2.87}$$

where f_F and f_B indicate forward and backward outgoing fermions, respectively. (We are assuming for the moment a polarization degree of the beam = 1, and will come back on this point in Chapter 8.) At the Z peak one may easily verify that

$$A_{FB}^{f,pol} = \frac{3}{4} \frac{g_{Lf}^2 - g_{Rf}^2}{g_{Lf}^2 + g_{Rf}^2} \tag{2.88}$$

showing that Eq. (2.87) is only dependent on the final state couplings, as we anticipated. Denoting the analogue of Eq. (2.85) for a fermion f

$$\mathcal{A}_f = \frac{g_{Lf}^2 - g_{Rf}^2}{g_{Lf}^2 + g_{Rf}^2} \,, \tag{2.89}$$

one finds that

$$A_{FB}^{f,pol} = \frac{3}{4}\mathcal{A}_f \,. \tag{2.90}$$

A second possibility is to define

$$A_{pol}^{f} = \frac{(\sigma_{f_{F,R}} - \sigma_{f_{F,L}}) - (\sigma_{f_{B,L}} - \sigma_{f_{B,R}})}{\sigma_{f_{F,R}} + \sigma_{f_{F,L}} + \sigma_{f_{B,R}} + \sigma_{f_{B,L}}} = \frac{\sigma_{f_R} - \sigma_{f_L}}{\sigma_{tot}} \tag{2.91}$$

where R and L indicate here the chirality of the final state fermion. One can see that, at the Z pole,

$$A_{pol}^{f} = -\mathcal{A}_f \,. \tag{2.92}$$

A very important conclusion stems from the observation that ratio of Eq. (2.85) can be expressed, using Eq. (1.116), in terms of one single parameter, the square of the sinus of the Weinberg angle $\sin^2\theta_W$. Moving from this observation, it is tempting to verify whether this feature survives in the remaining asymmetries. Actually for a transition from electron-positron to a $f\bar{f}$ pair, one has:

$$A_{FB}^{f} = \frac{3}{4}\mathcal{A}_e\mathcal{A}_f \tag{2.93}$$

as one can see by integrating in the forward and backward hemispheres (Eq. 2.86) the $e^+e^- \to Z \to f\bar{f}$ differential cross section.

From the general expression of the fermion chiral couplings given in Chapter 1, one realizes that each $\mathcal{A}_f$ can be expressed in terms of the single parameter $\sin^2\theta_W$. Thus, in conclusion, it appears that all the considered asymmetries, that are not vanishing as a consequence of the parity violation intrinsic in the Z exchange, can be expressed in terms of the genuine weak parameter $\sin^2\theta_W$. Although we proved this statement at the simple tree level, we shall see in the forthcoming Chapter 3 that this feature will be generalized to the one-loop level, leading to the definition of the phenomenological parameter $\sin^2\theta_{W,eff}$ that will play a fundamental rôle in the complete analysis of the available data, to be compared with the corresponding predictions of the Standard Model. Before moving to that, next Section provides a compact review on how the γZ interference modifies the asymmetries when the centre-of-mass energy is not equal to $s = m_Z^2$.

2.6 Asymmetries in the vicinity of the Z pole

Experimentally the asymmetries defined in the previous Section are measured at centre-of-mass energies close to the Z resonance that, normally, do not correspond exactly to the Z pole. The formulae discussed in this Section are useful to derive corrections, originating from the $Z\gamma$ interference, to the experimental data and, more in general, to describe the energy dependence of the asymmetries in the vicinity of the Z pole.

The differential cross section for $f\bar{f}$ production with polarized beam can be computed with the matrix element given in Eq. (2.81). For a detailed calculation we refer, again, to [31]. To describe the experimental data presented in next Chapters the cross section is given for unpolarized initial positrons colliding with longitudinally polarized electrons with polarization P_e. The production of a fermion f with helicity λ ($2\lambda = \pm 1$) at an angle θ with respect to the direction of the incoming e^- can be written in the following way:

$$\begin{aligned}\frac{d\sigma}{d\cos\theta}(s,\cos\theta,\lambda;P_e) = \frac{\pi\alpha^2(s)}{4s}N_c^f \\ \times \{ \left[(1+\cos^2\theta)\ G_1(s) + 2\cos\theta\ G_2(s)\right] \\ - 2\lambda\left[(1+\cos^2\theta)\ G_4(s) + 2\cos\theta\ G_3(s)\right] \\ - P_e\left(\left[(1+\cos^2\theta)\ G_3(s) + 2\cos\theta\ G_4(s)\right]\right. \\ \left. - 2\lambda\left[(1+\cos^2\theta)\ G_2(s) + 2\cos\theta\ G_1(s)\right]\right)\}\end{aligned} \tag{2.94}$$

where the value of N_c^f is one for leptons and three for quarks, while

$$\begin{aligned}G_1(s) &= Q_e^2Q_f^2 + 2Q_eQ_fg_{Ve}g_{Vf}\chi_{\gamma Z}(s) + (g_{Ve}^2+g_{Ae}^2)(g_{Vf}^2+g_{Af}^2)\chi_{ZZ}(s)\\ G_2(s) &= 2Q_eQ_fg_{Ae}g_{Af}\chi_{\gamma Z}(s) + 4g_{Ve}g_{Ae}g_{Vf}g_{Af}\chi_{ZZ}(s)\\ G_3(s) &= 2Q_eQ_fg_{Ae}g_{Vf}\chi_{\gamma Z}(s) + 2g_{Ve}g_{Ae}(g_{Vf}^2+g_{Af}^2)\chi_{ZZ}(s)\\ G_4(s) &= 2Q_eQ_fg_{Ve}g_{Af}\chi_{\gamma Z}(s) + 2(g_{Ve}^2+g_{Ae}^2)g_{Vf}g_{Af}\chi_{ZZ}(s)\ .\end{aligned}$$

The couplings g_V and g_A are related to the chiral couplings by $g_V = g_L + g_R$ and $g_A = g_L - g_R$ and

$$\begin{aligned}\chi_{\gamma Z}(s) &= F_G(s)\frac{s(s-m_Z^2) + s^2\Gamma_Z/m_Z\Im(\Delta\alpha)}{(s-m_Z^2)^2 + s^2\Gamma_Z^2/m_Z^2}\\ \chi_{ZZ}(s) &= F_G^2(s)\frac{s^2}{(s-m_Z^2)^2 + s^2\Gamma_Z^2/m_Z^2}\\ F_G(s) &= \frac{\mathrm{G_F}m_Z^2}{2\sqrt{2}\pi\alpha(s)}\end{aligned}$$

where $\alpha(s)$ indicates the energy-dependent fine-structure constant incorporating higher-order photonic corrections discussed in next Chapter. For completeness the effect of the imaginary parts of these corrections on the $Z\gamma$ interference, related to the photon-self energy and indicated as $\Im(\Delta\alpha)$, are also included. The coefficient F_G at the Z pole is $F_G(m_Z^2) \simeq 1.407$. The total cross section is obtained by summing on the helicities of the outgoing fermion, giving

$$\sigma(s) = \frac{4\pi\alpha^2(s)}{3s} N_c^f \left(G_1(s) - P_e G_3(s)\right) . \tag{2.95}$$

In Eqs. (2.94) and (2.95) the electron polarization is defined $P_e = +1$ for 100% right-handed electron polarization and $P_e = -1$ for 100% left-handed electron polarization.

The asymmetries defined in this Chapter can be computed using the differential cross section given by Eq. (2.94) as:

$$\begin{aligned}
A_{pol}(s) &= -\frac{G_4(s)}{G_1(s)} \\
A_{pol}^{FB}(s) &= -\frac{3}{4}\frac{G_3(s)}{G_1(s)} \\
A_{FB}(s) &= \frac{3}{4}\frac{G_2(s)}{G_1(s)} \\
A_{LR}(s) &= \frac{G_3(s)}{G_1(s)} \\
A_{FB}^{pol}(s) &= \frac{3}{4}\frac{G_4(s)}{G_1(s)} .
\end{aligned}$$

The energy dependence of the ratios G_i/G_1 near the Z pole is given by:

$$\begin{aligned}
\frac{G_2(s)}{G_1(s)} &= \mathcal{A}_e\mathcal{A}_f + S_2^f \frac{1}{F_G(m_Z^2)}\left[\frac{(s-m_Z^2)}{s} + \frac{\Gamma_Z}{m_Z}\Im(\Delta\alpha)\right] \\
\frac{G_3(s)}{G_1(s)} &= \mathcal{A}_e + S_3^f \frac{1}{F_G(m_Z^2)}\left[\frac{(s-m_Z^2)}{s} + \frac{\Gamma_Z}{m_Z}\Im(\Delta\alpha)\right] \\
\frac{G_4(s)}{G_1(s)} &= \mathcal{A}_f + S_4^f \frac{1}{F_G(m_Z^2)}\left[\frac{(s-m_Z^2)}{s} + \frac{\Gamma_Z}{m_Z}\Im(\Delta\alpha)\right]
\end{aligned} \tag{2.96}$$

where the asymmetries $\mathcal{A}_f$ are defined by Eq. (2.89) and the coefficients S_i^f

are:

$$
\begin{aligned}
S_2^f &= \frac{2Q_eQ_f}{(g_{V\mathrm{e}}^2+g_{A\mathrm{e}}^2)(g_{Vf}^2+g_{Af}^2)}\,(g_{A\mathrm{e}}g_{Af}-g_{V\mathrm{e}}g_{Vf}\mathcal{A}_{\mathrm{e}}\mathcal{A}_f)\\
S_3^f &= \frac{2Q_eQ_f}{(g_{V\mathrm{e}}^2+g_{A\mathrm{e}}^2)(g_{Vf}^2+g_{Af}^2)}\,g_{V\mathrm{e}}(g_{Af}-g_{Vf}\mathcal{A}_f) \qquad (2.97)\\
S_4^f &= \frac{2Q_eQ_f}{(g_{V\mathrm{e}}^2+g_{A\mathrm{e}}^2)(g_{Vf}^2+g_{Af}^2)}\,g_{Vf}(g_{A\mathrm{e}}-g_{V\mathrm{e}}\mathcal{A}_{\mathrm{e}}).
\end{aligned}
$$

Table 2.2 shows the numerical values of these functions.

Table 2.2 Numerical values of the couplings and of their functions computed assuming $\sin^2\theta_W = 0.2316$.

f	g_{Vf}	g_{Af}	$\mathcal{A}_f$	S_2^f	S_3^f	S_4^f
e,μ,τ	-0.036	-0.5	0.143	7.92	0.56	0.56
u,c,t	+0.191	+0.5	0.667	4.62	1.75	0.24
d,s,b	-0.346	-0.5	0.935	1.78	1.22	0.04

The brief review of the relevant expressions of the experimental observables, at the tree level accuracy, is now completed. It will represent a sufficient basis for deriving the more meaningful one-loop expressions of Chapter 3.

Chapter 3

Z Physics at One Loop for Final Leptonic States

We now arrive to the heart of Z pole physics: *electroweak radiative corrections*. Their accurate calculation, resulting from a remarkable theoretical effort of the late 80s [33], was motivated by two equally fundamental reasons. The first one was the evident desire of testing the renormalizability of the Glashow-Salam-Weinberg model. This could be done by checking that the shift between the simple tree level predictions and the corresponding calculations at the next order of the perturbative expansion was consistent with the wealth of measured quantities. If this had turned out to be the case, the MSM would have acquired the same respectability as its "ancestor", QED theory, the measurements at the Z pole playing a crucial rôle in this respect, essentially analogous to that of the fundamental measurements of the muon's g–2 in the QED case.

The second, perhaps more fascinating reason, is a *genuine* feature of the MSM that does not have any correspondence in QED and is, actually, deeply related to the non Abelian component ($SU(2)$) of its postulated symmetry group. In fact, as it was pointed out long ago by Veltman and Maiani [34] , the higher order corrections to the tree level predictions of the MSM *can* be sensitive to the existence of *heavy* particles, i.e. of particles that could not be directly produced at the energy scale of the process under consideration. This fascinating possibility of "communicating" with undiscovered matter is completely lacking in QED, where heavy objects are *decoupled* from measured quantities as a consequence of a theorem due to Appelquist and Carazzone [35], deeply related to the vector nature of the electromagnetic current associated with the photon. The consequences of this sensitivity to heavy objects are, indeed, fundamental and twofold. Essentially, one must decide whether the theoretical wish is simply that of achieving a fully satisfactory, overall test of the MSM or, more ambitiously,

that of providing strong support for the existence of possible more complete, or more theoretically appealing, competitor models, to be generally defined as of *new physics* type.

For what concerns the first issue of testing the model, the sensitivity to heavy matter has indeed led to one spectacular result, i.e. to the prediction of a very large top mass that was later confirmed by its experimental discovery at Fermilab [36]. In the case of the still lacking Higgs boson, the theoretical sensitivity to a possibly large mass is unfortunately (and accidentally) less powerful, being *screened* as originally pointed out by Veltman [37].

Still, interesting theoretical predictions can be derived, given the fact that several quantities have been measured which are sensitive to the Higgs mass. In particular, a widespread feeling exists that the Higgs boson should not be too "far away", i.e. within the reach of dedicated experiments in the near future.

In the case of searches of signals of new physics origin, the discussion becomes unavoidably less immediate and would require a long specific Chapter, which will not appear in this book. Here we can, though, anticipate that the final picture that has been reached, after several years of discussions and debates, is one where no evidence for any sort of deviations from the MSM predictions can be claimed. A significant rôle in this context, as we shall see, was actually played by the study of a particular decay of the Z boson, that into a $b\bar{b}$ couple, where in the theoretical prediction a sizeable contribution proportional to the squared top mass was involved. Even in this case, therefore, electroweak radiative corrections turned out to be an essential ingredient for a rigorous understanding of the hidden physical reality to be investigated.

This Chapter will be devoted to a general discussion of higher order radiative effects, with particular emphasis on those previously mentioned. The discussion will be complete at the one loop level and will deal with all the Z peak observables and, for reasons that will be fully explained, with the W mass. Although we shall try to avoid by as much as (realistically) possible to enter into fine details, the discussion will unavoidably become at times rather technical. For this reason we shall now provide, purely for the reader's convenience, a brief preliminary description of the main topics that will be reviewed.

Definition of physical input parameters and removal of infinities

From the description of the standard $SU(2)_L \times U(1)_{Y_L}$ model given in Chapter 1, it is clear that the calculation of the physical process $e^+e^- \to f\bar{f}$ requires, at tree level, the knowledge of 3 input parameters, for instance:

(1) the coupling constant g of the $SU(2)_L$ group;
(2) the coupling constant g' of the $U(1)_{Y_L}$ group;
(3) the mass m_Z of the intermediate vector boson Z (the photon mass vanishes by construction).

Of course, as we have seen, other equivalent sets of parameters might be used. One can replace g and g' by the electric charge $|e| \equiv \sqrt{4\pi\alpha} = gg'/\sqrt{g^2+g'^2}$, and by $\sin\theta_W = |e|/g$; alternatively, one can exploit the fact that, in the MSM, the masses of the W and Z bosons are related by the equality $m_W = m_Z \cos\theta_W$. This leads to the possibility of choosing a rather *natural* set of input parameters, i.e. the quantities α, m_W and m_Z. We shall call *natural* a parameter for which it is relatively simple and immediate to provide an operative definition, via a clearly defined physical measurement. For the electric charge and for the boson masses, we assume that this is intuitively possible (we shall discuss this statement in more detail later on).

The embarrassing feature that arises as soon as the calculation of higher order effects in the process $e^+e^- \to f\bar{f}$ is performed is that, as one will easily realize, several contributions to the scattering amplitude that must be computed are infinite.

This difficulty is not unexpected for those who did numerical calculations in QED; in fact, one solution to this problem is essentially similar to that given in that framework. As a first step, one can give a suitable operative definition of a chosen *physical* parameter, leading to a unambiguous (numerical) experimental determination valid to all orders of the theoretical estimate. The most immediate example is that of the electric charge, for which one possible definition is related to the value of a measurable cross-section (electron-muon, for instance) at zero momentum transfer. This (necessarily finite) value must be reproduced by the corresponding theoretical calculation. The latter, when performed beyond the tree level, will be affected in general as we will see by certain infinities, produced by higher order terms of the scattering amplitude; it will also contain some of the input parameters *of the Lagrangian* (in the MSM case, α, m_W, m_Z), that are

in the conventional terminology called *bare* parameters. It is obvious that the particular combination of *bare* parameters and higher order infinities that appears in the theoretical expression of a *physical* quantity will necessarily be finite, and numerically fixed by the measured experimental value of the physical quantity itself. It is also unavoidable to conclude that *bare* parameters will contain *suitable* infinities, to cancel those coming from the higher order effects. In the sneaky solution that is provided by the available theoretical treatment of this problem, both in the *bare* parameters and in the higher order effects one separates an infinite part from a finite one. The infinite parts of the bare parameters and of the higher order effects cancel out, leaving a finite residual component fixed by the experimental value of the *physical* quantity that has been used as an "infinity-killer". The important point is that, quite generally, a certain *bare*parameter will *differ* from its corresponding *physical* one. This will be the case in the MSM *both* for the bare charge α *and* for the bare masses m_W, m_Z. The corresponding *physical* parameters will be defined in an operative way, discussed in this Chapter, fixed by 'simple' and intuitive prescriptions.

One should have clearly understood at this point that in the MSM one can use *three* physical measurements, those of the electric charge and of the W and Z mass, to "kill" *three* possible infinities coming from higher order terms by *reabsorbing* them, as one commonly states, in the three bare corresponding (α, m_W, m_Z) parameters. But this would not be the final solution if infinities could proliferate endlessly. It is exactly at this precise moment that the virtue of a renormalizable model shows up: in such type of models, one actually knows that the overall number of "infinity killing" operations requested to get finite theoretical predictions at all orders is finite. This will necessarily happen in the MSM. In this Chapter, though, we shall not try to provide complicated proofs of this "miracle". We shall rather show, with simple numerical examples, that, for what concerns physics on the Z peak, the theoretical predictions for all *experimentally measurable* quantities become finite, once the three aforementioned "killings" have been properly carried through.

In the previous discussion, several fine details have been omitted. In particular, it should be mentioned that our presentation of the removal of infinities is neither unique, nor necessarily the most rigorous. It is, though, in our opinion, simple and understandable; as a matter of fact, it follows rather closely the original approach of Sirlin [38], defined "simple" by its author. We shall devote Section 3.1 to our presentation of this essential preliminary task.

Choice of the most convenient set of input** physical **parameters

The approach described above, based on the use of the *physical* squared electric charge and of the W, Z masses as input parameters of the theoretical calculations, has one important practical difficulty. For high precision measurements, like those at the typical permil level performed on top of the Z resonance, it is essential to start from adequately precise input parameters. The squared electric charge certainly meets this request, as it is determined with a precision of $\sim 10^{-8}$. The Z mass, we will see, is nowadays measured with an accuracy of 2×10^{-5}. But the W mass is, even today, "only" known with a relative precision of 5×10^{-4}, not sufficiently good at this extreme level of Z peak experiments.

Luckily, a way out to this difficulty exists and is provided by the fundamental Eq. (1.24) that becomes in the MSM scheme, using Eq. (1.105) and Eq. (1.126):

$$\frac{G_F}{\sqrt{2}} = \frac{\pi\alpha}{2m_W^2(1 - m_W^2/m_Z^2)} \tag{3.1}$$

and allows, at tree level, to express m_W in terms of α, m_Z and of the Fermi coupling G_F. Since the latter is known experimentally from the muon decay with an accuracy of 9×10^{-6}, the unavoidable theoretical attitude is that of replacing m_W via Eq. (3.1) and to use, as a proper set of input parameters, that composed by α, m_Z and G_F. The obvious problem that will arise is related to the appearance of infinities in the modifications of Eq. (3.1) at higher order. This will be solved in the previously explained conventional way, since the operative definition of the *physical* G_F will be intuitive and immediate, and will lead as expected to the cancellation of the new infinities that will arise and will be reabsorbed by the bare parameter G_F.

Having fixed the optimal set of parameters, it would be technically possible to begin the operations that lead to theoretical predictions. The first step in this direction is that of moving from the simplest *tree level* to the next order of perturbation theory, the so called *one loop* order, that typically corresponds to the diagram replacement shown in Fig. 3.1.

As soon as the computational process is actually performed, one realizes that, for pure convenience, i.e. practical purposes, the input parameter represented by the *physical* charge, measured at zero momentum transfer and defined conventionally from here on as $\alpha(0)$, can be safely replaced by a conveniently defined *effective* charge $\alpha(q^2)$, computed at $q^2 = m_Z^2$, where m_Z will be the physical Z mass, different from the *bare* $m_{Z(0)}$, to be

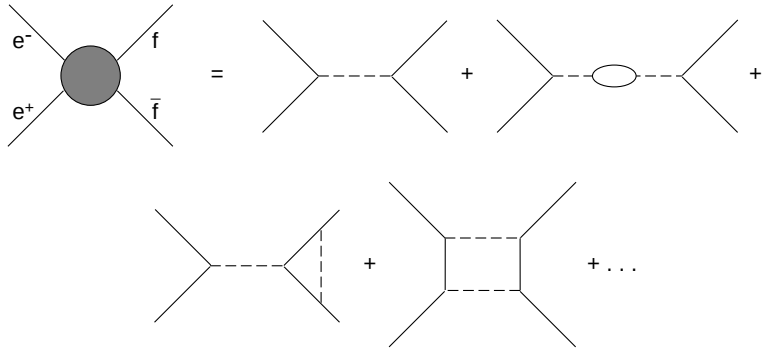

Fig. 3.1 Typical diagrams contributing to the process $e^+e^- \to f\bar{f}$ at one loop.

defined in the following Section. Thus the final set of input parameters will be, in fact, that composed by m_Z, G_F and $\alpha(m_Z^2)$. The actual definition and the precise calculation of $\alpha(m_Z^2)$ represent a very important theoretical exercise, and we shall devote a part of this Chapter to a detailed discussion of several of its most relevant features.

Calculation of the W mass

As a first example of full calculation at one loop, we shall derive the formula that gives the physical W mass in terms of the parameters $\alpha(m_Z^2), m_Z, G_F$ *and* of electroweak radiative corrections, whose appearance "shifts" the original tree level Eq. (3.1). As we shall see, the shift indeed goes in the "right" direction. We shall give a rather detailed discussion of this important formula, commonly known as Sirlin's equation, that we shall write in the form:

$$\frac{m_W^2}{m_Z^2}\left(1-\frac{m_W^2}{m_Z^2}\right) = \frac{\pi\alpha(m_Z^2)}{\sqrt{2}G_F(1-\Delta r^W)} \tag{3.2}$$

where Δr^W will be, in our conventions, the electroweak radiative correction. We shall provide in this Chapter an accurate estimate of some of its components, in particular those due to self-energy diagrams with fermion pairs (the second diagram on the r.h.s of Fig. 3.1). This will bring to light a few important features of Δr^W, related to the kinds of physical effects that can affect it in an observable way. As we shall show in the next parts of this Chapter, some of these effects will also influence the physical observables at the Z peak. More precisely, two of the three independent effects that

affect Δr^W will also be present, in different combinations, in *all* the Z peak observables. This will relate in a deep and fruitful way the measurements of the W mass and those performed at LEP1 and SLC.

Full treatment of Z peak observables at one loop and definition of the effective electroweak angle via the longitudinal polarization asymmetry

This fundamental part of Chapter 3 will be first devoted to a general discussion of how one can provide a simple and fully gauge invariant *effective* description of the process $e^+e^- \to f\bar{f}$ at one loop at general squared c.m. energy, in particular at the Z peak. From the discussion it will quite naturally follow the idea of defining an *effective* energy dependent electroweak parameter, the squared sine of the electroweak angle, to be called $\sin^2\theta_{W,eff}$ and to be estimated at m_Z^2 for what concerns predictions at the Z resonance. For this parameter, in contrast to $\alpha(m_Z^2)$ whose definition in the MSM is purely conventional, it will be possible to provide a simple and intuitive operative definition, that relates it to a measurable quantity called longitudinal polarization asymmetry A_{LR}. The rôle and the properties of A_{LR} will be thoroughly discussed in this Chapter, and a detailed derivation of the expression of the effective electroweak angle will be performed.

Definition of the effective Z lepton axial vector coupling: the Z leptonic width. Introduction of the gauge invariant parameters ϵ_1, ϵ_3 and ϵ_2

In this part of Chapter 3 we shall show that, in analogy with the effective electroweak angle $\sin^2\theta_{W,eff}$, one can give a convenient definition of the effective axial Z-lepton coupling on Z resonance $g_A(m_Z^2)$. This can be done, again, in a meaningful operative way by relating this parameter to the partial decay width of the Z into leptons, either charged or neutral. In this way, it will become natural to associate two of the outstanding theoretical features of the MSM, the chiral nature of the $Z - fermion$ interaction and the purely left-handed nature of its neutrinos, with two perfectly defined measurements, that of the longitudinal polarization asymmetry and that of the Z partial width into neutrinos.

As a byproduct of this description, we shall show that the full discussion of electroweak radiative corrections for Z physics at one loop and final leptonic states can be given in terms of two gauge-invariant param-

eters, originally called ϵ_1, ϵ_3 by Altarelli, Barbieri and Jadach [39]. The *same* two parameters, together with a third one (ϵ_2), will appear in the expression of the W mass.We shall derive this important result and conclude with a related discussion this long Chapter, that is only devoted to the process of production of final lepton-antilepton states. The reason for this choice is that, in such cases, only the purely electroweak component of the MSM Lagrangian is effective, for which a conventional one-loop perturbative treatment is apparently fully adequate. The generalization of the results obtained in Chapter 3 to the case of final hadronic states, where the rôle of strong interactions must be carefully taken into account, will be treated in Chapter 4.

3.1 Definition of *physical* input parameters and removal of infinities at one loop in e^+e^- annihilation on Z resonance

3.1.1 *The theoretical description at tree level*

For the specific case of electron-positron annihilation, the MSM description at the lowest order in a perturbative expansion is only based on those Feynman diagrams where either a Z or a photon (γ) appear in vertices with two fermions. To avoid unnecessary complications at the very beginning, let us consider an annihilation process whose final state is a fermion-antifermion couple *different* from electron-positron; in other words, we shall not consider the so called Bhabha scattering for the moment. For general values of the c.m. squared energy, defined as

$$(p_{e^+} + p_{e^-})^2 \equiv q^2 = (p_f + p_{\bar{f}})^2 \tag{3.3}$$

($p_{e^+}, p_{e^-}, p_f, p_{\bar{f}}$ = positron, electron, fermion, antifermion 4-momentum) the process is then described by the two Feynman diagrams where a Z and a γ are respectively exchanged in the s-channel.

In order to make meaningful theoretical predictions, one first writes the expression of the *invariant scattering amplitude* following a set of conventionally derived Feynman rules. If $f\bar{f}$ denotes the final fermion-antifermion pair and θ the scattering angle in the c.m. frame, the expression of the invariant scattering amplitude in the MSM can be written as

$$A_{ef}^{(0)}(q^2, \theta) = A_{ef}^{(0)(Z)}(q^2, \theta) + A_{ef}^{(0)(\gamma)}(q^2, \theta) \tag{3.4}$$

where the two terms correspond respectively to Z and γ exchange in the s-channel, as shown in Fig. 3.2 ($p_{e^-,e^+} = p_{1,2}; p_{f,\bar{f}} = p_{3,4}$), and the '0'

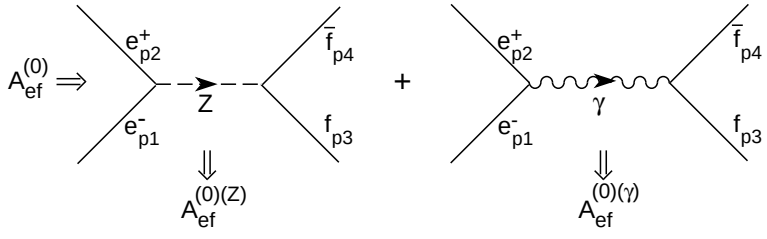

Fig. 3.2 Tree level Feynman diagrams description of the process $e^+e^- \to f\bar{f}$.

index on A_{ef} is a reminder of the fact that the theoretical prediction is performed at the lowest order in a perturbative expansion in the interaction Lagrangian responsible for the fermion-gauge boson coupling.

The theoretical expression for the invariant scattering amplitude (whose knowledge allows to compute differential and total cross-sections and scattering asymmetries, as summarised in Chapter 2), is given by standard Feynman rules and reads for the two components:

$$A_{ef}^{(0)(\gamma)}(q^2,\theta) = ij_f^{\mu(\gamma)}\left[\frac{-i}{q^2}\right] ij_{\mu e}^{(\gamma)} \tag{3.5}$$

$$A_{ef}^{(0)(Z)}(q^2,\theta) = ij_f^{\mu(Z)}\left[\frac{-i}{q^2-m_Z^2}\right] ij_{\mu e}^{(Z)} \tag{3.6}$$

where we have used the condensed notations:

$$j_{\mu e}^{(\gamma)} = |e_0|Q_e\bar{v}_e(\vec{p}_2)\gamma_\mu u_e(\vec{p}_1) \tag{3.7}$$

$$j_{\mu f}^{(\gamma)} = |e_0|Q_f\bar{u}_f(\vec{p}_3)\gamma_\mu v_f(\vec{p}_4) \tag{3.8}$$

$$j_{\mu e}^{Z} = \frac{|e_0|}{2\sin\theta_W\cos\theta_W}\bar{v}_e(\vec{p}_2)\gamma_\mu\left[g_{Ve}^{(0)} - \gamma_5 g_{Ae}^{(0)}\right] u_e(\vec{p}_1) \tag{3.9}$$

$$j_{\mu f}^{(Z)} = \frac{|e_0|}{2\sin\theta_W\cos\theta_W}\bar{u}_f(\vec{p}_3)\gamma_\mu\left[g_{Vf}^{(0)} - \gamma_5 g_{Af}^{(0)}\right] v_f(\vec{p}_4) \tag{3.10}$$

where $Q_{e,f}$ are the *electron* and *fermion* charges in unity of the *positron* one (so that $Q_e = -1$),

$$g_{Ve,f}^{(0)} = I_{3Le,f} - 2Q_{e,f}\sin^2\theta_W \tag{3.11}$$

$$g_{Ae,f}^{(0)} = I_{3Le,f} \tag{3.12}$$

and $1 - \cos^2\theta_W \equiv \sin^2\theta_W$ is defined in Eq. (1.82). The initial and final fermions Dirac spinors u_e, v_e, u_f, v_f have been previously defined in Chapter 2.

The quantities $g^{(0)}_{V,A}$ are given by the expressions

$$g^{(0)}_V = g^{(0)}_L + g^{(0)}_R \quad ; \quad g^{(0)}_A = g^{(0)}_L - g^{(0)}_R \tag{3.13}$$

where $g^{(0)}_{L,R}$ are defined by Eq. (1.116) and we have sticked to the definition of the Lagrangian Eq. (1.111).

A few words of comment are at this point appropriate. All the couplings that appear in Eqs. (3.7), (3.13) are by definition *bare* quantities, appearing in the definition of the Interaction Lagrangian. For this reason, they are labeled by a '0' index (the *same notation* should have been used in the derivation of the MSM Lagrangian in Chapter 1, but was avoided not to generate unnecessary complications.) Analogously, m_Z in Eq. (3.6) must also be considered as a *bare* (Lagrangian) parameter. Equations (3.5), (3.6) can be summarised by an (unorthodox) "thumb" Feynman rule, that associates in the construction of the invariant scattering amplitude of Fig. 3.2 geometrical entities to corresponding quantities as follows:

i) to the $e^+e^-, \bar{f}f$ vertices with γ or Z, the quantities $(ij^{(\gamma)(Z)}_{\mu e})$ (initial vertex) and $(ij^{(\gamma),(Z)}_{\nu f})$ (final vertex). Here μ, ν are Lorentz indexes.

ii) to the γ, Z line of four-momentum q the *bare propagators* $iP^{(\gamma,Z)}_{\nu\mu}(q)$:

$$-i\frac{g_{\nu\mu}}{q^2} \equiv iP^{(\gamma)}_{\nu\mu}(q) \; ; \quad -i\frac{g_{\nu\mu}}{q^2 - m_Z^2} \equiv iP^{(Z)}_{\nu\mu}(q) \; . \tag{3.14}$$

Note that, for the specific case of external massless fermions, one can systematically neglect from the beginning any hypothetical component $\sim q_\mu q_\nu$ of the bare propagators, since its contribution to the scattering amplitude would be (as a consequence of Dirac's equation) proportional to the fermion masses. In this particular case, one can identify therefore the bare propagator with its $\sim g_{\nu\mu}$ component. This simplification would not be valid in a process where (some of) the external fermion masses could not be neglected.

In general, the expression of $A^{(0)}_{ef}$ will contain four more indexes e.g. $\lambda_1, \lambda_2, \lambda_3, \lambda_4$ that indicate the possible initial and final fermion polarizations. We omit them for the moment since for unpolarized variables known rules exist for summing and/or averaging over these quantities in the expressions of the various cross-sections. Note that the latter ones will be obtained by computing the squared modulus of the scattering amplitude,

and as a consequence of this there will be in the cross-sections three independent Lorentz structures that could be indicated as (γ,γ), (Z,Z), (γ,Z) (or (Z,γ)) respectively and that correspond to the possible combinations of the $A_{ef}^{(0)(\gamma)}, A_{ef}^{(0)(Z)}$ components in the squared expression.

In a theoretical treatment truncated at the lowest *tree* level, the bare quantities have a precise meaning, since they can be directly related to measurable observables, as shown in detail in Chapter 2.

As soon as the theoretical description becomes more ambitious, and calculations are performed at next orders of perturbation theory, the original meaning of bare quantities is generally lost. This will have drastic and positive consequences, that we shall now begin to explore systematically in the case of the considered process of electron-positron annihilation. Here the rigorous MSM description will be given at the *next to the tree-level* order, the so called *one loop level*. In the following part of this Chapter we shall begin to investigate the theoretical ingredients that are introduced in order to carry on the required treatment.

3.1.2 *Renormalizability and gauge transformations in the MSM*

One of the main and substantial differences between the ancient Fermi description of weak interactions (Eq. (1.5)) and the MSM is that the latter one is a *renormalizable* quantum field theory. This fundamental property, whose derivation is due to a memorable 't Hooft's effort [5], has the consequence that theoretical computations can be in principle performed at any order of perturbation theory (leaving aside the practical difficulties e.g. due to the increasing number of Feynman diagrams), leading to *finite* (i.e. meaningful) predictions for *physical* (i.e. measurable) quantities.

The last sentence must be always and carefully taken into account. In fact, renormalizability will guarantee the finiteness of the theoretical predictions for *physical* observables. In the theoretical available perturbative framework the latter ones will be very often obtained as a sum of several components, each one (or some ones) turning out to be infinite. The cancellation of the various infinities in the physical quantity will be a recurrent feature in the MSM. In a sense, it will often turn out to be, rather than a complication, a useful check of the validity of the final (finite) prediction since every formally infinite component will leave a *finite* contribution to the overall physical observable.

From a more technical point of view, the MSM is in fact a non Abelian,

spontaneously broken gauge field theory. This has the consequence that, in the process of its quantization and in the proof of its renormalizability, a number of peculiar difficulties will arise, whose known existing solutions will enforce the presence of certain *unphysical* entities, due to the addition of corresponding *unphysical* terms to the Lagrangian Eq. (1.135), Chapter 1. Without entering the details of this known theoretical approach, we shall simply list these unphysical, but necessary, objects that are:

The 'ghosts'

They correspond to complex *scalar* field operators that obey Fermi statistic, and their appearance in any *unbroken* non Abelian gauge theory was first proposed by Faddeev and Popov (FP) [40] to cure unpleasant diseases, affecting the gauge bosons of the system, that might cause problems with unitarity. In the MSM the extra complication arises of the *spontaneous* breaking of the symmetry in the electroweak sector of the model. This will leave in the final formulation four FP ghosts, one for each gauge boson, to be conventionally called C^+, C^-, C_Z, C_γ.

As a consequence, Feynman diagrams will appear and will have to be computed with gauge boson-ghost-ghost couplings (the ghost do not interact with fermions). In the process of e^+e^- annihilation into a fermion pair, one will encounter e.g. the diagram of Fig. 3.3 where a (C^+, C^-) pair is produced by a virtual Z, in formal correspondence with the analogue W^+W^- pair. The important point to be kept in mind is that, although all contributions to observables like that of Fig. 3.3 must be accurately computed and taken into account, the ghosts do not correspond to any physical particle; they are rather introduced as a convenient purely mathematical trick to *retain* a physical request, that one does not want to abandon. One can

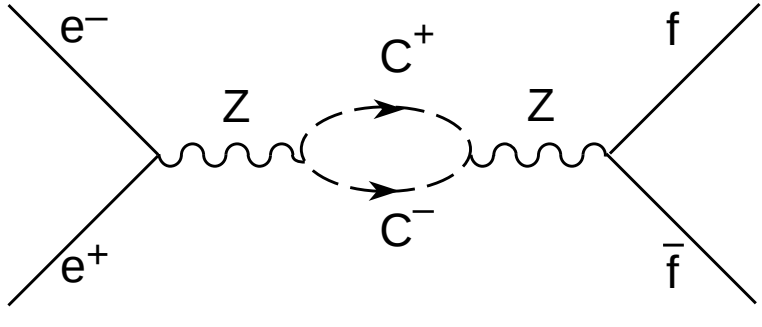

Fig. 3.3 Ghost loop in the process $e^+e^- \to f\bar{f}$.

easily imagine at this point that their numerical contribution to a physical quantity will have to be added to that of other *unphysical* entities that must be retained in the MSM for mathematical convenience, and that the *overall* unphysical contributions will cancel. This is precisely what happens, and we shall illustrate this fact with a simple and meaningful example in the following part of this Chapter, when discussing the properties of the photon propagator. More specifically, the extra unphysical entities to be retained are those already encountered in Chapter 1: the *would be* Goldstone bosons, to be discussed now in some detail.

The 'would be' Goldstone bosons

We already met in Chapter 1 the three scalar fields $\tilde{s_1}, \tilde{s_2}, \tilde{s_3}$ that would generate the unpleasant mixing term Eq. (1.61). In the same Chapter we have seen that these scalars can be *reabsorbed* by the corresponding gauge boson fields $A^1_\mu, A^2_\mu, A^3_\mu$ in the so called unitary gauge. But the price to pay, as discussed in Chapter 1, is that the renormalizability of the theory in this gauge is at first sight not achievable, owing to the form of the gauge boson propagator Eq. (1.29). Thus, the simultaneous elimination of both the unphysical scalars and of their mixing terms leads to a serious mathematical difficulty. This is not a problem at the tree level, but becomes such as soon as calculations at higher order, that involve unavoidably integrals of gauge boson propagators, begin to occur.

Loosely speaking, the solution proposed by 't Hooft appears as kind of a (clever) compromise, in which the *would-be* Goldstone bosons are allowed to remain, but their *mixing* is eliminated. At a qualitative level, it is not difficult to understand the logics of this procedure. In the mixing defined by Eq. (1.61), a sum of unwanted terms of the form $A^{(j)}_\mu \partial^\mu \tilde{s}_j$, $j = 1, 2, 3$ appears. In a completely rigorous way, since it is the Action, i.e. the integration of the Interaction Lagrangian over the full space-time, that has a physical meaning, and the field operators are assumed vanishing at the (infinite) contour of integration, one can make the replacement:

$$\begin{aligned} \int_{-\infty}^{+\infty} (A^{(j)}_\mu \partial^\mu \tilde{s}_j) dx &\equiv \int_{-\infty}^{+\infty} \left[\partial^\mu (A^{(j)}_\mu \tilde{s}_j) - \tilde{s}_j (\partial^\mu A^j_\mu) \right] dx \\ &= \int_{-\infty}^{+\infty} -\tilde{s}_j (\partial^\mu A^{(j)}_\mu) dx \end{aligned} \tag{3.15}$$

so that, *effectively*, one can write the Lagrangian part of Eq. (1.61) as the sum of terms $\sim \tilde{s}_j (\partial^\mu A^{(j)}_\mu)$. This is still, formally, of the previous mixing type. But in any local gauge theory it is possible to impose a condition

on the divergence of a gauge boson field. In fact, from the request of gauge invariance, one can always make a transformation of $A_\mu^{(j)}$, whose form for *infinitesimal* transformations is given in Eq. (1.203) for the $SU(2)_L$ case. This means that a (huge) *set* of different gauge fields exists that are absolutely equivalent for what concerns the physics of the system where they appear, and we can call generically "gauge" each particular choice of the fields. Starting for simplicity from Eq. (1.203), it is relatively easy to see that one can choose the 3 arbitrary components of $\vec{\epsilon}(x)$ so that the *divergences* of the transformed fields satisfy a suitable condition, and one can decide to restrict the (huge) set of different equivalent gauge fields to a *subset* where the chosen suitable condition on the divergences is satisfied. This suitable condition is then called a *gauge fixing* condition, since it clearly reduces the set of equivalent *gauges*.

In the case of the *effective* surviving mixing terms $\sim \tilde{s}_j(\partial^\mu A_\mu^{(j)})$ it will be therefore possible, if so wished, to "bargain" the component $\partial^\mu A_\mu^{(j)}$ with a suitable gauge fixing condition. Although this statement is certainly oversimplified, it is not surprising that, in order to avoid the replacement of a mixing term with a new term of the same nature, the immediate possibility is that of imposing the divergence of the gauge field $A_\mu^{(j)}$ to become proportional to the scalar $\tilde{s}_j$, so that the mixing terms $\sim \tilde{s}_j \partial^\mu A_\mu^{(j)}$ are replaced by $\sim \tilde{s}_j^2$ (which is a priori perfectly acceptable). This explains, in this qualitative way, the choice of the *gauge fixing* condition:

$$\partial^\mu A_\mu^{(j)} = -\xi_j g \frac{\langle s_0 \rangle}{\sqrt{2}} (\sqrt{2}\tilde{s}_j) = -\xi_j m_A (\sqrt{2}\tilde{s}_j)(j = 1, 2, 3) \tag{3.16}$$

where the $vev \langle s_0 \rangle_0$ is that generated by the spontaneous symmetry breaking mechanism *in the simplified version* Eq. (1.53) for the considered $SU(2)_L$ case, and the 3 real parameters ξ_j, all varying between zero and infinity, define an infinite subset of "gauges", each one specified by the values of the three parameters. The generalization to the MSM case with W_μ^+, W_μ^-, Z_μ is straightforward.

After imposing the gauge fixing conditions Eq. (3.16), we return to the original component of the Lagrangian that contains the mixing terms and write it in the equivalent way:

$$-g\langle s_0 \rangle_0 \sum_{j=1}^{3} [A_\mu^{(j)} \partial^\mu \tilde{s}_j] = g\langle s_0 \rangle_0 \sum_j \tilde{s}_j \partial^\mu A_\mu^{(j)} \tag{3.17}$$

(where the equality is an *effective* one, i.e. for what concerns the integrated Lagrangian).

Next, we perform a "trick" that is often played in gauge theories, adding to Eq. (3.17) a quantity that is identically vanishing in the previously defined class of gauges. This quantity is usually called *gauge fixing* (gf) Lagrangian, and its formal expression is:

$$\mathcal{L}_{gf} = \sum_j \left(\frac{-1}{2\xi_j}\right) \left(\partial^\mu A_\mu^{(j)} + \xi_j g \langle s_0 \rangle_0 \tilde{s}_j\right)^2 . \tag{3.18}$$

Adding Eq. (3.18) to Eq. (3.17) we obtain a quantity that is identical to Eq. (3.17), but whose formal expression reads:

$$\begin{aligned} & g\langle s_0\rangle_0 \sum_j \tilde{s}_j \partial^\mu A_\mu^{(j)} + \mathcal{L}_{gf} \\ \equiv & \sum_j \left[-\frac{1}{2\xi_j} (\partial^\mu A_\mu^{(j)})^2 - \frac{1}{2} (\xi_j m_A)^2 (\sqrt{2}\tilde{s}_j)^2 \right] . \end{aligned} \tag{3.19}$$

These two terms must now be added to the original corresponding quadratic terms (the first two on the r.h.s.) of Eq. (1.56). This produces the overall quadratic $(A_\mu, \tilde{s}_j)$ component:

$$\begin{aligned} \mathcal{L}_{\text{quad}}(A_\mu^{(j)}, \tilde{s}_j) = \sum_{j=1}^{3} \Bigg[& \frac{1}{2} m_A^2 A_\mu^{(j)} A^{\mu(j)} \\ - & \frac{1}{2\xi_j} (\partial^\mu A_\mu^{(j)})^2 + \frac{1}{2} (\partial_\mu \sqrt{2}\tilde{s}_j)(\partial^\mu \sqrt{2}\tilde{s}_j) \\ - & \frac{1}{2} (\xi_j m_A^2)(\sqrt{2}\tilde{s}_j)^2 \Bigg] . \end{aligned} \tag{3.20}$$

In the conventional field theory formalism, the first two terms describe three vector particles whose propagators are:

$$iP_{\mu\nu}^{(j)}(q) = \frac{-i}{q^2 - m_A^2} \left[g_{\mu\nu} + \frac{(\xi_j - 1) q_\mu q_\nu}{q^2 - \xi_j m_A^2} \right] . \tag{3.21}$$

These modified propagators vanish in the "infinite q" limit as $\sim 1/q^2$ like in the familiar case of the QED photon propagator, leading to a much softer kind of possible residual divergences after q-integration. Naively, one would hope that from this feature the desired renomalizability property should follow. Actually, this fact was proved by 't Hooft [5]. For this reason, the set of *gauges* where the gauge-fixing conditions Eq. (3.16) are satisfied are called *renormalizable ξ-gauges* or R_ξ gauges.

An important remark is appropriate now: the proof given by 't Hooft is valid for every choice of the gauge parameters ξ_j, even in the limit $\xi_j \to \infty$.

In this limit the gauge boson propagators Eq. (3.21) are re-transformed in those of the unitary gauge Eq. (1.63). The conclusion is that, contrary to naive expectations, even in the unitary gauge the MSM must be renormalizable. The only technical problem is that calculations in that gauge are formally more complicated, since "harder" infinities must be canceled.

The last two terms of Eq. (3.20) have also an immediate field-theory interpretation: they describe 3 real scalars, $\sqrt{2}\tilde{s}_j$, whose squared masses are $\xi_j m_A^2$, and whose propagators are consequently:

$$iP^{(j)}(q) = \frac{i}{q^2 - \xi_j m_A^2} \tag{3.22}$$

where m_A^2 is the squared mass of the associated gauge boson (when moving to the concrete SM case, there will be W^+, W^-, Z indexes for masses and scalar fields).

At this point, an apparently embarrassing picture appears: theoretical predictions seem to be based on properties of pseudo-particles, that can be eliminated in the special unitary gauge!

The answer to this problem is that it is only an apparent one. In fact, by definition, *physical* quantities must not depend on the choice of gauge: they must be *gauge-independent*. In terms of our parametrisation, this means that the final meaningful predictions will *not* have to depend on the ξ_j parameters. Since these quantities appear in the propagators of the $\tilde{s}_j$ and of their associated gauge bosons $A_\mu^{(j)}$, a number of delicate *cancellations* will have to occur between the possible contributions to *observable* quantities generated by Feynman diagrams where $\tilde{s}_j$ and $A_\mu^{(j)}$ are exchanged.

The same kind of philosophy must be adopted whenever contributions from the ghost fields also appear.

Without entering a detailed discussion, the main features of these entities is that they can only be coupled in trilinear vertices $\sim (ACC)$ to the gauge bosons, and always appear as a closed internal loop in our e^+e^- considered process, like in the *one-loop* diagram of Fig. 3.3. The propagator of the three ghosts associated to W^+, W^- and Z also depends on the choice of gauge, and reads:

$$iP_c^{(j)}(q) = \frac{-i}{q^2 - \xi_j m_A^2} \tag{3.23}$$

that also (as expected) disappears in the unitary gauge (note the opposite sign with respect to Eq. (3.22). Clearly, the overall contribution to any physical observable, including also (when necessary) the ghost term, must be ξ_j-independent.

Again, although this request might appear as an extra complication, one should consider it rather as a powerful test that must be passed by the final prediction for a physical quantity: the cancellation of the ξ_j-dependence.

In fact, after having checked the gauge-independence of the physical quantities, a choice of a certain gauge where the theoretical calculations should be performed must be made. Quite often, and almost systematically in this book, the choice $\xi_j = 1$ is performed, corresponding to the so called 't Hooft-Feynman gauge. The immediate reason is that, in this gauge, the expression of the gauge boson $P_{\mu\nu}$ propagator is of purely $\sim g_{\mu\nu}$ type, which makes calculations, usually, much simpler.

A final important point must still be stressed. Almost regularly, the various observable quantities to be computed will be obtained, in the chosen gauge, as a sum of several terms some (or all) of which will be formally infinite. Renormalizability ensures, though, that their *sum* in the observable quantity will be finite. In practice, a delicate mechanism of cancellation of infinities will be at work, and once again the finiteness of the final expression will be a (rather important) test of the accuracy of the theoretical prediction.

It remains now to be seen which mechanisms of cancellation of infinities will have to be used in the MSM. This will be shown in some detail in the next Subsections.

3.1.3 *Treatment of formally divergent quantities in e^+e^- annihilation: the divergences at one loop*

In this Subsection we shall illustrate the kind of infinities that are actually met in the calculations of the contributions to the invariant scattering amplitude of the process $e^+e^- \to f\bar{f}$ at the next perturbative order after the tree level, for what concerns the purely electroweak component of the interaction (in other words, strong interactions will be for the moment turned off). In the current language, this level is called the *one-loop* level. In terms of Feynman diagrams, it can be decomposed into three general and distinct categories, that are usually classified as:

'Self-energy' effects

These correspond to two classes of diagrams, represented in Figs. 3.4 and 3.5. The first class is a generalization of the corresponding QED one, with internal loops that include fermions, bosons, physical and unphysical scalars, ghosts.

The second class corresponds to another, typical, theoretical feature of

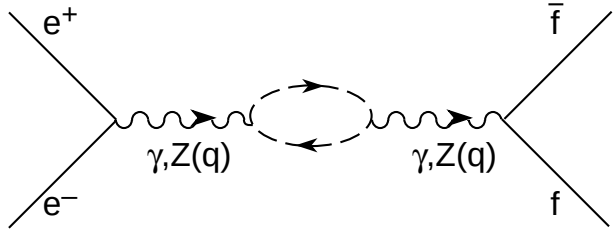

Fig. 3.4 *Self-energy* Feynman diagrams at one loop for $e^+e^- \to f\bar{f}$ (all combinations of γ and Z are allowed). The internal loop includes pairs of fermions, gauge bosons, physical and unphysical scalars, ghosts in all possible allowed combinations; $q = p_{e^+} + p_{e^-}$ is the total c.m. energy.

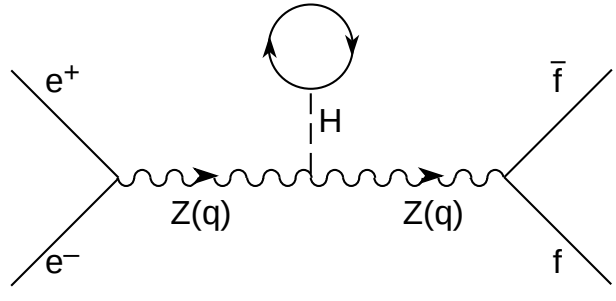

Fig. 3.5 *Tadpole* diagrams contributing the Z self-energy. The internal loop includes pairs of fermions, gauge bosons, physical and unphysical scalars in all possible allowed combinations. The overall c.m. energy is denoted as q.

the MSM that leads to the so called *tadpole* graphs, where a Higgs scalar is "produced" and "disappears" like in Fig. 3.5.

In our description of e^+e^- annihilation on Z resonance, we shall not insist particularly on the previous *tadpole* diagrams. As one can guess, they correspond to a theoretical trick rather than to a physical effect; actually, their presence is essential for the purposes of giving e.g. a gauge-invariant definition of the Z mass at one loop. We shall accept without proving it that this task can be satisfactorily fulfilled , and will not return on Fig. 3.5 for the rest of this book.

'Vertex' effects

These correspond to diagrams of the kind represented in Fig. 3.6, with all possible allowed virtual particles exchanges. Note that we include in this category also the various *external fermions self-energies* diagrams. Note, also, that we do not include the vertices with virtual photon exchange.

These belong to the specific QED sector, and must be treated separately. For our purposes of precision tests of the genuinely weak sector of the MSM, they can be considered as perfectly "known" quantities.

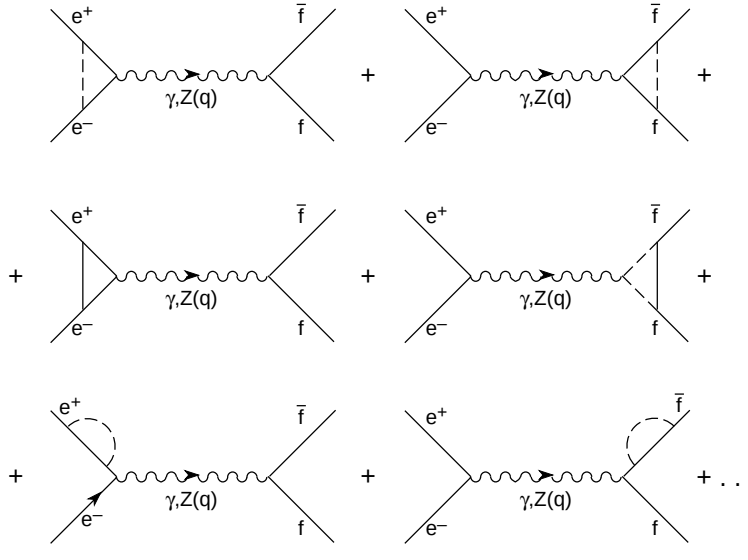

Fig. 3.6 Examples of *vertex* diagrams at one loop.

'Box' effects

These correspond to Fig. 3.7, with dots representing other possible diagrams with *weak* virtual bosons exchanges (but without photons for the reasons previously exposed).

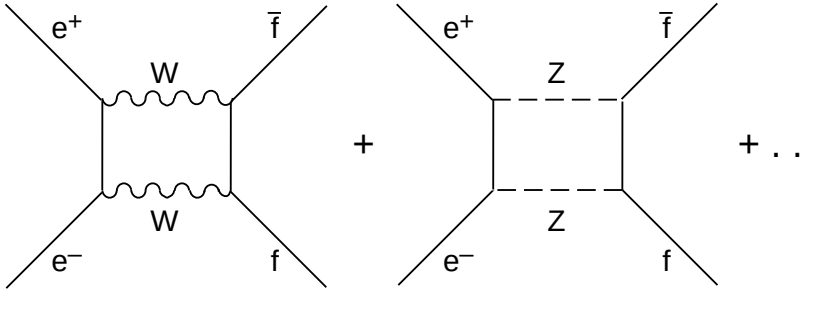

Fig. 3.7 Examples of *box* diagrams at one loop.

We now consider, as a first illustrative example, the calculation of one of the possible *self-energy* diagrams of Fig. 3.4, i.e. that with an initial and final virtual Z line and a pair of charged virtual leptons $L, \bar{L}$ in the loop, with mass m_L and four-momenta κ and $\bar{\kappa} = \kappa - q$. Working in the 't Hooft gauge and following conventional Feynman rules, moving from the right (final fermions) to the left (initial electron-positron), we can compute this contribution to the invariant scattering amplitude at one loop $A^{(1)}_{lf}(q^2, \theta)$. Denoting the four-vector indexes of the four vertices *from right* $(Zf\bar{f})$ to left (Ze^+e^-) by Lorentz symbols ν, ρ, σ, μ respectively, we can write this *contribution* as:

$$\begin{aligned} A^{(1)}_{ef}(q^2,\theta)(\text{Fig. 3.4}) &= i j^{(Z)}_{\nu f} \frac{(-ig^{\nu\rho})}{q^2 - m_Z^2} \\ &\times (i\Pi^{(Z)(L)}_{\rho\sigma}(q)) \frac{(-ig^{\sigma\mu})}{q^2 - m_Z^2} i j^{(Z)}_{\mu l} \qquad (3.24) \\ &= j^{\nu(Z)}_f \frac{1}{q^2 - m_Z^2} \left(i\Pi^{(Z)(L)}_{\nu\mu}(q) \right) \frac{1}{q^2 - m_z^2} j^{\mu(Z)}_l \end{aligned}$$

where the L-component, of the Z self-energy $i\Pi^{(Z)(L)}_{\nu\mu}(q)$ is pictorially depicted in Fig. 3.8 and, following the adopted Feynman rules, one has the familiar trace (Tr) of Dirac matrices:

$$\begin{aligned} & i\Pi^{(Z)(L)}_{\nu\mu}(q^2)(\text{Fig. 3.8}) \\ &= \int_{-\infty}^{+\infty} - \frac{d^4\kappa}{(2\pi)^4} Tr \left\{ \frac{i|e_0|}{2\sin\theta_W \cos\theta_W} \left[\gamma_\nu \left(-\frac{1}{2} + 2\sin^2\theta_W \right) + \frac{1}{2}\gamma_\nu\gamma_5 \right] \right. \\ &\times \frac{i(\hat{\kappa} + m_L)}{(\kappa^2 - m_L^2)} \frac{i|e_0|}{2\sin\theta_W \cos\theta_W} \left[\gamma_\mu \left(-\frac{1}{2} + 2\sin^2\theta_W \right) + \frac{1}{2}\gamma_\mu\gamma_5 \right] \\ &\left. \times \frac{i(\hat{\kappa} - \hat{q} + m_L)}{[(\kappa - q)^2 - m_L^2]} \right\} \; ; \quad (\hat{\kappa} \equiv \gamma^\rho \kappa_\rho) \; . \qquad (3.25) \end{aligned}$$

From inspection of Eq. (3.25) one can conclude immediately that the quantity to be computed is clearly infinite, since the integrand does not

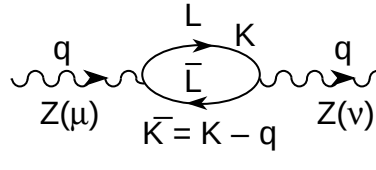

Fig. 3.8 Z self-energy diagram with a $L, \bar{L}$ fermion bubble and vector indexes ν (right), μ (left); $\kappa, \bar{\kappa}$ are the virtual $L, \bar{L}$ four-momenta.

vanish sufficiently quickly with κ when $\kappa \to \infty$. More precisely, one notices the presence of quadratic ($\sim \hat{\kappa}\hat{\kappa}/\kappa^4$), linear ($\sim \hat{\kappa}/\kappa^4$) and logarithmic ($\sim m_L/\kappa^4$) divergent integrand expressions, whose contributions to physical observables must be necessarily canceled, in a magic way that we shall illustrate.

In conclusion, one must expect for the general self-energy diagram at one loop the appearance of infinities. Let us examine now the situation for vertices, considering as a representative case that corresponding to the Feynman diagram of Fig. 3.9 where a couple of final charged *leptons* $L, \bar{L}$ is produced via a s-channel Z and a W is exchanged in the final vertex:

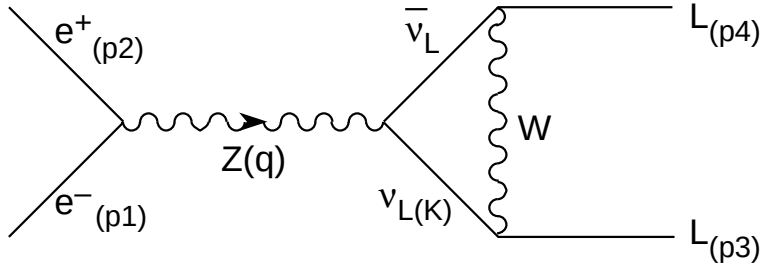

Fig. 3.9 *Vertex* diagram with two final charged leptons and virtual W exchange; κ is the virtual ν_L four-momentum.

In the $\xi_j = 1$ gauge, the contribution of the diagram of Fig. 3.9 to the invariant scattering amplitude at one loop can be written in a way formally similar to that of Eq. (3.6) i.e.:

$$A_{eL}^{(1)}(q^2,\theta)(\text{Fig. 3.9}) = \left[i\bar{u}_L(\vec{p}_3)\Gamma_{\nu,L}^{(Z)}v_L(\vec{p}_4)\right]\frac{(-ig^{\mu\nu})}{q^2 - m_Z^2}ij_{\mu e}^{(Z)} \tag{3.26}$$

where

$$\begin{aligned} i\Gamma_{\nu,L}^{(Z)}(\text{Fig. 3.9}) = &\int_{-\infty}^{+\infty}\frac{d^4\kappa}{(2\pi)^4}\frac{i|e_0|}{2\sqrt{2}\sin\theta_W}\gamma_\rho(1-\gamma_5) \\ &\times\frac{(-i\hat{\kappa})}{\kappa^2}\frac{i|e_0|}{2\sin\theta_W\cos\theta_W}\gamma_\nu\left(\frac{1}{2}-\frac{1}{2}\gamma_5\right) \\ &\times\frac{(-i)(\hat{\kappa}-\hat{q})}{(\kappa-q)^2}\frac{i|e_0|}{2\sqrt{2}\sin\theta_W}\gamma_\sigma(1-\gamma_5)\frac{(-i)g^{\rho\sigma}}{|(\kappa+p_3)^2 - m_W^2]}\,. \end{aligned} \tag{3.27}$$

One sees, again, that the quantity Eq. (3.28) is formally infinite, owing to the presence of terms $\sim \hat{\kappa}\hat{\kappa}/\kappa^6$ that induce a logarithmic divergence. Even in the general case of vertices, new cancellations will have therefore

to be produced in some clever way by the renormalizability of the model, for what concerns the contributions to observable quantities.

Finally, we move to the case of *box* effects and consider as a typical genuine weak contribution that corresponding to double W exchange with production of two final charged (and different from electron-positron) leptons $L, \bar{L}$ represented by the Feynman diagram of Fig. 3.10.

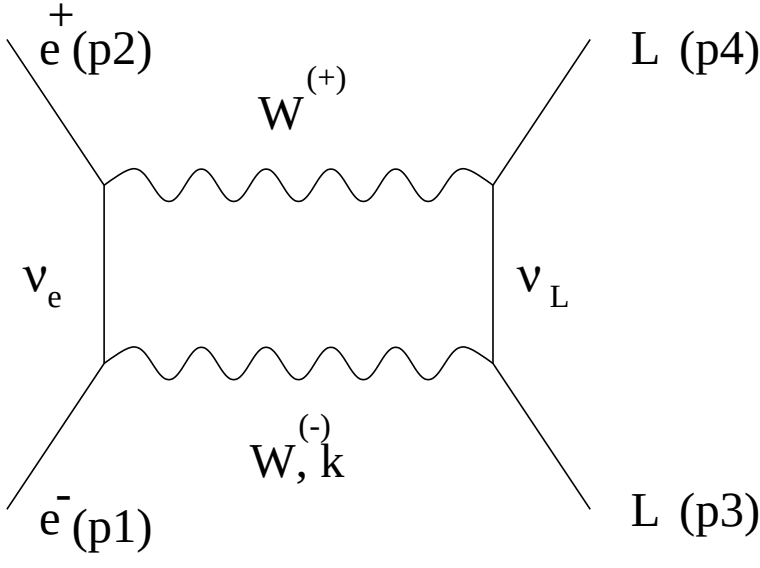

Fig. 3.10 Double virtual W *box* diagram with two final charged leptons $L, \bar{L}$; κ is the $W^{(-)}$ 4-momentum.

The contribution to the invariant scattering amplitude from this quantity can be written in a straightforward way, and corresponds to the following single integration (after taking into account all the four-momenta conservations at the various vertices):

$$
\begin{aligned}
A_{ef}^{(1)}(q^2,\theta)(\text{Fig. 3.10}) = i\bar{u}_L(\vec{p}_3) & \\
\times \int_{-\infty}^{+\infty} \frac{d^4\kappa}{(2\pi)^4} & \frac{i|e_0|}{2\sqrt{2}\sin\theta_W}\gamma_\mu(1-\gamma_5)\frac{(-i)(\hat{p}_3-\hat{\kappa})}{(p_3-\kappa)^2} \\
\times \frac{i|e_0|}{2\sqrt{2}\sin\theta_W} & \gamma_\rho(1-\gamma_5)v_L(\vec{p}_4)\frac{(-i)g^{\rho\sigma}}{[(\kappa-q)^2-m_W^2} \\
\times \bar{v}_e(\vec{p}_2) & \frac{i|e_0|}{2\sqrt{2}\sin\theta_W}\gamma_\sigma(1-\gamma_5)\frac{(-i)(\hat{p}_1-\hat{\kappa})}{(\kappa-p_1)^2}
\end{aligned}
$$

$$\times \frac{i|e_0|}{2\sqrt{2}\sin\theta_W}\gamma_\nu(1-\gamma_5)\frac{(-i)g^{\mu\nu}}{(\kappa^2-M_w^2)}u_e(\vec{p}_1)\ . \tag{3.28}$$

As one sees, the contribution from Eq. (3.28) is, this time, finite since the integrand behaves at worst as $\sim \hat{\kappa}\hat{\kappa}/\kappa^8$ at infinity, which does not give rise to divergent terms. This welcome simplification is valid in a general R_ξ gauge, with the exception of the unitary ($\xi_j \to \infty$) one. Here the two W propagators acquire each one an extra $\sim \kappa\kappa$ factor in the numerator, and the resulting contributions diverge, requiring a number of suitable extra cancellations that would not be necessary in a "finite ξ" gauge.

Until now, we have been vaguely talking of "canceling infinities". But this delicate procedure must be performed in a totally unambiguous way since, after the cancellation has been performed, a finite part will remain that will correspond to the prediction for a certain observable. Clearly, a convenient and clever algorithm should be adopted, to carry on this important program. This will be illustrated in the following Subsection.

3.1.4 *The dimensional regularization method*

In any renormalizable quantum field theory based on perturbative expansions, the problem generally arises of the unambiguous determination of the "meaningful" finite component of a combination of several terms, that are all formally infinite. Any computational scheme that succeeds in this goal is called *regularization* scheme.

For the special case of e^+e^- annihilation that we shall consider, a particularly convenient approach is provided by the so called *dimensional regularization* scheme, usually called the 't Hooft-Veltman scheme [41]. As we shall explicitly show, this method will lead to a determination of the relevant finite quantities that will be, thanks to a number of extra physical requests, completely unambiguous in the considered case of the MSM predictions for e^+e^- annihilation at the Z resonance at one loop, for *physical* quantities. We shall provide a few relevant examples of this statement, without entering a general discussion of the method and of its applications to other physical processes.

The main (and clever) idea of the dimensional regularization approach is that in general the quantities that one must compute and that diverge, to be specific those of Eqs. (3.25) and (3.28), are infinite because the integration in the virtual momentum κ is performed in a four-dimensional space, and

notoriously

$$\int_{-\infty}^{+\infty} d^4\kappa \left(\frac{1}{\kappa^2}, \frac{1}{\kappa^3}, \frac{1}{\kappa^4}\right) = \infty \ .$$

If *the same* integrations were performed on a space of "suitably" smaller dimension $n < 4$, they would lead to finite results for the previous terms since e.g. it would be possible to choose n so that:

$$\int_{-\infty}^{+\infty} d^n\kappa \left(\frac{1}{\kappa^2}, \frac{1}{\kappa^3}, \frac{1}{\kappa^4}\right) < \infty \ .$$

This leads to the idea of transforming the dimension n into a complex continuous variable and of defining the relevant integrals $\int d^n\kappa \left(\frac{1}{\kappa^2}, \cdots\right)$ as *analytic* functions of n. Once these functions have been determined, the final move is to define, for any given integrand in n dimensions $I(\kappa, n)$:

$$\int d^4\kappa I(\kappa; 4) = \lim_{n\to 4} \mu^\epsilon \int d^n\kappa I(\kappa; n) \tag{3.29}$$

where

$$n \equiv 4 - \epsilon \tag{3.30}$$

and the arbitrary scale parameter μ (with mass dimension), requested for purely dimensional reasons, is expected to disappear from the expressions of *physical observables*. In Eq. (3.29) $I(\kappa; n)$ represents the expression of the original integrand when '4' is replaced by 'n' in some expressions (e.g. $(2\pi)^4 \to (2\pi)^n$), with prescriptions that are fixed by the method.

In practice, for our purposes a limited number of divergent integrals will have to be treated, and we give here the list of those final expressions that we shall need, computed in the $\lim_{\epsilon\to 0^+}$, i.e. moving from values $n < 4$, in order of *decreasing* formal degree of divergence (with $\epsilon = 4 - n$):

$$\lim_{\epsilon\to 0^+} \frac{\mu^\epsilon}{(2\pi)^n} \int_{-\infty}^{+\infty} \frac{d^n\kappa \kappa_\mu \kappa_\nu}{[\kappa^2 - m_1^2][(\kappa + p)^2 - m_2^2]} \tag{3.31}$$

$$= \frac{i}{16\pi^2} \left[p_\mu p_\nu B_{21}(p^2, m_1^2, m_2^2) - g_{\mu\nu} B_{22}(p^2, m_1^2, m_2^2)\right] \ ,$$

$$\lim_{\epsilon\to 0^+} \frac{\mu^\epsilon}{(2\pi)^n} \int_{-\infty}^{+\infty} \frac{d^n\kappa \kappa_\mu}{[\kappa^2 - m_1^2][(\kappa + p)^2 - m_2^2]} \tag{3.32}$$

$$= \frac{i}{16\pi^2} p_\mu B_1(p^2, m_1^2, m_2^2) \ ,$$

$$\lim_{\epsilon\to 0^+}\frac{\mu^\epsilon}{(2\pi)^n}\int_{-\infty}^{+\infty}\frac{d^n\kappa}{[\kappa^2-m_1^2][(\kappa+p)^2-m_2^2]} = \frac{i}{16\pi^2}B_0(p^2,m_1^2,m_2^2)\ , \tag{3.33}$$

$$\lim_{\epsilon\to 0^+}\frac{\mu^\epsilon}{(2\pi)^n}\int_{-\infty}^{+\infty}\frac{d^n\kappa\kappa_\mu\kappa_\nu}{[\kappa^2-m_1^2][(\kappa+p)^2-m_2^2][(\kappa+p+p')^2-m_3^2]} = \frac{i}{16\pi^2}\left[g_{\mu\nu}C_{24}(p^2,p'^2,m_1^2,m_2^2,m_3^2)-p_\mu p_\nu C_{21}-\right.$$
$$\left. p'_\mu p'_\nu C_{22}-(p_\mu p'_\nu+p_\nu p'_\mu)C_{23}\right]\ . \tag{3.34}$$

Here p, p' denote arbitrary four-momenta of *external* particles of the considered reaction; m_1, m_2, m_3 are masses of virtual exchanged particles.

The functions $B_{21}, B_{22}, B_1, B_0, C_{24}$ are infinite. In the dimensional regularization approach they can be expressed [42] as the sum of an infinite part (to be canceled) and of a surviving finite term (that will contribute the expressions of the relevant observables).

Taking the simplest example of the function B_0 as an useful representative illustration, one finds in this case:

$$B_0(p^2,m_1^2,m_2^2)=\Delta-\int_0^1 dx\ln\left[\frac{D(x,p^2,m_1^2,m_2^2)}{\mu^2}\right] \tag{3.35}$$

where

$$\Delta=\lim_{\epsilon\to 0^+}\left(\frac{2}{\epsilon}\right)+(\ln 4\pi-\gamma)=\infty \tag{3.36}$$

$$D(x,p^2,m_1^2,m_2^2)=m_1^2(1-x)+m_2^2x-p^2x(1-x)\ . \tag{3.37}$$

In Eq. (3.35) μ is an arbitrary scale parameter and γ is the so called Euler-Mascheroni constant:

$$\gamma=0.5772\cdots \tag{3.38}$$

A number of comments on Eq. (3.35) are now appropriate:

i) The infinite part, Δ, is independent of four momenta and masses. The inclusion in Δ of the finite constant $(\ln 4\pi-\gamma)$ is a conventional prescription. We shall not comment its possible interpretation since, in all the cases that we shall illustrate, it will disappear from physical quantities together with the genuinely infinite term $2/\epsilon$.

ii) The arbitrary scale parameter μ that appears in the finite term will also disappear in the physical observables, through the same mechanism that will cancel the divergent term Δ. This is easily understandable since (forgetting for the moment dimensional considerations) the term $\sim \ln \mu^2$ in the finite part could be considered as an extra addition to Δ, that disappears when Δ disappears.

For what concerns the remaining infinite functions, the expression of the various B_s is relatively simple. For B_1 one finds the following result:

$$\begin{aligned} B_1(p^2, m_1^2, m_2^2) = & -\frac{1}{2} B_0(p^2, m_1^2, m_2^2) \\ & + \frac{1}{2p^2} \left[m_1^2 \left(1 - \ln \frac{m_1^2}{\mu^2} \right) - m_2^2 \left(1 - \ln \frac{m_2^2}{\mu^2} \right) \right. \\ & \left. + (m_1^2 - m_2^2) \int_0^1 dx \ln \left[\frac{D(x, p^2, m_1^2, m_2^2)}{\mu^2} \right] \right] \\ \equiv & -\frac{1}{2} \Delta + B_1^{(\text{finite})} \end{aligned} \tag{3.39}$$

in which the divergent part is given by the first term $= -(1/2)B_0$ on the r.h.s. The remaining term is finite (and regular in the limit $p^2 \to 0$, as it must be from the definition Eq. (3.32)).

Similar, slightly more complicated expressions can be derived for the remaining functions B_{21}, B_{22} (and C_{24}). Without exhibiting the complete formula for the moment, we only list the various divergent components. In a self-explaining notation, we shall have:

$$B_{21}(p^2, m_1^2, m_2^2) = \frac{1}{3} \Delta + B_{21}^{(\text{finite})}(p^2, m_1^2, m_2^2) \tag{3.40}$$

$$B_{22}(p^2, m_1^2, m_2^2) = \frac{1}{12} (p^2 - 3m_1^2 - 3m_2^2) \Delta + B_{22}^{(\text{finite})}(p^2, m_1^2, m_2^2) \tag{3.41}$$

$$C_{24}(p^2, p'^2, m_1^2, m_2^2, m_3^2) = \frac{1}{4} \Delta + C_{24}^{(\text{finite})}(p^2, p'^2, m_1^2, m_2^2, m_3^2) \, . \tag{3.42}$$

Equations (3.35)–(3.42) show us the nature of infinities (and related cancellations) that will be met in the dimensional regularization method, as a consequence of the bad asymptotic behaviour in the integration variable of the integrands that appear in the loop effects (*ultraviolet* divergences). The remarkable simplicity of the resulting divergent expressions leads already to the feeling that the process of their cancellations will turn out to be straightforward. This statement needs, though, some extra additional

discussion, since the aforementioned cancellation would not be performable without the additional contributions of new infinite quantities. These will appear at one loop as the consequence of the presence in the Lagrangian of *bare* parameters, whose original meaning is lost when one abandons the lowest order of perturbation theory and moves to the next one-loop level. This fact will have the tricky consequences that will be fully discussed in the forthcoming Subsection 3.1.5.

3.1.5 *Definition of physical parameters: renormalization of* m_W, m_Z

In any renormalizable quantum field theory all theoretical predictions for observable quantities are finite, at any order of perturbation theory. This is usually achieved by mutual cancellations of infinite quantities of the kind explicitly shown in the previous Subsection 3.1.3. In general, though, the process of cancellation is only successful if other infinities of a rather different kind are introduced in the game. This is the result of a process in which all (or some) or the original parameters of the Lagrangian (*bare* in the conventional definition) are replaced by new ones, the *renormalized* ones, plus an infinite term whose task is that of contributing the cancellation of infinities. In symbols, if we denote by P_0 a *bare* parameter of the Lagrangian, for the moment completely unspecified, the usual procedure is that of writing

$$P_0 = P_R + \delta P_R \tag{3.43}$$

where P_R is *finite* and δP_R generally infinite. Equation (3.43) defines the process of *renormalization* of the parameter P_0, that could be e.g. a mass, or a charge, in the original Lagrangian.

It must be stressed that the choice of P_R (and, consequently, of δP_R) is not unique. In fact, each choice defines a certain *renormalization scheme*. The criteria that motivate a particular choice are normally based on convenience, or common sense. Once the scheme has been chosen, the infinite quantity δP_R is uniquely fixed. The fundamental property of a renormalizable model is that a *finite* number of *renormalizations* of different bare parameters is sufficient to guarantee finiteness for the relevant theoretical calculations to each order of perturbation theory.

In what follows, we shall motivate in a qualitative way the choice of renormalization scheme that we shall adopt. With this purpose, a good starting point could be the observation that, when one abandons the lowest

order (*tree level*) description and moves e.g. to one loop, the original and characteristic property of a general bare parameter is usually lost. To be more definite, let us consider a bare mass parameter of the Lagrangian, for instance the Z mass m_Z defined by Eq. (1.79), which appears in the Lagrangian Eq. (1.69). In full generality, m_Z^2 can be defined as *the pole* in the q^2 variable of the lowest order Z propagator Eq. (3.14) in the $\xi_j = 1$ gauge. Alternatively, one can say that m_Z^2 is *the* value of q^2 corresponding to which the *real part* of the denominator of the lowest order Z propagator $P_{\mu\nu}^{(Z)}(q)$ vanishes in the $\xi_j = 1$ gauge.

When one moves to the next perturbative one-loop level, it is easy to see that the lowest order (Z) propagator is naturally replaced by a new expression that retains the same formal properties of the lowest order quantity. This modified expression contains also the bare parameter m_Z^2. But now m_Z^2 is no longer the zero of the real part of the modified propagator. To verify this statement, a few technical details are now requested. First of all, let us derive the formal expression of this "modified propagator". A glance to Eq. (3.25) shows that the one-loop Z self-energy contribution to the invariant scattering amplitude can be written in a way formally identical with that of the corresponding lowest order Z exchange term Eq. (3.6), with the replacement:

$$iP^{\nu\mu(Z)}(q) \Rightarrow iP^{\nu\rho(Z)} i\Pi_{\rho\sigma}(q) iP^{\sigma\mu(Z)} \tag{3.44}$$

which can be alternatively written as:

$$\frac{g^{\nu\mu}}{q^2 - m_Z^2} \Rightarrow \frac{1}{q^2 - m_Z^2} \Pi^{\nu\mu(Z)}(q) \frac{1}{q^2 - m_Z^2} \tag{3.45}$$

with $\Pi^{\nu\mu(Z)}(q)$ defined by Eq. (3.25) in the particular case of a charged lepton pair contribution. Leaving aside the specific "bubble" that enters Fig. 3.3, the most general expression of $\Pi^{\nu\mu(z)}$, that can be considered at one loop as due to the sum of all possible contributions represented by Figs. 3.3 and 3.4 (i.e. different types of fermions or gauge bosons or scalars or ghosts or tadpoles), must necessarily be (owing to its tensorial Lorentz structure):

$$i\Pi^{\nu\mu(Z)}(q) \equiv -i[g^{\nu\mu} A^{(Z)}(q^2) + q^\mu q^\nu B^{(Z)}(q^2)] \, . \tag{3.46}$$

The (Lorentz scalar) functions $A(q^2), B(q^2)$ are usually called the *transverse* (A) and the *longitudinal* (B) components of the self-energy tensor $\Pi^{\nu\mu}$. In the specific case of the electron-positron annihilation process on top of resonance, for which the possible final fermion are always *light* (i.e.

of a mass much smaller that that of the Z boson), the function B can be neglected. In fact, its contribution to the scattering amplitude in Eq. (3.25), owing to the contraction of $q_{\mu,\nu} = (p_1 + p_2)_{\mu,\nu} = (p_3 + p_4)_{\mu,\nu}$ with the Dirac γ matrices and to the properties of the Dirac equation, is always proportional to the electron or final fermion masses and thus, as one can easily verify, completely negligible. As a consequence of this kinematical simplification, one can rewrite Eq. (3.45) as:

$$\frac{g^{\nu\mu}}{q^2 - m_Z^2} \Rightarrow \frac{1}{q^2 - m_Z^2}(-)g^{\nu\mu}A^{(Z)}(q^2)\frac{1}{q^2 - m_Z^2} \; . \tag{3.47}$$

For the *total* scattering amplitude at one loop, sum of $A_{ef}^{(0)}$ and $A_{ef}^{(1)}$, the overall formal replacement is therefore the following:

$$\frac{g^{\nu\mu}}{q^2 - m_Z^2} \Rightarrow \frac{g^{\nu\mu}}{q^2 - m_Z^2}\left[1 - \frac{A^{(Z)}(q^2)}{q^2 - m_Z^2}\right] \; . \tag{3.48}$$

The self-energy tensor Eq. (3.25) and its components A, B are of order $|e_0|^2$ at one loop, and *within this one-loop approximation* $(1 - O(e_0^2) = 1/(1 + O(e_0^2))$ one finally has:

$$\begin{aligned} \frac{g^{\nu\mu}}{q^2 - m_Z^2} \equiv -P^{\nu\mu(Z)}|_{\xi=1} &\Rightarrow \frac{g^{\nu\mu}}{(q^2 - m_Z^2)}\frac{1}{\left[1 + \frac{A^{(Z)}(q^2)}{q^2 - m_Z^2}\right]} \\ &= \frac{g^{\nu\mu}}{q^2 + A^{(Z)}(q^2) - m_Z^2} \\ &= \frac{g^{\nu\mu}}{(q^2 + ReA^{(Z)}(q^2) - m_Z^2) + iImA^{(Z)}(q^2)} \end{aligned} \tag{3.49}$$

where we have used the fact that the transverse self-energy $A^{(Z)}(q^2)$ is, in general, a complex function (with an imaginary part not vanishing in the timelike $q^2 > 0$ region).

As one sees from inspection, the new expression in the r.h.s. of Eq. (3.49), that replaces the lowest order propagator, still contains m_Z^2 as a bare parameter. But clearly, since in general $ReA^{(Z)}(q^2) \neq O$, the value $q^2 = m_Z^2$ does not correspond any longer to a zero of the real part of the denominator, and the original lowest order interpretation of m_Z^2 is therefore lost at the one loop level.

If one wishes to define a new and *finite* renormalized Z squared mass such that its interpretation at one loop reproduces that of m_Z^2 at lowest order, one has to define

$$m_{Z(0)}^2 = m_Z^2 + \delta m_Z^2 \tag{3.50}$$

with the condition that, when $q^2 = m_Z^2$ in Eq. (3.49):

$$m_Z^2 + ReA^{(Z)}(m_Z^2) - m_{Z(0)}^2 = O \tag{3.51}$$

that, combined with Eq. (3.50), means:

$$\delta m_Z^2 = ReA^{(Z)}(m_Z^2)\ . \tag{3.52}$$

The choice of Eqs. (3.50)–(3.52) defines the so called *on shell* renormalization scheme and, also, gives a physical clean meaning to the Z mass. Naively, one understands that in correspondence to $q^2 = m_Z^2$ there will be a maximum in the squared modulus of the scattering amplitude, that is in the measurable differential and total production cross sections.

An immediate consequence of Eq. (3.52) is that δm_Z^2 will be infinite, if such will be $ReA^{(Z)}(m_Z^2)$. To clarify this point, let us consider Eq. (3.25) and generalize it so that is corresponds to a generic $f\bar{f}$ (fermion-antifermion) bubble of couplings to Z= $g_{Vf}^{(0)}, g_{Af}^{(0)}$ defined by Eqs. (3.11), (3.12). We can then write:

$$\begin{aligned}
i\Pi_{\nu\mu}^{(Z)(f)}(q^2) &= \frac{-e_0^2}{4\sin^2\theta_W\cos^2\theta_W} N_f \int_{-\infty}^{+\infty} \frac{d^4\kappa}{(2\pi)^4} \frac{1}{(\kappa^2 - m_f^2)[(\kappa - q)^2 - m_f^2]} \\
&\times Tr\left\{ \left[\gamma_\nu g_{Vf}^{(0)} - \gamma_\nu\gamma_5 g_{Af}^{(0)}\right](\hat{\kappa} + m_f) \left[\gamma_\mu g_{Vf}^{(0)-\gamma_\mu\gamma_5 g_{Af}^{(0)}}\right] \right. \\
&\times \left. (\hat{\kappa} - \hat{q} + m_f\} \right. \\
&= \frac{-e_0^2}{4\sin^2\theta_W\cos^2\theta_W} N_f \int_{-\infty}^{+\infty} \frac{d^4\kappa}{(2\pi)^2} \frac{1}{(\kappa^2 - m_f^2)[(\kappa - q)^2 - m_f^2]} \\
&\times \left\{ 4(g_{Vf}^{(0)^2} + g_{Af}^{(0)^2})\left[\kappa_\mu\kappa_\nu + \kappa_\nu\kappa_\mu - q_\nu\kappa_\mu - \kappa_\nu q_\mu \right.\right. \\
&\left.\left. -g_{\nu\mu}(\kappa^2 - \kappa q)\right] + 4(g_{Vf}^{(0)^2} - g_{Af}^{(0)^2}) m_f^2 g_{\mu\nu} \right\}
\end{aligned} \tag{3.53}$$

where $N_f = 1$ for leptons, 3 for quarks, takes into account the color factor.

From the definition Eq. (3.46), the expression of the relevant *transverse* component (the coefficient of $-ig_{\nu\mu}$) turns out therefore to be:

$$\begin{aligned}
A^{(Z)(f)}(q^2) &= \frac{-1}{16\pi^2} \frac{e_0^2}{\sin^2\theta_\omega\cos^2\theta_\omega} N_f \\
&\times \left\{ (g_{Vf}^{(0)^2} + g_{Af}^{(0)^2}) \left[q^2 \left(B_{21}(q^2, m_f^2, m_f^2) + B_1(q^2, m_f^2, m_f^2)\right) \right.\right. \\
&\left.\left. -2B_{22}(q^2, m_f^2, m_f^2)\right] - (g_{Vf}^{(0)^2} - g_{Af}^{(0)^2}) m_f^2 B_0(q^2, m_f^2, m_f^2) \right\}\ .
\end{aligned} \tag{3.54}$$

This has an infinite component, that will be expressed in our convention as:

$$A^{(Z)(f)(\infty)}(q^2) = \frac{e_0^2 N_f}{16\pi^2 \sin^2\theta_W \cos^2\theta_W} \Delta \left[\frac{q^2}{3} (g_{Vf}^{(0)2} + g_{Af}^{(0)2}) - 2m_f^2 g_{Af}^{(0)^2} \right] . \tag{3.55}$$

$A^{(Z)(f)}(q^2)$ will thus diverge for general q^2 values, in particular, at $q^2 = m_Z^2$ (numerically fixed in the on-shell scheme by the observed cross section peak). The Z squared mass shift δm_Z^2 defined by Eq. (3.52) will consequently be infinite. The result of Z mass renormalization is therefore that of introducing another infinite quantity in the game. Without entering the details, we can repeat the derivation in the case of the W boson, where the identical procedure will be that of defining a *physical* W mass starting from the bare one Eq. (1.75)

$$m_{W(0)}^2 = m_W^2 + \delta m_W^2 \tag{3.56}$$

with the on-shell condition

$$\delta m_W^2 = Re A^{(W)}(m_W^2) \tag{3.57}$$

and $A^{(W)}$ defined starting from the W self-energy function:

$$i\Pi^{\nu\mu(W)}(q) = -i \left[g^{\nu\mu} A^{(W)}(q^2) + q^\mu q^\nu B^{(W)} q^2) \right] \tag{3.58}$$

where the calculation of $i\Pi^{\nu\mu(W)}(q)$ can be performed following the same rules that we have illustrated for the Z case, with obvious changes of couplings, starting from a Feynman diagram like that of Fig. 3.3 with virtual W's replacing virtual γ, Z. The expression that would correspond to Eq. (3.25) can be derived in a straightforward way, and reads, for two members f_1, f_2 of a fermion doublet in the virtual bubble, of masses conventionally defined as m_{f_1}, m_{f_2} for the $I_{3L} = +(1/2), -(1/2)$ states:

$$i\ \Pi_{\nu\mu}^{(W)(f)}(q) = -N_f \int_{-\infty}^{+\infty} \frac{d^4\kappa}{(2\pi)^4} Tr \left\{ \frac{i|e_0|}{2\sqrt{2}\sin\theta_W} [\gamma_\nu - \gamma_\nu\gamma_5] \right.$$
$$\left. \times \frac{i(\hat{\kappa} + m_{f_1})}{(\kappa^2 - m_{f_1}^2)} \frac{i|e_0|}{2\sqrt{2}\sin\theta_W} [\gamma_\mu - \gamma_\mu\gamma_5] \frac{i(\hat{\kappa} - \hat{q} + m_{f_2})}{[(\kappa - q)^2 - m_{f_2}^2]} \right\} . \tag{3.59}$$

From Eq. (3.59) one derives the transverse component $A^{(W)(f)}(q^2)$, that reads:

$$A^{(W)(f)}(q^2) = -\frac{N_f}{32\pi^2} \frac{e_0^2}{\sin^2\theta_W}$$
$$2[q^2(B_{21}(q^2, m_{f_1}^2, m_{f_2}^2) + B_1(q^2, m_{f_1}^2, m_{f_2}^2)) - 2B_{22}(q^2, m_{f_1}^2, m_{f_2}^2)] \tag{3.60}$$

whose infinite part is:

$$A^{(W)(f)(\infty)}(q^2) = \frac{e_0^2 N_f}{16\pi^2 \sin^2\theta_W} \Delta \left[\frac{q^2}{3} - \frac{1}{2}(m_{f_1}^2 + m_{f_2}^2) \right] \tag{3.61}$$

so that $A^{(W)(f)}(q^2)$ diverges for general q^2 values, in particular for $q^2 = m_W^2$, which introduces another infinite squared mass shift δm_W^2 in the scheme, following the definition Eq. (3.57). Thus, from W, Z mass renormalization one has "gained" two more infinities, to use, expectedly, "against" those coming from virtual four-momenta integrations of one-loop effects.

Two comments are now appropriate. The first one is related to the fact that, in our oversimplified treatment of the W self-energy, we have assumed that the W couplings to a fermion doublet are of the form $\sim g_0\gamma_\mu(1-\gamma_5) = (|e_0|/\sin\theta_W)\gamma_\mu(1-\gamma_5)$ for both leptons and quarks.

For quarks, this statement is not fully correct since, following our discussion on the Cabibbo-Kobayashi-Maskawa matrix Eq. (1.173), the squared matrix element $|U_{f_1 f_2}|^2$ should be enclosed. In fact, one should sum over all the nine possible $f_1 \neq f_2$ combinations (i.e. ud, us, ub, cd, $cs, \cdots$) and isolate the various independent infinite, and finite, parts. In practice, one easily realizes that, owing to the unitarity property of the Cabibbo-Kobayashi-Maskawa matrix, it is sufficient to retain the three *diagonal* doublets (ud, cs, tb) using the simplified expression of Eq. (3.25) (as we shall do in the following), for all the relevant theoretical predictions. The second comment is related to the fact that we have considered, in the definition of the physical Z, W masses, effects of self-energy type that are due both to fermion and to *non fermion* virtual pairs (including ghosts and tadpoles).

The important point is that, in the *specific* kinematical configurations $q^2 = m_Z^2, m_W^2$, the sum of all the 'non fermion' contributions, which would be, at general q^2 values, gauge-dependent, is 'miraculously' gauge-independent, exactly like the fermion contributions (that are always gauge independent since no ξ_j parameters appear in the fermion propagators). We anticipate this claim, without proving it [43], because it makes it clear that the definition of the physical Z, W masses that we have given at one loop Eqs. (3.50), (3.52), (3.56), (3.57), is, as one would correctly expect, a gauge independent one. Operatively, the values of m_W, m_Z are supposed to be unambiguously fixed by the results of suitable experimental measurements, to be discussed separately but qualitatively intuitive (e.g. m_Z will be related to the peak of e^+e^- cross sections, and m_W can be analogously defined in experiments where W's are produced and decay).

In the electroweak Lagrangian, the list of bare parameters is not exhausted by $m^2_{W(0)}, m^2_{Z(0)}$. One still has e.g. $\sin^2\theta_W$. But Eq.(1.85) shows that this bare parameter can be expressed in terms of $m^2_{W(0)}, m^2_{Z(0)}$ in the MSM. Therefore, in the expression of the invariant scattering amplitude at tree level Eqs. (3.5)–(3.12), the only bare parameter to which a physically meaning renormalized one has not yet been associated it the QED coupling e_0. If the process were considered within a pure QED scheme, i.e. with weak interactions ignored, the renormalization of e_0 (or, as normally done, of $\alpha_0 \equiv (e_0^2/4\pi)$) would be a known procedure. Within the MSM one might expect a few differences since other changed particles, different from the familiar QED fermions (e.g. W^+, W^-, charged unphysical scalars, ghosts...) appear.

In fact, this is exactly what happens: in particular, from the non-Abelian nature of the symmetry group of the MSM, a number of essential differences with respect to the familiar QED case will be generated. Since the properties and the correct definitions of the electric charge play a prominent rôle for what concerns the physics at the Z resonance, we shall devote the next Subsection 3.1.6 to a rather detailed discussion of these topics.

3.1.6 *Charge renormalization and definition in the MSM*

In the previous Subsection we have illustrated an operative definition of the *physical* Z mass. This is naturally related to a measurement of a cross section at a particular squared four-momentum, to be identified with the Z squared mass. The value of this parameter remains therefore fixed by the empirical observation of a peak in a cross-section. This intuitively clear definition remains valid to any order of perturbation theory, although we have made explicit use of it in the limited case of a one loop treatment. As an immediate consequence of the chosen definition, we have shown that the numerical value of the "shift" between the *bare* and the *physical* squared Z mass is exactly the gauge independent, formally infinite, value of the real part of the *transverse* Z *self-energy* computed at the physical Z squared mass.

The aim of this Subsection is twofold. First, we shall illustrate a definition of the physical electric charge which exhibits a number of analogies with that of the Z mass. This will lead in a quite natural way to the identification of the shift between the *bare* and the *physical* squared electric charge with the value of a quantity that will be *defined* as the gauge-invariant

transverse photon self-energy. This value will be computed at the physical (zero) photon squared mass, and will turn out to be, formally, infinite. The new infinite quantity thus achieved will be added to the previous infinite (Z, W) mass "shifts" Subsection 3.1.5 and will manage together with them to kill all the infinities produced by the various Feynman diagrams at one loop that we have examined. This will lead, as wished, to finite predictions for all the physical observables of our considered process, to be examined in the rest of this Chapter. Our second aim will be that of suggesting the possibility that the couplings of the Z boson with fermions may be defined in an operative way that exhibits an essential analogy with the definition of the physical electric charge. This will be fully explored in the following Section 3.3, and will lead in a natural way to the operative definition of the *genuinely weak* parameter of the MSM, the effective electroweak angle.

To proceed in a pedagogical way, we shall now divide this Subsection 3.1.6 into three separate parts where three different, but deeply correlated, topics will be discussed. We shall avoid as much as possible the detailed analysis of a number of numerical calculations that are involved, and only stress those features that seem to us most relevant,and understandable.

The photon self-energy in the MSM

One of the basic universal postulates in physics is the assumption that photons are massless, exactly like in the original celebrated Einstein's proposal. In a field theory language, this corresponds to the mathematical request that the Lagrangian of a system where photons are involved, and interact with some charged matter, has an exact (unbroken) U(1) gauge symmetry, as already discussed in Chapter 1. This property would be destroyed by the presence in the Lagrangian of a quadratic *mass* term $\sim m_\gamma^2 A_\mu A^\mu$ (A_μ represents the vector photon field), that is therefore, from the very beginning, forbidden in the theoretical description. In other words, and using the same language as in Subsection 3.1.5, the *bare* photon mass must be equal to zero. An equivalent statement is that the lowest order photon propagator $P_{\nu\mu(\gamma)}(q)$ Eq. (3.14) has a *pole* at $q^2 = m_\gamma^2 = 0$, or that *zero*' is the value of q^2 corresponding to which the full denominator of the photon propagator in Eq. (3.14) vanishes.

The main difference with respect of the case of the Z mass is due to the fact that, contrary to what discussed in Subsection 3.1.5, the *same* formal property (of vanishing), that the photon mass has at the tree level, must

remain true at the next orders of perturbation theory, in particular at the one loop level. This means that, retaining the interpretation of the squared mass of the photon at one loop as the value of q^2 corresponding to which the modified photon propagator has a vanishing denominator (a *pole*), we must impose that the photon transverse self-energy $A^{(\gamma)}(q^2)$ vanishes at $q^2 = 0$. In fact, defining the photon self-energy tensor in analogy with that of the Z Eq. (3.46) i.e.:

$$i\Pi^{\nu\mu(\gamma)}(q) \equiv -i[g^{\nu\mu}A^{(\gamma)}(q^2) + q^\mu q^\nu B^{(\gamma)}(q^2)] \tag{3.62}$$

we would find, following exactly the various steps of Subsection 3.1.5, that the relevant correspondence between tree level and one loop quantities, represented in the Z case by Eq. (3.49), becomes now:

$$\frac{g^{\nu\mu}}{q^2} \Rightarrow \frac{g^{\nu\mu}}{[q^2 + ReA^{(\gamma)}(q^2)] + iImA^{(\gamma)}(q^2)} \; . \tag{3.63}$$

Imposing that $q^2 = 0$ corresponds to a zero of the denominator of Eq. (3.63) means therefore to require that:

$$ReA^{(\gamma)}(0) = 0 = ImA^{(\gamma)}(0) \tag{3.64}$$

(the photon must remain a massless particle).

Equation (3.64) has a consequence that will be essential for our next discussions. If we adopt for the general $(W, Z, \gamma \cdots)$ transverse self-energy the formal decomposition:

$$A^{(i)}(q^2) \equiv A^{(i)}(0) + q^2 F^{(i)}(q^2) \tag{3.65}$$

where the index (i) can correspond to a W, Z, γ self-energy, but also to a *mixed* $Z\gamma$ (or γZ) couple of virtual gauge bosons (in which case we shall use the notation $A^{(Z\gamma)} -$ or $A^{(\gamma Z)} -$), Eq. (3.64) implies that:

$$A^{(\gamma)}(q^2) \equiv q^2 F^{(\gamma)}(q^2) \; . \tag{3.66}$$

Equation (3.66) will be fundamental, as it will represent the starting point of our next definition of physical charge. For this reason, we shall now spend some time to discuss the validity of the request imposed by Eq. (3.64), showing a simple and illustrative numerical example.

In the explicit calculation of the photon self-energy, several contributions arise that originate from different Feynman diagrams. It is convenient, at this point, to make a clean separation between two classes of diagrams, to be called for simplicity the *fermionic* (f) and the *non fermionic* (Nf) ones. The first class, represented diagrammatically in Fig. 3.11, includes

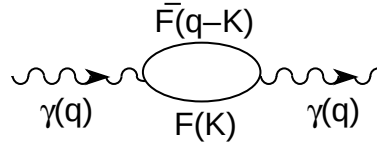

Fig. 3.11 Photon self-energy diagram with virtual fermion-antifermion pair.

all those contributions due to a virtual fermion-antifermion (both leptons and quarks) pair.

The second class in represented diagrammatically in Fig. 3.12. As one sees, it includes both *physical* (i.e. W pairs) and *unphysical* (would be Goldstone bosons, ghosts) contributions. In any $\xi \neq \infty$ gauge, the unphysical terms cannot be ignored, and we shall show explicitly how relevant their presence will be, working as usually in the 't Hooft $\xi = 1$ gauge.

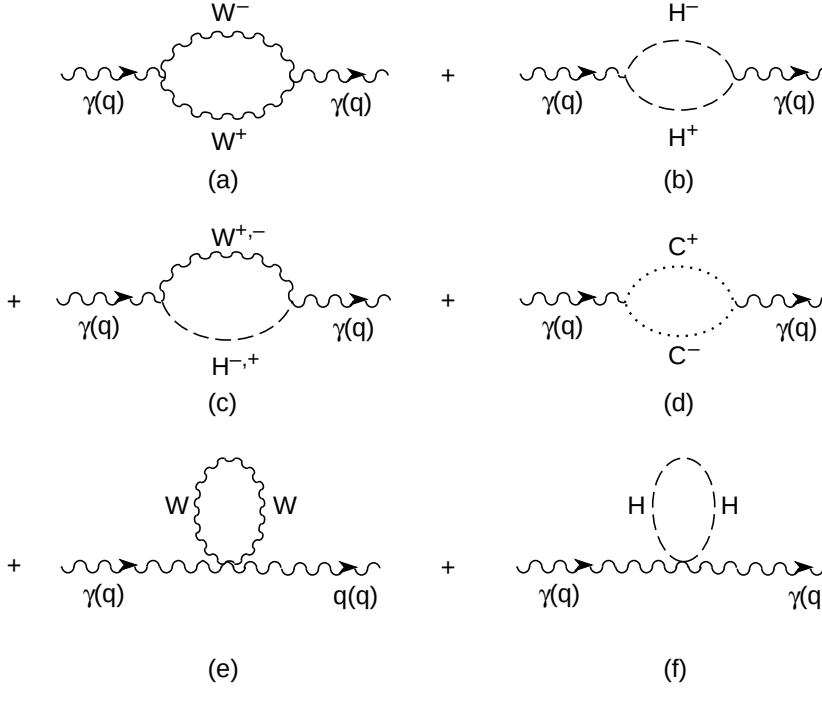

Fig. 3.12 Non-fermionic contributions to the photon self-energy: (a) W pairs; (b) 'would be' pairs; (c) W-'would be' pairs; (d) 'ghost' pairs; (e), (f) 'seagull' diagrams.

The separation into the two classes depicted in Figs. 3.11 and 3.12 corresponds to an essential difference: the contributions to $A^{(\gamma)}(q^2)$ from the various fermion pairs components of Fig. 3.11 are all gauge-independent, those from the various components of Fig. 3.12 are not. This is true both for the separate diagrams and for their sum, with the only remarkable exception of the point $q^2 = 0$, where the contribution to $A^{(\gamma)}(0)$ of the *sum* of all diagrams of Fig. 3.12 will manage to be gauge independent.

It is not difficult to understand qualitatively the reason of the aforementioned difference. The fermion propagators do not depend on the gauge parameters ξ_i, and consequently cannot induce any ξ dependence in the photon propagator of Fig. 3.11, after integration over κ, the virtual fermion four-momentum. This is not true for the various graphs of Fig. 3.12 where *all* the internal bubbles are ξ dependent, and after κ -integration this dependence can partially "migrate" to the relevant transverse part of the photon self-energy that will actually become, at general q^2 values, gauge (i.e. ξ) dependent. This has a remarkable exception in the case $q^2 = 0$, for the *sum* of all diagrams of Fig. 3.12.

To prove the last statement, one should compute all contributions of that figure to $A^{(\gamma)}(0)$ at variable ξ, and verify the cancellation of the ξ-dependent part. We shall proceed in a more modest, intuitive way, based on our previous discussion according to which the condition $A^{(\gamma)}(0) = 0$ ensures that the photon remains massless, and thus that the theory remains gauge-invariant. Turning this argument, gauge-invariance requires that $A^{(\gamma)}(0)$ should be necessarily zero. We shall check now whether this request is fulfilled by Figs. 3.11, 3.12, "at least" in the 't Hooft gauge.

The calculation of the first contribution, Fig. 3.11, can be easily performed in the dimensional regularization scheme. The starting point is the formal expression of the relevant term. For a fermion f of electric charge $Q_f|e_0|$ and mass m_f, from conventional Feynman rules, one derives for the $f\bar{f}$ component of the photon self-energy tensor $\equiv \Pi^{\nu\mu(f)(\gamma)}(q^2)$ Eq. (3.62):

$$i\Pi^{\nu\mu(f)(\gamma)}(q^2) = -\int_{-\infty}^{+\infty} \frac{d^4\kappa}{(2\pi)^4} Q_f^2 e_0^2 \times Tr\left[\gamma^\nu \frac{(\hat{\kappa}+m_f)}{(\kappa^2-m_f^2)}\gamma^\nu \frac{(\hat{\kappa}-\hat{q}+m_f)}{[(\kappa-q)^2-m_f^2]}\right] . \tag{3.67}$$

The trace (Tr) of the matrix contained in the square bracket can be easily computed and the infinite part of Eq. (3.68) is determined following the prescriptions given in Subsection 3.1.4. This leads in a straightforward way

to the expression of the transverse self energy $A^{(\gamma)}(q^2)$ Eq. (3.62):

$$A^{(f)(\gamma)}(q^2) = q^2 \left[\frac{Q_f^2 e_0^2}{12\pi^2}\right] \left\{[\Delta] - 6\int_0^1 dx\, x(1-x) \ln\left|\frac{D_f(q^2)}{\mu^2}\right|\right\} \quad (3.68)$$

where Δ is the infinite quantity defined by Eq. (3.36), μ^2 is an arbitrary scale parameter that must disappear in the theoretical expression of the physical *observables*, and

$$D_f(q^2) = m_f^2 - q^2 x(1-x)\ . \quad (3.69)$$

From Eq. (3.68) it is immediate to conclude that any fermionic contribution to $A^{(\gamma)}(q^2)$ *vanishes* at $q^2 = 0$. Since such contributions are separately gauge independent, this is exactly what we expected to find.

The calculation of the six diagrams of Fig. 3.12 can also be easily performed in our chosen approach, following the prescriptions given in this Chapter. Without entering the detailed analysis of each separate term, we list here in order the six relevant contributions, using the same notations as in Fig. 3.12, i.e. Figs. 3.12(a)–(f) correspond to $A^{(\mathrm{a}),(\mathrm{b}),(\mathrm{c})\ldots(\mathrm{f})}(q^2)$:

$$\begin{aligned} A^{(\mathrm{a})(\gamma)}(q^2) = {} & \frac{-e_0^2}{16\pi^2} \\ & \times \int_0^1 dx \left\{[\Delta][9R^2 + q^2(5 - 2x(1-x))]\right. \\ & + R^2\left[7 - 9\ln\left|\frac{R^2}{\mu^2}\right|\right] - q^2 \ln\left|\frac{R^2}{\mu^2}\right| [5 - 2x(1-x)]\Big\} \end{aligned} \quad (3.70)$$

$$\begin{aligned} A^{(\mathrm{b})(\gamma)}(q^2) = {} & \frac{-e_0^2}{16\pi^2} \\ & \times \int_0^1 dx \left\{[\Delta][2R^2] + 2R^2\left[1 - \ln\left|\frac{R^2}{\mu^2}\right|\right]\right\} \end{aligned} \quad (3.71)$$

$$\begin{aligned} A^{(\mathrm{c})(\gamma)}(q^2) = {} & \frac{+e_0^2}{16\pi^2} \\ & \times \int_0^1 dx \left\{[\Delta][2m_W^2] - 2m_W^2 \ln\left|\frac{R^2}{\mu^2}\right|\right\} \end{aligned} \quad (3.72)$$

$$\begin{aligned} A^{(\mathrm{d})(\gamma)}(q^2) = {} & \frac{+e_0^2}{16\pi^2} \\ & \times \int_0^1 dx \left\{[\Delta][R^2] + R^2\left[1 - \ln\left|\frac{R^2}{\mu^2}\right|\right]\right\} \end{aligned} \quad (3.73)$$

$$A^{(\mathrm{e})(\gamma)}(q^2) = \frac{+e_0^2}{16\pi^2} \times \int_0^1 dx \left\{ [\Delta][6m_W^2] + 6m_W^2 \left[1 - \ln \frac{m_W^2}{\mu^2} \right] \right\} \tag{3.74}$$

$$A^{(\mathrm{f})(\gamma)}(q^2) = \frac{+e_0^2}{16\pi^2} \times \int_0^1 dx \left\{ [\Delta][2m_W^2] + 2m_W^2 \left[1 - \ln \frac{m_W^2}{\mu^2} \right] \right\} \tag{3.75}$$

where

$$R^2(q^2) = m_W^2 - q^2 x(1-x) \; . \tag{3.76}$$

As one sees from the previous expression, all the separate six contributions to the photon transverse self-energy are neither vanishing nor finite at $q^2 = 0$. When one computes the sum of all the terms, though, one finds the following results for the overall *non fermionic* (Nf) function: (separate contributions are denoted by the corresponding letter)

$$\begin{aligned} A^{(Nf)(\gamma)}(q^2 = 0) = \frac{-e_0^2}{16\pi^2} \int_0^1 dx \\ \times \Big\{ [\Delta][(9m_W^2)^{(\mathrm{a})} + (2m_W^2)^{(\mathrm{b})} - (2m_W^2)^{(\mathrm{c})} - (m_W^2)^{(\mathrm{d})} \\ - \quad (6m_W^2)^{(\mathrm{e})} - (2m_W^2)^{(\mathrm{f})}] \\ + m_W^2 \left[\left(7 - 9 \ln \frac{m_W^2}{\mu^2} \right)^{(\mathrm{a})} + \left(2 - 2 \ln \frac{m_W^2}{\mu^2} \right)^{(\mathrm{b})} \right. \\ + \left(2 \ln \frac{m_W^2}{\mu^2} \right)^{(\mathrm{c})} - \left(1 - \ln \frac{m_W^2}{\mu^2} \right)^{(\mathrm{d})} \\ \left. - \left(6 - 6 \ln \frac{m_W^2}{\mu^2} \right)^{(\mathrm{e})} - \left(2 - 2 \ln \frac{m_W^2}{\mu^2} \right)^{(\mathrm{f})} \right] \Big\} = 0 \; . \end{aligned} \tag{3.77}$$

As one sees, the (due) vanishing of $A^{(\gamma)}(0)$ is in this case ($\xi = 1$ gauge) the final result of a "professionally" coordinated team work, where a bunch of unphysical creatures (would be Goldstone bosons, ghosts...) combine their efforts with that of the physical ones (Ws) to obtain the "meaningful" results. This is in fact the reason why we have shown in some detail the previous calculation, and for similar reasons we shall spend some time, in

the first part of Chapter 4, to illustrate a similar situation, that arises in the case where the final fermion state is a $b\bar{b}$ pair.

From the result of Eq. (3.77) we can only conclude, strictly speaking, that the full transverse photon self-energy $A^{(\gamma)}(q^2)$, i.e. the sum of the fermionic and of the non fermionic component, vanishes at $q^2 = 0$ in the $\xi = 1$ gauge. To prove that this property remains valid in any gauge requires a more formal calculation,that can be found elsewhere [43]. The conclusion is that, indeed, $A^{(\gamma)}(0)$ is vanishing *and* gauge-independent. This feature is analogous to that of the Z, W transverse self-energies that are also (when *all* the relevant contributions are included) gauge independent at the q^2 value that corresponds to the *physical squared mass* of their related (Z, W) gauge boson (in the photon case, this is exactly $q^2 = 0$). As we shall explicitly show in the following part of this Chapter, all the previous transverse self-energies become gauge dependent as soon as one moves away from the physical squared mass value of q^2. Note that the previous "exceptional" gauge independence only applies to the function $A^{(\gamma),(Z),(W)}$. In particular, for the relevant case of the photon that we are now considering, this property will *not* apply for the function $F^{(\gamma)}(q^2)$, defined by Eq. (3.65), at $q^2 = 0$. One can easily verify this statement by computing, in analogy with what done for $A^{(\gamma)}(0)$, the non fermionic contribution to $F^{(\gamma)}(0)$ in a general $\xi \neq \infty$ gauge. We shall, as usually, provide an indirect argument in the following part of this Chapter, when we shall define a *generalized* gauge-invariant self-energy obtained by adding to the function $F^{(\gamma)}(q^2)$ a precisely fixed amount of vertex effects.

The main result that has been obtained in the previous paragraphs is that it is possible to write the transverse photon self-energy in the form of Eq. (3.66) i.e. without $A^{(\gamma)}(0)$. This fact will be the basic point of our next definition of physical charge.

Definition of the physical charge in the MSM

We have repeatedly stressed in this Chapter the fact that our chosen operative definition of the Z mass is based on the measurement of a cross section at the kinematical point that corresponds to the Z mass, where the Z exchange dominates. This procedure is fairly clear and understandable, and for this reason we shall adopt a similar definition of the electric charge that is also based on the measurement of a cross-section at the kinematical point that corresponds to the photon mass, i.e. at zero four momentum

square. Although this is not the only conceivable valid definition of the electric charge, we shall insist on it, to make our overall presentation of physics at the Z resonance as homogeneous as possible.

Quite generally, the idea of identifying the electric charge with the result of the measurement of an interaction between charged particles at zero momentum transfer has an obvious classical ancestor, since the measurement of the electric force between two particles is, classically, the result of such a static operation. At the quantum field theory level it is not difficult to realize that an essentially similar definition survives. A rather simplified way is that of considering the process of elastic scattering of an electron by a "heavy" target, e.g. a muon. To the lowest order this is represented by the Feynman diagrams of Fig. (3.13), where one photon or one Z is exchanged in the t-channel. Here we shall denote by p_e, p_μ, p'_e, p'_μ the initial and final electron-muon four momenta, with

$$p_e + p_\mu = p'_e + p'_\mu \tag{3.78}$$

and

$$t = (p_e - p'_e)^2 = (p_\mu - p'_\mu)^2 \equiv \kappa^2 \tag{3.79}$$

with $\kappa = p_e - p'_e = p'_\mu - p_\mu$.

From conventional Feynman rules one can easily derive the expression of the invariant scattering amplitude that corresponds to the photonic *zero* order Fig. 3.12(a). Denoting this quantity as $A^{(0)(\gamma)}_{e\mu,e'\mu'}$, one finds:

$$A^{(0)(\gamma)}_{e\mu,e'\mu'} = \left[i\bar{u}(p'_\mu)\gamma^\nu u(p_\mu)\bar{u}(p'_e)\gamma_\nu u(p_e)\right]\left[\frac{e_0^2}{t}\right] \equiv [A^{(0)(E)(\gamma)}][A^{(0)(I)(\gamma)}(t)] \tag{3.80}$$

where we have introduced two quantities, that correspond to the two squared brackets on the r.h.s. of Eq. (3.80), and represent the components of $A^{(0)(\gamma)}$ due to the real external (E) structure and to the internal (I) virtual exchanges. In this particularly simple case:

$$A^{(0)(I)(\gamma)}(t) = \frac{e_0^2}{t} \tag{3.81}$$

where e_0 is the *bare* electric charge that appears in the starting Lagrangian, assumed to be that of the considered MSM. In practice Eq. (3.81) is the contribution to the scattering amplitude coming from the bare charge and the bare photon propagator $P_{\nu\mu}(\kappa)$, which is the analogue of Eq. (3.14) but in the κ variable, where κ is now the virtual photon four-momentum of Fig. 3.13.

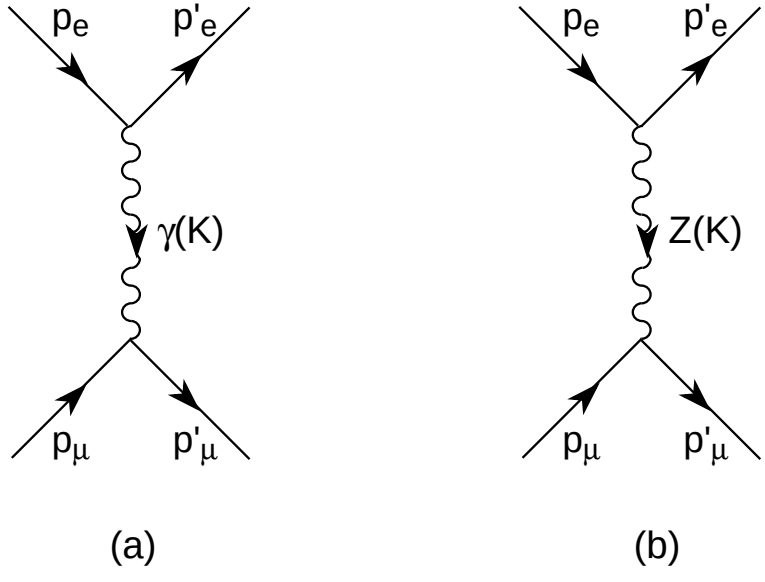

Fig. 3.13 Elastic electron-muon scattering in (a) the one photon t-channel exchange approximation. (b) the one Z t-channel exchange approximation.

From Eq. (3.81) we can derive an important property of the bare squared charge e_0^2, or alternatively of the more commonly used $\alpha_0 \equiv (e_0^2/4\pi)$, i.e. that:

$$4\pi\alpha_0 = \lim_{t\to 0}[tA^{(0)(I)(\gamma)}(t)] \; . \tag{3.82}$$

In mathematical language this can be expressed by saying that the bare $e_0^2 = 4\pi\alpha_0$ is the *residue* of the function $A^{(0)(I)(\gamma)}(t)$ at the *pole* at $t = 0$ (where $A^{(0)(I)(\gamma)}(t)$ becomes formally infinite,as shown by Eq. (3.81). Apparently, this is a purely mathematical property, and little physical information has been gained until now.

To realize that Eq. (3.82) can be viewed as a very meaningful definition it is, though, sufficient to compute the expression of the differential cross section for the considered process. In the approximate description that corresponds to Fig. 3.13, defining the usual Mandelstam variables:

$$\begin{aligned} &s = (p_e + p_\mu)^2 = (p'_e + p'_\mu)^2; \quad t = (p_e - p'_e)^2; \\ &u = (p_e - p'_\mu)^2; \quad s + t + u = 2m_e^2 + 2m_\mu^2 \end{aligned} \tag{3.83}$$

one finds after some straightforward calculation the expression of the unpolarized differential cross section. Considering the separate purely photonic

contribution, i.e. ignoring for the moment Z exchange, this reads:

$$\frac{1}{4\pi}d\sigma_{e\mu}^{(0)(\gamma)} = \frac{(4\pi\alpha_0)^2}{t^2}\frac{\left\{[s-(m_e^2+m_\mu^2)]^2+st+\frac{1}{2}t^2\right\}}{[s-(m_e+m_\mu)^2][s-(m_e-m_\mu)^2]}dt\ . \qquad (3.84)$$

Equation (3.84) leads immediately to the following property:

$$\lim_{t\to 0}\frac{1}{4\pi}t^2\frac{d\sigma_{e\mu}^{(0)(\gamma)}}{dt} = (4\pi\alpha_0)^2\frac{[s-(m_e^2+m_\mu^2)]^2}{[s-(m_e+m_\mu)^2][s-(m_e-m_\mu)^2]}\ . \qquad (3.85)$$

Assuming $s \gg m_e^2, m_\mu^2$, although this is not requested in principle, leads to a simplified expression i.e.(neglecting terms of order $\frac{m_{e,\mu}^2}{s}$):

$$\lim_{t\to 0}\frac{1}{4\pi}t^2\frac{d\sigma_{e\mu}^{(0)(\gamma)}}{dt} = (4\pi\alpha_0)^2 \equiv \left[\lim_{t\to 0}(tA^{(0)(I)(\gamma)}(t))\right]^2\ . \qquad (3.86)$$

Equation (3.86) can be viewed as the desired operative definition of the bare quantity α_0^2. In fact, in the considered kinematical limit $t \to 0$, the other contribution to the differential cross-section from Z exchange in the t-channel is not of the form $\sim 1/t^2$ and thus vanishes when multiplied by t^2. Therefore one can identify in Eq. (3.86) the photon component with the full differential cross section $d\sigma^{(0)}$ ($\gamma + Z$ exchange) and write

$$\lim_{t\to 0}\frac{1}{4\pi}t^2\frac{d\sigma^{(0)}}{dt} \equiv \lim_{t\to 0}\frac{1}{4\pi}t^2\frac{d\sigma^{(0)(\gamma)}}{dt} = (4\pi\alpha_0)^2\ . \qquad (3.87)$$

The extrapolation process in the t variable requested in Eq. (3.87) is in principle a perfectly meaningful one, since the considered limit can be obtained from measurements in the *physical* kinematical region ($t \leq 0$) of the process. It involves the properties of the collision of two charged particles in the region of vanishing four-momentum exchange, as one would naively expect from the classical definition of electric charge. For the purposes of our future discussion, Eq. (3.87) will provide a useful and understandable operative definition.

Two important comments must be added at this point. The fact that the differential cross section Eq. (3.84) becomes, formally, infinite at $t = 0$ is expected, since in the non relativistic limit one simply recovers the well known forward singularity of the Rutherford cross section. Actually, in the practical calculations, suitable *screening* effects should be thus included. Having clarified this feature, it remains obvious that the presence of an infinite term $\sim 1/t^2$ in Eq. (3.84) is the consequence of the presence of an infinite term $\sim 1/t$ in the scattering amplitude. In fact, $d\sigma \simeq |A_{e\mu,e'\mu'}|^2$ (spin sums and averages are understood). In particular, the relevant part of $A^{(0)(I)}(t)$ Eq. (3.80), that enters the definition of the bare charge, is *only*

that which becomes infinite $\sim 1/t$ when $t \to 0$, as summarized mathematically by Eq. (3.82).

After these premises, we may now propose a definition of the *physical* electric charge. Following our general philosophy, we shall simply generalize the tree level definition Eq. (3.87) and write, at the next one-loop level(neglecting again $\sim m_e^2, m_\mu^2$ terms):

$$\lim_{t\to 0} \frac{1}{4\pi} t^2 \frac{d\sigma^{(1)}_{e\mu}}{dt} \equiv (4\pi\alpha)^2 \ . \tag{3.88}$$

The previous definition is evidently an operative one. To proceed towards a corresponding theoretical expression of the physical charge, one can first remark that, at the considered one loop level, the expression of the scattering amplitude (whose square generates the differential cross section) can be separated in two parts i.e.

$$A^{(1)}_{e\mu,e'\mu'} = A^{(1)(\gamma)}_{e\mu,e'\mu'} + [A^{(1)}_{e\mu,e'\mu'} - A^{(1)(\gamma)}_{e\mu,e'\mu'}] \tag{3.89}$$

where the first term on the r.h.s. represents all those contributions to the amplitude that can be written in the form:

$$A^{(1)(\gamma)}_{e\mu,e'\mu'} \equiv A^{(0)(E)(\gamma)} \cdot A^{(1)(I)(\gamma)} \tag{3.90}$$

i.e. retaining the same *external* Lorentz structure as at the tree level, Eq. (3.80), but with a modified *internal* function $A^{(1)(I)(\gamma)}$.

In terms of Feynman diagrams, it is relatively easy to understand which kind of virtual exchanges will contribute the *photonic* component Eq. (3.90). Clearly, at least one of the internal particles will necessarily be a photon, since the external Lorentz structure must be the same as that of the tree level photon exchange i.e. $A^{(0)(E)(\gamma)}$ Eq. (3.80). Examples of such diagrams are shown in Fig. 3.14.

Looking at Fig. 3.14 it is immediate to understand that the *external* structure of Figs. 3.14(b) and 3.14(c) is exactly the same as that of Fig. 3.14(a). Actually this is not true for the following Figs. 3.14(d)–(g). In these cases one must *project* from the involved W vertices the *photonic* Lorentz component $\sim \gamma_\mu$ and combine it with the remaining photon-electron (or muon) vertex. The *non photonic* component of the W vertex can be ignored for the present discussion.The reason will become clear, and will be throughly discussed, in the forthcoming Section 3.3.

One important point can be understood from our previous discussion: all the Feynman diagrams that we have depicted in Fig. 3.14 generate contribution to $A^{(I)(\gamma)}$ that are singular $\sim 1/t$ in the limit $t \to 0$, exactly like the tree level one of Fig. 3.14(a). Considering for instance the first three

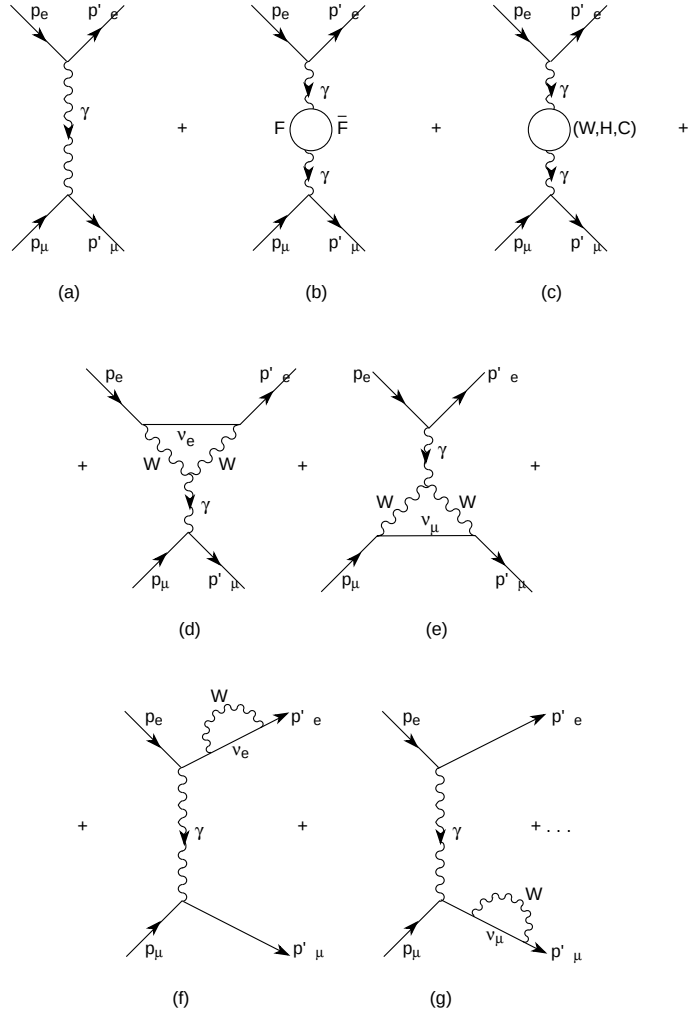

Fig. 3.14 Examples of Feynman diagrams contributing the *photonic* component of the scattering amplitude $A_{e\mu,e'\mu'}$ to the one-loop level. In (b) and (c) the *fermionic* (F) and *non fermionic* (W,H,C) contributions to the photon self-energy are separately shown.

Figs. 3.14(a),(b),(c) and using the notation of Eq. (3.62) for the photon transverse self-energy, it is clear from Eq. (3.63) that the overall contribution to the *photonic* component $A^{(I)(\gamma)}$ from these figures is:

$$A^{(1)(I)(\gamma)(\mathrm{a+b+c})}(t) = \frac{4\pi\alpha_0}{t}\left[\frac{1}{1+F^{(f)(\gamma)}(t)+F^{(Nf)(\gamma)}(t)}\right] \qquad (3.91)$$

where we have retained the definitions of Eqs. (3.68), (3.77) for the *fermionic* and *non fermionic* component of the photon transverse self-energy.

Equation (3.91) has been obtained by simply adding to the bare photon propagator of Fig. 3.14(a) the similar expressions of Figs. 3.14(b),(c) that lead to the modified one-loop formula Eq. (3.63). In a quite similar way, one can take into account the contributions due to the remaining graphs Figs. 3.14(d)–(g).

We shall discuss in detail in Section 3.3 the complete derivation of the relevant expressions, that involves a preliminary discussion on how the request of gauge invariance fixes at one loop the combinations of self-energies and vertices (and, generally, boxes) that must necessarily contribute each observable quantity in *gauge blocks*. For the moment we shall be limited to the intuitive observation that the extra contributions to $A^{(1)(I)(\gamma)}(t)$ coming from Figs. 3.14(d)–(g) will be necessarily of the form

$$A^{(1)(I)(\gamma)(\mathrm{d+e+f+g})}(t) = \frac{4\pi\alpha_0}{t}[-F^{(V)(W)(\gamma)}(t)] \tag{3.92}$$

where the function $F^{(V)(W)(\gamma)}(t)$ represents the *photonic* component of the various *vertices*, i.e. that multiplied by $\bar{v}_\ell \gamma_\mu u_\ell$, where ℓ is the lepton in the one-loop vertex.

At the one-loop level, making use of the known formal recipes (that in this case consist of equating $1/1+0(\alpha)$ to $1-0(\alpha)...$) one has in conclusion the total expressions of $A^{(1)(I)(\gamma)}$ that corresponds to Fig. 3.14. This will be written in the form:

$$A^{(1)(I)(\gamma),(a)\to(f)}(t) = \frac{4\pi\alpha_0}{t} \times \left[\frac{1}{1+F^{(f)(\gamma)}(t)+F^{(Nf)(\gamma)}(t)+F^{(V)(W)(\gamma)}(t)}\right] . \tag{3.93}$$

Equation (3.93) becomes clearly infinite $\sim 1/t$ at $t = 0$ since, as we guess and shall show, the denominator on its r.h.s. is not vanishing at this point. We shall assume now without proving it (but postponing the discussion to Section 3.3) that no other contributions to the *full* scattering amplitude become infinite $\sim 1/t$ at $t = 0$. We anticipate that, to fully understand this statement, a rigorous definition of the gauge-invariant 'gauge blocks' is requested. As we shall see, this will automatically eliminate the apparent contribution from the mixed $\gamma - Z$ transverse self-energy, i.e. will cancel it at the point $t = 0$ after combination with the associated vertex in the 'block'.

We can now return to Eq. (3.88) where the definition of the physical charge is given. From the previous discussion it is clear that the only contribution that survives in the limit when $t \to 0$ for negligible lepton masses is that from the function $A^{(1)(I)(\gamma)}$ (whose square behaves like $1/t^2$). We can therefore adjust the tree level expression Eq. (3.86) and conclude that

$$\begin{aligned}\lim_{t\to 0} \frac{1}{4\pi} t^2 \frac{d\sigma_{e\mu}^{(1)}}{dt} &\equiv (4\pi\alpha)^2 \\ &= \left[\lim_{t\to 0}(tA^{(1)(I)(\gamma)}(t)\right]^2 \\ &= (4\pi\alpha_0)^2 \frac{1}{[1 + F^{(f)(\gamma)}(0) + F^{(Nf)(\gamma)}(0) + F^{(V)(W)(\gamma)}(0)]^2}\end{aligned} \tag{3.94}$$

which can be recast in the form:

$$\alpha_0 = \alpha[1 + F^{(f)(\gamma)}(0) + F^{(Nf)(\gamma)}(0) + F^{(V)(W)(\gamma)}(0)] \,. \tag{3.95}$$

Equation (3.95) gives the desired connection between the *bare* and the *physical* electric charges. In the conventional notation one writes:

$$\alpha_0 = \alpha + \delta\alpha \equiv \alpha \left[1 + \frac{\delta\alpha}{\alpha}\right] \tag{3.96}$$

with

$$\frac{\delta\alpha}{\alpha} = \left[F^{(f)(\gamma)}(0) + F^{(Nf)(\gamma)}(0) + F^{(V)(W)(\gamma)}(0)\right] \,. \tag{3.97}$$

The physical electric charge corresponds to the experimentally measured fine-structure constant

$$\alpha \equiv e^2/4\pi = \frac{1}{137.03599911(46)} \,. \tag{3.98}$$

Having defined the physical electric charge, we still have to compute the theoretical expression given by Eq. (3.97), that represents the 'shift' between the meaningless (bare) and the meaningful (physical) quantities. From our previous experience, we expect to find an infinite quantity. From our general philosophy, we expect that this infinity is canceled by other infinities in the theoretical expressions of the observables. We shall first compute, formally, Eq. (3.97) in the forthcoming pages.

Calculation of the charge shift in the MSM

We now proceed to the formal calculation of Eq. (3.97). This will involve a number of relatively straightforward operations, to be carried on numerically in the $\xi = 1$ gauge as usually. The important point to be stressed before entering the procedure is that the definition of the physical charge α, being related to a measurable operation, must be obviously gauge independent. Since the bare parameter α_0 cannot depend on ξ_i , the shift $\delta\alpha$ will have to be gauge-independent as well. In order to enforce this request in a simple way, it is convenient to separate Eq. (3.97) into two different pieces, the first one coming from the fermion pairs contribution to the photon self-energy and the second one from the remaining graphs i.e. (W, H, C) self-energies and W vertices. Thus, we shall write:

$$\frac{\delta\alpha}{\alpha} = \left[\frac{\delta\alpha}{\alpha}\right]^{(f)} + \left[\frac{\delta\alpha}{\alpha}\right]^{(Nf)} \tag{3.99}$$

where

$$\left[\frac{\delta\alpha}{\alpha}\right]^{(f)} = F^{(f)(\gamma)}(0) \tag{3.100}$$

and

$$\left[\frac{\delta\alpha}{\alpha}\right]^{(Nf)} = F^{(Nf)(\gamma)}(0) + F^{(V)(W)(\gamma)}(0)\ . \tag{3.101}$$

It is obvious from the previous discussions that the first component Eq. (3.100) will be automatically gauge-invariant, being the result of integration of fermion ξ_i-independent propagators. For what concerns its explicit expression, this can be easily derived from Eq. (3.68) summing over the fermions of one generation and leaving the generation number N_f unspecified (although $N_f = 3$ in the MSM). This gives:

$$\left[\frac{\delta\alpha}{\alpha}\right]^{(f)} = \frac{\alpha}{12\pi}\Delta\left[\frac{32}{3}N_f\right] - \frac{\alpha}{3\pi}\sum_f Q_f^2 \ln\frac{m_f^2}{\mu^2} \tag{3.102}$$

where in the second term on the r.h.s a sum over all charged fermions (that includes the color factor for quarks) is understood. Note that the charge that appears on the r.h.s. can be safely identified with the physical one rather than with the bare one; this can be easily understood at the one loop level (the difference would be of higher perturbative order).

As one sees, the *fermionic* charge shift is infinite, and has a μ^2 dependent finite term. We expect, and will verify soon our expectation, that both disturbing features disappear in the expression of the physical observables.

To compute the charge shift due to the (W, H, C) contributions to the photon self-energy, Fig. 3.14(c), is also immediate from the given expressions Eqs. (3.70)–(3.75). Summing all the terms one finds the result (we shall now leave the notation $\xi = 1$):

$$\begin{aligned}\left[\frac{\delta\alpha}{\alpha}\right]_{\xi=1}^{(W,H,C)} &\equiv F^{(Nf)(\gamma)}(0)|_{\xi=1} \\ &= \frac{\alpha}{12\pi}\Delta\left[-\left(\frac{19}{2}\right)-1+\left(\frac{1}{2}\right)\right] \\ &- \frac{\alpha}{4\pi}\left\{\left[\frac{1}{3}-\frac{19}{6}\ln\frac{m_W^2}{\mu^2}\right]+\left[\frac{1}{3}\ln\frac{m_W^2}{\mu^2}\right]\right. \\ &\left.+\left[-\frac{1}{6}\ln\frac{m_W^2}{\mu^2}-\frac{1}{3}\right]\right\} \\ &= \frac{\alpha}{12\pi}\Delta[-10]+\frac{3\alpha}{4\pi}\ln\frac{m_W^2}{\mu^2} \end{aligned} \tag{3.103}$$

where the contributions from the different diagrams of Fig. 3.14(c) have been separately listed. One notices again the presence of an infinite and of a finite scale dependent part, like in the fermion case. The infinite part is of opposite sign (negative) with respect to that of the fermionic contribution Eq. (3.102). This fact is not accidental, and will be rediscussed later on.

The last contribution depicted in Figs. 3.14(d),(e) is that coming from the (WW) vertices. The calculation can be easily performed starting from the expression given in Subsection 3.1.4. The result can be cast in the following form:

$$\begin{aligned}\left[\frac{\delta\alpha}{\alpha}\right]_{\xi=1}^{(W\text{ vertex})} &\equiv F^{(V)(W)(\gamma)}(0)|_{\xi=1} \\ &= \frac{\alpha}{12\pi}\Delta[-12]+\frac{2\alpha}{4\pi}\ln\frac{m_W^2}{\mu^2} \\ &\equiv 16\pi\alpha I_{WW}(0) \end{aligned} \tag{3.104}$$

where we have introduced the auxiliary function:

$$I_{WW}(q^2) = \lim_{n\to 4} i\mu^{4-n}\int_{-\infty}^{+\infty}\frac{d^n\kappa}{(2\pi)^n}\frac{1}{(\kappa^2-m_W^2)[(\kappa+q)^2-m_W^2]} \tag{3.105}$$

The derivation of Eq. (3.104) requires a couple of technical details, that we shall summarize here briefly. The first step is that of computing the sum of the one loop γW vertices of Fig. 3.14.

From its expression proportional to $\gamma_\mu(1-\gamma_5)$ (since only left-handed fermions are involved), only the *photonic* component $\sim \gamma_\mu$ has to be

projected out. This will produce the quantity defined as $F^{(V)(W)(\gamma)}(t)$ in Eq. (3.93), that will finally lead to the corresponding charge shift Eq. (3.101). The remaining Lorentz *non photonic* component of the γW vertex will then *cancel* the corresponding Lorentz structure of the γZ self energy at $t = 0$, which can thus be safely ignored.

One should still prove that the total charge shift defined by Eqs. (3.99)–(3.101) is indeed gauge independent. At this stage, the rigorous procedure would be its evaluation in a general ξ gauge. This would show that the ξ dependent parts do cancel in the sum. We shall not perform this technical proof here but rather leave it as a useful exercise to the interested reader, suggesting to follow the procedure illustrated in [43].

In conclusion, the total charge shift acquires the following expression:

$$\frac{\delta\alpha}{\alpha} = \frac{\alpha}{12\pi}\Delta\left[\frac{32}{3}N_f - 22\right] + \frac{\alpha}{12\pi}\left[-4\sum_F Q_F^2 \ln\frac{m_F^2}{\mu^2} + 15\ln\frac{m_W^2}{\mu^2}\right] . \tag{3.106}$$

The procedure to be followed from now on is at this point clear. In the theoretical expressions to be computed at one loop the *bare* Z, W masses $m_{Z,W}$ and the *bare* charge α_0 that enter the various Feynman rules will be replaced by the corresponding physical parameters and by the related 'shifts' defined by Eqs. (3.52), (3.57), and (3.106). The infinities and the scale dependence thus introduced will have to cancel those produced by the ultraviolet divergences of the one-loop integrals that are involved in the expressions of the physical observables, leaving in all cases a finite scale independent result expressed in terms of only physical parameters. The next part of this Chapter will be devoted to some numerical illustrations of the procedure. But before entering this sector, we shall briefly introduce a subject that will turn out to be extremely useful in the following, i.e. that of *effective* or 'running' QED coupling in the MSM.

3.1.7 *The 'running' of α_{QED} in the MSM*

We shall now very briefly review, for the limited purpose of this book, the concept of *running* coupling, that appears in the so-called *Renormalization Group* (RG) approach, whose main details can be found elsewhere [44].

In this Subsection we shall show how the general features discussed in that Chapter can be more concretely exhibited, with a simple calculation

that exploits those made in the previous Subsection, considering the specific case of the electromagnetic charge.

With this purpose we notice that, in the *renormalization scheme* that we have adopted, the electric charge (in fact, its square) has been defined choosing the scale $t = 0$. Introducing a scale variable p with mass dimension, we would say that

$$\alpha \equiv \alpha(p = 0) \; . \tag{3.107}$$

A priori, though, one could have given a different and quite respectable definition of the electric charge using a different scale $p_0 \neq 0$, obtaining a quantity to be called $\alpha(p_0)$. More generally, one can imagine that an infinite continuous set of definitions is possible, each one specified by a choice of scale p. Defining the dimensionless parameter

$$h = \ln p/p_0 \tag{3.108}$$

the *running* α in the RG approach will be the quantity (p_0 is supposed to be fixed)

$$\alpha^R(h; p_0) \equiv \alpha(p) \tag{3.109}$$

such that

$$\alpha(h = 0; p_0) \equiv \alpha(p_0) \; . \tag{3.110}$$

This *running* coupling will satisfy the RG equation [44]:

$$\frac{d}{dh}\alpha^R(h; p_0) = \beta(\alpha^R) \; . \tag{3.111}$$

The connection between the running α, that may be supposed to correspond in any case to an acceptable definition (leading to a finite value) and the *bare* quantity α_0 is usually written in the form

$$\alpha^R(h; p_0) \equiv \alpha(p) = Z_2\alpha_0 \; . \tag{3.112}$$

The quantity Z_2 is a (generally infinite) number. If its numerical calculation were performed using a cutoff Λ for the (divergent) integration in the virtual four-momentum that usually appears (consider e.g. (3.68)), it would contain typically logarithmic terms $\sim \ln \Lambda$. Being adimensional, it will also necessarily only depend on Λ/p (and on the fixed bare α_0). Thus we shall write:

$$\alpha(p) = Z_2\left(\frac{\Lambda}{p}; \alpha_0\right)\alpha_0 \; . \tag{3.113}$$

In our treatment, strictly limited at the one loop level, dimensional regularization has been used and infinities are expressed via the parameter Δ.

Without entering the proof of this statement, we shall simply enunciate here that the following formal correspondence exists between the two approaches:

$$\Delta \Rightarrow 2 \ln \frac{\Lambda}{p} \, . \tag{3.114}$$

We can now compute the β function at one loop using a rather simplified approach. With this aim, we start from the obvious remark that the bare parameter α_0 is p-independent, and write:

$$0 = \frac{d\alpha_0}{dp} = \frac{d}{dp}\left[\frac{\alpha(p)}{Z_2}\right] = \frac{1}{Z_2}\frac{d\alpha(p)}{dp} - \frac{\alpha(p)}{(Z_2)^2}\frac{dZ_2}{dp} \, . \tag{3.115}$$

This can be rewritten as:

$$\frac{d\alpha(p)}{dp} = \alpha(p)\frac{d}{dp}\ln Z_2 = \alpha(p)\left[\frac{d}{d\left(\ln\frac{\Lambda}{p}\right)}\ln Z_2\right]\left(-\frac{1}{p}\right) \, . \tag{3.116}$$

Introducing the adimensional variable h Eq. (3.108) finally gives ($p\frac{d}{dp} \equiv \frac{d}{dh}$):

$$\frac{d}{dh}\alpha^R(h;p_0) = \left[-\frac{d}{d\left(\ln\frac{\Lambda}{p}\right)}\ln Z_2\right]\alpha^R(h;p_0) \tag{3.117}$$

which is the RG Eq. (3.111) with:

$$\beta(\alpha^R) = \left[-\frac{d}{d\left(\ln\frac{\Lambda}{p}\right)}\ln Z_2\right]\alpha^R \, . \tag{3.118}$$

To compute the β function, one must therefore isolate the coefficient of the logarithmically divergent term $\sim \ln\Lambda$ in Z_2. Since, intuitively, this term will be the same for every choice of the scale p, one can compute it in the limiting case $p = 0$, which corresponds to the case that we have discussed in this Chapter. That means that one can write, for what concerns the divergent term:

$$\alpha \equiv \alpha(0) \equiv Z_2(p=0)\alpha_0 = \alpha_0\left[1 - \frac{\delta\alpha}{\alpha}\right] = \alpha_0\left[1 - \left(\frac{\delta\alpha}{\alpha}\right)^{(f)} - \left(\frac{\delta\alpha}{\alpha}\right)^{(Nf)}\right] \tag{3.119}$$

having used Eqs. (3.96), (3.99) and the usual one-loop approximations. Forgetting for the moment dimensional rigor, we can write for the infinite components:

$$Z_2^{(\infty)}(p=0) = \left[1 - \frac{\delta\alpha}{\alpha}\right]^{(\infty)} \tag{3.120}$$

and, formally $(\ln(1-\epsilon) \simeq -\epsilon \cdots)$

$$\ln Z_2^{(\infty)}(p=0) = -\left[\frac{\delta\alpha}{\alpha}\right]^{(\infty)} \simeq -\frac{\alpha}{6\pi}\ln\Lambda\left[\frac{32}{3}N_f - 22\right] \tag{3.121}$$

where the formal correspondence Eq. (3.114) has been used in Eq. (3.106). Generalization to the $p \neq 0$ case then gives:

$$\beta(\alpha^R) = \left[-\frac{d}{d\left(\ln\frac{\Lambda}{p}\right)}\ln Z_2(p\neq 0)\right]\alpha^R = \frac{\alpha^R}{6\pi}\left[\frac{32}{3}N_f - 22\right] \quad (\alpha^R \equiv \alpha(p))\ . \tag{3.122}$$

Using Eq. (3.122), the *RG* Eq. (3.111) can be solved obtaining the solution:

$$\alpha^R(h;p_0) = \frac{\alpha(p_0)}{1 - \left[\frac{1}{12\pi}\left(\frac{32}{3}N_f - 21\right)\ln\frac{p^2}{p_0^2}\right]\alpha(p_0)}\ . \tag{3.123}$$

Equation (3.123) gives the *RG* 'running' of α in the MSM. It deserves a number of remarks, that we shall now expose in a very concise way. More precisely:

a) The expression of the β function Eq. (3.122) can be separated into two distinct pieces. The first one $\sim N_f$ is due to the fermion pairs contribution. This is essentially the same that one would have in a purely QED theory. As one notices, it is *positive*. The corresponding expression of the β function does *not* lead therefore to an *asymptotically free* behaviour in the RG approach. Since QED has a Abelian U(1) symmetry, this is perfectly in agreement with what one expects [18]. Also, the second contribution to Eq. (3.122) is *negative*, and would lead (if it were the only term) to an *asymptotically free* behaviour. We have shown that this contribution is exactly that coming from the triple γWW gauge couplings, where the *non Abelian* features of the MSM show up. One expects therefore [18] that is produces a negative effect in the β function, as it does.

b) In the MSM, the overall sign of the β function Eq. (3.122), with $N_f = 3$, is positive. Thus α^R will *increase* with increasing p. This will have very interesting consequences in a more advanced approach based on the concept of *Grand Unification* [46].

c) The quantity that multiplies $\alpha(p_0)$ in the denominator of Eq. (3.123) is the product of $(\ln(p^2/p_0^2))$ with the coefficient of $(\alpha\Delta)$ in the shift $(\delta\alpha/\alpha)$ Eq. (3.106).

d) It is convenient to define the following quantity:

$$\left[\frac{1}{12\pi}\left(\frac{32}{3}N_f - 22\right)\ln\frac{p^2}{p_0^2}\right]\alpha(p_0) \equiv \Delta\alpha^R(p, p_0)\ . \tag{3.124}$$

From Eq. (3.123) one derives the physical interpretation of the previous quantity. In fact:

$$\Delta\alpha^R(p, p_0) \equiv \frac{\alpha(p) - \alpha(p_0)}{\alpha(p)} \tag{3.125}$$

which represents the *relative* shift of the *running* α when one moves from the scale p_0 to the scale p.

e) In our previous treatment we have implicitly assumed that fermions are massless. In the particular case of choice $p = 0$ one must be more careful and treat correctly the mass terms, which remain the only residual scale in this situation. In other words, the Z_2 function will exhibit in this case logarithms of fermion masses that will remain in the final finite expressions, as we shall explicitly show.

Having defined the concept of RG-*running* α, we now introduce the relevant (for our discussion of Z physics) concept of *effective* α. The simplest way is that of considering the parametrization given in Eq. (3.91) for the *photonic* component of the scattering amplitude that becomes singular when $t \to 0$. To begin with, it is useful to retain only the (gauge invariant) fermion pairs contributions to the photon self-energy, which means to work in an essentially QED-type scheme. In this approximation we can write.

$$A^{(1)(I)(\gamma)(f)}(t) \equiv \frac{4\pi\alpha}{t}\frac{1}{1 + F^{(f)(\gamma)}(t) - F^{(f)(\gamma)}(0)} \tag{3.126}$$

having used Eqs. (3.96), (3.97) and having retained systematically at the one-loop level the fermionic components.

Equation (3.126) can be formally rewritten introducing an *effective* coupling that depends on the squared four-momentum that is involved in the virtual photon exchange Figs. 3.14(a),(b). We shall write symbolically:

$$A^{(1)(I)(\gamma)(F)}(t) \equiv \frac{4\pi}{t}\alpha(t) \tag{3.127}$$

where the *effective* coupling $\alpha(t)$ is defined as:

$$\alpha(t) = \frac{\alpha}{1 - [F^{(f)(\gamma)}(0) - F^{(f)(\gamma)}(t)]} \tag{3.128}$$

and $\alpha \equiv \alpha(0)$ is the physical coupling previously defined in this Chapter.

One notices immediately a formal analogy between the RG Eq. (3.123) satisfied by the RG-*running* $\alpha^R(p)$ and the *definition* Eq. (3.128). Following the interpretation given in Eqs. (3.124), (3.125) we argue immediately that it will be possible to introduce the quantity:

$$\Delta\alpha(t)^{(f)} \equiv F^{(f)(\gamma)}(0) - F^{(f)(\gamma)}(t) = \frac{\alpha(t) - \alpha(0)}{\alpha(t)} \tag{3.129}$$

that will represent the fermion pairs contribution to the *relative* shift of the *effective* squared charge from its physical value at the four-momentum square t that is being considered.

It should be stressed that the relative shift Eq. (3.129) is *not* the RG relative shift Eq. (3.125). There exists, though, an important analogy with the RG treatment. To make evident this similarity, it is sufficient to consider the change of the effective α when moving to the four momentum square t from an arbitrary (different from zero) value t_0. Within the usual one-loop approximations, one easily sees from Eq. (3.128) that

$$\alpha(t) = \frac{\alpha(t_0)}{1 - \Delta^{(f)}\alpha(t, t_0)} \tag{3.130}$$

where $\Delta^{(f)}\alpha(t, t_0) \equiv F^{(f)(\gamma)}(t_0) - F^{(f)(\gamma)}(t)$ is the analogue of the RG shift Eq. (3.124). In the limit of *large* t, for $t_0 \gg m_F^2$, its expression can be simply computed from Eq. (3.68), obtaining:

$$\alpha(t) \longrightarrow \frac{\alpha(t_0)}{1 - \left[\frac{1}{12\pi}\left(\frac{32}{3}N_f\right)\ln\frac{t}{t_0}\right]\alpha} \tag{3.131}$$

where (usual one-loop situation) one can set $\alpha = \alpha(t_0)$ in the denominator. Thus, in other words, the asymptotic behaviour of the *effective* coupling Eq. (3.128) is *exactly* that predicted by the corresponding *purely fermionic* sector of the RG approach, Eq. (3.123). For this reason one often identifies the *effective* α with the *running* one, in the QED-like fermionic approximation. But when bosonic components to Eq. (3.123) are considered, the definition of an *effective* coupling, that has the same asymptotic behaviour as the RG one, becomes more involved, since problems of gauge independence must be carefully solved. We shall return on this point later on, at the end of this Chapter. For the moment we conclude this discussion with the definition of the effective coupling Eq. (3.128). This will turn out to be of fundamental importance in the next Section 3.2, where the treatment of e^+e^- collisions of Z resonance will be finally given in full details. The starting point will be the *operative* definitions of the three physical parameters m_Z, m_W, α that have been given in this pedagogical Section 3.1.

3.2 Theoretical description of the Z physics observables at one loop in the MSM

3.2.1 *Choice of the most convenient input parameters: definition of the physical G_F*

From now on, we shall concentrate our analysis on the process of electron-positron annihilation *on top* of the Z resonance, i.e. at a c.m. energy $\sqrt{q^2} = m_Z$, treated at the one-loop level, and we shall try to illustrate a systematic procedure to derive theoretical predictions for all the measurable observables of the process. In the framework that we have discussed until now, we have at disposal at this point a *basic* input whose three parameters are the physical electric charge $\alpha(0)$, the physical Z mass m_Z and the analogous W quantity m_W. This starting set will appear in all the finite theoretical predictions at one loop , whose accuracy must be evidently ,at least, at the level of the experimental one.

Actually,the numerical values of these input parameters are by definition provided by their available experimental measurements. In particular, $\alpha(0)$ is determined nowadays with a relative precision of about 3×10^{-8}. The Z mass is assumed to be determined by looking at the so called *lineshape* of the Z resonance in the annihilation process; this will lead, as we shall see, to a relative precision of about 2×10^{-5}.

The situation is certainly worse for what concerns the experimental value of m_W, for which at the beginning of LEP1, SLC operations the available relative precision was of about 2×10^{-3} (it is at the moment around 0.5×10^{-3}). The latter point raises an immediate and pragmatically unavoidable theoretical problem: in fact, the final (actually reached) experimental precision of LEP1 measurements of various observables was expected to be at the one permil level. As a consequence of this remarkable experimental precision, the intrinsic error induced by the use of m_W as input parameter for the theoretical predictions was evidently too dangerously large. Fortunately, this problem can be avoided by resorting to a celebrated formula generally known as Sirlin's equation [38], that allows to replace, in the theoretical predictions, m_W by the Fermi coupling G_F defined to lowest order by Eq. (1.24). Since the relative experimental accuracy on G_F is of about 9×10^{-6}, the replacement is fully satisfactory for what concerns Z resonance physics. Given the fundamental consequences of Sirlin's equation, we shall now devote the rest of this Chapter to a fairly detailed derivation of its mains relevant features.

Our starting point will be a clean definition of the *physical* parameter to be associated with the *bare* quantity defined, strictly speaking, by Eq. (1.24). Following the discussion that was given immediately after that equation, we shall now rewrite it in the more appropriate way as:

$$\frac{G_F^{(0)}}{\sqrt{2}} = \frac{g_0^2}{8m_W^2} = \frac{e_0^2}{8m_W^2 \sin^2\theta_W} = \frac{e_0^2}{8m_W^2} \frac{1}{(1-\frac{m_W^2}{m_Z^2})} \tag{3.132}$$

where we have used the property that in the MSM $\cos^2\theta_W = \sin^2\theta_W \equiv m_W^2/m_Z^2$ Eq. (1.85).

Note that Eq. (3.132) is clearly an equality between *bare* parameters. To transform it into a meaningful relationship between measurable quantities, we have to define a *physical* parameter G_F that generalizes the *bare* l.h.s of Eq. (3.132). This is *conventionally* done by relating G_F to the muon lifetime τ_μ, *measured* in the weak decay $\mu \to e + \nu_\mu + \bar{\nu}_e$, by means of Eq. (1.13):

$$G_F \equiv \left\{ \left[\frac{1}{\tau_\mu}\right] \frac{192\pi^3}{m_\mu^5} \left[F\left(\frac{m_e^2}{m_\mu^2}\right)\right]^{-1} [1+\Delta Q]^{-1} \right\}^{\frac{1}{2}} \tag{3.133}$$

where ΔQ is a pure QED correction that takes into account the *muon and electron* photon vertex effects, calculable (and finite) in this particular case, whose expression at one-loop reads [45]:

$$\Delta Q^{O(\alpha)} = \alpha/2\pi[1 + 2\alpha/3\pi \ln m_\mu/m_e][25/4 - \pi^2] \,. \tag{3.134}$$

The complete QED two-loop correction can be found in Ref. [15].

In the MSM, it is possible to compute the muon lifetime τ_μ in a conventional way, i.e. upon integration on the final four-momenta of a quantity proportional to the squared modulus of the invariant decay amplitude $A_\mu \to e\nu\bar{\nu}$.

To proceed in strict analogy with the approach developed in Subsection 3.1.6, we shall introduce the *tree level* decay amplitude $A^{(0)}_{\mu\to e\nu_\mu\bar{\nu}_e}$, related to the Feynman diagram shown in Fig. 3.15. Following the notations of Eq. (3.80) we shall write:

$$\begin{aligned} & A^{(0)}_{\mu\to e\nu_\mu\bar{\nu}_e}(q^2) \\ &= -\left[i\bar{u}(\nu_\mu)\gamma_\mu(1-\gamma_5)u(\mu)\bar{u}(\nu_e)\gamma^\mu(1-\gamma_5)u(e)\right]\left[\frac{g_0^2}{8\,(m_W^2-q^2)}\right] \\ &= -\left[A^{(0)(E)(W)}\right]\left[A^{(0)(I)(W)}\left(q^2\right)\right] \end{aligned} \tag{3.135}$$

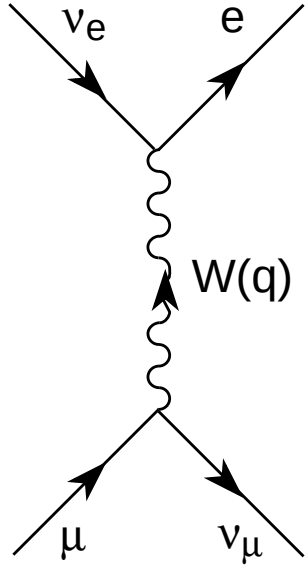

Fig. 3.15 Feynman diagram associated to the decay $\mu \to \nu_\mu e \bar{\nu}_e$ to lowest order in the MSM.

where the two quantities represent the external (E) and internal (I) structure of Fig. 3.15, and

$$A^{(0)(I)(W)}\left(q^2\right) = \frac{-g_0^2}{8\left(q^2 - m_W^2\right)} \,. \tag{3.136}$$

Note the choice of sign in $A^{(0)(I)(W)}(q^2)$, that corresponds to the overall *minus one* factorised in Eq. (3.135). This is formally due to the conventional definition of the Fermi Lagrangian, that reads for leptons:

$$L_F = -\frac{G_F^{(0)}}{\sqrt{2}}[J^+_{\lambda,\ell} J^{\lambda,\ell} + h.c.] \tag{3.137}$$

where

$$J_{\lambda,\ell} = \bar{\psi}_{\nu e}\gamma_\lambda(1-\gamma_5)\psi_e + (\mu,\tau) \tag{3.138}$$

Equating Eq. (3.135) to the corresponding expression obtained in the Fermi formulation for the muon decay amplitude leads then to the correspondence

$$\frac{G_F^{(0)}}{\sqrt{2}} = A^{(0)(I)(W)}(q^2=0)\left(\equiv \frac{g_0^2}{8m_W^2}\right) \tag{3.139}$$

having neglected the involved lepton masses as usually.

It is now relatively easy to realize that the tree level definition of G_F Eq. (3.139) is identical, at the same lowest perturbative order, with the *operative* definition via the muon lifetime expressed by Eq. (3.133). This can be qualitatively understood by rewriting that equation in a less rigorous way, i.e.:

$$G_F^2 \sim \frac{1}{\tau_\mu} \sim \sum |A_{\mu \to e\nu\bar{\nu}}|^2 \tag{3.140}$$

where the sum includes the standard operations (spin average, momentum integration...) that now essentially affect the *external* amplitude component, so that the final result relates G_F to the *internal* component as shown by Eq. (3.139). Of course, the rigorous derivation can be performed, but it will be omitted at this stage.

Having accepted the equality of the operative definition Eq. (3.133) and of Eq. (3.139) at tree level, it becomes now reasonably simple to generalize both expressions at the next one loop order. We shall proceed by steps, trying to stress as much as possible a number of analogies with the previous approach that we have used to derive the expression of the physical charge.

For what concerns the operative definition of the *physical* G_F, Eq. (3.133) can be used at any order of perturbation theory. Once again one sees that the definition of a physical quantity involves a measurement of a well defined physical process. In the case of G_F, this is a decay rather than a cross section, which represents the difference with respect to the cases of the Z, W masses and of the electric charge. For what concerns the involved squared four-momentum, this will be equal to the squared muon mass, that we shall assume to be equal to zero, consistently with our overall approach.

Having defined both the *physical* G_F via Eq. (3.133) and the *bare* one via Eq. (3.139), we shall now write in full generality, as we did when we wrote Eq. (3.96):

$$G_F^{(0)} = G_F + \delta G_F = G_F \left[1 + \frac{\delta G_F}{G_F} \right] . \tag{3.141}$$

To provide the theoretical expression of the *shift* δG_F, we shall work as usually at the one loop level. In this approximation, the calculation of δG_F will be then performed by adding a number of Feynman diagrams to the simplest tree level one of Fig. 3.15, to obtain the value of the muon lifetime in the MSM. Some of these diagrams are listed in Fig. 3.16, to make the previous statement more quantitative.

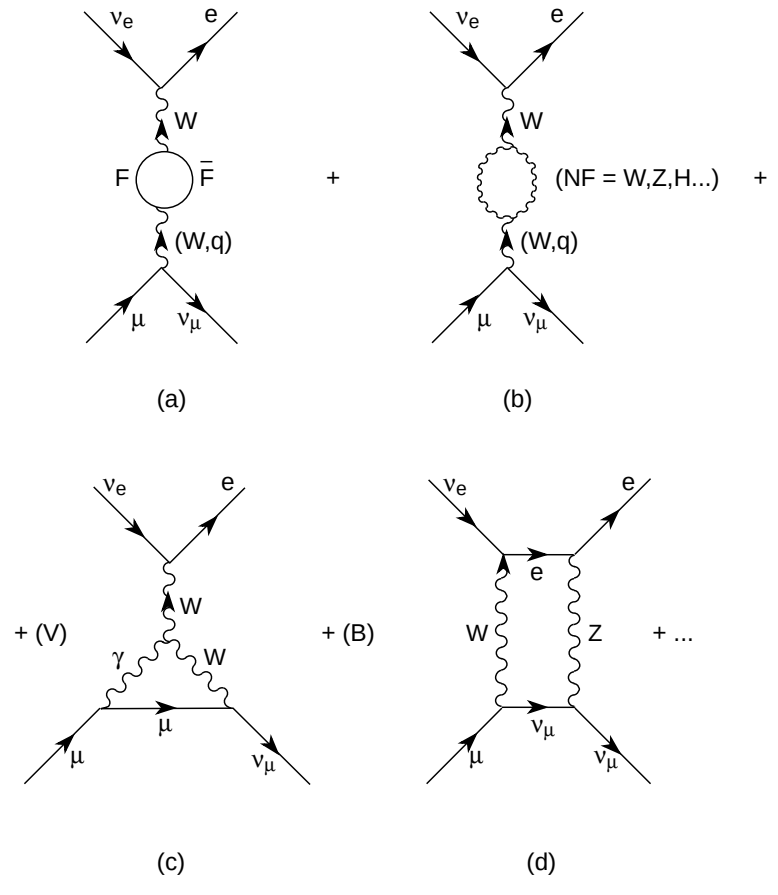

Fig. 3.16 examples of Feynman diagrams contributing the muon decay at one loop in the MSM.

In full generality, we shall therefore write an expression for the shift δG_F that corresponds to four separate kinds of Feynman diagrams, and reads:

$$\delta G_F = \delta G_F^{(f)} + \left[\delta G_F^{(Nf)} + \delta G_F^{(V)} + \delta G_F^{(B)}\right] \tag{3.142}$$

where the first term on the r.h.s. is due to the set of fermion pairs contributions to the W self-energy (Fig. 3.16(a)). The three remaining ones correspond to self-energy diagrams with non fermionic pairs (Fig. 3.17(b)), to Vertex diagrams (like Fig. 3.16(c)) and to Box diagrams (like Fig. 3.16(d)), and of course all relevant diagrams should be included in Fig. 3.16. Note

that we have grouped the last three terms in a single bracket. The reason is that only their *sum* is gauge independent, and therefore these contributions must be computed together (we shall return on this point, that can be qualitatively understood from our previous discussions, at the end of this Chapter). On the contrary, the fermion self-energy contribution is separately gauge-independent. Since its calculation is relatively easy, and quite similar to that of the corresponding part of the charge shift, we shall now concentrate our attention on its explicit derivation.

Let us assume therefore, for an initial approximate approach, that one loop contributions not due to fermion pairs can be safely ignored (*turned off*). In this "fermion pairs self-energy dominance" spirit, the only difference between the descriptions of the muon decay at tree level and at one loop comes from the first diagram (a) of Fig. 3.16. Since its contribution to the scattering amplitude is only affecting the internal component Eq. (3.136) [and is only dependent on q^2, unlike the box diagram of Fig. 3.16(d)], the shift $\delta G_F^{(f)}$ will be very simply obtained by computing the approximate theoretical value that the physical G_F would acquire in this approximation.

If we denote by $A^{(1)(I)(F)}(q^2)$ the expression that the internal component of the decay amplitude (Eqs. (3.135), (3.136) at tree level) would acquire at one loop owing to Fig. 3.16(a), and $G_F^{(f)}$ the corresponding approximate *theoretical* expression of the physical G_F, it is now understandable that the two quantities will be related by an equality that is the immediate generalization of Eq. (3.139), i.e.:

$$\frac{G_F^{(f)}}{\sqrt{2}} = A^{(1)(I)(f)}(q^2 = 0) \tag{3.143}$$

(the external component of the scattering amplitude remains unchanged).

By a straightforward application of the rules that we have illustrated e.g. with Eq. (3.49) we can now conclude that:

$$G_F^{(f)} = \frac{-g_0^2}{8[q^2 + A^{(W)(f)}(q^2) - m^2_{W(0)}]_{q^2=0}} = \frac{+g_0^2}{8[m^2_{W(0)} - ReA^{(W)(Ff}(0)]} \tag{3.144}$$

where $A^{(W)(f}(q^2)$ is the fermion-pairs component of the W transverse self-energy Eq. (3.58), that is purely real at $q^2 = 0$.

Equation (3.144) can be rewritten at one loop in the equivalent way:

$$G_F^{(f)} = \frac{g_0^2}{8m^2_{W(0)}\left[1 - \frac{ReA^{(W)(f)}(0)}{m^2_{W(0)}}\right]} = \frac{G_F^{(0)}}{\left[1 - \frac{ReA^{(W)(f)}(0)}{m^2_W}\right]}$$

$$= G_F^{(0)} \left[1 + \frac{ReA^{(W)(f)}(0)}{m_W^2} \right] \tag{3.145}$$

where the bare W mass $m_{W(0)}$ has been replaced by the physical one m_W in the denominator $ReA^{(W)(f)}(0)/m_W^2$ (this is formally valid in the usual one loop approximations).

From Eq. (3.145) we can finally derive the approximate shift as:

$$G_F^{(0)} - G_F^{(f)} \equiv \delta G_F^{(f)} = -G_F^{(f)} \frac{ReA^{(W)(f)}(0)}{m_W^2} \,. \tag{3.146}$$

In our usual one-loop approximation the difference between the complete theoretical expression of G_F and that obtained in the fermion-pairs contribution approximation is (formally) of $0(\alpha)$ like $A^{(W)}(0)$, which allows us finally to conclude that:

$$\delta G_F^{(f)} = -G_F Re \frac{A^{(W)(f)}(0)}{m_W^2} \,. \tag{3.147}$$

Combining this equation with Eqs. (3.141), (3.142) leads to the expression that will be used in the following, i.e.:

$$\begin{aligned} G_F^{(0)} &= G_F \left[1 + \frac{\delta G_F^{(f)}}{G_F} + \frac{\delta G_F^{(Nf,V,B)}}{G_F} \right] \\ &= G_F \left[1 - \frac{ReA^{(W)(f)}(0)}{m_W^2} + \frac{\Delta G_F^{(Nf,V,B)}}{G_F} \right] \end{aligned} \tag{3.148}$$

where the last term corresponds to all the effects that are not fermion pairs contributions the W self-energy.

Equation (3.148) is the analogue of Eqs. (3.96), (3.97), (3.100) that relate the bare and the physical charge. In particular, one finds from Eq. (3.147) the (familiar) correspondence:

$$\frac{\delta G_F^{(f)}}{G_F} = -Re \frac{A^{(W)(f)}(0)}{m_W^2} \tag{3.149}$$

which appears a generalization of Eq. (3.100).

An important comment at this point is that, within the one-loop approximation to which we shall stick, we have to retain the convention that the definition of G_F Eq. (3.133) is by assumption freed from the photonic QED muon and electron vertex effects. This means that, when computing the decay amplitude $A^{(1)}_{\mu \to e\nu\bar{\nu}}$ from the Feynman diagrams partially depicted in Fig. 3.15, those corresponding to the aforementioned effects should *not* be included in the summation.

We have now concluded the discussion of all the *operative* definitions of physical parameters that will be needed to develop the theoretical description of physics on Z resonance. In the forthcoming Subsection 3.2.2 we shall begin to illustrate the practical procedure that is followed. As anticipated in the initial part of this Chapter, we shall proceed first of all to the replacement of the physical input parameter m_W by the physical input parameter G_F, deriving the formula that is generally known as Sirlin's equation.

3.2.2 *Derivation of Sirlin's equation: introduction and definition of the fundamental parameter* Δr

At tree level, the possibility of replacing the bare W mass, $m_{W(0)}$, with a combination of the bare parameters $m_{Z(0)}, e_0, G_F^{(0)}$ is an immediate consequence of the fundamental equality Eq. (3.132). To transform this equality into one for the corresponding physical quantities is relatively simple after the discussions of this Chapter. With this purpose, one can simply rewrite Eq. (3.132) using physical parameters and "shifts". Proceeding step by step, we begin by writing:

$$\frac{G_F^{(0)}}{\sqrt{2}} \equiv \frac{G_F}{\sqrt{2}}\left[1+\frac{\delta G_F}{G_F}\right] = \frac{4\pi\alpha_0}{8m_{W(0)}^2\left(1-\frac{m_{W(0)}^2}{m_{Z(0)}^2}\right)}$$
$$= \frac{\pi\alpha}{2m_{W(0)}^2(1-m_{W(0)}^2/m_{Z(0)}^2)}\left[1+\frac{\delta\alpha}{\alpha}\right] (\alpha_0 \equiv 4\pi e_0^2)\ . \quad (3.150)$$

To eliminate the bare W, Z masses that enter Eq. (3.150) one uses Eqs. (3.56), (3.57) for $m_{W(0)}^2$; for $m_{W(0)}^2/m_{Z(0)}^2$ one writes:

$$1-\frac{m_{W(0)}^2}{m_{Z(0)}^2} \equiv 1-\frac{m_W^2+\delta m_W^2}{m_Z^2+\delta m_Z^2} = (\text{at one loop})$$
$$= 1-\frac{m_W^2}{m_Z^2}\left(1+\frac{\delta m_W^2}{m_W^2}-\frac{\delta m_Z^2}{m_Z^2}\right)$$
$$= 1-\frac{m_W^2}{m_Z^2}\left(1+\frac{ReA^{(W)}(m_W^2)}{m_W^2}-\frac{ReA^{(Z)}(m_Z^2)}{m_Z^2}\right). \quad (3.151)$$

The previous equation can be identically rewritten in a more useful way, that is:

$$\left[1-\frac{m_{W(0)}^2}{m_{Z(0)}^2}\right] = \left[1-\frac{m_W^2}{m_Z^2}\right] - \frac{m_W^2}{m_Z^2}\left[\frac{ReA^{(W)}(m_W^2)}{m_W^2}-\frac{ReA^{(Z)}(m_Z^2)}{m_Z^2}\right]\ . \quad (3.152)$$

This corresponds to the following renormalization prescription of the bare parameter $\sin^2\theta_W = 1 - m_W^2/m_Z^2$ (Eq. (1.85))

$$\sin^2\theta_W = \left(1 - \frac{m_W^2}{m_Z^2}\right) + \delta^{(W,Z)}\sin^2\theta_W \tag{3.153}$$

where the quantity $\delta^{(W,Z)}\sin^2\theta_W$ is defined as

$$\delta^{(W,Z)}\sin^2\theta_W = -\frac{m_W^2}{m_Z^2}\left[\frac{ReA^{(W)}(m_W^2)}{m_W^2} - \frac{ReA^{(Z)}(m_Z^2)}{m_Z^2}\right] \tag{3.154}$$

which is formally of $O(\alpha_0)$ and, as one can easily verify from our previous Eq. (3.55), Eq. (3.61), infinite.

Combining the previous formulae within the usual one loop approximations we are led to the following expression:

$$\frac{G_F}{\sqrt{2}} = \frac{\pi\alpha}{2m_W^2(1 - m_W^2/m_Z^2)}[1 + \Delta r] \tag{3.155}$$

where

$$\Delta r = \left[\frac{\delta\alpha}{\alpha} - \frac{\delta G_F}{G_F} - \frac{ReA^{(W)}(m_W^2)}{m_W^2} + \frac{m_W^2}{m_Z^2\left(1 - \frac{m_W^2}{m_Z^2}\right)}\right.$$
$$\left.\times\ Re\left(\frac{A^{(W)}(m_W^2)}{m_W^2} - \frac{A^{(Z)}(m_Z^2)}{m_Z^2}\right)\right]. \tag{3.156}$$

Equation (3.155) is the one-loop modification of Eq. (3.132) and is commonly known as Sirlin's equation. It relates the four *physical* quantities m_W, G_F, m_Z, α operatively defined in the previous part of this Chapter, and involves a one-loop electroweak correction called Δr. Clearly, it can be used to eliminate, if so wished, one of the four quantities (for instance, m_W) in terms of the three remaining ones *and* of Δr. Given the fundamental rôle that Eq. (3.155) will play in the following part of this Chapter, we shall make a couple of comments that are appropriate at this stage.

The first comment is that Eq. (3.155) relates four *physical* parameters i.e. G_F, m_W, m_Z, α. These must be, obviously, both *finite* and *gauge-independent*. As a consequence, the same two properties will necessarily be valid for the one-loop parameter Δr. We shall verify, at least partially, this important statement in the following part of this Chapter.

The second comment is that Δr, as defined by Eq. (3.156), is a mixture of effects that might be called of *conventional QED* type (like e.g. the fermion pairs contribution to the electric charge shift $\delta\alpha$) and of effects that might be called of *genuinely weak* type (like e.g. all those involving

W, Z exchanges). Intuitively, the second, weak component, will be sensitive to the deep theoretical features of the MSM, like the properties of the Higgs, or the mass of the top quark, as we shall explicitly show. Thus, a clean separation between the *conventional* and the *genuine* component of Δr will be useful, and will be shown in detail in what follows.

To illustrate the previous statements with a concrete example, we shall first proceed to compute the component of Δr that is only due to the existence of fermion pairs self-energy one-loop effects. Clearly, this component is by construction gauge-independent. We shall now show that it is finite, although the various terms that appear in the definition Eq. (3.156) are, separately, infinite.

Following our notational convention, we shall call $\Delta r^{(f)}$ this component, that will be given by the following expression:

$$\begin{aligned}\Delta r^{(f)} &= \left[\frac{\delta\alpha^{(f)}}{\alpha} - \frac{\delta G_F^{(f)}}{G_F} - \frac{Re A^{(f)(W)}(m_W^2)}{m_W^2}\right. \\ &+ \left.\frac{m_W^2}{m_Z^2(1-m_W^2/m_Z^2)} Re\left(\frac{A^{(f)(W)}(m_W^2)}{m_W^2} - \frac{A^{(f)(Z)}(m_Z^2)}{m_Z^2}\right)\right] \\ &= \left[F^{(f)(\gamma)}(0) + \frac{A^{(f)(W)}(0)}{m_W^2} - Re\frac{A^{(f)(W)}(m_W^2)}{m_W^2}\right. \\ &+ \left.\frac{m_W^2}{m_Z^2\left(1-\frac{m_W^2}{m_Z^2}\right)} Re\left(\frac{A^{(f)(W)}(m_W^2)}{m_W^2} - \frac{A^{(f)(Z)}(m_Z^2)}{m_Z^2}\right)\right]\end{aligned} \tag{3.157}$$

having used Eqs. (3.100), (3.149) ($A^{(W)}(q^2)$ is real, as one can easily guess, at $q^2 = 0$) and having defined, in analogy with the remaining cases, $A^{(f)(Z)}(q^2)$ as the fermion pairs component of the Z self-energy.

We shall now show that the r.h.s. of Eq. (3.157) is *finite*. With this aim, we shall explicitly compute the separate contributions that appear in the square bracket on its r.h.s. Using Eqs. (3.55), (3.61) and (3.68), it will be sufficient to compute the overall effect for one single fermion family, since the procedure will be identical for each additional family to be considered. Also, we must consider lepton and quark contributions separately. Denoting

by (e,ν_e) and (u,d) these general terms, we find for the lepton component:

$$\Delta_r^{(e,\nu_e)(\infty)} = \Delta\left[\frac{e_0^2}{12\pi^2} - \frac{1}{m_W^2}\left(\frac{e_0^2}{16\pi^2\sin^2\ theta_W}\right)\frac{m_W^2}{3}\right.$$
$$+\frac{m_W^2/m_Z^2}{1-\frac{m_W^2}{m_Z^2}}\left(\frac{e_0^2}{16\pi^2\sin^2\theta_W\cos^2\theta_W}\right)\left(\frac{1}{3}-\frac{m_e^2}{2m_W^2}\right)$$
$$-\frac{m_W^2/m_Z^2}{1-\frac{m_W^2}{m_Z^2}}\left(\frac{e_0^2}{16\pi^2\sin^2\theta_W\cos^2\theta_W}\right)$$
$$\left.\times\left(\frac{1}{3}(g_{Ve}^{(0)2}+g_{Ae}^{(0)2}+g_{V\nu_e}^{(0)2}+g_{A\nu e}^{(0)2})-\frac{m_e^2}{2m_Z^2}\right)\right] \tag{3.158}$$

where Δ is defined by Eq. (3.36).

To proceed with the calculation, one uses again the fact that, within a one-loop approximation like the one that we are adopting, the physical quantities $(1-m_W^2/m_Z^2), m_W^2/m_Z^2$ can be identified, *inside* one-loop corrections, with the bare parameters $\sin^2\theta_W, \cos^2\theta_W$. This is due to the presence of the overall multiplicative factor e_0^2 appearing in Eq. (3.13), that makes the difference between physical and bare parameters to be of order e_0^4, and therefore not contributing at this one-loop order. Then it is easy to verify that the square bracket of Eq. (3.158), containing the charged and neutral lepton contribution to the photon, W and Z self-energies, is actually *vanishing* when one uses the expressions of the Z vector and axial vector couplings to e and ν_e defined by Eqs. (3.11) and (3.12). Note that, contrary to what will be systematically done for the *finite* component of Δr, the values of the relevant fermion masses have not been equated to zero, since they appear now as coefficients of infinite terms, and a mutual cancellation between the various different masses must be systematically verified. In Eq. (3.158) this is easily checked, since the term proportional to m_e^2 contains the difference

$$e_0^2\left(\frac{1}{m_W^2}-\frac{1}{\cos^2\theta_W m_Z^2}\right) = e_0^2\left(\frac{1}{m_W^2}-\frac{1}{\frac{m_W^2}{m_Z^2}m_Z^2}\right)+0(e_0^4) = 0(e_0^4)$$

i.e. it vanishes at one loop. Analogous procedures then lead to the cancellation of the terms that are m_e^2 independent, and to the conclusion that, as one should expect, the considered component of Δr is indeed finite. The same result can be obtained in a rather straightforward way for the (u,d) quark contribution, by computing its infinite part and checking that the coefficient of Δ is, again, vanishing. We leave this as an exercise to the interested reader.

Having verified the finiteness of the quantity $\Delta r^{(f)}$ that appears in Eq. (3.157), the next important step is now that of computing the meaningful finite component. This will be done in some detail in the following part of this Chapter.

3.2.3 *Calculation of $\Delta r^{(f)}$: identification of four classes of physical effects*

To proceed with the calculation, it is convenient to rewrite, using Eq. (3.65), the expression for $\Delta r^{(f)}$ Eq. (3.157) in the following equivalent form:

$$\Delta r^{(f)} = Re\left\{ F^{(\gamma)}_{(0)} - \frac{m_W^2/m_Z^2}{(1-m_W^2/m_Z^2)}\left[\frac{A^{(Z)}(0)}{m_Z^2} - \frac{A^{(W)}(0)}{m_W^2}\right] \times \frac{+(2m_W^2/m_Z^2-1)}{(1-m_W^2/m_Z^2)}F^{(W)}(m_W^2) - \frac{m_W^2/m_Z^2}{(1-m_W^2/m_Z^2)}F^{(Z)}(m_Z^2)\right\}^{(f)} . \tag{3.159}$$

A first impression that one derives from a glance to the previous equation is that several terms of different physical origin appear and contribute, as one would naively guess. In fact, the considered process to which our procedure has been applied is of typical *electroweak* nature. As a consequence, one expects to be able to identify both *genuinely* QED and *genuinely* weak features and effects. This feeling is certainly correct, but Eq. (3.159) does not fully exhibit in the most evident way this property. To get a better understanding of the previous statement, some formal reshuffling of the equation is very useful. In particular, it is convenient to reintroduce the (unphysical) $W_\mu^{(3)}$ gauge boson, defined as in Eq. (1.84) in terms of the physical Z and photon.

$$W_\mu^{(3)} = \cos\theta_W Z_\mu + \sin\theta_W A_\mu \tag{3.160}$$

and its transverse self-energy $A^{(3)}(q^2)$, defined in complete analogy with the corresponding $Z, \gamma, Z\gamma$ ones and formally identical to:

$$A^{(3)}(q^2) \equiv \cos^2\theta_W A^{(Z)}(q^2) + \sin^2\theta_W A^{(\gamma)}(q^2) + 2\sin\theta_W\cos\theta_W A^{(Z\gamma)}(q^2) \tag{3.161}$$

where the mixed $Z-\gamma$ self-energy $A^{(Z\gamma)}(q^2)$ in the lepton pair case can be immediately obtained from Eq. (3.25), by a simple replacement of one Z-fermion vertex

$$\left(\frac{i|e_0|}{2\sin\theta_W\cos\theta_W}[\gamma_\nu g_{Ve}^{(0)} - \gamma_\nu\gamma_5 g_{Ae}^{(0)}]\right)$$

with the corresponding $(-i|e_0|\gamma_\nu)$ photon one, retaining in the second Z-fermion vertex only the *vector* coupling $g_{Ve}^{(0)}$ (analogous straightforward rules lead to the expression of $A^{(Z\gamma)}(q^2)$ in the quark pair case).

Since both the photon self-energy $A^{(\gamma)}(q^2)$ and the $Z-\gamma$ self-energy $A^{(Z\gamma}(q^2)$ are vanishing at $q^2=0$ (only *fermion* pairs are considered), one sees that the second term in the curly bracket of the r.h.s of Eq. (3.159) can be written as

$$\begin{aligned}&\frac{-m_W^2/m_Z^2}{(1-m_W^2/m_Z^2)}\left[\frac{A^{(Z)}(0)}{m_Z^2}-\frac{A^{(W)}(0)}{m_W^2}\right]^{(f)}\\&=\frac{-m_W^2/m_Z^2}{(1-m_W^2/M_W^2)}\left[\frac{A^{(3)}(0)-A^{(W)}(0)}{m_W^2}\right]^{(f)}\end{aligned}\tag{3.162}$$

(at one loop)

$$\equiv\frac{-m_W^2/m_Z^2}{(1-m_W^2/m_Z^2}\Delta_1(0)$$

where we have introduced the notation

$$\Delta_1(0)=\left[\frac{A^{(3)}(0)-A^{(W)}(0)}{m_W^2}\right]^{(f)}\equiv\left[\frac{A^{(f)(Z)}(0)}{m_Z^2}-\frac{A^{(f)(W)}(0)}{m_W^2}\right]\ .\tag{3.163}$$

One easily verifies that the quantity $\Delta_1(0)$ defined by the previous equation is *finite*.

It is therefore quite natural to associate it to a well defined physical phenomenon, that will necessarily be related to effects that act differently within (self-energies of) the same $\mathrm{SU}(2)_L$ triplet (i.e. $A^{(3)}(0), A^{(W)}(0)$), in a way that is energy (i.e. q^2) independent. Remembering the discussion given in Subsection 1.4.3 about the so called ρ_0-parameter, one expects that $\Delta_1(0)$ will take into account *custodial SU(2) violating* effects, and for this reason one often finds in the literature the notation $\Delta\rho(0)$ for this term (since, however, a certain amount of different quantities is sometimes indicated by the same symbol $\Delta\rho$ by different authors, we prefer to retain our definition Eq. (3.161) in what follows, and whenever necessary we shall work out the relationships with other notations). As an immediate example of such a possible energy independent custodial SU(2) violating effect, we can think of the contribution to $\Delta_1(0)$ from a doublet of fermions of not vanishing and definitely different *mass*, like a bottom quark-top quark pair, that will be investigated in Subsection 3.2.5.

It is quite natural at this point to try to ensemble effects that might be formally related to custodial SU(2) violations that are energy *dependent*. An immediate possibility is that of adding and subtracting to $\Delta r^{(f)}$

Eq. (3.159) the term

$$\frac{(2m_W^2/m_Z^2-1)}{1-m_W^2/m_Z^2)}F^{(f)(3)}(m_Z^2)\ ,$$

with $F^{(3)}(q^2)$ defined bas in Eq. (3.65), and of defining the quantity

$$\begin{aligned}\Delta_2 &= Re[F^{(W)}(m_W^2)-F^{(3)}(m_Z^2)]^{(f)}\\ &\equiv Re\left[F^{(f)(W)}(m_W^2)-m_W^2/m_Z^2F^{(f)(Z)}(m_Z^2)-\left(1-\frac{m_W^2}{m_Z^2}\right)F^{(f)(\gamma)}(m_Z^2)\right.\\ &\qquad\left.-2m_W/m_Z\sqrt{1-m_W^2/m_Z^2}F^{(f)(Z\gamma)}(m_Z^2)\right]\ . \qquad (3.164)\end{aligned}$$

One easily verifies again that Δ_2 is finite. This supports the previous idea of relating it to physical effects, that we shall discuss in Subsection 3.2.5. Thus, Eq. (3.159) can be formally rewritten at this stage as:

$$\begin{aligned}\Delta r^{(f)} = Re\Bigg\{&F^{(f)(\gamma)}(0)-\frac{m_W^2/m_Z^2}{(1-m_W^2/m_Z^2)}\Delta_1(0)\\ &+\frac{(2m_W^2/m_Z^2-1)}{(1-m_W^2/m_Z^2)}\Delta_2+\frac{(2m_W^2/m_Z^2-1)}{(1-m_W^2/m_Z^2)}F^{(Ff(3)}(m_Z^2)\\ &-\frac{m_W^2/m_Z^2}{(1-m_W^2/m_Z^2)}F^{(f)(Z)}(m_Z^2)\Bigg\} \qquad (3.165)\end{aligned}$$

The last step of our process of separation of $\Delta r^{(f)}$ into "physically meaningful" components starts from the qualitative statement that the two first quantities that have been until now isolated, i.e. Δ_1 and Δ_2, describe the consequences of the fact that W_3 is *different* from the physical *charged bosons* W^+, W^-. One would naively expect that $\Delta r^{(f)}$ also contains a component that takes into account the extra fact that W_3 is *different* from the physical *photon*, to which it is related by Eq. (1.84). To make this statement more quantitative, it is sufficient to rewrite the first, fourth and fifth terms of Eq. (3.165) as follows:

$$\begin{aligned}&\left[F^{(\gamma)}(0)+\frac{(2m_W^2/m_Z^2-1)}{(1-m_W^2/m_Z^2)}F^{(3)}(m_Z^2)\frac{-m_W^2/m_Z^2}{(1-m_W^2/m_Z^2)}F^{(Z)}(m_Z^2)\right]^{(f)}\\ &\equiv 2\left[\frac{m_W^2}{m_Z^2}F^{(\gamma)}(m_Z^2)-\frac{m_W^2}{m_Z^2}F^{(Z)}(m_Z^2)+\frac{m_W/m_Z(2m_W^2/m_Z^2-1)}{\sqrt{1-m_W^2/M_z^2}}\right.\\ &\qquad\left.\times F^{(Z\gamma)}(m_Z^2)\right]^{(f)}+[F^{(\gamma)}(0)-F^{(\gamma)}(m_Z^2)]^{(f)}\ . \qquad (3.166)\end{aligned}$$

We define now the quantity:

$$\Delta_3(m_Z^2) \equiv Re\left[\frac{m_W^2}{m_Z^2}\left(F^{(\gamma)}(m_Z^2) - F^{(Z)}(m_Z^2)\right)^{(f)} + \frac{m_W/m_Z}{\sqrt{1-m_W^2/m_Z^2}}(2m_W^2/m_Z^2 - 1)F^{(f)(Z\gamma)}(m_Z^2)\right] \quad (3.167)$$

and verify immediately that it is finite. For what concerns its physical interpretation, it is easy to realize that this quantity can also be written, at any q^2, as:

$$\Delta_3(q^2) = Re\left[\frac{1}{\sqrt{1-m_W^2/m_Z^2}}F^{(\gamma)}(q^2) - F^{(3)}(q^2)\right]^{(f)} . \quad (3.168)$$

Loosely speaking, Δ_3 reflects the fact that the unphysical gauge boson field $W_{3\mu}$ is *different* from the photon field A_μ rescaled by a $1/\sqrt{1-m_W^2/m_Z^2}$ factor, which can be viewed as a consequence of the presence of the extra $U(1)_{Y_L}$ gauge boson field B_μ in Eq. (1.84). Clearly, this has little to do with the custodial symmetry violation effects described by Δ_1, Δ_2. One consequently expects that Δ_3 may be responding in a quite different way (compared to $\Delta_{1,2}$) to a given physical input, and we shall provide illustrative examples of this statement in the following Subsections.

The quantity defined by Equation (3.166) can be, at this point, expressed as the sum of $\Delta_3(m_Z^2)$ with the difference $Re[F^{(f)(\gamma)}(0) - F^{(f)(\gamma)}(m_Z^2)]$. The latter is exactly the shift due to fermion pairs $\Delta\alpha$ of the *effective* α, Eq. (3.129), computed at four-momentum square $= m_Z^2$. We see therefore that the parameter $\Delta r^{(f)}$ can be written in conclusion as a sum of *four* independent finite components, each one of rather different and understood physical origin, combined in the final expression as follows:

$$\Delta r^{(f)} = \left\{[\Delta\alpha(m_Z^2)] - \frac{m_W^2/m_Z^2}{(1-m_W^2/m_Z^2)}[\Delta_1(0)] + \frac{(2m_W^2/m_Z^2 - 1)}{1-m_W^2/m_Z^2)}[\Delta_2] + 2[\Delta_3(m_Z^2)]\right\}^{(f)} . \quad (3.169)$$

As anticipated in the previous discussion, we recognize the existence of three effects (those expressed by $\Delta_1, \Delta_2, \Delta_3$) that can be correctly classified as of *genuinely* weak type. In fact, their existence is a direct consequence of some specific physical property of the massive gauge bosons. On the contrary, the fourth parameter $\Delta\alpha(m_Z^2)$ is fully entitled to be classified as of *genuinely QED type*, since it does not feel in any way the presence (or absence) of the massive gauge partners of the photon. This has a practical

consequence that is, in a sense, funny. In fact, it is clear that the *interesting* features of $\Delta r^{(f)}$ (and of the full Δr in general) will *not* be contained in $\Delta\alpha$, but rather in the remaining component. For $\Delta r^{(f)}$ this means that the *weak* (W) quantity

$$\Delta r^{(f)W} \equiv \Delta r^{(f)} - \Delta\alpha(m_Z^2) \tag{3.170}$$

will be that for which theoretical predictions and accurate precision measurements will have to be compared. On the other hand, it should be clear already at this stage that the measurable quantity will be the *full* Δr (see e.g. Eq. (3.155). This will be obtained adding to $\Delta r^{(f)}$ another component where massive gauge bosons always enter (see Eq. (3.156). In full generality, adding these new *genuinely weak* components to $\Delta r^{(f)}$ will lead to the final separation:

$$\Delta r^{W} \equiv \Delta r - \Delta\alpha(m_Z^2)\ . \tag{3.171}$$

In order to derive, from the (assumed) measured value of Δr, that of the *interesting* weak quantity Δr^W, it is thus necessary to have at our disposal a theoretical estimate of $\Delta\alpha(m_Z^2)$ that is sufficiently precise and reliable to compete with the experimental accuracy of the measurement of Δr. Thus, the *not-interesting* component $\Delta\alpha(m_Z^2)$ must be computed in a way that is extremely accurate and, also, model-independent at the same time. We shall devote the next Subsection 3.2.4 to a brief illustration of how this computation is actually performed.

3.2.4 *Numerical estimate of* $\Delta\alpha(m_Z^2)^{(f)}$

We now proceed to the numerical estimate of $\Delta\alpha(m_Z^2)^{(f)}$, i.e. of the quantity:

$$\Delta\alpha(m_Z^2)^{(f)} = Re[F^{(f)(\gamma)}(0) - F^{(f)(\gamma)}(m_Z^2)]\ . \tag{3.172}$$

To perform the practical calculation, the fermion pairs contribution to the photon self-energy must be separated, for computational purposes, into its lepton and its quark component. The first one can be derived in a rather straightforward way from Eq. (3.68); using Eq. (3.66) immediately leads to the results;

$$F^{(\ell)(\gamma)}(q^2) = \frac{\alpha}{3\pi}\Delta + F^{(\ell)(\gamma)(\text{finite})}(q^2) \tag{3.173}$$

where, for the *finite* part, one obtains the following expression:

$$F^{(\ell)(\gamma)(\text{finite})}(q^2) = -\frac{2\alpha}{\pi}\int_0^1 dx\, x(1-x)\ln\left[\frac{m_\ell^2 - q^2x(1-\gamma)}{\mu^2}\right] \tag{3.174}$$

as it can be verified from the properties of the various functions defined by Eqs. (3.35), (3.37). One obtains therefore for the lepton component $\Delta\alpha$ $(1, 2, 3 = e, \mu, \tau)$:

$$\Delta\alpha(q^2)^{(\ell)} = -\frac{2\alpha}{\pi}\sum_{\ell=1}^{3}\int_0^1 dx\, x(1-x)\ln\left|1 - \frac{q^2 x(1-x)}{m_\ell^2}\right| . \qquad (3.175)$$

Setting $q^2 = m_Z^2 \gg m_\ell^2$ and retaining the dominant term inside the argument of the logarithm leads to the known expression:

$$\Delta\alpha(m_Z^2)^{(\ell)} = \frac{2\alpha}{3\pi}\left[\ln\frac{m_Z}{m_e} + \ln\frac{m_Z}{m_\mu} + \ln\frac{m_Z}{m_\tau} - \frac{5}{2}\right] . \qquad (3.176)$$

Inserting the experimental values of m_Z, m_e, m_μ and m_τ finally leads to the result:

$$\Delta\alpha(m_Z^2)^{(\ell)} = 0.0314 . \qquad (3.177)$$

Two comments are at this point appropriate and, in a sense, correlated. The first one is the realization that, numerically, the one-loop correction that is taken into account by Eq. (3.114) is "not small". A relative three percent represents in fact quite large an effect in situations where the experimental accuracy is supposed to be at the permil level, which will be the case for measurements on Z resonance. The second comment is a qualitative statement about the next estimate of the quark contribution to $\Delta\alpha(m_Z^2)$. A priori, one can guess that its numerical value should be of a size comparable with that of Eq. (3.177), which implies a relevant contribution. One also sees from Eq. (3.175) that a large part of the effect is produced by the smaller masses, and one consequently expects that a major rôle should be played by exchanges of "light" (u, d, s, c, b) quarks. On this very precise point, a calculation like that performed for the leptons appears to be from the beginning in serious trouble for two rather strong reasons. In first place, the precise definition (and the value) of the light quark *masses* is not unambiguously known. This would unavoidably lead to an intrinsic theoretical error in the calculation, whose size would be rather difficult to fix. Secondly, in the light quark diagrams, the extra correction due to gluon exchanges cannot be ignored, and its perturbative estimate in such a region of essentially "quasi zero" momentum transfer is certainly unreliable. This leads to the conclusion that, for such an expectedly relevant contribution, some different computational strategy should be utilized.

Luckily enough, a well known and general approach to this problem exists, based on the use of the old fashioned *dispersion relations* technique [8].

This is essentially based on the assumption that the hadronic (quark) photon self-energy $F^{(h)(\gamma)}(q^2)$ is an analytic function of the variable q^2 for generalized complex q^2 values, so that the Cauchy theorem can be written as:

$$F^{(h)(\gamma)}(q^2) = \frac{1}{2\pi i}\oint_c \frac{F^{(h)(\gamma)}(q'^2)}{q'^2 - q^2} dq'^2 \tag{3.178}$$

where c denotes a closed contour in the complex q^2 plane. By choosing the closed contour c as the infinite limit of a special finite circle surrounding the real axis and cut along the positive q^2 values, it is always possible to express the real part of any analytic function that vanishes at infinity as the integral over only the real axis of its imaginary part. Choosing this function as $1/q^2[F^{(\gamma)}(q^2) - F^{(\gamma)}(0)]^{(h)}$, one therefore writes:

$$Re\left[\frac{F^{(\gamma)}(q^2) - F^{(\gamma)}(0)}{q^2}\right]^{(h)} = \frac{1}{\pi} P \int_{q_0'^2}^{\infty} \frac{dq'^2}{q'^2 - q^2} Im\left[\frac{F^{(\gamma)}(q'^2) - F^{(\gamma)}(0)}{q'^2}\right]^{(h)} \tag{3.179}$$

where P denotes the so called *principal value* of the integral, that avoids the infinite at $q'^2 = q^2$ and $q_0'^2$ represents the threshold value after which an imaginary part begins to develop. According to a sort of generalization of the optical theorem, this imaginary part is then proportional to the total cross section σ_h of the process of electron-positron annihilation into hadrons, so that the final expression is obtained:

$$Re\frac{[F^{(\gamma)}(q^2) - F^{(\gamma)}(0)]^{(h)}}{q^2} = \frac{1}{4\pi^2\alpha} P \int_{4m_\pi^2}^{\infty} \frac{dq'^2}{q'^2 - q^2} \sigma_h(q'^2) \tag{3.180}$$

with a physical threshold at $q_0'^2 = 4m_\pi^2$. The evaluation of the hadronic component $\Delta^{(h)}\alpha(m_Z^2)$ proceeds now from Eq. (3.180) using as a "theoretical" input the experimental values of the hadronic electron-positron annihilation cross section, since one has:

$$\Delta\alpha(m_Z^2)^{(h)} \equiv Re[F^{(\gamma)}(0) - F^{(\gamma)}(m_Z^2)]^{(h)} = \frac{m_Z^2}{4\pi^2\alpha} P \int_{4m_\pi^2}^{\infty} \frac{dq'^2}{m_Z^2 - q'^2} \sigma_h(q'^2) \tag{3.181}$$

and this equation is valid to all orders of strong interactions.

For practical (and, also, theoretical) purposes it is more useful to rewrite Eq. (3.181) by replacing inside the integral the hadronic cross section by the ratio $R^{(\gamma)} \equiv \sigma_h/\sigma_\mu$ of the hadronic to the muonic electron-positron cross sections. Since one has, to lowest order in the QED coupling:

$$\sigma_\mu(q'^2) \equiv \sigma_{e^+e^-\to\mu^+\mu^-}(q'^2) = \frac{4}{3}\pi q'^2 \alpha^2 \tag{3.182}$$

one gets, to the considered one-loop level:

$$\Delta\alpha(m_Z^2)^{(h)} = \frac{\alpha m_Z^2}{3\pi} P \int_{4m_\pi^2}^{\infty} \frac{dq'^2}{q'^2(m_Z^2 - q'^2)} R^{(\gamma)}(q'^2) \; . \tag{3.183}$$

The usual approach to a numerical estimate of Eq. (3.183), consists of a first separation of the contribution coming from "light" hadrons, thought as composed by the five "light" (u, d, s, c, b) quarks, from the remaining term usually identified with that produced by the top quark (no other fermion families are present in the MSM). For what concerns the light contribution, one understands from a glance to Eq. (3.182) that it will be mainly produced by the relatively low energy region, e.g. for $\sqrt{q'^2} \leq$ 40 GeV, where experimental data with a related error are available; for higher energies, a theoretical (e.g. QCD...) asymptotic fit must be used. Clearly, this calculation will lead to a prediction whose error is mostly given by that on the available experimental data below 40 GeV (in the theoretical QCD fit the error is practically negligible). A proper estimate of this error is quite important, since its size might damage, if it turned out to be dangerously large, the accuracy of the MSM predictions. This explains the great number of dedicated papers that were written, starting from the original calculation [47] to the most recent work [48]. A complete list of authors can be found in Ref. [49] with a table of all results and uncertainties, that varied with time following the improvements of the relevant low energy measurement of the e^+e^- hadronic cross section. The value used in this book for $\Delta\alpha^{(5)}(m_Z^2)$, $(5) = u, d, s, c, b$, is

$$\Delta\alpha(m_Z^2)^{(5)} = 0.02758 \pm 0.00035 \tag{3.184}$$

i.e. of the same size as the leptonic contribution Eq. (3.177).

Two comments are now relevant. The first one is that the main source of error in Eq. (3.184) comes from the experimental error on the data in the region 1 GeV $\leq \sqrt{q'^2} \leq$ 10 GeV. The second one is that the top-quark contribution must still be added. This does not represent a problem, given the fact that the value of the top mass is large, $m_t \simeq 2m_Z$, and its contribution is consequently highly depressed in the integral. Note that in the top case one can ascribe a meaning, and thus use an experimental value, to the concept of *top mass*. This fact, and the smallness of the related contribution (plus the large energy scale intrinsically associated to the top, that makes strong interactions perturbatively treatable, and essentially negligible) lead to the conclusion that the top component can be computed by using Eq. (3.175), with the insertion of a color ($N_t = 3$) and of a charge

(4/9) factor, but assuming this time $m_t^2 \gg m_Z^2$, that produces the result:

$$\Delta\alpha(m_Z^2)^{(\mathrm{top})} \simeq -\frac{\alpha}{15\pi}\frac{m_Z^2}{m_t^2} \simeq -0.00004 \tag{3.185}$$

much smaller than the error of Eq. (3.183) and thus totally negligible.

From a general theoretical point of view, this conclusion is predictable. The top contribution to the photon self-energy at $q^2 = m_Z^2$ is in fact a typical effect coming from a particle, of squared mass m_t^2 sufficiently larger than the involved squared moment, to a purely vectorial self-energy. As such, it must fulfill the request of the *decoupling theorem* of Appelquist and Carazzone [35], according to which this type of effects behaves like $\sim q^2/m_t^2$ and thus *decouples* as actually shown by Eq. (3.185).

In conclusion, the theoretical statement that is nowadays available is that the overall value of $\Delta\alpha(m_Z^2)^{(f)}$ is the following:

$$\Delta\alpha(m_Z^2)^{(f)} = 0.05901 \pm 0.00035 \tag{3.186}$$

obtained as a sum of leptonic and (quark) hadronic contributions. This corresponds to a value of the effective QED coupling Eq. (3.128):

$$[\alpha(m_Z^2)]^{-1} = 128.9495 \pm 0.045\ . \tag{3.187}$$

It should be stressed that the contribution Eq. (3.186) to Δr is rather large, almost six percent. This will affect the MSM predictions in a substantial way. However, the induced theoretical error of the predictions will be systematically negligible. We shall discuss this point in detail in the final part of this Book, and we shall assume its validity for the moment. In this spirit, we shall consequently write Eq. (3.155), using Eq. (3.171), as follows:

$$\begin{aligned}\frac{G_F}{\sqrt{2}} &= \frac{\pi\alpha}{2m_W^2(1-m_W^2/m_Z^2)}[1+\Delta\alpha(m_Z^2)+\Delta r^W] \\ &= \frac{\pi\alpha}{2m_W^2(1-m_W^2/m_Z^2)}[1+\Delta\alpha(m_Z^2)][1+\Delta r^W] \\ &= \frac{\pi\alpha(m_Z^2)}{2m_W^2(1-m_W^2/m_Z^2)}[1+\Delta r^W]\end{aligned} \tag{3.188}$$

where the usual one-loop approximation has been used.

Equation (3.188) contains an implicit statement, that we anticipated in the introduction to this Chapter. This may be essentially expressed by saying that, if one wants to replace the input parameter m_W by a "more convenient" set that includes (almost unavoidably) the extremely precisely determined G_F, the involved theoretical operation automatically involves both the Z mass and the effective charge at the squared Z mass $\alpha(m_Z^2)$.

This set $(G_F, m_Z, \alpha(m_Z^2))$ appears therefore as the natural one to be used as the fixed input of the different theoretical predictions, and we shall adopt this pragmatic attitude from now on.

The previous statement still requires a final "detail" to be fixed. This is, as one can guess from Eq. (3.188), the precise determination (or the theoretical expression at least) of the *genuine* weak parameter Δr^W. We shall devote the next Subsection 3.2.5 to a detailed investigation of this problem.

3.2.5 *Determination of Δr^W and calculation of the W mass*

3.2.5.1 *Numerical estimate of* $\Delta_1(0)$

As a first example of electroweak calculation at one loop, we shall now compute the expression of the W mass. This can be obtained by Eq. (3.188) once the value of Δr^W has been determined. With this aim we shall first consider, again, the fermion pairs contribution to self energies, $\Delta r^{(f)W}$, Eqs. (3.169), (3.170). The example will have two major motivations. The first one will be the derivation of a clean *prediction* (for the W mass), that can be considered as a crucial test of the MSM; the second one will be the fact that, as we shall see soon, some of the parameters that enter Δr^W will *also* be involved in the expression of the various Z peak observables. In this sense, the discussion that will be given in this Subsection 3.2.5 will remain valid for the rest of this Chapter, that will be more strictly related with physics at the Z resonance.

To make the previous discussion more concrete, we now begin by considering the contribution to $\Delta_1(0)$ Eq. (3.163) from a fermion doublet, more precisely from a pair of (u, d) quarks (u, d simply denote the states with $I_{3L} = \pm 1/2$), whose masses m_u, m_d will now be not ignored, but carefully retained in the calculation. In fact, since $\Delta_1(0)$ is supposed to react to (custodial) SU(2) violating effects, one expects that these can be originated e.g. by a mass *difference* $\sim m_u - m_d$ inside the doublet, as we shall explicitly verify.

The expression of $\Delta_1(0)$ corresponding to one quark doublet (u, d) can be derived from Eqs. (3.54), (3.61), and reads:

$$\Delta_1^{(u,d)}(0) = \frac{3\alpha}{8\pi m_W^2 (1 - m_W^2/m_Z^2)}$$

$$\times \int_0^1 dx \left\{ m_u^2 \ln \frac{m_u^2}{\mu^2} + m_d^2 \ln \frac{m_d^2}{\mu^2} \right.$$
$$\left. -2[m_u^2(1-x) + x m_d^2] \ln \left[\frac{m_u^2}{\mu^2}(1-x) + x \frac{m_d^2}{\mu^2} \right] \right\} \tag{3.189}$$

where the first two terms come from $A^{(Z)}(0)$, the last one from $A^{(W)}(0)$, and a factor 3 that takes into account the colour degree of freedom has been inserted.

A glance to Eq. (3.189) immediately shows that it vanishes in the case of *equal* quark masses, $m_u = m_d$. This confirms the discussion previously given about the intrinsic sensitivity of $\Delta_1(0)$ to custodial SU(2) violating effects. In this spirit, it becomes clear that only situations of sizeable mass difference should be relevant and potentially interesting. In fact, this can be evidenced by performing the x-integration, which leads to the expression:

$$\Delta_1^{(u,d)}(0) = \frac{3\alpha}{8\pi m_W^2 (1 - m_W^2/m_Z^2)}$$
$$\times \left[\frac{1}{2}(m_u^2 + m_d^2) - \frac{m_u^2 m_d^2}{(m_u^2 - m_d^2)} \ln \frac{m_u^2}{m_d^2} \right] . \tag{3.190}$$

In the limit e.g. $m_u^2 \gg m_d^2$ this reads:

$$\Delta_1^{(m_u \gg m_d)}(0) \simeq \frac{3\alpha}{16\pi(1 - m_W^2/m_Z^2)} \frac{m_u^2}{m_W^2} . \tag{3.191}$$

One sees, and this point must be stressed, that $\Delta_1^{(u,d)}(0)$ develops a contribution that is *quadratic* in the dominant fermion mass. This will remain unchanged also if $m_u^2 \gg m_W^2$. This property, first stressed by Veltman [34], is orthogonal to the one met in the case of $\Delta\alpha(m_Z^2)$ where the decoupling theorem [35] was effective. The reason for this difference is the presence of a non-vectorial (i.e. essentially of not purely QED type) component in the Z, W self-energy, that leads to a *genuinely weak* violation of the theorem.

From a numerical point of view, one immediately realizes that Eq. (3.191) can lead to an appreciable contribution in the case of a sufficiently heavy quark mass. Writing, in first approximation, $(1 - m_W^2/m_Z^2) \simeq 1/4$, we obtain:

$$\Delta_1^{(m_u \gg m_d)}(0) \simeq \frac{\alpha}{\pi} \frac{m_u^2}{m_Z^2} . \tag{3.192}$$

One sees that, unless $m_u > m_Z$, the size of the term will be always less than $\alpha/\pi \simeq$ two permil (with an even worse situation in the lepton case, as one can easily guess, due to the absence of the colour factor). The only

remarkable exception to this negative statement is provided by the (top, bottom) doublet contribution. Here, with $m_t \simeq 2\ m_Z$, $\Delta_1(0)$ reaches the one percent size, that will be relevant for Z resonance physics. This fact will lead to the extremely interesting consequence that precision measurements on top of the Z resonance where, we anticipate, $\Delta_1(0)$ will be one of the input parameters, will be sensitive to the actual value of the top mass, and as such they will be, so to say, directly comparable with the independent experimental measurement of this quantity, as we shall discuss in detail in the final part of this Book.

One comment at this point is relevant, and concerns the naive expectation that a similar feature might characterize the *non fermionic* virtual contributions (to e.g. self-energies) where a Higgs boson is involved. If this were the case, precious indications on the still unknown value of the Higgs mass would be derived, that would be of great practical value for actual searches. Unfortunately, at the considered one-loop level, this is not the case. As first shown by Veltman [37], the virtual Higgs contribution at this level is *screened* i.e. it is only of logarithmic type in the large Higgs mass regime and thus very difficult to be practically detected. We shall return on this point at the end of this Chapter, when a few relevant formulae will be explicitly shown.

To conclude this Subsection 3.2.5.1, we have shown that the presence of custodial SU(2) violations can lead to observable effects at the one-loop level via $\Delta_1^{(0)}$. In the next Subsection 3.2.5.2, we shall investigate in some details the properties of one extra quantity, $\Delta_3\left(m_Z^2\right)$, that will be much less sensitive to custodial violations features, but whose rôle in the process of precision tests of the MSM will also turn out to be rather crucial.

3.2.5.2 *Numerical estimate of* $\Delta_3(m_Z^2)$

We shall now illustrate the main properties of $\Delta_3(m_Z^2)$ by explicitly performing the calculation of the contribution to this quantity coming from a quark pair, to be generically indicated Eq. (3.190) by a (u, d) doublet. Starting from the definition Eq. (3.167) and using Eq. (3.54), that can be easily modified to provide the expressions of both $F^Z(q^2)$ and $F^{(Z\gamma)}(q^2)$ by simple changes of the fermion vertices, it is straightforward to obtain the finite expression:

$$\Delta_3(m_Z^2) = -\frac{\alpha}{4\pi(1 - m_W^2/m_Z^2)}$$

$$\times \left\{ \left[\int_0^1 dx\, x(1-x) \ln \left| \frac{m_u^2 - m_Z^2 x(1-x)}{m_d^2 - m_Z^2 x(1-x)} \right| \right] \right.$$
$$\left. + \frac{3}{2} \left[\frac{m_u^2}{m_Z^2} \ln \left| 1 - \frac{m_Z^2 x(1-x)}{m_u^2} \right| + \frac{m_d^2}{m_Z^2} \ln \left| 1 - \frac{m_Z^2 x(1-x)}{m_d^2} \right| \right] \right\} . \tag{3.193}$$

We can consider now two quite different extreme situations. The first one is that in which $m_u \gg m_Z \gg m_d$, and corresponds (with the extra request $m_Z \gg m_d$) to the non-decoupling case of the previous Subsection. By approximation of the integrands with their dominant terms, we derive in the considered limit:

$$\Delta_3^{(u,d)}(m_Z^2) \simeq -\frac{\alpha}{4\pi\,(1 - m_W^2 m_Z^2)} \left\{ \left[\frac{1}{6} \ln \frac{m_u^2}{m_Z^2} + \frac{5}{18} \right] - \left[\frac{3}{18} \right] \right\}$$
$$m_u \gg m_Z \gg m_d$$
$$\simeq \frac{-\alpha}{24\pi \left(1 - \frac{m_W^2}{m_Z^2} \right)} \ln \frac{m_u^2}{m_Z^2} \, . \tag{3.194}$$

Numerically, for the top quark case with $m_t \simeq 2m_Z$, the contribution is well below the one permil, more than one order of magnitude smaller than the corresponding contribution to $\Delta_1(0)$ Eq. (3.192). This confirms the expectation, already discussed in Subsection 3.2.5.2, that $\Delta_3(m_Z^2)$ will not react like $\Delta_1(0)$ to custodial symmetry violating inputs. In fact, the sensitivity of $\Delta_3(m_Z^2)$ to such situations is practically negligible.

The second interesting situation to be considered is that where $m_u = m_d \gg m_Z$. We know from the previous discussions that both $\Delta_\alpha(m_Z^2)$ and $\Delta_1(0)$ will be totally unaffected in this case, owing to the decoupling property of the first quantity and to the custodial symmetry peculiar constraints on the second one Eq. (3.189). For Δ_3, the numerical estimate of Eq. (3.193) leads, on the contrary, to the conclusion:

$$\Delta_3^{(u,d)}(m_Z^2) \simeq \frac{\alpha}{8\pi\,(1 - m_W^2/m_Z^2))} \tag{3.195}$$
$$m_u = m_d \gg m_Z \, .$$

Numerically, this contribution is just above one permil, which does not represent a remarkable effect. Still, and quite generally, this shows the totally *orthogonal* nature of $\Delta_3(m_Z^2)$ compared with $\Delta_1(0)$. In principle, the existence of a sizeable number of new *super* heavy quarks degenerate in mass would be detectable in $\Delta_3(m_Z^2)$, but not in $\Delta_1(0)$.

To conclude this qualitative study of the three parameters appearing in Eq. (3.170), we still have to discuss the Δ_2 term. This will be done in the forthcoming part of the Section.

3.2.5.3 *Numerical estimate of* Δ_2

From its definition Eq. (3.164) and from the expressions given in Eqs. (3.54, (3.61) it is again straightforward to derive the contribution of a general (u,d) quark doublet to Δ_2, that reads:

$$\begin{aligned}\Delta_2^{(u,d)} = & \frac{3\alpha}{4\pi(1-m_W^2/m_Z^2)} \\ & \times \left\{ \int_0^1 dx\, x(1-x) \ln \left[\frac{m_u^2 - m_Z^2 x(1-x)}{m_u^2(1-x) + m_d^2 x - m_W^2 x(1-x)} \right] \right. \\ & + \int_0^1 dx\, x(1-x) \ln \left[\frac{m_d^2 - m_Z^2 x(1-x)}{m_u^2(1-x) + m_d^2 x - m_W^2 x(1-x)} \right] \\ & + \int_0^1 dx \left[(1-x)\frac{m_u^2}{m_W^2} + x m_d^2 m_W^2 \right] \\ & \qquad \times \ln \left[\frac{m_u^2(1-x) + m_d^2 x - m_W^2 x(1-x)}{m_u^2(1-x) + m_d^2 x} \right] \\ & - \frac{1}{2} \int_0^1 dx \left[\frac{m_u^2}{m_Z^2} \ln \left| 1 - \frac{m_Z^2 x(1-x)}{m_u^2} \right| \right. \\ & \left. \left. + \frac{m_d^2}{m_Z^2} \ln \left| 1 - \frac{m_Z^2 x(1-x)}{m_d^2} \right| \right] \right\} . \end{aligned} \tag{3.196}$$

In the limiting case $m_u \gg M_{Z,W} \gg m_d$ that was already considered in the previous part of the Section one finds the following expression:

$$\begin{aligned} & \Delta_2^{(u,d)} \simeq \frac{-3\alpha}{4\pi(1-m_W^2/m_Z^2)} \left[\frac{1}{6} \ln \frac{m_u^2}{m_Z^2} + \frac{1}{12} \right] \\ & m_u \gg M_{W,Z} \gg m_d \end{aligned} \tag{3.197}$$

showing that the contribution carried by the energy dependent component of the custodial symmetry violation $\simeq F^{(3)}(m_W^2) - F^{(W)}(m_W^2)$ is only of logarithmic type and numerically, for $m_u = m_t \simeq 2m_Z$, at the negligible one permil level. For what concerns the second considered situation $m_u = m_d \gg M_{Z,W}$ that was not irrelevant for $\Delta_3(m_Z^2)$, one finds in this case:

$$\begin{aligned} & \Delta_2^{(u,d)} \simeq \frac{-3\alpha}{2\pi(1-m_W^2/m_W^2)} \int dx\, x^2(1-x)^2 \frac{(m_Z^2 - m_W^2)}{m_u^2} \\ & m_u = m_d \gg M_{W,Z} \end{aligned} \tag{3.198}$$

showing that this contribution to Δ_2 is indeed negligible. In fact, at least within the MSM, Δ_2 seems to play a not particularly meaningful rôle, since most of the possible considered one loop effects do not affect it in a sensible way. On top of this, this parameter will not enter into the theoretical

predictions for physics on Z resonance, as we shall immediately see. As a consequence of these two facts, we shall not concentrate our attention on it any longer in what follows.

Our discussion of the weak fermionic component of Δr is at this point concluded. Keeping in mind the fact that we did not illustrate the calculation of the non fermionic component, we are now in a position to present the derivation of the theoretical prediction for the W mass in the MSM. This will be the subject of the forthcoming part of this Section.

3.2.5.4 *Calculation of the W mass*

Let us return to Eq. (3.188). By multiplying and dividing it by m_Z^2, it is possible to rewrite it in the more convenient way:

$$\frac{m_W^2}{m_Z^2}\left(1-\frac{m_W^2}{m_Z^2}\right)=\frac{\pi\alpha(m_Z^2)}{\sqrt{2}m_Z^2G_F}[1+\Delta r^W]\,. \tag{3.199}$$

The l.h.s. of Eq. (3.199) is a quadratic expression in the adimensional variable m_W^2/m_Z^2. The r.h.s. contains the three input parameters that we have decided to adopt, $\alpha(m_Z^2), G_F, m_Z$, and the weak parameter Δr^W. The latter will contain typical quantities of the MSM (of particular relevance, the top mass) and also, as shown e.g. by Eq. (3.169), (3.189), (3.193), (3.196), it will depend again in general on m_W^2/m_Z^2. Thus Eq. (3.199) is not, rigorously, a second order equation in m_W^2/m_Z^2 and it must be solved e.g. by recurrence. This does not represent a problem, but prevents us from providing a simple algebraic solution. We can, though, derive an approximate m_W^2/m_Z^2 solution that should be, intuitively, rather close to the complete one. This approximate solution is defined c_0^2 and satisfies the equation:

$$c_0^2s_0^2=\frac{\pi\alpha(m_Z^2)}{\sqrt{2}m_Z^2G_F} \tag{3.200}$$

with $s_0^2\equiv 1-c_0^2$. Of the two solutions of Eq. (3.200), c_0^2 will be chosen as that which almost coincides with the actual experimental value of $m_W^2/m_Z^2\simeq 0.77$. This means that

$$c_0^2=\frac{1}{2}\left[1+\sqrt{1-\frac{4\pi\alpha(m_Z^2)}{\sqrt{2}m_Z^2G_F}}\right]\,. \tag{3.201}$$

Numerically, using the experimental result for m_Z, one obtains the value:

$$c_0^2\simeq 0.769 \tag{3.202}$$

or

$$s_0^2 = 1 - c_0^2 \simeq 0.231 \; . \tag{3.203}$$

Clearly, Eq. (3.202) (or Eq. (3.203)) does *not* represent the complete MSM prediction for the quantity m_W^2/m_Z^2. This can be obtained, as we said, by solving numerically Eq. (3.199) for given values of the *free* MSM parameters (at the beginning of SLC, LEP1 operations: m_t, m_H). We shall not pursue this operation here, but rather embed it into the final overall numerical fit to be discussed at the end of this Book. The reason why we illustrated at this stage the calculation of m_W is that we were able in this way to introduce, and to endow them with a clear physical meaning, a number of parameters and of quantities that will be needed for the complete description of Physics on Z resonance. This will start, in fact, in the forthcoming Section 3.3.

3.3 Formulation of Z physics at one loop: introduction of the *effective* weak parameter $\sin^2\theta_{W,eff}$

3.3.1 *Operative definition of the electroweak mixing angle: the longitudinal polarization asymmetry*

We have already stressed in Chapter 1 the point that a fundamental difference between a photon and a Z boson is represented by the fact that the latter couples in a different way with left-handed and right-handed fermions. An immediate consequence of this is that, in a process that can be described to a very good approximation as a pure s-channel Z exchange from an initial to a final fermion-antifermion state, it will be possible to define and to measure an observable quantity, that would be vanishing if the same process could be approximated by a pure s channel photon exchange. This quantity, that has played from the very beginning a major rôle in the development of the experimental strategies for testing the MSM on top of Z resonance, is the so called *longitudinal polarization asymmetry*. If the considered process is that of annihilation of an initial electron-positron state, with a left (right) handed electron $\equiv e_{L,R}$, into a final fermion-antifermion $(f\bar{f})$ pair, and $\sigma_{L,R}^{(f)}(q^2)$ denote the respective cross sections at variable squared c.m. energy q^2, the longitudinal polarization asymmetry at the Z peak is conventionally defined as:

$$A_{LR}^{(f)}(m_Z^2) \equiv A_{LR}^{(f)} = \frac{\sigma_L^{(f)}(m_Z^2) - \sigma_R^{(f)}(m_Z^2)}{\sigma_L^{(f)}(m_Z^2) + \sigma_R^{(f)}(m_Z^2)} \; . \tag{3.204}$$

We shall begin to investigate the most relevant theoretical features of this observable at the simplest tree level approximation, since as we shall see they remain *essentially* unchanged when one moves to the one-loop description. In particular, we shall make the initial approximation that, on top of the Z resonance, the considered process can be described as a pure Z exchange i.e. by only retaining the first Feynman diagram in Fig. 3.2. This approximation corresponds, for what concerns the expression of any integrated cross section, to neglecting the squared photon with respect to the squared Z contribution (the γZ interference vanishes exactly on Z resonance). This clearly introduces an error that can be exactly estimated, and does not significantly modify any of the following conclusions.

In the described Z-dominance approximation, the expression of $A_{LR}^{(f)}$ at tree level can be easily derived by straightforward application of our relevant formulae shown in detail in Chapter 2. But for an easier and immediate understanding of the main characteristic theoretical features of this quantity, it may be useful to follow a less rigorous, more intuitive approach, that is based on the following simple remark. Consider the process of resonant production and subsequent decay into an arbitrary final $f\bar{f}$ state of a Z, that is created by a left (right) handed electron and by the corresponding positron (whose chirality is uniquely fixed by that of the partner electron in the model, see Eq. (1.114)). This process is described by a related cross section $\sigma_{L,R}^{(f)}(m_Z^2)$; quite generally, this will be proportional to the product of the squared Z-lepton left (right) coupling with an awkward, complicated function that describes the subsequent decay of the Z into the final $f\bar{f}$ fermionic state. Reabsorbing a universal normalization factor in this function, one will consequently write:

$$\sigma_{L,R}^{(0)(f)}(m_Z^2) = g_{L,R\ell}^{(0)^2} f_{L,R}^{(f)}(m_Z^2) \tag{3.205}$$

(the *zero* apex is a reminder of the fact that we are now working at the lowest tree level).

The key observation is now represented by the fact that, once the Z is produced by a polarized electron (with a *strength* proportional to $g_{L,R}^{(0)^2}$), it decays into the final state in a way that is independent of the initial electron polarization. Otherwise stated, one will have that:

$$f_L^{(f)}(m_Z^2) = f_R^{(f)}(m_Z^2) \equiv f^{(f)}(m_Z^2)\ . \tag{3.206}$$

The immediate consequence is that, no matter how complicated $f^{(f)}(m_Z^2)$ is, it will factorize and *cancel* in the ratio of Eq. (3.141), leaving as a final

result

$$A_{LR}^{(0)(f)} = \frac{g_{L,\ell}^{(0)^2} - g_{R,\ell}^{(0)^2}}{g_{L,\ell}^{(0)^2} + g_{R,\ell}^{(0)^2}} \equiv A_{LR}^{(0)} \tag{3.207}$$

i.e. the longitudinal polarization asymmetry (in the used approximation) is actually *independent of the final state*, and only depends on the *initial* lepton-Z couplings.

The previous conclusion has been reached to the lowest order in *weak and strong interactions* in a Z dominance approximation. But, to lowest order of weak interactions, one can immediately generalize it to all orders for what concerns *strong* interactions affecting the final state. In fact, the only consequence of these extra forces will be that of making the function $f^{(f)}(m_Z^2)$ to become even more awkwardly complicated, without, though, introducing in it any dependence on the initial electron polarization. To all orders in the strong interactions and to the lowest order in the electroweak ones, A_{LR} will be thus final state independent. In particular, it will be the same for the production of final lepton pairs and for that of all possible hadronic states, assumed to be the result of the initial creation of the five possible elementary quark couples. This means that it will become possible to measure a genuinely *weak* parameter like that of Eq. (3.207) by simply counting the number of final *hadronic* states (of any possible flavor) produced by left handed and by right handed electrons, thus achieving a much more enhanced statistics with respect to that provided by the analogous measurement of the final leptonic states, with the consequent understandable benefit for what concerns the purely statistical experimental error. This remarkable property will not be spoiled by strong interactions, but rather from the consideration of possible higher order electroweak effects. As a consequence of this fact, one would expect that is should *essentially* survive at the considered one-loop level, which was explicitly shown in Ref. [50].

Having listed the main theoretical reasons that privileged A_{LR}, from the very beginning, as a rather special quantity for accurate tests of the MSM, we now want to specify more precisely what particular genuinely weak parameter would be fixed by its precise measurement. This can be immediately seen by looking at Eq. (1.116), that allows to rewrite Eq. (3.207) as follows:

$$A_{LR}^{(0)} = \frac{2(1 - 4\sin^2\theta_W)}{1 + (1 - 4\sin^2\theta_W)^2} \ . \tag{3.208}$$

In full generality, we conclude that Eq. (3.208) can be viewed as one that provides a realistic *operative* definition of the weak parameter that essentially characterizes the MSM, i.e. $\sin^2\theta_W$. In agreement with our general treatment of input parameters, $\sin^2\theta_W$ turns out to be fixed (modulo small calculable one photon exchange QED corrections) by a prescribed measurement of cross sections, at a precisely defined value of the squared four-momentum equal to the squared Z mass.

Although one should always interpret a tree level definition with some care, a basic analogy with the corresponding QED situation remains, still, impressive. We have actually seen e.g. from Eq. (3.87) and related discussion that the genuine bare QED quantity α_0 can be, in principle, extracted from a prescribed measurement of a (differential) cross section at the precisely defined value of the squared four-momentum equal to the squared *photon* mass. This corresponds nicely to the situation occurring for $\sin^2\theta_W$.

The previous tree level analogy becomes even more interesting if we now consider the way in which the *physical* QED coupling α was defined at the next one-loop level. We have presented the example of Eq. (3.88), showing that the *same* physical cross section, computed at one loop, defines the *physical* charge α. This fact, and the underlying symmetry between electric and weak parameters of the model, leads in an natural way to the idea of introducing a physical or *effective* weak parameter, associated to the bare quantity $\sin^2\theta_W$, to be called conventionally $\sin^2\theta_{W,eff}$, operatively defined at *the one-loop* level from the generalization of Eq. (3.208):

$$A_{LR} \equiv \frac{\sigma_L^{(\ell)} - \sigma_R^{(\ell)}}{\sigma_L^{(\ell)} + \sigma_R^{(\ell)}}|_{q^2=m_Z^2} \equiv \frac{2(1-4\sin^2\theta_{W,eff})}{1+(1-4\sin^2\theta_{W,eff})^2} \ . \tag{3.209}$$

A couple of points should be now stressed. The first one is that Eq. (3.209) now prescribes a measurement of final leptonic states. In fact, at the one loop level, the final state dependence of $A_{LR}^{(f)}$ is not identically vanishing, and in particular the expressions for leptonic and hadronic final states are, in principle, different. This difference is, as previously stated, *small* and calculable and in principle one can therefore use $A_{LR}^{(had.)}$ to define $\sin^2\theta_{W,eff}$ as well. We shall return on this point later, but for the moment we shall stick to the definition of Eq. (3.209). The second point is that the definition of a *physical* $sin^2\theta_{W,eff}$ is rather arbitrary, much like the analogous definition of the *physical* α. Actually, a number of different definitions of the physical mixing angle exists in the literature; however, that provided by Eq. (3.209) has become nowadays largely accepted. In view of this fact, not to generate unnecessary confusion, we shall not try to make a list of

comparisons with alternative definitions.

The next step of our approach is now evidently that of deriving the theoretical expression of $\sin^2\theta_{W,eff}$ in the MSM. This will be done, in the forthcoming Subsection.

3.3.2 *Calculation of* $\sin^2\theta_{W,eff}$ *at one loop: fermion pairs contributions to self-energies*

We now proceed to the derivation of the MSM expression of the effective parameter $\sin^2\theta_{W,eff}$ defined by Eq. (3.209). Following our systematic criterion, we shall first work within a well defined set of approximations, whose generalization to the complete situation will be intuitive and given without a rigorous proof. As usually, we shall stick to the one-loop level. At this order, we shall assume that, on top of the Z resonance, the pure Z contributions to all cross sections, and consequently to all their ratios like that defining A_{LR}, will be the largely dominant ones. Since any cross section is expressed as the result of an operation that involves the squared modulus of the scattering amplitude, we shall concentrate our attention on the *effective* amplitude i.e. on those modifications of the pure Z exchange Feynman diagram at tree level that contribute effectively A_{LR} at one loop. To begin with, we shall be limited to the consideration of the gauge invariant subset of diagrams that correspond to the fermion pairs contributions to self-energies, exactly as we did in the treatment of Sirlin's equation. In terms of Feynman diagrams, they correspond to the following Figure 3.17 and, in our notations, they involve the fermion pairs components of the Z transverse self-energy function $A^{(f)(Z)}(q^2)$ and of the γZ self-energy functions $A^{(f)(Z\gamma)}(q^2)$, $A^{(f)(\gamma Z)}(q^2)$, evaluated in the case of interest at $q^2 = m_Z^2$. Note that we have adopted a notation that defines the mixed self-energies $A^{(Z\gamma)}, A^{(\gamma Z)}$ according to whether the incoming boson is a $Z(A^{(Z\gamma)})$ or a $\gamma(A^{(\gamma Z)})$. This distinction is purely conventional at the self-energy level, but will acquire a more definite meaning when extra non universal corrections (vertices and boxes) of possibly not separately gauge-invariant type will be considered.

If the quantity to be estimated is A_{LR}, one extra simplification occurs. In fact, one immediately realizes that the first two types of corrections corresponding to the diagrams (a) and (b) of Fig. 3.17 will cancel at one loop in the involved ratio of cross sections. This is due to the fact that these contributions will simply fall into components of the function $f^{(f)}(q^2)$ defined by an immediate generalization of Eqs. (3.205), (3.206), given the fact

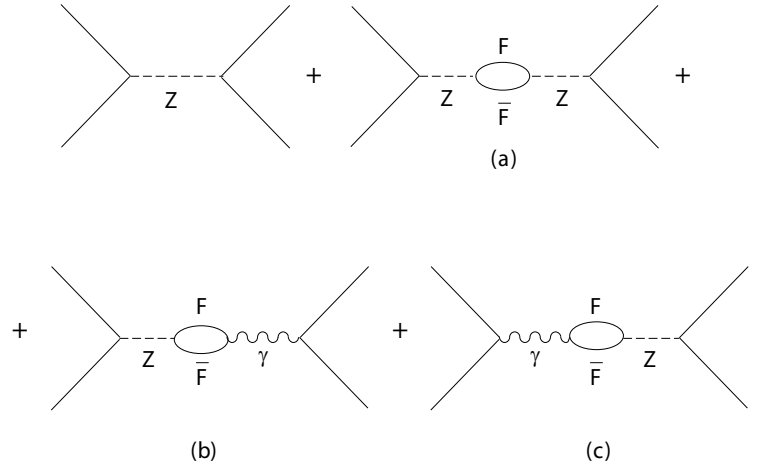

Fig. 3.17 Fermion (F) pairs self-energies modifications of the tree level Z exchange in electron-positron annihilation: (a) Z self-energy (b) $Z\gamma$ self-energy (c) γZ self-energy. The final state is a fermion-antifermion pair.

that the initial vertex has remained unchanged. This is not conversely true for the contribution coming from the diagrams of (c) type, that modify the initial leptonic vertex. We can therefore conclude that, for what concerns the calculation of $A_{LR}^{(f)}$ at one loop for an *arbitrary* final fermion-antifermion state, an *effective* component of the scattering amplitude can be associated with the two diagrams represented in Fig. 3.18 and conventionally defined as $A_{ef,eff}^{(1)(f)}$.

To compute this quantity, a simple possibility is provided by the following observation. As a consequence of the additional one-loop diagram of Fig. 3.18, the overall *effective* amplitude can be written as the sum of two terms. Following the prescriptions and the definitions of Eqs. (3.5)–

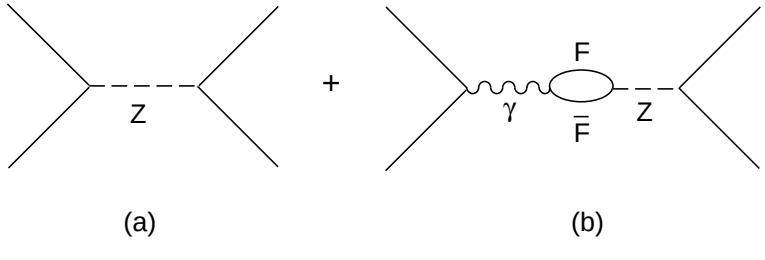

Fig. 3.18 Diagrams that contribute at one loop in the calculation of $A_{LR}^{(f)}$.

(3.12), (3.46) and (3.62) (with a straightforward replacement of the Z or γ self-energy with the $\gamma - Z$ self-energy) leads to the expression:

$$A^{(1)(f)}_{ef,eff}(q^2) =$$

$$\left[\frac{i}{(q^2-m_Z^2)}\frac{|e_0|}{2\sin\theta_W\cos\theta_W}\bar{v}_e(\vec{p}_2)\gamma^\mu(g^{(0)}_{Ve}-\gamma_5 g^{(0)}_{Ae})u_e(\vec{p}_1)\right.$$
$$\left.+\frac{i}{q^2}|e_0|\bar{v}_e(\vec{p}_2)\gamma^\mu Re\frac{A^{(F)(\gamma Z)}(q^2)}{q^2-m_Z^2}u_e(\vec{p}_1)\right] j^{(Z)}_{\mu f} =$$
$$\frac{|e_0|}{2\sin\theta_W\cos\theta_W}\frac{i}{(q^2-m_Z^2)}\bar{v}_e(\vec{p}_2)\gamma^\mu$$
$$\left[g^{(0)}_{Ve}\left(1+\frac{2\sin\theta_W\cos\theta_W}{g^{(0)}_{Ve}}Re\frac{A^{(F)(\gamma Z)}(q^2)}{q^2}\right)-\gamma_5 g^{(0)}_{Ae}\right]u_e(\vec{p}_1)j^{(Z)}_{\mu f}\ . \tag{3.210}$$

As one sees, the only difference between the tree level amplitude and the *effective* one is that, in the latter, the vector Z-electron coupling $g^{(0)}_{Ve} = -\frac{1}{2}(1-4\sin^2\theta_W)$ has been replaced by the *effective* coupling

$$g^{(0)}_{Ve} \Rightarrow g^{(1)(f)}_{Ve,eff}(q^2) = g^{(0)}_{Ve}\left(1+\frac{2\sin\theta_W\cos\theta_W}{g^{(0)}_{Ve}}Re\frac{A^{(f)(\gamma Z)}(q^2)}{q^2}\right)$$
$$= g^{(0)}_{Ve}\left(1-\frac{4\sin\theta_W\cos\theta_W}{(1-4\sin^2\theta_W)}Re\frac{A^{(f)(\gamma Z)}(q^2)}{q^2}\right) \tag{3.211}$$

whilst the axial coupling $g^{(0)}_{Ae}$ has remained unchanged. For what concerns the expression of A_{LR}, it is now convenient to rewrite the tree level Eq. (3.207) in terms of $g^{(0)}_{Ve}$ and $g^{(0)}_{Ae}$. This gives:

$$A^{(0)}_{LR} \equiv \frac{2g^{(0)}_{Ve}g^{(0)}_{Ae}}{g^{(0)2}_{Ve}+g^{(0)2}_{Ae}}\ . \tag{3.212}$$

From the previous discussion it is now clear that the new expression at one loop will be obtained by simply replacing $g^{(0)}_{Ve}$ with its modification Eq. (3.211), by definition computed at $q^2 = m_Z^2$. Performing the usual operations formally valid at one loop, and introducing for simplicity the auxiliary variable

$$v_W = 1-4\sin^2\theta_W \tag{3.213}$$

one arrives in a straightforward way to the following result:

$$A^{(1)(f)}_{LR} = \frac{2g^{(1)(f)}_{Ve,eff}(m_Z^2)g^{(0)}_{Ae}}{(g^{(1)(f)}_{Ve,eff}(m_Z^2))^2+g^{(0)^2}_{Ae}}$$

$$= \frac{2g_{Ve}^{(0)}g_{Ae}^{(0)}}{(g_{Ve}^{(0)^2}+g_{Ae}^{(0)2})}\left[1-\frac{4\sin\theta_W\cos\theta_W}{v_W}\frac{(1-v_W^2)}{(1+v_W^2)}Re\frac{A^{(f)(\gamma Z)}(m_Z^2)}{m_Z^2}\right]$$

$$+\text{'small' QED}=$$

$$\equiv A_{LR}^{(0)}\left[1-\frac{4\sin\theta_W\cos\theta_W}{v_W}\frac{(1-v_W^2)}{(1+v_W^2)}Re\frac{A^{(f)(\gamma Z)}(m_Z^2)}{m_Z^2}\right]. \quad (3.214)$$

From this formula, by simply equating it to the operative definition given in Eq. (3.209), we can now derive the expression of the fermion pairs component of the self-energy contribution to $\sin^2\theta_{W,eff}$. This can be done immediately by writing the *formal* generalization of Eq. (3.209):

$$A_{LR}^{(1)(f)} \equiv \frac{2(1-4\sin^2\theta_{W,eff}^{(f)})}{1+(1-4\sin^2\theta_{W,eff}^{(f)})^2}. \quad (3.215)$$

Equating Eqs. (3.215) and (3.214) and using Eq. (3.208) one is then led, after a few straightforward steps, to the result

$$\sin^2\theta_W = \sin^2\theta_{W,eff}^{(f)} - \sin\theta_W\cos\theta_W Re\frac{A^{(f)(\gamma Z)}(m_Z^2)}{m_Z^2}. \quad (3.216)$$

A simpler attitude is that of realizing that, at the considered fermion pairs contribution approximation level, the only crucial replacement is that of the bare vector Z-lepton coupling, $g_{Ve}^{(0)} = -\frac{1}{2}+2\sin^2\theta_W$, by the effective coupling defined by Eq. (3.211). This can equally well be interpreted as a replacement of $\sin^2\theta_W$ with $\sin^2\theta_{W,eff}^{(f)}$, by simply defining:

$$g_{Ve,eff}^{(1)(f)}(m_Z^2) \equiv g_{Ve}^{(0)} + 2\sin\theta_W\cos\theta_W Re\frac{A^{(f)(\gamma Z)}(m_Z^2)}{m_Z^2}$$

$$= -\frac{1}{2}+2\sin^2\theta_W + 2\sin\theta_W\cos\theta_W Re\frac{A^{(f)(\gamma Z)}(m_Z^2)}{m_Z^2}$$

$$\equiv -\frac{1}{2}+2\sin^2\theta_{W,eff}^{(f)} \quad (3.217)$$

from which , again, we find[1]:

$$\sin^2\theta_{W,eff}^{(f)} = \sin^2\theta_W + \sin\theta_W\cos\theta_W Re\frac{A^{(f)(\gamma Z)}(m_Z^2)}{m_Z^2}. \quad (3.218)$$

[1] A word of caution is now worthwhile. Equation (3.218) (or (3.216)) contain a quantity $\sin^2\theta_{W,eff}^{(f)}$, meaningfully defined only in the "fermion pairs contribution to self-energies approximation", i.e. to the extent that all one loop contributions of different nature are neglected. This means that, if one wants to eliminate in Eq. (3.218) the bare parameter $\sin^2\theta_W$ using e.g. Eqs. (3.153), (3.154), only the fermion pairs contribution to Eq. (3.154) should be retained, to guarantee a self-consistent procedure in this preliminary and approximate treatment.

as in Eq. (3.216).

Equation (3.218) provides the formal definition of the component of the effective electroweak mixing angle that takes fermion pairs contributions to self-energy effects at one loop into account. We shall now show that it can be rewritten in a more fashionable way, as a sum of physical parameters and of quantities previously defined in this Chapter. As a first and mandatory step in this direction, we shall verify that the quantity defined by Eq. (3.218) as the sum of a bare parameter and of a transverse self-energy, both separately infinite, is actually finite. As we did in Subsection 3.2.2, Eq. (3.158), we shall be limited to the consideration of the contribution to $\sin^2\theta_W, A^{(\gamma Z)}$ from a lepton family $\equiv (\ell, \nu_\ell)$. To compute its infinite part, we shall use our previous equations (3.153), (3.154) and work consistently following the comment given in the footnote after Eq. (3.218), i.e. only retaining fermion pairs contributions on both sides of it. In this way, we obtain from Eq. (3.218):

$$\sin^2\theta^{(f)}_{W,eff} = \left[1 - \frac{m_W^2}{m_Z^2}\right] + \frac{m_W^2}{m_Z^2} Re\left[\frac{A^{(Z)}(m_Z^2)}{m_Z^2} - \frac{A^{(W)}(m_W^2)}{m_W^2}\right]^{(f)} + \sin\theta_W \cos\theta_W Re\frac{A^{(f)(\gamma Z)}(m_Z^2)}{m_Z^2} \,. \tag{3.219}$$

The calculation of the coefficient of the infinite contribution from a (ℓ, ν_ℓ) family proceeds now in the known way, leading to the result:

$$\sin^2\theta^{(\ell,\nu_\ell)(\infty)}_{W,eff} = \Delta\left[e_0^2 192\pi^2 \sin^2\theta_W\right] \times \left\{\left[3 - 6\frac{m_e^2}{m_Z^2} + (1 - 4\sin^2\theta_W)^2 - 4 + 4\sin^2\theta_W + 6\frac{m_e^2}{m_Z^2}\right] + 4\sin^2\theta_W(1 - \sin^2\theta_W)\right\} = 0 \tag{3.220}$$

(the terms in the square bracket correspond to the $A^{(Z)}, A^{(W)}$ contribution). Analogous conclusion, suggested as an useful exercise to the reader, can be derived for the general contribution from a (u, d) quark couple.

Having checked that the definition of Eq. (3.218) is actually physically acceptable (i.e. infinity free) we can rewrite Eq. (3.219) in the more understandable way:

$$\sin^2\theta^{(f)}_{W,eff} = \left[1 - \frac{m_W^2}{m_Z^2}\right] + O(\alpha) \tag{3.221}$$

where the *finite* $O(\alpha)$ one loop effect is fully given by the fermion pairs contribution to transverse self-energies.

A first important conclusion that can be already drawn at this point is the fact that the effective mixing angle is *not* equal to $[1-(m_W^2/m_Z^2)]$, and will differ from that quantity as the result of the presence of one-loop corrections. This is quite different from the situation met at the tree level, where the *same* bare parameter $\sin^2\theta_W$ was defined both by the bare mass ratio, $\sin^2\theta_W = [1-(m_W^2/m_Z^2)]$, and by the bare expression of $A_{LR}^{(0)}$ Eq. (3.208). To give the previous conclusion a more quantitative content, we return to Eq. (3.219) and, working consistently at the one-loop order and using the definitions of Eq. (3.169), re-express it in the equivalent way:

$$\sin^2\theta_{W,eff}^{(f)} = \left[1-\frac{m_W^2}{m_Z^2}\right] + \left[\frac{m_W^2}{m_Z^2}\left(\Delta_1(0)-\Delta_2\right) - \left(1-\frac{m_W^2}{m_Z^2}\right)\Delta_3\left(m_Z^2\right)\right]. \quad (3.222)$$

In the previous equation, an apparent dependence on the (unwanted) parameter m_W is exhibited. This can be eliminated exploiting the fact that, at the one-loop level, one can write:

$$\left[1-\frac{m_W^2}{m_Z^2}\right] = s_0^2 + \frac{c_0^2 s_0^2}{2c_0^2-1}\Delta r^W \quad (3.223)$$

having used Eqs. (3.204), (3.206). Inserting the previous equality in Eq. (3.222), one obtains the final expression:

$$\sin^2\theta_{W,eff}^{(f)} = s_0^2 + \frac{s_0^2}{2c_0^2-1}\left[\Delta_3\left(m_Z^2\right) - c_0^2\Delta_1(0)\right] \quad (3.224)$$

and, inside $\Delta_1(0)$, $\Delta_3\left(m_Z^2\right)$, one can safely set $\frac{m_W^2}{m_Z^2} = c_0^2 \simeq 0.769$.

Equation (3.224) shows the expression of the effective mixing angle in the MSM, in the approximation of only retaining the fermion pairs contribution to self-energies at one loop. As anticipated in this Chapter, the result does *not* depend on the Δ_2 parameter. It will be numerically fixed by the values of the input quantities $\alpha(m_Z^2)$, G_F, m_Z that determine s_0^2, and by those of the other parameters that appear at one loop, in particular the top mass m_t that affects $\Delta_1(0)$. Keeping in mind the fact that we have only derived an *approximate* expression of the weak mixing angle,

we shall now perform in the next Subsections a systematic investigation of the various relationships between $\sin^2\theta_{W,eff}$ and the various experimental observables at the Z peak, always retaining the same "fermion pairs dominance" approximation. The reason, that we must anticipate, is the fact that the set of formulae that we shall obtain in this way will be simple and understandable and, more important, easily generalizable to the realistic situation in which *all* the one-loop effects will be consistently taken into account.

3.3.3 *Relationship between* $\sin^2\theta^{(f)}_{W,eff}$ *and* m_Z

As the first example of the interconnection between the weak effective mixing angle and the quantities that can be measured at the Z peak, we shall now derive the formula that relates, at one loop, the value of the Z mass to that of $\sin^2\theta_{W,eff}$. This derivation is rather simple if one starts from the definition of $c_0^2 s_0^2$ Eq. (3.200) and rewrites it in the equivalent form:

$$m_Z^2 = \frac{\alpha\left(m_Z^2\right)\pi}{\sqrt{2}G_F}\frac{1}{c_0^2 s_0^2}\,. \tag{3.225}$$

The next step is provided by Eq. (3.224) that, in the usual one-loop philosophy, can be rewritten as follows:

$$s_0^2 c_0^2 = \sin^2\theta^{(f)}_{W,eff}\left(1-\sin^2\theta^{(f)}_{W,eff}\right)\left[1+\Delta_1(0)-\frac{\Delta_3\left(m_Z^2\right)}{c_0^2}\right]. \tag{3.226}$$

Combining the previous equations we can finally write the equality:

$$m_Z^2 = \frac{\alpha\left(m_Z^2\right)\pi}{\sqrt{2}G_F}\frac{1}{\sin^2\theta^{(f)}_{W,eff}\left(1-\sin^2\theta^{(f)}_{W,eff}\right)} \times \frac{1}{\left[1+\Delta_1(0)-\frac{\Delta_3\left(m_Z^2\right)}{c_0^2}\right]}\,. \tag{3.227}$$

Equation (3.227) is a simple relationship between different observables that are measurable at the Z peak. It is fixed by the numerical values of m_Z, G_F, $\alpha(m_Z^2)$ and by those of the two weak parameters $\Delta_1(0)$, $\Delta_3(m_Z^2)$. The third weak parameter Δ_2 does not appear, as we have anticipated. We shall find the same properties in all the following examples that will be provided for other observables in the following Subsections.

3.3.4 *The Z leptonic width at one loop in the 'fermion pairs' approximation*

A typical observable that can be measured with very high precision at the Z peak is the Z partial decay width into a specific final fermion-antifermion state. We shall now consider in some detail the derivation of the corresponding MSM expression at one loop, as a useful illustrative example. To begin with, we shall consider the simplest possible realistic case, that of of a purely leptonic charged final state; the generalization to hadronic production will be treated in the following Chapter.

We already derived in Chapter 2 the tree-level expression of the leptonic width Γ_ℓ, that we shall rewrite as:

$$\frac{\Gamma_\ell^{(0)}}{m_Z} = \left[\frac{G_F^{(0)} m_Z^2}{6\pi\sqrt{2}}\right]\left[|g_{V\ell}^{(0)}|^2 + |g_{A\ell}^{(0)}|^2\right] \tag{3.228}$$

(we are now using bare parameters, and the identity of Eq. (3.127)).

To generalize the previous definition at one loop, several approaches are possible. In this Subsection we shall continue to work in the spirit of the previous part of this Book. To begin with, we shall redefine the Z leptonic width at tree level by considering the corresponding expression of the *pure* Z component of the cross section for the process of electron-positron annihilation into a charged lepton-antilepton $(\ell\bar{\ell})$ pair at variable squared c.m. energy q^2, given in Chapter 2. For our purposes, we shall write it as follows:

$$\frac{\sigma_\ell^{(0)(Z)}\left(q^2\right)}{q^2} = \frac{12\pi}{\left(q^2 - m_Z^2\right)^2}\left[\frac{\Gamma_e^{(0)}\Gamma_\ell^{(0)}}{m_Z^2}\right] . \tag{3.229}$$

The previous equality is a tree level one, and as such it must be handled with some caution. It can, though, provide a useful operative definition if it is rewritten as follows:

$$\lim_{q^2 \to m_Z^2} \frac{\sigma_\ell^{(0)(Z)}\left(q^2\right)}{12\pi q^2}\left[D_Z^{(0)}\left(q^2\right)\right]^2 = \left[\frac{\Gamma_e^{(0)}\Gamma_\ell^{(0)}}{m_Z^2}\right] \tag{3.230}$$

where $D_Z^{(0)}(q^2) = q^2 - m_Z^2$ is the denominator that appears in the *bare* Z propagator.

Following the procedure already illustrated in this Chapter, when the definition of the *physical* electric charge at one loop was just the generalization of that given at tree level for the bare one, we shall define the *physical* leptonic width at one loop as the simple generalization of Eq. (3.230), i.e.:

$$\lim_{q^2 \to m_Z^2} \frac{\sigma_\ell^{(1)(Z)}\left(q^2\right)}{12\pi q^2} |D_Z^{(1)}\left(q^2\right)|^2 = \left[\frac{\Gamma_e^{(1)}\Gamma_\ell^{(1)}}{m_Z^2}\right] \tag{3.231}$$

where $D_Z^{(1)}(q^2)$ is the denominator that appears in the *physical* Z propagator at one loop, that does *not* vanish at $q^2 = m_Z^2$. This allows to rewrite Eq. (3.231) in the more useful form:

$$\lim_{q^2 \to m_Z^2} \frac{\sigma_\ell^{(1)(Z)}\left(q^2\right)}{12\pi q^2} = \frac{1}{|D_Z^{(1)}\left(m_Z^2\right)|^2} \left[\frac{\Gamma_e^{(1)}\Gamma_\ell^{(1)}}{m_Z^2}\right] . \tag{3.232}$$

The l.h.s. of Eq. (3.232) is essentially the result of the process of squaring the Z-component of the invariant scattering amplitude of the process (summing and averaging over polarizations). This suggests that to derive the quantity on the r.h.s. it will be sufficient to write the modified expression of the square of the Z component of the invariant scattering amplitude at one loop, in the limit $q^2 \to m_Z^2$. This can be done starting from the expression of that amplitude at tree level Eq. (3.6), that can be written in the equivalent form:

$$\begin{aligned} A_{e\ell}^{(0),(Z)}\left(q^2,\theta\right) = & \left[i\sqrt{2}G_F^{(0)}\frac{m_Z^2}{q^2-m_Z^2}\right] \\ & \times \left[\bar{u}_\ell\left(\vec{p}_3\right)\gamma_\mu\left(g_{V\ell}^{(0)} - \gamma_5 g_{A\ell}^{(0)}\right)v_\ell\left(\vec{p}_4\right)\right. \\ & \left. \times\ \bar{v}_e\left(\vec{p}_2\right)\gamma^\mu\left(g_{Ve}^{(0)} - \gamma_5 g_{Ae}^{(0)}\right)u_e\left(\vec{p}_1\right)\right] . \end{aligned} \tag{3.233}$$

In this Section, we shall only consider those modifications of the scattering amplitude at one loop that are due to the fermion pairs contribution to self-energies. In the considered case of the Z component of $A_{e\ell}$, only the corresponding effects on the bare Z propagator will have to be retained. Quite generally, these can be divided into two distinct sets. The first one is *not* altering the "external" Lorentz structure of tree level Feynman diagram, that appears in the second square bracket on the r.h.s. of Eq. (3.233), and simply modifies the "internal" structure represented by the first square

bracket on the r.h.s. of the same Equation. This corresponds to the insertion of the Z self-energy diagrams like that shown in Fig. 3.7. The second set also modifies the external structure and is given, in the approximation that is being used, by the insertion of $Z\gamma$ self-energy diagrams with a photon entering either the initial or the final vertex. The effect of the first set of Feynman diagrams can be easily computed. By a straightforward applications of the simple prescriptions that were given in this Chapter one derives that:

$$\begin{aligned}\frac{m_Z^2}{q^2-m_Z^2} &= \frac{m_Z^2+ReA^{(Z)}\left(m_Z^2\right)}{q^2-m_Z^2-ReA^{(Z)}\left(m_Z^2\right)} \\ &\to \frac{m_Z^2+ReA^{(Z)}\left(m_Z^2\right)}{q^2-m_Z^2-ReA^{(Z)}\left(m_Z^2\right)+A^{(Z)}\left(q^2\right)}\end{aligned} \tag{3.234}$$

where the transverse self-energy function $A^{(Z)}\left(q^2\right)$ will have in general both a real (Re A) and an imaginary (Im A) component.

The previous Equation can be rewritten, by straightforward repeated applications of those allowed one- loop tricks that we have often illustrated (that we suggest as useful exercise to the reader), in the more appealing form:

$$\begin{aligned}\frac{m_Z^2}{q^2-m_Z^2} \to \frac{m_Z^2}{D_Z^{(1)}\left(q^2\right)}\Bigg[1 &+ \frac{ReA^{(Z)}\left(m_Z^2\right)}{m_Z^2} \\ &- Re\left(\frac{A^{(Z)}\left(q^2\right)-A^{(Z)}\left(0\right)}{q^2}\right) \\ &- m_Z^2 Re\left(\frac{F^{(Z)}\left(q^2\right)-F^{(Z)}\left(m_Z^2\right)}{q^2-m_Z^2}\right)\Bigg]\end{aligned} \tag{3.235}$$

where the definition $A^{(Z)}\left(q^2\right)=A^{(Z)}\left(0\right)+q^2F^{(Z)}\left(q^2\right)$ has been used and $D_Z^{(1)}\left(q^2\right)$ is the denominator of the physical Z propagator, whose explicit expression is:

$$D_Z^{(1)}\left(q^2\right)=q^2-m_Z^2+iq^2\frac{\Gamma_Z\left(q^2\right)}{m_Z}\ . \tag{3.236}$$

The real quantity $\frac{\Gamma_Z\left(q^2\right)}{m_Z}$ is defined as:

$$\frac{\Gamma_Z\left(q^2\right)}{m_Z}=\frac{ImF^{(Z)}\left(q^2\right)}{1+ReF^{(Z)}\left(q^2\right)+m_Z^2Re\left(\frac{F^{(Z)}(q^2)-F^{(Z)}\left(m_Z^2\right)}{q^2-m_Z^2}\right)}$$

$$= ImF^{(Z)}\left(q^2\right) + O\left(\alpha^2\right) \simeq ImF^{(Z)}\left(q^2\right) \tag{3.237}$$

and is called the energy-dependent Z (total) width. One verifies immediately that each contribution from a given fermion-antifermion pair $F\bar{F}$ reproduces, modulo $O\left(\alpha^2\right)$ terms, the partial Z width Γ_F into $F\bar{F}$ defined in Chapter 2 at $q^2 = m_Z^2$.Thus one can safely omit at one-loop the q^2 dependence and simply write Γ_Z $(= \sum_F \Gamma_F$)in Eq. (3.236).

One still has to replace the bare coupling $G_F^{(0)}$ in Eq. (3.233) with the physical one and perform the limit $q^2 \to m_Z^2$. Using the expression of the shift δG_F Eq. (3.143) finally leads to the expression of the modification of the Z component of the scattering amplitude due to the fermion pairs (f) contribution to the Z transverse self-energy:

$$\begin{aligned}\lim_{q^2 \to m_Z^2} A_{e\ell}^{(1)}\left(q^2,\theta\right) D_Z^{(1)}\left(m_Z^2\right) &= i\sqrt{2} G_F m_Z^2 \\ &\times \left[1 + \Delta_1(0) - m_Z^2 \dot{F}^{(f),(Z)}\left(m_Z^2\right)\right] \\ &\times \left[\bar{u}_\ell\left(\vec{p}_3\right)\gamma_\mu \ldots\ldots\right]\end{aligned} \tag{3.238}$$

where $\dot{F}\left(m_Z^2\right)$ denotes the q^2 derivative of F at $q^2 = m_Z^2$ and the second square bracket on the r.h.s. is still equal to the tree level one.We now assume universality for the Z-charged lepton couplings so that $\Gamma_e = \Gamma_\ell$. Then the l.h.s. of the previous equation is exactly that which produces the *internal* shift of the partial width.This will be obtained by the simple formal replacement:

$$\begin{aligned}\frac{G_F^{(0)} m_Z^2}{6\pi\sqrt{2}} &\to \frac{G_F m_Z^2}{6\pi\sqrt{2}} \\ &\times \left[1 + \Delta_1(0) - m_Z^2 \dot{F}^{(f),(Z)}\left(M_z^2\right)\right] .\end{aligned} \tag{3.239}$$

The second modification of the tree level partial width is due to the change of the *external* structure, corresponding to the second square bracket on the r.h.s. of Eq. (3.228) and due, in our approximation, to the insertion of the γZ self-energy. Without entering a formal discussion, we can easily guess what effect will arise. In fact, the rôle of the external structure, after spin summation and averaging, is that of generating the term $\simeq \left[g_{V\ell}^{(0)2} + g_{A\ell}^{(0)2}\right] = \frac{1}{4}\left[1 + \left(1 - 4\sin^2\theta_W\right)^2\right]$. From the discussion given in Subsection 3.3.2 we already know that the fermion pairs contribution to

the γZ self-energy will simply generate at one loop the formal replacement $\sin^2\theta_W \to \sin^2\theta^{(f)}_{W,eff}$, where the latter parameter is defined e.g. by Eq. (3.212). Therefore we can conclude that, within the *fermion pairs* approximation, the final expression of the Z charged leptonic width Γ_ℓ will be at one loop:

$$\begin{aligned}\frac{\Gamma^{(1)(f)}_\ell}{m_Z} &= \frac{G_F m_Z^2}{24\pi\sqrt{2}} \\ &\times \left[1 + \Delta_1(0) - m_Z^2 \dot{F}^{(f)(Z)}\left(m_Z^2\right)\right] \\ &\times \left[1 + \left(1 - 4\sin^2\theta^{(f)}_{W,eff}\right)^2\right] . \end{aligned} \tag{3.240}$$

The previous equation gives the first example of the deep interconnection between different observables at the Z peak. It shows that the *same* parameter $\sin^2\theta_{W,eff}$ that is measured by the longitudinal polarization asymmetry also enters the expression of the Z leptonic width, together with a set of electroweak one-loop corrections to the tree level formula. The latter ones will depend in general on some of the characteristic MSM parameters $(m_t, m_H ....)$, whose numerical values will have to be in agreement with those of the various measured quantities in a suitable overall numerical fit.

Given the relevance of this statement, we shall now devote the remaining part of this Chapter to a more general analysis, that also includes those one-loop effects (non fermionic contributions to self-energies, vertices, boxes) that we have neglected until now. This will lead to the *complete* one-loop expression of the fundamental parameter $\sin^2\theta_{W,eff}$ and, also, to the generalization of all those equations that were written in the *fermion pairs* contribution approximation. As we shall see, the final form of all the relevant expressions will be obtained by an immediate and simple modification of the "approximate" ones, that will be discussed in the forthcoming Section.

3.4 The complete expression of $\sin^2\theta_{W,eff}$ at one loop

Our derivation of the MSM expression of the physical observables at the Z peak at one loop has only considered, until now, the addition to the tree level Z exchange of those effects that are due to the fermion-pairs contri-

butions to the gauge bosons self-energies. As a result of this procedure we have obtained approximate formulae, whose numerical reliability still has to be discussed. But, independently of this important "detail", it must be stressed that the approximation thus derived can be considered as a *physical* one, since it is evidently *gauge-invariant*. This property, that must be obviously a common feature of every theoretical prediction, is a simple consequence of the fact that in the fermion propagators, that must be integrated in their virtual four-momentum to obtain their contribution to the *transverse* gauge bosons self-energies $A_{\gamma,W,Z\ldots}\left(q^2\right)$, there is no dependence on the gauge-fixing parameters ξ_j that can be transmitted to A.

The previous feature is no longer valid as soon as we consider contributions to the gauge bosons self-energies that involve a non fermionic loop (to be generally called *bosonic contributions*). In the case of electron-positron annihilation, the simplest representative example is that of a W bosons bubble represented in Fig. 3.19.

The related complication can be summarized as follows: the Feynman diagram of that Figure generates a contribution to the γ, Z self-energies that will be the result of an integration over a virtual four-momentum κ analogous to that of Eq. (3.26), but with the fermion propagators replaced by the W ones that are of the form given in Eq. (3.17), with a ξ_W dependence in their *longitudinal* parts.Thus, in full generality, one expects for the self-energy tensor $\Pi^{\gamma,Z}_{\mu,\nu}$ a dependence on ξ_W from that integration.

The delicate point is the fact that the ξ dependence of the *longitudinal* components of the integrands "migrates" into (also) the *transverse* component of the integrated function A, so that, using a self-explaining notation in which (W, W) denotes the W pairs contribution:

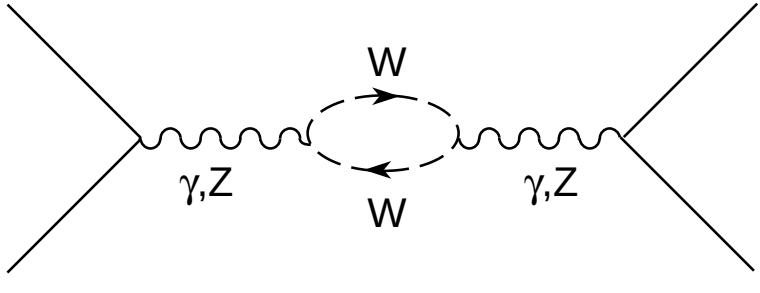

Fig. 3.19 Self-energy diagram including a W^+W^- pair.

$$A^{(W,W)(\gamma,Z)} = A^{(W,W)(\gamma,Z)}\left(q^2, \xi_W\right) \ . \tag{3.241}$$

Technically speaking, the reason of this "migration" is the fact that, after κ integration, a term of the form $\simeq \kappa_\mu \kappa_\nu$ can generate a Lorentz tensor $\simeq g_{\mu\nu}$ that contributes the transverse part of the self-energy. As a consequence of this fact, there will be, in the expression of the invariant scattering amplitude at one loop,some contributions from self-energies that will *not* be gauge-invariant.Since the scattering amplitude *must* conversely be the same in any arbitrary gauge, at any order of perturbation theory, there will have to be necessarily, at the considered one-loop level, contributions of different nature that add up to the previous ones and *cancel* the previous ξ dependence.

Clearly, the immediate candidate diagrams are those of vertex and of box type, represented by Figs. 3.6 and 3.7. In particular, on pure intuitive arguments, one expects that a gauge dependence is generated by diagrams where two W's are exchanged, like those represented in Fig. 3.19.

In fact, this feeling is correct, since one can easily verify that both diagrams do depend on the parameter ξ_W. The next expectation is then that there will be special "intelligent" combinations of transverse self-energies, vertices and boxes that will make up physically meaningful gauge-invariant "blocks", calculable in any arbitrary gauge obtaining the same expressions, exactly like in the case of the fermion pairs contribution to the transverse self-energies.To determine such combinations represents a quite useful exercise. One clean way of obtaining these combinations is that of computing rigorously all the separate Feynman diagrams, with their explicit ξ dependence; then its elimination is relatively straightforward. A simpler attitude that we shall follow is that of showing how the "intelligent" combinations

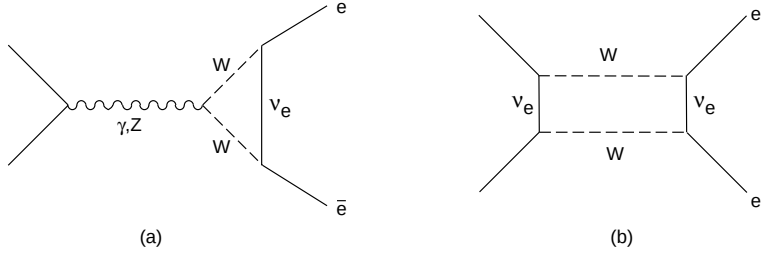

Fig. 3.20 Vertex diagram (a) and box diagram (b) involving double W exchange, for a final leptonic state.

must be, on quite general grounds. Then they will be computed in a special ($\xi = 1$) gauge, and will lead to the requested *physical* predictions for all the relevant observables. This will be done in the remaining part of this Chapter.

3.4.1 *A gauge-invariant classification of one-loop effects*

The starting point of this discussion will be the consideration of the invariant scattering amplitude for the process of electron-positron annihilation into a charged lepton-antilepton $\ell\bar{\ell}$ pair; the generalization to the case of a final quark-antiquark pair will then be straightforward. As usually, we shall work in the approximation of considering massless *external* fermions. At the tree level the MSM expression is given by Eqs. (3.5),(3.6) and consists of the sum of two components that we shall call the $\gamma\gamma$ and ZZ Lorentz structures. These correspond to the two products $j_\ell^{\mu(\gamma)} j_{e\mu}^{(\gamma)}$ and $j_\ell^{\mu(Z)} j_{e\mu}^{(Z)}$ whose terms are defined by Eqs. (3.7)–(3.10) ($f = \ell$ now), and correspond to the propagation of a photon and of a Z in the s-channel. Since we shall not consider Bhabha scattering in this Chapter, these are the only independent Lorentz structures at tree level.

The previous statement is no longer true when one moves to the next one-loop level. The simplest example is provided by the two self-energy diagrams represented in Fig. 3.21, that we shall conventionally indicate as of "γZ" and of "$Z\gamma$" type, following the order (from left to right) of the initial and final state in the diagrams.

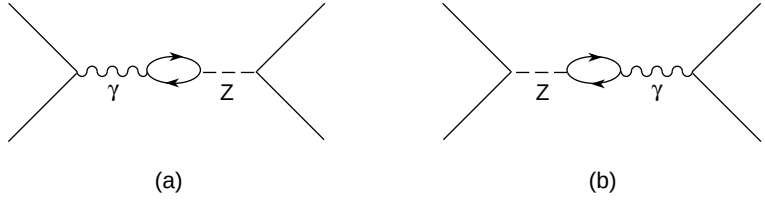

Fig. 3.21 Self-energy diagrams (a) of "γZ" type and (b) of "$Z\gamma$" type. The internal loops represent both fermionic and bosonic contributions.

These contribute the scattering amplitude in the way that we write, from our prescriptions, as follows:

$$A_{e\ell}^{(1)(a)}\left(q^2,\theta\right) + A_{e\ell}^{(1)(b)}\left(q^2,\theta\right) =$$

$$-ij_\ell^{\mu(Z)}\left[\frac{1}{q^2-m_Z^2}A^{(\gamma Z)}\left(q^2\right)\frac{1}{q^2}\right]j_{e\mu}^{(\gamma)}$$
$$-ij_\ell^{\mu(\gamma)}\left[\frac{1}{q^2}A^{(\gamma Z)}\left(q^2\right)\frac{1}{q^2-m_Z^2}\right]j_{e\mu}^{(Z)} \tag{3.242}$$

($A^{(\gamma Z)}$ is the transverse γZ self-energy, for which the ordering of γ, Z indexes is irrelevant). The previous equation shows that two new Lorentz structures $\simeq j_\ell^{\mu(Z)}j_{e\mu}^{(\gamma)}, j_\ell^{\mu(\gamma)}j_{e\mu}^{(Z)}$ have now appeared. In the process that we are considering, as a consequence of the assumed universality of electroweak interactions, the two structures are identical. For final hadronic states $\ell \to f = u, d, s, c, b$ they will not coincide, and for this reason we retain the apparently useless double leptonic index.

It is straightforward to verify that no new Lorentz structures are introduced by the remaining one-loop diagrams. Consider first the remaining self-energy diagrams represented in Fig. 3.21, that modify the photon and the Z propagators.

These will simply act as multiplicative correction factors to the corresponding tree-level $\gamma\gamma$ and ZZ structures, since from an immediate application of our rules we obtain from them the following contributions to the scattering amplitude:

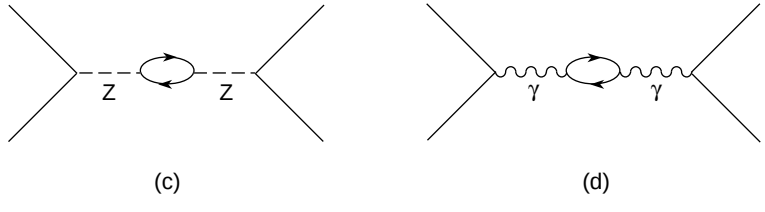

Fig. 3.22 (c) Z self-energy and (d) γ self-energy diagrams at one loop, with both fermionic and bosonic pairs included.

$$A_{e\ell}^{(1)(c)}\left(q^2,\theta\right) = ij_\ell^{\mu(Z)}\left[\frac{1}{q^2-m_Z^2}\left(1-\frac{A^{(Z)}\left(q^2\right)}{q^2-m_Z^2}\right)\right]j_{e\mu}^{(Z)} \tag{3.243}$$

$$A_{e\ell}^{(1)(d)}\left(q^2,\theta\right) = ij_\ell^{\mu(\gamma)}\left[\frac{1}{q^2}\left(1-F^{(\gamma)}\left(q^2\right)\right)\right]j_{e\mu}^{(\gamma)}\,. \tag{3.244}$$

Note that in all Eqs. (3.237), (3.238), (3.239) the transverse self-energies contain *all* contributions i.e. both those from fermion pairs and those of *bosonic* type, that implies in general a gauge-dependent contribution.

The key and simple observation is now that, *within the MSM and for massless external fermions*, also the remaining diagrams of vertex and box type do not introduce extra Lorentz structures.For vertices, the two typical diagrams are those depicted in Figs. 3.23–3.24, where the bubbles contain all possible *weak* contributions (purely QED vertices have known features and can be computed separately, together with other QED effects, in a known way).

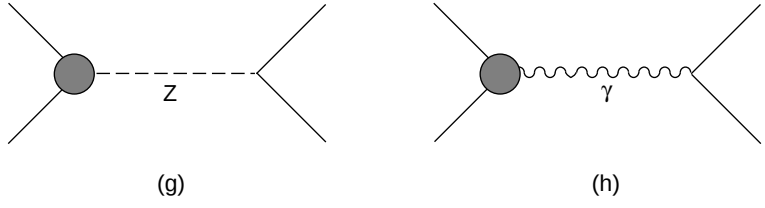

Fig. 3.23 Examples of vertex diagrams at one loop: (g) initial Z vertex, (h) initial γ vertex.

We shall define their contribution to the scattering amplitude with the following notations:

$$A_{e\ell}^{(1)(g)}\left(q^2,\theta\right) = ij_\ell^{\mu(Z)}\frac{1}{q^2-m_Z^2}\Gamma_{e\mu}^{(Z)} \tag{3.245}$$

$$A_{e\ell}^{(1)(h)}\left(q^2,\theta\right) = ij_\ell^{\mu(\gamma)}\frac{1}{q^2-m_Z^2}\Gamma_{e\mu}^{(\gamma)} \tag{3.246}$$

where the functions $\Gamma_{e\mu}^{(\gamma)}, \Gamma_{e\mu}^{(Z)}$ take into account vertices like those shown in Fig. 3.10 and similar ones, and for the moment we only need the fact that, under our assumptions, their only possible Lorentz decomposition will be:

$$\Gamma_{e\mu}^{(Z)} = a_1 j_{e\mu}^{(Z)} + a_2 j_{e\mu}^{(\gamma)} \tag{3.247}$$

$$\Gamma_{e\mu}^{(\gamma)} = a_3 j_{e\mu}^{(Z)} + a_4 j_{e\mu}^{(\gamma)} \tag{3.248}$$

where $a_{1,2,3,4}$ are certain functions that will depend on the bare parameters of the MSM.

The previous equations are simply a consequence of the fact that, for massless external fermions, any diagram of vertex type can only be a combination of a vector $\simeq \gamma_\mu$ and of an axial-vector $\simeq \gamma_\mu\gamma_5$ Lorentz component, owing to the form of the electroweak interaction Lagrangian of the

MSM.This will generate an immediate decomposition of the $\Gamma_{e\mu}$ functions along two Lorentz vector and Lorentz axial-vector "axes":

$$\Gamma_{e\mu}^{(Z)} = b_1 \bar{v}_e\left(\vec{p}_2\right) \gamma_\mu \gamma_5 u_e\left(\vec{p}_1\right) + b_2 \bar{v}_e\left(\vec{p}_2\right) \gamma_\mu u_e\left(\vec{p}_1\right) \tag{3.249}$$

$$\Gamma_{e\mu}^{(\gamma)} = b_3 \bar{v}_e\left(\vec{p}_2\right) \gamma_\mu \gamma_5 u_e\left(\vec{p}_1\right) + b_4 \bar{v}_e\left(\vec{p}_2\right) \gamma_\mu u_e\left(\vec{p}_1\right) \tag{3.250}$$

where $b_{1,2,3,4}$ are other functions that also depend on the bare parameters.

To move from the decompositions of Eqs. (3.249), (3.250) on the Lorentz vector-axial vector components to those of Eqs. (3.247), (3.248) along the photon-Z ones is like a change of axes in a two-dimensional space. From the expressions of $j_\mu^{(\gamma)}$, $j_\mu^{(Z)}$ Eqs. (3.7)–(3.10) one obtains easily the connections between the a_i and the b_i functions, that reads:

$$a_1 = -\frac{1}{|e_0|}\left[\frac{2\sin\theta_W \cos\theta_W}{g_{Ae}^{(0)}} b_1\right] \tag{3.251}$$

$$a_2 = \frac{1}{|e_0| Q_e}\left[\frac{g_{Ve}^{(0)}}{g_{Ae}^{(0)}} b_1 + b_2\right] \tag{3.252}$$

$$a_3 = -\frac{1}{|e_0|}\left[\frac{2\sin\theta_W \cos\theta_W}{g_{Ae}^{(0)}} b_3\right] \tag{3.253}$$

$$a_4 = \frac{1}{|e_0| Q_e}\left[\frac{g_{Ve}^{(0)}}{g_{Ae}^{(0)}} b_3 + b_4\right] . \tag{3.254}$$

It is convenient at this point to introduce the *projections* of the $\Gamma_{e\mu}$ functions on the two photon and Z "axes" as from Eqs. (3.247), (3.248). Using the conventional notation for ordinary vectors, we shall write [51]:

$$a_{1,2} = \left(j_{e\mu}^{(Z),(\gamma)}, \Gamma_{e\mu}(Z)\right) \tag{3.255}$$

$$a_{3,4} = \left(j_{e\mu}^{(Z),(\gamma)}, \Gamma_{e\mu}(\gamma)\right) . \tag{3.256}$$

Using the previous notations it is now possible to rewrite the considered vertices contributions to the scattering amplitude in the following useful way:

$$A_{e\ell}^{(1)(g)}\left(q^2,\theta\right) = ij_\ell^{\mu(Z)}\left[\frac{1}{q^2-m_Z^2}\left(j_{e\mu}^{(Z)},\Gamma_{e\mu}^{(Z)}\right)\right]j_{e\mu}^{(Z)} + ij_\ell^{\mu(Z)}\left[\frac{1}{q^2-m_Z^2}\left(j_{e\mu}^{(\gamma)},\Gamma_{e\mu}^{(Z)}\right)\right]j_{e\mu}^{(\gamma)} \qquad (3.257)$$

$$A_{e\ell}^{(1)(h)}\left(q^2,\theta\right) = ij_\ell^{\mu(\gamma)}\left[\frac{1}{q^2-m_Z^2}\left(j_{e\mu}^{(Z)},\Gamma_{e\mu}^{(\gamma)}\right)\right]j_{e\mu}^{(Z)} + ij_\ell^{\mu(\gamma)}\left[\frac{1}{q^2-m_Z^2}\left(j_{e\mu}^{(\gamma)},\Gamma_{e\mu}^{(\gamma)}\right)\right]j_{e\mu}^{(\gamma)}\,. \qquad (3.258)$$

From these equations one clearly sees how the overall effect of the initial vertex diagrams can be redistributed between the four independent Lorentz structures of the process, and begins to understand which combinations of self-energies and vertices will form the separate gauge-invariant "blocks".These will be precisely the combinations that fall into the *same* Lorentz structure. In fact, the scattering amplitude must be, by definition, independent of the considered gauge.*This property must be valid for all the independent Lorentz structures that we have defined.* One can provide as support of this statement a simple physical motivation, since there would be no way that a possible gauge-dependence of a structure that only takes into account e.g. photon exchanges were "cured" by another one that only feels Z exchanges. In a strictly mathematical language, there is no possible migration of ξ_i factors from one of the considered Lorentz structures to any different one.

In a perfectly analogous way, with obvious modifications, one can treat the effect of the diagrams of final weak vertex type, represented in Fig. 3.24.

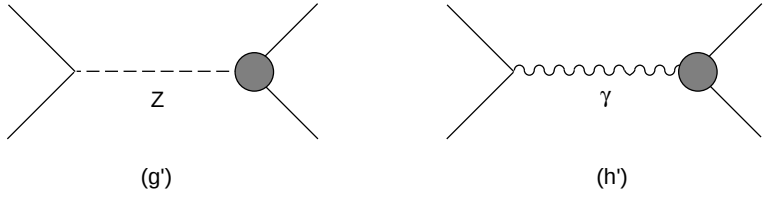

Fig. 3.24 Vertex diagrams at one loop: (g') final Z vertex, (h') final γ vertex.

The corresponding contribution to the scattering amplitude will be written in the form:

$$A_{e\ell}^{(1)(g')+(h')} = i\Gamma_{\ell}^{\mu(Z)} \frac{1}{q^2 - m_Z^2} j_{e\mu}^{(Z)} + i\Gamma_{\ell}^{\mu(\gamma)} \frac{1}{q^2} j_{e\mu}^{(\gamma)} \,. \tag{3.259}$$

The final vertex functions Γ_{ℓ}^{μ} can be decomposed along their photon and Z components exactly like in the case of the initial vertex ones. We shall identify the relevant projections with the notations $(j_{\ell}^{\mu}, \Gamma_{\ell}^{\mu})$ and γ, Z indexes on the corresponding quantities, and write the contribution of Fig. 3.24 to the scattering amplitude in full analogy with Eqs. (3.257), (3.258) i.e.:

$$\begin{aligned} A_{e\ell}^{(1)(g')}\left(q^2,\theta\right) = {} & ij_{\ell}^{\mu(Z)} \left[\frac{1}{q^2 - m_Z^2} \left(j_{\ell\mu}^{(Z)}, \Gamma_{\ell\mu}^{(Z)}\right)\right] j_{e\mu}^{(Z)} \\ & + ij_{\ell}^{\mu(Z)} \left[\frac{1}{q^2 - m_Z^2} \left(j_{\ell\mu}^{(\gamma)}, \Gamma_{\ell\mu}^{(Z)}\right)\right] j_{e\mu}^{(\gamma)} \end{aligned} \tag{3.260}$$

$$\begin{aligned} A_{e\ell}^{(1)(h')}\left(q^2,\theta\right) = {} & ij_{\ell}^{\mu(\gamma)} \left[\frac{1}{q^2 - m_Z^2} \left(j_{\ell\mu}^{(Z)}, \Gamma_{\ell\mu}^{(\gamma)}\right)\right] j_{e\mu}^{(Z)} \\ & + ij_{\ell}^{\mu(\gamma)} \left[\frac{1}{q^2 - m_Z^2} \left(j_{\ell\mu}^{(\gamma)}, \Gamma_{\ell\mu}^{(\gamma)}\right)\right] j_{e\mu}^{(\gamma)} \,. \end{aligned} \tag{3.261}$$

The previous notations are at this point purely conventional. We shall provide a simple, illustrative and relevant example with a complete calculation of the *projections* in the special case of the $Z_{b\bar{b}}$ vertex in Chapter 4, and retain for the moment the abstract terminology that has been introduced.

The last contribution to be considered is that coming from *weak* boxes, i.e.diagrams like those of Fig. 3.10 where W's or Z's are exchanged.In the configuration of *massless* external fermions it is easy to realize that, in the MSM, these diagrams can only contribute the four Lorentz structures that we have defined, as one can directly verify by a numerical calculation.

Using a self-explaining notation, we shall therefore write the weak boxes $(w.b.)$ contribution to the scattering amplitude as:

$$\begin{aligned} (-i)\, A_{e\ell}^{(1)(w.b.)}\left(q^2,\theta\right) = {} & j_{\ell}^{\mu(Z)} \left[A_{e\ell,ZZ}^{(w.b.)}\left(q^2,\theta\right)\right] j_{e\mu}^{(Z)} \\ & + j_{\ell}^{\mu(\gamma)} \left[A_{e\ell,\gamma\gamma}^{(w.b.)}\left(q^2,\theta\right)\right] j_{e\mu}^{(\gamma)} \\ & + j_{\ell}^{\mu(Z)} \left[A_{e\ell,\gamma Z}^{(w.b.)}\left(q^2,\theta\right)\right] j_{e\mu}^{(\gamma)} \end{aligned}$$

$$+j_\ell^{\mu(\gamma)}\left[A_{e\ell,Z\gamma}^{(w.b.)}\left(q^2,\theta\right)\right]j_{e\mu}^{(Z)}\,. \qquad (3.262)$$

The overall expression of the invariant scattering amplitude at one loop, obtained as the sum of contributions from self-energies ($s.e.$), weak vertices ($w.v.$) and weak boxes ($w.b.$), can be finally written as the sum of four different, necessarily gauge-invariant, terms that correspond to the four chosen Lorentz structures in the form:

$$\begin{aligned}
&(-i)\,A_{e\ell}^{(1)(s.e.+w.v.+w.b.)}\left(q^2,\theta\right)= \\
&=j_\ell^{\mu(Z)}\left[\frac{1}{q^2-m_Z^2}\left(1-\frac{\hat{A}_{e\ell}^{(Z)}\left(q^2,\theta\right)}{q^2-m_z^2}\right)\right]j_{e\mu}^{(Z)} \\
&+j_\ell^{\mu(\gamma)}\left[\frac{1}{q^2}\left(1-\hat{F}_{e\ell}^{(\gamma)}\left(q^2,\theta\right)\right)\right]j_{e\mu}^{(\gamma)} \\
&-j_\ell^{\mu(Z)}\left[\frac{1}{q^2-m_Z^2}\frac{\hat{A}_{e\ell}^{(\gamma Z)}\left(q^2,\theta\right)}{q^2}\right]j_{e\mu}^{(\gamma)} \\
&-j_\ell^{\mu(\gamma)}\left[\frac{1}{q^2-m_Z^2}\frac{\hat{A}_{e\ell}^{(Z\gamma)}\left(q^2,\theta\right)}{q^2}\right]j_{e\mu}^{(Z)}\,. \qquad (3.263)
\end{aligned}$$

The four functions that appear in the different square brackets are the "intelligent" combinations of self-energies, vertices and boxes that were mentioned in the introduction of Section 3.4. By construction, they must be gauge-invariant. Their explicit expressions can be easily derived by simply summing the various contributions explicitly, using the notations of this Section. They read:

$$\begin{aligned}
&\frac{\hat{A}_{e\ell}^{(Z)}\left(q^2,\theta\right)}{q^2-m_Z^2}=\frac{A^{(Z)}\left(q^2\right)}{q^2-m_Z^2}-\left(j_{e\mu}^{(Z)},\Gamma_{e\mu}^{(Z)}\right) \\
&-\left(j_\ell^{\mu(Z)},\Gamma_\ell^{\mu(Z)}\right)-\left(q^2-m_Z^2\right)A_{e\ell,ZZ}^{(w.b.)}\left(q^2,\theta\right) \qquad (3.264)
\end{aligned}$$

$$\begin{aligned}
&\hat{F}_{e\ell}^{(\gamma)}\left(q^2,\theta\right)=F^{(\gamma)}\left(q^2\right)-\left(j_{e\mu}^{(\gamma)},\Gamma_{e\mu}^{(\gamma)}\right) \\
&-\left(j_\ell^{\mu(\gamma)},\Gamma_\ell^{\mu(\gamma)}\right)-q^2A_{e\ell,\gamma\gamma}^{(w.b.)}\left(q^2,\theta\right) \qquad (3.265)
\end{aligned}$$

$$\frac{\hat{A}_{e\ell}^{(\gamma Z)}\left(q^2,\theta\right)}{q^2}=\frac{A^{(\gamma Z)}\left(q^2\right)}{q^2}-\left(j_{e\mu}^{(\gamma)},\Gamma_{e\mu}^{(Z)}\right)$$

$$-\frac{q^2-m_Z^2}{q^2}\left(j_\ell^{\mu(Z)},\Gamma_\ell^{\mu(\gamma)}\right)-\left(q^2-m_Z^2\right)A_{e\ell,\gamma Z}^{(w.b.)}\left(q^2,\theta\right) \quad (3.266)$$

$$\frac{\hat{A}_{e\ell}^{(Z\gamma)}\left(q^2,\theta\right)}{q^2}=\frac{A^{(\gamma Z)}\left(q^2\right)}{q^2}-\frac{q^2-m_Z^2}{q^2}\left(j_{e\mu}^{(Z)},\Gamma_{e\mu}^{(\gamma)}\right)$$
$$-\left(j_\ell^{\mu(\gamma)},\Gamma_\ell^{\mu(Z)}\right)-\left(q^2-m_Z^2\right)A_{e\ell,Z\gamma}^{(w.b.)}\left(q^2,\theta\right)\ . \quad (3.267)$$

Note that the full dependence on the scattering angle θ is produced by the box components; self-energies *and* vertices are functions of q^2 only.As a consequence of this fact, one can already guess that at the Z peak the relevant combinations will exhibit no θ dependence.

A rather useful simplification arises now if we are strictly confined within the one-loop approximation. In this case, one can rewrite Eq. (3.263) in the equivalent, simple form that is strongly reminding the starting tree level expression of Eqs. (3.5)–(3.10):

$$A_{e\ell}^{(1)(s.e.+w.v.+w.b.)}\left(q^2,\theta\right)=ij_\ell^{\mu(\gamma)}\left[\frac{1}{q^2}\left(1-\hat{F}_{e\ell}^{(\gamma)}\left(q^2,\theta\right)\right)\right]j_{e\mu}^{(\gamma)}$$
$$+ij_\ell^{(1)\mu(Z)}\left[\frac{1}{q^2-m_Z^2}\left(1-\frac{\hat{A}_{e\ell}^{(Z)}\left(q^2,\theta\right)}{q^2-m_Z^2}\right)\right]j_{e\mu}^{(1)(Z)} \quad (3.268)$$

where $\hat{F}_{e\ell}^{(\gamma)}$, $\hat{A}_{e\ell}^{(Z)}$ are given by Eqs. (3.265), (3.264) and we have introduced the modified one-loop quantities:

$$j_{e\mu}^{(1)(Z)}=-\frac{|e_0|}{2\sin\theta_W\cos\theta_W}\bar{v}_e\left(\vec{p}_2\right)\gamma_\mu\left[g_{Ve}^{(1)}\left(q^2,\theta\right)-\gamma_5 g_{Ae}^{(0)}\right]u_e\left(\vec{p}_1\right) \quad (3.269)$$

$$j_\ell^{(1)\mu(Z)}=-\frac{|e_0|}{2\sin\theta_W\cos\theta_W}\bar{u}_\ell\left(\vec{p}_3\right)\gamma^\mu\left[g_{V\ell}^{(1)}\left(q^2,\theta\right)-\gamma_5 g_{A\ell}^{(0)}\right]v_\ell\left(\vec{p}_4\right)\ . \quad (3.270)$$

The modified one-loop vector couplings are expressed in terms of the previous gauge-invariant combinations in the following form:

$$g_{Ve}^{(1)}\left(q^2,\theta\right)=g_{Ve}^{(0)}-2\sin\theta_W\cos\theta_W Q_e\frac{\hat{A}_{e\ell}^{(\gamma Z)}}{q^2} \quad (3.271)$$

$$g_{V\ell}^{(1)}\left(q^2,\theta\right)=g_{V\ell}^{(0)}-2\sin\theta_W\cos\theta_W Q_\ell\frac{\hat{A}_{e\ell}^{(Z\gamma)}}{q^2}\ . \quad (3.272)$$

Using the definition of the bare vector couplings Eqs. (3.11), the previous expressions can be rewritten in the equivalent final form:

$$g_{Ve,\ell}^{(1)}\left(q^2,\theta\right) = I_{3Le,\ell} - 2Q_{e,\ell}s_{e,\ell}^2\left(q^2,\theta\right) \tag{3.273}$$

where:

$$s_e^2\left(q^2,\theta\right) = \sin^2\theta_W + \sin\theta_W\cos\theta_W\frac{\hat{A}_{e\ell}^{(\gamma Z)}\left(q^2,\theta\right)}{q^2} \tag{3.274}$$

and

$$s_\ell^2\left(q^2,\theta\right) = \sin^2\theta_W + \sin\theta_W\cos\theta_W\frac{\hat{A}_{e\ell}^{(Z\gamma)}\left(q^2,\theta\right)}{q^2}\,. \tag{3.275}$$

The two functions s_e^2, s_ℓ^2 are by construction gauge-invariant.Assuming lepton universality, they are obviously identical. This will not be true when final hadronic states will be examined; in that case, ℓ will become a light quark $q = u, d, s, c, b$ and the relevant quantity s_q^2 will differ from s_e^2, as we shall show in detail in Chapter 4. In Eqs. (3.274)–(3.275) an extra simplification can be introduced, once again related to the adopted one-loop conventions. To the extent that cross sections or their ratios are considered, one must always compute the squared modulus of a component of the scattering amplitude. The latter contains a *real* tree level $\simeq O(1)$ term and a complex $\simeq O(\alpha)$ one-loop correction, sum of a real and of an imaginary term. In the squared modulus, the latter generates a higher perturbative order compared to the product of the tree level with the real term; therefore, at this order, it can be consistently neglected in the expressions of the various one-loop quantities. Also, in the same self-consistency spirit, all those bare parameters that *multiply* a one-loop quantity will be systematically replaced by their *physical* corresponding ones. In particular, $m_{Z(0)}^2$ will become m_Z^2. This allows to conclude that, at the Z peak $q^2 = m_Z^2$, the θ dependence of $s_{e,\ell}^2\left(q^2,\theta\right)$ carried by the box contribution will completely disappear and we shall be entitled to write:

$$\begin{aligned} s_e^2\left(m_Z^2,\theta\right) &= s_e^2\left(m_Z^2\right) = \sin^2\theta_W \\ &+ \sin\theta_W\cos\theta_W Re\left[\frac{A_{e\ell}^{(\gamma Z)}\left(m_Z^2\right)}{m_Z^2} - \left(j_{e\mu}^{(\gamma)}, \Gamma_{e\mu}^{(Z)}\left(m_Z^2\right)\right)\right] \end{aligned} \tag{3.276}$$

and analogously:

$$s_\ell^2\left(m_Z^2,\theta\right) = s_\ell^2\left(m_Z^2\right) = \sin^2\theta_W$$

$$+\sin\theta_W\cos\theta_W Re\left[\frac{A_{e\ell}^{(\gamma Z)}\left(m_Z^2\right)}{m_Z^2}-\left(j_{\ell\mu}^{(\gamma)},\Gamma_{\ell\mu}^{(Z)}\left(m_Z^2\right)\right)\right] \quad (3.277)$$

where the real part (Re) of the corrections appears.

The gauge-invariant quantities defined by the two last equations are built of contributions to the involved self-energies $A^{(\gamma Z)}$ and vertices coming from *all* the possible particles of the MSM, i.e. both fermions *and* bosons. One immediately realizes that the *approximate* definition of the *effective* weak angle given previously in this Chapter in Eq. (3.218) was only taking the fermion pairs contribution to self-energies in Eq. (3.277) into account(final leptonic states were considered in that derivation). It appears thus natural and immediate to consider Eq. (3.277) as the *complete* definition of the effective electroweak angle, and write:

$$\sin^2\theta_{W,eff}=s_e^2\left(m_Z^2\right)=\sin^2\theta_W$$

$$+\sin\theta_W\cos\theta_W Re\left[\frac{A_{e\ell}^{(\gamma Z)}\left(m_Z^2\right)}{m_Z^2}-\left(j_{e\mu}^{(\gamma)},\Gamma_{e\mu}^{(Z)}\left(m_Z^2\right)\right)\right]. \quad (3.278)$$

Equation (3.278) is, at this point, just a formal definition. We shall prove in the remaining part of this Chapter that the quantity there defined retains the properties of its "fermion pairs approximation", and enters *all* the Z peak observables. This will be done in a pedagogical way, starting with the simplest and most intuitive case of the Z peak leptonic asymmetries, to be illustrated in the forthcoming part of the Section.

3.4.2 *Operative definition of* $\sin^2\theta_{W,eff}$*: the leptonic asymmetries at the Z peak*

From a formal point of view, a first check on the validity of the definition of the effective electroweak angle given by Eq. (3.278) is that it is *finite*. This implies the explicit calculation of all its infinite terms, to verify their overall cancellation. The latter will be the result of a process that involves both the infinite parts of the self-energy and of the vertex components of $\hat{A}_{e\ell}^{(\gamma Z)}$ *and* those of the bare parameter $\sin^2\theta_W$ that appears in the definition. For the "fermion pairs approximation" Eq. (3.219) we have already verified that the various infinite terms are actually mutually canceling, Eq. (3.220). To verify the same result for the "non fermionic" (Nf) component requires the calculation of a number of diagrams analogous to that performed in the case of the photon self-energy Eqs. (3.70)–(3.75) since once again *all*

the (physical and unphysical) particles of the MSM will contribute. The W's, *would-be* Goldstone bosons and ghosts will appear in the (γZ) self-energy, in the Z vertex and, also, in the W and Z self-energies that enter the renormalization of $\sin^2\theta_W$ Eq. (3.154). This leads to a rather long list of contributions and to the final expected cancellation of infinities, that is recommended as a useful exercise to the reader but will not be shown here.

The next fundamental point is to relate the parameter $\sin^2\theta_{W,eff}$ thus defined to measurable quantities. For physics at the Z resonance, this can be done in a quite simple way if one makes the first reasonable approximation of only retaining, in that configuration, the s-channel Z exchange. In fact we have seen in the previous Subsection that in this case, at the one-loop level, the only changes in the scattering amplitude with respect to the tree level description consist of replacing the bare Z propagator with the modified expression that appears in the second square bracket on the r.h.s. of Eq. (3.268) *and* of replacing the bare Z-lepton *vector* coupling $g^{(0)}_{Ve}$ by its modified expression Eq. (3.271), while the axial Z coupling remains unchanged. This "effective" description leads in a quite immediate way to the derivation of corresponding expressions for all those observables that are defined as *ratios* of cross sections. In fact, in such cases, the modification of the Z propagator (that is θ independent at $q^2 = m_Z^2$) acts as a common multiplicative factor both in the numerator and in the denominator, and is consequently canceled in the ratio. Thus, the final expression can be immediately obtained by taking that given at tree level, with the simple replacement of the bare Z vector coupling with its one-loop modified expression. Alternatively, one can consider the tree level ratio

$$\frac{g^{(0)}_{Ve}}{g^{(0)}_{Ae}} = 1 - 4\sin^2\theta_W \tag{3.279}$$

and replace it with the modified expression:

$$\frac{g^{(1)}_{Ve}}{g^{(0)}_{Ae}} = 1 - 4\sin^2\theta_{W,eff} \tag{3.280}$$

that corresponds to simply replacing the bare parameter $\sin^2\theta_W$ with the effective angle $\sin^2\theta_{W,eff}$ in the tree level ratios.

The previous conclusion is valid if one neglects the QED photon exchange at the Z resonance. Intuitively, given the scarce numerical relevance of that term, one expects that the prescription that was given remains

valid modulo "small and calculable" QED corrections, which is actually the case. These terms will be indicated from now on using the notation: "small QED". With this convention, we shall now list the effective expressions of the various relevant (i.e. measurable) leptonic asymmetries at the Z peak, starting from the tree level ones that can be found in Chapter 2. More precisely, we shall consider the following quantities:

a) **The longitudinal polarization asymmetry A_{LR}.**

This was already defined in Eq. (3.209). Keeping in mind the previous discussion, and that given after Eq. (3.209), we shall write its one-loop expression as follows:

$$A_{LR}^{(1)(\ell)}\left(q^2 = m_Z^2\right) = \mathcal{A}_e + \text{'small QED(LR)'}$$

$$= 2\frac{1 - 4\sin^2\theta_{W,eff}}{1 + \left(1 - 4\sin^2\theta_{w,eff}\right)^2} + \text{'small QED(LR)'}\,. \qquad (3.281)$$

Strictly speaking we are considering at this point leptonic final states (in practice $\mu^+\mu^-$ and $\tau^+\tau^-$, since for the e^+e^- final state the t-channel exchange is relevant). For hadronic final states one expects from the discussion given in Subsection 3.3.1 to find "essentially" the same expression, even after having taken into account the final-state strong interaction.

b) **The μ (τ) forward-backward asymmetry A_{FB}^{μ} (A_{FB}^{τ}).**

From the tree level expression of this observable derived in Chapter 2, one derives immediately the "effective" A_{FB}^{μ} at one loop:

$$A_{FB}^{\mu(1)}\left(q^2 = m_Z^2\right) = \frac{3}{4}\mathcal{A}_\ell^2 + \text{'small QED(FB)'} \qquad (3.282)$$

where $\mathcal{A}_\ell = \mathcal{A}_e$ is defined by Eq. (3.281) and lepton universality is assumed. The same expression holds for A_{FB}^{τ}. Note that the small QED extra terms in Eq. (3.281) and Eq. (3.282) are in principle different, which explains the extra added symbols. Also, as a matter of fact, in the expression of the forward-backward asymmetry one usually adds one more contribution from the *imaginary* part of the scattering amplitude, which seems to contradict our previous statement of ignoring it systematically. The pragmatic reason is that, for pure accidental reasons that are a consequence of the small numerical value of $\mathcal{A}_\ell^2$, the real component of A_{FB}^{μ} is so small that the imaginary component, although of a higher perturbative order, cannot be safely

neglected. This extra contribution is a *number* that has been computed [86] and we shall include it in the discussion given in the final Chapter of this book.

c) **The τ polarization asymmetry A_{pol}^{τ}.**

This quantity was defined at the tree level in Chapter 2 (Eq. 2.92), and was given by the same expression that defined $\mathcal{A}_\ell$. Thus, even at one loop, we shall continue to have, neglecting "small" QED corrections:

$$A_{pol}^{\tau(1)}\left(q^2 = m_Z^2\right) = -\mathcal{A}_\tau = -\mathcal{A}_\ell \ . \tag{3.283}$$

The three previous leptonic asymmetries represent a set of realistic observables that all provide operative definitions of the *same* fundamental weak parameter $\sin^2\theta_{W,eff}$. This can be therefore measured in a clean way using the previous observables, since it is the only weak parameter that enters their expressions. As argued previously, this can be viewed as a consequence of having considered *ratios* of cross sections at the one-loop level, which cancels the contribution from the modifies Z propagator. But at the Z peak one can also define a number of observables that are *not* ratios of cross sections. For these quantities the theoretical expression will be in general less simple e.g. containing other genuinely weak parameters different from $\sin^2\theta_{W,eff}$. The most immediate example is that of the leptonic Z partial width, that was already examined in the *fermion pairs* approximation in Subsection 3.3.4. We shall derive in the forthcoming Section its *complete* expression at one loop. This will then lead in a natural way to the introduction and to the operative definition of a *second* genuinely weak parameter, the Z -lepton effective axial vector coupling, as we shall show in some detail.

3.5 A two-parameters description of Z physics for final leptonic states

3.5.1 *Complete expression of the Z leptonic width at one-loop*

We have already sketched in Subsection 3.3.4 the derivation of the expression of the Z leptonic width in the *fermion pairs* approximation. To derive the complete one-loop formula requires a straightforward generalization of that discussion, where essentially the Z self-energy is replaced by its gauge-invariant generalization given by Eq. (3.264). To better clarify

the procedure, it is convenient to rewrite the one-loop *effective* expression of the Z component of the scattering amplitude, given in Eq. (3.268), in the more explicit way:

$$\begin{aligned} A_{e\ell}^{(Z)(1)} &= i\sqrt{2}G_F^{(0)}\left[\frac{1}{q^2-m_Z^2}\left(1-\frac{\hat{A}_{e\ell}^{(Z)}\left(q^2,\theta\right)}{q^2-m_Z^2}\right)\right] \\ &\times\left[\bar{u}_\ell\left(\vec{p}_3\right)\gamma_\mu\left(g_{V\ell}^{(1)}-\gamma_5 g_{A\ell}^{(0)}\right)v_\ell\left(\vec{p}_4\right)\right. \\ &\times\left.\bar{v}_e\left(\vec{p}_2\right)\gamma^\mu\left(g_{Ve}^{(1)}-\gamma_5 g_{Ae}^{(0)}\right)u_e\left(\vec{p}_1\right)\right] \end{aligned} \tag{3.284}$$

where the modified Z vector couplings are defined in Eq. (3.273). Starting from this expression, one simply reproduces the steps leading from Eq. (3.228) to Eq. (3.240). The only difference will be the presence of non fermionic contributions. They will affect the Z self-energy and also the shift δG_F of the vertex contributions to the generalization of the Z self-energy in the "internal" modification (first square bracket on the l.h.s. of Eq. (3.228)). Note that this quantity is not affected by boxes that disappear at $q^2 = m_Z^2$. Moreover there will be an appearance in the second square bracket on the l.h.s. of Eq. (3.228) of the *complete* $\sin^2\theta_{W,eff}$. This can be seen in the final expression, that reads:

$$\begin{aligned} \frac{\Gamma_\ell^{(1)}}{m_Z} &= \frac{G_F m_Z^2}{6\pi\sqrt{2}} \\ &\times\left[1+\frac{\delta G_F}{G_F}+\frac{A^{(Z)}(0)}{m_Z^2}-m_Z^2 Re\dot{F}^{(Z)}\left(m_Z^2\right)\right. \\ &+\left. Re\left(j_{e\mu}^{(Z)},\Gamma_{e\mu}^{(Z)}\left(m_Z^2\right)\right)+Re\left(j_\ell^{\mu(Z)},\Gamma_\ell^{\mu(Z)}\left(m_Z^2\right)\right)\right] \\ &\times g_{Ae}^{(0)2}\left[1+\left(1-4\sin^2\theta_{W,eff}\right)^2\right] \end{aligned} \tag{3.285}$$

where we have used the definition of $\sin^2\theta_{W,eff}$ given in Eq. (3.280).

In the previous equation, only real parts appear. This is not an approximation, since the imaginary component of the generalization of the Z self-energy has been reabsorbed exactly in the definition of the Z width, that is contained in the modified Z propagator and disappears from the expression of the *partial* Z width. The shift of the Fermi coupling contains a *fermion pairs* component and a *bosonic* one, as already exhibited in Eqs. (3.148),(3.149). The first one, summed to the *fermion pairs* component

of $A^{(Z)}(0)$ produces the quantity $\Delta_1(0)$ that appears in the approximate Eq. (3.240).

The first square bracket on the r.h.s. of the previous equation contains the unity and the weak parameter introduced in Ref. [39] and called ϵ_1. (Other definitions of ϵ_1 exist that incorporate a QED factor that can be factorized separately.) Following our prescription of ignoring for the moment such effects, we shall only retain the genuinely weak component of the Z width. For what concerns the leptonic index ℓ that appears, assuming as we did universality of weak interactions implies that one can identify the two vertices that appear in Eq. (3.285), $\Gamma_e = \Gamma_\ell$. This would not be allowed if a final quark pair were considered, to be denoted as $f\bar{f}$. Then the contribution of Γ_f would be in principle different from that of Γ_e, leading to a different contribution (of *non universal* kind) to Γ_f.

In conclusion, the expression of the Z leptonic width will be, under the previous assumptions, the following:

$$\begin{aligned}\frac{\Gamma_\ell^{(1)}}{m_Z} &= \frac{G_F m_Z^2}{6\pi\sqrt{2}}\left[1+\epsilon_1\right] g_{Ae}^{(0)2}\left[1+\left(1-4\sin^2\theta_{W,eff}\right)^2\right] \\ \epsilon_1 &= \frac{\delta G_F}{G_F}+\frac{A^{(Z)}(0)}{m_Z^2}-m_Z^2 Re\dot{F}^{(Z)}\left(m_Z^2\right) \\ &\quad + 2Re\left[\left(j_e^{\mu(Z)},\Gamma_e^{\mu(Z)}\left(m_Z^2\right)\right)\right] . \end{aligned} \tag{3.286}$$

The previous parameter (ϵ_1) is by construction a *gauge-invariant* quantity. This can be split into a sum of two separately gauge-invariant components. The first one is given by the *fermion pairs* approximation that has been already extensively illustrated, and is of universal (self-energy) type. The second one is given by the sum of the non fermionic contributions to the self-energies that appear in its definition *and* of the Z- component of the $Ze\bar{e}$ vertex at $q^2 = m_Z^2$. These two terms must be added *together*, since each one is separately gauge-dependent, so that only their sum has a physical meaning.

A subtle question might arise at this point: how can the gauge-dependence of the *universal* non fermionic contributions to a self-energy be canceled by an essentially *non universal* quantity like a vertex? The answer to this objection is that, between the diagrams that contribute a vertex, there exists a subset of *universal* kind. Such are for example all vertices with *two* W's stemming from the Z. As one can see in detail,

the cancellation of the gauge dependence of the self-energies in Eq. (3.286) is provided by these universal components of the vertex. One guesses at this point that the non-universal components of vertices might be in general gauge-invariant themselves, and we shall return to this point in the forthcoming Chapter.

In the *fermion pair* ("f ") approximation ϵ_1 is given by the expression:

$$\epsilon_1^{(f)} = \Delta_1(0) - m_Z^2 Re\dot{F}^{(f)(Z)}\left(m_Z^2\right) \ . \tag{3.287}$$

One easily realizes from the previous expressions that the dominant dependence on the top mass of the *complete* parameter ϵ_1 will be the quadratic one of $\Delta_1(0)$, already derived in Eq. (3.191). In fact, it is straightforward to verify that the derivative of the Z self-energy function $F^{(Z)}$ has an m_t dependence that vanishes in the large m_t limit. In first approximation this means that:

$$\epsilon_1^{(top)} \simeq \frac{3\alpha}{16\pi s_0^2 c_0^2}\frac{m_t^2}{m_Z^2} = \frac{3G_F m_t^2}{8\sqrt{2}\pi^2} \ . \tag{3.288}$$

For $m_t \simeq 2m_Z$, this generates a relative effect in Γ_ℓ of about one percent, "large" and visible at an experimental accuracy of few permil. One sees therefore in this simple preliminary example how fundamental the rôle of the top mass is in the interpretation of the leptonic measurements at the Z peak, and this will be shown in more detail in the discussion given in the corresponding Chapter.

In the expression of the Z leptonic width one sees at this point *two* weak parameters i.e. $\sin^2\theta_{w,eff}$ and ϵ_1. The first one has been endowed with a clean operative definition from the leptonic asymmetries, and we would like to ascribe an equally meaningful property to the second one. This can be done with a simple redefinition of the second weak parameter; with this purpose we first rewrite Eq. (3.286), using Eq. (3.279), in the equivalent form:

$$\begin{aligned}\frac{\Gamma_\ell^{(1)}}{m_Z} &= \frac{G_F m_Z^2}{6\pi\sqrt{2}}\left[g_{Ae}^{(0)2}\left(1+\epsilon_1\right)\right] \\ &\times \left[1 + \frac{g_{Ve}^{(1)2}\left(m_Z^2\right)}{g_{Ae}^{(0)2}}\right] \ .\end{aligned} \tag{3.289}$$

The last expression leads in a quite natural way to the idea of defining the *effective* axial Z-lepton coupling, to be called g_{Ae}, as:

$$g_{Ae} = \sqrt{1+\epsilon_1} \quad g_{Ae}^{(0)} \approx (1+\frac{\epsilon_1}{2}) g_{Ae}^{(0)} \ . \tag{3.290}$$

Using systematically this parameter in Eq. (3.289), in particular in its second square bracket, leads in the same natural way to the idea of introducing also an *effective* vector Z lepton coupling, to be called g_{Ve} and to be defined as:

$$g_{Ve} = \sqrt{1+\epsilon_1} \quad g_{Ve}^{(1)}\left(m_Z^2\right) \approx (1+\frac{\epsilon_1}{2}) g_{Ve}^{(1)}\left(m_Z^2\right) \ . \tag{3.291}$$

In terms of these quantities we shall now write the final expression of the Z leptonic width as:

$$\begin{aligned} \frac{\Gamma_\ell^{(1)}}{m_Z} &= \frac{G_F m_Z^2}{6\pi\sqrt{2}} \left[g_{Ae}^2 + g_{Ve}^2\right] \\ &= \frac{G_F m_Z^2}{6\pi\sqrt{2}} g_{Ae}^2 \left[1 + \left(1 - 4\sin^2\theta_{W,eff}\right)^2\right] \end{aligned} \tag{3.292}$$

where the weak parameter $\sin^2\theta_{W,eff}$ is defined in two equivalent ways, i.e.:

$$\begin{aligned} \sin^2\theta_{W,eff} &= \frac{1}{4}\left[1 - \frac{g_{Ve}^{(1)}\left(m_Z^2\right)}{g_{Ae}^{(0)}}\right] \\ &= \frac{1}{4}\left[1 - \frac{g_{Ve}}{g_{Ae}}\right] \ . \end{aligned} \tag{3.293}$$

In conclusion, all the considered leptonic observables at the Z peak can be expressed in terms of the *two* weak parameters $\sin^2\theta_{W,eff}$ and g_{Ae}. Both parameters are naturally and intrinsically related to one of the most characteristic features of the MSM, the presence of a neutral massive Z boson that is *mixed* with the photon and has extra *axial* couplings with fermions. For both parameters, an operative definition can be given, and we have already discussed that of the mixing angle. For the axial coupling, a simple and consistent definition can be immediately provided. This is given by the expression of the partial Z width into a neutrino-antineutrino pair, that an immediate extension of our procedure allows to write as:

$$\Gamma_\nu^{(1)} = \frac{G_F m_Z^2}{3\pi\sqrt{2}} g_{Ae}^2 \ . \tag{3.294}$$

Note that one could use as well, as independent parameters of the model, the couple of the *effective* Z lepton couplings, g_{Ae} and g_{Ve} defined by Eqs. (3.290), (3.291). Even in this case, the prescription for writing the expressions of the various leptonic observables at one loop remains that of writing the corresponding tree level expressions and of replacing there the bare couplings $g^{(0)}_{A,V}$ with the effective ones.

The previous couples of weak parameters are perfectly satisfactory to describe the leptonic observables at the Z peak, and we could conclude this Chapter at this point, if the only topics to be illustrated were the MSM. For a slightly more ambitious discussion, in which the possibility of evidencing from high precision measurements possible small deviations from the MSM predictions due to the presence of still undiscovered "new physics", those parameters did not represent the most "clever" choice at the time of the beginning of the Z physics operations. The point is that all parameters exhibit a quadratic dependence on the (at the time, unknown) top mass. This is certainly a *good* feature if one tries to derive indications on m_t from precision measurements; it is also certainly a *bad* feature if one tries to extract small extra new physics effects from these parameters, since they would be obscured by the ignorance of the value of the top mass.

A clever compromise might be the introduction of a new couple of parameters, one of which retains the large quadratic dependence on m_t, while the second one *does not*. This idea led to the proposal [39] of a new weak parameter, ϵ_3, to be used, together with ϵ_1, to provide an elegant description of the leptonic sector of Z physics. We shall review this proposal in the last forthcoming part of this Chapter.

3.5.2 *The Z peak leptonic observables in terms of the ϵ_1, ϵ_3 parameters*

One simple way of performing the useful change of parameters that was mentioned is to start from the expression of the effective electroweak angle given in Eq. (3.278).

This still contains the bare parameter $\sin^2\theta_W$, which can be eliminated using Eqs. (3.153), (3.154), obtaining the following equation:

$$\sin^2\theta_{W,eff} = \left[\quad 1 \quad - \frac{m_W^2}{m_Z^2} \right] - \frac{m_W^2}{m_Z^2} Re \quad \left[\frac{A^{(W)}\left(m_W^2\right)}{m_W^2} - \frac{A^{(Z)}\left(m_Z^2\right)}{m_Z^2} \right]$$

$$+ \sin\theta_W \cos\theta_W Re \frac{\hat{A}_{e\ell}^{(\gamma Z)}\left(m_Z^2\right)}{m_Z^2} \ . \tag{3.295}$$

The next step consists of eliminating the first square bracket on the r.h.s. of the previous equation. This can be done using Eq. (3.223) and introduces the quantities c_0^2, s_0^2 defined by Eqs. (3.200), (3.201) and the *weak* component of $\Delta_r{=}\Delta_r^W$ defined by Eq. (3.171). Working systematically at the one-loop level and exploiting the allowed known "tricks" leads, after a number of steps that one can easily perform as a useful exercise, to the relevant desired expression:

$$\sin^2\theta_{W,eff} = s_0^2 \left[\quad 1 - \quad \frac{c_0^2}{2c_0^2-1} \quad \epsilon_1 + \frac{1}{2c_0^2-1} \quad \epsilon_3 \right] . \tag{3.296}$$

The parameter ϵ_3 that appears in the square bracket is the m_t *smooth* quantity originally introduced in Ref. [39]. It is a gauge-invariant combination of self-energies, of their derivatives and of vertices. To better understand its relevant properties, we shall decompose it, as usually, into the sum of its component coming from the fermion pairs contributions to the self-energies (and to their derivatives), specified by an index (f), and by the remaining component, that includes different (Nf) contributions to self energies (and to their derivatives), and to vertices. In this spirit, we shall write:

$$\begin{aligned}
\epsilon_3 = & \quad \left[\quad \Delta_3\left(m_Z^2\right) - \quad c_0^2 m_Z^2 \quad Re\dot{Z}^{(f)(Z)}\left(m_Z^2\right) \right] \\
& + \left[\frac{c_0}{s_0}\left(2c_0^2-1\right) \quad Re\frac{A^{(Nf)(\gamma Z)}\left(m_Z^2\right)}{m_Z^2} - \quad c_0^2 \quad ReF^{(Nf)(Z)}\left(m_Z^2\right) \right. \\
& \left. - \ c_0^2 m_Z^2 \quad Re\dot{F}^{(Nf)(Z)} + \quad c_0^2 \frac{\delta\alpha^{(Nf)}}{\alpha} \right] \\
& + \left[2c_0^2 \quad Re\left(j_{e\mu}^{(Z)}, \Gamma_{e\mu}^{(Z)}\left(m_Z^2\right)\right) - c_0 s_0\left(2c_0^2-1\right) \quad Re\left(j_{e\mu}^{(\gamma)}, \Gamma_{e\mu}^{(Z)}\left(m_Z^2\right)\right) \right]
\end{aligned} \tag{3.297}$$

where the *non fermion pairs* shift of the electric squared charge $\delta\alpha^{(Nf)}$ is defined by Eqs. (3.101),(3.92) and by the related discussion of Subsection 3.1.6.

To check that the overall expression Eq. (3.297) is finite is a straightforward useful exercise that was already performed for its *fermion pairs* component. Very important for our purposes is the fact that, as one sees

from the previous equation, the complete m_t dependence of ϵ_3 will be contained in the first square bracket on its r.h.s.. In particular, given the already mentioned m_t independence of the derivative $\dot{F}^{(Z)}$ in the large m_t limit, this dependence will be the *smooth* logarithmic one of Δ_3, i.e.:

$$\begin{aligned}\epsilon_3\,(\text{large } m_t) &\simeq -\frac{\alpha}{12\pi}\frac{1}{\left(1-\frac{m_W^2}{m_Z^2}\right)}\ln\frac{m_t}{m_Z}\\ &= -\frac{m_W^2}{6\sqrt{2}}\frac{G_F}{\pi^2}\ln\frac{m_t}{m_Z}\end{aligned} \tag{3.298}$$

having exploited Eq. (3.297).

We can thus conclude that one can describe the leptonic Z peak observables that we have considered in terms of two *gauge-invariant* parameters, ϵ_1, ϵ_3, the first one of which is strongly (quadratically) m_t dependent, while the second one is *smooth* i.e. only logarithmically dependent. This fact will have quite relevant consequences for the discussion of the validity of certain electroweak models alternative to the MSM, that will be mentioned in Chapter 11. To compute the explicit dependence of all the observables on ϵ_1, ϵ_3 is simple. We already know that of $\sin^2\theta_{W,eff}$ given in Eq. (3.296). This leads immediately to the expressions of all the leptonic asymmetries, that only depend on the effective electroweak angle. For the leptonic Z width it is sufficient to start e.g. from Eq. (3.292) and to use Eq. (3.290). This gives the following result:

$$\begin{aligned}\frac{\Gamma_\ell^{(1)}}{m_Z} &= \frac{G_F}{24\pi\sqrt{2}}m_Z^2\left(1+v_0^2\right)\\ &\times\left[1+\epsilon_1\left(1+8\frac{v_0}{1+v_0^2}\frac{s_0^2c_0^2}{2c_0^2-1}\right)\right.\\ &\left.-\epsilon_3\left(8\frac{v_0}{1+v_0^2}\frac{s_0^2}{2c_0^2-1}\right)\right]\end{aligned} \tag{3.299}$$

where, using the value of $\alpha\left(m_Z^2\right)$ Eq. (3.187), one has:

$$v_0 = 1-4s_0^2 \simeq 0.0756\,. \tag{3.300}$$

Numerically, using the value $s_0^2 \simeq 0.231$ given in Eq. (3.203), one obtains:

$$\frac{\Gamma_\ell^{(1)}}{m_Z} = \frac{G_F}{24\pi\sqrt{(2)}}m_Z^2\left(1+v_0^2\right)\left[1+1.199\epsilon_1-0.258\epsilon_3\right]\,. \tag{3.301}$$

This shows that the leptonic Z width is much more dependent on ϵ_1 than on ϵ_3. The case of the asymmetries is different. The basic quantity $\mathcal{A}_e$ Eq. (3.281) has actually the following expression:

$$\mathcal{A}_e = \frac{2v_0}{1+v_0^2}\left[1 + \quad \epsilon_1 \quad \frac{4s_0^2c_0^2}{2c_0^2-1}\left(\frac{1}{v_0} - \frac{8v_0}{1+v_0^2}\right)\right.$$
$$\left. - \ \epsilon_3 \quad \frac{4s_0^2}{2c_0^2-1}\left(\frac{1}{v_0} - \frac{2v_0}{1+v_0^2}\right)\right] . \tag{3.302}$$

Numerically, this gives:

$$\mathcal{A}_e = 0.150\left[1 + 16.69\epsilon_1 - 22.48\epsilon_3\right] . \tag{3.303}$$

From the previous expression one immediately obtains that of the μ, τ forward-backward asymmetry $A_{FB}^{\ell} = \frac{3}{4}\mathcal{A}_e^2$:

$$A_{FB}^{\ell} = \frac{3}{4}\mathcal{A}_e^2 = 0.01695\left[1 + 33.37\epsilon_1 - 44.96\epsilon_3\right] . \tag{3.304}$$

One notices that, in the leptonic asymmetries, the weight of the m_t − *smooth* parameter ϵ_3 is larger than that of the m_t − *sensitive* one ϵ_1, contrary to the case of the Z leptonic width. Those observables will play therefore a complementary rôle with respect to that of the Z leptonic width.

An analogous situation occurs in the complete expression that relates the Z mass to the effective electroweak angle and generalizes the approximate one given by Eq. (3.227). This can be easily derived starting from the definition of $\sin^2\theta_{W,eff}$ Eq. (3.296), that can be reformulated in the following way:

$$\sin^2\theta_{W,eff}\left(1 - \sin^2\theta_{W,eff}\right) = s_0^2c_0^2\left[1 - \epsilon_1 + \frac{1}{c_0^2}\epsilon_3\right] . \tag{3.305}$$

From the previous equation, using the definition of the product $s_0^2c_0^2$ given by Eq. (3.200) and working self-consistently at the one-loop level, one obtains the complete relationship:

$$m_Z^2 = \frac{\alpha\left(m_Z^2\right)\pi}{G_F\sqrt{2}}\frac{1}{\sin^2\theta_{W,eff}\left(1 - \sin^2\theta_{W,eff}\right)}\frac{1}{1 + \epsilon_1 - \frac{\epsilon_3}{c_0^2}} \tag{3.306}$$

that appears the "obvious" generalization of the approximate Eq. (3.227).

Our analysis of the leptonic observables at the Z peak is now almost concluded. In fact, a fundamental discussion is at the moment still missing.

Until now, we have focused our attention on the rôle of the top mass in the MSM predictions for the considered Z peak observables. A natural question that arises at this point is that of the sensitivity of the previous observables to the remaining still unknown MSM parameter, the Higgs mass m_H. We said at the beginning of this book that at the one-loop level the Higgs effect is *screened* i.e. it is of only logarithmic type. This property must be valid then in both ϵ_1 and ϵ_3. Contrary, though, to the m_t dependence, the rôle of ϵ_3 in this case is now relevant. We shall devote the forthcoming Subsection to a simple derivation of these important properties of the two weak parameters. This will also have a pedagogical content since, once again, we shall see how a physical result will be obtained from a common effort where certain unphysical particles will be involved, that is recurrent feature of the calculations performed in the $\xi = 1$ 't Hooft gauge.

3.5.3 *Dependence of the weak parameters ϵ_1, ϵ_3 on the Higgs mass*

To compute the Higgs effect on Z peak leptonic observables is relatively easy and also instructive. We shall perform here the explicit calculation in the simpler case of the $m_t - smooth$ parameter ϵ_3. This can be done starting from its definition Eq. (3.297) and noticing that, under our working assumption of massless external fermions and taking into account the fact that photons do not couple to a neutral particle like the Higgs, only the contribution from the Z self-energy (and, in principle, from its derivative) must be retained. In the 't Hooft gauge the relevant contributions will imply not only the physical Higgs particle, but also its related neutral *would-be* Goldstone boson s_3 defined in Chapter 1, Eq. (1.41). They correspond to the two Feynman diagrams depicted in Fig. 3.25.

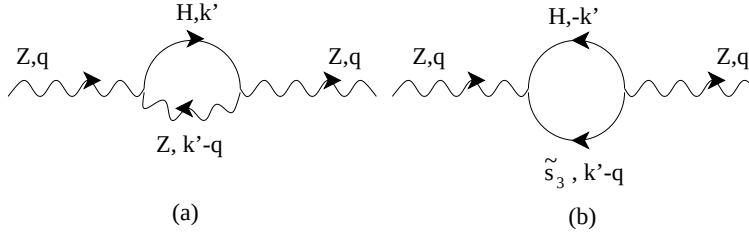

Fig. 3.25 Contribution to the Z self-energy from a physical Higgs (a) and from a Higgs-would be pair (b).

From the conventional Feynman rules valid in the MSM one derives in a straightforward way the expression of the *finite* (i.e. not proportional to Δ) part of $F^{(Z)}\left(q^2\right)$, corresponding to the two diagrams (a) and (b):

$$ReF^{(Z)(a)}\left(q^2\right)(\textit{finite}) = -\sqrt{2} \quad \frac{m_Z^2 G_F}{4\pi^2}$$
$$\times \int_0^1 dx \frac{m_Z^2}{q^2} \ln|\frac{m_H^2(1-x)+m_Z^2 x - q^2 x(1-x)}{m_H^2(1-x)+m_Z^2 x}| \qquad (3.307)$$

$$ReF^{(Z)(b)}\left(q^2\right)(\textit{finite}) = \sqrt{2} \quad \frac{m_Z^2 G_F}{4\pi^2}$$
$$\times \int_0^1 dx \quad \left[-\frac{m_Z^2}{q^2}\ln|\frac{m_H^2(1-x)+m_Z^2 x - q^2 x(1-x)}{m_H^2(1-x)+m_Z^2 x}|\right.$$
$$+\frac{m_H^2(1-x)+m_Z^2 x - q^2 x(1-x)}{2q^2}\ln|\frac{m_H^2(1-x)+m_Z^2 x - q^2 x(1-x)}{m_H^2(1-x)+m_Z^2 x}|$$
$$\left.-\frac{x(1-x)}{2}\ln|\frac{m_H^2(1-x)+M_z^2 x}{m_Z^2}|\right]. \qquad (3.308)$$

At $q^2 = m_Z^2$ it is immediate to verify that the leading contribution in the *large* m_H limit comes entirely from the *unphysical* diagram (b) where one *would-be* Goldstone boson is also exchanged!! This result, that reproduces a recurrent feature of calculations performed in the $\xi = 1$ 't Hooft gauge, can be expressed saying that the contribution to ϵ_3 from the Higgs $=\epsilon_3^{(H)}$ for large Higgs masses (again, the derivative of the Z self-energy is depressed in this limit) is:

$$\epsilon_3^{(H)}(\text{large } m_H) \simeq \frac{G_F m_W^2}{12\sqrt{2}\pi^2}\ln\frac{m_H}{m_Z} \qquad (3.309)$$

which shows that the Higgs contribution to ϵ_3 is, particularly for m_H larger than m_t, well competitive with that of the top given in Eq. (3.298). This is quite different from the case of ϵ_1, where the quadratic top contribution Eq. (3.288) is faced with a Higgs term that again, as one can easily verify, is "only" logarithmic and has the expression:

$$\epsilon_1^{(H)}(\text{large } m_H) \simeq -\frac{3G_F m_W^2}{4\sqrt{2}\pi^2}\frac{s_0^2}{c_0^2}\ln\frac{m_H}{m_Z}\,. \qquad (3.310)$$

The previous discussion has shown that the two electroweak parameters ϵ_1, ϵ_3 have quite different sensitivities to the most relevant MSM parameters, m_t and m_H. From a formal point of view, the two previous parameters

are the generalization of the weak quantities Δ_1, Δ_3 introduced in Subsection 3.2.2. To conclude this Chapter in a satisfactory way, we shall now define the quantity that generalizes the third weak parameter Δ_2 also defined in that Subsection, and discuss its rôle and its relevance within the context of the MSM. Strictly speaking, this generalization will not have connections with the description of physics at the Z peak that we have provided until now. As we shall see, it will be, though, quite relevant for what concerns the predictions that can be derived from those measurements on the W mass. For this reason we shall include it in this Chapter although, rigorously speaking, it does not "belong" to Z physics in a technical sense.

3.5.4 *The ϵ_2 parameter and the complete expression of the W mass*

A relatively easy and self-consistent way of introducing the weak parameter that generalizes the quantity Δ_2 defined by Eq. (3.164) is that of starting from the original, rigorous definition of the "weak" component $\Delta r^W = \Delta r - \Delta\alpha\left(m_Z^2\right)$, that can be written in the usual one-loop approximations as:

$$\Delta r^W = Re\left[\frac{\delta\alpha}{\alpha} - \frac{\delta G_F}{G_F} - \frac{A^{(W)}\left(m_W^2\right)}{m_W^2} + \frac{c_0^2}{s_0^2}\left(\frac{A^{(W)}\left(m_W^2\right)}{m_W^2} - \frac{A^{(Z)}\left(m_Z^2\right)}{m_Z^2}\right)\right] - \Delta\alpha\left(m_Z^2\right) \ . \quad (3.311)$$

One can now proceed using the previous definitions of the two weak parameters ϵ_1, ϵ_3. After a few "steps and tricks" that can be omitted the result is that the previous equation can be rewritten in the identical way:

$$\Delta r^W = -\frac{c_0^2}{s_0^2}\epsilon_1 + 2\epsilon_3 + \frac{2c_0^2 - 1}{s_0^2}\epsilon_2 \ . \quad (3.312)$$

The weak parameter ϵ_2 was also introduced in Ref. [39]. It is a *gauge-invariant* combination of self-energies and their derivatives, and vertices. In the conventional notations that we have introduced, its complete expression is the following:

$$\epsilon_2 = Re\left[F^{(W)}\left(m_W^2\right) - c_0^2 F^{(Z)}\left(m_Z^2\right) - s_0^2 F^{(\gamma)}\left(m_Z^2\right) - 2s_0 c_0 \frac{A^{(\gamma Z)}\left(m_Z^2\right)}{m_Z^2} - c_0^2 m_Z^2 \dot{F}^{(Z)}\left(m_Z^2\right)\right.$$

$$- \; s_0^2 \left(F^{(Nf,\gamma)}(0) - F^{(Nf,\gamma)}\left(m_Z^2\right)\right) + \frac{\delta G_F^{(V,B)}}{G_F}$$
$$+ \; 4c_0^2 \left(\Gamma_{\mu l}^{(Z)}\left(m_Z^2\right), j_{\mu l}^{(Z)}\right) + 2s_0 c_0 \left(\Gamma_{\mu l}^{(Z)}\left(m_Z^2\right), j_{\mu l}^{(\gamma)}\right)\Big] \; . \quad (3.313)$$

To verify the finite nature of the previous expression is a useful recommended exercise. For what concerns its gauge-invariance, this is an automatic consequence of the fact that, as we have already seen, all the remaining quantities that enter Eq. (3.312) i.e. Δr^W, ϵ_1, ϵ_3 enjoy this property. Thus ϵ_2 can be viewed as a *physical* weak parameter, whose dependence on the top and Higgs masses deserves to be investigated like we did in the case of ϵ_1, ϵ_3. As one sees from its definition, the self-energy *fermion pairs* component of $\epsilon_2 = \epsilon_2^{(f)}$ is simply given by the expression:

$$\epsilon_2^{(f)} = \Delta_2 - c_0^2 m_Z^2 \dot{F}^{(Z),(f)}\left(m_Z^2\right) \; . \quad (3.314)$$

Therefore, the dependence of ϵ_2 on m_t will be practically the same as that of Δ_2, that we have shown Eq. (3.197) to be of logarithmic type, more precisely of the form:

$$\epsilon_2 \,(\text{large } m_t) \simeq -\frac{G_F m_W^2}{2\sqrt{2}\pi^2} \ln \frac{m_t}{m_Z} \; . \quad (3.315)$$

Even "worse" is the dependence on m_H that, in the large m_H limit, can be practically ignored, as one can verify by a straightforward calculation. For what concerns the latter parameter, the only information that can be derived at this stage is therefore that provided by the two Z peak weak parameters ϵ_1, ϵ_3.

Starting from Eq. (3.312) and inserting it into Eq. (3.223) it is now possible to derive the complete one-loop expression of the W mass in terms of the three ϵ_i, that is:

$$\begin{aligned} m_W^2 &= m_Z^2 c_0^2 \left[1 - \frac{s_0^2}{2c_0^2 - 1}\Delta r^W\right] \\ &= m_Z^2 c_0^2 \left[1 + \frac{c_0^2}{2c_0^2 - 1}\epsilon_1 - \epsilon_2 - \frac{2s_0^2}{2c_0^2 - 1}\epsilon_3\right] \\ &= m_Z^2 c_0^2 \left[1 + 1.430\epsilon_1 - \epsilon_2 - 0.859\epsilon_3\right] \end{aligned} \quad (3.316)$$

(the numerical value of c_0^2=0.769 given by Eq. (3.202) has been used). One sees that all the three weak parameters enter the prediction of the W mass with comparable weight.

A final comment is at this point spontaneous. If we combine the previous Eq. (3.316) with the expression of $\sin^2\theta_{weff}$ given by Eq. (3.305) we obtain the following one-loop identity:

$$1 - \sin^2\theta_{weff} = \frac{1}{\rho}\frac{m_W^2}{m_Z^2} \tag{3.317}$$

where

$$\rho = \left[1 + \epsilon_1 - \epsilon_2 - \frac{s_0^2}{c_0^2}\epsilon_3\right] . \tag{3.318}$$

One sees that, at the one loop level, the tree level identity between *bare* quantities $1 - sin^2\theta_w = \frac{m_W^2}{m_z^2}$ typical of the MSM is transformed into a meaningful equation, that gives an *operative* definition of a parameter (ρ), often mentioned in the current literature with several possibly different definitions. We have now completed the calculation of the fermionic and of the Higgs contributions to $\epsilon_{1,2,3}$ and the calculation of the fermionic contributions to $\Delta\alpha(m_Z^2)$. Before moving to the next Chapter, we feel that two additional comments are worthwhile. The first one concerns the remaining boson contributions. For what concerns $\Delta\alpha(m_Z^2)$, their calculation has been performed [52], and shows that they are indeed negligible, even at the extremely accurate precision levels of LEP1. (The same conclusion applies to the gauge boson contribution to Δr^W.) Following this information, we shall therefore identify, from now on, the quantity $\Delta\alpha(m_Z^2)^{(f)}$, that we have computed, with the full parameter $\Delta\alpha(m_Z^2)$. The second comment concerns the possible relevance of those higher orders effects that we have systematically neglected. Infact, a calculation exists, of the two-loop electroweak effect on $\Delta_{1(o)}$ [53]. The conclusion is that, for values of the top mass in agreement with the measurements (Chapter 10), these two-loop effects can be neglected. A different conclusion must be drawn for the contribution to $\Delta_{1(o)}$ coming from electroweak-strong interference. This has been computed [54] and shows that the final value of $\Delta_{1(o)}$ becomes, roughly

$$\Delta_{1(o)} \to \Delta_{1(o)}(1 - \alpha_s) . \tag{3.319}$$

For a value of $\alpha_s \approx 0.12$ this effect must be properly taken into account.

These final remark conclude Chapter 3, in which the expressions of those *genuinely* electroweak quantities that can be measured with extreme precision at the Z peak (with the inclusion of the W mass) have been derived at one loop in a rather detailed way. By definition, these quantities are *not* affected by the strong interactions and therefore only allow leptons in the final state. Since the variety of Z peak measurements also includes

final hadronic states, we shall devote the next Chapter 4 to a detailed analysis of those processes, whose inclusion in the final overall analysis will turn out , for the reasons that we shall illustrate, quite relevant.

Chapter 4

Z Physics at One Loop for Final Hadronic States

Until now, our treatment of Z physics at one loop has only been considering the production of a (charged) lepton-antilepton pair. In the numerical examples that were given, only contributions to the various observables due to self-energy corrections were explicitly computed. These effects are of *universal* type, since they do not depend on the nature of either the initial or the final state. As one would guess, their calculation in the theoretical expressions that describe quark-antiquark production (for instance,that of the Z partial width into a quark-antiquark pair) is identical with that performed for final leptonic pairs. All the conclusions and the features that were stressed in Chapter 3 remain valid and do not require any extra comment.

There are, obviously, significant theoretical differences between the cases of lepton-antilepton and quark-antiquark production. For what concerns Z physics at the one loop level, two main and quite relevant additional features must be taken into account. The first one is of purely electroweak origin, and is due to the rôle of *not universal* one loop effects, in particular those that depend on the properties of the *final* state. From the discussion given in Subsection 3.4.1, in particular from the expression provided by Eqs. (3.264)–(3.267), it is clear that the only new quantities to be considered will be the final vertices Γ_f^μ (f now indicates the final quark of the process), since all contributions from boxes are automatically canceled on Z resonance.

Starting from the precise definition of Γ_f^μ Eq. (3.245), it is relatively easy to perform the numerical calculation in the approximation of considering massless quarks. However, the most spectacular theoretical consequences appear in a rather special case where this approximation must be abandoned, that for Z physics corresponds to the production of a final $b\bar{b}$ pair.

Here, vertex diagrams allow virtual top quarks to be exchanged. From the theoretical calculation, a "large" electroweak contribution proportional to the squared top mass (and also, not negligibly, to its logarithm) emerges. This reminds the similar effect that appears in the self-energy correction $\Delta_1(0)$ Eq. (3.192), although the physical interpretation in the case of the vertex is quite different (and uncorrelated to custodial symmetry violations). Given the relevance that this vertex contribution, we shall devote the first part of this Chapter, Section 4.1, to its detailed calculation. In particular, we shall discuss the relevance of the effect for the predicted theoretical value of the partial decay width of the Z into a $b\bar{b}$ pair Γ_b. We shall also review more quickly the theoretical predictions for a number of unpolarized and polarized heavy quark pairs asymmetries , and stress the relevant and measurable consequences of the presence of *not universal* one loop effects that enter their theoretical expressions at the pure electroweak one loop level.

The last sentence is a remainder of the fact that there is a second essential and relevant feature still to be taken in account for a final non leptonic state: the presence of strong interactions. In the final part of this Chapter, Section 4.2, we shall provide a short discussion of the strong interactions' effect on final quark-antiquark pairs. This will be consistently described by a *running* strong coupling $\alpha_s(q^2)$, to be evaluated at the resonant squared energy $q^2 = m_Z^2$. Rather than insisting on the conventional QCD features that will appear in the calculation, that can be found in previous excellent dedicated reviews [55], we shall concentrate our attention on the practical consequences of the introduction in the theoretical description of a fourth input parameter $\alpha_s(m_Z^2)$. This point, in particular the deep correlation between the values of the strong coupling constant, of the top mass and of the Higgs mass will be discussed in Chapter 11.

4.1 The rôle of the $Zb\bar{b}$ vertex in Z physics

The theoretical expression of the partial Z decay width into a final quark-antiquark pair, to be indicated as $f\bar{f}$, exhibits a fundamental difference with respect to the case of final lepton pairs. Understanding the origin of this difference is relatively simple if one considers the relevant vertex diagrams where virtual W, Z are exchanged, shown in Fig. 4.1.

At the Z peak, for final u, d, s, c quarks, both the final physical fermion f and the corresponding virtual one f_1 of Fig. 4.1 can be treated as if

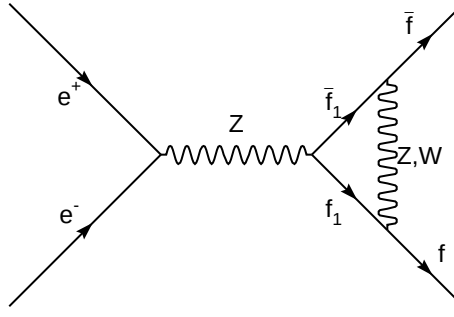

Fig. 4.1 Examples of vertex diagrams with W, Z exchange.

they were rigorously massless. This approximation must be abandoned when the final quark is a b. Here the corresponding f_1 in the virtual W diagram of Fig. 4.1 is a top quark, and one expects that in this case the top mass will play a rôle. Furthermore, looking at the same diagram with W exchange, one also expects that the top mass will only affect the left-handed component of the $Zb\bar{b}$ coupling. This statement would be obvious in the unitary gauge, where no other unphysical particles can be exchanged in the considered $Zb\bar{b}$ vertex. Since the physical top mass effect must be gauge-independent, the previous conclusions must remain valid in any other "finite ξ" gauge, in particular in the $\xi = 1$ one where we shall perform the numerical analysis.

After this general preliminary heuristic discussion, we now proceed in the forthcoming Subsection to the explicit calculation of the $Zb\bar{b}$ vertex.

4.1.1 *Calculation of the electroweak component of the $Zb\bar{b}$ vertex*

To understand the origin of the top mass dependence of the $Zb\bar{b}$ vertex is relatively simple in the $\xi = 1$ t'Hooft gauge. The main point is that, in this gauge, one must add to the graphs with W exchange Fig. 4.1 the analogous ones with virtual contributions coming from diagrams where the

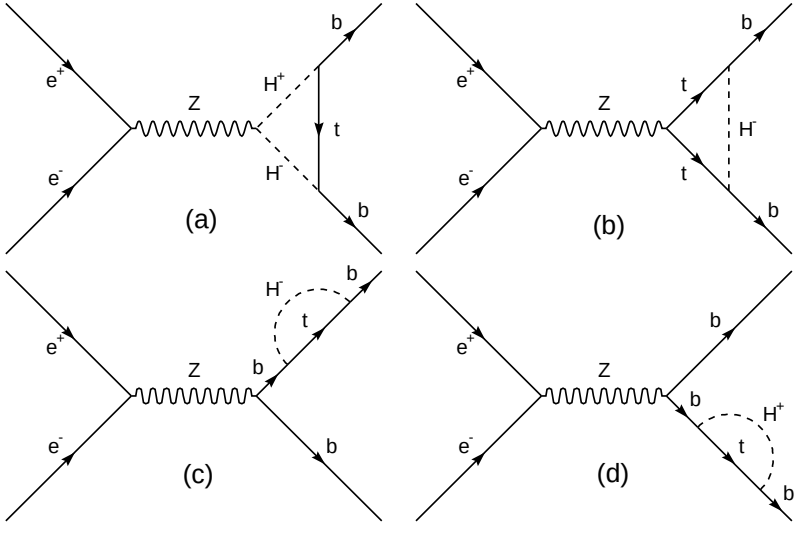

Fig. 4.2 $Zb\bar{b}$ vertex diagrams with charged would-be Goldstone boson exchange.

unphysical charged *would-be* Goldstone bosons H^+, H^- are exchanged, as shown in Fig. 4.2.

Let us examine the contribution coming from the latter diagrams first. From the Feynman rules valid in the MSM, the Hff' vertex is given by the following expression:

$$H^- f f' = \frac{-igU^{KM}_{ff'}}{2\sqrt{2}m_W} \left[m_f \left(1-\gamma_5\right) - m_{f'} \left(1+\gamma_5\right)\right] \tag{4.1}$$

where U^{KM} is the Cabibbo-Kobayashi-Maskawa matrix defined by Eq. (1.173), and from the discussion given in Chapter 1 we can safely retain only its diagonal elements that correspond to (u, d), (s, c), (b, t) pairs. Given the values of the quark masses, to be compared with the process scale m_Z, it is intuitively clear that the contribution of the charged would-be Goldstone bosons to vertices with final u, d, s, c quarks will be negligible. This conclusion does not apply to the case of a final b, where the term proportional to m_t in the r.h.s. of Eq. (4.1) cannot be simply ignored. A priori, we would therefore expect the appearance of terms proportional to m_t^2 in the diagrams of Fig. 4.2.

Note that this conclusion might not be drawn now for the set of diagrams of Fig. 4.1, since in the $\xi = 1$ gauge the W propagator is purely transverse

and cannot generate a $\approx m_t^2$ dependence (which would be allowed in the unitary gauge, where H^+, H^- are absent but a longitudinal component of the W propagator exists).

This short discussion leads naturally to the conclusion that the contribution of diagrams that introduce couplings like that of Eq. (4.1) might be the most relevant for the calculation of the $Zb\bar{b}$ vertex, and possibly important for the calculation of the $Z \to b\bar{b}$ partial width. We shall now verify with a detailed calculation that this is actually the case.

Following our notations, we shall denote the four contributions of Figs. 4.2(a)–(d) to the invariant scattering amplitude as $A_{lb}^{a,b,c,d}(q^2)$. Each contribution will be associated to a component of the $Z_{b\bar{b}}$ vertex, according to the definition given in Eq. (3.259) i.e.:

$$A_{lb}^{a,b,c,d}(q^2) = \frac{i\Gamma_b^{\mu(Z)(a,b,c,d)}(q^2) j_{\mu l}^{(Z)}}{[q^2 - m_Z^2]} \ . \tag{4.2}$$

From the canonical Feynman rules valid in the MSM we can easily derive the expression of the four vertices. For the first one we have:

$$\begin{aligned}
\Gamma_b^{\mu(Z)a} &= i\overline{u}_b(\vec{p}_3) \int \frac{d^4k}{(2\pi)^4} \left[\frac{ig_0 m_t (1+\gamma_5)}{2\sqrt{2} m_W}\right] \\
&\times i \frac{\hat{k} + \hat{p}_3 + m_t}{\left[(p_3+k)^2 - m_t^2\right]} \left[\frac{-ig_0 m_t (1-\gamma_5)}{2\sqrt{2} m_W}\right] \frac{i}{(k^2 - m_H^2)} \\
&\times \left[-ig_0 \left(\cos^2\theta_W - \sin^2\theta_W\right) \frac{(q-k)^\mu}{\cos\theta_W}\right] \\
&\times \frac{i}{\left[(k+p_3+p_4)^2 - m_H^2\right]} v_b(\vec{p}_4) + O\left(\frac{m_b^2}{m_W^2}\right).
\end{aligned} \tag{4.3}$$

In writing Eq. (4.3), we have only retained the term proportional to m_t in Eq. (4.1), assuming $m_b = 0$ and $U_{bt}U_{bt}^* = 1$ from now on. All the couplings that appear are, formally, bare ones. In practice, though, since Eq. (4.1) is already at the one loop level, all those bare quantities that will not be reabsorbed into either a $j_b^{\mu(Z)}$ or a $j_b^{\mu(\gamma)}$ structure will be safely bargained with corresponding physical parameters. For this reason, the W mass that appears can be identified with the physical one. This also applies to the would-be Goldstone mass m_H (which in the t'Hooft gauge coincides with the W one, although we shall write m_H in the following formulae).

A glance to Eq. (4.3) shows that, as expected, the integral is formally divergent, and therefore the by now familiar dimensional regularization approach must be followed. After a few straightforward operations on the various γ matrices that appear in the numerator, one is led to the expression ($\varepsilon = 4 - n$):

$$\Gamma_b^{\mu(Z)a}(q^2) = \lim_{\varepsilon \to 0^+} \frac{\mu_0^{\varepsilon}}{(2\pi)^n} \left[\left(\cos^2\theta_W - \sin^2\theta_W \right) \frac{g_0^2 m_t^2}{2m_W^2} \right]$$
$$\times \quad \overline{u}_b(\vec{p}_3) \int \frac{d^n k}{2} \frac{(k-q)^{\mu}}{(k^2 - m_H^2)} \frac{\left(\hat{p}_3 + \hat{k} \right)}{\left[(k+p_3)^2 - m_t^2 \right]}$$
$$\times \frac{(1-\gamma_5)\, v_b(\vec{p}_4)}{\left[(k+p_3+p_4)^2 - m_H^2 \right]} \tag{4.4}$$

where μ_0 is the scale parameter involved in the approach, that will eventually disappear in the final physical expression.

For what concerns the divergent nature of the integral, this is only due to the term proportional to $k^{\mu}\hat{k}$ in the numerator. Equation (3.34) shows that the (logarithmic) divergence will only be coming from the function C_{24}. The remaining components of the integral, both those corresponding to the extra functions C_{21} ,C_{22} , C_{23} defined by Eq. (3.34) and those coming from the terms in the numerator that are not quadratic in the k-variable, are finite. Moreover, one easily realizes that, at the end of a reasonable number of "$\gamma - matrices$ reshufflings", they give rise to terms in which either a $\hat{p}_3$ or a $\hat{p}_4$ can be glued to the external Dirac spinors, thus generating a finite contribution proportional to m_b that can be safely thrown away. The conclusion is that the relevant part of Eq. (4.4) can be simply written as:

$$\Gamma_b^{\mu(Z)a}(q^2) = -\frac{g_0}{2\cos\theta_W} \overline{u}_b(\vec{p}_3)\, \gamma^{\mu}(1-\gamma_5)\, v_b(\vec{p}_4)$$
$$\times \left[\frac{\left(\cos^2\theta_W - \sin^2\theta_W \right)}{32\pi^2} g_o^2 \frac{m_t^2}{m_W^2} \right]$$
$$\times C_{24}\left(q^2; m_H, m_t, m_H \right) \tag{4.5}$$

where $q^2 = (p_3 + p_4)^2$ and $m_b = 0$ in all the finite expressions. Using Eq. (3.42) to isolate the infinite component (=Δ) of C_{24} , one writes at

this point:

$$\Gamma_b^{\mu(Z)a}(q^2) = -\frac{g_0}{2\cos\theta_W}\overline{u}_b(\vec{p}_3)\,\gamma^\mu(1-\gamma_5)\,v_b(\vec{p}_4)$$
$$\times\left[\frac{\left(\cos^2\theta_W-\sin^2\theta_W\right)}{32\pi^2}g_o^2\frac{m_t^2}{m_W^2}\right]$$
$$\times\left[\frac{\Delta}{4}+C_{24}^{(fin.)}\left(q^2;m_H,m_t,m_H\right)\right] \tag{4.6}$$

where Δ is defined by Eq. (3.36).

The next contribution to be computed is that represented in Fig. 4.2(b). Repeating the procedure that we have previously illustrated and using the canonical Feynman rules at disposal, one is led to the following preliminary expression:

$$\Gamma_b^{\mu(Z)b}(q^2) = -i\frac{g_0}{\cos\theta_W}\overline{u}_b(\vec{p}_3)\,\frac{g_0^2m_t^2}{8m_W^2}\lim_{\varepsilon\to0^+}\frac{\mu_0^\varepsilon}{(2\pi)^n}\int d^nk\,(1+\gamma_5)$$
$$\times\left[\frac{\hat{k}-m_t}{k^2-m_t^2}\frac{\gamma^\mu\gamma_Lg_{Lt}+\gamma^\mu\gamma_Rg_{Rt}}{(k+p_3)^2-m_H^2}\frac{m_t-\hat{k}}{(k+p_3+p_4)^2-m_t^2}\right]$$
$$\times(1-\gamma_5)\,v_b(\vec{p}_4)\,. \tag{4.7}$$

In the previous expression, only the component proportional to m_t of the coupling in Eq. (4.1) has been retained, as in the case of the first contribution $\Gamma_b^{\mu(Z)a}$. The quantities in the square bracket are defined as follows:

$$\gamma_{L,R} = \frac{1-\gamma_5, 1+\gamma_5}{2}\;; \tag{4.8}$$

$$g_{Lt} = \frac{1}{2} - \frac{2\sin^2\theta_W}{3}\;; \qquad g_{Rt} = -\frac{2\sin^2\theta_W}{3} \tag{4.9}$$

according to Eq. (1.117).

Equation (4.7) is also affected by a logarithmic divergence, generated by the component of the numerator that is proportional to $\hat{k}\hat{k}$. One major difference with respect to the case of Eq. (4.3) is given by the fact that now the finite components of the integral will not be proportional to m_b, due to the lack of terms proportional to $\hat{p}_3$ in the numerator. This leads to the appearance of one new finite integral, not met in Subsection 3.1.4, defined as:

$$\int d^4k \frac{1}{(2\pi)^4} \frac{1}{k^2 - m_1^2} \frac{1}{(k+p_3)^2 - m_2^2} \frac{1}{(k+p_3+p_4)^2 - m_3^2} =$$
$$-\frac{i}{16\pi^2} C_0\left(p_3^2, p_4^2, q^2; m_1, m_2, m_3\right) \tag{4.10}$$

where $q^2 = (p_3 + p_4)^2$. Note that this integral is finite,and one can work with $n = 4$ from the beginning, finding in a straightforward way that:

$$C_0\left(p_3^2, p_4^2, q^2; m_1, m_2, m_3\right) = \int_0^1 dx \int_0^x dy \frac{1}{ax^2 + by^2 + cxy + dx + ey + f} \tag{4.11}$$

and

$$\begin{aligned} &a = p_4^2 \; ; \quad b = p_3^2 \; ; \quad c = q^2 - p_3^2 - p_4^2 \; ; \\ &d = m_2^2 - m_3^2 - p_4^2 \; ; \quad e = m_1^2 - m_2^2 + p_4^2 - q^2 \; ; \\ &f = m_3^2 \end{aligned} \tag{4.12}$$

(a small imaginary part should be added to the denominator to avoid integration problems). In terms of the function C_0 and of those defined by Eq. (3.34) one finds after a small number of "tricks":

$$\begin{aligned} &\Gamma_b^{\mu(Z)b}(q^2) = \frac{g_0}{\cos\theta_W} \frac{g_0^2 m_t^2}{32\pi^2 m_W^2} \\ &\times \quad \overline{u}_b\left(\vec{p}_3\right) \gamma^\mu \gamma_L v_b\left(\vec{p}_4\right) \qquad \left\{ m_t^2 g_{tL} C_0\left(q^2; m_t, m_H, m_t\right) \right. \\ &\left. + g_{tR} \left[-q^2 C_{23}\left(q^2; m_t, m_H, m_t\right) - \frac{1}{2} + 2C_{24}\left(q^2; m_t, m_H, m_t\right) \right] \right\} \end{aligned} \tag{4.13}$$

(as usually, we set $p_3^2 = p_4^2 = m_b^2 = 0$). Equation (4.13) can be rewritten separating its infinite part from the finite one, as it was done with Eq. (4.4). This leads to the final expression:

$$\begin{aligned} &\Gamma_b^{\mu(Z)b}(q^2) = -\frac{g_0}{\cos\theta_W} \frac{g_0^2 m_t^2}{32\pi^2 m_W^2} \\ &\times \quad \overline{u}_b\left(\vec{p}_3\right) \gamma^\mu \gamma_L v_b\left(\vec{p}_4\right) \left[\frac{1}{3} \sin^2\theta_W \Delta + \text{“}finite\text{”} \right] \end{aligned} \tag{4.14}$$

where the "finite" contribution comes from all the components of the curly bracket in Eq. (4.13) that are not proportional to Δ (and contain C_0, C_{23} and the finite term of C_{24}, as defined by Eq. (3.34)).

Adding Eq. (4.14) to Eq. (4.6) one obtains, for the sum of the two Feynman diagrams Figs. 4.2(a),(b), the following expression:

$$\Gamma_b^{\mu(Z)a+b}(q^2) = \frac{g_0}{\cos\theta_W}\frac{g_0^2 m_t^2}{32\pi^2 m_W^2}\overline{u}_b(\vec{p}_3)$$
$$\times\gamma^\mu\gamma_L v_b(\vec{p}_4)\left[\frac{\sin^2\theta_W - \cos^2\theta_W}{4}\Delta - \frac{\sin^2\theta_W}{3}\Delta + \text{“}finite\text{”}\right] \tag{4.15}$$

where the first and the second coefficient of Δ inside the curly bracket comes respectively from the first and second contribution to the vertex, Fig. 4.2. One sees therefore that the sum of these two Feynman diagrams is still divergent, and thus not yet physically meaningful (leaving aside for the moment the extra question of gauge dependence on which we shall soon return).

In fact, we still must add the last two contributions corresponding to Fig. 4.2. To treat the latter ones consistently, we shall now provide a small concise discussion. With this aim, let us assume that a certain meaning can be given to the concept of “quark mass”, for instance identifying it (as one normally does for “conventional” particles) with the position of the pole of the complete quark propagator. For definiteness, let us consider the case in which we are interested now, that of a b-quark. Its bare propagator, conventionally depicted as in Fig. 4.3(a) is written, if p denotes its four-momentum, as

$$\frac{i}{\hat{p} - m_{b0}} = i\frac{\hat{p} + m_{b0}}{p^2 - m_{b0}^2}. \tag{4.16}$$

Next, consider the modification of the quark propagator that is depicted in Fig. 4.3(b). In our conventions, we shall associate Fig. 4.3(b) to the quantity called $i\Gamma_{b,H}$. The latter will be then rewritten as follows:

$$i\Gamma_{b,H} = i\hat{p}\delta_{b,H}. \tag{4.17}$$

The calculation of $\Gamma_{b,H}$ proceeds formally via conventional Feynman rules, leading to the preliminary expression:

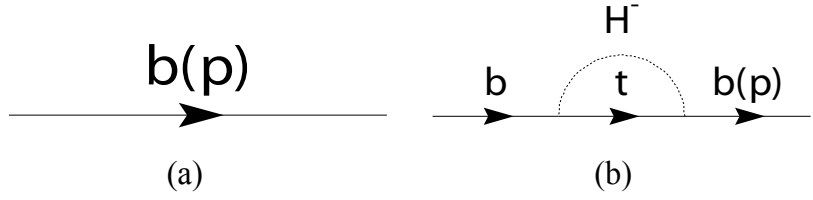

Fig. 4.3 (a) bare b quark propagator with four-momentum p; (b) modification of the bare b-propagator due to virtual H^-, t emission.

$$
\begin{aligned}
i\Gamma_{b,H} &= \int d^4k \frac{1}{(2\pi)^4} i g_0 m_t \left(1+\gamma_5\right) \frac{1}{2\sqrt{2}m_W} \\
&\times i\frac{\hat{k}}{k^2-m_t^2} \frac{-ig_o m_t \left(1-\gamma_5\right)}{2\sqrt{2}m_W} \frac{i}{\left(k-p\right)^2 - m_H^2} \\
&= \lim_{\varepsilon\to 0^+} \frac{\mu_o^{\varepsilon}}{(2\pi)^n} \frac{-g_o^2 m_t^2}{2m_W^2} \int d^n k \frac{\hat{k}}{k^2-m_t^2} \frac{\gamma_L}{\left[\left(k-p\right)^2 - m_H^2\right]} \\
&= i\hat{p}\left[-\frac{g_0^2 m_t^2}{32\pi^2 m_W^2} B_1\left(p^2; m_t^2, m_H^2\right)\gamma_L\right] \qquad (4.18)
\end{aligned}
$$

having exploited Eq. (3.32). We conclude that, once again,an infinite quantity appears since:

$$
\delta_{b,H} = -\frac{g_0^2}{32\left(\pi\right)^2} \frac{m_t^2}{m_W^2} \left[-\frac{\Delta}{2} + B_1^{finite}\left(p^2, m_t^2, m_H^2\right)\right] \qquad (4.19)
$$

as one sees from Eq. (3.39).

The divergent quantity $\delta_{b,H}$ can be naturally interpreted as a redefinition of the bare quark mass at one loop. This can be done in strict analogy with the case of the W, Z masses treated in Subsection 3.1.5. For our purposes, it can be advantageous to consider the modification at one loop of the expression that describes the propagation of a b quark originated at a certain vertex (that can be one with a Z but also with one photon or one W), to be called in full generality $V^{\mu(0)}$. At tree level the correspondence will be given by the forthcoming graphical equation:

$$
\text{VERTEX} \to V^{\mu(0)} \frac{i}{\hat{p} - m_{b,0}} \,. \qquad (4.20)
$$

Adding the modification of Fig. 4.3 will lead to the modified expression:

$$\begin{aligned}
&\text{VERT.+E.S.E.} \to V^{\mu(0)} \frac{i}{\hat{p} - m_{b,0}} \left[1 + i\Gamma_{b,H} \frac{i}{\hat{p} - m_{b,0}}\right] \\
&= V^{\mu(0)} \frac{i}{\hat{p} - m_{b,0} + \hat{p}\delta_{b,H}} = V^{\mu(0)} \frac{i}{(\hat{p} - m_b)\,(1 + \delta_{b,H})} \\
&= \left[V^{\mu(0)}\,(1 - \delta_{b,H})\right] \frac{i}{\hat{p} - m_{b,H}}
\end{aligned} \tag{4.21}$$

where "E.S.E." means *external self-energy* and we have defined a *candidate* b mass

$$m_{b,H} = m_{b,0}\,(1 - \delta_{b,H}) \tag{4.22}$$

which intuitively appears as a proper *pole* of the quark propagator, and the tricks that are formally allowed at one loop (typically, $1 + \delta_{b,H} = \frac{1}{1-\delta_{b,H}}$) have been extensively used.

The qualitative conclusion at this point is that one can reabsorb the effect of the graph Fig. 4.3 into two different operations. The first one is a redefinition of the quark mass; the second one is a formal modification of the initial bare quark vertex (in our case, this will be the $Zb\bar{b}$ one) that corresponds to the addition of a quantity

$$\delta V^{\mu} = -V^{\mu(0)} \delta_{b,H} \tag{4.23}$$

to the bare vertex. Note, to avoid confusion, that this quantity must now be computed following the conventional Feynman rules prescriptions; for a $Zb\bar{b}$ vertex this gives:

$$\begin{aligned}
V^{\mu(0)}_{Zb\bar{b}} &= \frac{g_0}{2\cos\theta_W} \gamma^{\mu} \left[g^0_{Vb} - \gamma_5 g^0_{Ab}\right] \\
&= \frac{g_0}{\cos\theta_W} \gamma^{\mu} \left[\gamma_L g_{Lb} + \gamma_R g^0_{Rb}\right]
\end{aligned} \tag{4.24}$$

where $g^0_{Lb} = -\frac{1}{2} + \frac{1}{3}\sin^2\theta_W$; $g^0_{Rb} = \frac{1}{3}\sin^2\theta_W$.

Let us apply these qualitative conclusions to the two graphs represented in Figs. 4.2(c), (d). Without proving it explicitly, we shall assume that the shift $\delta_{b,H}$ is the same in both cases. Also, from the conventional rules, we

shall consider the half of the sum of the two contributions. This leads to the conclusion that:

$$\Gamma_b^{\mu(Z)(c+d)} = -\bar{u_b}\left(\vec{p}_3\right)\left[V_{Z_{b\bar{b}}}^{\mu(0)}\delta_{b,H}\right]v_b\left(\vec{p}_4\right) =$$
$$-\bar{u_b}\left(\vec{p}_3\right)\frac{g_0}{\cos\theta_W}\gamma^\mu\left[\gamma_L g_{L,b}+\gamma_R g_{R,b}\right]\left[-\frac{g^2}{32\pi^2}\frac{m_t^2}{m_W^2}\right]$$
$$\times\gamma_L\left[-\frac{\Delta}{2}+B_1^{finite}\left(p_3^2,m_t,m_H\right)\right]v_b\left(\vec{p}_4\right)$$
$$=\left[\frac{g}{\cos\theta_W}\right]\bar{u_b}\left(\vec{p}_3\right)\gamma^\mu\gamma_L v_b\left(\vec{p}_4\right)\left[\frac{g^2}{32\pi^2}\frac{m_t^2}{m_W^2}\right]$$
$$\times\left[-\frac{1}{2}+\frac{1}{3}\sin\theta_W{}^2\right]\left[-\frac{1}{2}\Delta+B_1^{finite}\left(p_3^2,m_t,m_H\right)\right]. \qquad (4.25)$$

The overall $Zb\bar{b}$ vertex can now be explicitly computed adding Eq. (4.25) to Eq. (4.15). One sees immediately that, when this operation is performed, the overall coefficient of the infinite component Δ vanishes, since:

$$\Gamma_b^{\mu(Z)(a+b+c+d)(infinite)} = \Gamma_b^{\mu(Z)(infinite)}$$
$$=\frac{g}{\cos\theta_W}\bar{u_b}\left(\vec{p}_3\right)\gamma^\mu\gamma_L v_b\left(\vec{p}_4\right)\left[\frac{g^2}{32\pi^2}\frac{m_t^2}{m_W^2}\right]$$
$$\times\Delta\left[\left(\frac{1}{4}\sin\theta_W{}^2-\frac{1}{4}\cos\theta_W{}^2\right)-\left(\frac{1}{3}\sin\theta_W{}^2\right)+\left(\frac{1}{4}-\frac{1}{6}\sin\theta_W{}^2\right)\right]$$
$$=0. \qquad (4.26)$$

The sum of the four contributions is therefore finite, and is given by the following expression:

$$\Gamma_b^{\mu(Z)(finite)} = \Gamma_b^{\mu(Z)}$$
$$=\frac{g}{\cos\theta_W}\bar{u_b}\left(\vec{p}_3\right)\gamma^\mu\gamma_L v_b\left(\vec{p}_4\right)\left[\frac{g^2}{32\pi^2}\frac{m_t^2}{m_W^2}\right]$$
$$\times\left[finite+\left(\frac{1}{3}\sin\theta_W{}^2-\frac{1}{2}\right)B_1^{finite}\left(0;m_t,m_H\right)\right] \qquad (4.27)$$

where the first *finite* term in the square bracket is defined by Eqs. (4.6),(4.14),(4.15) and the b mass has been systematically equated to zero in all the (now finite) contributions.

We see that, as expected from the discussion given at the beginning of this Chapter, the leading m_t contribution of Fig. 4.2 to the $Zb\bar{b}$ vertex is purely left-handed. The reader can verify that this property applies to all four diagrams separately.

Equation (4.27) is quite general and does not consider yet the (relevant) situation $m_t >> m_W$. This case will be examined in detail in the following Subsection; before doing that, we shall conclude this part of Chapter with an illustration of how the *projection* procedure on the different Lorentz structures actually proceeds in this specific case. With this purpose, it is convenient to rewrite Eq. (4.27) in the condensed form:

$$\Gamma_b^{\mu(Z)} = \frac{g}{\cos\theta_W} \bar{u_b}\left(\vec{p}_3\right) \gamma^\mu \gamma_L v_b\left(\vec{p}_4\right) F\left(q^2, m_t, m_W, m_H\right) \tag{4.28}$$

where $F(q^2, ...)$ corresponds to the finite terms contained in the square brackets on the r. h. s. of Eq. (4.27). From Eq. (4.28) we can now derive the expression that we need simply by readjusting it as follows:

$$\begin{aligned} &\Gamma_b^{\mu(Z)}\left(q^2\right) = \frac{g}{2\cos\theta_W} F\left(q^2, ...\right) \\ &\times \left[-\bar{u_b}\left(\vec{p}_3\right)\gamma^\mu\gamma_5 v_b\left(\vec{p}_4\right) + \bar{u_b}\left(\vec{p}_3\right)\gamma^\mu v_b\left(\vec{p}_4\right)\right] \\ &= b_{1b}\bar{u_b}\left(\vec{p}_3\right)\gamma^\mu\gamma_5 v_b\left(\vec{p}_4\right) + b_{2b}\bar{u_b}\left(\vec{p}_3\right)\gamma^\mu v_b\left(\vec{p}_4\right) \end{aligned} \tag{4.29}$$

where we have used the definition of Eq. (3.248), with

$$b_{1b} = -b_{2b} = -\frac{g}{2\cos\theta_W} F\left(q^2, m_t, m_W, m_H\right) . \tag{4.30}$$

For our derivation, we must now rewrite the $Zb\bar{b}$ vertex in the equivalent way:

$$\Gamma_b^{\mu(Z)}\left(q^2\right) = a_{1b}\left(q^2\right) j_b^{\mu(Z)} + a_{2b}\left(q^2\right) j_b^{\mu(\gamma)} \tag{4.31}$$

where $j_b^{\mu(Z)}$ and $j_b^{\mu(\gamma)}$ are defined by Eqs. (3.10), (3.8):

$$j_b^{\mu(Z)} = \frac{|e_0|}{2\sin\theta_W\cos\theta_W} \bar{u_b}\left(\vec{p}_3\right)\gamma^\mu\left[g_{Vb}^0 - \gamma_5 g_{Ab}^0\right] v_b\left(\vec{p}_4\right) \tag{4.32}$$

$$j_b^{\mu(\gamma)} = -\frac{1}{3}|e_0|\bar{u_b}\left(\vec{p}_3\right)\gamma^\mu v_b\left(\vec{p}_4\right) \tag{4.33}$$

and $g_{Vb}^0 = -\frac{1}{2} + \frac{2}{3}\sin\theta_W{}^2$; $g_{Ab}^0 = -\frac{1}{2}$.

Using Eqs. (3.250), (3.251) of Chapter 3 we can now derive the expressions of the *projections* of the $Zb\bar{b}$ vertex on the "Z" and "γ" Lorentz structures:

$$\begin{aligned} &\left(\Gamma_b^{\mu(Z)}\left(q^2\right), j_b^{\mu(Z)}\right) = a_{1b}\left(q^2\right) \\ &= \frac{4b_{1b}}{|e_0|}\sin\theta_W\cos\theta_W = -2F\left(q^2, m_t, m_W, m_H\right) \end{aligned} \tag{4.34}$$

$$\left(\Gamma_b^{\mu(Z)}\left(q^2\right), j_b^{\mu(\gamma)}\right) = a_{2b}\left(q^2\right) =$$
$$-\frac{3}{|e_0|}\left[\left(\frac{g_{Vb}^0}{g_{Ab}^0}-1\right)b_{1b}\right] = -2\frac{\sin\theta_W}{\cos\theta_W}F =$$
$$-2\frac{s_0}{c_0}F\left(q^2, m_t, m_W, m_H\right) \tag{4.35}$$

and in the last step of Eq. (4.35) we have exploited, as usually, the fact that we are working at the one loop level which allows to replace the bare parameters that are involved with corresponding physical quantities. In the same spirit we shall replace systematically from now on, inside the function $F\left(q^2, ...\right)$, the bare parameter g_0^2 by $\frac{4\pi\alpha}{s_0^2}$, with s_0 defined by Eq. (3.200).

Equations (4.34), (4.35) with F given by Eq. (4.28) are all that we need for our forthcoming discussion, that will proceed in the following Subsection.

4.1.2 *Observable effects of the $Zb\bar{b}$ vertex at the Z peak: the large m_t limit*

Until now, all our derivation has been quite general and no special assumption has been made on the size of the top mass. The relevance of the $Zb\bar{b}$ vertex becomes, however, enhanced when m_t increases and becomes larger than, say, m_W, as it results from the available experimental measurement (Chapter 10). In order to provide a satisfactory description of this important effect, we shall consider from now on the extreme situation $m_t \to \infty$, and concentrate our attention on the *leading* m_t terms in the asymptotic m_t expressions of those analytic functions that contribute the $Zb\bar{b}$ vertex as e.g. from Eq. (4.27). As we shall see, two features become evident in the considered configuration, whose combination makes it possible to consider the $Zb\bar{b}$ vertex as the manifestation of a *physical* effect at the Z peak: first of all, the effect is "large" at the level of the related experimental accuracy; secondly, it is manifestly (although a priori not obviously) gauge-invariant. To prove the first statement, it is sufficient to compute the limit of the finite quantity $F(m_Z^2, m_t, m_W, m_H)$ in Eq. (4.28). In terms of the functions B_1, C_{24}, C_{23} that have been defined by Eqs. (3.32), (3.34) this reads:

$$F\left(m_Z^2, m_t, m_W, m_H\right) = \frac{\alpha}{8\pi s_0^2}\frac{m_t^2}{m_W^2}\left\{\left[-\frac{1}{2}+\frac{1}{3}s_0^2\right]B_1^{finite}\left(0; m_t, m_H\right)\right.$$
$$\left.-\left[c_0^2-s_0^2\right]C_{24}^{finite}\left(q^2; m_H, m_t, m_H\right)+m_t^2\left[\frac{1}{2}-\frac{2}{3}s_0^2\right]C_0\left(q^2; m_t, m_H, m_t\right)\right.$$

$$+\frac{2}{3}s_0^2\left[q^2C_{23}\left(q^2;m_t,m_H,m_t\right)+\frac{1}{2}-2C_{24}^{finite}\left(q^2;m_t,m_H,m_t\right)\right]\Bigg\}. \tag{4.36}$$

The calculation of the leading term for large m_t leads to the expression:

$$\lim_{m_t\to\infty}F\left(m_Z^2;m_t,m_W,m_H\right)=\frac{\alpha}{8\pi s_0^2}\frac{m_t^2}{m_W^2}\left[\frac{1}{2}+next-to-leading\right] \tag{4.37}$$

where, for the moment, we do not consider the next-to-leading terms (that will turn out to be not negligible, as we shall discuss later).

To get a feeling of the relevance of the expression written in Eq. (4.37) for what concerns the modification of physical quantities, it is convenient to write the complete theoretical expression of the partial width $\Gamma_b^{(1)}=\Gamma_{Z\to b\bar{b}}^{(1)}$ at one loop. By an immediate and straightforward generalization of the procedure that led to the derivation of the corresponding formula for the leptonic width one is led to the following equation, valid in the approximation $m_b=0$:

$$\begin{aligned}\Gamma_b^{(1)}&=N_{QCD,b}\frac{G_F}{\sqrt{2}}\frac{m_Z^2}{6\pi}\left[1+\varepsilon_{1b}\right]\left[g_{Ab}^2+g_{Vb}^2\right]=N_{QCD,b}\\&\times\frac{G_F}{\sqrt{2}}\frac{m_Z^2}{24\pi}\left[1+\varepsilon_{1b}\right]\left[1+\left(1-\frac{4}{3}s_b^2\left(m_Z^2\right)\right)^2\right]\end{aligned} \tag{4.38}$$

(we did not yet include a small multiplicative purely QED correction $1+\frac{3}{4}\frac{\alpha}{\pi}$) where $N_{QCD,b}$ is the strong interactions effect on the final $b\bar{b}$ pair, to be discussed in the second part of this Chapter, and:

$$\begin{aligned}\varepsilon_{1b}&=\varepsilon_1-2Re\left(\Gamma_l^{\mu(Z)}\left(m_Z^2\right),j_l^{\mu(Z)}\right)\\&+2Re\left(\Gamma_b^{\mu(Z)}\left(m_Z^2\right),j_b^{\mu(Z)}\right)\\&=\varepsilon_1+2Re\left(\Gamma_b^{\mu(Z)}\left(m_Z^2\right),j_b^{\mu(Z)}\right)^{NU}\end{aligned} \tag{4.39}$$

$$\begin{aligned}&s_b^2\left(m_Z^2\right)=\left(\sin\theta_{W,eff}\right)^2\\&+s_0c_0Re\left[\left(\Gamma_{\mu l}^{(Z)}\left(m_Z^2\right),j_{\mu l}^{(\gamma)}\right)-\left(\Gamma_b^{\mu(Z)},j_b^{\mu(\gamma)}\right)\right]\\&=\left(\sin\theta_{W,eff}\right)^2-s_0c_0Re\left(\Gamma_b^{\mu(Z)}\left(m_Z^2\right),j_b^{\mu(\gamma)}\right)^{NU}\end{aligned} \tag{4.40}$$

where we have used the definitions of Eqs. (3.281), (3.286) and the usual one loop approximations. These are supposed to be valid at the requested level of accuracy, and do not need a special discussion in each separate case to be considered. The latter statement is, on the opposite, not true for another approximation that has been systematically adopted until now, that of treating the final physical quarks as genuinely massless objects. In the case of a Z partial width, taking into account the quark mass (assuming that a proper definition can be given of this quantity) introduces a small modification of the formulae that we have derived. For a "light" quark of a mass much smaller than m_Z, neglecting terms of order m_q^4,one obtains the relevant expression by simply performing in Eq. (4.38) the single following modification:

$$g_{A,b}^2 \to g_{A,b}^2 \sqrt{1 - \frac{4m_b^2}{m_Z^2}} (1 - \frac{4m_b^2}{m_Z^2}) \tag{4.41}$$

(the vectorial coupling remains unchanged at this level of accuracy), where for the b mass a value of approximately 4.5 GeV can be taken, that is intuitively related to that of the upsilon resonance. Numerically, the change induced on Γ_b is of approximately a (relative) one percent, that is comparable with the experimental accuracy and must consequently be taken into account. This remark only applies, at the Z peak, to final bottom pair production. For this reason we have not derived the general formula valid for massive fermions from the beginning, since in all other cases the zero mass approximation is perfectly valid. We shall return on this b mass dependence later on, when treating other properties of $b\bar{b}$ production in this Chapter.

In Eqs. (4.39), (4.40) the symbol "NU" means "not universal", and denotes the fact that the only difference in this case between a final charged lepton ℓ and a final quark b is the appearance in the vertex of non universal terms. These are clearly exhibited by the $\simeq m_t^2$ charged would-be $H^{+,-}$ contribution. In the relevant situation $m_t \to \infty$ we can then safely retain the leading component of the effect, and write:

$$\begin{aligned} &\varepsilon_{1b}\left(m_t \to \infty\right) \simeq \varepsilon_1 + 2a_{1b} = \varepsilon_1 - 4F\left(m_Z^2; m_t ...\right) \\ &\times s_b^2\left(m_Z^2\right)\left(m_t \to \infty\right) \simeq \left(\sin\theta_{W,eff}\right)^2 - s_0 c_0 a_{2b} \\ &= \left(\sin\theta_{W,eff}\right)^2 + 2s_0^2 F\left(m_Z^2; m_t, m_W, m_H\right) . \end{aligned} \tag{4.42}$$

From the value given in Eq. (4.37) we conclude that:

$$\begin{aligned}\varepsilon_{1b} &\simeq \varepsilon_1 - \frac{\alpha}{4\pi s_0^2 c_0^2}\frac{m_t^2}{m_Z^2} \\ &= \varepsilon_1 - \frac{\alpha}{2.232} m_t^2 m_Z^2 \end{aligned} \tag{4.43}$$

$$\begin{aligned}s_b^2\left(m_Z^2\right) &\simeq \left(\sin\theta_{W,eff}\right)^2 + \frac{\alpha}{8\pi c_0^2}\frac{m_t^2}{m_Z^2} \\ &= \left(\sin\theta_{W,eff}\right)^2 + \frac{\alpha}{19.315}\frac{m_t^2}{m_Z^2} \end{aligned} \tag{4.44}$$

having used the value of s_0^2 given in Eq. (3.203).

Combining Eqs. (4.43) and (4.44) with Eq. (4.38) we can compute in leading m_t^2 order the relative shift on the partial width Γ_b. We stress that we are now interested in the non-universal effect that is not present for final leptonic or light quark states. With this aim, we shall not include the universal component of ϵ_1 and $\sin^2\theta_{W,eff}$ already given by Eq. (3.288) and Eq. (3.296), and call "NU" the remaining contributions, which give, after a few one-loop tricks:

$$\begin{aligned}\frac{\Gamma_b^{1,m_t(NU)}}{\Gamma_b^1} &= \left[1 - \frac{\alpha}{4\pi s_0^2 c_0^2}\frac{m_t^2}{m_Z^2}\right] \\ &\times \left[1 - \frac{16 s_0^2}{3}\frac{1-\frac{4s_0^2}{3}}{1+\left(1-\frac{4s_0^2}{3}\right)^2}\frac{\alpha}{16\pi s_0^2 c_0^2}\frac{m_t}{m_Z^2}\right] \\ &\simeq \left[1 - \frac{\alpha}{2.32}\frac{m_t^2}{m_Z^2} - \frac{\alpha}{15.46}\frac{m_t^2}{m_Z^2}\right] \end{aligned} \tag{4.45}$$

where the first correction is generated by ε_{1b} and the (much smaller) second one comes from $s_b^2\left(m_Z^2\right)$. In correspondence with the experimental value $m_t \simeq 2m_Z$, a relative correction of about two percent appears in this first rough estimate.

As a matter of fact, in a situation of large m_t, a second term arises in F that is of the form $\sim \left(\ln\frac{m_t^2}{m_Z^2}\right)^2$, with a numerically large coefficient, that practically doubles the previous $\sim m_t^2$ contribution. Leaving aside the details of the derivation [56], one reaches the conclusion that relative non-universal shifts of a few $(\sim 3-4)$ percent appear in the expression of the Z partial width Γ_b. This is, a priori, a quite sizeable effect that certainly requires a proper treatment and a careful theoretical calculation.

The previous conclusion would be acceptable provided that one could claim that this *large* m_t effect is a gauge-independent one. Since the overall calculation was performed in the t'Hooft $\xi = 1$ gauge, this statement is not in principle obvious (in fact, we left in the theoretical expression the notation $m_H = \xi m_W$ as a remainder of this intrinsic ξ dependence). It turns out, though, that the *large* m_t contribution that we have isolated is actually gauge-independent. This can be proved in different ways; we shall present here a simple and intuitive argument, mostly based on self-consistency considerations. In fact, we have shown in Chapter 3 that, in order to cancel the gauge-dependence of the *universal* self-energies, a precisely defined amount of boxes and vertices must be added to generate the gauge-independent combinations, as shown e.g. by Eqs. (3.263), (3.266). At the Z peak, the box contribution is kinematically canceled, and the previous operation must be carried on by vertices. From the universality of self-energies, it is clear that only the universal parts of the related vertices can be (suitably) gauge dependent to perform the requested cancellation. Thus, the non universal "NU" components of the vertices must be individually gauge-independent *at the Z peak*. This is evidently the case of the components of the $Zb\bar{b}$ vertex that are depending on m_t, which proves our statement. Given the large size of the effect, we can thus consider it as a physical, observable one. In the forthcoming Subsection we shall provide, an *operative* definition that relates it to measurable quantities.

4.1.3 *Operative definition of the $Zb\bar{b}$ vertex at the Z peak: the δ_{bV} parameter*

A simple way to provide an operative definition of the non-universal component of the $Zb\bar{b}$ vertex that has been discussed until now, arises from the observation that its effect, as already stated, only involves at the Z peak the Z decay into a $b\bar{b}$ pair, and none of the remaining Z partial widths. Since the latter quantities are, in principle, measurable, one immediate proposal is that of considering *ratios* of the $Z \to b\bar{b}$ width (Γ_b) with other "suitable" ones. To specify the meaning of the word "suitable", it is useful (anticipating the specific discussion to be given in this Subsection) to consider the fact that Γ_b is affected by strong interactions effects (generally treated in a conventional QCD scheme), whose presence might obscure the electroweak details that we are trying to isolate, particularly if residual sizeable theoretical uncertainties were present in the QCD sector. To eliminate, or at least to reduce drastically, the previous difficulty, a simple possibility is that of

considering ratios of the $Z \to b\bar{b}$ width with other *hadronic* Z widths. To a very good approximation, to be discussed later on, the QCD effect in the production of *light* quark-antiquark pairs at the Z peak can be treated in the usual *zero quark mass* limit. In such a situation, the effect of the strong interactions factorizes in the same way both in the numerator and in the denominator (a fact that is somehow reminiscent of the similar property of the longitudinal polarization asymmetry A_{LR} for final hadronic states), and consequently disappears, leaving the $\sim m_t$ vertex effect unambiguously defined. The simplest possibility in this spirit would then be measuring, as originally proposed in Ref. [57], the non universal $Zb\bar{b}$ vertex from the ratio of Γ_b to Γ_s (the Z decay width into a $s\bar{s}$ pair) i.e.:

$$\frac{\Gamma_b}{\Gamma_s} = 1 + \delta_{bV} \tag{4.46}$$

where the parameter δ_{bV} has the following expression:

$$\delta_{bV} = -F\left(m_Z^2; m_t\right)\left[4 + \frac{16 s_0^2}{3}\frac{1 - \frac{4s_0^2}{3}}{1 + \left(1 - \frac{4s_0^2}{3}\right)^2}\right] \tag{4.47}$$

which can be obtained combining Eqs. (4.34)–(4.40). Note that, in the ratio of Eq. (4.46), the universal components of $\epsilon_{1,3}$ cancel exactly, only leaving the non-universal term.

Note also that, in Eq. (4.47), the b mass cannot be totally neglected, as stated. Its effect of the observable quantities will be discussed later on. Equations (4.46), (4.47) provide an operative definition of the quantity δ_{bV}. This is directly proportional to $F\left(m_Z^2; m_t\right)$ defined by Eq. (4.36). Using Eq. (4.37) one can derive immediately the *leading* m_t expression of δ_{bV}, and write:

$$\begin{aligned}\delta_{bV} = &-\frac{\alpha}{4\pi s_0^2 c_0^2}\left[1 + \frac{4s_0^2}{3}\frac{1 - \frac{4s_0^2}{3}}{1 + \left(1 - \frac{4s_0^2}{3}\right)^2}\right] \\ &\times \left[\frac{m_t^2}{m_Z^2} + \frac{13}{6}\left(ln\frac{m_t^2}{m_Z^2}\right)^2 + ...\right]\end{aligned} \tag{4.48}$$

where the coefficient of the logarithmic term, that makes the total contribution quite competitive (roughly 4%), has been computed in previous papers [56].

From a strictly practical point of view, the $Z \to s\bar{s}$ decay cannot be measured at the permil level of accuracy. A better quantity to be used in order to define and measure δ_{bV} is actually the ratio $\frac{\Gamma_b}{\Gamma_h}$, where Γ_h is the *full* hadronic Z width i. e.

$$\Gamma_h = \Gamma_u + \Gamma_d + \Gamma_s + \Gamma_c + \Gamma_b \tag{4.49}$$

whose experimental measurement can be performed with the required accuracy. Intuitively, the same theoretical considerations about QCD cancellations will remain valid for this ratio. For what concerns the electroweak component, an elementary calculation leads to the following theoretical expression:

$$\begin{aligned} R_b \equiv \frac{\Gamma_b}{\Gamma_h} &= \frac{\Gamma_s\,(1+\delta_{bV})}{\Gamma_u + \Gamma_d + \Gamma_s + \Gamma_c + \Gamma_b} \\ &= \frac{\Gamma_d\,(1+\delta_{bV})}{2\Gamma_u + \Gamma_d\,(3+\delta_{bV})} \\ &= \frac{1+\delta_{bV}}{3+2r_{ud}+\delta_{bV}}\,. \end{aligned} \tag{4.50}$$

In deriving the final expression of Eq. (4.50) we have assumed:

$$\Gamma_u = \Gamma_c\,;\, \Gamma_d = \Gamma_s \tag{4.51}$$

and defined the ratio

$$\frac{\Gamma_u}{\Gamma_d} = r_{ud}\,. \tag{4.52}$$

Note that, for what concerns the quantities that appear in Eq. (4.50), the modifications due to *quark mass* differences in the QCD corrections are totally negligible for the four lightest u, d, s, c quarks, that can be consistently treated as massless. In the usual one-loop approximation philosophy, we can rewrite Eq. (4.50) as follows:

$$\frac{\Gamma_b}{\Gamma_h} = \frac{1}{3+2r_{ud}}\left[1+\delta_{bV}\left(1-\frac{1}{3+2r_{ud}}\right)\right]\,. \tag{4.53}$$

The ratio r_{ud} that enters Eq. (4.53) must be computed theoretically at the one loop level. For what concerns its contribution *inside* the square bracket on the r.h.s. of that equation, which multiplies the $O\,(\alpha)$ parameter δ_{bV}, it can be approximated by its lowest order expression. This corresponds to writing $\frac{\Gamma_u}{\Gamma_d}$ in the following form:

$$\frac{\Gamma_u}{\Gamma_d} = r_{ud} = \frac{\left[1+\left(1-\frac{8}{3}s_0^2\right)^2\right]}{\left[1+\left(1-\frac{4}{3}s_0^2\right)^2\right]}\,(1+O\,(\alpha)) \tag{4.54}$$

and to only retaining the square bracket in the final expression. In this way one is led to the theoretical formula:

$$\frac{\Gamma_b}{\Gamma_h} = \frac{1}{3+2r_{ud}}\left[1+\delta_{bV}\left(1-\frac{1}{3+2\frac{1+\left(1-\frac{8}{3}s_0^2\right)^2}{1+\left(1-\frac{4}{3}s_0^2\right)^2}}\right)\right]$$
$$= \frac{1}{3+2r_{ud}}\left[1+0.780\delta_{bV}\right] \tag{4.55}$$

where the numerical value of s_0^2 given in Eq. (3.203) has been used.

For what concerns the remaining r_{ud} contribution in Eq. (4.55), this must be computed without approximations, starting from the definition Eq. (4.54) that can be rewritten, using again Eq. (3.203), as:

$$r_{ud} = 0.7759\left[1+O\left(\alpha\right)\right]. \tag{4.56}$$

The $O(\alpha)$ term is expected, on general grounds, to be small. In fact, the large$\sim m_t^2$ contribution coming from the self-energy component $\Delta_1(0)$ is predominantly contained in $\varepsilon_{1u,d}$ whose expression can be easily derived by a generalization of Eq. (4.39), i.e.

$$\varepsilon_{1u,d} = \varepsilon_1 + 2Re\left(\Gamma_{u,d}^{\mu(Z)}\left(m_Z^2\right), j_{u,d}^{\mu(Z)}\right)^{NU}. \tag{4.57}$$

One sees that the $\sim m_t^2$ contribution from $\Delta_1(0)$ is the same in the two parameters (the non universal vertex has no $\sim m_t^2$ components) and therefore, essentially, cancels out. This does not apply to the $\sim m_t^2$ contributions from the $s_{u,d}^2$ parameters are defined by a generalization of Eq. (4.38) as follows:

$$s_{u,d}^2\left(m_Z^2\right) = \left(\sin\theta_{W,eff}\right)^2 - s_0c_0Re\left(\Gamma_{u,d}^{\mu(Z)}\left(m_Z^2\right), j_{u,d}^{\mu(\gamma)}\right)^{NU}. \tag{4.58}$$

From the expression of $\left(\sin\theta_{W,eff}\right)^2$ given in Eq. (3.307) one can evaluate the $\sim m_t^2$ effect in the ratio that appears in the generalization of Eq. (4.54):

$$\left[\frac{1+\left(1-\frac{8}{3}s_u^2\left(m_Z^2\right)\right)^2}{1+\left(1-\frac{4}{3}s_d^2\left(m_Z^2\right)\right)^2}\right]^{(m_t)} \simeq \frac{\left[1+\left(1-\frac{8}{3}s_0^2+\frac{8}{3}\frac{s_0^2c_0^2}{2c_0^2-1}\varepsilon_1\right)^{2(m_t)}\right]}{\left[1+\left(1-\frac{4}{3}s_0^2+\frac{4}{3}\frac{s_0^2c_0^2}{2c_0^2-1}\varepsilon_1\right)^{2(m_t)}\right]}$$
$$= \frac{1.1473\left(1+0.5894\varepsilon_1\right)^{(m)t)}}{1.4787\left(1+0.4123\varepsilon_1\right)^{(m_t)}}$$
$$= 0.7759\left(1+0.1771\varepsilon_1\right)^{(m_t)}$$
$$= 0.7759\left(1+0.1771\Delta_1\left(0\right)\right)^{(m_t)}. \tag{4.59}$$

One sees in conclusion that, as in the case of the $\varepsilon_{1u,d}$ ratio, the $\sim m_t^2$ effect from the generalized weak angles is very diluted. This means that the theoretical value of r_{ud} to be used in Eq. (4.55) will be very stable with respect to the input parameter m_t. In practice, one expects that the complete value, that can be computed by the existing programs [86], does not differ significantly from the lowest order calculation =0.7759 that appears in Eq. (4.56).

This long discussion should have illustrated, we hope in a reasonably understandable way, the calculation of the $Z \to b\bar{b}$ decay at the Z resonance. To conclude this subject, we still have to review a few peculiar properties that make this quantity a rather *special* one. More precisely, the two following facts should be stressed:

a) the parameter δ_{bV}, that represents a reasonable parametrization of the $Zb\bar{b}$ effect, does *not* depend on the Higgs mass m_H. In fact, in the conventional approach, the physical Higgs exchange in the vertex would be proportional to the b mass and therefore vanishing, in first realistic approximation;
b) the quadratic dependence of F Eq. (4.37) on m_t^2 has nothing to do with the custodial symmetry violation $\sim \left(m_t^2 - m_b^2\right)$ that enters the quantity $\Delta_1(0)$ Eqs. (3.190), (3.191) and therefore the parameter ε_1 Eq. (3.288).

The conclusion of the two previous observations is that the $Zb\bar{b}$ vertex, as parametrized e.g. by the quantity δ_{bV}, represents a genuine and unique "top mass indicator", that only depends on the fundamental SM parameter m_t. This should make it clear why the measurement of the Z partial width into a $b\bar{b}$ pair has represented, in the long period of time that was devoted to the measurements at the Z peak, a fundamental issue. In Chapter 10 we shall discuss the effect of the $b\bar{b}$-production data on the determination of the top mass.

To conclude this part of the Chapter, we still have to analyze the possible sensitivity to the δ_{bV} parameter of the measurable $Z \to b\bar{b}$ asymmetries, in analogy with what we did in the case of production of a final charged lepton pair when we examined the dependence on the custodial symmetry breaking parameter $\Delta_1(0)$. We shall see that, in the case of final $b\bar{b}$ pairs, the relevant asymmetries are in practice insensitive to δ_{bV}. Having shown this fact, we shall also discuss in a qualitative way the reason why this lack of sensitivity has to be expected, on very general, and simple, grounds.

The technical proof of our statement is based on the definition of the $Z \to b\bar{b}$ *chiral asymmetry* $\mathcal{A}_b$ defined in detail in Chapter 2 Eq. (2.89). At tree level, this has the expression:

$$\mathcal{A}_b^{(0)} = \frac{g_{bL}^{(0)2} - g_{bR}^{(0)2}}{g_{bL}^{(0)2} + g_{bR}^{(0)2}} = 2\frac{g_{bV}^{(0)} g_{bA}^{(0)}}{g_{bV}^{(0)2} + g_{bA}^{(0)2}} \,. \tag{4.60}$$

At one loop, following our general prescription illustrated in Chapter 3, we shall write:

$$\begin{aligned}
\mathcal{A}_b^{(1)} &= 2\frac{g_{bV}^{(1)}\left(m_Z^2\right) g_{bA}^{(0)}}{g_{bV}^{(1)2}\left(m_Z^2\right) + g_{bA}^{(0)2}} = \frac{2}{1 + \frac{g_{bV}^{(1)2}\left(m_Z^2\right)}{g_{bA}^{(0)2}}} \frac{g_{bV}^{(1)}\left(m_Z^2\right)}{g_{bA}^{(0)}} \\
&= 2\frac{\left[1 - \frac{4}{3}s_b^2\left(m_Z^2\right)\right]}{1 + \left[1 - \frac{4}{3}s_b^2\left(m_Z^2\right)\right]^2} \\
&\simeq 2\frac{\left[1 - \frac{4}{3}\left(\sin\theta_{W,eff}\right)^2 - \frac{8}{3}s_0^2 F\left(m_Z^2; m_t\right)\right]}{1 + \left[1 - \frac{4}{3}\left(\sin\theta_{W,eff}\right)^2 - \frac{8}{3}s_0^2 F\left(m_Z^2; m_t\right)\right]^2} \\
&\times (1 + \text{“QCD”})
\end{aligned} \tag{4.61}$$

and moving from the first to the second equations and from the second to the third line of the previous equation, Eqs. (4.40) and (4.35) have been exploited. In Eq. (4.61) a (small) calculable QCD correction has not been explicitly written down. The reason is that we are now interested in the particular electroweak $\sim m_t^2$ contribution appearing in F. In this spirit, we can neglect the QCD contribution (to be discussed later) and approximate F with Eq. (4.47). In this way, we obtain explicitly, using the numerical value for s_0^2 given in Eq. (3.203) and working “inside” the one loop level where $s_0^2 = \left(\sin\theta_{W,eff}\right)^2$:

$$\begin{aligned}
\mathcal{A}_b^{(1)(m_t)} &= 2\frac{1 - \frac{4}{3}s_0^2}{\left[1 + \left(1 - \frac{4}{3}s_0^2\right)^2\right]} \\
&\times \left[1 - \frac{8}{3}F\left(m_Z^2; m_t\right) \quad \frac{s_0^2}{1 - \frac{4}{3}s_0^2} \quad \frac{1 - \left(1 - \frac{4}{3}s_0^2\right)^2}{1 + \left(1 - \frac{4}{3}s_0^2\right)^2}\right] \\
&= 2\frac{1 - \frac{4}{3}s_0^2}{\left[1 + \left(1 - \frac{4}{3}s_0^2\right)^2\right]} \left[1 + \frac{8}{9} \quad \frac{s_0^4}{1 - \frac{4}{3}s_0^2}\delta_{bV}\right] \\
&= 0.936\left[1 + 0.069\delta_{bV}\right].
\end{aligned} \tag{4.62}$$

One sees therefore from a comparison with Eq. (4.55) that the sensitivity of the b asymmetry $\mathcal{A}_b$ to δ_{bV} is roughly ten times smaller than that of the ratio $\frac{\Gamma_b}{\Gamma_h}$, whose relative experimental accuracy will be, as discussed later, definitely better. Since the two relevant (polarization and forward-backward) $Z \to b\bar{b}$ asymmetries are simply defined in terms of $\mathcal{A}_b$ from the expressions given in Chapter 2, we can confirm the statement that, in practice, these quantities are unaffected by the contribution of the $Zb\bar{b}$ vertex within the MSM framework.

An intuitive understanding of this situation can be obtained by looking at the tree level definitions of $\mathcal{A}_b$ and Γ_b, Eqs. (4.60) and (2.79). In the case of Γ_b, the line of equation $\Gamma_b = constant$ in the plane of the "shifts" δg_{bV}, δg_{aB} would correspond to the relationship:

$$\delta\Gamma_b = 0 \to \delta g_{bV} = -\frac{g_{bA}}{g_{bV}}\delta g_{bA} \simeq$$
$$-\frac{1}{1-\frac{4}{3}s_0^2} \quad \delta g_{bA} \simeq -1.4\delta g_{bA}\ . \tag{4.63}$$

For $\mathcal{A}_b$, one would find the line of equation:

$$\delta\mathcal{A}_b = 0 \to \delta g_{bV} = \frac{g_{bV}}{g_{bA}}\delta g_{bA}$$
$$= \left(1-\frac{4}{3}s_0^2\right)\delta g_{bA} \simeq 0.7\delta g_{bA}\,. \tag{4.64}$$

The shifts produced by the $Zb\bar{b}$ vertex, that is of purely left-handed type, obey on the other hand the condition:

$$\delta g_{bR} = 0 \to \delta g_{bV} = \delta g_{bA}\ . \tag{4.65}$$

This line is "almost" parallel to that of constant $\mathcal{A}_b$ Eq. (4.64), and "almost" orthogonal to that of constant Γ_b Eq. (4.63). One understands therefore why the $Zb\bar{b}$ vertex effect is practically irrelevant on $\mathcal{A}_b$, and much stronger on Γ_b, a feeling that is numerically confirmed by our previous detailed calculation.

This final discussion concludes the first part of this Chapter, devoted to a meticulous derivation of the theoretical expressions that enter the electroweak sector of the $Z \to b\bar{b}$ decay. In the second part of the Chapter, as announced, we shall try to incorporate in the simplest and useful way the still lacking topics of the strong interaction effects, treated in the conventional QCD approach.

4.2 The rôle of strong interactions in Z physics

4.2.1 *Strong interactions effects at the Z peak*

Our discussion has been until now concentrated on the pure electroweak features of the $e+e-$ annihilation process on top of the Z resonance. With this aim, we have analyzed in detail both the production of final (charged) lepton-antilepton pairs and that of quark-antiquark pairs using the same theoretical mechanisms (the special treatment of a final $b\bar{b}$ pair only differs from the remaining cases because the top mass cannot be neglected in the $Zb\bar{b}$ vertex). As often emphasized, we have worked consistently within a perturbation theory expansion truncated at one loop, whose validity has been discussed at the end of Chapter 3 for what concerns the pure electroweak sector of the calculations.

When strong interactions of the final states must be estimated, the first and immediate question that arises is that of whether their effect can be taken into account in a way that is both (reasonably) simple and realistic. In practice, the most favourable situation in which both conditions are simultaneously met is one where perturbative QCD can be satisfactorily used, with a strong coupling α_s sufficiently small to justify the truncation of a power series that has α_s as the expansion parameter. We know from the general QCD features that the preliminary request will be that the relevant four-momentum square q^2, identifiable in this case with the c. m. squared energy of the electron-positron pair, is sufficiently larger than the squared characteristic scale of strong interactions. Intuitively and conventionally, this is identifiable with the nucleon squared mass $m_N^2 \simeq 1$ GeV^2. At the Z peak, the value of $q^2 = m_Z^2$ is two orders of magnitude larger than m_N^2, and the possibility of using a perturbative expansion in a "small" effective coupling $\alpha_s(m_Z^2)$ appears, a priori, to be substantially reasonable.

The previous conclusion is, clearly, qualitative. Let us assume for the moment that it is, at least in first approximation, correct and let us examine the practical problems that would arise in the explicit calculation of QCD corrections to a typical $Z-peak$ electroweak process. The simplest example that can be provided is that of the Z decay into a quark-antiquark pair. We have already derived, in the first part of this Chapter, the theoretical expression of the Z partial width, in the special case of a $b\bar{b}$ pair, and we have shown in Fig. 4.2 a set of electroweak Feynman diagrams that contribute at one loop. The detailed numerical discussion that we have given was also motivated by the ambition of showing that the sum of the four diagrams was

actually finite, in spite of the fact that all the separate contributions were infinite. In all cases the divergences were of ultraviolet origin, i.e. due to the bad behaviour of the (virtual) integrand in the asymptotic integration variable (= k) region, as shown e.g. by Eqs. (4.5), (4.8) and (4.20).

From a strictly formal point of view, the cancellation of the ultraviolet divergences in the considered Z vertex was completely achieved within the *invariant scattering amplitude*, to be more specific within *linear* one loop expressions (vertices, in this case). This can be restated by saying that the cancellation of the electroweak ultraviolet divergences at one loop in the process represented in Fig. 4.2 is an "internal affair" between diagrams with the *same* set of incoming and outgoing *real* particles (in our specific case, electron-positron into quark-antiquark) and different types of *virtual* exchanges , e.g. Fig. (4.2).

One would expect the same formal property to remain true when considering possible extra ultraviolet divergences of QCD origin affecting the same physical process, $e + e \to q\bar{q}$ at the Z peak. In terms of Feynman diagrams, these effects are represented at one loop by Fig. 1.6. Without entering the details of the QCD framework, we shall simply quote the relevant expressions of the gluon propagator and of the gluon-quark vertex. In our conventional notations, they read:

$$\begin{aligned} &\text{gluon propagator} \to P_{\nu\mu}(k) = \\ &= -\frac{\delta ab}{k^2}\left[g_{\nu\mu} + (\xi - 1)\frac{k_\nu k_\mu}{k^2}\right] \end{aligned} \tag{4.66}$$

$$\text{gluon-quark vertex} \to i g_s \gamma_\mu \frac{\lambda^a_{ij}}{2} \tag{4.67}$$

where a, b are color $SU(3)$ indexes, a, b=1...8, and the remaining quantities are defined as follows: λ_a are the Gell-mann matrices, i, j=1, 2, 3 are the quark color indexes; ξ is the $SU(3)$ gauge parameter, whose rôle is essentially similar to that of the electroweak gauge parameters ξ_W, ξ_Z (we shall not enter the discussion of the Faddeev-Popov *ghosts* in what follows and simply state that in the considered process $e^+e^- \to q\bar{q}$ these unphysical creatures can be safely ignored); g_s is the strong coupling, $\frac{g_s^2}{4\pi} = \alpha_s$.

The elimination of the gluon ultraviolet divergence in the $Zq\bar{q}$ vertex proceeds along the conventional approach that we have exhaustively illustrated in the corresponding electroweak case in the first part of this Chapter. The extra feature that we shall try to summarize will rather be the fact

that the cancellation of the ultraviolet divergences in the gluon vertex is not yet the final word for what concerns QCD divergences. Actually, another, essentially different, kind of infinities arises in this case, that is deeply connected with a characteristic property of the gluons. The latter ones are supposed to be massless particles, exactly like the photons. As a consequence of this feature, *infrared* divergences appear, exactly like in QED. Since the cancellation of these infinities is achieved by a procedure that is intrinsically different from those that we have previously examined, and a number of important papers exists [29] where all the details of the procedure are exhaustively discussed, we shall simply start from the pragmatic statement that, in conclusion, the finite expression of the strong interaction effect on the Z partial width into a massless quark pair, to lowest order in the strong coupling α_s, can be written as:

$$\Gamma_q^{1,s} = \Gamma_q^{\alpha^s=0} \left[1 + \frac{\alpha_s}{\pi}\right] \tag{4.68}$$

where $\Gamma_q^{\alpha_s=0}$ represents the purely electroweak component of the partial width.

Although Eq. (4.68) seems remarkably simple and attractive, it still cannot be utilized to generate a meaningful theoretical prediction, i.e. one directly comparable with an experimental measurement. The two main difficulties that still persist are related to the following problems:

a) what can actually be measured at the Z peak is the fraction of Z's decaying into well defined types of *hadrons*. Equation (4.68) only gives the fraction of Z's decaying into well defined *quarks*. In the commonly used theoretical description, the Z decay into quarks is the "first step" of its hadronic decays. This is followed by the next transformation of quarks into hadrons, via their *hadronization* process. The description of the latter is less simple and general, and requires a separate dedicated discussion of those non perturbative effects that are responsible for the formation of the bound states. This discussion can be (and has been) given, e.g. in the exhaustive analysis of [29]. However, the unavoidable introduction of new *ad hoc* phenomenological parameters makes the overall theoretical picture less favourable to the explicit goal of a high precision test of the genuine electroweak sector of the SM, that represents the main purpose of this book;
b) the numerical size of the one-loop effect in Eq. (4.68) depends on the precise value to be assigned to the strong coupling α_s. Assuming that, as one would intuitively guess, the proper quantity to be used is the

running coupling $\alpha_s\left(q^2\right)$ computed at $q_2 = m_Z^2$ (although, as we shall discuss, this statement only makes sense if at least the next contribution $\sim \alpha_s^2$ is computed), the available value before the start of LEP1-SLC operations would have been that obtained by previous different measurements [58], roughly leading to a value

$$\alpha_s\left(m_Z^2\right) \simeq 0.11 \pm 0.1\,. \tag{4.69}$$

When inserted in Eq. (4.68), this leads to a relative effect of approximately four percent, well above the conceivable permil experimental limit. Under these conditions, that are a consequence of the fact that the value of the strong coupling constant $\alpha_s\left(m_Z^2\right)$ is more than ten times larger than that of the corresponding QED coupling $\alpha\left(m_Z^2\right)$, the computation of the strong interaction effect at "only" one loop in Eq. (4.68) appears evidently insufficient for the purposes of Z physics. In fact, with a coefficient of the next $\sim \left(\frac{\alpha_s}{\pi}\right)^2$ of order one, which a priori cannot be excluded, the second order contribution would be at the few permil level, which represents a quite sizeable effect at the Z peak. One sees therefore that the calculation of (at least) the next term in the perturbative expansion in α_s of Eq. (4.68) is practically unavoidable from a strictly pragmatic point of view. As we shall see, this calculation will be indeed theoretically fundamental, since it will allow to clarify the meaning of the choice $q^2 = m_Z^2$ at which to compute the running parameter $\alpha_s\left(q^2\right)$.

Let us consider problem (a) first. A simple and realistic solution to this difficulty can be found by observing that the relative effect of the strong interactions in Eq. (4.68) is the same for all the five (assumed massless) *light* quarks that can be produced at the Z peak. This means that the theoretical expression of the partial Z width into the five light quarks, $\Gamma_5 = \Gamma_u + \Gamma_d + \Gamma_s + \Gamma_c + \Gamma_b$, will automatically be given for what concerns the strong interaction effect by the same simple formula found for the particular quark pair, that is:

$$\Gamma_5^{1,s} = \Gamma_5^{\alpha_s=0}\left[1 + \frac{\alpha_s}{\pi}\right]\,. \tag{4.70}$$

Equation (4.70), unlike Eq. (4.68), can be realistically compared with experiment. The simple reason is that the fraction of Z bosons decaying into *all* possible kinematically allowed hadrons (that is measured at the Z peak) is also equal to the fraction of Z bosons decaying into *all* possible allowed quarks, no matter what the separate hadronization schemes are. Otherwise

stated, the probability that *all* light quarks, after their production at the Z peak, transform into *all* detectable hadrons, is equal to one. One sees therefore that reasons of theoretical simplicity select the Z partial hadronic width Γ_5 as a clean and promising observable to be used, if the final goal is that of an unbiased test of the electroweak sector of the SM. In what follows, we shall accept these qualitative arguments and insist on Γ_5 and on its theoretical calculation.

The next step at this point becomes that of the computation of the higher order coefficients in the α_s expansion. Given the relevance of the subject, we shall devote next Subsection to a summary of the results that were obtained.

4.2.2 *Higher order strong coupling contributions*

In the calculation of the Z hadronic width beyond the lowest $\sim \alpha_s$ contribution a number of extra complications arises. Before listing and (briefly) discussing them, it is perhaps opportune to recall an important theoretical feature, that is deeply connected with the possibility of exploiting in a not ambiguous way the notion of *running* strong coupling $\alpha_s\left(q^2\right)$. A simple way of illustrating the problem is that of starting from the differential renormalization group (RG) equation satisfied by α_s. For our purposes, we shall rewrite it as follows:

$$\mu^2 \frac{d\alpha_s\left(\mu^2\right)}{d\mu^2} = -b_0 \alpha_s^2\left(\mu^2\right) \tag{4.71}$$

where $b_0 = \frac{33-2N_f}{12\pi}$.

As one sees from Eq. (4.71), varying the scale μ^2 by an arbitrary amount, $\mu^2 \to c\mu^2$, one can only reveal the change of $\alpha_s\left(\mu^2\right)$ at the next order α_s^2. If the theoretical expansion that one uses is truncated at the lowest $\sim \alpha_s$ order, at a given scale $\mu^2 = q^2$ ($=m_Z^2$ in our case), it does not make much sense to identify the running coupling α_s with $\alpha_s\left(q^2\right)$. This becomes possible if the expansion is prolongated, at least to the next $\sim \alpha_s^2$ order.

When carrying on this task, (at least) two new difficulties arise, that can be summarized as follows:

c) in general, going beyond the lowest α_s order, the terms of the perturbative QCD expansion may depend on the chosen *renormalization scheme*. Of course, the sum of *all* the terms of the expansion must not depend on the scheme for any chosen observable, but this property does not necessarily apply to the individual terms. We shall adopt in what

follows the commonly used attitude of performing QCD perturbative expansions in the so called *barred minimal subtracted* ($\overline{MS}$) scheme in a kinematical configuration ($q^2 = m_Z^2$) where five quarks may be produced. The running coupling that will enter the theoretical formulae should therefore, strictly speaking, be denoted as $\alpha_s^{(5),(\overline{MS})}\left(m_Z^2\right)$, but for simplicity we shall write it as $\alpha_s\left(m_Z^2\right)$;

d) in the calculation of higher order diagrams, an unavoidable dependence on the top mass arises, in some formal analogy with the case of the electroweak $Zb\bar{b}$ vertex Fig. 4.2.

It should be stressed at this point that, as already anticipated in this Chapter, for what concerns the mass of the five (udscb) light quarks, the approximation of setting it equal to zero in the computation of the QCD expansion is quite satisfactory with one (predictable) exception provided by the b-quark case. Here the value m_b different from zero must be retained at first order in α_s, leading to contributions$\sim \alpha_s \frac{m_b^2}{m_Z^2}$. The precise expression of such terms can be found e.g. in [33]. For what concerns our Eq. (4.38), the overall (i.e. including electroweak corrections as well) effect corresponds to the following formal replacements to the lowest α_s order:

$$\frac{g_{Vb}^2\left(m_b, \alpha_s\right)}{g_{Vb}^2\left(m_b = 0, \alpha_s = 0\right)} = \left[1 + \frac{\alpha_s}{\pi} + \frac{3\alpha_s}{\pi}\frac{4m_b^2}{m_Z^2}\right] \tag{4.72}$$

$$\frac{g_{Ab}^2\left(m_b, \alpha_s\right)}{g_{Ab}^2\left(m_b = 0, \alpha_s = 0\right)} = \left[1 - \frac{6m_b^2}{m_Z^2} + \frac{\alpha_s}{\pi} - \frac{6\alpha_s}{\pi}\frac{m_b^2}{m_Z^2}\left(1 + 2\ln\frac{m_b^2}{m_Z^2}\right)\right] . \tag{4.73}$$

One sees from Eqs. (4.72), (4.73) that the b *mass* corrections generate in the $Zb\bar{b}$ width $\sim \left(g_{Ab}^2 + g_{Vb}^2\right)$, on top of the ~ 1 percent correction at the electroweak lowest level, another one of approximately *five permil* at the α_s order, both effects being sizeable at the Z peak.

The next step in our analysis is now the stud of the higher order α_s effects. Here we shall assume that, as intuitively suggested by the previous numerical estimate, all quark masses, including the b mass, can be neglected. This leads to a numerical estimate that has been performed up to the third perturbative order α_s^3. The motivations for such an "extremely" accurate calculation will be discussed soon in this Chapter, and one will see immediately why the theoretical attention was concentrated for a rather long period on the last third perturbative order. Before entering

this discussion, we now summarize the results that were obtained for the second order terms.

To shorten the treatment, since we are assuming that all quark masses can be neglected, we shall write directly the α_s^2 correction to the full Z hadronic width Γ_5, that is of "universal" type i.e. has the same expression for each separate quark component. In the notation of a recent dedicated Review [59] this has the form (for three quark families):

$$\Gamma_5^{\left(\alpha_s^2\right)} = \Gamma_5^{(\alpha_s=0)} \left[1 + \frac{\alpha_s\left(m_Z^2\right)}{\pi} \left(1 + O\left(m_b^2\right)\right) \right.$$
$$\left. +1.41 \frac{\alpha_s^2\left(m_Z^2\right)}{\pi^2} + c_2 \frac{\alpha_s^2\left(m_Z^2\right)}{\pi^2} \right] . \tag{4.74}$$

The coefficient c_2 in Eq. (4.74) is exhibiting the m_t dependence, embodied in a function I_2 of m_t that must be computed numerically, and is related to c_2 as follows:

$$c_2 = -\frac{1}{12\Sigma_q \left[g_{V,q}^2 + g_{A,q}^2\right]} I_2\left(m_Z, m_t\right) \tag{4.75}$$

where

$$I_2\left(m_Z, m_t\right) \simeq 9.25 - 1.037 \frac{m_Z^2}{4m_t^2} - 0.632 \frac{m_Z^4}{16 m_t^4} + 6 \ln \frac{m_t}{m_Z} . \tag{4.76}$$

Numerically, for m_t ranging between 50 GeV and 200 GeV, I_2 varies from ~ 6 to ~ 12. For values of α_s in the range $0.11 - 0.12$ this corresponds to an overall α_s^2 contribution that is negative and of the five permil size, relevant at the Z peak accuracy level. This is perfectly in line with the qualitative expectation expressed at the beginning of this Chapter, when the motivations in favour of a second order calculation were roughly explained.

From a numerical point of view, one notices that the relative size of the second order α_s^2 effect is roughly one tenth of the first order one. Naively, one would expect a similar reduction factor for the following third order term. Were this the case, the related contribution would be of a relative size below the "visibility threshold " that for Γ_5 could be fixed at the permil level. Actually, one finds a coefficient numerically equal to -12.8 for the $\frac{\alpha_s^3}{\pi^3}$ term [59], whose relative negative effect is below the one permil and, in conclusion, not visible. This fact does not diminish the relevance of the hard calculation and the consequent possibility of declaring the perturbative α_s

expansion at the Z peak officially fully under control, for what concerns the theoretical estimate of the full hadronic Z width Γ_5 [60]. In the final part of this book, we shall make use of this variable , whose relevance in the overall numerical fit will be, least to say, remarkable.

As a matter of fact, there is another quantity that is measured at the Z peak and plays a very relevant rôle in the final numerical analysis. This is the forward-backward asymmetry for production of $b\bar{b}$ pairs, A_{FB}^b. Here the rôle of strong interactions is less immediate to explain than in the previous Γ_5 case. The simple reason is that in the case of A_{FB}^b a precise definition of *scattering angle* must be provided. This requires a series of technical steps that we shall discuss in Chapter 8, leading to then general expression

$$A_{FB}^{b,(\alpha_s)} = A_{FB}^{b,(\alpha_s=0)} \left[1 - k_b \frac{\alpha_s}{\pi}\right] \tag{4.77}$$

where

$$k_b = 1 - \frac{2\pi}{3}\mu \tag{4.78}$$

and $\mu = \frac{2m_b}{m_Z}$. This corresponds to a value of the $\frac{\alpha_s}{\pi}$ coefficient of approximately 0.8. In terms of the corresponding effect on the asymmetry, whose electroweak value is close to 0.10 (see Chapter 2), this produces a shift of about 0.003. Since the final experimental accuracy will be of the two-three permil level, one sees that the effect must be included. We shall return to this point in Chapter 8 since the rôle of the forward-backward b-asymmetry will turn out to be particularly relevant for the final averaged determination of the Weinberg $\sin\theta_W$ angle.

In conclusion, for the two observables Γ_5 and A_{FB} the strong interaction effects can be and have been computed at the proper accuracy. For what concerns the b partial width Γ_b, we have anticipated that the more practical experimental quantity $R_b = \frac{\Gamma_b}{\Gamma_5}$ Eq. (4.50) is in fact measured. For the latter, the relevant strong interaction effect can be derived in a straightforward way starting from the Equations that have been written in this Chapter for the numerator and for the denominator. As one can guess, the effect is largely diluted in the ratio, being essentially due to b-mass terms (mostly in the numerator).

Chapter 4 is at this point concluded. Its main results will be combined in Chapter 11 with those obtained in Chapter 3. Since the overall number of formulae and Equations is at this point rather large, we have summarized, for the reader's convenience, in Table 4.1 the most relevant expressions derived in those two long and, hopefully, useful Chapters.

As already mentioned, Chapters 1–4, have been devoted to a summary of the considerable theoretical effort that was developed by several physicists to indicate the best measurable quantities that would have provided high precision tests of the Standard Model. In the following Chapters the corresponding memorable experimental effort will analogously be summarized and illustrated, starting with the discussion of the fundamental measurement of the Z lineshape.

Table 4.1 Reference to most relevant formulae derived in Chapters 3 and 4.

Z leptonic width	Eq. (3.292)	$\frac{\Gamma_\ell^{(1)}}{m_Z} = \frac{G_F m_Z^2}{6\pi\sqrt{2}} \left[g_{Ae}^2 + g_{Ve}^2\right]$
effective axial Z-lepton coupling	Eq. (3.290)	$g_{Ae} = \sqrt{1+\epsilon_1}\, g_{Ae}^{(0)}$
effective vector Z-lepton coupling	Eq. (3.291)	$g_{Ve} = \sqrt{1+\epsilon_1}\, g_{Ve}^{(1)}\left(m_Z^2\right)$
$\sin^2\theta_{W,eff}$	Eq. (3.293)	$\sin^2\theta_{W,eff} = \frac{1}{4}\left[1 - \frac{g_{Ve}^{(1)}(m_Z^2)}{g_{Ae}^{(0)}}\right]$
longitudinal polarization asymmetry A_{LR}	Eq. (3.302)	$\mathcal{A}_e = \frac{2v_0}{1+v_0^2}[1 + \epsilon_1 \frac{4s_0^2 c_0^2}{2c_0^2-1}(\frac{1}{v_0} - \frac{8v_0}{1+v_0^2}) - \epsilon_3 \frac{4s_0^2}{2c_0^2-1}(\frac{1}{v_0} - \frac{2v_0}{1+v_0^2})]$
mu and tau forward-backward asymmetry	Eq. (3.304)	$A_{FB}^\ell = \frac{3}{4}\mathcal{A}_e^2 = 0.01695[1 + 33.37\epsilon_1 - 44.96\epsilon_3]$
tau polarization asymmetry	Eq. (3.283)	$A_{pol}^\tau = -\mathcal{A}_\tau = -\mathcal{A}_e$
R_b	Eqs. (4.55) and (4.56)	$\frac{\Gamma_b}{\Gamma_h} = \frac{1}{3+2r_{ud}}[1 + 0.780\delta_{bV}]$ with $r_{ud} = 0.7759[1 + O(\alpha)]$
chiral b asymmetry $\mathcal{A}_b$	Eq. (4.62)	$\mathcal{A}_b^{(1)(m_t)} = 0.936[1 + 0.069\delta_{bV}]$
W mass	Eqs. (3.316) and (3.202)	$m_W^2 = m_Z^2 c_0^2[1 + 1.430\epsilon_1 - \epsilon_2 - 0.859\epsilon_3]$ with $c_0^2 \simeq 0.769$

Chapter 5

Accelerators and Detectors for Z and W Physics

The experimental results presented in next Chapters have been achieved thanks to many years of successful operation of three major accelerators, LEP, SLC, Tevatron, and of their detectors. Their main features are outlined below, together with some of the details that are necessary to understand the rest of the book.

5.1 LEP

LEP, the CERN's Large Electron Positron collider, was situated in the region between the Geneva lake and the Jura mountains, in the underground tunnel now used for the Large Hadron Collider (LHC). It reached the highest energies in e^+e^- collisions and it was characterized by a very precise beam-energy calibration. The tunnel has a length of 26.7 kilometer and is 3.8-meter wide. Four large underground halls, located at a depth varying between 50 and 150 meters, housed the ALEPH, DELPHI, L3 and OPAL detectors. A sketch of LEP and its detectors can be seen in Fig. 5.1. The accelerator was approximately circular, consisting of eight arcs of 2.8-km length and eight straight sections. The electrons and positrons were accelerated at 20 GeV by the CERN accelerators complex and injected into LEP, where they were further accelerated at their maximum energy. The beam energy was about 45 GeV for the Z run that took place in the years 1989–1995 (LEP1 phase) and reached the maximum energy of 104.5 GeV in year 2000, after five years of operation above the WW threshold (LEP2 phase).

In the LEP1 phase the beams were accelerated by copper radio-frequency (RF) cavities positioned in the straight sections on either side of the experimental halls. The RF cavities were replaced by superconduct-

ing cavities in the second, higher energy, LEP2 phase. The replacement was required to compensate the higher energy loss per turn at LEP2, that was about 2 GeV to be compared with 125 MeV at LEP1. The beams were bended in the eight arcs by 3400 dipole magnets and focused by 800 quadrupoles and 500 sextupoles magnets. Electrons and positrons were grouped in bunches and circulated in opposite directions with a frequency of about 11 kHz. Typically four bunches were used at LEP, during the LEP1 phase a fraction of data was delivered with 8 bunches and even with bunch trains. Most of the LEP1 data was collected closely to the Z peak, but a sizeable fraction of the data was also delivered at side centre-of-mass energies, up to 3 GeV above and below the peak of the Z resonance. Such energy scans were essential for the measurement of the Z lineshape. The beams were colliding at the centre of the four experimental apparatus, interacting in a region approximately 300 μm wide along the LEP bending radius, 60 μm wide in the vertical direction and 2 mm wide along the beam direction. LEP achieved a record luminosity of $2.3 \times 10^{31} cm^{-2} s^{-1}$ during the Z runs, and went above $10^{32} cm^{-2} s^{-1}$ in the LEP2 phase. The total integrated luminosity delivered at the Z was about 150 pb^{-1} per experiment; the four experiments collected a total statistics of more than 15 millions hadronic Z decays and 1.7 millions leptonic Z decays. At LEP2 about 600 pb^{-1} per experiment were delivered, for a total of about ten thousand WW interactions per experiment. The techniques employed to achieve an absolute beam energy calibration with a precision of 2×10^{-5} are described in Chapter 6.

5.2 SLC

The SLC (Stanford Linear Collider), operating from 1989 to 1998, was the first example of a high energy linear collider and provided longitudinal polarization of the electron beam. Its length was 3.2 kilometer and the accelerator was running at a centre-of-mass energy in the vicinity of the Z peak. The layout of SLC is shown in Fig. 5.2. Alternate bunches of electrons and positrons were produced and, after damping in rings designed to reduce the phase space, they were accelerated to 45.6 GeV in two separate arcs. A single interaction point was provided, housing the Mark II detector in 1989 and subsequently, from 1990 onward, SLD. The luminous region had very small dimensions, a few microns in the directions orthogonal to the beams. The rate at the interaction point was low, about 120 Hz. The operation

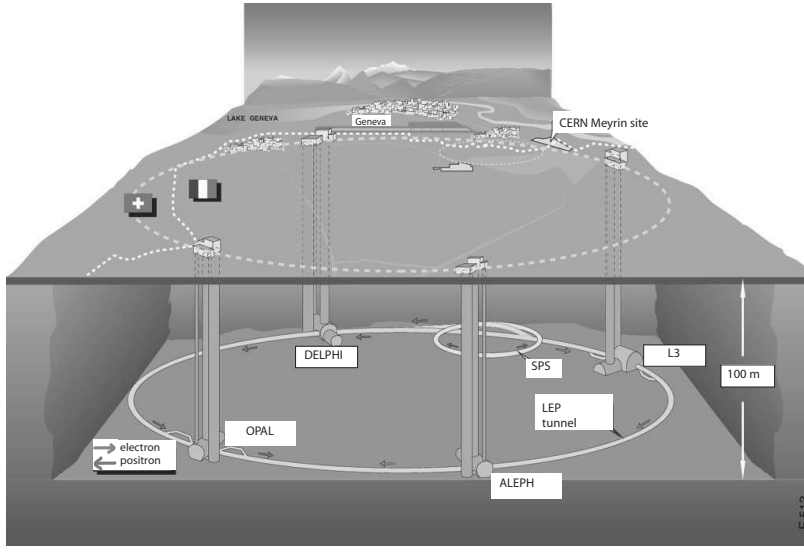

Fig. 5.1 A sketch of LEP with its experiments.

with polarized electron beams started in 1992, with the commissioning of an electron gun based on a GaAs cathode hit by polarized laser light. After 1994 an electron-beam polarization of about 77% was achieved. At this average polarization, about 150000 Z decays were recorded by the SLD experiment, complemented by about 70000 Z decays collected at lower beam polarization. More details about polarized beams at SLC are given in Chapter 8.

5.3 Tevatron

The Tevatron is presently reaching the highest centre-of-mass energies in $p\bar{p}$ collisions; at this accelerator the top quark was discovered. It is located at Fermilab in Illinois, about 40 km east of Chicago. The use of antiprotons in high energy colliders was pioneered at the CERN Sp$\bar{p}$S. Both CERN Sp$\bar{p}$S and Fermilab proton synchrotrons had originally been constructed as fixed-targed accelerators. The possibility of injecting high-intensity antiproton

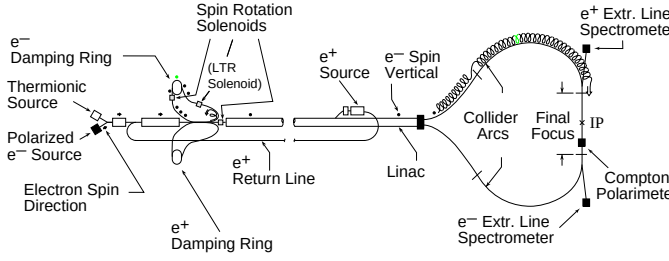

Fig. 5.2 The schematic layout of the SLC.

beams in the same storage ring was made possible in the early 1980s thanks to a technique called *stochastic cooling* [61]. This technical breakthrough allowed the discovery of the W and Z bosons at the Sp$\bar{\text{p}}$S.

At the Tevatron 10^8 antiprotons with an energy of 8 GeV are made every few seconds by bombarding a Nickel target with 10^{12} 120 GeV protons. About 30000 pulses of antiprotons need to be collected and stored in an accumulator before injection into the main accelerator. To produce a bunch of antiprotons of limited spatial dimensions and low momentum spread their six-dimensions phase space must be reduced (*cooled*) by nine order of magnitudes. The Tevatron layout is shown in Fig. 5.3. Hydrogen ions are produced by a ion source, injected into the Linac and then accelerated to 8 GeV in the Booster. In the Main Injector they reach the energy of 120 GeV for antiproton production and of 150 GeV to fill the Tevatron ring. Antiprotons of 8 GeV coming from the Accumulator are accelerated to 150 GeV in the Main Injector, too. Both beams are then injected in the Tevatron superconducting ring, a collider of 6-km circumference, to reach an energy of 980 GeV. The beams collide in two experimental areas housing the CDF and D0 experiments.

The Tevatron collider started its operations in 1988. In the period 1992-1995 (Run I) an integrated luminosity of about 110 pb^{-1} was delivered to the experiments. In Run I the Main Injector did not exist, a ring inside the Tevatron tunnel was used. The number of bunches was six and the beam energy 920 TeV. In 2002 the Main Injector and other upgrades were operational, the number of bunches increased to 36 and the beam energy to 980 TeV. The peak instantaneous luminosity during Run II has exceeded $10^{32} cm^{-2} s^{-1}$. The Run II period is foreseen to end in 2009, with a target integrated luminosity of 8 fb^{-1}.

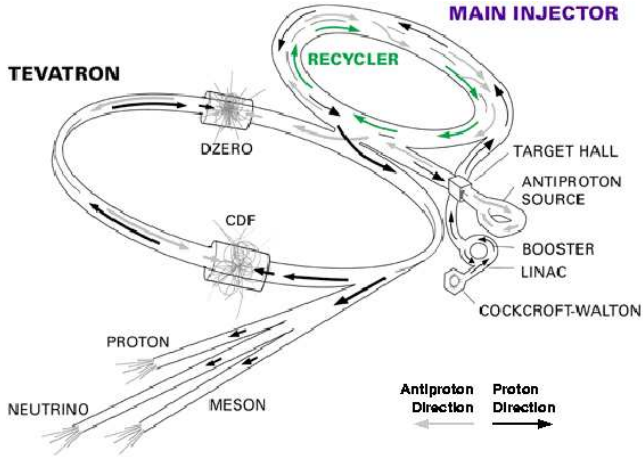

Fig. 5.3 The schematic layout of the Tevatron Collider, for the Run II data-taking period.

5.4 Beyond LEP, SLC and Tevatron: next colliders

The second half of 2007 will see the birth of the Large Hadron Collider (LHC) at CERN. The LHC is presently being completed in the already-existing 27 km LEP tunnel. It will provide head-on collisions of two proton beams of 7 TeV each, with a design luminosity of $10^{34} cm^{-2} s^{-1}$. The LHC proton bunches are spaced 25 ns, yielding a collision rate of 40 MHz. The aim of LHC is the search for the Higgs boson and for physics beyond the Standard Model; nevertheless the large cross sections, at proton-proton centre-of-mass energy of 14 TeV, and the high LHC luminosity will provide huge rates of Standard Model (W,Z, top-quark) events.

In order to deliver e^+e^- collisions at centre-of-mass energies higher than LEP, while keeping electric power consumption to a manageable level, a linear collider is needed. The International Linear Collider (ILC), based on high-field superconducting RF cavities, is presently being designed. The electric field in the cavities will reach 25 MVolt/m, to be compared with 6 MVolt/m at LEP2. Even with these strong cavities, the accelerator length will exceed 30 km. It should yield e^+e^- collisions at a maximum centre-of-mass energy from 500 to 800 GeV, with instantaneous luminosities around $10^{34} cm^{-2} s^{-1}$. Even higher centre-of-mass energies (3 TeV) could potentially be reached with the CLIC accelerator, being designed at CERN.

CLIC would receive its power from an intense low energy linac acting as a driver and replacing the conventional RF cavities. The main features of present and future accelerators are summarized in table 5.1.

Table 5.1 Present and future accelerators for W and Z physics. Expected parameters are given for future accelerators. For Tevatron the RUN II figures are shown. Integrated luminosity is for experiment.

	LEP	SLC	Tevatron	LHC	ILC	CLIC
Beams	e^+e^-	e^+e^-	$p\bar{p}$	pp	e^+e^-	e^+e^-
C.o.m. energy (GeV)	89-209	91	1900	14000	500-800	3000
luminosity $cm^{-2}s^{-1}$	10^{32}	10^{29}	10^{32}	10^{34}	10^{34}	10^{34}
Int. luminosity (pb^{-1})	750	8	8000	10^5	10^5	10^5

5.5 Detectors

Collider detectors follow a typical onion-like layout, covering large part of the 4π solid angle (as an example see Fig. 5.5). They are composed of several subsystems arranged in cylindrical structures, surrounding the beam line and centered on the nominal beam crossing point. This is typically the mid point of the straight section between the two final quadrupoles of the accelerator. The main components of collider detectors are briefly described in next paragraphs; detailed descriptions can be found elsewhere [62]. A general introduction on particle detectors can be found in Ref. [63]; see also [13] and references therein.

Charged particle tracking

Charged particle trajectories are measured in tracking devices by detecting the particle ionization in the detector material at increasing distance from the beam line; the result of the measurement is generally a set of three-dimensional coordinates describing the trajectory. Tracking devices are immersed in the axial magnetic field provided by a surrounding coil. Charged particles are bent by the magnetic field and their three-momenta can be measured by reconstructing the trajectory. The error on the momentum measurement is related to the geometry of the detectors and to the magnetic field as follows. If the strength of the axial magnetic field is B, the trajectory of a particle of momentum p, projected on a plane orthogonal to the field, follows a circle of radius $R = \frac{p_T}{eB}$ where e is the particle charge and $p_T = p\cos\lambda$ its transverse momentum (λ represents

the pitch angle with respect to the plane). If the tracking device is a cylinder of radius L the particle is bent by the magnetic field (Fig. 5.4) by an angle ϕ with $2\sin\frac{\phi}{2} = \frac{L}{R} = \frac{eBL}{p_{\mathrm{T}}}$. The deviation of the particle path from a straight line is determined by the sagitta of the circular trajectory, defined as $s = R - R\cos\frac{\phi}{2} \approx \frac{R\phi^2}{8}$, giving $s = \frac{eBL^2}{8p_{\mathrm{T}}}$. The uncertainty on the measurement of the sagitta, δs is a function of the uncertainty on the measurements of the coordinates x_i of the trajectory: $\delta s = f(\delta x_i)$. It follows that

$$\frac{\delta p_{\mathrm{T}}}{p_{\mathrm{T}}} = \frac{f(\delta x_i) 8 p_{\mathrm{T}}}{eBL^2}\,. \tag{5.1}$$

Equation (5.1) shows that good momentum measurement requires large tracking devices and high magnetic fields. Magnetic fields higher than 1 Tesla on large volumes can be obtained with superconducting coils. Equation (5.1) shows also that the uncertainty on transverse momentum grows with the transverse momentum itself. In a real detector the uncertainty on the sagitta measurement depends on the geometry and on the detector resolution in measuring the spatial coordinates; it depends also on multiple scattering, i.e. on multiple deflections of a particle in traversing the detector medium, generally due to Coulomb scattering from nuclei. The deflection caused by multiple scattering between two measurements of positions is proportional to the square root of the medium thickness, expressed in radiation lengths (X_0), and proportional to the inverse of the particle momentum ($\frac{1}{p}$). Multiple scattering adds to $\delta s = f(\delta x_i)$ a component which is proportional to $\frac{1}{p}$ and therefore adds to Eq. (5.1) a term independent on the transverse momentum. In order to suppress the effect of multiple scattering it is important to keep the material budget of tracking devices as low as possible. The transverse momentum resolution of collider tracking devices is generally parametrised as $\frac{\delta p_{\mathrm{T}}}{p_{\mathrm{T}}} = (A \times p_{\mathrm{T}} \oplus B)$, where $\oplus$ represents the sum in quadrature of the geometrical and multiple scattering terms. For the experiments considered in this book typical values of the two parameters are $A \approx 10^{-3}(\mathrm{GeV}/c)^{-1}$ and $B \approx 10^{-2}$. The momentum p can be computed from the measurement of p_{T} and of the pitch angle, λ. The latter one can be determined by measuring the coordinates of the trajectory in direction parallel to the magnetic field.

An important aspect of charged particle tracking concerns the detection of secondary vertices originating from the decay of long-lived particles; this is discussed in details in Chapter 7.

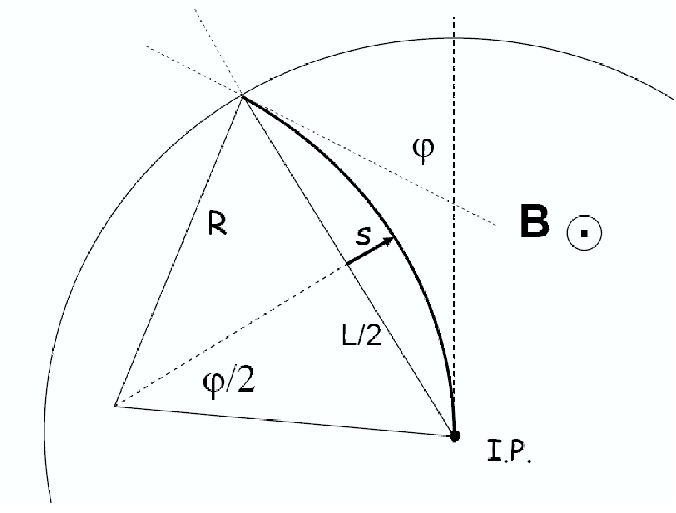

Fig. 5.4 Trajectory (bold line) of a charged particle in a cylindrical tracker of radius L, immersed in a magnetic field **B** parallel to the beam line. The view orthogonal to the beam line is shown. The curvature radius of the charged particle and the bending angle are indicated by R and ϕ, respectively. The sagitta is represented by the arrow s.

Calorimeters

Neutral particles cannot be measured by tracking devices and their detection requires the formation of a shower, which is a destructive process. The basic principles of shower development can be understood by considering a high energy photon, of energy E_0, impinging on a dense medium. In this case an electromagnetic shower is formed and the basic parameter regulating its development it's the medium radiation length (X_0). The probability that the photon converts into an electron-positron pair after traversing a depth of thickness x is $(1 - e^{-\frac{7}{9}\frac{x}{X_0}})$, i.e. about 50% after one radiation length. On average, the electron and positron will equally share the primary photon energy ($E_1 = E_0/2$) and their energy will decrease, on average, to $E_2 = E_1/e = E_0/2e$ in next radiation length. At high energies the electron and positron energy loss is caused, typically, by the emission of a bremsstrahlung photon. The process continues until all particle energies fall below a critical energy (E_c) at which the main processes involved in energy loss are no longer pair-creation and bremsstrahlung. For lead this happens below 10 MeV. The critical energy is reached, on average, after having crossed a thickness nX_0, where $n = \ln \frac{E_0}{E_c} / \ln 2$. This longitudinal

position is called shower maximum and features an average of $N = \frac{E_0}{E_c}$ particles.

Calorimeters are detectors made with dense material, with the capability of detecting the charged particles belonging to the shower. If they are dedicated to the measurement of electromagnetic showers, as the ones originating from photons and electrons/positrons, are called electromagnetic calorimeters. The detection can take place by measuring the ionization, or the Cherenkov light emitted by charged particles. The signal detected by an homogeneous calorimeter is proportional to the total track length T, that is the sum of all path lengths of electrons and positrons. In the simplified scheme described in previous paragraph the total track length is $T \approx \frac{2}{3} X_0 \sum_{\nu=1}^{n} 2^\nu \approx \frac{4}{3} X_0 \frac{E_0}{E_c}$ showing that it is linearly related to the initial photon energy. In real devices the drop in detection efficiency does not necessarily correspond to the critical energy, still it is found that

$$T = F(\frac{E_d}{E_c}) X_0 \frac{E_0}{E_c} \tag{5.2}$$

where E_d represents the real detection threshold and F is a function depending on the medium (it essentially depends on the medium Z/A ratio).

The previous discussion shows that calorimetric measurements are essentially a stochastic process and the measured energy fluctuates with the fluctuation of the detected total track length. The latter one, in turn, is proportional to the total charged particle yield (N_{ch}) which, according to Poisson statistics, fluctuates with $\sigma = \sqrt{N_{ch}}$. Therefore the relative energy resolution of a calorimeter has a stochastic component described by $\sigma(E)/E = A/\sqrt{E}$, where $E = E_0$ is the energy of the primary particle. Similar arguments hold for sampling calorimeters, consisting of inactive layers of dense materials interleaved with detector layers, typically made with gas detectors. In sampling calorimeters only a fraction of the total track length is detected, leading to additional sampling fluctuations. The relative energy resolution of a calorimeter decreases with increasing the energy of the primary particle; the resolution is eventually dominated by detector non-uniformities and uncertainties on the calorimeter calibration, adding a constant term to the stochastic component. The resolution effects can be parametrised as

$$\frac{\sigma(E)}{E} = \frac{A}{\sqrt{E/GeV}} \oplus B \tag{5.3}$$

where B is the constant term. Electromagnetic calorimeters for collider detector have typical values of A ranging from a few % for homogeneous

calorimeters to 10–20 % for sampling calorimeters. The constant term is of the order of (typically less than) 1%. Another important parameter of a calorimeter is its total thickness, as the shower longitudinal development goes as $\ln E$. A thickness of about 20 X_0 at collider energies is required for shower containment.

Electromagnetic calorimeters are also used to measure the primary particle position, at its entrance into the calorimeter. The position resolution depends on the transverse dimension of the shower, which scales with the Molière radius ($R_M = \frac{21MeV}{E_c} X_0$), and with the transverse granularity of the calorimeter. The position resolution includes a stochastic term and a constant term, similarly to Eq. (5.3). For high energy electrons and photons position uncertainties of a few mm are obtained at collider detectors. Calorimeter transverse granularity is also important to keep low the frequency of overlapping showers caused by nearby particles (for instance from two photons originating from the same π^0 decay).

The previous discussion applies, strictly speaking, to electromagnetic showers. Some general features can be extended, however, to hadronic showers produced by charged or neutral hadrons. Hadronic showers develops through a variety of inelastic interactions and are subject to important stochastic fluctuations. In hadronic interactions several secondaries, such as pions, kaons, protons, neutrons, etc. can be produced. Subsequent interactions lead to the formation of an hadronic cascade which can be detected by a hadron calorimeter. Only part of the energy is visible in the calorimeter: neutrinos and muons from pion and kaon decays escape the calorimeter and a fraction of the energy is lost in nuclear excitation and undetected low-energy nuclear fragments. When a neutral pion is created in the hadronic cascade, the subsequent decay into two photons induces the development of an electromagnetic shower. The response of detectors to electromagnetic showers is different, as the fraction of detectable electromagnetic energy is larger, and this has an important effect on the stochastic component of the calorimeter energy resolution. For hadron calorimeters the A term in Eq. (5.3) ranges from 40% to 100% mainly depending on the equalization of the electromagnetic component. The main parameter regulating the hadronic shower is the nuclear interaction length (λ_I), which is the mean free path for an hadron before the first inelastic interaction; the probability that an inelastic interaction occurs after crossing a layer of thickness x is $(1 - e^{-\frac{x}{\lambda_I}})$. As an example, for lead one interaction length is about 17 cm, to be compared to 0.56 cm for one radiation length. The longitudinal depth of hadronic showers depends on the energy, E, of the

primary hadron and its proportional to $\ln E$; typically at least 7 interaction lengths are required for detectors relevant to this book. Hadron calorimeters are very massive objects weighting thousands of tons. At colliders iron is often used to incorporate the hadron calorimeter in the return yoke of the solenoid; the hadron calorimeter is external to the electromagnetic calorimeter and it acts also as a filter for muons. An important parameter of hadron calorimeters is hermeticity: as neutrinos can only be detected as missing energy or missing transverse energy (Chapter 9) it is important to cover as much as possible the solid angle with sensitive detectors, in order to limit the undetected energy of the event.

Particle identification

The combination of calorimeters and tracking devices provides important information on the identification of particles. As already mentioned calorimeters act as filters for muons since they are not destroyed by shower formation; muons are generally detected by dedicated muon chambers placed externally to the calorimeters. Electrons are characterized by electromagnetic showers matching, in position and energy, with charged tracks measured by tracking devices. Isolated electromagnetic showers, instead, are a signature for photons.

Pions and other charged hadrons are detected as tracks depositing a limited amount of their energy in the electromagnetic calorimeter, accompanyed by a shower in the hadron calorimeter. The identification of neutral hadrons is more complex. The detection of K_S^0's and Λ's takes place from their decay in a pair of charged particles forming a typical V-shaped displaced vertex in the tracking device. Only a fraction of K_S^0's and Λ's can be detected, the detection efficiency depends on the momentum and the geometry of the central tracker. Measurement of K_L^0's and neutrons, instead, involves searching for hadronic showers not associated to charged tracks. Their identification is complicated by the presence of other hadrons: the lateral extension of hadronic showers is considerably larger than the electromagnetic ones, and typically reaches tens of centimetres. It also depends on other factors as the calorimeter noise.

The classification of charged hadrons in pions, kaons and protons is highly valuable for the measurements described in Chapters 7 and 8. The separation of charged hadrons with momentum p in individual species requires the measurement of quantities related to β, the particle velocity. In addition to their main rôle, tracking devices can often measure the specific

energy loss by ionization, $\mathrm{d}E/\mathrm{d}x$. The $\mathrm{d}E/\mathrm{d}x$ is described by a universal function of β, the Bethe-Bloch formula. Specific ionization measurements allow statistical separation of pion to kaons at about 2 σ level, in the momentum range 2-20 GeV/c. The $\mathrm{d}E/\mathrm{d}x$ measurement is also interesting for low momentum electrons, typically up to a few GeV, as they can be easily separated from other charged particles because of their relativistic behaviour. A powerful technique to separate individual hadron species relies on the measurement of the Cherenkov-light emission-angle, θ_C, related to the velocity by the relation $\theta_C = \frac{1}{\beta n}$, where n is the refractive index of a transparent medium. This method allows a good statistical separation of $\pi/K/p$ up to a momentum of about 30 GeV/c, but the identification efficiency is sensitive to the Cherenkov-photon statistics and to various technical issues [13].

Forward detectors

The forward region is differently instrumented in e^+e^- and hadron colliders. In the first case precise forward calorimeters are employed to measure the luminosity from the Bhabha scattering rate (luminosity monitors, treated in Chapter 6). At hadron colliders forward calorimeters extend the coverage to the high pseudo-rapidity region. (The pseudorapidity is defined as $\eta = -\ln\tan(\frac{\theta}{2})$, where θ is the angle with respect to the beam line.) This region is usually populated by soft interactions or, in high-p_T interactions, by hadronization products of the spectator quarks (underlying event). The very forward region in hadron colliders is studied for diffractive physics, and can provide information on the instantaneous luminosity.

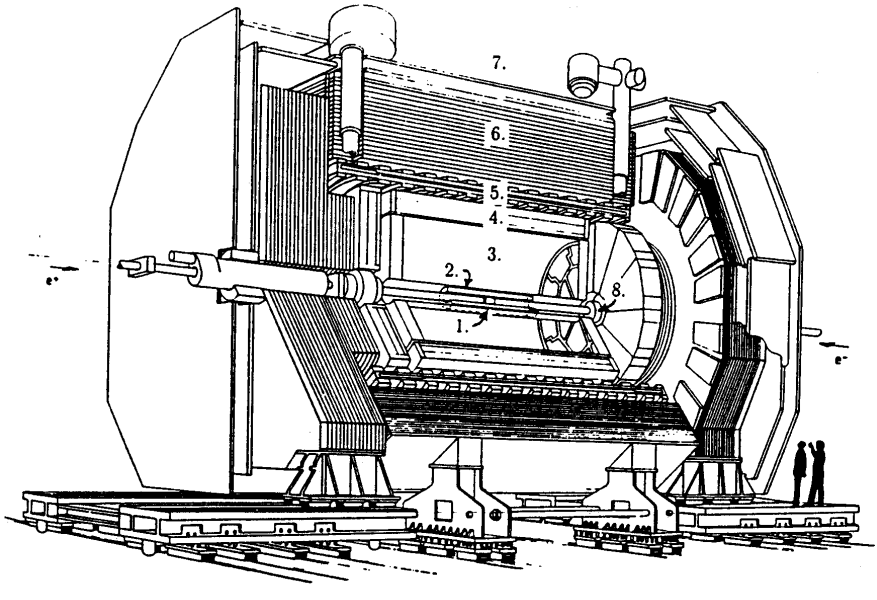

Fig. 5.5 Example of collider detector. Cut view of the LEP detector ALEPH with its main elements: (1) the silicon vertex detector; (2) the inner tracking chamber; (3) the time projection chamber; (4) the electromagnetic calorimeter; (5) the superconducting coil; (6) the hadron calorimeter; (7) the muon chambers; (8) the luminosity monitors.

This page intentionally left blank

Chapter 6

The Z Lineshape

The energy scan of the Z resonance provides two of the most important parameters of the Minimal Standard Model: the mass of the Z vector boson and its width. Experimentally, the cross sections at different e^+e^- center-of-mass energies around the Z peak are measured independently for hadronic and leptonic Z decays. The latter can be further separated in different lepton species, allowing the determination of four partial widths, one for Z decays to hadrons and three for Z decays to electron pairs, muon pairs and tau pairs, respectively.

In order to set the absolute scale of the scan a precise calibration of the center-of-mass energy at the collision points is required. At LEP this was done with a technique, called resonant depolarization, allowing a precision of the order of one part over one hundred thousand. As a consequence, the Z mass is one of the most precisely known physical quantities.

In this chapter we will describe the various ingredients of the measurement of the Z lineshape, i.e. the centre-of-mass dependence of the hadronic and leptonic cross sections. The important effects caused by initial state radiation will be addressed. The luminosity determination and the LEP energy calibration will be discussed. As we shall see the lineshape analysis provides also a precise measurement of the strong coupling constant and one of the most important measurements at LEP, the determination of the number of light neutrino species.

There will be no attempt to separate different flavours in hadronic Z decays, as quark flavour tagging allows to distinguish events in a statistical way only. These studies are left to the next Chapter.

6.1 Initial state radiation in e^+e^- collisions

The simple Breit–Wigner shape of the Z resonance is distorted by the radiation of photons by the electron and positron beams. The effect is sizeable: the production cross section at the peak is strongly reduced and the resonance shape becomes asymmetric, as a result of the shift in effective centre-of-mass energy. The main features of the treatment of initial state radiation (ISR) in colliding e^+e^- beams can be understood from the well known properties of bremsstrahlung in elastic electron scattering [64] . The two processes are related by crossing invariance: the emission of a photon for an e^+e^- process with cross section independent of the centre-of-mass energy can be directly related to the corresponding elastic scattering equations. In this case the tree level cross section, σ_0, is modified by radiation of one real photon by the factor

$$\delta = \frac{2\alpha}{\pi}(\ln\frac{s}{m_e^2} - 1)\int\frac{\delta\omega}{\omega} = \beta\int\frac{\delta\omega}{\omega} \tag{6.1}$$

where s is the transfer momentum of the process i.e. the square centre-of-mass energy for e^+e^- collisions. The first term comes from the angular integration over the photon emission angle and the second term represents the typical bremsstrahlung spectrum, for the emission of a photon of energy ω, affected by the infrared divergence. The divergence is related to the fact that the emission of a single real soft photon is unphysical [65] and an infinite number of photons should be considered.

Experimentally a minimum photon energy is required for detection, or for acceptance by the analysis cuts. By integrating between this minimum energy, ΔE , and the maximum possible energy, E, one gets

$$\delta = \beta\ln\frac{E}{\Delta E}\,. \tag{6.2}$$

In this scheme $\sigma = (1-\delta)\sigma_0$ is the cross section for the events where an ISR photon is not detected (or accepted by the analysis cuts). If the emission of ISR does not prevent the event to be accepted, $\Delta E = E$ and σ is unaffected.

The difficulty of summing an infinite number of photons is overcome by a procedure called exponentiation [66], where $\sigma = (1-\delta)\sigma_0$ is replaced by $\sigma = e^{-\delta}\sigma_0$, giving

$$\sigma = (\frac{\Delta E}{E})^{\beta}\sigma_0 \tag{6.3}$$

a relation that, as anticipated, is valid only if the tree level cross section does not vary with energy, which is not true for a resonance. The energy dependence can be introduced by generalizing Eq. (6.3) to [67]

$$\sigma = \beta \int_0^{\Delta E} \frac{d\omega}{\omega} (\frac{\omega}{E})^{\beta} \sigma_0(E-\omega)\,. \tag{6.4}$$

The integral can be carried out by taking a Breit-Wigner shape for the resonance of mass m_Z and width Γ_Z. By assuming $\Delta E > \Gamma_Z$ the integral yields

$$\begin{aligned}\sigma(s) = &(\frac{(\sqrt{s}-m_Z)^2+(\Gamma_Z/2)^2}{m_Z^2/4})^{\beta/2} \\ &\times (1+2\beta\frac{\sqrt{s}-m_Z}{\Gamma_Z}(\frac{\pi}{2}+\arctan(\frac{\sqrt{s}-m_Z}{\Gamma_Z/2})))\,\sigma_0(s)\,.\end{aligned} \tag{6.5}$$

One can observe that the result does not depend upon ΔE : the width of the resonance acts as a natural cutoff and the emission of photons with $\Delta E > \Gamma_Z$ is suppressed. The second term in Eq. (6.5) shows that the radiative corrections induce an asymmetry in the shape of the resonance.

A complete calculation requires the addition of virtual and soft corrections independent of the infrared singularity. For example at $\mathcal{O}(\alpha)$ [68] the corrected cross section is increased by

$$\delta_1 = \frac{13}{12}\beta + \frac{\alpha}{\pi}(\frac{\pi^2}{3}-\frac{17}{18})\,. \tag{6.6}$$

At the Z pole $\beta \sim 0.11$ and $\delta_1 \sim 10\%$ yielding a reduction of 75% of the peak cross section. The correction at the resonance is large because of the suppression of hard photon emission leaving the colliding e^+e^- system with not enough energy to produce a Z.

For the LEP analysis of the Z lineshape the treatment of initial state radiation has been improved by computing $\mathcal{O}\left(\alpha^2\right)$ [69] radiative corrections complemented by soft photon corrections to all orders in exponentiated form [71]. Figure 6.1 shows the theoretical prediction for the Z lineshape through successive approximations.

6.2 The reduced cross sections

For the extraction of the Z parameters it is useful to employ cross sections which are already corrected for the effect of initial state radiation. This can

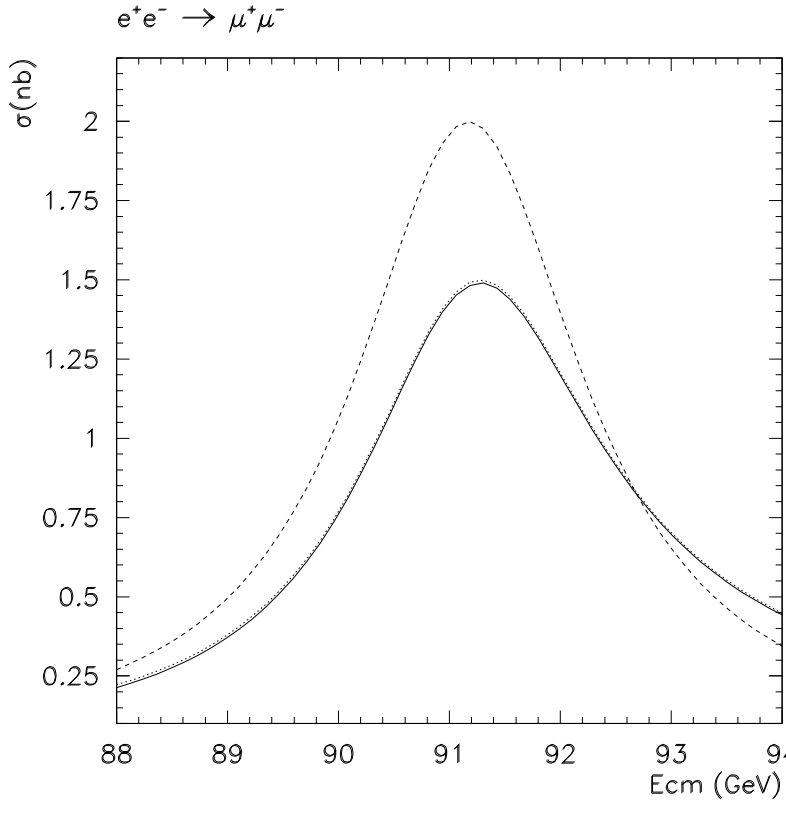

Fig. 6.1 Effect of QED initial state radiative corrections on the muon-pair production cross section near the Z pole. Cross section without initial state radiation (dashed line), $\mathcal{O}(\alpha)$ exponentiated initial state radiation (dotted line), $\mathcal{O}(\alpha^2)$ exponentiated initial state radiation (solid line).

be accomplished by fitting the measured cross sections using a formula that convolutes a reduced cross section $\hat{\sigma}$, with a radiator function $H(s, s')$:

$$\sigma_{f\bar{f}}(s) = \int_{4m_f^2}^{s} ds' H(s, s') \hat{\sigma}_{f\bar{f}}(s') \ . \tag{6.7}$$

The radiator function, peaking at $s' = s$ and with a long tail toward lower values of s' [70], incorporates all QED radiative effects described in the previous Section.

The $\hat{\sigma}$ reduced cross section

$$\hat{\sigma}_{f\bar{f}}(s) = \sigma_{f\bar{f}}^{peak} \cdot \frac{s\Gamma_Z^2}{\left(s - m_Z^2\right)^2 + \left(\frac{s\Gamma_Z}{m_Z}\right)^2} \; + \text{“}(\gamma - Z)\text{”} + \text{“}|\gamma|^2\text{”} \qquad (6.8)$$

is composed by three terms. The first represents the Z exchange; the width of the relativistic Breit-Wigner distribution is energy-dependent to take into account, in an approximate way, the dependence of the Z self-energy (Eq. (3.235), (3.236)) near the resonance [72]. With respect to the usual relativistic Breit-Wigner formula, where the second term in the denominator is given by $m_Z^2\Gamma_Z^2$, this ansatz gives a 34 MeV higher Z mass. The second term, $|\gamma|^2$, corresponds to the photon exchange and is only a few percent of the Z term. It can reliably be predicted by QED. The interference term $(\gamma - Z)$ is the smallest one and is zero when $s = m_Z^2$. It can either be fixed to the Standard Model prediction or fitted by using data far from the resonance, where the sensitivity to the $\gamma - Z$ interference is much higher. Particular care has to be taken in defining the reduced cross section for Bhabha scattering, $f = e$, because the t-channel photon- and Z-exchange diagrams have to be taken into account.

The peak cross section depends on the Z mass and width, on the Z partial width to the initial state, Γ_e, and the Z partial width to final fermions, Γ_f. It can be written as (Eq. (3.231)):

$$\sigma_{f\bar{f}}^{peak} = \sigma_{f\bar{f}}^{0}\left(\frac{1}{1+\delta_{QED}}\right) = \frac{12\pi}{m_Z^2} \cdot \frac{\Gamma_e\Gamma_f}{\Gamma_Z^2} \cdot \frac{1}{1+\frac{3\alpha}{4\pi}} \; . \qquad (6.9)$$

where Γ_f represents the physical partial width of $Z \to f\bar{f}$ and includes by definition all radiative corrections. The convolution with the radiator function in Eq. (6.7), however, takes already into account the initial state radiation; in order to have a consistent definition for Γ_e and Γ_f the QED final state radiative corrections δ_{QED} is removed in (6.9) from the initial state width Γ_e.

6.3 Luminosity

The precision measurement of the cross section, σ_i , of a given process i requires the precise determination of the collider luminosity. Indeed a cross section is measured through the relation

$$\sigma_i = \frac{N_i - N_{bk}^i}{\epsilon_i L} \; . \qquad (6.10)$$

where N_i is the number of selected events of type i corrected for the contribution of background events N_{bk}^i and ϵ_i is the selection efficiency. The integrated luminosity L is required for the normalization.

The instantaneous luminosity of two colliding e^+e^- beams of horizontal dimension σ_x and vertical dimension σ_y can be written as

$$L = \frac{N_{b+}N_{b-}f_{rev}k_b\xi}{\sigma_x\sigma_y} \tag{6.11}$$

where N_{b+} and N_{b-} are the number of electrons and positrons per bunch, k_b the number of bunches per beam, f_{rev} the revolution frequency. The ξ factor represents many systematic effects, due for instance to the offset between the two beams, the beam dispersion, etc. To give an example at LEP, with $\sigma_x = 100\mu m$, $\sigma_y = 10\mu m$, $k_b = 4$, $f_{rev} = 11245.5Hz$, $N_{b-} = N_{b+} = 3.10^{12}$, instantaneous luminosities up to $10^{32}cm^{-2}s^{-1}$ were achieved.

The above relation can be used only for a rough evaluation of the integrated luminosity, because of the many systematic uncertainties. In practice the only way to measure precisely the luminosity of a collider is by using Eq. (6.10) with a process of known cross section.

At an e^+e^- collider the Bhabha scattering process $e^+e^- \to e^+e^-$ is chosen because the cross section is large and is dominated by t-channel photon exchange, a well understood QED process. To obtain a precise measurement of the luminosity, the background, N_{bk}^i, has to be small and well known, the efficiency, ϵ_i, has to be high and under control, and the cross section should be computed precisely from the theory.

At small scattering angle, θ , the Bhabha cross section is given, at lowest order QED, by the Rutherford formula:

$$\frac{d\sigma_{bh}^{th}}{d\Omega} = \frac{16\alpha^2}{s}\left(\frac{1}{\theta^4}\right) ,$$

which integrated over the acceptance gives

$$\sigma_{bh}^{th} \sim \frac{16\pi\alpha^2}{s}\left(\frac{1}{\theta_{min}^2} - \frac{1}{\theta_{max}^2}\right) ,$$

where θ_{min} and θ_{max} are the polar angles defining the inner and outer acceptance, respectively, of the detector dedicated to the measurement of luminosity.

Typical luminosity detectors for experiments at e^+e^- colliders consist of two cylindrical calorimeters located at low angles at both sides of the

interaction point. A tracking device in front can help in the position measurement. If this is not available, fine granularity in the calorimeter is mandatory.

To compute the expected cross section (σ^{th}) precisely, the position R_{min} of the inner edge of the detector with respect to the beam needs to be known. Since $\theta_{min} \sim \frac{R_{min}}{z}$, where z is the distance of the detector from the interaction point, one has

$$\frac{\Delta\sigma}{\sigma} \simeq 2\frac{\Delta\theta_{min}}{\theta_{min}} \simeq 2(\frac{\Delta R_{min}}{R_{min}} \oplus \frac{\Delta z}{z}) \; . \tag{6.12}$$

At LEP excellent mechanical precision of the order of 20 microns was achieved in controlling the position of the inner edge of the detectors. For typical values of R_{min} around 60 mm these 20 microns correspond to an uncertainty in the luminosity $\Delta L/L \simeq 2\Delta R_{min}/R_{min} \simeq 7 \cdot 10^{-4}$. A much lower precision, $\Delta z \sim$ 1mm, was required for the knowledge of the position with respect to the interaction point, as the luminosity detectors were placed at few meters with respect to it.

The precise measurement of θ requires both the detector position and the position of the luminous region to be well understood. The luminosity is measured by requiring two coincident signals from the two detectors, placed symmetrically with respect to the interaction point. In this case, for cylindrical detectors, a common radial displacement, ΔR, of the inner and outer limits of the detectors (or of the beam itself) results in a reduction of the acceptance (and, hence, of the measured luminosity) by

$$\frac{\Delta\sigma}{\sigma} \propto \frac{2\Delta R}{R_{min}} \left(\frac{1 + R_{min}^3/R_{max}^3}{1 - R_{min}^2/R_{max}^2} \right) \; .$$

An appropriate choice of the event selection cuts can largely remove the dependence of the luminosity on the relative position between the beams interaction point and the detector, as proposed in [73]. If two different fiducial regions are defined for the two luminosity detectors positioned at the left and right sides with respect to the interaction point, the luminosity measurement can be made independent of transverse misalignments. One can show that this can be achieved if the difference in size between the "loose" fiducial region and the "tight" fiducial region is at least bigger than twice the maximum expected misalignment. The dependence on longitudinal misalignments is also largely canceled if the definition of loose and tight is changed from one side to the other side randomly on an event by event basis. In order to have a reduced dependence on the detector simulation the precise radial acceptance is normally defined by studying the energy

asymmetry across calorimeter pad boundaries, or by taking advantage of a tracker device positioned in front of a luminosity calorimeter.

Random coincidences of off-momentum beam particles can simulate a Bhabha scattering signal. The rate of this kind of background can be measured directly from the data using samples obtained through events triggering only one of the two luminosity detectors, and studying acoplanar coincidences. Backgrounds due to physical processes are small and below the permil level at $\sqrt{(}s) \approx m_Z$. Their contribution to the systematic error is very small. The overall experimental error obtained at LEP was between 0.07% and 0.1% , depending on the experiment. The tolerances in the mechanical structure was the cause of the largest uncertainty. Since the geometrical uncertainties are not correlated among experiments, the combined LEP experimental error was close to 0.05%.

A calculation of the theoretical cross section at the permil level is required to take advantage of the high experimental accuracy. Such a calculation implies a careful treatment of radiative corrections. Since photon radiation is collinear with the outgoing electrons and positrons, the electromagnetic showers originating from bremsstrahlung are superimposed to the electron (or positron) shower in the luminosity calorimeter. This and other acceptance effects have to be taken into account in the computation of the theoretical cross section. An uncertainty of 0.11% is estimated for the overall precision of the Bhabha cross section calculation [74]. The main component comes from missing sub-leading $\mathcal{O}(\alpha^2 L)$ corrections, where $L = \log(-t/m_e^2)$.

6.4 Centre-of-mass energy calibration in e^+e^- collisions

A precise measurement of the average center-of-mass energy at the collision points is required for three important electroweak parameters: the mass and width of the Z boson, discussed in this chapter, and the W mass, as measured in e^+e^- collisions, that will be discussed later.

The average energies of the electrons (positrons) going around the collider (E_{beam}) is given by:

$$\langle \mathrm{E}_{beam} \rangle = \frac{e}{2\pi} \oint \mathrm{B}\ \mathrm{dl},$$

where B is the vertical magnetic field sampled by the beam, of electric charge e, on its orbit. Therefore a precise knowledge of the sampled magnetic field is required for an accurate measurement of the centre-of-mass

energy. At LEP each magnet was equipped with one-turn induction coil, forming a closed electrical loop threading all the dipoles in one octant of the accelerator. The magnetic field could be measured by applying a current cycle (including a variation of the current sign) and integrating the induced voltage in the flux loop. A reference magnet powered in series with the accelerator dipoles was used for frequent monitoring, by using a rotating coil. The flux loop measurements were checked by filling the machine with protons. Protons, in contrast to electrons, are not ultra-relativistic and their velocity could be measured by the frequency of the RF acceleration voltage, determining the momentum of positrons on the same orbit. These methods allowed a relative energy error of about $3 \cdot 10^{-4}$.

An order of magnitude could be gained thanks to a method called resonant depolarization. The technique relies on the precession of the spin of the electrons about the vertical bending field. The precession follows the Thomas-BMT equation [75] :

$$\begin{aligned} \frac{d\vec{S}}{dt} &= \vec{\Omega} \times \vec{S} \\ \vec{\Omega} &= -\frac{e}{\gamma m_e}(1 + a\gamma)\vec{B} \end{aligned} \tag{6.13}$$

where the B field has been assumed to be transverse to the particle velocity; e is the electron charge, m_e is its mass, a the magnetic moment anomaly and γ the Lorentz factor. In an e^+e^- collider the average polarization can be different from zero because the emission of synchrotron radiation polarizes the beam in the vertical transverse direction (Sokolov-Ternov effect [76]). The amount of polarization depends on the bending radius of the accelerator, on the beam energy and on several depolarizing effects. At LEP a 10% vertical polarization was achieved when the beams were not colliding after compensation of the magnetic fields of the solenoids and accurate steering of the orbit in the vertical plane. The degree of polarization of a beam can be measured with a laser by switching the polarization of the laser light. Indeed the differential Compton scattering cross section depends on the initial polarization of electrons and photons. The change in rate of back-scattered photons when the circular polarization of the laser light is switched from left to right measures the electron beam polarization (Compton polarimetry). The Compton polarimeter used at LEP had a precision of about 2%.

The component of the spin vector parallel to the B field is conserved, as can be seen from Eq. (6.13), therefore a vertical polarization is maintained,

if no perturbation occurs. If an additional B field, directed along the radius of the ring, is applied at a point along the orbit, the vertical spin vector gets kicked toward the horizontal direction and start precessing $a_e\gamma$ times during one turn around the ring. If the additional radial B is made oscillating with a frequency in phase with the precession, the electron spin can be rotated to the horizontal plane after a number of turns. This is called resonance condition (see Fig. 6.2). Because of stochastic synchrotron radiation horizontal polarization is unstable in e^+e^- colliders and its quickly destroyed, i.e. the beam is *depolarized* by the resonance condition.

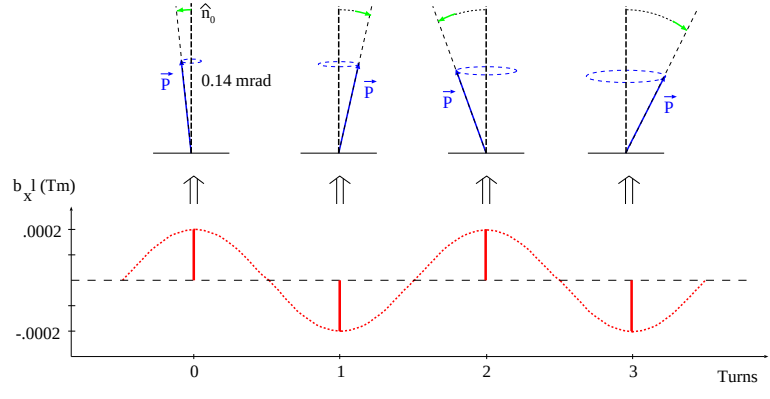

Fig. 6.2 Resonance condition between the nominal spin precession with $[\nu] = 0.5$ and the radial perturbation $\int b_x l$ from the RF-magnet. In an ideal storage ring the polarization vector is initially along the vertical direction. After being tilted $\vec{P}$ precesses with ν about its direction. If the perturbation is in phase with the nominal spin precession (in this example $f_{dep} = 0.5 \times f_{rev}$) the polarization vector is resonantly rotated away from the vertical direction. (From Ref. [78].)

The $a_e\gamma$ term is call *spin tune* and the time-averaged spin tune, ν_0, of each electron is proportional to the average beam energy, E_{beam}:

$$\nu_0 = a_e\gamma = \frac{a_e E}{m_e c^2} = \frac{\mathrm{E}_{\mathrm{beam}}}{440.6486(1)[\mathrm{MeV}]},$$

where m_e is the mass of the electron and c is the speed of light.

At LEP the resonance condition was induced by a radial oscillating field from a coil. About 10^4 turns ($\approx$ 1 second) were needed to bring the polarization vector into the radial plane. The resonance condition between the perturbing radial field and the nominal spin precession is $f_{\mathrm{dep}} = [\nu] \cdot f_{\mathrm{rev}}$, where f_{dep} is the frequency of the oscillating field, f_{rev} is the revolution

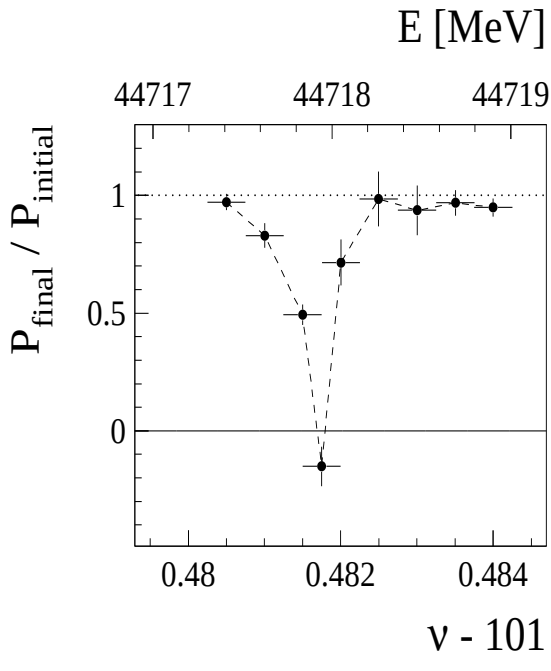

Fig. 6.3 Width of the depolarizing resonance excited for energy calibration at LEP.

frequency of the particles, which is precisely known, and $[\nu]$ denotes the non-integer part of the spin tune. Its integer part is known accurately enough from the setting of the bending field. The depolarization occurred slowly compared to the revolution period and each electron sampled the whole energy distribution during the process. For this reason the depolarizing resonance was very narrow, about 0.1 MeV, and E_{beam} could be determined with a precision of ~ 200 KeV, as can be seen from Fig. 6.3.

The spurious effects that can induce systematic errors have been studied theoretically and experimental bounds on the magnitude of each effect have been established in dedicated experiments concluding that the upper bound on the systematic error on a single measurement of E_{beam} was 1.1 MeV. The largest contribution to this error was due to the radial magnetic fields sampled by the beam inside the quadrupoles and is not correlated between two measurements done after different optimization of the machine.

The average beam energy could not be measured continuously since in standard LEP running conditions the beams were not polarized. Indeed

Table 6.1 Size (Δ) and error (σ) of the effects changing the LEP center-of-mass energy as a function of time, separated in three categories : (i) effects changing the dipole field; (ii) effects changing the vertical quadrupole field sampled by the orbit; (iii) effects changing the energy at the interaction point.

Effect	Δ	σ
Temperature variations	~ 3 MeV	0.3 MeV
Rise per fill	~ 3 MeV	1.0 MeV
Horizontal correctors setting	~ 1 MeV	0.4 MeV
Earth Tides (daily)	~ 10 MeV	0.1 MeV
Geological shifts (weeks)	~ 10 MeV	0.3 MeV
RF corrections	~ 10 MeV	0.5 MeV
Vertical collision offsets	< 1 MeV	0.3 MeV

the beam-beam interaction prevented the building up of the polarization. Several quantities had to be monitored, such as currents in the magnets, temperatures, measurement of magnetic fields, status of RF units, in order to follow the evolution of the energy as a function of time. The main effects are summarized in Table 6.1.

The magnetic field of the dipoles was monitored measuring the field of few dipoles instrumented with a NMR. This allowed to discover an unexpected rise of the dipole magnetic field during fills, correlated to vagabond currents that flow along the beam pipe mainly due to return currents of electrical trains that do not go back to the power supply along the railtracks.

Another important effect was related to the tides of Lake Geneva and even the earth tides ! Indeed while earth was deformed by the gravitational forces between earth and sun, the LEP diameter changed by a few mm with a period of 12 hours. Since the length of the LEP orbit was constrained by the synchronisation of radio-frequency (RF) the diameter variation was effectively pushing the electrons and positrons off-center in the quadrupoles where they received an extra deflection. A variation of 13μm of the average relative position of the beam with respect to the center of the quadrupole magnets induced a change of E_{beam} of about 1 MeV. The effect was monitored by measuring the variation of the position of the beams with respect to the center of the quadrupoles using the beam position pickups.

A further correction was related to the beam dispersion. The energy distribution of the particles in each bunch, at LEP was almost gaussian with a spread (rms) of about 40 MeV at $\sqrt{s} \simeq m_Z$. The average center-of-mass energy E_{cm} is, to first approximation, the sum of the average beam energies at the interaction point. A correlation between the transverse position of

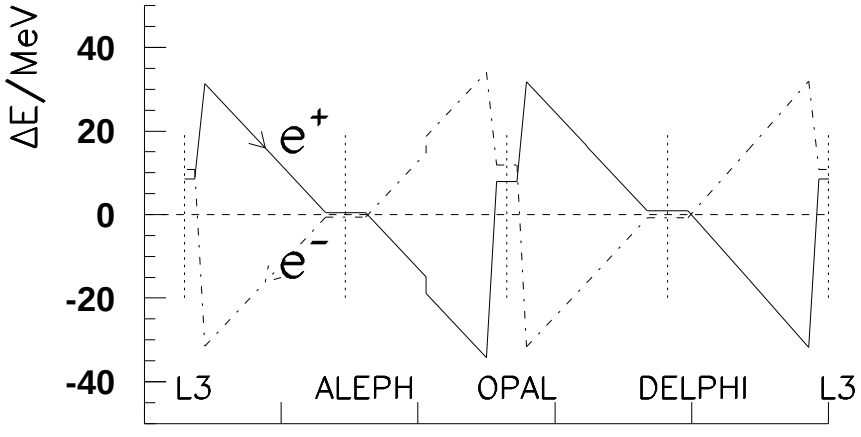

Fig. 6.4 Deviation from the beam mean energy in the LEP arcs.

the particles in the bunch and their energy (dispersion) may induce a shift in E_{cm}. This correction is proportional to the offset of the centers of the two bunches at collision point and to the difference between their dispersions.

It has to be mentioned that the mean beam energy is not constant as it goes around the ring. At LEP for a 45 GeV beam the energy loss due to synchrotron radiation in the arcs is about 125 MeV per turn. This energy loss was compensated by the RF cavities placed symmetrically on either side of L3 and OPAL interaction points (see Fig. 6.4).

Since the RF stations were symmetrically placed the average beam energy at the interaction points was close to E_{beam}. Deviations occurred if the accelerating fields seen by the beam at the four RF stations were not equal or because of misalignment errors of the RF stations with the interaction points. The alignment was carefully measured and the operating status of the RF well monitored, implying a precision on these corrections of a fraction of MeV.

In conclusion, after all the above mentioned effects were taken into account, the final LEP luminosity-weighted centre of mass energies for the running at the Z pole were known with the amazing precision of two parts in 10^5 at each collision point, allowing uncertainties on m_Z and Γ_Z of about 1.5 MeV [77, 78].

6.5 Selection of hadronic and leptonic Z decays

At e^+e^- centre-of-mass energies around m_Z the production rate of Z bosons is two order of magnitudes larger than other processes, within typical experimental acceptance. The most important background comes from the interaction of two photons of low virtuality radiated from the colliding beams. Such a background typically consists of low multiplicity events, with a total visible energy much lower than $\sqrt(s)$ and can be easily distinguished from the Z decays.

Most of Z decays consist in multihadronic events, produced by the fragmentation of $q\bar{q}$ pairs. They account for about 70% of the total cross section and carry most of the weight in the lineshape analysis. As can be seen in Fig. 6.5, where the sum of charged track momenta versus the charged track multiplicity is shown, they show a large visible energy and multiplicity in contrast to the two-photon background. They can also be easily separated from the very low multiplicity leptonic Z decays. The typical efficiency of selection cuts, based on the analysis of charged tracks, is greater than 97% for multihadronic Z decays, with a contamination of two-photon events and leptonic (mostly tau-pair) events of less than 1%. The efficiency can be increased to values larger that 99% if the information coming from calorimeters is added. The main cause of inefficiencies is due to low-multiplicity hadronic decays going down the beam pipe. At LEP each experiment accumulated about four million hadronic Z decays, corresponding to a statistical error below 0.1% on the hadronic cross section. The most important systematic error is related to the understanding of the two-photon background. Since the latter is not resonating it can be studied by varying the selection criteria and measuring the effect of the variation at different centre-of-mass energies.

Only about 10% of Z bosons decay to charged lepton pairs. However, these events have very distinctive signatures, such as low multiplicity accompanied by large visible energy. The three classes (electron, muon and tau pairs) can be separated by identifying the energy deposits in the electromagnetic calorimeter (electrons) and by their penetration through the iron of hadron calorimeters (muons). The identification efficiency for electron and muon pair is typically larger than 95%. Tau pair events feature two neutrinos (ν_τ) produced in the decays of the two tau leptons. The two ν_τ's are emitted essentially in opposite directions; this signature can be exploited by requiring events with large missing mass. Typical identification efficiencies for tau pairs are around 85%. Another source of inefficiency

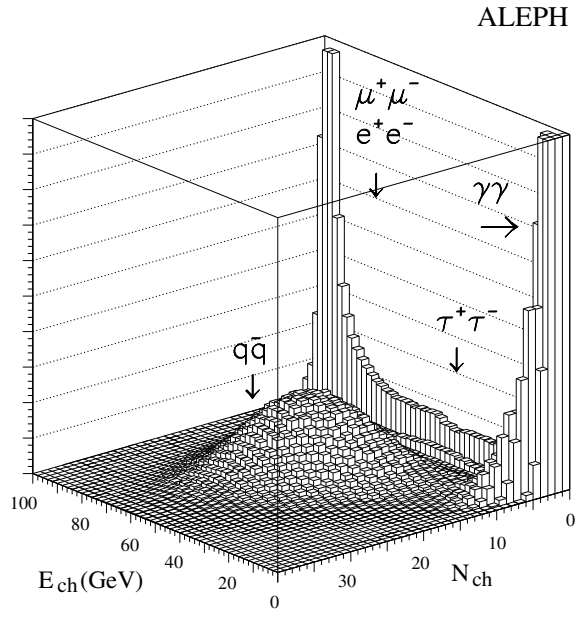

Fig. 6.5 The sum of charged track momenta versus the track multiplicity, for various final states at centre-of-mass energies around the Z peak.

is due to the geometrical acceptance, defined by a cut on the production angle of the scattered lepton (θ), measured with respect to the direction of the electron beam. The cut on $|\cos\theta|$ ranges from 0.8 to 0.95, depending on the experiment. For $e^+e^- \to e^+e^-$ scattering it is useful to define an asymmetric acceptance cut in order to reduce the effect of the t-channel contribution that is particularly important for low values of θ. Indeed this contribution has to be subtracted in order to extract the Z parameters; the uncertainty on the subtraction is an important source of systematic error. At LEP the $e^+e^- \to e^+e^-$ scattering cross section is measured for $\cos\theta < 0.7$. The two photon contamination is small and is essentially affecting only the tau pair channel (about 2%). The cross contamination among different lepton classes has to be taken into account when measuring the individual cross sections; if lepton universality is assumed this source of systematic uncertainty can be avoided by designing a common lepton selection. At LEP each experiment collected about half million Z decays into charged leptons.

6.6 Measuring the Z lineshape parameters

In order to optimize sensitivity in the determination of the peak position and the width of a resonance, data have to be collected on both peak sides, where the cross section is approximatively at half maximum. At LEP most of the integrated luminosity was collected at three scan points, namely at peak and at the two sides, separated by about 1.8 GeV. The errors on the Z mass and width depend on the measurement of the cross sections at the two off-peak points. The statistical error on the cross section can be made small by collecting enough integrated luminosity; in this condition the errors on the two parameters are dominated by the knowledge of E_{-2} and E_{+2} , the luminosity-weighted center-of-mass energies at the two off-peak points. One can write

$$\Delta m_Z \approx 0.5\Delta(\mathrm{E}_{+2} + \mathrm{E}_{-2}) \tag{6.14}$$

$$\Delta\Gamma_Z \approx \frac{\Gamma_Z}{(\mathrm{E}_{+2} - \mathrm{E}_{-2})}\Delta(\mathrm{E}_{+2} - \mathrm{E}_{-2}) = 0.71\Delta(\mathrm{E}_{+2} - \mathrm{E}_{-2}) \tag{6.15}$$

showing that the error on the mass depends on the error on the sum and the error on the width depends on the error of the difference of centre-of-mass energies. As discussed in Section 6.4 the energy of the accelerator was measured at LEP with the amazing precision of 2×10^{-5} , yielding an error of 1.5 MeV on the Z mass. This error is given by the correlated centre-of-mass energy error between the two off-peak points added in quadrature to $\frac{1}{\sqrt{2}}$ of their uncorrelated error. When the statistical error on the cross sections is included a total error of 2 MeV on the Z mass is obtained. As far as the width is concerned only the uncorrelated errors in E_+ and E_- contribute, yielding again an error of 1.5 MeV. The width is also affected by the centre-of-mass energy spread ($\epsilon_{CMS} \sim 56$ MeV) that modifies the cross-section by

$$\delta\sigma \simeq -0.5\frac{d^2\sigma}{dE^2}\epsilon^2_{CMS}\,. \tag{6.16}$$

The energy spread causes an apparent reduction of the cross section of 1.1 permil at $\sqrt{s} = m_Z$ and an apparent increase of 0.5 permil at ± 2 GeV from the Z peak, increasing the apparent Z width by about 4 MeV. This correction is determined with a precision of 2.5% from the machine optics, giving a negligible systematic error. A total error of 2.5 MeV on the Z

Table 6.2 Average line shape parameters from the results of the four LEP experiments assuming lepton universality. The values of R_e, R_μ, R_τ are also indicated.

Parameter	Average Value
m_Z(GeV)	91.1875±0.0021
Γ_Z(GeV)	2.4952±0.0023
σ^0_{had}(nb)	41.540±0.037
R_ℓ	20.767±0.025
R_e	20.804±0.050
R_μ	20.785±0.033
R_τ	20.764±0.045

width is obtained when the statistical error and the uncertainty on the background from non-resonating processes are taken into account.

As described in the previous Section the cross sections are measured separately for the Z decay to hadrons and to the three lepton species. The reduced cross sections are then extracted from the data by applying the formalism described in Section 6.2. The experimentally-measured reduced cross sections are compared to Eqs. (6.8), (6.9) and the lineshape parameters are determined in a global fit to the data. Because of the larger statistics the hadronic decays are dominating the measurements of the mass and the width. In the global fit the decays into charged lepton pairs are incorporated either by introducing in the reduced cross sections the three leptonic partial widths (Γ_e, Γ_μ and Γ_τ) or by assuming lepton universality. This assumption implies three equal leptonic widths, after small corrections for mass effects. With the current experimental precision, only the correction for the tau is non-negligible (0.23%). When lepton universality is assumed, a common leptonic width, Γ_ℓ , is determined, corresponding to the width of any single flavour as if it were massless. In this case four parameters are needed to describe the centre-of-mass dependence of the hadronic and leptonic cross sections. The set of parameters chosen for the LEP measurements are the Z mass (m_Z), the Z width (Γ_Z), the ratio of hadronic to leptonic partial width $R_\ell = \Gamma_h/\Gamma_\ell$ and the hadronic peak cross section σ^0_h. The choice of these parameters is motivated by their small correlations. If lepton universality is not assumed, R_ℓ is replaced by three analogous quantities, R_e, R_μ, R_τ.

The result of the four-parameter fit to the Z lineshape is given in table 6.2. The values of R_e, R_μ and R_τ from the six-parameter fit, are also

shown, demonstrating that the lineshape analysis does not unveil violation of lepton universality. As can be seen in Figs. 6.6 and 6.7 [1], the Z width is sensitive to the values of the top and Higgs masses, while R_ℓ, being a ratio of widths, is essentially independent of these parameters. Indeed for R_ℓ, the dependence on the top and Higgs masses originating from self-energy effects cancels, leaving a small residual dependence coming from the non-universal final state vertex correction (the same feature is discussed in Subsection 4.1.3 for the R_b case). Because of its dependence on the strong coupling constant, R_ℓ is an excellent variable for determining $\alpha_s(m_Z^2)$ by assuming the validity of the electroweak theory to compute the ratio of couplings of quarks and leptons to the Z. Using the measured value of R_ℓ one obtains:

$$\alpha_s(m_Z^2) = 0.122 \pm 0.004$$

where the formulas relating R_ℓ with the QCD prediction [79], known to $\mathcal{O}(\alpha_s^3)$, have been used. The residual dependence on the Higgs mass, calculated by varying M_{Higgs} from 114 GeV to 1 TeV accounts for 0.002 on the error on $\alpha_s(m_Z^2)$.

The measurement by the four LEP collaborations of the hadronic cross section as a function of the centre-of-mass energy is shown in Fig. 6.8. Decays of the Z bosons to neutrino pairs accounts for about 20% of the total decays, if three species (families) of light neutrino (i.e. much lighter than $\frac{m_Z}{2}$) are assumed. Within the Standard Model the ratio of the partial Z decay width to a neutrino species (Γ_ν) over the partial decay width to a lepton species (Γ_ℓ) is $\Gamma_\nu/\Gamma_\ell = 1.991 \pm 0.001$. The small error in the prediction for this ratio results from the large cancellations of the top and Higgs mass dependences. As can be seen in Fig. 6.8 the hadronic cross section at peak is strongly dependent on the number of light neutrino families. Additional families yield a reduction of the peak cross section and an increase of the total width of the resonance. On the other hand the dependence of the hadronic peak cross section on other parameters, such as the top mass, the Higgs mass or the strong-coupling constant is very small. The hadronic peak cross section is an ideal variable to measure possible Z decays to additional invisible modes or to probe deviations from the Standard Model without the uncertainty related to the lack of knowledge in some of its parameters. For example, a hypothetical extra heavy neutral boson, Z', mixing to the Z would modify the expected cross section at peak. The main contribution to the error on the hadronic cross section

[1] Similar figures for other observables can be found in Ref. [80].

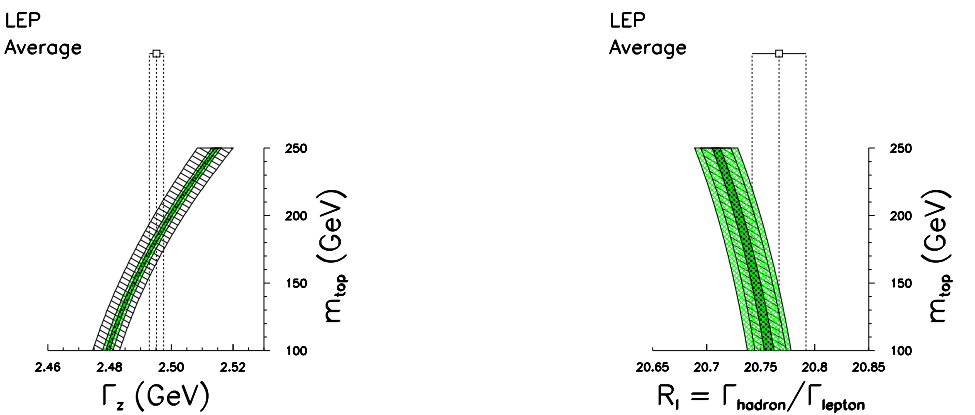

Fig. 6.6 Dependence on the top mass of the prediction on Γ_Z (left) and R_ℓ (right). The hatched bands shows the uncertainty on the prediction when varying other input parameters. These are the Higgs mass, the strong coupling constant and the fine structure constant at the m_Z scale, respectively. The Higgs mass is varied in the range [114-1000 GeV]. The strong couplings constant is varied by 3% and $\alpha(m_Z^2)$ by $7 \cdot 10^{-4}$ (this value is for illustration only). The experimental measurements of Γ_Z and R_ℓ are indicated by the error bar.

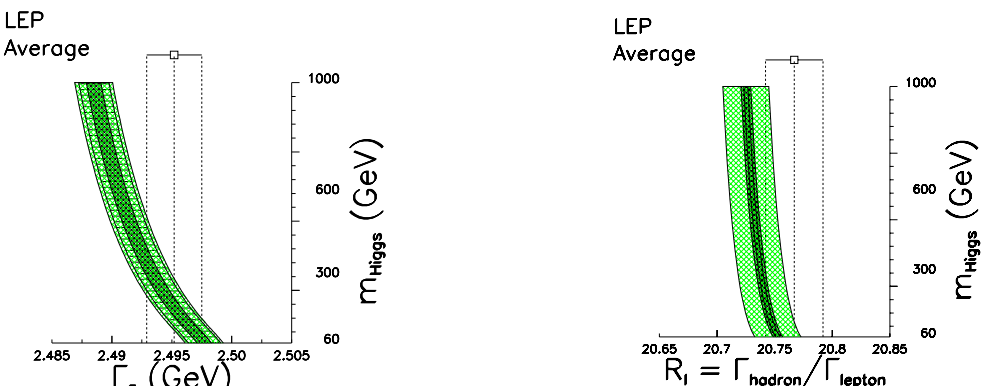

Fig. 6.7 Dependence on the Higgs mass of the prediction on Γ_Z (left) and R_ℓ (right). The hatched bands shows the uncertainty on the prediction when varying other input parameters. These are the top mass, the strong coupling constant and the fine structure constant at the m_Z scale, respectively. The top mass is varied in the range [170-180 GeV], for illustration only. The strong couplings constant is varied by 3% and $\alpha(m_Z^2)$ by $7 \cdot 10^{-4}$ (this value is for illustration only). The experimental measurements of Γ_Z and R_ℓ are indicated by the error bar.

at peak is given by the theoretical error on the small-angle Bhabha cross section used for the luminosity calculation (Section 6.3).

The width of the Z to invisible states , Γ_{inv}, can be written as

$$\Gamma_{inv} = \Gamma_Z - \Gamma_h - 3\Gamma_\ell .$$

The number of light neutrino families N_ν can be obtained from the ratio of the invisible width to the leptonic width, assuming that the invisible width is only due to neutrino final states:

$$\frac{\Gamma_{inv}}{\Gamma_\ell} = \frac{\Gamma_Z}{\Gamma_\ell} - \mathrm{R}_\ell - 3 = (\frac{12\pi \mathrm{R}_\ell}{\sigma^0_{had} m_Z^2})^{1/2} - \mathrm{R}_\ell - 3 = N_\nu \cdot \frac{\Gamma_\nu}{\Gamma_\ell} \qquad (6.17)$$

where the dependence on σ^0_{had} has been made explicit. Using the Standard Model prediction for Γ_ν/Γ_ℓ the result is

$$N_\nu = 2.984 \pm 0.008$$

in agreement (within 2 σ !) with the existence of 3 light neutrino families. The number of light neutrino generations can be measured also from the rate of single photon events above the Z peak. These events, showing only a photon of energy

$$E_\gamma = \frac{s - m_Z^2}{2\sqrt{(}s)}$$

in the apparatus, originate from the initial state radiation process $e^+e^- \rightarrow \gamma\nu\bar{\nu}$ and their rate is proportional to the number of families. The result obtained with this process [81] is in agreement with the lineshape analysis, but its precision is one order of magnitude worst.

In conclusion from the analysis of the lineshape the following fundamental results are obtained:

- a precise measurement of the Z mass, a physical constant known with the precision of 2×10^{-5} ,
- a measurement of Γ_Z , an observable sensitive to the top and Higgs mass through one loop radiative corrections ,
- a measurement of the strong coupling constant with little theoretical dependence, from the ratio between the hadronic to leptonic widths, R_ℓ ,
- the determination of the number of light neutrino families.

The study of observables sensitive to the top and Higgs mass through loops continues in the next Chapters, with the measurement of the decay width of the Z to $b\bar{b}$ pairs, the measurement of the electroweak mixing angle ($\sin^2\theta_W$), and the measurement of the mass of the W boson.

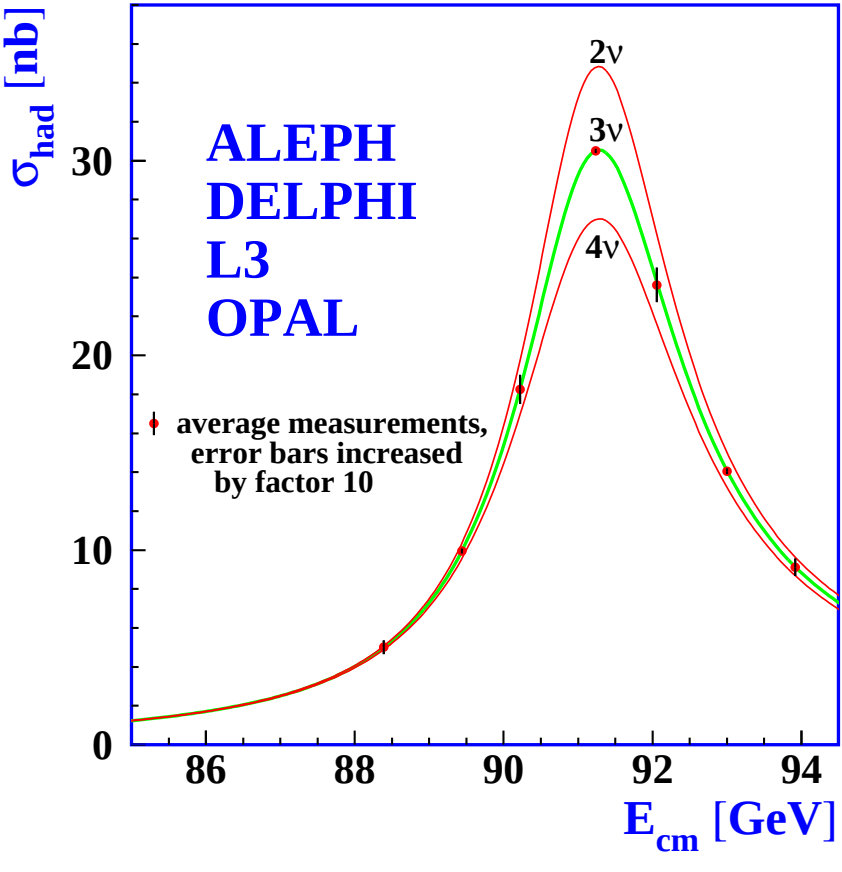

Fig. 6.8 The hadronic cross section, as a function of the centre-of-mass energy, from the combination of the measurements of the four LEP experiments. The predicted cross section assuming 2, 3 or 4 light neutrino families is shown.

Chapter 7

Z Decays to Heavy Quarks

The detailed study of Z decays to a pair of heavy quarks ($c\bar{c}$ or $b\bar{b}$) constitutes one of the important heritages of LEP and SLC. The relevance of hadronic Z decays as a tool to test electroweak interactions has already been stressed in Chapter 4. The $Zb\bar{b}$ vertex, in particular, plays an important rôle in precision tests of the MSM as it is very sensitive to electroweak corrections involving the top quark. A precise determination of the partial width of Z decays to b quarks, $R_b = \Gamma(Z \to b\bar{b})/\Gamma(Z \to \text{hadrons})$, measures these corrections and constrains the main parameter that regulates them, the mass of the top quark. The corresponding charm-quark quantity, $R_c = \Gamma(Z \to c\bar{c})/\Gamma(Z \to \text{hadrons})$, is largely independent from electroweak parameters and its measurement provides an important cross-check.

From the experimental point of view the presence of two heavy-flavoured hadrons in the final state has important consequences. Such events have distinctive properties, and can be experimentally disentangled from light-quark Z decays on a statistical basis, i.e. samples with reasonably low contamination from other Z decays can be selected. The data selection procedure is called tagging: cuts are applied on suitable discriminating variables and interesting events are selected with higher efficiency than background. The quality of a tagging procedure is defined by two parameters: the efficiency of selecting interesting events and the purity, i.e. the fraction of interesting events over the total. Heavy quark tagging is discussed in detail in the present Chapter. This discussion is required to understand the heavy quark measurements presented here and in Chapter 8, dedicated to the measurement of asymmetries. Heavy quark tagging is described in the typical experimental environment of e^+e^- colliders; many concepts, however, can be translated in the more difficult experimental condition typical of hadron colliders as will be recalled at Chapter 10.

Before discussing heavy-quark tagging and the partial widths measurements, some general properties of hadronic events in e^+e^- collisions are briefly reviewed.

7.1 General properties of hadronic events at the *Z*

Hadronic events are characterized by high particle multiplicity: at the Z resonance on average about twenty charged particles per event are produced (Fig. 6.5), accompanied by a similar number of neutral particles. As the Z boson is considerably heavier than quarks, final state particles tend to be relatively collimated around a specific axis, as shown in the event represented in Fig. 7.1. The main axis of the event can be evaluated as the direction of the unit vector $\hat{n}$ that maximises the thrust T:

$$T = \frac{\sum_i \mid \vec{p}_i \cdot \hat{n} \mid}{\sum_i \mid \vec{p}_i \mid} \ , \tag{7.1}$$

where $\vec{p}_i$ represents the momentum of particle i and the sum is calculated over all reconstructed particles of the event. The thrust axis is taken as an estimator of the quark-antiquark flight direction: a plane perpendicular to the thrust axis and containing the interaction vertex, i.e. the point where the Z is produced, divides the event in two halves (called hemispheres), of which one typically contains the quark and the other the antiquark.

Emission of hard gluons in hadronic Z decays is a relatively frequent process. Hemispheres containing hard gluons feature broader jets of particles and can show a "multi-jet" structure. The value of T itself ($0.5 \leq T \leq 1$) is an indicator of the presence of hard gluons: broader jets or multi-jet events tend to yield a lower T. A satisfactory definition of jets requires the introduction of jet clustering algorithms. Such algorithms are based on iterative procedures and on the definition of a metric, i.e. a "distance" y_{ij} between particle i and particle j. A widely used metric [88] is related to the invariant mass of the two-particle system

$$y_{ij} = \frac{2E_iE_J(1-\cos\theta_{ij})}{E_{vis}^2} \tag{7.2}$$

where E_i, E_j are the particles' energies and θ_{ij} their opening angle. The term E_{vis}^2 is the square of the energy of all particles used in the event. The iterative algorithm proceeds as follows: the pair of n particles with the smallest value of y_{ij} is replaced by a pseudoparticle (*jetlet*). The four-momentum of the jetlet is recomputed according to a recombination scheme.

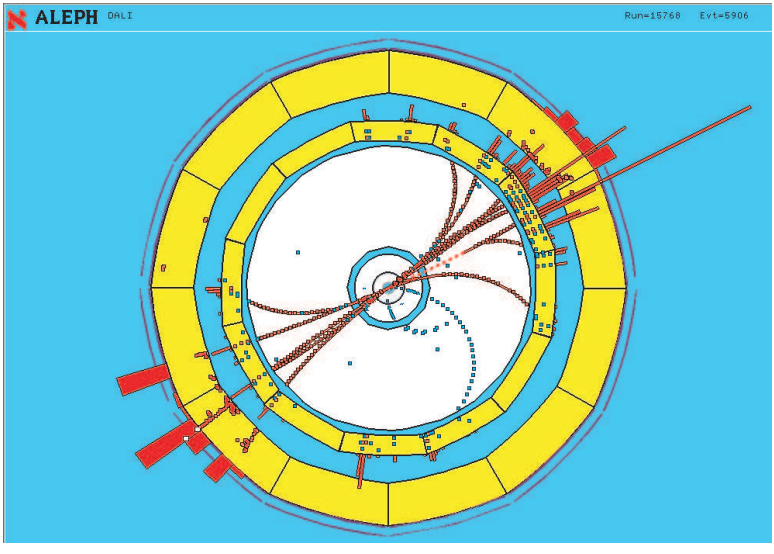

Fig. 7.1 Display of a Z hadronic decay collected by ALEPH. The reconstructed particles are clustered in two back-to-back "jets".

In a widely used scheme ("E" scheme) the four momentum of the jetlet is simply the sum of the four momenta of the two particles. The clustering procedure is then iterated with $n-1$ objects with the jetlet treated as a new particle. The procedure is repeated until all y_{ij} are larger than a predefined value, y_{cut}, called jet resolution parameter. At the end of the procedure N jets, with definite four-momentum, are obtained. The term E_{vis}^2 in Eq. (7.2) simply represents a normalization allowing similar values of y_{cut} to be used when different sets of particles are employed in the event reconstruction. In some of the measurements charged particles only are used, as measured by tracking devices, accounting typically for about 65% of the visible energy at LEP. In most of the final LEP measurements, however, jets were reconstructed using also neutral particles detected from their energy deposits in the calorimeters (Chapter 5). In this case the visible energy is much closer to the centre-of-mass energy. The N-jet rate depends on the chosen value of y_{cut}: as an example for hadronic Z decays $y_{cut} = 0.01$ yields about 65% of two-jet events, about 30% of three-jet events and 5% of events with higher jet multiplicities.

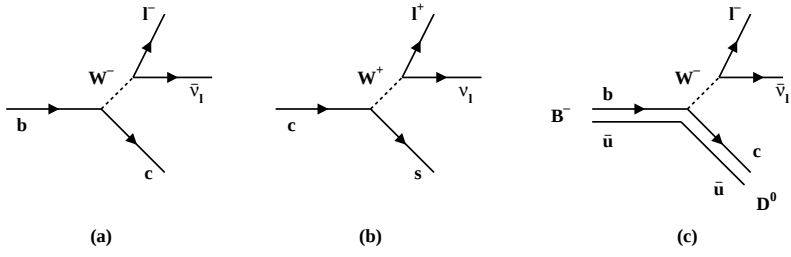

Fig. 7.2 Diagram of the $b \to \ell^-$ decay (a). Diagram of the $c \to \ell^+$ decay (b). Example of a specific exclusive decay: $B^- \to D^0 \ell^- \bar{\nu}_\ell$ (c).

7.2 Tagging Z decays to b and c quarks

A variety of methods have been used to select samples enriched in Z decays to heavy quarks; the most important of such methods exploits the nonzero lifetime of heavy-flavoured particles and the decay channels with leptons (electrons or muons). A review of the different heavy quark tagging methods is given below.

7.2.1 *Lepton tagging*

Heavy flavoured hadrons have sizable decay widths into final states containing an electron or a muon and the corresponding neutrino. The decay width into final states with a tau is suppressed by phase space, because of the large tau mass; in addition, the identification of tau leptons in hadronic environment is exceptionally challenging, therefore final states with tau leptons are not interesting for b tagging (unless the tau subsequently decays to an electron or a muon): in the following the word *lepton* is used to indicate electrons or muons only. Diagrams for heavy quark semileptonic decays are shown in Fig. 7.2; the light quarks inside the decaying hadron (*spectator quarks*) remain available for the hadronization of the final state quark.

The average semileptonic branching ratios of b and c hadrons produced in Z decays $BR(b \to \ell)$ and $BR(c \to \ell)$ are both around 10%. The third main source of leptons in heavy flavour Z decays is the cascade of b decaying to c, with the c hadron decaying semileptonically (Fig. 7.3): the branching ratio $BR(b \to c \to \ell)$ is again around 10%, as almost all b decays yield a charmed hadron in the final state. There are several other decay chains

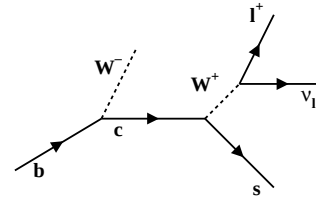

Fig. 7.3 The cascade $b \to c \to \ell^+$ decays.

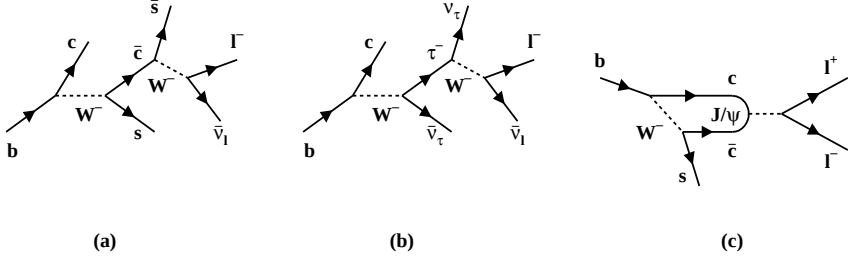

Fig. 7.4 Other semileptonic decays: $b \to \bar{c} \to \ell^-$ (a), $b \to \tau^- \to \ell^-$ (b), and $b \to J/\psi \to \ell^+\ell^-$ (c).

yielding an electron or a muon in the final state; the most relevant, with branching ratios of the order of 1%, are the b decay chains $b \to c\bar{c}, \bar{c} \to \ell^-$, usually abbreviated as $b \to \bar{c} \to \ell^-$, and $b \to \tau^- \to \ell^-$; in addition, b hadrons can produce a J/ψ (or a ψ'), which in turn can decay into two opposite-sign leptons $b \to J/\psi \to \ell^+\ell^-$. The corresponding diagrams are shown in Fig. 7.4. It should be noted that all the decay channels have the correct correlation between the lepton charge and the parent quark charge, except the $b \to c \to \ell^+$ channel, that has the wrong correlation, and the $b \to J/\psi \to \ell^+\ell^-$ channel, where if one lepton only is selected the charge information is random.

The sources of leptons described so far are usually refereed to as *prompt leptons*, *i.e.* leptons that are produced from the decay of a heavy hadron, without any long-lived particle in the decay chain. A summary of the prompt lepton sources with their abundance is shown in Table 7.1.

Table 7.1 Sources of prompt leptons in b and c decays. The branching ratios quoted refer to the b hadron and c hadron mixtures produced in the hadronization of quarks from Z decays.

Source	Branching ratio
$b \to \ell^-$	0.106 ± 0.002
$b \to c \to \ell^+$	0.081 ± 0.002
$b \to \bar{c} \to \ell^-$	0.016 ± 0.004
$b \to \tau^- \to \ell^-$	0.0042 ± 0.0006
$b \to J/\psi \to \ell^+\ell^-$	0.00072 ± 0.00006
$c \to \ell^+$	0.098 ± 0.003

Another important source of leptons are the decay in flight of pions and kaons to muons. Charged pions are produced in large multiplicity in events of any flavour from the hadronization of the primary quarks; they are produced also in many decay channels of the heavy-flavoured particles in b and c events. The average energy of pions produced in Z decays is in the GeV range, therefore the decay inside the tracking volume (typically around 1 m diameter) is a relatively rare event; however, when such a decay happens, the resulting muon is indistinguishable from a prompt muon in the calorimeters and muon detectors of the experiment. The production of kaons in the parton shower is suppressed by about a factor of 10 compared to pions. However, kaons are produced in the hadronization of the primary quarks in $Z \to s\bar{s}$ decays, and are frequently produced also in many decay channels of b and c hadrons. Charged kaons decay frequently to muons and, less frequently, also to electrons. Although the production of kaons in hadronic Z decays is overall almost a factor of 10 less copious than the pion production, they have substantially higher mass, and therefore higher probability of decaying inside the tracking volume. Overall, the contributions of $\pi \to \mu$ and $\mathrm{K} \to \mu$ decays to a sample of muon candidates selected in hadronic Z decays are often of comparable size. Another source of leptons is the conversion of photons in the detector material. The size of such a source obviously depends on the detector, and is one of the reasons why the material budget of tracking systems should be kept as low as possible. Particularly relevant is the material close to the interaction region (beam pipe and vertex detector), as photons converted near the primary vertex of the event give rise to charged particles that appear to come from the Z decay, and are therefore difficult to reject.

These sources of leptons are referred to as *non-prompt leptons*, and, as

mentioned above, are virtually indistinguishable from prompt leptons in the calorimeter system of the detector. However, it is possible to build discriminating variables that can be used to reduce their contribution to the sample of lepton candidates. If the tracking system provides some measurement of the ionisation of the charged particles, such information can be used to reject some $\mathrm{K} \to \mu$ decays: if the decay happened sufficiently far from the interaction point the average ionisation measured will be closer to that expected for a kaon than to that expected for a muon. The criterion is not effective for pion decays, as there is basically no difference in the ionisation of pions and muons at the energies considered. Another useful criterion is the quality of the measured trajectory: if there is a decay in flight inside the tracking volume, the trajectory should contain a kink, giving a poorer χ^2 of the fit used to determine the trajectory; in some cases the kink can even be identified by reconstructing the two track segments separately; this criterion is again more effective for kaon decays than for pion decays, as the higher q-value gives on average more pronounced kinks. Electrons from photon conversions can be rejected by looking for tracks that fulfil loose electron identification criteria and that form a good vertex with the electron candidate, in a region of the detector with substantial material density.

The third class of lepton candidates are *fake leptons*, *i.e.* hadrons that fulfil the lepton identification criteria. A fake muon can be selected when a pion produced in the hadronic shower inside the hadron calorimeter decays to a muon, and this muon is sufficiently collimated with the parent hadron that originated the shower (this mechanism is sometimes called *punch through*). Alternatively, the hadron can profit from regions with reduced material inside the calorimeters to cross them without interacting and reach the muon detectors (*sail through*). For electrons, the misidentification can happen when a photon enters the calorimeter very close to a charged particle, producing an electromagnetic shower that is geometrically compatible with the incoming charged track. If the photon energy is close enough to the charged particle energy (within the calorimeter resolution), the charged particle can be identified as an electron. For the LEP detectors and SLD the hadron rejection is of the order of 10^{-3}, giving low hadron contamination in the lepton samples, despite the initial unfavourable ratio of hadrons to prompt leptons in hadronic events, of about 100:1.

The different sources of leptons can be discriminated on the basis of their kinematic properties and of the topology of the jets to which they be-

long. The discriminating variables typically provide also further rejection against the background of fake leptons. Because of the large mass of b and c hadrons, the radiation of gluons is suppressed in $Z \to b\bar{b}$ and $Z \to c\bar{c}$ events: on average 70% of the beam energy is carried away by the heavy-flavoured hadron in b events, and 50% in c events, giving high-energy leptons in the decay chain. Another important feature, especially for semileptonic b decays, that is still a consequence of the high mass of the decaying hadron, is that the lepton in primary ($b \to \ell^-$) decays tends to have a larger transverse momentum with respect to the jet to which it belongs. The experiments have optimised over the years the algorithms to cluster the reconstructed particles into jets, and to calculate the transverse momentum of the lepton candidates, in order to maximise the separation between primary and cascade decays, that is crucial especially for the forward-backward asymmetry measurements (because of the wrong charge information carried by the lepton in $b \to c \to \ell^+$ decays).

An example of discriminating variables between the different lepton components is given in Fig. 7.5, from the ALEPH simulation. The two variables shown are the lepton momentum and its transverse momentum with respect to the jet axis, where the jet is re-clustered excluding the lepton: $b \to \ell^-$ decays are characterised by a higher average momentum p and transverse momentum $p_\perp$, $c \to \ell^+$ decays have smaller $p_\perp$ and $b \to c \to \ell^+$ decays have small p and $p_\perp$. Selecting leptons with high p and $p_\perp$, a purity of about 80% of primary $b \to \ell^-$ decays can be obtained, with an efficiency around 25%, thus retaining about 6% of jets associated to b quarks from Z decays [89].

The lifetime tag, discussed in the next Subsection, has an intrinsically superior performance as a tool to select $Z \to b\bar{b}$ decays and it is therefore the main way to measurements of the partial widths. However the lepton tag has two specific interesting features, that makes it competitive for the measurement of forward-backward asymmetries:

- lepton identification mostly relies on calorimeters, and is typically effective in a wide angular range ($|\cos\theta| < 0.95$); the lifetime tag, instead, is fully effective in a restricted angular range defined by the vertex detector acceptance (typically $|\cos\theta| < 0.7$), while the forward region carries larger statistical weight in the asymmetry measurements;
- the lifetime tag does not provide any straightforward and effective way of telling the quark charge, while in the lepton tag such information is directly provided by the lepton charge.

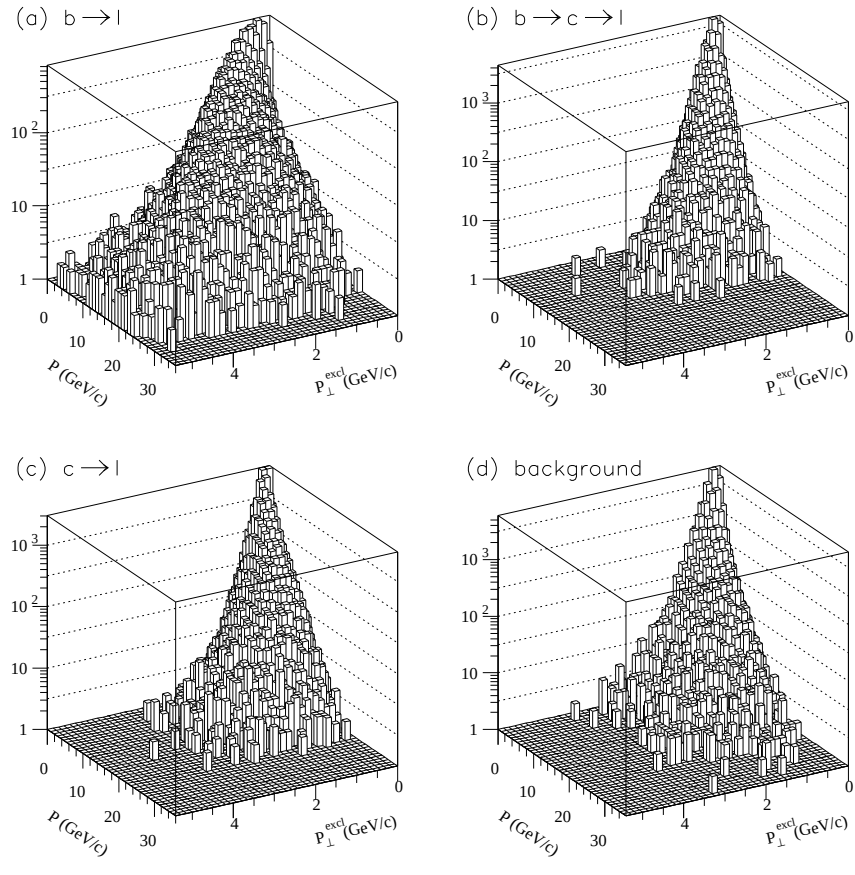

Fig. 7.5 Distribution in the (p,$p_\perp$) plane of lepton candidates originating from $b \to \ell^-$ decays (a), from $b \to c \to \ell^+$ decays (b), from $c \to \ell^+$ decays (c), and of non-prompt or fake leptons (d). The transverse momentum $p_\perp$ is computed with respect to the jet axis, after excluding the lepton from the jet. (Courtesy of Duccio Abbaneo).

For these reasons the identification of leptons in hadronic environment has been the first method used for the measurement of the heavy flavour asymmetries and one of the design requirements for the detectors.

From the discussion of this Section it appears evident that any lepton selection will tag $Z \to b\bar{b}$ decays more efficiently than $Z \to c\bar{c}$ decays, for two main reasons:

1. the lepton yield in $Z \to b\bar{b}$ events is roughly twice the yield of $Z \to c\bar{c}$ events, due to the presence of direct and cascade decays;
2. leptons from b decays (especially from $b \to \ell^-$ direct decays) have distinctive kinematic properties and can be efficiently separated from the background of fake and non-prompt leptons, while leptons from c decays have intermediate properties between $b \to \ell^-$ decays and background.

Therefore a lepton selection is not by itself a mean to select a high-purity sample of $Z \to c\bar{c}$ decays; nonetheless discriminating variables as those presented above can be used to select samples with different relative content of $Z \to c\bar{c}$ and $Z \to b\bar{b}$ decays: a comparative analysis of such samples may allow to extract R_b and R_c (or the b and c forward-backward asymmetries), at the same time.

7.2.2 *Lifetime tagging*

The most effective way of selecting $Z \to b\bar{b}$ decays relies on the nonzero lifetime of particles containing a b quark. The average lifetime of b hadrons is around 1.5 ps, with small differences among the various species; combined with the average boost at the Z cms energy ($\gamma \approx 6$), it gives a decay length of about 2.7 mm on average: $\langle L \rangle = \langle \gamma\beta \rangle c\tau$, where τ is the particle mean lifetime. Such a distance is one order of magnitude larger than the typical precision on the secondary vertex reconstruction, if the charged decay products of the b hadron are within the vertex detector acceptance. An example of good separation between the primary vertex of the event and the b hadron decay vertex is shown in Fig. 7.6.

Alternatively, instead of identifying the b decay products and fitting them to a common vertex, the b hadron can be tagged in a more inclusive way by the presence of tracks that are incompatible with the primary vertex. The *impact parameter* of a track is defined as the minimum distance of the track from the primary vertex of the event; its sign is defined using the direction of the jet to which the track belongs (taken as an estimator of the b flight direction), as in the sketch of Fig. 7.7. The sign is considered as positive when the track crosses the jet direction before the primary vertex and negative otherwise. The impact parameter of a track is $\delta = \gamma\beta ct \sin\phi$, where t is the lifetime of the parent particle and ϕ is the decay angle. As the average decay angle is $\langle \sin\phi \rangle = 1/\beta\gamma$, the average impact parameter can be written as $\langle \delta \rangle = c\tau$, where τ is the parent particle mean lifetime. Particles from b decays are expected to have a positive impact parameter of about 450 μm, that is again about one order of magnitude larger than

Table 7.2 Production fractions of the different b hadron species in the hadronization of b quarks from Z decays, along with their measured lifetimes and masses. The fraction quoted for Λ_b also accounts for heavier b baryons.

Particle	Fraction	Lifetime	Mass
B^0	0.388	1.542 ± 0.016 ps	5.279 GeV
B^-	0.388	1.674 ± 0.018 ps	5.279 GeV
B_s	0.106	1.461 ± 0.057 ps	5.370 GeV
Λ_b	0.118	1.229 ± 0.080 ps	5.624 GeV

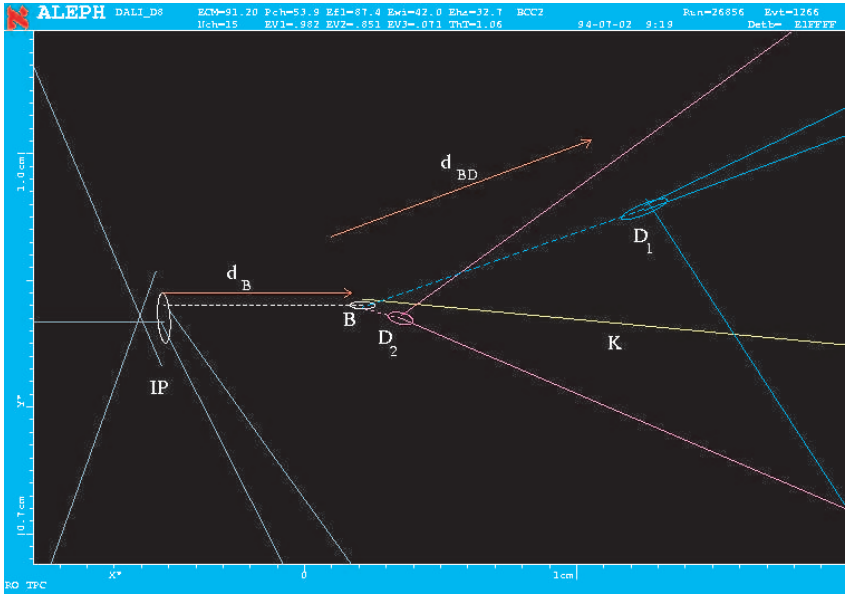

Fig. 7.6 Event with a reconstructed b decay vertex, recorded by the ALEPH detector. The ellipses around the primary and the secondary vertexes represent the estimated uncertainties in the reconstructed positions.

the resolution, if the track is measured in the vertex detector.

Charmed particles also have significant lifetime, typically around 0.5 ps, except for the D^+, that has a lifetime of about 1 ps. The hadronization of charm quarks from Z decays produces a ratio of vector (D^{*+}, D^{*0}) to scalar (D^+, D^0) to mesons of about 1.6. While the D^{*0} always decays to a

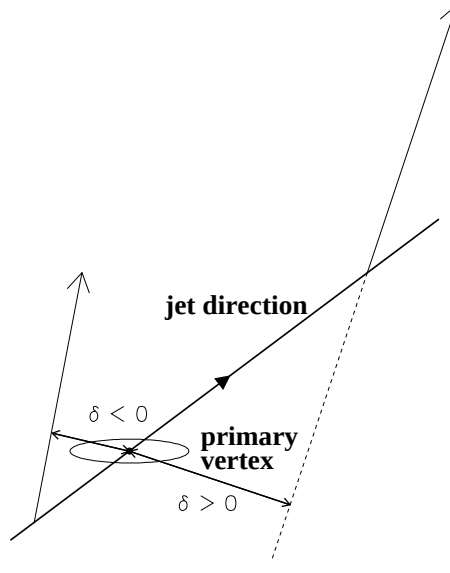

Fig. 7.7 Definition of the track impact parameter and of its sign.

Table 7.3 Production fractions of the different c hadron species in $Z \to c\bar{c}$ events, along with their measured lifetimes and masses. The fraction quoted for Λ_c also accounts for heavier c baryons.

Particle	Fraction	Lifetime	Mass
D^+	0.234	1.051 ± 0.013 ps	1.869 GeV
D^0	0.545	0.412 ± 0.003 ps	1.865 GeV
D_s	0.125	0.490 ± 0.009 ps	1.968 GeV
Λ_c	0.096	0.200 ± 0.006 ps	2.285 GeV

D^0 (with a photon or a π^0), the D^{*+} decays to D^+ with a branching ratio of about 32%, the rest decaying in the channel $D^0\pi^+$. For this reason, in terms of the weakly-decaying hadrons, $Z \to c\bar{c}$ events contain many more neutral than charged mesons, as shown in Table 7.3.

Charm events represents the largest background to b tagging. Additional discrimination between the two flavours can be achieved exploiting the larger mass of b hadrons (Tables 7.2 and 7.3), and the larger charged particle multiplicity of b hadron decays (about 5 charged particles on average) compared to c hadron decays (about 2.2 charged particles).

Also in light quark events there can be particles that do not originate, or do not appear to originate from the primary vertex, and can therefore be mistaken as decay products of heavy-flavoured particles. Such particles can be:
- products of early decays of Λ, Σ^+, K^0_S, K^+ or π^+;
- electrons from photon conversions;
- electrons that radiate a bremsstrahlung photon early in the tracking system, and therefore have a kink in their trajectory;
- similarly, pions that make a soft nuclear interaction in the tracking system, and therefore have a kink in their trajectory.

Such sources of background can be reduced by identifying and rejecting photon conversions, as well as Λ and K^0_S decays, and imposing cuts on the quality of the reconstructed particle tracks.

The determination of the primary vertex

The first crucial step in building a lifetime tag is an accurate determination of the Z decay point, usually called primary vertex of the event. This applies both to algorithms based on the impact parameter significance of individual tracks, and to algorithms based on the reconstruction of vertices with significant separation from the primary vertex.

The luminous region depends on the optics of the accelerator, and can vary with time. At LEP it had a typical size of about 10 μm in y, 100 μm in x and 1 cm in z. The position of the luminous region is determined using chunks of events (typically 100) and calculating the impact parameter of the tracks with respect to a nominal position. The information on the position of the luminous region is then used as a constraint in the determination of the primary vertex of each event of the chunk.

The reconstruction of the primary vertex in heavy flavour Z decays is a non-trivial problem because of the presence of the decay products of the heavy hadrons, that are actually not originating from the primary vertex. A common solution consists in reconstructing jets (with a clustering parameter optimized for the purpose) and using only the projection of the tracks on the plane orthogonal to the jet direction to measure the position of the primary vertex: in the case of the decay of a heavy hadron, the effect due to its nonzero lifetime is eliminated to the extent to which the jet direction is a good approximation of its flight direction (see sketch of Fig. 7.8). The precision can be further improved in a second step, by adding also the component parallel to the jet direction for the tracks that are compatible with

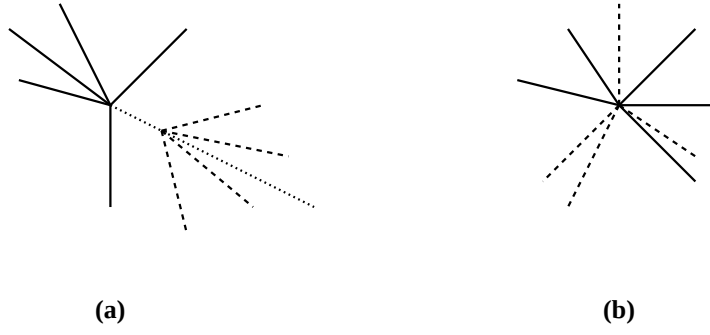

Fig. 7.8 Tracks coming from the decay of a heavy hadron, represented with dashed lines (a), appear to come from the Z decay point (b) when projected onto a plane perpendicular to the hadron flight direction, represented with the dotted line. In the analyses, the b hadron flight direction is approximated by the reconstructed jet direction.

the first determination of the primary vertex. The precision that can be achieved with such an algorithm is about 50 μm $\times$ 10 μm $\times$ 60 μm in the $x \times y \times z$ coordinates, where the precision in the y view is entirely dominated by the constraint on the luminous region. In the final R_b analyses, in order to control some specific systematic effects, the LEP collaborations have chosen to determine independently the position of the primary vertex in the two event hemispheres (defined as usual using the thrust axis). Each of the two determinations is degraded by about 30% in the x and z views, but the loss of precision is more than compensated by a better understanding of the correlations between the two hemispheres (see Subsection 7.3.1).

At SLC the beam spot was much narrower than at LEP. In the xy plane the beam size was of the order of a micron, while the beam motion resulted in a spread of about 7 μm. Such a value is considerably smaller than the resolution that would be achieved by fitting the tracks to a common vertex event by event. Therefore the average beam position (measured on about 30 events) was taken as estimate of the primary vertex in the xy plane. In the z projection the beam spot was about 700 μm long. Event-by-event reconstruction yields a precision of about 15 μm in light quark events, that degrades to about 30 μm in $Z \to b\bar{b}$ events, due to the presence of heavy-

flavoured particles.

Tagging with track impact parameters

The relevant variable that can be used to tag the presence of particles with nonzero lifetime is the impact parameter significance $\mathcal{S}$ of the tracks of reconstructed charged particles, that is the impact parameter defined as in Fig. 7.7, divided by its estimated uncertainty. The uncertainty results from the propagation of the estimated error on the primary vertex, and the uncertainty on the track parameters, including the effect of multiple scattering. The impact parameter resolution can be parametrized as an asymptotic term, given by the precision and position of the reconstructed coordinates closer to the primary vertex, a momentum-dependent term accounting for the uncertainty due to multiple scattering, and a polar-angle dependent term that accounts for the increase of the extrapolation length from the interaction point to the vertex detector layers. At LEP the impact parameter resolution for 45 GeV muons at $\cos\theta \approx 0$ was typically between 15 μm and 30 μm in the $r\phi$ view, and between 10 μm and 100 μm in the z view. At SLD a resolution better than 10 μm was achieved in both views, thanks to the smaller beam spot and a high precision vertex detector very close to the interaction point.

Tracks that originate from the Z decay point are expected to have an impact parameter significance normally distributed around zero, while the presence of a few tracks with large and positive impact parameter significance can be used as a tag of a Z decay to heavy quarks. The tracks that populate the negative side of the impact parameter distribution constitutes an important control sample that is used to measure the resolution directly from the data and calibrate the tag. The negative side of the impact parameter distribution is fit with a functional form $\mathcal{D}(\mathcal{S})$ (typically a Gaussian plus some exponential components), and then for a track with measured positive impact parameter significance $\mathcal{S}$, a variable $\mathcal{P}$ is defined as [90]:

$$\mathcal{P}(\mathcal{S}) = \int_{-\infty}^{-\mathcal{S}} \mathcal{D}(x)dx \ . \tag{7.3}$$

The variable $\mathcal{P}(\mathcal{S})$ has the physical meaning of the probability that a track with positive impact parameter significance $\mathcal{S}$ originates from the primary vertex (or, better, the probability that a track originating from the primary vertex has an impact parameter significance larger than the measured one). Tracks coming from the primary vertex have a flat distribution of $\mathcal{P}$ between 0 and 1. By construction $\mathcal{P}$ accounts for effects due to non-gaussian

resolution tails in the data, as it is derived from $\mathcal{D}(\mathcal{S})$ that is measured on the data.

Probabilities measured for different tracks can be combined: given a group of N tracks, the quantity

$$\mathcal{P}_N = \Pi \sum_{j=0}^{N-1} \frac{(-\ln \Pi)^j}{j!} \ , \tag{7.4}$$

with

$$\Pi = \prod_{j=1}^{N} \mathcal{P}_j \ , \tag{7.5}$$

represents the probability that the N tracks are originating from the primary vertex (or that a group of N tracks originating from the primary vertex have a set of impact parameters equally or more incompatible with it). An example for all tracks in a given hemisphere is shown in Fig. 7.11. This technique can be used to define tagging variables on set of tracks of particular interest: typically in R_b measurements the analysis is made on hemispheres, for other applications individual jets are considered, or even the whole event.

The performance of the method depends crucially on the use of sets of well reconstructed tracks, with minimal tails on the negative $\mathcal{S}$ distribution. The analyses heavily relying on the impact parameter lifetime tag are typically restricted to the acceptance of the vertex detector, and apply stringent quality cuts on the tracks considered, including rejection of photon conversions and decays of long-lived particles, as discussed above. Another important point is the optimization of the jet direction reconstruction, which is used to sign the impact parameter: signing errors give rise to tails in the negative side of the impact parameter distribution, spoiling the performance of the tag.

It is worth noting that such a tag implicitly takes advantage of the larger decay multiplicity of b hadrons compared to c hadrons, when the probability of all tracks of a hemisphere (jet or event) are combined. As for the lepton tag, the method is suitable for selecting high-purity $Z \to b\bar{b}$ samples, while c events have intermediate properties between b events and light quark background.

Decay length reconstruction

The impact parameter tag described above relies on the presence of tracks that are measured to be incompatible with the Z decay point: no informa-

tion is used about the compatibility of those tracks with the hypothesis of coming from a common point in space: the decay point of the heavy hadron. Such a fact on one side is indeed a limitation of the impact parameter tag, but on the other hand it is also an advantage, because in fact in the vast majority of b decays the decay products are not originating from a single secondary vertex, but from two or even three vertices, often significantly separated among them (some examples are shown in Fig. 7.6). The presence of such a variety of topologies is a severe limitation for the construction of high-performance b tagging algorithm based on the reconstruction of the b decay length. Nonetheless such algorithms have been developed by the LEP experiments, and used successfully for R_b analyses, in particular by OPAL [91].

Tracks belonging to a jet are fit to a common vertex, after applying quality cuts to reject badly measured tracks and decay products of long-lived particles. The χ^2 of the fit is computed; then tracks are removed in turn one by one, and the χ^2 difference in the vertex fit is evaluated, selecting the track that gives the largest $\Delta\chi^2$; if such $\Delta\chi^2$ exceeds a given threshold ($\Delta\chi^2 > 4$) the track is removed, the vertex is recomputed and the procedure is reiterated. The procedure yields a good reconstructed secondary vertex, unless too few tracks are left (less than four in the OPAL analysis) in which case no vertex is found.

The distance between the secondary and the primary vertex, projected along the jet direction, is taken to be the decay length of the heavy hadron. When the secondary vertex appears to be behind the primary vertex, the decay length is given a negative sign. The uncertainty on the measured decay length is evaluated by propagating the fit uncertainty on the primary and secondary vertices, and the decay length significance L/σ_L is used as tagging variable.

Events without lifetime yield a symmetric distribution of measured decay lengths, therefore the negative side of the distribution provides a measurement of the resolution directly from the data.

The decay length tag is intrinsically more robust than the impact parameter method with respect to single badly measured tracks, because of the requirement on the compatibility of the tracks forming the secondary vertex. In addition it is less sensitive to a limited resolution in the jet direction reconstruction, which in this case contributes to degrade the decay length resolution but does not cause signing mistakes.

The efficiency is limited by the complicated topology of b decays, as discussed above, and drops to zero for low charged multiplicity decays.

Overall the performance remains lower than that of the impact parameter tag.

At SLD the high precision tracking in the vicinity of the interaction point allows efficient reconstruction of secondary vertices; the identification of the b decay products, however, is exploited to calculate the mass of the parent particle (rather than its decay length), which is used as discriminating variable. The method is discussed below.

Mass tag

The large b hadron mass can be used to improve the discriminating power between b and c events. The most direct method consists in reconstructing a secondary vertex, and calculating the invariant mass of the particles assigned to that vertex. In the case of a charm decay, the mass is in principle limited to about 1.8 GeV, while the region between 1.8 GeV and 5 GeV is mostly populated by b decays. This method was particularly effective at SLD, thanks to the high precision tracking at small radii [92]. For an evaluation of the decaying particle mass corrections are needed, because;

1. the vast majority of b decays proceed through a cascade decay to charm: decay products of the charmed particle may be incompatible with the secondary vertex;
2. neutral particles are not accounted for.

Decay products of secondary charmed particles in b cascade decays can be recovered with a dedicated procedure: tracks that are inconsistent with the primary vertex, and that pass within 1 mm (in space) from the axis that contains the PV-SV axis are included in the secondary vertex.

The tracks selected are used to calculate the invariant mass of the vertex. A further correction to the calculated mass is obtained by comparing the direction of the total momentum with the direction of the PV-SV axis: in general the two vectors are significantly acollinear, due to missing neutral particles and possibly missing neutrinos. A kinematic correction to the mass is defined, based on the transverse momentum P_t of the reconstructed momentum with respect to an axis tangent to the error boundaries of the two reconstructed vertices (sketch of Fig. 7.9): P_t represents the minimum amount of transverse momentum needed to make the two vectors compatible, so avoiding large corrections due to resolution effects that would increase the contamination non-$b\bar{b}$ events. The corrected mass is then written as

$$M_{\rm corr} = \sqrt{M^2 + P_t^2} + \mid P_t \mid , \tag{7.6}$$

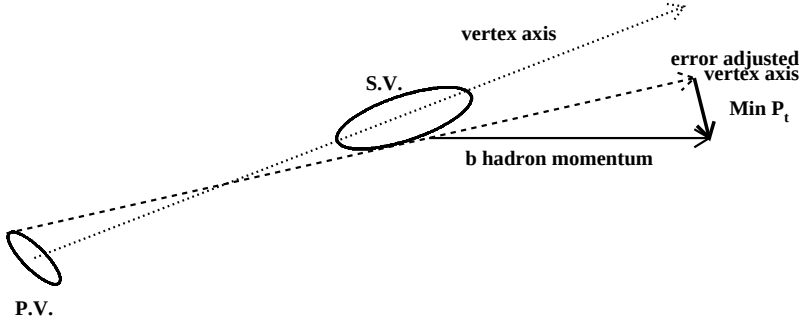

Fig. 7.9 Definition of the "minimum P_t" used to calculate the vertex corrected mass at SLD. The b candidate momentum is compared with the vertex axis (dottet arrow). A new vector tangent to the Primary Vertex and Secondary Vertex error boundaries is defined (dashed arrow), and the transverse momentum of the b candidate with respect to this axis is considered.

with M indicating the uncorrected mass. Hemispheres where $M_{\rm corr} > 2M$ are rejected.

The corrected mass provides excellent separation between b, c and uds quarks, as shown in Fig. 7.10, and is used in conjunction with the vertex momentum in the R_b and R_c analyses. The discrimination is further improved by combining, through a neural network, additional information such as the decay length and charged particle multiplicity of the reconstructed vertex. Through this technique SLD was able to select inclusively high-purity charm samples, an achievement that was not attainable for LEP detectors.

A different approach has been taken by ALEPH: tracks are ordered according to their impact parameter significance and their invariant mass is calculated. When such mass exceeds 1.8 GeV, the impact parameter significance of the last track added is taken as the discriminating variable. In the case of a charm decay, such a track is expected to be that of a fragmentation particle, originating from the decay vertex. In the case of a b decay, the last track added can be that of a b decay product, and therefore have a significant impact parameter. The distribution of the discriminating variable obtained is shown in Fig. 7.11b. This method is not necessarily more powerful than the previous one in terms of discrimination between b and c

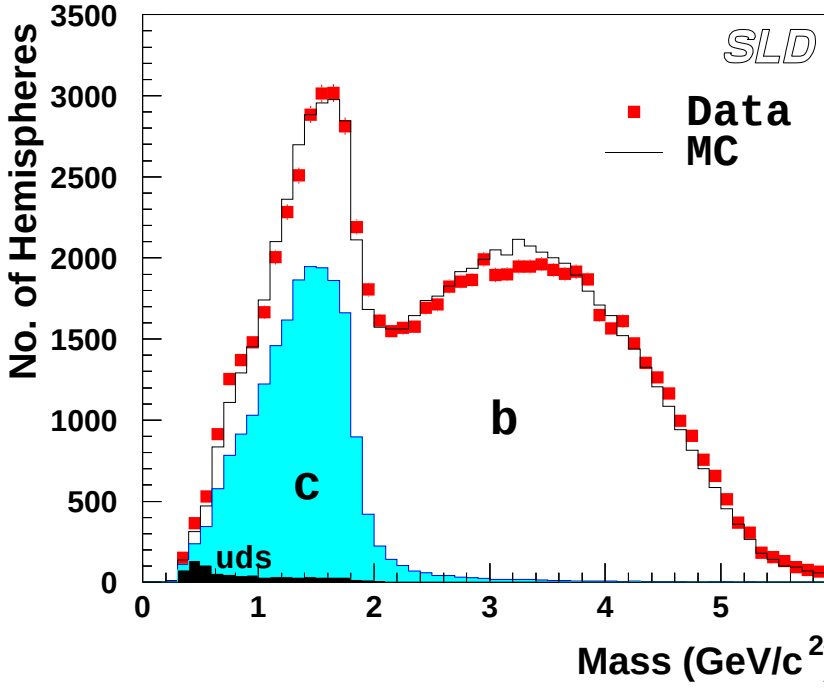

Fig. 7.10 Distribution of the corrected mass for reconstructed secondary vertices at SLD. Thanks to the precise tracking near the interaction point, this variable provides excellent separation between b, c and light quark events.

decays, but it is interesting if one needs to use the simulation to evaluate the residual charm background: in the previous case such estimate is sensitive to the details of the hadronization process (multiplicity and kinematic properties of fragmentation particles), while in this case the background mostly arises, as for the impact parameter tag, from the decay products of long-lived particles, photon conversions, hadronic interactions etc.

This long discussion on lifetime tagging was motivated by the superior performance of these methods compared to other ones (e.g lepton or event-shape tagging). At LEP experiments, jets associated to b quarks originating from Z decays were selected with efficiencies ranging from 20% to 30%, for a purity of 98%. Even higher efficiencies (about 60%) were obtained at SLD, for the same purity.

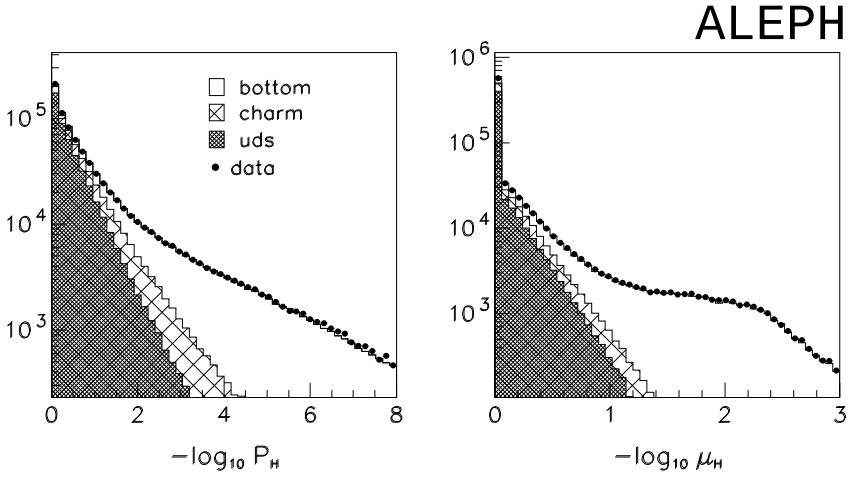

Fig. 7.11 Lifetime and mass tagging. (a) Negative logarithm of the tagging probability defined by Eq. (7.5) for all tracks in a given hemisphere. (b) Negative logarithm of the tagging probability for the first track exceeding the charm mass (details are given in the text); in the case of charm or light quark events this particles is expected to originate from the primary vertex.

7.2.3 *Reconstruction of charmed hadrons*

Several charm states were reconstructed at LEP and SLC. Due to the small branching ratios of the decay channels considered (typically of the order of a few percent), this tagging technique was more useful at LEP, where larger statistics were available, as a mean of tagging heavy flavour Z decays. In $Z \to c\bar{c}$ decays charm hadrons carry away a larger fraction of the beam energy compared to secondary charm hadrons from b decays in $Z \to b\bar{b}$ events. This property is often employed to obtain high-purity charm samples, by using the energy of the reconstructed charm state as a discriminating variable. Other useful complementary variables are the lifetime of the reconstructed particle, and the properties of the opposite hemisphere (lifetime tag, lepton tag, event shape).

Reconstruction of ground state charmed hadrons

The reconstruction of ground state D mesons (D^0, D^+,D_s) and of Λ_c baryons is typically performed in the "golden" channels $D^0 \to K^-\pi^+$,

$D^+ \to K^-\pi^+\pi^+$, $D_s{}^+ \to K^-K^+\pi^+$ (possibly with the K^-K^+ pair forming the ϕ resonance), and $\Lambda_c^+ \to pK^-\pi^+$, as such channels offer the best background conditions. The reconstruction consists in the calculation of the invariant mass of good quality charged tracks, typically complemented with the available particle identification information (energy loss measurement, information from Cerenkov or time of flight detectors, when present) to improve the efficiency in the assignment of the pion and kaon masses to the selected tracks.

The resulting mass spectra are shown in Fig. 7.12 in the case of the ALEPH experiment. The selection of the events falling in the mass window provides samples with a substantial amount of combinatorial background (typically more than 50%), that can be estimated directly from the data by fitting the sidebands with a polynomial. The signal of correctly reconstructed hadrons contains contribution from $Z \to c\bar{c}$ events, where the charmed hadron is generated in the hadronization of the primary quark, and from $Z \to b\bar{b}$ events, where the reconstructed particle comes from the decay of a b hadron. In the analyses the two components are disentangled using information from the opposite hemisphere (typically lifetime tag), or from the same hemisphere (*e.g.* lifetime and momentum of the reconstructed particle).

Reconstruction of $\mathbf{D^*}$ *mesons*

The reconstruction of D^* mesons offers particularly clean samples, due to the peculiar kinematics of the decay $D^{*+} \to D^0\pi^+$. The mass difference between D^* and D^0 is 145.5 MeV, very close to the kinematic threshold, leaving only 6 MeV of q-value.

In the laboratory frame, the D^* energy is limited by the beam energy, giving a maximum boost of $\gamma \approx 20$, which translates to a kinematic limit for the momentum of the pion from the D^* decay, usually denominated as "soft pion" π_s, of $P_{\pi_s} \approx 3$ GeV. Therefore the experimental signature of the $D^* \to D^0\pi_s$ decay is a track with momentum limited at 3 GeV, highly collinear with the D^0 candidate (or with the axis of the jet to which it belongs, reconstructed with a suitable clustering parameter).

The calculation of the mass difference between the reconstructed D^* and the reconstructed D^0 gives a narrow peak with low background, as shown in Fig. 7.13(a). The low background conditions are essentially due to the fact that the signal is at the end of the phase space: random combinations

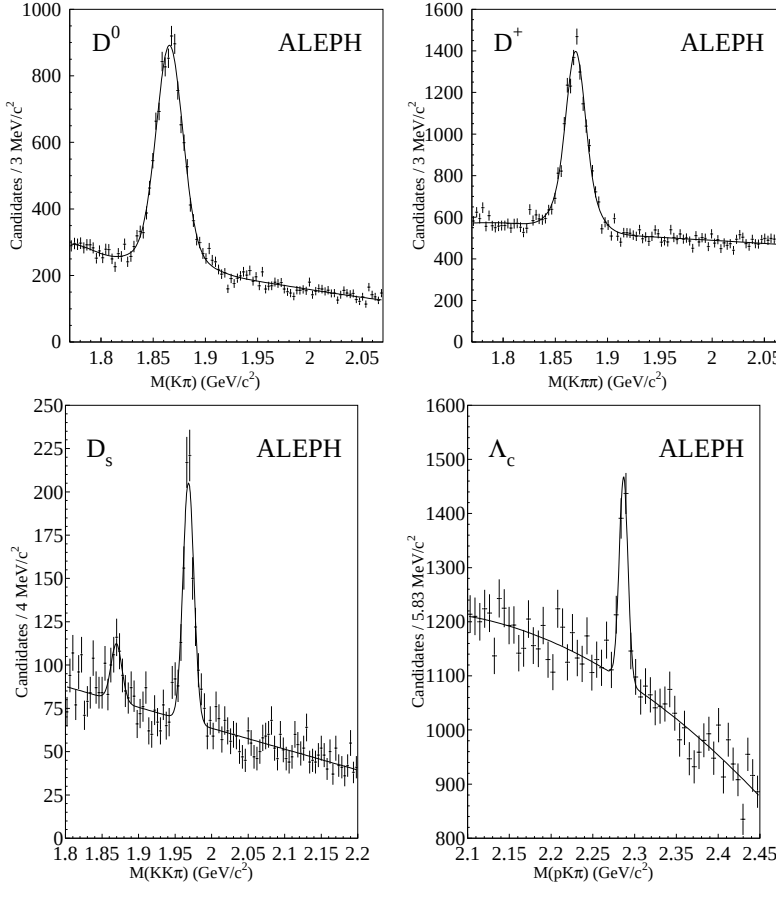

Fig. 7.12 Reconstructed mass distributions for $D^0 \to K^-\pi^+$, $D^+ \to K^-\pi^+\pi^+$, $D_s \to K^-K^+\pi^+$ and $\Lambda_c \to pK^-\pi^+$ from ALEPH. The fitted functions are the sum of polynomials for the combinatorial background and Gaussian functions for the signals.

of tracks have little probability of being so collinear, and therefore tend to give a larger measured mass difference. The method is effective even if the D^0 is not fully reconstructed, as shown in Fig. 7.13(b) and 7.13(c). Due to the fact that the D^0 decay products are typically ultrarelativistic and well collimated, the effect of the missing particle(s) largely cancels in the mass difference, giving a moderate increase of the peak width.

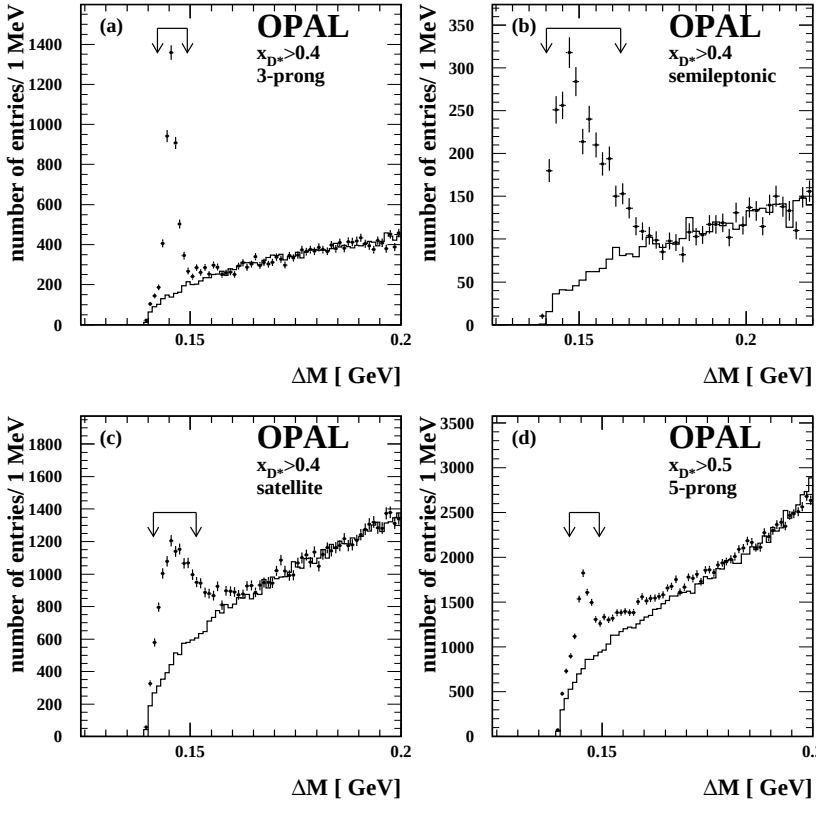

Fig. 7.13 Mass difference $\Delta M = m(\mathrm{D}^0\pi^+) - m(\mathrm{D}^0)$ reconstructed by OPAL in different channels. Fully reconstructed $\mathrm{D}^0 \to \mathrm{K}^-\pi^+$ candidates (a) give a narrow peak with small background, while the channel $\mathrm{D}^0 \to \mathrm{K}^-\pi^+\pi^-\pi^+$ (d) has equally good resolution but higher combinatorial background, because of the higher multiplicity. The semileptonic channel $\mathrm{D}^0 \to \mathrm{K}^-\ell^+\nu_\ell$ (b) yields a broader signal peak because of the missing neutrino, but the resolution on the mass difference is still sufficient to find a high-purity signal region. Similarly for the channel $\mathrm{D}^0 \to \mathrm{K}^-\pi^+\pi^0$ (c), with the π^0 not reconstructed. In all four plots the solid histogram shows the estimated combinatorial background.

The technique can be pushed even further, by looking for a "soft pion" signature without attempting any reconstruction of the D^0 particle. A sample enriched in pions from D^* decays can be selected by searching for

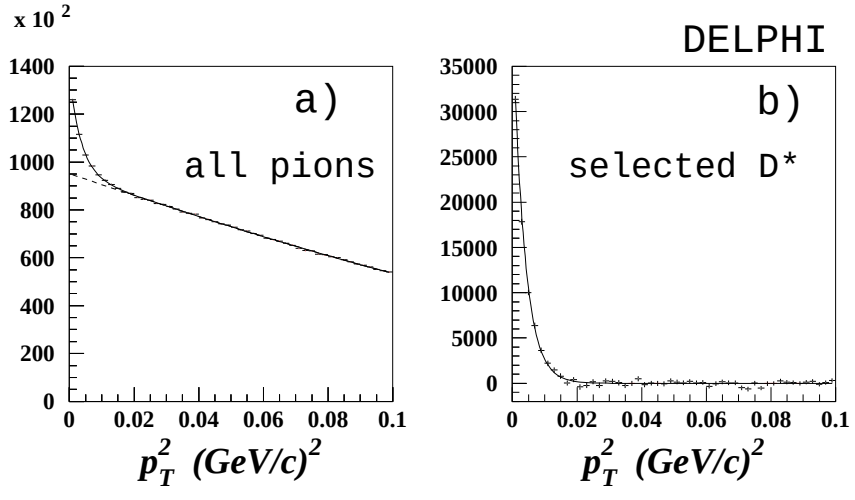

Fig. 7.14 Distribution of the squared transverse momentum with respect to the jet axis at DELPHI for (a) inclusive pions, (b) pions from selected D^*.

charged particles of momentum lower than 3 GeV and collinear with the jet axis, as shown in Fig. 7.14.

The method has the advantage of being effective for any D^0 decay mode, but requires the subtraction of a large background below the low $p_\perp^2$ peak, complicated by the presence of the contribution from b hadron decays, that produce a broad accumulation in the same region.

7.2.4 *Event shape tagging*

The hard fragmentation and the large mass of b quarks result in distinctive topological properties of $Z \to b\bar{b}$ decays, that can be exploited to define global discriminating variables.

In b events gluon radiation is suppressed, and a large fraction of the beam energy (70% on average) is carried away by the b hadron (and subsequently, its decay products). In light quark events, instead, many particles are produced in the fragmentation process, with a soft momentum spectrum.

Due to the large b hadron mass, b decay products may have a relatively large transverse momentum with respect to the b quark direction, while

light quark events tend to produce more collimated jets.

In summary, b events tend to have two broad jets carrying a large fraction of the beam energy, while light quark events typically show a softer particle spectrum and particles have lower transverse momentum with respect to the fragmenting partons.

A variety of discriminating variables have been defined by the experiments to exploit the topological differences between b events and light quark events; some of these variables rely on a few of the most energetic tracks of the events, that in b events are typically b decay products: examples are the invariant mass and sphericity of the three most energetic particles of the leading jet in each hemisphere; other variables are defined using all particles of a jet, of even on the whole hemisphere.

Event shape b tagging typically offers substantially worse performance than lifetime tagging, and the purity of the selected samples is more difficult to estimate with the simulation, because the efficiency for selecting light quark events depends on the details of the fragmentation process. If several variables are defined, they tend to have substantial statistical correlations (as they largely exploit the same information), and neural network techniques are needed to combine them in a fully efficient way. Event shape variables are typically used to complement lifetime tagging, especially in techniques where the non-b background can be estimated directly from the data (like multi-tag R_b analyses).

7.2.5 *Gluon splitting to heavy quarks*

A special background to any type of b or c tagging is represented by events containing a gluon splitting to heavy quarks (Fig. 7.15). Such a process can happen independently of the flavour of the event, yielding Z decays to light quarks that actually contain heavy-flavoured hadrons. Therefore events with a gluon splitting to heavy quarks represent an irreducible background for the tagging of heavy flavour Z decays: their only peculiarity is that the heavy-flavoured hadrons tend to be close in phase space (*i.e.* in the same hemisphere, and possibly even in the same jet, depending on the clustering parameter chosen) and have a much softer energy spectrum.

The background from $g \to b\bar{b}$ events at some point turned out to be limiting the precision of the R_b measurement; then the LEP collaborations and SLD made an effort to measure the $g \to b\bar{b}$ and $g \to c\bar{c}$ rates from their data samples, to improve the precision on the subtraction of such irreducible background. Most of the measurements were aiming to identifying Z decays

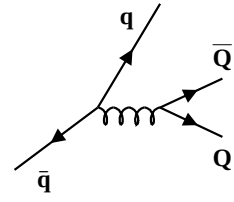

Fig. 7.15 In hadronic Z decays a hard gluon can split to a pair of heavy quarks ($Q\bar{Q}$), yielding heavy flavoured particles in events of any flavour.

to light quarks containing one gluon splitting to heavy quarks. The selection was based on events with 3-jet topologies, where the softer jet was tagged by a lepton, by lifetime, or by a D^*, and it had large invariant mass, while the two most energetic jets were not b- or c-tagged. The $g \to b\bar{b}$ rate was also measured in 4-jet topologies using a fine clustering parameter.

The world average of the available measurements [93] of the rate of Z hadronic decays containing gluon splitting to heavy quarks are:

$$g \to c\bar{c} = 0.030 \pm 0.004 \ , \tag{7.7}$$

$$g \to b\bar{b} = 0.0025 \pm 0.0005 \ . \tag{7.8}$$

7.3 R_b measurements

The large data samples collected by the LEP experiments and SLD, together with the high b tagging capability, yield R_b measurements with a statistical precision in the few permil range. Such a high statistical power calls for extreme care in addressing possible systematic effects.

The breakthrough for achieving a good control of systematic effects has been the use of the single/double tag method, discussed below in Subsection 7.3.1. All the analyses are based on a lifetime tag, sometimes enhanced with information related to vertex mass or lepton transverse momentum. Some experiments have enhanced the method to include other complementary tags (Subsection 7.3.2), obtaining a further gain in precision.

The experimental results measure the ratio of the production cross sections $\sigma_{b\bar{b}}/\sigma_{\rm had}$. The ratio of Z partial widths R_b =

$\Gamma(Z \to b\bar{b})/\Gamma(Z \to \text{hadrons})$ is derived by applying small corrections to account for photon exchange and $\gamma - Z$ interference (typically around $+0.0002$). (The corrected quantity is often indicated as R_b^0 in the experimental papers.)

7.3.1 *The single/double tag method*

The so-called single/double tag methods take advantage of the fact that the hadronization of the two b quarks from the z decay is largely uncorrelated. Therefore it is useful to divide the event in two hemispheres, using the thrust axis, and apply a tag (*e.g.* a lifetime tag) in each hemisphere. The number of hemispheres that fulfil the tag N_h^t and the number of events where both hemispheres fulfil the tag N_{ev}^t, can be measured in a sample of preselected hadronic events N_{ev}, and written in terms of the hemisphere tagging efficiency and Z partial widths for the different quark flavours, as follows

$$N_h^t = 2\,N_{ev}\,\left[R_b\epsilon_b + R_c\epsilon_c + (1 - R_b - R_c)\epsilon_{uds}\right]\ , \tag{7.9}$$

$$N_{ev}^t = N_{ev}\,\left[R_b\epsilon_b^2(1+\rho_b) + R_c\epsilon_c^2 + (1 - R_b - R_c)\epsilon_{uds}^2\right]\ , \tag{7.10}$$

where ϵ_b and ϵ_c are the heavy flavour hemisphere tagging efficiencies, and ϵ_{uds} represents the average tagging efficiency for light quark hemispheres; the sum of the partial widths to the five quark species is taken to be unity. The parameter ρ_b is a correction factor that accounts for possible correlations between the b tagging efficiency in the two hemispheres, discussed in detail below. In principle such a correction is present also for the charm and the light quark terms, but in practice it can be neglected in all existing analyses, because ϵ_c and ϵ_{uds} are much smaller than ϵ_b.

The Eqs. (7.9) and (7.10) can be solved for R_b and ϵ_b; the b tagging efficiency is therefore measured directly from the data and it is not a source of systematic error. Charm and light quark efficiencies, as well as the hemisphere correlation correction, have to be estimated with the simulation.

It is instructive to introduce some approximations in the Eqs. (7.9) and (7.10). Neglecting the charm and light quark contributions, solutions for R_b and ϵ_b can be written as

$$R_b \approx (1+\rho_b)\left(\frac{N_h^t}{2N_{ev}}\right)^2\left(\frac{N_{ev}}{N_{ev}^t}\right)\ , \tag{7.11}$$

$$\epsilon_b \approx \frac{1}{1+\rho_b}\left(\frac{N_{ev}^t}{N_{ev}}\right)\left(\frac{2N_{ev}}{N_h^t}\right)\ . \tag{7.12}$$

The statistical error on R_b is dominated by the double tagging fraction N^t_{ev}/N_{ev}, that has the largest uncertainty (simply because it involves smaller numbers). A shift in the values assumed for ρ_b, ϵ_c and ϵ_{uds} translates to a shift in the measured value of R_b as follows:

$$\frac{\Delta R_b}{R_b} \approx -\,\Delta\rho_b \ , \tag{7.13}$$

$$\frac{\Delta R_b}{R_b} \approx -\,\frac{R_c}{R_b}\,\frac{\epsilon_c}{\epsilon_b}\,\frac{\Delta\epsilon_c}{\epsilon_c} \ , \tag{7.14}$$

$$\frac{\Delta R_b}{R_b} \approx -\,\frac{1-R_b-R_c}{R_b}\,\frac{\epsilon_{uds}}{\epsilon_b}\,\frac{\Delta\epsilon_{uds}}{\epsilon_{uds}} \ . \tag{7.15}$$

The relation (7.13) shows that the error on ρ directly reflects to a relative shift in R_b; therefore a measurement of R_b at a few permil level implies that the hemisphere correlation correction must be controlled at the permil level. The other two equations show that systematic effects due to ϵ_c and ϵ_{uds} scale with the ratios between those efficiencies and the ϵ_b, therefore a tag with high efficiency and purity not only gives more statistical power but also helps reducing the systematic uncertainties from the background efficiencies estimated with the simulation.

Hemisphere-hemisphere correlations

Hemisphere-hemisphere correlations turn out to be the most challenging source of systematic uncertainty.

Correlations may arise from many different effects. One simple example of detector-related effect is the polar angle dependence of the tag efficiency, especially relevant for lifetime tags, that have full performance only if the b decay products are inside the vertex detector acceptance: the two b jets tend to be back-to-back, and therefore tend to be both inside or both outside the high performance region, which gives a positive correlation. Limiting this effect is one of the reasons to restrict the lifetime-based analyses to events well contained in the vertex detector. Also inefficient regions due to detector failures may give rise to correlations, as the two b jets cannot both cross the faulty detector: in this case the induced correlation is negative.

An example of physics source of correlation is the radiation of energetic gluons in the final state: in events with substantial gluon emission both b hadrons than to be less energetic, thus having both lower tagging probability than average, which gives a positive correlation. In about 2% of the events a hard gluon is emitted, that produces the most energetic jet of the event and dominates the calculation of the thrust axis; the two b jets are

reconstructed in the same hemisphere, leading to a negative correlation.

The most complicated effects, however, arise through the reconstruction of the primary vertex. As discussed in Subsection 7.2.2, the precision obtained in the determination of the primary vertex position is degraded in heavy flavour events, due to the presence of particles that originate from the heavy hadron decay points. The degradation has a large dependence on the heavy flavour hadron momentum: in the case of energetic hadrons, the fragmentation tracks are fewer and softer (and therefore less precisely measured because of multiple scattering), and therefore the primary vertex position measurement is less precise. As a result, an event that has in one hemisphere a high-energy hadron, with higher-than-average tagging probability, will have the primary vertex determination spoiled, and therefore the tagging probability for the other hemisphere lower than average; therefore a negative correlation between the two hemispheres. Such an effect can be as large as several percent, and cannot be reliably estimated with the simulation, because it depends on the b hadron momentum spectrum as well as on all other details of the fragmentation. With the increase of the statistics collected, the experiments have decided to perform the primary vertex determination separately in the two hemispheres, so avoiding this kind of effects, at the expenses of some statistical power. The information on the beam spot position can be safely used for both hemispheres, as it has no interplay with the b hadron production and decay properties.

The different effects contributing to the hemisphere correlation correction cannot really be disentangled, as they are all correlated. However some test variables can be defined, to check the accuracy of the simulation. First of all one has to identify a variable that is related to the effect to be investigated. For example, effects related to the variation of the tagging efficiency in the different detector regions can be investigated using the polar and azimuthal angle of the thrust axis. Effects related to gluon emission can be studied using the jet momentum. A dependence of the tagging efficiency in one hemisphere upon the variable calculated in the other hemisphere (or on the variable itself, if defined on the whole event as in the case of the thrust axis) is an indication of an underlying source of correlation.

The quantity

$$\rho_b^v = \frac{\int f_b(v)\epsilon_b^{\mathrm{same}}(v)\epsilon_b^{\mathrm{oppo}}(v)dv}{\left[\int f_b(v)\epsilon_b^{\mathrm{same}}(v)dv\right]^2} - 1 \ , \tag{7.16}$$

is taken as an estimator of the contribution of the effect associated with the variable v to the correlation correction. In the formula, $f_b(v)$ is the distri-

bution of b hemispheres as a function of v, and "same"/"oppo" refer to the same/opposite hemisphere where the variable v is calculated. The difficulty is that the formula has to be evaluated on b events, and it is therefore not directly accessible on data. An approximate procedure consists in estimating ρ_b^v in a data sample enriched in b events by applying a mild b tag cut; the remaining udsc background as well as the bias introduced by the b tag cut are corrected for with the simulation, allowing for large uncertainties associated with such corrections; the result obtained gives an indication of the size of the effect, and allows a comparison with the corresponding quantity measured in simulated data.

Other sources of systematic uncertainty

The other sources of systematic uncertainty are related to the estimate of the light quark and charm efficiencies from simulated data.

As discussed in Subsection 7.2.2, light quark events can be selected because of mis-measured tracks, long-lived particles, photon conversions, interactions with the detector material, or gluons splitting to heavy quarks, that is by far the largest source. The experimental error on the rates $g \to b\bar{b}$ and $g \to c\bar{c}$ is used to assess the associated uncertainties.

The charm background is much more relevant, and needs careful treatment. The measured fractions of weakly-decaying c hadrons (Table 7.3) and their lifetimes are implemented in the simulation, and their experimental errors are used to estimate the associated uncertainty. The decay channels of the c hadrons are also relevant, but unfortunately many of them are rather poorly known. The decay properties that have the largest impact on the tagging probability are the number of charged particles produced; therefore the inclusive measurement of the decay multiplicities from MARK III [94] are used. A special treatment is needed, however, for the decay $\mathrm{D} \to \mathrm{K}^0 X$, where the K^0 typically carries away a large fraction of the energy, yielding a particularly low tagging probability. For this specific channel the measured exclusive branching ratio is used.

In order to solve Eqs. (7.9) and (7.10), an input value is needed also for R_c. Typically the experiments use as input the Standard Model value, and compute the dependence (derivative) of the measured R_b value on the R_c input value, which is then used as input to a global fit to all the measured heavy flavour electroweak observables [142].

7.3.2 *Multi-tag methods*

The single/double tag method can be extended to include several mutually exclusive tags, having different efficiencies for the different flavours. In the final ALEPH and DELPHI measurements [95] five tags were used: one main b-tag with high efficiency and purity, two other complementary b-tags (with lower performance), one c-tag and one uds-tag. For N tags, there are N single-tag rates and $N(N+1)/2$ double tag rates to measure. If events are divided in three flavour classes: b, c and light quarks (as in the single/double tag method), those observables can be expressed in terms of R_b, R_c, $3N$ hemisphere tag efficiencies, and $3N(N+1)/2$ hemisphere correlation corrections (one per flavour class and per tag combination). In the actual measurements the charm and light quark efficiencies for the main tag are estimated from the simulation, as well as the 45 correlations, while the remaining 13 efficiencies are extracted from the fit to the 20 observables. The fact that the efficiencies of the complementary tags are extracted from the data, allows to use fairly complicated algorithm, since an accurate simulation of their performance is not required. The statistical power of the method improves by about $10-20\%$ compared to a single/double tag method based on the main tag only. The increased statistical power can be used to tighten the selection cut on the main tag, or to further restrict the fiducial region where the analysis is performed, to reduce the systematic uncertainty from background sources. The sensitivity to the hemisphere correlation of the primary tag is also reduced compared to a single/double tag method, however the uncertainties coming from the other correlation coefficients have to be estimated.

7.3.3 R_b *results*

The combination of the R_b measurements from SLD and the LEP experiments [95] is performed with a global fit that includes the R_c measurements described below and the heavy-flavour forward-backward asymmetries described in Subsection 8.3.2. This common procedure takes into account the correlations among various measurements and treats in an optimal way the systematic uncertainties [142]. The photon exchange and $\gamma-Z$ interference corrections are applied by the individual experiments before the combination, as they can be slightly affected by the event selection cuts. The result is

$$R_b = 0.21629 \pm 0.00066$$

in agreement with the MSM expectation. Within the MSM this result depends solely on the top mass and can be used to set an indirect limit on its value (Section 10.3).

7.4 R_c measurements

As previously discussed, charm events have intermediate properties between b events and light quark events, for nearly all discriminating variables. As a consequence, charm tags have significantly worse efficiency/purity figures compared to b tags, and the R_c analyses reach statistical precision in the few percent range, rather than few permil.

Several methods have been employed by SLD and the LEP experiments to measure R_c, that can be classified as follows:

- single-double tag methods, using the same tag in the two hemispheres (as for the R_b analyses);
- single-double tag methods, using an exclusive tag in one hemisphere, and an inclusive tag in the other hemispheres;
- charm counting analyses;
- measurements based on leptons.

The four types of analyses contribute with approximately equal weights in the overall combination.

In general, in R_c analyses the remaining b background is extracted from the data by applying a b tagging in the hemisphere opposite to the selected charm candidate; therefore R_c results have typically a small dependence on the assumed value of R_b.

As in the case of R_b, a small correction (≈ 0.0002) accounting for photon exchange and $\gamma - Z$ interference has to be applied.

7.4.1 *Single/double tag*

This method is most effective at SLD, where the particularly favourable experimental conditions allow a high performance c-tag to be obtained (about 14% efficiency for 67% purity), with the method discussed in Subsection 7.2.2. The SLD result has approximately the same precision as the combination of all the LEP analyses [96].

At LEP a single/double tag analysis has been performed by ALEPH using a reconstructed D meson tag, and by DELPHI using a soft pion

tag. The ALEPH analysis is severely limited by the statistics (the selection yields 89% purity but only 2.5% efficiency), while the DELPHI analysis is limited by the understanding of the background in the single-tag sample.

7.4.2 *Inclusive/exclusive tag*

As discussed in the above paragraph, the measurement of R_c at LEP is limited either by the systematic uncertainty in the composition of the single-tag sample, if an inclusive tag is used, or by the poor statistics of the double-tag sample, in the case of exclusive tags. An effective compromise consists in using an exclusive tag for the single-tag sample, and combine it with an inclusive tag for the double tag sample.

First, the rate of hemispheres with a reconstructed $\mathrm{D}^{*+} \to \mathrm{D}^0\pi^+$ is measured. The D^0 is reconstructed in the "golden" channel $\mathrm{K}^-\pi^+$ plus possibly other channel with known branching ratios. Unfolding the D^0 branching ratios and the reconstruction efficiency (taken from the simulation) the measured rate can be written in terms of $R_c \times P(c \to \mathrm{D}^*) \times \mathrm{BR}(\mathrm{D}^{*+} \to \mathrm{D}^0\pi^+)$.

Then, a sample of events enriched in charm is selected by requiring a high energy fully reconstructed D^* in one hemisphere, and the D^* rate in the opposite hemisphere is measured by selecting soft pions: such a rate is proportional to $P(c \to \mathrm{D}^*) \times \mathrm{BR}(\mathrm{D}^{*+} \to \mathrm{D}^0\pi^+)$ (unfolding selection efficiency and background), so that the ratio of the two measured rates gives R_c.

The method still requires that the efficiencies and purities for the exclusive reconstruction of the D^*, and for the inclusive selection of π_s, are correctly estimated with the simulation, while uncertainties in the fragmentation of the charm quark cancel in the ratio.

7.4.3 *Lepton analyses*

The R_c parameter can also be inferred from the measured rate of prompt leptons in hadronic Z decays. Higher precision is obtained if the lepton yield is analysed as a function of the lepton momentum and transverse momentum, as such variables discriminate the different sources (Subsection 7.2.1). The total lepton spectrum can be written as

$$\begin{aligned} \mathcal{F}(p, p_\perp) \quad &= R_b\, P_b(p, p_\perp)\epsilon_b(p, p_\perp) \\ &+ R_c\, P_c(p, p_\perp)\epsilon_c(p, p_\perp) \\ &+ (1 - R_b - R_c)\, f_{uds}(p, p_\perp)\ , \end{aligned} \tag{7.17}$$

where $P_{b,c}(p, p_\perp)$ describe the total lepton yields in b and c events, $\epsilon_b(p, p_\perp)$ are the identification efficiencies, and $f_{uds}(p, p_\perp)$ is the probability of selecting a lepton candidate in light quark events.

The shape of the b contribution (including selection efficiency) can be extracted from the data, by applying a b tag in one hemisphere, and studying the lepton yield in the opposite hemisphere. Small corrections have to be applied to subtract the residual non-b background, and to account for distortions in the $(p, p_\perp)$ spectrum caused by the b-tag cut, through kinematic correlations between the b hadrons in the two hemispheres (discussed in Subsection 7.3.1).

The shape of the light quark background can be also studied in the data, by selecting samples of photon conversions and identified hadrons.

The $(p, p_\perp)$ shape of the charm contribution is obtained from a fit to data collected at e^+e^- experiments above the charm production threshold.

Once the three shapes are known, a fit to the spectrum measured on the data is performed leaving the normalization of the b and c contributions free. The normalization of the c contribution can be written as $R_c \times BR(c \to \ell)$. The inclusive $c \to \ell^+$ branching ratio is measured independently at LEP by studying the lepton yield opposite to a high-energy D^*.

7.4.4 *Charm counting*

The final state c hadrons can be fully reconstructed at LEP, as shown in Fig. 7.12, in particularly convenient decay channels. Taking as example the $\mathrm{D}^0 \to \mathrm{K}^-\pi^+$ channel, the measured yield after background subtraction can be written as $R_c\, f(\mathrm{D}^0)\, \mathrm{BR}(\mathrm{D}^0 \to \mathrm{K}^-\pi^+)\epsilon_{\mathrm{D}^0 \to \mathrm{K}^-\pi^+}$, where $f(\mathrm{D}^0)$ is the probability that a c quark from the Z decay eventually produces a D^0, and ϵ is the selection efficiency. The subtraction of the b contribution and of the combinatorial background is performed as explained in Subsection 7.2.3. Folding the known value of the decay branching ratio and the reconstruction efficiency estimated with the simulation, $R_c\, f(\mathrm{D}^0)$ can be extracted. If the measurement is repeated for the four c hadron species of Fig. 7.12, one can assume that the four production probabilities add up to one, with a small correction for the unmeasured charmed strange baryon yield. Such a correction is taken to be 15% of the Λ_c rate.

Imposing the constraint

$$f(\mathrm{D}^0) + f(\mathrm{D}^+) + f(\mathrm{D_s}) + 1.15 \pm 0.05 f(\Lambda_c) = 1 \ , \qquad (7.18)$$

R_c can be extracted from the four measured rates, deriving at the same

time the production probabilities (Table 7.3), that are used to estimate the c background in the R_b analyses.

7.4.5 R_c^0 results

The R_c results from SLD and the LEP experiments [96] are combined with the procedure mentioned in Subsection 7.3.3, yielding

$$R_c = 0.1721 \pm 0.00030$$

in agreement with the MSM expectation. Within the MSM this result is essentially independent of parameters as the top, the Higgs mass or the strong coupling constant, which cancel in the ratio.

The precise determinations of R_b and R_c presented in this Chapter are compared to the MSM expectation in Fig. 7.16.

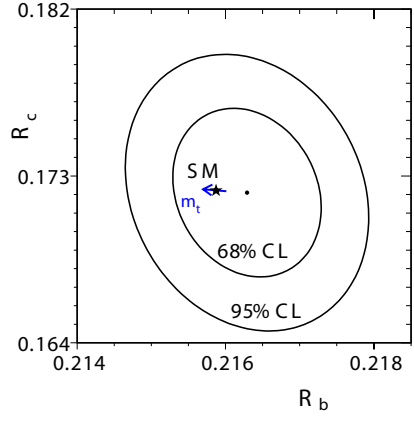

Fig. 7.16 The 68% CL contour for R_b and R_c compared to the prediction of the MSM. The star indicates the prediction of the SM for a top mass of 172 GeV, and the arrow the direction of growing top mass. The size of the arrow corresponds to a top mass variation of about 9 GeV. (Courtesy of the LEP Electroweak Working Group.)

Chapter 8

Asymmetries at the Z pole

A distinct feature of electroweak neutral interactions is the difference between right-handed and left-handed currents. This difference is regulated by the Weinberg electroweak mixing angle $\sin^2\theta_W$, that enters the vector coupling of the Z to right-handed and left-handed fermions. The different behaviour of the Z in presence of fermions of opposite chiral states has a direct consequence on experimental data, causing measurable asymmetries that can be used to determine the mixing angle and, using information from the Z partial widths, the couplings themselves.

As a first example, if a polarized electron beam collides with unpolarized positrons at a centre-of-mass energy equal to m_Z, the total cross section will be different, and much higher, if left-handed polarization is used. The relative difference between the two cross sections ($\sigma_{_L}$ and $\sigma_{_R}$) is the left-right asymmetry (A_{LR}) introduced in Section 2.5, related to the right-handed (g_{Le}) and left-handed (g_{Re}) electron couplings by

$$A_{LR} = \frac{\sigma_{e^-_{_L}} - \sigma_{e^-_{_R}}}{\sigma_{e^-_{_L}} + \sigma_{e^-_{_R}}} = \frac{g^2_{Le} - g^2_{Re}}{g^2_{Le} + g^2_{Re}} \equiv \mathcal{A}_{\rm e}\,. \tag{8.1}$$

As $g_{_L} = \frac{g_{V{\rm e}}+g_{A{\rm e}}}{2}$ and $g_{_R} = \frac{g_{V{\rm e}}-g_{A{\rm e}}}{2}$ one can see that $\mathcal{A}_{\rm e}$ depends on the ratio between vector ($g_{_{V{\rm e}}}$) and axial vector($g_{_{A{\rm e}}}$) coupling constants of the electron:

$$\mathcal{A}_{\rm e} = \frac{2\ g_{_{V{\rm e}}} g_{_{A{\rm e}}}}{(g_{_{V{\rm e}}})^2 + (g_{_{A{\rm e}}})^2} = \frac{2\ g_{_{V{\rm e}}}/g_{_{A{\rm e}}}}{1 + (g_{_{V{\rm e}}}/g_{_{A{\rm e}}})^2}\ . \tag{8.2}$$

The ratio of leptonic couplings is used for the operative definition of $\sin^2\theta_{W,eff}$, the *effective* electroweak mixing angle, introduced in Section 3.3:

$$\sin^2\theta_{W,eff} \equiv \frac{1}{4}\left(1 - \frac{g_{V\ell}}{g_{A\ell}}\right)\ . \tag{8.3}$$

In the reaction $e^+e^- \to Z \to f\bar{f}$ with unpolarized beams, the same effect causes the Z to be polarized along the direction of the beams. Indeed, because of angular momentum conservation, left-handed (right-handed) electrons interact with opposite-helicity positrons only (Eq. (2.45)) and the different cross sections of the two processes cause parity violation and a net Z polarization opposite to the direction of the electron beam. The amount of polarization is exactly $\mathcal{A}_e$. The Z polarization, and therefore $\mathcal{A}_e$, can be measured by analysing the polarization of the fermion emitted by the Z boson since, once again, angular momentum conservation relates the two quantities. In practice this is possible only if the emitted fermion is a tau lepton, by measuring the tau polarization in $e^+e^- \to Z \to \tau\bar{\tau}$. Alternatively, one can take advantage of parity violation in the decay of the Z, causing the emitted anti-fermion ($\bar{f}$) being directed preferentially along the direction of the Z spin, with the fermion (f) in the opposite direction. This effect originates a forward-backward asymmetry of the fermion emission with respect to the initial electron beam. The forward-backward asymmetry is defined as (Eq. (2.86))

$$A_{FB} = \frac{\sigma_F - \sigma_B}{\sigma_F + \sigma_B} \tag{8.4}$$

where σ_F is the cross section for fermions emitted in the hemisphere centered along the direction of the electron beam, while σ_B is for fermions in the opposite hemisphere. The relationship between the forward-backward asymmetry and the couplings is given by Eq. (2.93).

In next Sections the main issues related to the measurements of the left-right asymmetry, of the tau polarization in Z decays and of the forward-backward asymmetry are discussed in some detail. The various measurements are compared in the last Section where combined values of $\sin^2\theta_{W,eff}$ and of the lepton couplings are given.

8.1 Measurement of the left-right asymmetry (A_{LR})

The measurement of A_{LR} requires the avalaibility of longitudinally polarized beams. At SLC longitudinal polarization of the electron beam was achieved by a circularly polarized laser source hitting a GaAs photocathode [98], allowing SLC to be operated with an electron beam polarization of about 75%. Since a fully polarized electron beam cannot be produced, Eq. (8.1) has to be modified to take into account the average beam polar-

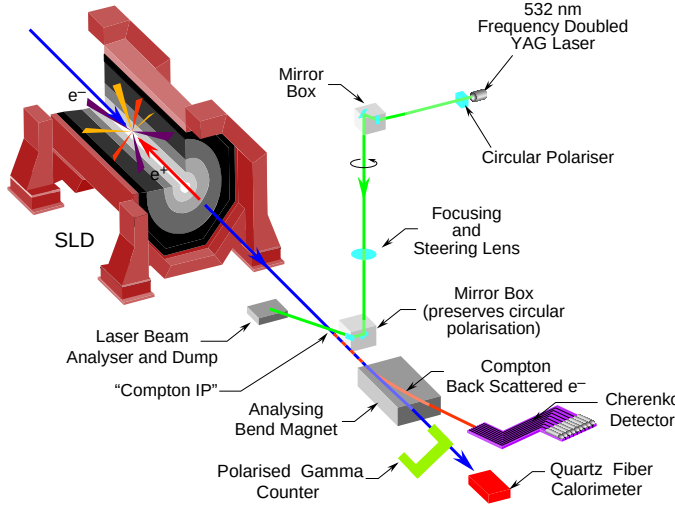

Fig. 8.1 The schematic layout of the SLD compton polarimeter.

ization ($\mathcal{P}_e$), becoming

$$A_{LR} = \frac{1}{\mathcal{P}_e} \frac{\sigma_L - \sigma_R}{\sigma_L + \sigma_R}. \tag{8.5}$$

The main experimental issue, for a precise measurement of A_{LR}, is an accurate determination of the beam polarization. This need could be overcome if both electron and positron beams could be independently polarized. By performing three independent measurements, the first with polarized electrons and unpolarized positrons, the second with polarized positrons and unpolarized electrons, and a third one with both polarized beams, A_{LR} and the two beam-polarizations could be determined without the need of external inputs. This scheme was originally proposed for LEP [97], but never went into operation. The standard SLC operating cycle consisted of two close electron bunches, the first of which was polarized, while the other was used to produce unpolarized positrons. The sign of the electron polarization was randomly chosen, so that the measurement was not affected by time variations of the apparatus efficiency.

The SLD experiment monitored the longitudinal SLC-beam polarization with a polarimeter based on Compton scattering of electrons by circularly polarized light of a Nd:YAG laser beam. The measurement took place after the interaction point, as shown in Fig. 8.1. The Compton cross sections

for spin-parallel (j=3/2) and spin anti-parallel (j=1/2) interactions are different, and this difference is a function of the normalized scattered-photon energy fraction (x). The difference can be written, in terms of x, as

$$\frac{d\sigma^{3/2}}{dx} - \frac{d\sigma^{1/2}}{dx} = \frac{d\sigma}{dx}(1 - \mathcal{P}_\gamma \mathcal{P}_\mathrm{e} A(x)) \tag{8.6}$$

where $A(x)$ is the Compton asymmetry function [99]. The asymmetry reaches its maximum at the kinematic endpoints (full forward- or back-scattering). At SLD the Compton-scattered electrons were deflected by the first beam line dipole after the interaction point and entered a threshold Cerenkov detector segmented in seven cells transverse to the beam line (Fig. 8.1). Many Compton interactions were produced at every laser pulse and all channels of the polarimeter integrated the signal of several Compton scatters and background. The laser fired every 7th beam crossing (SLD frequency was 120 Hz) and the other six were used to monitor the background in the Cerenkov counters. The laser beam polarization, typically 99.8%, was continuously monitored. The statistical accuracy on $\mathcal{P}_\mathrm{e}$ was of $\pm 1\%$ every three minutes. The relative systematic uncertainties [100, 101] in the polarization measurement are summarized in Table 8.1. The last entry of this table is the uncertainty on the difference between the measured polarization and the polarization at the interaction point (IP). The latter is computed as $\mathcal{P}_\mathrm{e}(1+\eta)$, where η is a small correction. It is mainly due to off-energy electrons which do not contribute to the effective luminosity and to the small spin precession of the electron beam in the focusing elements between the interaction point and the Compton polarimeter. The depolarization of the electron beam during the $\mathrm{e^+e^-}$ collision was checked by measuring the polarization with and without beam collisions and was found to be negligible. To derive the left-right asymmetry, the mean luminosity-weighted electron polarization

$$\langle \mathcal{P}_\mathrm{e} \rangle = (1+\eta)\frac{1}{\mathrm{N_Z}} \sum_{\mathrm{i}=1}^{\mathrm{N_Z}} \mathcal{P}_\mathrm{i} \ , \tag{8.7}$$

estimated from measurements of $\mathcal{P}_\mathrm{e}$ made when Z events were recorded was used. The total contribution of the systematic uncertainty on the beam polarization to the measurement of A_{LR} was 0.52 % (high-statistics 1997/8 run); this is the main source of systematic uncertainty in the left-right asymmetry measurement.

The asymmetry of the left-right rates was measured with a simple event selection, since A_{LR} does not depend on the final state as long as this

Table 8.1 Relative (%) systematic uncertainties on the electron beam polarization at SLD in two data-taking periods.

Source of uncertainty	1994/5 (%)	1997/8 (%)
Laser Polarization	0.2	0.1
Detector Linearity	0.5	0.2
Detector Calibration	0.29	0.40
Electronic Noise	0.20	0.20
Transport from polarimeter to SLD IP	0.17	0.15

is an s-channel process. Care must be only taken in rejecting Bhabha scattering events, because of the t-channel contribution to $e^+e^- \rightarrow e^+e^-$. The event selection was focused on high-multiplicity events: at least four charged tracks and at least 22 GeV of visible energy in the calorimeters were required, with an energy imbalance (ratio of vector to scalar energy sum in the calorimeter) less than 0.6. The total sample comprised approximately 537000 Z decays and was mostly made of hadronic events, with a small tau contributions ($\sim 0.3\%$). The events produced with left-handed (N_L) and right-handed (N_R) polarization were counted and their asymmetry $A_m = (N_L - N_R)/(N_L + N_R) \sim 0.12$ was measured. The measured asymmetry is related to A_{LR} by the following expression

$$A_{LR} = \frac{A_m}{\langle \mathcal{P}_e \rangle} + \frac{1}{\langle \mathcal{P}_e \rangle}[f_b(A_m - A_b) - A_L + A_m^2 A_{\mathcal{P}} \\ -E_{cm}\frac{\sigma'(E_{cm})}{\sigma(E_{cm})}A_E - A_\epsilon + \langle \mathcal{P}_e \rangle \mathcal{P}_p] \quad (8.8)$$

where a number of small corrections, listed below, are incorporated. In Eq. (8.8) A_X indicates the left-right asymmetry of X, defined as $A_X \equiv \frac{X_L - X_R}{X_L + X_R}$. The first term in the square bracket represents the correction for the background: f_b is the background fraction and A_b the background left-right asymmetry. The second term represents the asymmetry of the integrated luminosity, while the third term takes into account the asymmetry in the beam left and right absolute polarizations. The fourth term corrects for the different centre-of-mass energies when left or right beams are used: $\sigma'(E_{cm})$ is the derivative of the cross section with respect to E_{cm}. The fifth term represents the left-right asymmetry in selection efficiency: it is totally negligible for an apparatus with symmetric acceptance in polar angle. Finally, the last term corrects for possible longitudinal polarization of the positron beam. This was measured with a dedicated experiment based

on Möller scattering and found negligible. The sum of the corrections in the square brackets of Eq. (8.8) gives $[+0.16 \pm 0.07]\%$ for the 1997/8 high luminosity run.

The left-right asymmetry depends on the centre-of-mass energy because of the Z - γ s-channel interference. The energy dependence can be computed from Eq. (2.96) as

$$A_{LR}(s) = \mathcal{A}_{\mathrm{e}} + 0.00002\Delta E(MeV) + 0.00005 \tag{8.9}$$

where ΔE is the difference between m_Z and the actual centre-of-mass energy, while the constant term accounts for the correction due to the imaginary part of $\Delta\alpha$. In order to apply the correction and compute the asymmetry at the Z pole the centre-of-mass energy of the experiment must be precisely known. SLC employed two energy spectrometers (one for the electron and one for the positron beam) calibrated, through an energy scan, to the precise measurement of m_Z at LEP. The measured average offset was -46 MeV and the total centre-of-mass energy uncertainty 29 MeV. The measured left-right asymmetry is also corrected for the effect of initial state radiation (the most sizeable QED correction, which lowers the asymmetry as expected from Eq. (8.9)), for the effect of pure photon exchange (which slightly dilutes the asymmetry) and for other higher order QED/electroweak effects (as the already mentioned imaginary part of $\Delta\alpha$). The total correction (including the centre-of-mass energy offset) is 0.00358 ± 0.00058, the error being essentially due to the uncertainty on the beam energy. (The corrected measurement is indicated as $A^0_{LR\cdot}$.) When this uncertainty is added in quadrature to the uncertainty on the electron beam polarization and the uncertainty on the corrections of Eq. (8.8) a total systematic error on A^0_{LR} of 0.64 % is obtained.

The final result, including the statistical errors, is

$$A^0_{LR} = 0.15138 \pm 0.00216 \tag{8.10}$$

$$\sin^2\theta_{W,eff} = 0.23097 \pm .00027 \tag{8.11}$$

giving the most precise measurement of the weak mixing angle.

8.2 Measurement of the tau polarization in Z decays

Each Z decay into an $f\bar{f}$ pair can be characterized by the direction and the chiral state of the emitted fermion f. Defining as forward the hemisphere where the electron beam is pointing, the events can be subdivided

into four categories: FR, BR, FL and BL corresponding to right-handed (R) or left-handed (L) fermions emitted in the forward (F) or backward (B) direction. The forward-backward polarization asymmetry and the polarization asymmetry can be defined as:

$$A_{pol}^{FB} = \frac{\sigma_{F,R} - \sigma_{F,L} + \sigma_{B,L} - \sigma_{B,R}}{\sigma_{tot}} \tag{8.12}$$

$$A_{pol} = \frac{\sigma_{F,R} + \sigma_{B,R} - \sigma_{F,L} - \sigma_{B,L}}{\sigma_{tot}} = \frac{\sigma_R - \sigma_L}{\sigma_{tot}} \tag{8.13}$$

where σ_{tot} is the total cross section, measured adding up the cross sections of the four categories. The forward-backward polarization asymmetry A_{pol}^{FB} depends on the polarization of the Z produced in the e^+e^- collision while is not sensitive to the flavour of the fermion emitted in the Z decay. The polarization asymmetry A_{pol} corresponds to Eq. (2.91), depends only on the chiral state of the fermions emitted in the decay of the Z and is not sensitive to parity violation at production. Indeed, by means of the cross sections given in Eqs. 2.68-2.71 and integrating over the two hemispheres one gets

$$A_{pol}^{FB} = -\tfrac{3}{4}\mathcal{A}_{\mathrm{e}} \tag{8.14}$$

$$A_{pol} = -\mathcal{A}_f. \tag{8.15}$$

For massless fermions the chiral states, defined in Section 2.2 using the operators $\frac{1 \pm \gamma_5}{2}$, are equal to to the helicity states. For fermions with masses much smaller than the Z mass this is still true, up to corrections $\mathcal{O}(\frac{m_f^2}{m_Z^2})$, justifying the use of the name "polarization" for these asymmetries. Experimentally, the two asymmetries require the measurement of the polarization of the fermion and this can be done, statistically, only for the channel $Z \to \tau^+\tau^-$.

The helicity of the two taus from Z decay are nearly 100% anti-correlated, again except for very small $\mathcal{O}(\frac{m_f^2}{m_Z^2})$ corrections. In order to determine the two asymmetries defined by Eqs. (8.13) and (8.12) it is convenient to measure the τ polarization as a function of the angle (θ) between the τ^- and the electron beam. The definition of the tau polarization for any $\cos\theta$ bin is given by

$$P_\tau = \frac{\sigma_R - \sigma_L}{\sigma_R + \sigma_L}, \tag{8.16}$$

where σ_R is the cross section to produce a right-handed τ^- and σ_L is the cross section to produce a left-handed τ^-. The polarization asymmetry

(A_{pol}) is equal to the tau polarization measured on the entire $\cos\theta$ range and the forward-backward polarization asymmetry (A_{pol}^{FB}) is given by the tau polarization measured in the forward and in the backward direction.

The dependence of the tau polarization on θ is readily computed in improved Born approximation at the Z pole from Eqs 2.68–2.71. The ratio of the two equations

$$\frac{d(\sigma_R - \sigma_L)}{d\cos\theta} = -\frac{3}{8}\sigma_{f\bar{f}}^{tot}[\mathcal{A}_\tau(1+\cos^2\theta) + 2\mathcal{A}_\mathrm{e}\cos\theta] \tag{8.17}$$

$$\frac{d(\sigma_R + \sigma_L)}{d\cos\theta} = \frac{3}{8}\sigma_{f\bar{f}}^{tot}[(1+\cos^2\theta) + 2\mathcal{A}_\mathrm{e}\mathcal{A}_\tau\cos\theta] \tag{8.18}$$

gives

$$P_\tau(\cos\theta) = \frac{A_{pol}(1+\cos^2\theta) + \frac{8}{3}A_{pol}^{FB}\cos\theta}{(1+\cos^2\theta) + \frac{8}{3}A_{FB}\cos\theta} \tag{8.19}$$

where A_{FB} indicates the forward-backward asymmetry of the tau pairs. All four LEP experiments have measured the two asymmetries by means of a fit to the observed $P_\tau(\cos\theta)$ distribution to Eq. (8.19). This procedure gives better total error than measurements integrated over the hemispheres by giving more weight to $\cos\theta$ bins with higher sensitivity. This fit allows $\mathcal{A}_\mathrm{e}$ and $\mathcal{A}_\tau$ to be measured simultaneously and, assuming universality, gives a determination of $\sin^2\theta_{W,eff}$.

The polarization of the τ is measured exploiting the parity violation of its weak decay [102], that is mediated by a pure V-A current. Five tau decay channels, amounting to a branching ratio of about 90% are used ($\tau \to \pi\nu$, $\tau \to \rho\nu$, $\tau \to \mathrm{a}_1\nu$, $\tau \to \mathrm{e}\nu\bar{\nu}$, $\tau \to \mu\nu\bar{\nu}$). Tau decays to charged kaons, having relatively low branching ratio, are included in the corresponding pion channels. Tau decay modes with more than three pions in the final states are not used in the measurement because the corresponding experimental samples show a significant background contamination; furthermore the description of their decays depends on model assumptions.

The principle of the polarization analysis is more easily understood by taking the simplest channel, $\tau \to \pi\nu$. The tau decay in this channel, for the two helicity cases, is sketched in Fig. 8.2. Because of the left-handedness of the neutrino, in case of decays of right-handed taus, the pion is boosted in the direction of the tau. The opposite is true for decays of left-handed taus. It follows that the energy of the pion discriminates between the two parent-tau helicity states. The tau differential decay width, given in term of the scaled pion energy $x_\pi = \frac{E_\pi}{E_{beam}}$ is

$$\frac{1}{\Gamma}\frac{d\Gamma}{dx_\pi} = 1 + P_\tau(2x_\pi - 1) \tag{8.20}$$

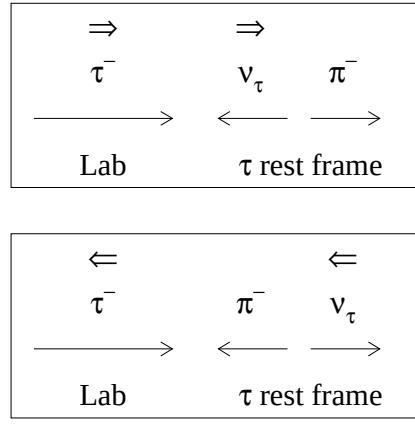

Fig. 8.2 The principle of the tau polarization analysis taking the $\tau \to \pi\nu$ channel as an example.

as can be shown by boosting into the laboratory frame the rest-frame decay angular distribution of a spin 1/2 particle decaying into two particles of spin 1/2 and spin 0, respectively. (The rest-frame angular distribution is $\sim (1 + P_\tau \cos\theta^*)$, where θ^* is the decay angle of the pion in the rest frame of the tau.)

The measurement of the polarization uses two sets of reference decay distributions, one for $P_\tau = -1$ and one for $P_\tau = 1$, obtained applying the $\tau \to \pi\nu$ selection cuts to simulated data. These are produced by generating Monte Carlo events according to Eq. (8.20); each generated event is passed through the full detector simulation. The tau polarization can be extracted by performing a binned maximum likelihood fit of the measured distributions to the sum of the corresponding simulated distributions normalized by the coefficients $N(1 + P_\tau)$ and $N(1 - P_\tau)$. Background events, mostly coming from cross-contamination from other τ decays passing the $\tau \to \pi\nu$ selection, are included in the simulated data. Since decay distributions of a τ^- with given helicity are identical to those of a τ^+ with opposite helicity, the decay distributions of a τ^+ decaying at angle θ can be simply added to the distributions of the τ^- decaying at $\pi - \theta$. Figure 8.3 illus-

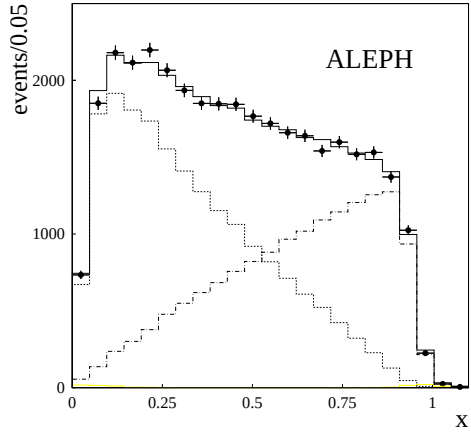

Fig. 8.3 Distribution of the normalized pion energy, x, for $\tau \to \pi\nu$ decays selected by the Aleph experiment. The dotted and dashed lines corresponds to the contributions of left- and right-handed τ's, respectively.

trates this procedure for a sample of $\tau \to \pi\nu$ events collected by the Aleph experiment. The departure of the positive- and negative-helicity reference histogram from the simple linear behaviour given in Eq. (8.20) is due to the selection cuts and to the smearing caused by the experimental resolution. An excess of τ^- with negative helicity is clearly seen.

Multi-pion $\tau \to (2,3)\pi\nu$ hadronic decays, going through vector (ρ) and axial vectors (a_1) resonances, are more complex and more than one variable is needed to fully extract the information on the tau polarization. It has been shown [103] that in each decay channel the tau polarization can be measured in an optimal way by distributions showing a linear dependence on the polarization. The tau decay products can be described by a vector of n observables ($\mathbf{x}$) distributed according to

$$W(\eta) = f(\mathbf{x}) + P_\tau g(\mathbf{x}) \tag{8.21}$$

where the f and g functions satisfies

$$\int f(\mathbf{x}) d^n\mathbf{x} = 1, \int g(\mathbf{x}) d^n\mathbf{x} = 0, \; f \geq 0, \text{ and } |g| \leq f\,. \tag{8.22}$$

As demonstraded in [103] the optimal variable, giving maximal sensitivity to the polarization is

$$\omega = \frac{f(\mathbf{x})}{g(\mathbf{x})} \tag{8.23}$$

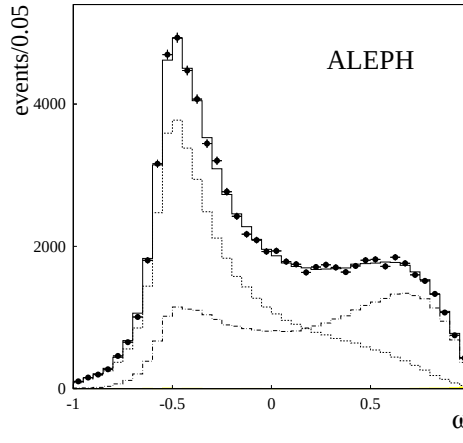

Fig. 8.4 Distribution of the ω variable (see text) for for $\tau \to \rho\nu$ decays selected by the Aleph experiment. The dotted and dashed lines corresponds to the contributions of left- and right-handed τ's, respectively.

which can be represented in the reduced form

$$\begin{aligned}\hat{W}(\omega) &= \hat{f}(\omega)[1 + P_\tau \omega] \\ &= \frac{1}{2}[(1 + P_\tau)\hat{W}^+(\omega) + (1 - P_\tau)\hat{W}^-(\omega)] \end{aligned} \tag{8.24}$$

where the distributions for negative and positive helicities are indicated as W^- and W^-, respectively. The distribution of the ω variable for $\tau \to \rho\nu$ decays is shown in Fig. 8.4; again a clear excess excess of τ^- with negative helicity is observed. The ideal sensitivity for the measurement of the tau polarization in various channels is given in Table 8.2. (The sensitivity is defined as $\frac{1}{\sigma\sqrt{N}}$, where σ is the relative statistical error expected for a sample of N events.) Due to the undetected neutrinos the τ direction cannot be precisely reconstructed and all polarization estimators are defined in the laboratory reference system. For events in which both τ's decay to hadrons, however, it is possible to make an approximated measurement of the τ direction [106] which is used to gain sensitivity, as shown in Table 8.2. For $\tau \to \ell\nu\bar{\nu}$ leptonic decays the only available information is the momentum of the charged particle: they show reduced sensitivity because of two undetected neutrinos.

The tau polarization measurement requires the selection of $Z \to \tau^+\tau^-$ events and the identification of the τ decay channel. Typical signatures for

Table 8.2 Ideal sensitivities for the polarization measurement in the tau decay channels. Two cases, without and with the measurement of the tau direction, are shown.

Channel	Sensitivity without tau direction	Sensitivity with tau direction
$\tau \to \pi\nu$	0.58	0.58
$\tau \to \rho\nu$	0.49	0.58
$\tau \to a_1\nu$	0.45	0.58
$\tau \to \ell\nu\bar{\nu}$	0.22	-

the decay of the Z boson in two τ's are

- two very collimated jets almost back-to-back,
- a small multiplicity of charge particles,
- large missing energy,
- unbalanced transverse momentum.

The last two features are due to the undetected neutrinos. The selected tau events are divided into two hemispheres along the thrust axis and each hemisphere is analysed to classify the tau decay. The individual tau decay channels are first classified using the multiplicity of the charge particles in the hemisphere. Pions, electrons and muons are separated thanks to the particle identification capabilities of the detectors. Photon reconstruction and π^0 identification is necessary to properly classify tau decays to hadrons. Additional information is provided by the invariant mass of the visible state. Pions are not separated from kaons since they have similar decay distributions. The main background consists of Z decays into electron and muon pairs. It is normally rejected by applying cuts on the hemisphere opposite to the tau under study in order to minimize the energy dependence of the efficiency. Typical selection efficiencies range from 60% to 80%. When both τ's from the same Z decay are used in the polarization measurement the correlated decay distribution [104] has to be used. The main background in the distributions used to measured the tau polarization is the cross-contaminations among different channels. In the $\pi\nu$ channel this is coming from tau decays into $2\pi\nu$ with the photons from the π^0 decays unidentified, similarly in the $2\pi\nu$ channel the main source of background is from τ decays with more than one π^0. The measurement of the polarization is dominated by these two channel ($\tau \to \pi\nu$ and $\tau \to 2\pi\nu$) because of their high sensitivity, large branching ratios and because they can be selected with high purity (ranging from 80% to 95%).

It follows from the analysis procedure that the main systematic errors

are related to inconsistency between data and Monte Carlo. The validity of the Standard Model in describing tau decays has been checked by measuring the tau decay parameters [13] and is assumed in the tau polarization analyses. The decay distributions of $\tau \to \pi\nu$, $\tau \to \rho\nu$ and $\tau \to \ell\nu\bar{\nu}$ are completely determined by Lorentz invariance. This is not true for the $\tau \to \mathrm{a}_1\nu$ decay that depends on "structure functions" [105]. The dependence on the model used for the simulation of this decay is taken into account by varying the model parameters within the limits allowed by the data. This systematic uncertainty is correlated among the various experiments and has to be properly taken into account in combining the measurements. As many kinematic variables used in the fit depend on the momentum, an important source of systematic error is related to the momentum dependence of the selection efficiency. Since the two main channels are affected by the correctness of the photon reconstruction, the simulation of showers in the electromagnetic calorimeter is another important source of systematics. Other source of uncertainties are related to the non-tau background contamination (mainly Bhabha events) and to the cross talk among different tau decay channels. The systematic uncertanties are more important for the measurement of A_{pol} than for A_{pol}^{FB} , since the latter is only affected by sources that are at the same time forward-backward and charge asymmetric.

The angular dependence of the tau polarization has been measured by ALEPH [106], DELPHI [107], L3 [108] and OPAL [109], as can be seen in Fig. 8.5. The experimental data are fitted to Eq. (8.19) in order to extract A_{pol} and A_{pol}^{FB}. The A_{FB} term in Eq. (8.19) is small (~ 0.02) and treated differently by different experiments. In some experiments is expressed in the fitting formula in terms of A_{pol} and A_{pol}^{FB}, in others the measured A_{FB} value or the Standard Model is assumed. The corresponding uncertainties have no effect on the final result. The LEP average [142] is

$$\mathcal{A}_{\mathrm{e}} = -\frac{4}{3}A_{pol}^{FB} = 0.1498 \pm 0.0049 \tag{8.25}$$

$$\mathcal{A}_{\tau} = -A_{pol} = 0.1439 \pm 0.0043. \tag{8.26}$$

The correlation between $\mathcal{A}_{\mathrm{e}}$ and $\mathcal{A}_{\tau}$ is small (+1.2%). To the measurements of A_{pol} and $\frac{4}{3}A_{pol}^{FB}$ a small correction is applied to take into account the difference between the centre-of-mass energy and the Z pole, the effects of the photon exchange, the $Z-\gamma$ interference and initial and final state radiation. The correction amounts to $\sim +0.005$ in both cases and its uncertainty (~ 0.0002) is smaller than in the A_{LR} case because of the precise

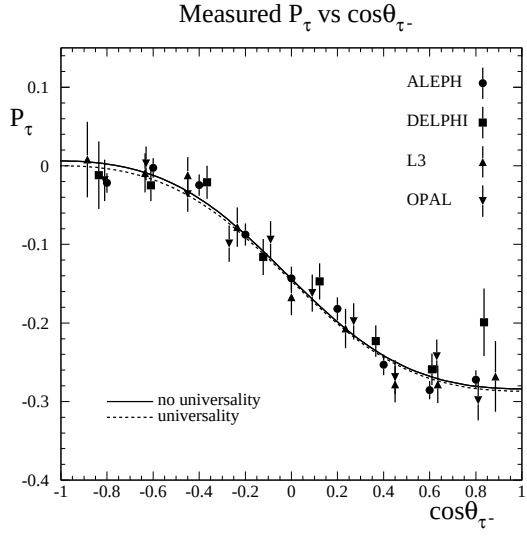

Fig. 8.5 Angular distribution of the tau polarization measured by the four LEP experimets. The solid and dashed lines represents the result of fits without and with the assumption of lepton universality, respectively. (Courtesy of the LEP Electroweak Working Group.)

knowledge of the beam energy at LEP. Assuming lepton universality the two measurements can be eventually combined, giving

$$\mathcal{A}_\ell = 0.1465 \pm 0.0033.$$

The error on this measurement is statistically dominated, the systematic component is equal to 0.0015. The corresponding value of the effective weak mixing angle is

$$\sin^2 \theta_{W,eff} = 0.23159 \pm 0.00041.$$

The $\mathcal{A}_\mathrm{e}$ and $\mathcal{A}_\tau$ measurements from the four LEP Collaborations are shown in Fig. 8.6 and compared to the $\mathcal{A}_\mathrm{e}$ measurement of SLD.

8.3 Forward-backward asymmetries

The measurement of the forward-backward asymmetry (Eq. (8.4)) requires the identification of the charge of the fermion and the measurement of its

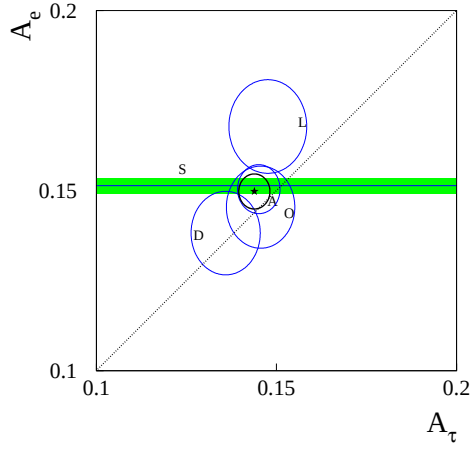

Fig. 8.6 Comparison of the $\mathcal{A}_e$ and $\mathcal{A}_\tau$ measurements by the ALEPH (A), DELPHI (D), L3 (L) and OPAL (O) experiments. The elipses give the standard error countours (corresponding to 39% CL for a two-dimension gaussian). The combination of the four experiments is represented by a star (central value) and a thicker elipse. The horizontal band indicates the $\mathcal{A}_e$ measurement by SLD (S) from the left-right asymmetry; the allowed range is given by plus and minus one standard deviation with respect to the central value.

direction. A_{FB} has been measured for individual lepton species (e, μ, τ), for heavy quarks (c and b) and inclusively for hadrons. Assuming lepton universality the ratios of the couplings of the Z to charged leptons are equal, therefore the asymmetries involving leptons provide a direct determination of the effective mixing angle (Eq. (8.3)) using the relation $A_{FB} = \frac{3}{4}\mathcal{A}_e\mathcal{A}_f$, where the fermion f in this case represents the final state lepton. The quark forward-backward asymmetries depends on $\mathcal{A}_f = \frac{2g_{Vq}/g_{Aq}}{1+(g_{Vq}/g_{Aq})^2}$ where the subscript q indicates the quark flavour. The ratio of quark couplings can be expressed in terms of $\sin^2\theta_{W,eff}$ and non-universal corrections as [84]:

$$\frac{g_{Vq}}{g_{Aq}} = 1 - \frac{2Q_q}{I_{3L,q}}(\sin^2\theta_{W,eff} + C_q)\ . \tag{8.27}$$

The residual vertex correction C_q can be computed assuming the Standard Model. For *udsc* quarks it is small and has very little dependence on the parameters of the model, while for b it depends on the top mass because of the additional $Z \to b\bar{b}$ vertex corrections (see Eq. (4.44)). It amounts to $+0.0014$ for a top mass of 175 GeV. In case of quarks the term $\mathcal{A}_f$ is large

and weakly dependent on $\sin^2\theta_{W,eff}$ leaving most of the dependence on the weak mixing angle to $\mathcal{A}_e$. It follows that for quarks A_{FB} is essentially linearly dependent on $\sin^2\theta_{W,eff}$, while for leptons it shows a quadratic dependence (Eq. (3.282)). The consequence of this behaviour is shown in Table 8.3 where the magnitude of A_{FB} and its sensitivity to $\sin^2\theta_{W,eff}$ is given for leptons, for u-type and d-type quarks.

The forward-backward asymmetries can be determined either by measuring the cross section in the forward and backward hemisphers and then computing $A_{FB} = \frac{\sigma_F - \sigma_B}{\sigma_F + \sigma_B}$, or by fitting the data to the differential angular distribution

$$\frac{dN}{d\cos\theta} = C(\cos\theta) \cdot \left(1 + \cos^2\theta + \frac{8}{3} A_{FB}\cos\theta\right) \tag{8.28}$$

where θ is the scattering angle of the fermion in the centre-of-mass system and $C(\cos\theta)$ is an acceptance function modifying the differential cross section (Eq. (2.94)). The measurements can be divided in two classes:

- measurements where the selection of both fermions is required, as for the leptonic asymmetries described in Section 8.3.1;
- measurements where at least one fermion must be tagged, as for the measurement of heavy quark asymmetries described in Section 8.3.2.

In both cases the acceptance is a symmetric function, provided the selection efficiency is charge- or forward-backward symmetric. This can be seen by defining $F(\cos\theta)$, the efficiency to detect a fermion at scattering angle θ. If the efficiency is charge-simmetric the same function, F, gives the efficiency for anti-fermions. Hence for the first class of measurements one has $C(\cos\theta) = F(\cos\theta)F(-\cos\theta) = C(-\cos\theta)$, similarly for the second class $C(\cos\theta) = F(\cos\theta) + F(-\cos\theta) = C(-\cos\theta)$. Similar arguments hold for forward-backward symmetric efficiencies.

The symmetry of the acceptance has important consequences. One can see that in the $(\cos\theta)$-dependent forward-backward asymmetry, defined as

$$A_{FB}(\cos\theta) = \frac{\frac{dN}{d\cos\theta}(\cos\theta) - \frac{dN}{d\cos\theta}(-\cos\theta)}{\frac{dN}{d\cos\theta}(\cos\theta) + \frac{dN}{d\cos\theta}(-\cos\theta)} = \frac{8}{3} A_{FB} \frac{\cos\theta}{(1+\cos\theta^2)} \tag{8.29}$$

the $C(\cos\theta)$ acceptance cancels, showing that it is possible to make a measurement independent on the acceptance by exploiting the differential angular distribution. This is an important advantage over the simple counting of forward and backward events, because it makes the measurement insensitive to most intrumental effects, under the assumption of a given angular

behaviour. Another advantage is a more accurate determination of A_{FB} since the whole angular distribution is used, and more weight is given to the most sensitive angular regions. It is convenient to take advantage of these properties by using an unbinned log-likelihood method to fit the data. If $\mathcal{L} = \prod_i \mathcal{P}_i$ is the likelihood function defined as product of event probabilities $\mathcal{P}_i$, with the product extended to all events, one can write the negative log-likelihood as

$$\begin{aligned} -\ln\mathcal{L} &= -\sum_i \ln\mathcal{P}_i \\ &= -\sum_i \ln\frac{3}{8}C(\cos\theta_i)\cdot\left(1+\cos^2\theta_i+\frac{8}{3}A_{FB}\cos\theta_i\right) \\ &= -\sum_i \ln\frac{3}{8}C(\cos\theta_i) - \sum_i \ln\left(1+\cos^2\theta_i+\frac{8}{3}A_{FB}\cos\theta_i\right) \end{aligned}$$

where Eq. (8.28) has been used. The value of the A_{FB} parameter giving the maximum likelihood does not depend on the angular correction, therefore the first term in Eq. (8.30) can be ignored in the data analysis. This unbinned likelihood method cannot be applied to Bhabha scattering, since the presence of the t-channel requires a forward-backward asymmetric term, computed from theory, to be added to Eq. (8.29). Because of this additional term the acceptance does not decouple anymore from A_{FB} and the knowledge of the efficiency as a function of the scattering angle is required.

The energy dependence near the Z peak, caused by the interference between the photon and the Z exchange depends on the electric charge of the final fermion and on its axial coupling and has very little dependence on other electroweak parameters. This can be shown with Eq. (2.96), giving

$$A_{FB}^f(s) \simeq A_{FB}^f(m_Z^2) + \frac{(s-m_Z^2)}{s}\frac{3\pi\alpha(s)}{\sqrt{2}\mathrm{G_F}m_Z^2}\frac{2Q_eQ_fg_{Ae}g_{Af}}{(g_{Ve}^2+g_{Ae}^2)(g_{Vf}^2+g_{Af}^2)}\ . \quad (8.30)$$

The dependence is maximal for leptons ($\Delta A_{FB}^\ell/\Delta E_{CM} \simeq 0.00009/\mathrm{MeV}$), while the down-type quarks show the smallest energy dependence. This effect is corrected for using the precise energy determination of the LEP beam energy, by running the measured asymmetry to m_Z. All forward-backward asymmetries are also corrected for the effect of initial state radiation, for imaginary parts of the couplings (in particular for $\mathrm{Im}(\Delta\alpha)$), for the effect of pure photon exchange and the presence of box diagrams. Specific corrections, described later, are also applied for final state photon radiation (leptons) and gluon emission (hadrons). The uncertainty of this correction

Table 8.3 Magnitude of A_{FB} and its sensitivity on $\sin^2\theta_{W,eff}$ for various fermion species at the pole of the Z. The value of 0.2316 is used for $\sin^2\theta_{W,eff}$. For comparison the last line gives the magnitude and the sensitivity for A_{LR}.

	A_{FB}	$\frac{\partial A_{FB}}{\partial \sin^2\theta_{W,eff}}$
leptons	.02	-1.7
u and c quarks	.07	-4.0
d, s and b quarks	.10	-5.6
A_{LR}	.15	-7.8

is, in all cases, much smaller than the present total error, dominated by the statistical uncertainty for all measurements. The corrected asymmetry for a fermion f will be indicated as $A_{FB}^{0,f}$ in the following pages.

The most important issues related to the lepton measurements are discussed next, before moving to quarks.

8.3.1 *Lepton forward-backward asymmetries*

The selection of $e^+e^- \to \ell^+\ell^-(\gamma)$ events at LEP has been already described in the Chapter dedicated to the measurement of the Z lineshape. The forward-backward asymmetry is determined by fitting the data to Eq. (8.28); θ is defined by the scattering angle of the final-state negative lepton. For tau leptons the direction is given by the sum of the momenta of charge particles associated to the tau decays; the tau charge is measured in the same way.

In the case of e^+e^- final state, the t-channel photon-exchange process induces an important asymmetric correction and requires a careful treatment. The contribution of this process is taken into account subtracting it from the measured angular distribution. Semi-analytical calculations incorporating leading-log photonic corrections, first-order non-log terms and first-order weak corrections are available [85] and are used for this correction. The t-channel influence is reduced by analysing the data in a restricted angular region, typically in the $-0.9 \leq \cos\theta \leq +0.7$ range. (Within this range the t-channel contributes 12% to the total cross section, therefore calculations with 1% precision yield an uncertainty of 0.1%.) In the fit of the subtracted data to the form given by Eq. (8.28) an extended maximum-likelihood procedure is used, where the overall normalization is a free parameter of the fit.

The scattering angle of the final leptons in the laboratory system is affected by initial- and final-state radiation; the main effect is due to hard collinear radiation from one of the initial state leptons. The latter can be corrected for by using the scattering angle in the effective centre-of-mass system, that is

$$\cos\theta^* = \frac{\cos[\frac{1}{2}(\theta_{\ell^-} - \theta_{\ell^+} + \pi]}{\cos[\frac{1}{2}(\theta_{\ell^-} + \theta_{\ell^+} + \pi]} \tag{8.31}$$

where θ_{ℓ^-} and θ_{ℓ^+} are the scattering angles of the lepton and anti-lepton, respectively. In practice, since initial-state radiation (ISR) is forward-backward symmetric, the use of (8.31) is not strictly required; it simplifies, however, the definition of the acceptance, particularly for the e^+e^- final state. The ISR affects the observed asymmetry for another reason: the steep dependence of the asymmetry on $\sqrt{s}$ (Eq. (8.30)), changes the effective centre-of-mass and therefore the observed asymmetry itself. As photons produced in final-state radiation are not used in the definition of the scattering angle, their effect is a small reduction of the observed asymmetry. Semi-analytical programs can be used to correct for final-state photon emission [86].

The asymmetries A_{FB}^{ℓ} ($\ell = e, \mu$ and τ) measured at LEP [82] are extracted with a fit to the measured $A_{FB}(s)$ using data collected near the Z peak and at the off-peak points used to measure the Z lineshape. It has been already stressed that, since the vector couplings of the leptons are small, the slope of $A_{FB}^{\ell}(s)$ as a function of the beam energy is mainly sensitive to the axial couplings. The fitting formula takes into account the energy dependence of the asymmetry and the fit is done simultaneously with the lineshape data to account for the effect of the energy uncertainty. In the simultaneous fit of the lineshape data and $A_{FB}^{\ell}(s)$ the axial couplings are essentially determined by the lineshape and they are used to transport the off-peak measurements of $A_{FB}^{\ell}(s)$ to $\sqrt{s} = m_Z$. In an alternative method [83], the slope of the asymmetry is described by a free parameter. This different approach allows to check the consistency in the determination of the axial couplings between the lineshape and the forward-backward asymmetries.

The measurement of $A_{FB}^{0,\ell}$ is a rather straightforward measurement and has low systematic uncertainties. For the μ and τ channels the systematic uncertainties are related to the applied corrections, to the presence of background and to possible detector asymmetries. Typical systematic errors quoted by the LEP experiments are of the order of $\Delta A_{FB} = 0.0005 \div 0.001$

for muons and $\Delta A_{FB} = 0.001 \div 0.003$ for taus, depending on the experiment. For electrons, the theoretical uncertainty introduced in the treatment of the t-channel terms (≈ 0.0014) has to be taken into account increasing the typical error to $\Delta A_{FB} \approx 0.002$. The uncertainty on the center-of-mass energies gives a contribution of $\Delta A_{FB}^{0,\ell} = 0.0004$, comparable to the experimental systematics. This last two uncertainties are common to the four experiments and have to be treated in a correlated way when averaging the measurements.

The combination of the results of the four LEP experiments gives

$$A_{FB}^{0,e} = 0.0145 \pm 0.0025\,, \tag{8.32}$$

$$A_{FB}^{0,\mu} = 0.0169 \pm 0.0013\,, \tag{8.33}$$

$$A_{FB}^{0,\tau} = 0.0188 \pm 0.0017\,. \tag{8.34}$$

These measurements can be used to determine the ratios $g_{V\ell}/g_{A\ell}$ for the three charged leptons up to a common sign (Section 8.4.2). The three measurement can be combined assuming lepton universality, giving

$$A_{FB}^{0,\ell} = 0.0171 \pm 0.0010\,. \tag{8.35}$$

This result can be converted into

$$\sin^2\theta_{W,eff} = 0.23099 \pm 0.00053.$$

The dependence of the asymmetries on the centre-of-mass energy, $A_{FB}^{\ell}(s)$, is consistent with the expected value and sign of the lepton axial couplings and it is shown in Fig. 8.7.

8.3.2 *Heavy quark asymmetries*

8.3.2.1 *Lepton tagging*

As discussed in Section 7.2.1 the presence of a lepton is a tag for $Z \to b\bar{b}$ or $Z \to c\bar{c}$ events, while lepton kinematics can be used to discriminate the different lepton sources, on a statistical basis.

The simplest approach consists in selecting high-$p_\perp$ leptons, which give a high-purity sample of b events, with enhanced $b \to \ell^-$ content. Such a sample can be used to measure the b asymmetry by fitting the polar angle distribution of the thrust axis signed by the lepton charge[1] according to Eq. (8.28).

[1]The thrust axis is oriented towards the hemisphere containing the lepton if this is negatively charged, towards the other hemisphere otherwise.

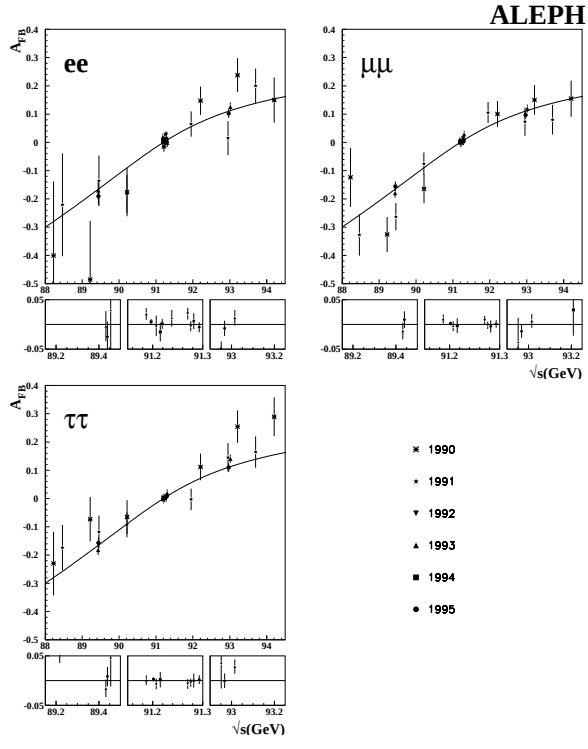

Fig. 8.7 Measurement of the forward-backward asymmetries for the three lepton species at various centre-of-mass energies.

The sample selected through high-$p_\perp$ leptons is enhanced in $b \to \ell^-$ decays (carrying the correct charge correlation between quark and tagging lepton), yielding a visible forward-backward asymmetry in the oriented thrust axis polar angle distribution, as shown in Fig. 8.8.

The observed asymmetry can be written in terms of the contributions of the different components of the selected sample:

$$\begin{aligned} A_{FB}^{obs} = \quad & (1-2\bar{\chi})(f^b_{\text{r.s.}} - f^b_{\text{w.s.}})A^b_{FB} + f^b_{\text{bkg}}\eta^b_{\text{bkg}}A^b_{FB} \\ & - f^{c\to\ell^+}A^c_{FB} - f^c_{\text{bkg}}\eta^c_{\text{bkg}}A^c_{FB} \\ & + f^{uds}\overline{A^{uds}_{FB}}\ , \end{aligned} \tag{8.36}$$

where $f^b_{\text{r.s.}}$ and $f^b_{\text{w.s.}}$ are the fractions of prompt leptons from b decays with right/wrong charge correlation between the lepton charge and the b quark charge, η^b_{bkg} and η^c_{bkg} describe the (small) correlation between the charge

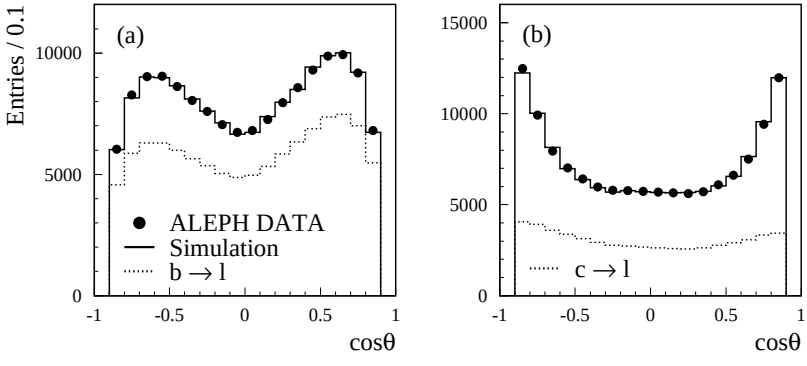

Fig. 8.8 Polar angle distribution of the oriented thrust axis at the peak energy for the ALEPH high-$p_\perp$ lepton analysis.The curve superimposed shows the result of the fit, that is restricted to the range$|\cos\theta| < 0.9$ to avoid regions with small detector acceptance.

of fake and non-prompt leptons and the charge of the primary quark in b and c events, and the last term accounts for the contribution of light quark background. The term $(1-2\bar{\chi})$ is introduced to correct for neutral b meson mixing: $\mathrm{B_d^0}$ and $\mathrm{B_s^0}$ mesons oscillate between the B and the $\overline{\mathrm{B}}$ state, thus diluting the charge information carried by the final state lepton. $\mathrm{B_s^0}$ oscillations are fast compared to the $\mathrm{B_s^0}$ lifetime, therefore a $\mathrm{B_s^0}$ meson arising from the hadronization of a b quark has 50% probability of decaying as a $\mathrm{B_s^0}$ and 50% probability of decaying as a $\overline{\mathrm{B_s^0}}$. $\mathrm{B_d^0}$ oscillations are much slower, giving $\chi_d \approx 0.18$. The average mixing parameter for inclusive b decays can therefore be expressed as:

$$\bar{\chi} = 0.5\, f_s + \chi_d f_d \ , \tag{8.37}$$

where the values of f_s and f_d are about 0.12 and .38, respectively.

High-$p_\perp$ leptons can be selected in both hemispheres, and the counting of same sign and opposite sign pairs ($N_{\mathrm{o.s.}}$, $N_{\mathrm{s.s.}}$) gives the possibility to measure from the data the charge correlation in b events $\mathcal{P}_b = (1-2\bar{\chi})(f^b_{\mathrm{r.s.}} - f^b_{\mathrm{w.s.}})$, once the small contribution from charm and light quark events has been subtracted:

$$f_{\mathrm{o.s.}} \ = \ \frac{N_{\mathrm{o.s.}}}{N_{\mathrm{o.s.}} + N_{\mathrm{s.s.}}} \ = \ \mathcal{P}_b^2 + (1-\mathcal{P}_b)^2 \ + \ \text{c and uds corrections.} \tag{8.38}$$

The analysis of the dilepton sample to evaluate $\mathcal{P}_b$ from the data, lowers considerably the dependence of the measurement upon the knowledge of semileptonic b decays (rates and kinematic properties), as well as b meson mixing. It should be also noted that since the measurement makes use of both forward negative leptons and backward positive leptons to tag forward b quarks, the detector acceptance has nearly no effect on the extracted value of the asymmetry: a sizeable effect could arise only in case of inefficiencies that are both forward-backward asymmetric and different for positive and negative leptons, which is very unlikely for LEP detectors.

The extraction of A_{FB}^b depends on the evaluation and on the modelling of the charm component, and on the assumed value of A_{FB}^c. The branching ratio $c \to \ell^+$ is measured at LEP studying the lepton yield opposite to a reconstructed high-energy D mesons; the modelling of semileptonic decays relies on the study of D^0 and D^+ semileptonic decays performed by the DELCO and MARK III experiments, at centre-of-mass energies below the Z peak.

An extension of the high-$p_\perp$ lepton analysis consists in studying the whole $p_\perp$ spectrum of lepton candidates, extracting A_{FB}^b and A_{FB}^c simultaneously. The sample is analysed in bins of $p_\perp$ (or other discriminating variables) and polar angle, and in each bin the observed asymmetry is written in terms of the b and c asymmetries: the different b/c content of the different bins gives sensitivity to both variables. Also in this case the sample composition as a function of the discriminating variable needs to be estimated with the simulation, but the study of events with identified leptons in both hemispheres gives information on $\mathcal{P}_b$, the charge correlation in b events.

In the most precise analyses lifetime-based discriminating variables have been used in conjunction with the lepton kinematics, to enhance the separation between the b and the c constributions, gaining further statistical power. The use of the lifetime introduces a significant complication in the treatment of B meson mixing: B_s^0 oscillations are so fast that the probability of mixing can be assumed to be 50% independently of the value of the lifetime variable, but B_d^0 oscillations have a period that is about twelve times the b lifetime, therefore events with short lifetime are enhanced in "non-oscillated" mesons, while events with long lifetime are enhanced in "oscillated" mesons. The dependence of the effective mixing parameter $\bar{\chi}$ on the lifetime variable is relevant and needs to be treated correctly.

8.3.2.2 *Inclusive measurements*

As discussed in Chapter 7, tagging methods based on lifetime have high performance, but they do not provide information about the quark charge. Inclusive methods have been developed to estimate the charge of the b quark, to complement lifetime tags for the measurement of forward-backward asymmetries.

The jet charge is usually defined as

$$Q_{\mathrm{h}} = \frac{\sum_i q_i p_{\parallel i}^k}{\sum_i p_{\parallel i}^k} \ , \tag{8.39}$$

where $p_{\parallel i}$ is the momentum of a particle parallel to the thrust axis, and the sum runs over all charged particles in a hemisphere. Alternative definitions can be constructed using the rapidity instead of the projected momentum, or using the axis of the leading jet instead of the thrust axis, or restricting the sum to the particles belonging to the leading jet. The parameter k can be tuned to obtain high sensitivity to the quark charge, while keeping low correlation between the charge of the two hemispheres (discussed below): typical values are between 0.3 and 1.

In a pure sample of b events, the forward-backward asymmetry is proportional to the mean charge flow between the two hemispheres

$$Q_{FB}^b \equiv \langle Q_F^b - Q_B^b \rangle = \delta_b A_{FB}^b \tag{8.40}$$

where δ_b is a parameter called charge separation. At parton level δ_q (the charge separation for a generic quark q) is equal to twice the quark charge, but hadronization and decays lower its value, diluting the measured charge flow. A precise determination of the forward-backward asymmetry requires an eveluation of δ_q with the lowest possible uncertainty. The advantage of high-purity single-flavour samples, that in practice can be obtained for b quarks only, lies on the possibility of measuring δ_q from the data, lowering considerably the use of theoretical assumptions in the evaluatiuon of this parameter, and therefore lowering its uncertainty. Hemispheres containing the b or the $\bar{b}$ quark have average measured charge

$$\langle Q_b \rangle = \delta_b/2 + \langle \mathcal{R}_b \rangle \tag{8.41}$$

$$\langle Q_{\bar{b}} \rangle = -\delta_b/2 - \langle \mathcal{R}_{\bar{b}} \rangle \ , \tag{8.42}$$

where $\mathcal{R}_b$ and $\mathcal{R}_{\bar{b}}$ are small corrections which account for interactions with the detector material, that introduce a bias between positively and negatively charged reconstructed particles. The total charge measured in the

event is $\langle Q^b_{TOT}\rangle = \langle \mathcal{R}_b - \mathcal{R}_{\bar{b}}\rangle$, which is very close to zero. The product of the two hemisphere charges can be written as:

$$\langle Q^b_F Q^b_B\rangle = \langle Q_b Q_{\bar{b}}\rangle = -\frac{1}{4}\delta_b^2 - \frac{1}{2}\delta_b\left(\langle \mathcal{R}_b\rangle + \langle \mathcal{R}_{\bar{b}}\rangle\right) - \langle \mathcal{R}_b \mathcal{R}_{\bar{b}}\rangle \ , \qquad (8.43)$$

where the term $\langle \mathcal{R}_b \mathcal{R}_{\bar{b}}\rangle$ accounts for correlations between the charge measurements in the two hemispheres, due to total charge conservation and kinematic correlations between the b hadrons.

The charge separation δ_b can be measured by comparing the widths of the distributions of the charge flow and of the total charge, as demonstrated below:

$$\begin{aligned}\sigma^2\left(Q^b_{FB}\right) - \sigma^2\left(Q^b_{TOT}\right) &= \langle \left(Q^b_{FB}\right)^2\rangle - \langle Q^b_{FB}\rangle^2 - \langle \left(Q^b_{TOT}\right)^2\rangle + \langle Q^b_{TOT}\rangle^2 \\ &= -4\langle Q^b_F Q^b_B\rangle - \langle Q^b_{FB}\rangle^2 + \langle Q^b_{TOT}\rangle^2 \\ &\approx \delta_b^2 - \langle Q^b_{FB}\rangle^2 + \langle Q^b_{TOT}\rangle^2 \ . \end{aligned} \qquad (8.44)$$

The last expression relates δ_b to physical observables, having dropped the corrections for material interactions and hemisphere correlations (introduced above in Eq. (8.43)), that in the analyses are estimated with the simulation. A sketch illustrating the physical meaning of the above quantities is presented in Fig. 8.9.

In an asymmetry analysis, pure b samples cannot be selected, therefore the above formalism has to be developed taking into account also the contributions of the other flavours; for instance, the charge flow can be written as

$$Q_{FB} \ = \ f_b\,\delta_b\,A^b_{FB} \ + \ f_c\,\delta_c\,A^c_{FB} \ + \ f_{uds}\,\delta_{uds}\,A^{uds}_{FB} \ , \qquad (8.45)$$

where the f_b, f_c, f_{uds} are the fraction of b, c and light quark events in the selected sample, and light quark have been, as usual, treated as a single class.

In a simple approach, the sample composition as well as the charm and light quark charge separations can be estimated with the simulation, δ_b can be extracted from the data (using the simulation to subtract the non-b contributions and correct for hemisphere correlations) and the b asymmetry can be derived from the observed charge flow. In the more sophisticated approaches double tagging techniques, similar to the ones employed for the measurement of R_b can be used to derive most parameters from data. The measurement of the b forward-backward asymmetry using these techniques, as well as the measurement described before using semileptonic events, are affected by systematic uncertainties much smaller than the statistical error obtained at LEP.

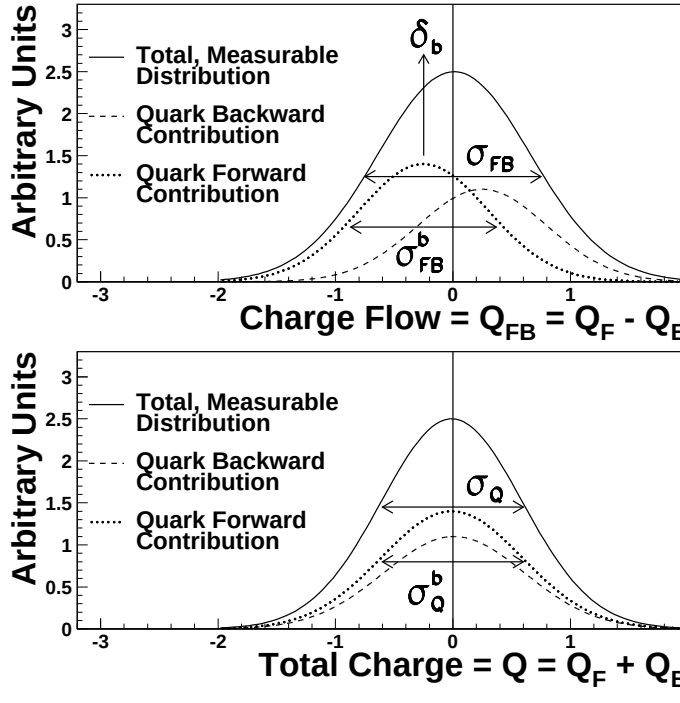

Fig. 8.9 Sketch showing the distributions of charge flow and total charge: the difference in width between the two distribution is related to the charge separation, as explained in the text.

8.3.2.3 *Measurement of the jet charge asymmetry using all flavours*

As already mentioned, direct measurements of the charge separation for non-b quark flavours are more difficult. Nevertheless charm samples selected by requiring the presence of a D^* meson can be employed to evaluate δ_c with moderate model-dependence. Lifetime-tagged samples with varying charm content can also be examined to infer the value of δ_c. The charm charge separation is reduced by the presence of the soft pion in the D^* decay (section 7.2.3). The soft pion retains memory of the original charm charge, but being low momentum it gets a low weight from the jet charge definition, Eq. (8.39). Individual charge separations for lighter quarks cannot be measured separately, however the average δ_{uds} can be inferred from the difference in width of the $\langle Q_F - Q_B \rangle$ and $\langle Q_F + Q_B \rangle$ distributions, by a procedure similar to the one based on Eq. (8.44). When b tagging is not

used, Eq. (8.45) can be rewritten as:

$$Q_{\rm FB} = C \sum_{q=u,d...}^{b} \delta_q A_{\rm FB}^q \frac{\Gamma_{q\bar{q}}}{\Gamma_{had}} = C\frac{3}{4} \sum_{q=u,d...}^{b} \delta_q \mathcal{A}_e \mathcal{A}_q \frac{\Gamma_{q\bar{q}}}{\Gamma_{had}} \qquad (8.46)$$

where C indicates the geometrical acceptance. This relation shows a linear dependence on $\mathcal{A}_{\rm e}$ and, through this parameter, can be used to extract $\sin^2\theta_{W,eff}$. Since the $\mathcal{A}_q$ are only weakly dependent on $\sin^2\theta_{W,eff}$ their expected SMS value can be used; the same is done for $\frac{\Gamma_{q\bar{q}}}{\Gamma_{had}}$. The electroweak mixing angle determined from $Q_{\rm FB}$ using untagged hadronic samples is dominated by the systematic uncertanties on the charge separations, δ_q's. In particular detailed Monte Carlo studies are needed to disentangle the δ_u, δ_d and δ_s contributions, and the the simulation has to be carefully tuned to the measured kaon and Λ production rates in order to have a realistic description of strangeness production.

8.3.2.4 *D meson measurements at LEP*

Prompt $\rm D^*$ produced in $Z \to c\bar{c}$ decays can be be exploited to measure the forward-backward asymmetry. These vector mesons give clear signatures, since a narrow peak with low background can be obtained in the ΔM distribution (Fig. 7.13). The $\rm D^*$ charge is correlated with the one of the parent c quark charge. The background consists essentially of $\rm D^*$ produced in the b quark cascade of $Z \to b\bar{b}$ events. This background can be suppressed using the $\rm D^*$ energy, which is higher for $\rm D^*$ originating from $Z \to c\bar{c}$ than for charm mesons from b decays. The thrust axis direction, signed by the $\rm D^*$ charge, is used and a log-likelihood fit to the angular distribution is performed.

The amount of b background must be carefully monitored. The correlation with the $\rm D^*$ charge is opposite for $Z \to b\bar{b}$ events, therefore the presence of contaminating b's considerably dilutes the observed asymmetry. The b and c components can be determined by a fit of the $\rm D^*$ energy distribution. The effect of b mixing on the b asymmetry needs to be accounted for in a way which differs from an unbiased sample: the $b \to \rm D^*$ process selects preferentially B_d hadrons, therefore the effective χ parameter is dominated by χ_d. Sidebands of invariant mass peaks can be used to evaluate the background asymmetry which is generally close to zero. In order to evaluate the background from data and in an unbiased way, the events mixing method is often used. This technique allows to evaluate the background from data by taking the D meson and the slow pion forming

the D^* from opposite hemispheres or from different events. In this way the contamination caused by partially reconstructed events is treated without the need of Monte Carlo simulations.

8.3.2.5 *Heavy quark asymmetries: combined results and QCD corrections*

The LEP measurements of b and c forward-backward asymmetries from semileptonic events, from inclusive samples and from D mesons [110] can be combined to merge the experimental information in an optimal way. The combination procedure follows a χ^2 minimisation and it is described in Ref. [112]. The measurements of R_b and R_c (Subsections 7.3.3, 7.4.5) are included in the same procedure. Some measurements depend on parameters determined analysing the same data, for example the semileptonic events used to measure the b and c asymmetries provide also information on the b semileptonic branching ratios or on $B\bar{B}$ oscillations. These ancillary measurements must be taken into account in the combination. The covariance matrix used in the fit includes the statistical and systematic correlation among various measurements. Statistical correlations exist for measurements performed with the data collected by the same experiment. On the other hand measurements of the same parameter by different experiments are affect by common systematic uncertainties.

As mentioned at the introduction of this Section, the extraction of the effective electroweak mixing angle requires the evaluation of the corrected b and c asymmetries $A_{FB}^{0,b}$ and $A_{FB}^{0,c}$, from the measured asymmetries. Heavy quark asymmetries are affected by radiative effects due to strong interactions, as described in Subsection 4.2.2. They are related to virtual vertex and gluon bremsstrahlung diagrams which modify the angular distribution of the fermions emitted in the final state. The emission of an hard gluon, for example, may scatter both b and $\bar{b}$ in the same hemisphere (forward or backward): in such events the original electroweak asymmetry is destroyed. The effect of such radiative effects is to lower the experimentally observed asymmetry by a few percent, as can be seen from Eq. (4.77). Detailed calculation based on perturbative QCD, including second-order corrections for massless quarks and quark mass effects at first-order, are available [113]. An important ingredient of these theoretical calculations is the definition of the b quark direction, which should closely match the experimental definition based on thrust axis reconstruction. In practice experimental cuts reduce considerably the QCD corrections [114]. For instance the momen-

tum cut which is applied in lepton tagging selects events with reduced gluon radiation. Furthermore in some cases the effect of hard gluon radiation is automatically incorporated by analysis procedure. This is the case for the inclusive measurements based on jet charge techniques, because the b charge separation, measured with data, is an effective parameter that includes the QCD smearing.

The present world averages for the b and c forward-backward asymmetries at the Z pole, as given in [142], are:

$$A_{FB}^{0,b} = 0.0992 \pm 0.0016$$
$$A_{FB}^{0,c} = 0.0707 \pm 0.0035 \ .$$

There is a +15% correlation between the two results. Both results are dominated by the statistical uncertanties. In particular, for the b asymmetry, the systematic uncertainties related to the QCD corrections is a factor three lower than the statistical error.

The dependence of the b and c asymmetries on the centre-of-mass energy, $A_{FB}^{b}(s)$ and $A_{FB}^{c}(s)$, is regulated by the quark electric charge and its axial coupling (Eq. (8.30)). Their observed energy dependence is shown in Fig. 8.10 and compared to the MSM prediction. (The value of $\sin^2\theta_{W,eff}$ given in Section 8.4 is used to normalize the vertical scale for the MSM prediction). The different slope for b and c quarks is due to the absolute value of their electric charge, that is twice larger for up-type quarks. The asymmetry is increasing in both cases because the two quark types have opposite sign (and same absolute value) for the axial couplings.

8.3.2.6 *HF asymmetries with polarized beams*

The quark asymmetries discussed above, based on measurements employing unpolarized beams, are probing the product of initial and final state couplings, $\mathcal{A}_e\mathcal{A}_q$. On the other hand the polarized forward-backward asymmetry ($A_{FB}^{pol}(q)$), defined by Eq. (2.87), is solely dependent on $\mathcal{A}_q$. The polarized forward-backward asymmetry of b and c quarks have been measured by SLD [111] using flavour tagging methods very similar to the ones used for the unpolarized case. Inclusive samples of $Z \to b\bar{b}$ events selected thanks to the long b lifetime provide a precise determination of $\mathcal{A}_b$ using jet-charge techniques. Semileptonic b and c decays give a simultaneous determination of $\mathcal{A}_b, \mathcal{A}_c$ through the analysis of their inclusive lepton spectra; D and D* mesons have been used to measure $\mathcal{A}_c$. These measurements are corrected for QCD effects, which are similar to the unpolarized case. The

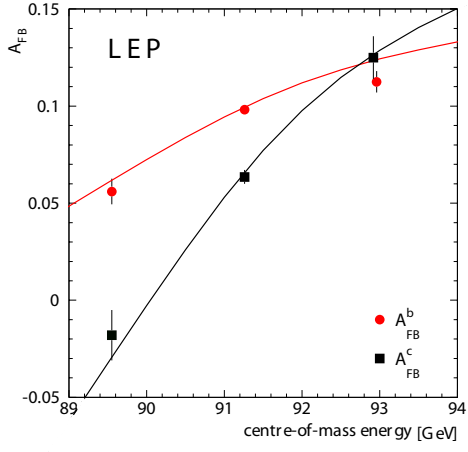

Fig. 8.10 Measurement of the b and c forward-backward asymmetries as a function of the centre-of-mass energy. The MSM expectation for the two quark types is shown. (Courtesy of the LEP Electroweak Working Group [142].)

correction depends on the channel and on the tagging method and amounts to a few percent.

The SLD results are combined [142], yielding:

$$\mathcal{A}_b = 0.923 \pm 0.020$$
$$\mathcal{A}_c = 0.670 \pm 0.027\,.$$

The correlation between $\mathcal{A}_b$ and $\mathcal{A}_c$ is small (11%). The measurements are consistent with the MSM predictions giving $\mathcal{A}_b = 0.935$ and $\mathcal{A}_c = 0.668$, respectively. These predictions have a small uncertainty (≈ 0.001 for b quarks) because the quark $\mathcal{A}_q$ parameters are only weakly dependent on $\sin^2\theta_{W,eff}$. Indeed, as can be seen by using Eq. (8.27), $\delta\mathcal{A}_b \approx -0.63\,\delta\sin^2\theta_{W,eff}$.

8.4 Interpretations

8.4.1 *The determinations of* $\sin^2\theta_{W,eff}$

The measurements of the asymmetries presented in the previous Sections can be interpreted as a measurement of $\sin^2\theta_{W,eff}$. For the leptonic forward-backward asymmetries, for the measurements of $\mathcal{A}_e$ and $\mathcal{A}_\tau$ from tau polarization, and for the measurement of A^0_{LR} the interpretation requires the only assumption of lepton universality. The derivation of $\sin^2\theta_{W,eff}$ from hadronic measurements requires the knowledge of the $\mathcal{A}_q$ terms that, as already discussed, have only a mild dependence on $\sin^2\theta_{W,eff}$ in the MSM. For this class of measurements the validity of the MSM for the $\mathcal{A}_q$ terms is assumed; this assumption is corroborated by the direct measurements of $\mathcal{A}_b, \mathcal{A}_c$ using polarized beams, which agree with the MSM.

A compilation of the various results is shown in Fig. 8.11, where the dependence of $\sin^2\theta_{W,eff}$ on the Higgs boson mass is also indicated. The six results shown in the figure are obtained, respectively, from the lepton forward-backward asymmetry, the tau polarization, the left-right asymmetry, the b forward-backward asymmetry, the c forward-backward asymmetry and the jet charge asymmetry using all quark flavours. The average of the six measurements gives:

$$\sin^2\theta_{W,eff} = 0.23153 \pm 0.00016$$

with a χ^2 of 11.8 for five degrees of freedom corresponding to a confidence level of 3.7%. This confidence level is relatively low, because the most precise determinations, based on A^0_{LR} and on the b asymmetry are about 3 σ apart. From the experimental point of view both measurements are dominated by statistical errors, with accurate studies of the much lower systematic uncertainties. On the other hand a departure of the b couplings from their MSM expectation seems to be excluded by the precise measurements of $\mathcal{A}_b$ and R_b. Therefore this discrepancy is assumed to be related to a statistical fluctuation.

8.4.2 *Extraction of the neutral current couplings*

The couplings of the neutral current to leptons ($\ell = e, \mu, \tau$) can be determined using three ingredients:

- the leptonic partial widths,
- the $\mathcal{A}_\ell$ parameters as determined by the leptonic asymmetries,

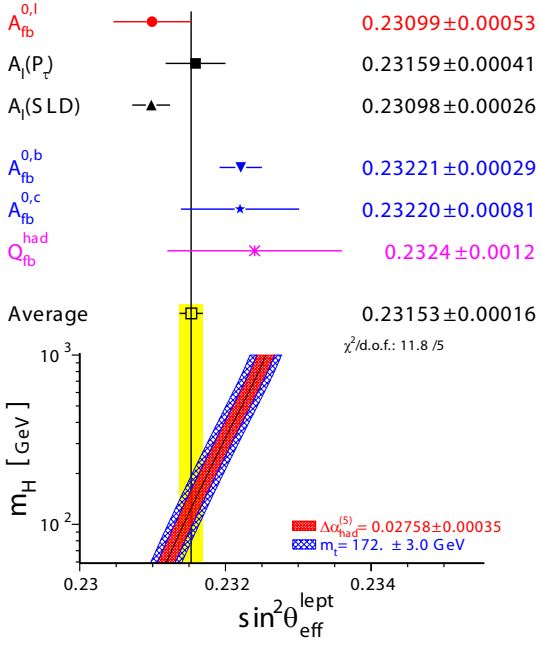

Fig. 8.11 The determinations of $\sin^2\theta_{W,eff}$ from the measurements described in this Chapter and their average. The measurements are, starting from the top, the lepton forward-backward asymmetry, the tau polarization, the left-right asymmetry, the b forward-backward asymmetry, the c forward-backward asymmetry and the jet charge asymmetry using all quark flavours. The results are compared to the MSM prediction, as a function of the Higgs boson mass. The uncertainty due to $\alpha(m_Z^2)$ on the MSM predictions is indicate by a band. The effect of varying the top mass within the range indicated in the figure is added as two extra side bands. (Courtesy of the LEP Electroweak Working Group [142].)

- the energy dependence of the leptonic forward-backward asymmetries.

The partial width of the decay $Z \to \ell^+\ell^-$, (Section 6.6) gives the sum of the squares of the couplings using Eq. (2.79). The ratio of the vector and axial couplings is given by the leptonic measurements of $\mathcal{A}_\ell$ (Eq. (8.2)), i.e. by the measurement of A_{LR}, of the tau polarization and of the leptonic forward-backward asymmetries. The energy dependence of the asymmetries (Eq. (8.30)) fixes the value of the axial couplings, up to a common sign.

This last ingredient is required, since the widths and asymmetries do not change if $g_{V\ell}$ and $g_{A\ell}$ replace each other, as can be seen from Eqs. (2.79) and (8.2).

The measured vector and axial couplings to electron, muon and tau are compared in Fig. 8.12 to test the hypothesis of lepton universality. The measurements are in agreement and lepton universality is tested to less than 0.1% for axial couplings and to a few percent for the smaller vector couplings:

$$\frac{g_{V\mu}}{g_{Ve}} = 0.961 \pm 0.063 \;\; \frac{g_{A\mu}}{g_{Ae}} = 1.0002 \pm 0.00064$$
$$\frac{g_{V\tau}}{g_{Ve}} = 0.958 \pm 0.030 \; \frac{g_{A\tau}}{g_{Ae}} = 1.0019 \pm 0.00073 \; .$$

These results improves by two order of magnitudes the tests of neutral currents lepton-universality available before the start of LEP and SLC, based on νe and $\nu\mu$ scattering.

The b and c quark couplings can be extracted with the same procedure adopted for the lepton case, by using the measurements of R_b, R_c, the values of $\mathcal{A}_b$, $\mathcal{A}_c$ determined by the polarized heavy quark asymmetries, and the energy dependence of the b and c forward-backward asymmetries. With this method the axial (vector) b couplings can be tested to a precision of approximately 2% (3%). Similar precisions are obtained with the tests of the c couplings (the bounds in this case are somewhat weaker mainly because of the larger uncertainty on the measured value of R_c). All couplings are found to agree with the MSM.

The $\mathcal{A}_q$ parameters for b and c quarks can also be evaluated from the unpolarized b and c asymmetries using Eq. (2.86) and the value of $\mathcal{A}_e$ derived from $A_{FB}^{0,\ell}$, from the tau polarization and from A_{LR}^0. This interpretation of the heavy quark unpolarized asymmetries is bound to lead, however, to a rather low value of $\mathcal{A}_b$ (0.881 ± 0.017, compared to the MSM expectation of 0.935) because of the 3 σ discrepancy between $A_{FB}^{0,b}$ and A_{LR}^0 already mentioned in the discussion concerning the determination of $\sin^2\theta_{W,eff}$. As a consequence a rather high (low) value of the axial (vector) b couplings is obtained and the agreement with the MSM is marginal for both couplings. It must be stressed, however, that this discrepancy is totally correlated with the one seen in Fig. 8.11.

The measurements of the vector and axial couplings for various fermion species are depicted in Fig. 8.13. The regions allowed by the experimental measurements at 68% CL are shown. As expected the precision obtained for the lepton measurements is impressive. With the scale used by this

figure the three measurements are represented by three superimposed dots. Considerable precision is obtained also for the heavy quark couplings. Constraints are obtained on the couplings of lighter quarks by measurements of forward-backward asymmetries using kaons [115] and high-momentum stable particles [116]. As the large uncertanties of these measurements do not allow the study of the energy dependence, the contours indicating the allowed regions are symmetric with respect to the line $g_{Vf} = g_{Af}$. The constraints on neutrino couplings are computed from the measurement of the invisible width (Section 6.6), assuming three neutrino families with identical neutral couplings. In this case the experimentally allowed region is represented by a very thin ring.

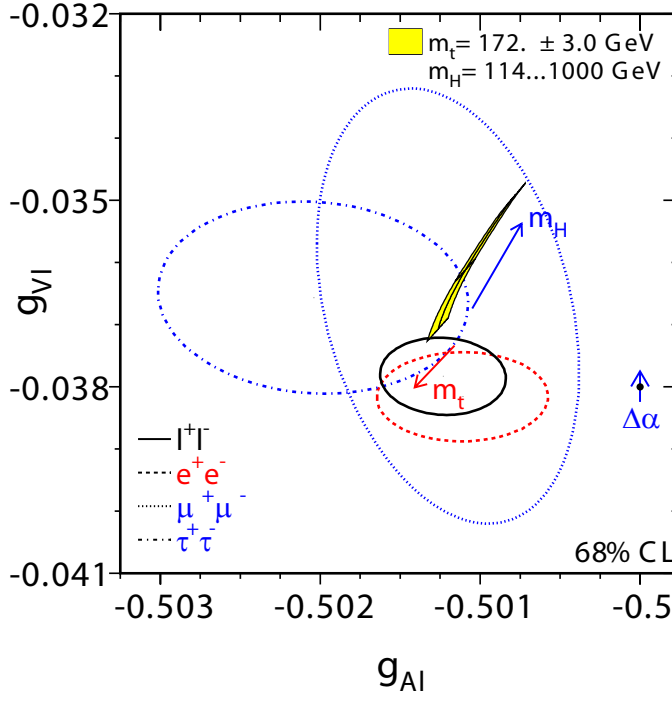

Fig. 8.12 The vector and axial couplings of the neutral current to electrons, muons and taus. The 68% CL allowed regions are shown with dashed, dotted and dash-dotted lines, respectively. The combination of the measurements from the three lepton species, assuming lepton universality, is also shown (full line). The shaded area shows the MSM prediction, within the allowed values for the top and Higgs boson masses. The uncertainty on $\alpha(m_Z)$ is indicated by the small arrow. (Courtesy of the Lep Electroweak Working Group.)

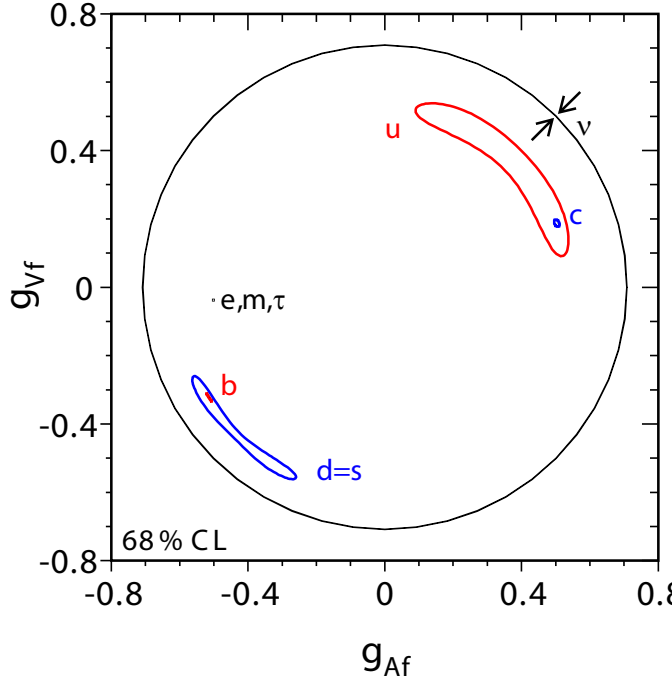

Fig. 8.13 The vector and axial couplings of the neutral current to various fermion species. The regions allowed by the experimental measurements (68% CL) are shown. (Courtesy of the Lep Electroweak Working Group.)

This page intentionally left blank

Chapter 9

Electroweak Measurements with W Bosons

The discovery of the W boson in 1983 [25, 26] was the first experimental evidence in favour of the model of Glashow, Weinberg and Salam [2]. Since then W physics has played a growing role in tests of electroweak interactions. The mass of the W is very sensitive to pure electroweak radiative corrections, through the relation (Eq. (3.188))

$$m_W^2(1 - \frac{m_W^2}{m_Z^2}) = \frac{\pi\alpha(m_Z^2)}{\sqrt{2}G_F}(1 + \Delta r^W) \tag{9.1}$$

where $\alpha(m_Z^2)$ is the fine structure constant evolved at $q^2 = m_Z$ (as explained in Subsection 3.2.4), m_Z and G_F come from precise measurements of the Z mass and of the muon lifetime, and Δr^W indicates the genuine electroweak corrections. The relation can either be used to compare a direct measurement of the W mass to the indirect value, computed with Δr^W taken from other observables, or to evaluate Δr^W itself. The W mass has been measured with increasing precision at the $Sp\bar{p}S$, Tevatron and LEP colliders, leading to a growing evidence for the need of radiative corrections, beyond the pure QED effects that are incorporated in the effective $\alpha(m_Z^2)$. This can be seen in Fig. 9.1 where the value of the W mass computed with Eq. (9.1), and assuming $\Delta r^W = 0$, is compared to the W mass world average, over the years.

This Chapter starts with a description of W boson production and mass measurement at hadron colliders, followed by W physics measurements at LEP. The study of $WW\gamma$ and WWZ triple gauge couplings is the main subject of the final Section.

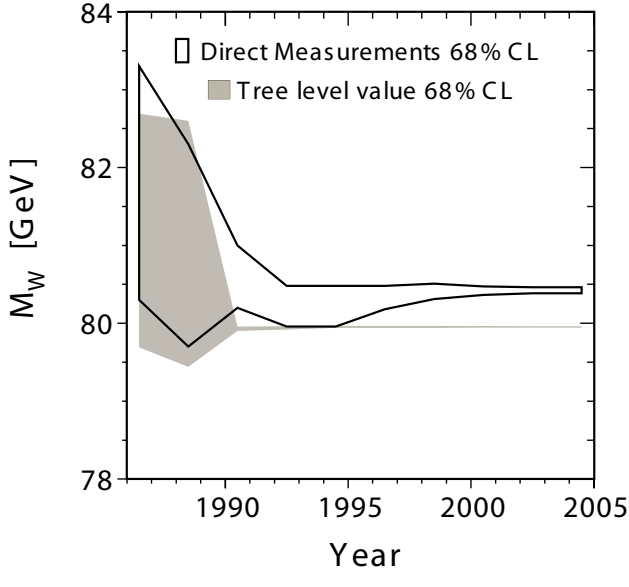

Fig. 9.1 The time evolution of the W mass World Average (Particle Data Group) compared to the value extrapolated from Eq. (9.1) with $\Delta r^W = 0$, in the same years. The areas represent the 68% CL contours. The difference has reached 12 σ's in year 2005, showing the need of genuine electroweak corrections to describe the experimental data.

9.1 *W* mass measurement at hadron colliders

The main W production mechanism at hadron colliders is the $q\bar{q}' \to W$ Drell-Yan process shown in Fig. 9.2. The initial quarks can either be valence or see quarks.

The study of W bosons at $p\bar{p}$ and pp colliders naturally leads to two different streams of investigation. One can use W (and Z) bosons to probe the internal structure of the proton, i.e. to measure the momentum distribution of initial partons within the proton (anti-proton) target, the so-called Parton Density Functions (PDF's). A detailed treatment of this topic goes beyond the scope of this book. The second stream of investigations is re-

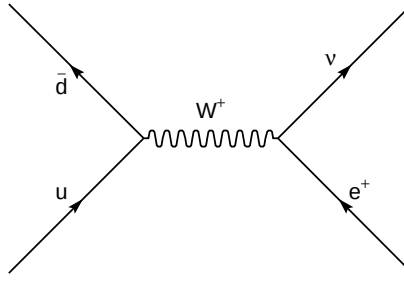

Fig. 9.2 An example of W production and decay through the Drell-Yan process.

lated to the electroweak properties of the W boson, in particular to its mass.

The W production cross section at hadron colliders can be written as

$$\sigma(h_1 h_2) = \int_0^1 dx_1 dx_2 f_{h1}^a(x_1) f_{h2}^b(x_2) d\sigma^{DY}(\hat{s}) \tag{9.2}$$

where $f_{h1}^a(x_1)$ ($f_{h2}^b(x_2)$) represents the probability that quark a (b) carries a fraction x_1 (x_2) of the initial hadron momentum and $d\sigma^{DY}(\hat{s})$ is the cross section of the Drell-Yan subprocess at transfer momentum $\hat{s}$. The $f_{h1}^a(x_1)$ function represents the PDF for quark a. For the subprocess $u\bar{d} \to W^+ \to e^+\nu$ the cross section is described by the Breit-Wigner ansatz

$$d\sigma^{DY}(\hat{s}) = \frac{1}{3}\frac{\pi}{s}\frac{\Gamma_{u\bar{d}}\Gamma_{e\nu}}{(\sqrt{\hat{s}} - m_W)^2 + \frac{\Gamma^2}{4}} \tag{9.3}$$

where Γ_i and Γ are the partial and total width for the W decay. The factor $1/3$ comes from the need of matching the colours of the initial quarks. At the $Sp\bar{p}S$ collider ($\sqrt{s}$ = 540 GeV) the W production cross section times the $W \to e\nu$ branching ratio was 0.3 nb , it is 2 nb at the Tevatron ($\sqrt{s}$ = 2 TeV) (Fig. 9.3) and will be about 15 nb ($\sqrt{s}$ = 14 TeV) at the LHC.

The PDF's in Eq. (9.2) are relevant at $x_1 \approx x_2 \approx \frac{m_W}{\sqrt{s}}$ making valence quarks less and less important at higher energy. At LHC, that is a pp collider, the production through valence quarks will be absent.

The W production cross section has to be compared to the total $p\bar{p}$ (pp) cross section, that is eight orders of magnitude larger at the Tevatron. Because of the large hadronic background W decays must be detected into the

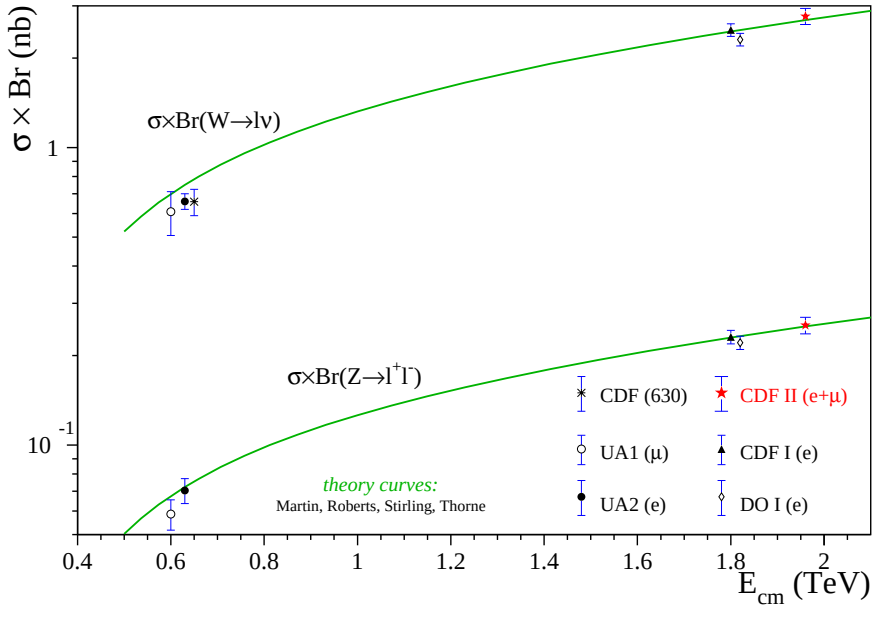

Fig. 9.3 The W production cross section at $p\bar{p}$ colliders. The cross section is multiplied by the $W \to e\nu$ branching ratio.

leptonic channels, by requiring an isolated lepton (electron or muon) with high transverse momentum and large missing transverse energy due to the undetected neutrino. At hadron colliders the longitudinal component of the missing momentum cannot be measured because of the collision fragments, directed along the beam axis, that are not detected. The W invariant mass cannot be measured and is replaced by the transverse mass defined using the transverse components of the momenta as

$$M_W^T = \sqrt{(E_T^{lepton} + E_T^{\nu})^2 - (\mathbf{p}_T^{lepton} + \mathbf{p}_T^{\nu})^2} = \sqrt{2p_T^{lepton} p_T^{\nu}(1 - \cos\phi)} \tag{9.4}$$

where ϕ is the angle between the lepton and the missing momentum measured on the transverse plane and $(E_T^i)^2 = (p_T^i)^2 + m_i^2$. The missing transverse momentum is measured by taking into account the total transverse momentum of the recoiling hadronic system, in addition to the lepton information.

The transverse mass distribution peaks at $\approx m_W$, as can be seen by the differential cross section

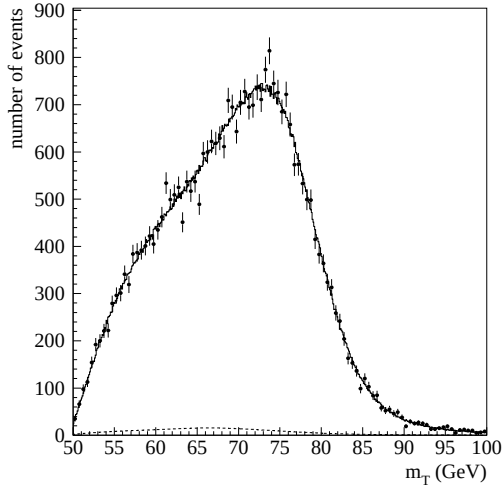

Fig. 9.4 Transverse mass distribution from high p_T electrons collected by the D0 experiment at the Tevatron Collider.

$$\frac{d\sigma}{dM_W^T} = \frac{d\sigma}{dcos\theta}\frac{dcos\theta}{dM_W^T} = \frac{d\sigma}{dcos\theta}(\frac{M_W^T}{2m_W})(m_W^2 - (M_W^T)^2)^{-\frac{1}{2}} \tag{9.5}$$

where θ is the polar decay angle in the W decays frame and $M_W^T \approx 2p_T^{lepton}$ has been used. The divergence in Eq. (9.5) translates in a relatively broad *Jacobian peak* when the natural width of the W boson and the effect of detector smearing, originating from finite energy and momentum resolutions and from undetected particles, are taken into account (Fig. 9.4).

An important experimental source of systematic error in the measurement of the W mass at hadron colliders is related to the determination of the absolute energy scale. The momentum scale of tracking detectors can be determined, using the known J/ψ mass and selecting $J/\psi \to \mu^+\mu^-$ decays, to a typical precision of less than permil. Calorimeters can be calibrated with high-energy electron pairs from Z decays, by computing the pair invariant mass and then comparing to the Z mass precisely measured at LEP. The comparison requires correcting for the electron bremsstrahlung in the tracking detectors. The uncertainty on the lepton energy scale gave systematic

errors of about 80 MeV at the Tevatron for earlier data (Run I, Ref. [117]) and recently lowered to less than 30 MeV (Run II, Ref. [118]). The W mass measurement is performed by fitting the data to distributions obtained with Monte Carlo simulations at different masses. The modeling of the M_W^T distribution used for the fitting procedure is another source of systematic uncertainty. Relevant inputs to the Monte Carlo models are the electron energy and muon momentum resolutions, the response of the detector to the recoiling hadronic system and the distributions of the W transverse and longitudinal momentum. Leptonic decays of the Z boson obtained during the same experimental conditions can be used to calibrate the first two effects. The latter is constrained using the measurement of the forward-backward charge asymmetry in W decays. The average of the measurements of the W mass from $p\bar{p}$ colliders is $m_W = 80.429 \pm 0.039$ GeV [118].

9.2 W production in e^+e^- collisions

At centre-of-mass energies greater than $2m_W \approx 161$ GeV W pairs can be produced in e^+e^- collisions. Three diagrams, usually called *CC03 diagrams* (CC stands for Charged Currents) contribute at Born level, as shown in Fig. 9.5. The first two diagrams involve vertexes with three interacting gauge bosons (Triple Gauge Couplings, or TGC's) while the third represents the exchange of a neutrino in the t channel. The Born-level matrix element depends on the electron beam helicity (κ) [1], on the outgoing W's helicities (λ_-, λ_+), on the s,t Mandelstam variables and is given by

$$\mathcal{M}(\kappa, \lambda_-, \lambda_+, s, t) = \frac{e^2}{2s_W^2}\frac{1}{t}\mathcal{M}_1\delta_{\kappa -} + e^2[\frac{1}{s} - \frac{c_W}{s_W}g_{eeZ}\frac{1}{s - M_Z^2}]2(\mathcal{M}_2 - \mathcal{M}_3) \tag{9.6}$$

where $\delta_{\kappa -}$=1 for left-handed electrons and zero otherwise, $c_W = \frac{m_W}{m_Z}$, $s_W = \sqrt{1 - c_W^2}$, and g_{eeZ} is the Z-electron coupling. The expressions for $\mathcal{M}_1, \mathcal{M}_2, \mathcal{M}_3$ can be found in [119]. For small values of the W velocity $\beta = \sqrt{1 - 4\frac{m_W^2}{s}}$, i.e. close to the WW threshold, the t-channel process dominates:

$$\frac{\mathcal{M}_2}{\mathcal{M}_1} \approx \frac{\mathcal{M}_3}{\mathcal{M}_1} \approx \beta \tag{9.7}$$

[1] The positron beam helicity must be equal and with opposite sign.

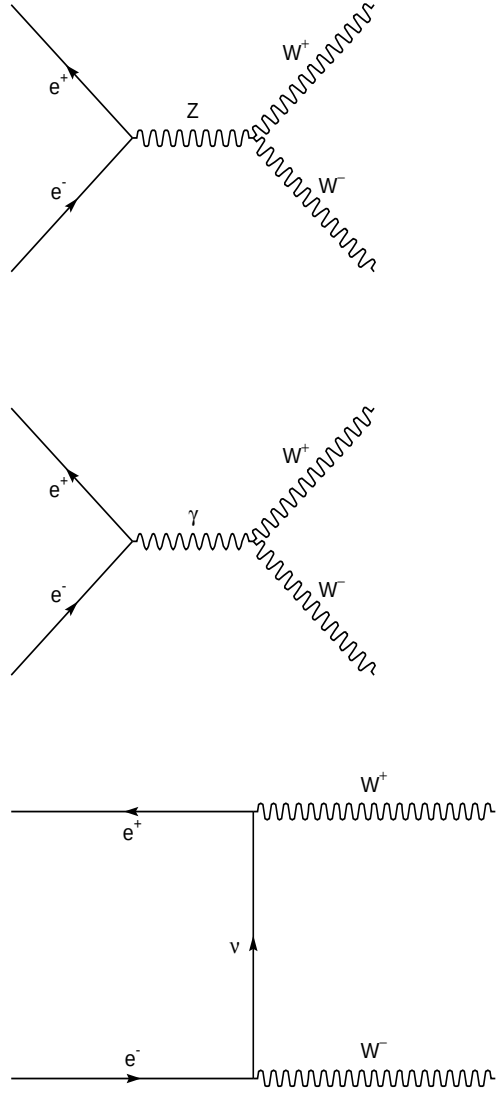

Fig. 9.5 Diagrams contributing to WW production at LEP.

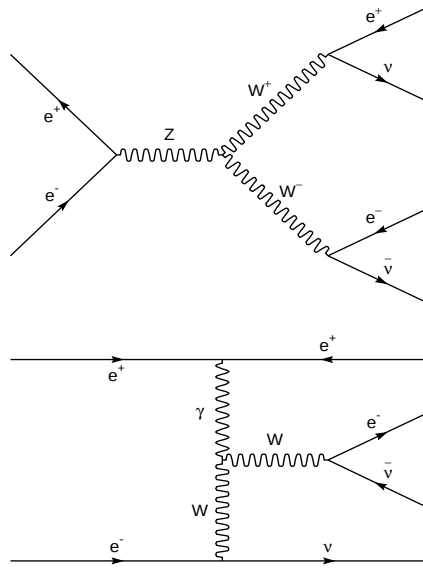

Fig. 9.6 Example of two diagrams contributing to 4f final states at LEP. The second diagram represents an example of single-W production.

and the cross section for unpolarized beams and W's can be computed as [120]

$$\frac{d\sigma}{d\Omega} = \frac{\beta}{64\pi^2 s} \sum_{\kappa,\lambda_-,\lambda_+} \frac{1}{4} |\mathcal{M}(\kappa, \lambda_-, \lambda_+, s, t)|^2$$
$$\approx \frac{\alpha^2}{s} \frac{1}{4s_W^4} \beta [1 + 4\beta cos\theta \frac{3c_W^2 - 1}{4c_W^2 - 1} + \mathcal{O}(\beta^2)] \quad (9.8)$$

showing the dominant term proportional to the W velocity entirely due to the t-channel.

Above threshold Eq. (9.8) does not hold and a cross section computed using the t-channel diagram only would grow as $log(s)$ with increasing centre-of-mass energy and eventually violate unitarity. The negative interference with the WWZ and $WW\gamma$ processes yields, for LEP energies above 180 GeV, a weakly increasing cross-section of about 17 pb^{-1}. It must be pointed out that a cross-section definition based only on the three CC03 diagrams is not gauge invariant. The physical process is $e^+e^- \rightarrow W^+W^- \rightarrow ffff$ where $ffff$ indicates the final state made of

four fermions. In principle all four fermion final states must be taken into account, see for instance Fig. 9.6 for an example of two processes with identical final states (the second process is called single-W production and is important for the study of TGC's, described in the last Section). In practice in this context, within typical experimental cuts, the cross sections computed with the full set of four fermion diagrams and the CC03 only turn out to be numerically very similar.

While at the Z pole decays of the Z boson can be selected in an essentially background-free environment, $e^+e^- \to W^+W^-$ events at higher energies have to be separated from the dominant two-photon [121] and two-fermion [122] processes (Fig. 9.7). The two-photon processes (as $e^+e^- \to q\bar{q}e^+e^-$) have a large cross section but low visible energy in the experimental apparatus and are characterized by low transverse momentum particles. They can be rejected relatively easily by simple selection cuts. The two-fermion events are mainly related to the radiative tail of the Z resonance and consist in the production of an on-shell Z boson together with the emission of a ISR photon of energy

$$E_\gamma = \frac{s - M_Z^2}{2\sqrt{s}}. \tag{9.9}$$

These $e^+e^- \to f\bar{f}\gamma$ events are typically longitudinally unbalanced, since the ISR photon is often lost along the beam line and the Z boson is boosted in the laboratory frame. The visible energy in this case is close to the Z mass. These features can be used to tag these events and considerably reduce the background. Two-fermion events with the ISR photon emitted within the apparatus acceptance can be rejected by detecting high energy isolated photons.

Decays of W bosons to hadrons are twice as frequent as decays to leptons. This is a consequence of quarks' three colours and the top mass being too large for the W to decay to the third quark family. Essentially only W^+ decays to $u\bar{d}$ and $c\bar{s}$ are allowed (other allowed combinations are suppressed by low CKM matrix elements) for a total of six states when three colours are taken into account. Three kind of leptonic decays are allowed ($W \to e\nu, \mu\nu, \tau\nu$), resulting in a branching ratio of 2/3 for the hadronic decays. Since W's are produced in pairs, the four-fermion $e^+e^- \to W^+W^- \to ffff$ events are classified in three topologies:

- fully hadronic decays ($e^+e^- \to W^+W^- \to qqqq$, about 45% of the

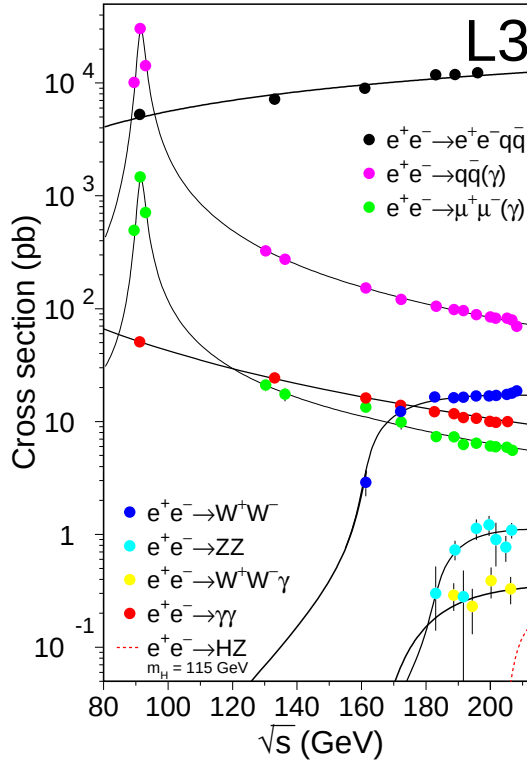

Fig. 9.7 Cross sections for various processes at LEP. (Courtesy of Salvatore Mele.)

events), characterized by four jets in the apparatus [2];

- semileptonic decays ($e^+e^- \to W^+W^- \to qql\nu$, about 44% of the events), with two jets, an high energy lepton and missing energy due to the undetected neutrino;
- fully leptonic decays ($e^+e^- \to W^+W^- \to l\nu l\nu$, about 11% of the events), characterized by two high-energy acollinear leptons and missing energy.

Experimentally three different event selections correspond to the three topologies. Fully hadronic decays are selected by requiring high multiplicity

[2]The label q indicates a generic quark (or anti-quark).

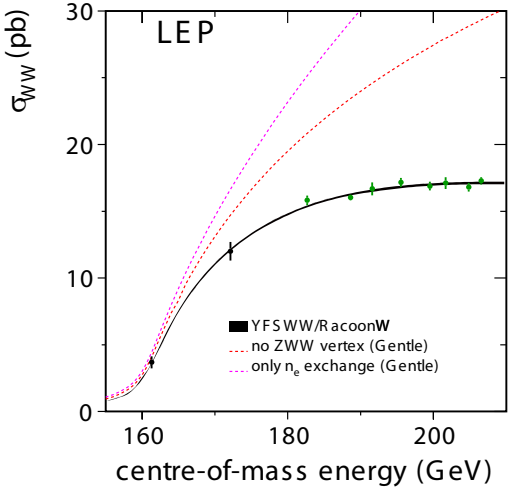

Fig. 9.8 The $e^+e^- \to W^+W^-$ cross section as a function of the centre-of-mass energy. The experimental measurements are compared to theoretical predictions. (Courtesy of the LEP Electroweak Working Group).

events and four hadronic jets. Selections are based on event properties as sphericity, jet angles, and other event-shape variables, often combined with neural network techniques. Typical efficiencies are $\approx 85\%$ with background contaminations of $\approx 15\%$. Semileptonic decays selections are based on the requirement of one isolated lepton, two reconstructed jets and missing momentum. The isolated lepton can be an electron, a muon or a tau, selected as a low multiplicity jet. In this channels the typical selection efficiency is $\approx 70\%$ and the background contamination very low, of the order of a few percent. Leptonic decays selections require low multiplicity events, with two isolated acoplanar leptons with missing transverse momentum. The lepton candidates can be low multiplicity jets to account for taus and final state radiation. Efficiencies around 50% are obtained with low background contamination ($\approx 10\%$). While in events with one or two leptons can be further classified according to the lepton species (for example semileptonic-tau events or electron-muon leptonic decays) in fully hadronic decays the quark flavours are not distinguished and all sub-channels are treated together.

The cross sections of the various channels are computed in a common likelihood fit with poissonian statistics in order to take into account cross contaminations among channels (i.e. the fraction of event of one kind selected in a different class). Backgrounds from non-four-fermion events, as computed from Monte Carlo simulations, are subtracted in the fit. The cross sections are corrected for the effect of non-WW four-fermion events (see, for instance, the single-W process of Fig. 9.6). The latter correction is of the order of 1%. The total cross section as measured at LEP and compared to recent calculations [123] is shown in Fig. 9.8. The measurements are a strong indication in favour of the existence of WWZ and $WW\gamma$ TGC's. From the individual cross sections [124] the W decay branching ratios can be computed. The hadronic branching ratio amounts to $(67.48 \pm 0.28)\%$ in agreement with the Standard Model expectation (67.51%). The individual leptonic branching ratios are $BR(W \to e) = (10.65 \pm 0.17)\%$, $BR(W \to \mu) = (10.59 \pm 0.15)\%$, and $BR(W \to \tau) = (11.44 \pm 0.22)\%$. The branching ratios of W into electron and muon are in good agreement with the hypothesis of lepton universality, while the tau channel shows an higher value (2.8 standard deviations higher, if electron and muon are combined together and correlations taken into account). If the three leptonic channels are combined, assuming lepton universality, the leptonic branching ratio is $BR(W \to \ell) = (10.84 \pm 0.09)\%$, in agreement with the MSM expectation (10.83%).

9.3 W mass measurement in e^+e^- collisions

Data taken with e^+e^- collisions provide information on the the W mass in two ways. At threshold the cross section itself is sensitive on the W mass value, beyond threshold W bosons, and their invariant mass, can be reconstructed from their decay products.

The total cross section at threshold is obtained by integrating Eq. (9.8) over the angles, giving

$$\sigma \approx \frac{\pi\alpha^2}{s}\frac{1}{4s_W^4}4\beta + \mathcal{O}(\beta^3)]. \tag{9.10}$$

The linear dependence on the W velocity translates into a dependence on the W mass, entirely due to the t channel neutrino exchange. The contribution of diagrams involving trilinear couplings, that are tested with limited precision and could be modified by new physics (see next chapter),

is $\mathcal{O}(\beta^3)$, keeping the model dependence small. Because of the limited statistics collected by LEP experiments at the WW threshold the result from this technique is affected by a rather large uncertainty. The cross section from data taken at a centre-of-mass-energy of 161 GeV is $\sigma = 3.69 \pm 0.45\, pb$, corresponding to $m_W = 80.40 \pm 0.22$ GeV/c^2.

An order of magnitude in precision is gained with direct W reconstruction. The measurement is based on the $W^+W^- \to qqqq$ and $W^+W^- \to qql\nu$ channels ; information on the W mass can also be provided by the fully leptonic $l\nu l\nu$ channel, but the precision is limited by the lower branching ratio and the presence of two undetected neutrinos. Jet reconstruction is the first step of the measurement: two jets (four jets) are reconstructed in the semileptonic (fully hadronic) channel. An iterative procedure (Section 7.1) based on a metric, typically related to the invariant mass, is used to build the jets. The closest particles are joined together to form a new pseudoparticle (*jetlet*) and the process ends when only two (or four for fully hadronic events) jets are left. In the procedure the four-momentum of the new jetlet is normally computed from the sum of the two four-momenta of the previous jetlets and the new object acquires a mass from the invariant mass of the resulting four-momentum. The W mass is computed from the invariant mass of the two-jet system:

$$m_W = \sqrt{4E_iE_j(1 - \beta_i\beta_j \cos(\theta))} + m_i^2 + m_j^2 \tag{9.11}$$

where i and j refer to the two jets. In the fully hadronic channel there are three possible pairs of two-jet combinations; a criterion is needed to choose the best combination, based for instance on discarding clearly wrong pairings (out of a large window around 80 GeV/c^2) or on choosing the largest value of the CC03 matrix element (Eq. (9.6)). If the latter criterion is used the four vectors of the two jets and a nominal value of the W mass are used as input.

Since in e^+e^- collisions the four momentum of the initial state is known the W mass resolution can be greatly improved by applying a constrained kinematic fit to the four momenta of the reconstructed jets, leptons and missing momentum. The constraint is

$$\sum_k (E_k, \vec{P}_k) = (\sqrt{s}, 0, 0, 0) \tag{9.12}$$

where the sum is over all reconstructed objects. A further constraint can be applied by requiring the two W invariant masses to be equal, within

the expected W width. In semileptonic decays the mass of the leptonically decaying W is computed from the lepton and the missing momentum. In the kinematic fitting the four momenta of the reconstructed objects are allowed to vary within their expected uncertainties (hence, for example, since the energy of a jet is less well measured than the energy of a lepton a larger variation is allowed); typically a χ^2 is constructed and the constraints are imposed by Lagrange multipliers. As can be seen in Fig. 9.9 a sizeable improvement can be obtained.

The kinematic fit can be applied if the centre-of-mass energy, i.e. the beam energy of the accelerator, is precisely known. From Eq. (9.11) one gets

$$\frac{\delta m_W}{m_W} \approx \frac{\delta E_{beam}}{E_{beam}} \tag{9.13}$$

showing that the uncertainty on the centre-of-mass energy directly reflects on the mass uncertainty. At LEP the resonant depolarization technique, described in Section 6.4 and allowing a relative precision of 10^{-5}, worked only for beam energies up to 60 GeV and extrapolations were needed to calibrate the higher energies reached at LEP2. The extrapolation was controlled by the extensive use of NMR probes in the LEP magnets and cross checked in several ways. A special spectrometer was installed in the beam line to directly measure the beam momentum; the energy loss by synchrotron radiation, which is proportional to the fourth power of the beam energy, was measured by the frequency of the accelerating field. Finally the beam energy was measured directly with the data by means of Z radiative returns (see Eq. (9.9)), i.e. two-fermion events where a real Z is boosted in the laboratory system. In this events the opening angle of the two fermions produced in the Z decay depends on the centre-of-mass energy. The final uncertainty on the LEP2 beam energy [125] was about 20 MeV (the exact value depends on the year of data taking), corresponding to $\delta m_W \approx 17\,\mathrm{MeV/c^2}$.

Invariant mass distributions as measured at LEP, taking as an example the semileptonic channel, are shown in Fig. 9.10. The Breit-Wigner distribution of the W resonance is distorted by several effects:

- the emission of Initial State Radiation (ISR),
- phase space constraints, especially important at threshold,
- detector resolution,
- wrong particle assignment to the W's,

- background contamination,
- selection cuts.

These effects need to be taken into account to extract the W mass from the experimental distributions. The differential cross section as a function of the two W masses ($m_{1,2}$) can be written as

$$\frac{d^2\sigma}{dm_1 dm_2} = H \times \sigma_{CCO3} \times \rho_1 \times \rho_2 \tag{9.14}$$

where H is a radiator similar to the one described for the Z lineshape (Section 6.2) , σ_{CCO3} is the Born level matrix element (Eq. (9.6)) and $\rho_{1,2}$ are the relativistic Breit-Wigner distributions for the two W bosons. Detector effects can be taken into account by a resolution function and included by a convolution integral as

$$\Phi = \int dM_1 \int dM_2 \, G(M_1, M_2, m_1, m_2) \frac{d^2\sigma}{dm_1 dm_2} \tag{9.15}$$

where G is the transfer resolution function. The W mass can be evaluated by maximazing the likelihood

$$\mathcal{L} = \prod_{i=1}^{N} \Phi(M_1, M_2; m_W) \tag{9.16}$$

running over all the N events, with $M_{1,2}$ as measured masses and m_W as free parameter (and result) of the fit. The result is biased (because in practice it is impossible to take analytically into account all effects) and the method must be calibrated on Monte Carlo events. Alternatively the Monte Carlo simulation can be directly used by generating simulated distribution with various input W masses and by choosing the Monte Carlo sample that best fits the data. This technique is free of bias (provided that the Monte Carlo simulation includes all effects!) and calibrated by definition. Since the production of an infinite number of Monte Carlo samples is impossible a finite number of samples with a grid of input masses is used, and intermediate W mass input values are interpolated. The interpolation takes place with a technique called *re-weighting*. Each Monte Carlo event (i) is given a weight (w_i) that is 1 for all events in the grid, while for interpolated events is

$$w_i(m_W) = \frac{|\mathcal{M}(m_W, p_1^i, p_2^i, p_3^i, p_4^i)|}{|\mathcal{M}(m_W^{gen}, p_1^i, p_2^i, p_3^i, p_4^i)|} \tag{9.17}$$

where m_W^{gen} is the input values for the closest sample in the grid and p_j^i is the four vector of the fermion j in $e^+e^- \to W^+W^- \to f_1f_2f_3f_4$. Since the typical mass resolution obtained with kinematic fits is 1–2 GeV/c^2 the experimental distributions are sensitive to the W width, Γ_W. Within the Standard Model this is fixed by the W mass and the Fermi constant by the relation $\Gamma_W = \frac{3G_F}{2\sqrt{(2)}\pi} m_W^3 \approx 2.1$ GeV/c^2 . The methods discussed here are often generalized to a simultaneous measurement of two parameters: m_W and Γ_W .

The separation of the decay vertexes of the two W's in $e^+e^- \to W^+W^- \to ffff$ is smaller than the typical hadronization scale (1 fm) since $\Gamma_W \sim 10\Lambda_{QCD}$. When both W's are hadronically decaying interconnection phenomena in the final state may link the decay products: final hadrons cannot longer be labeled as belonging to the decay stream of a specific W boson. The colour flow between two quarks originating from two different W bosons is called *colour reconnection*, a phenomenon that has been observed in b hadron decays as $B_d^0 \to J/\Psi K_s^0$. Another effect that can correlate hadrons from different W's is the symmetrization of the wave functions arising from Bose–Einstein statistics. It has been shown [126] that both phenomena can lead to an important bias ($O(100)$ GeV/c^2) in the measured W mass. The exact size of these effects is difficult to predict since they are non computable in perturbative QCD. Fortunately the W mass shift is not the only effect of interconnection phenomena. Colour reconnection modifies the flow of low momentum particles, especially in the region between jets, while Bose–Einstein correlations bring same–sign pions close in momentum phase space. The effects can be monitored with distributions measured on experimental data.

The W mass measured in e^+e^- collisions by LEP in the two channels is [127, 143]

$$m_W = 80.372 \pm 0.036\ (W^+W^- \to qql\nu)$$
$$m_W = 80.387 \pm 0.059\ (W^+W^- \to qqqq)$$

and the combined value is $m_W = 80.376 \pm 0.033$. The purely statistical error for both channel is about 30 MeV/c^2, the total error is larger for the $qqqq$ channel because of the systematic uncertainty related to colour reconnection effects. The combination of the LEP measurements with the Tevatron results obtained with the techniques described in Section 9.1 gives [118]

$$m_W = 80.398 \pm 0.025\,. \tag{9.18}$$

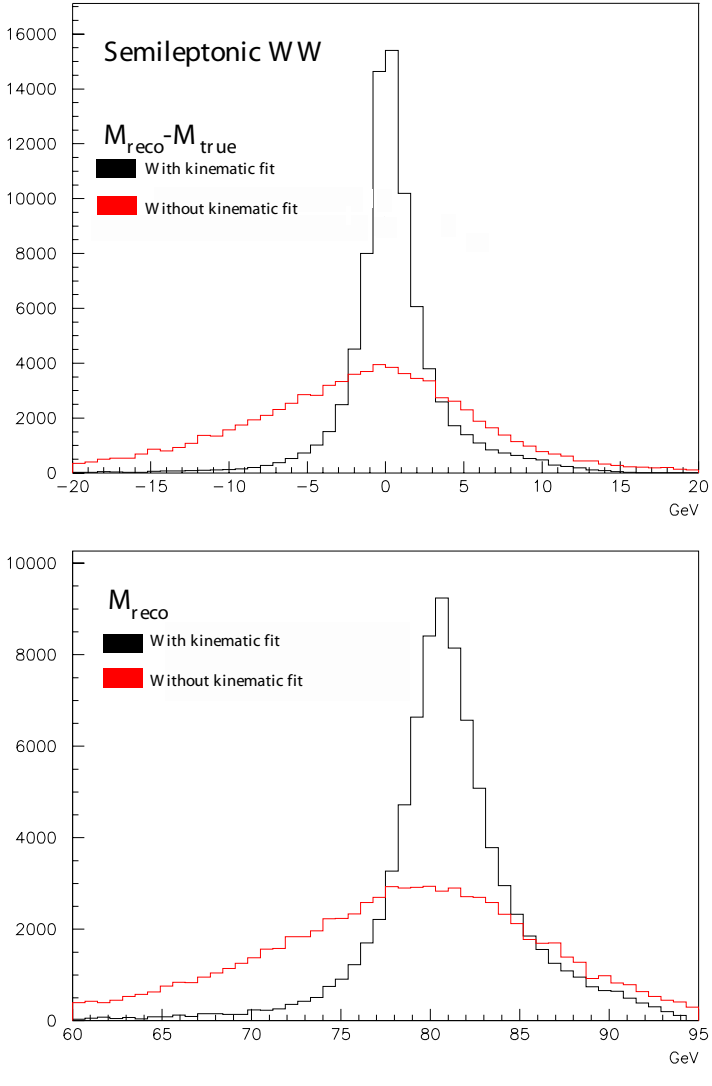

Fig. 9.9 Effect of the kinematic fit on the W mass reconstruction at LEP2. (Courtesy of Andrea Venturi.)

This result is compared to the W mass predicted by the one-loop calculations of Chapter 3, shown as a function of the Higgs mass, in Fig. 9.11.

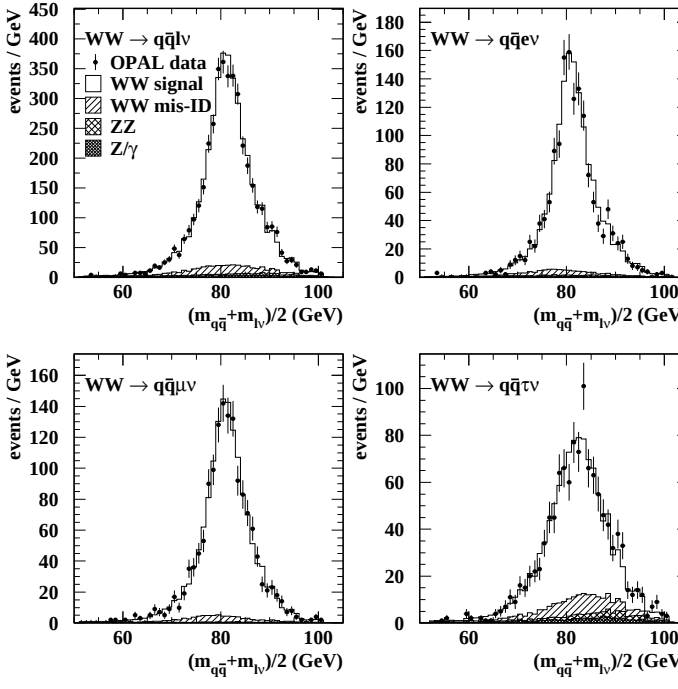

Fig. 9.10 Examples of invariant mass distributions used to measure the W mass at LEP. The plots are made with semileptonic WW events. The first plot shows the three lepton channels combined, while in the other plots the electron, muon and tau events are separately shown. The points with error bars represents the data, while the histograms show the simulation. The background contamination is indicated by the hatched histograms. For each event the average of the two measured masses is used.

9.4 Triple gauge couplings

The presence of tree level triple gauge boson interactions is a distinct signature of the non–abelian nature of the Standard Model and a consequence of its $SU(2)_L \times U(1)_Y$ gauge structure. The model predicts the same coupling g for the interaction of weak bosons to matter and among themselves. The existence of triple gauge couplings (TGC's) is proved by the behaviour of the $e^+e^- \to W^+W^-$ total cross section (Fig. 9.8); its energy dependence is consistent with the presence of both $WW\gamma$ and WWZ interactions and

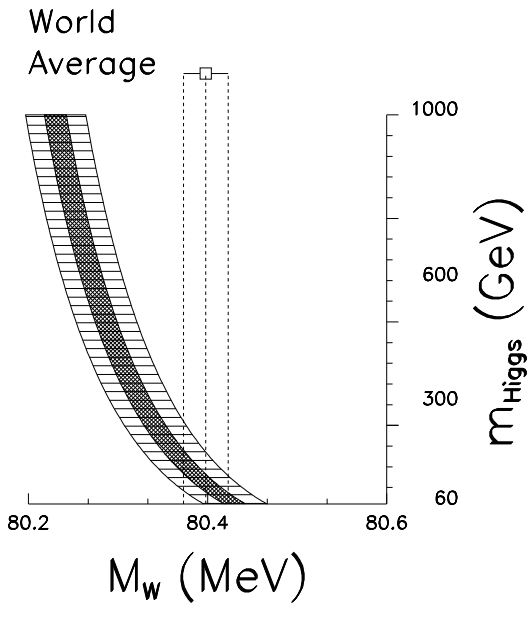

Fig. 9.11 Dependence on the Higgs mass of the prediction on m_W. The hatched bands shows the uncertainty on the prediction when varying other input parameters. These are the top mass and the fine structure constant at the m_Z scale, respectively. The same ranges as for Fig. 6.7 are used, for illustration only. The experimental measurements of m_W are indicated by the error bar.

of a universal g coupling. Triple gauge interactions are also seen in other processes, such as single W production in e^+e^- interactions (Fig. 9.6) or associated Wγ production at hadron colliders, both testing the $WW\gamma$ vertex.

Triple gauge couplings do not only affect production rates, but also angular distributions of emitted weak bosons and of their decay products. Precision tests of triple gauge couplings, and of $SU(2)_L \times U(1)_Y$ predictions, require detailed measurements of differential cross sections. Angular distributions analyse different weak boson helicity states: since the longitudinal component of the helicity is directly linked to the symmetry breaking mechanism and to the mass generation these are fundamental tests of the theory.

Neutral triple gauge boson couplings, as ZZZ, $ZZ\gamma$ or $Z\gamma\gamma$, do not exist in the Standard Model at tree level. The existence of anomalous neutral couplings would affect processes as $e^+e^- \to ZZ$ or $e^+e^- \to Z\gamma$.

No departure from the cross sections predicted by the Standard Model for these processes has been detected, todate.

Next Subsection is dedicated to the measurement of the angular differential cross sections and of the W polarization in the $e^+e^- \to W^+W^-$ channel. The general charged TGC analysis follows.

9.4.1 *The $e^+e^- \to W^+W^-$ angular analysis and the W polarization*

If initial state radiation and the finite W width are neglected, the $e^+e^- \to W^+W^-$ process is described by 5 angles

- the angle θ_W between the W^- and initial e^- in the W^+W^- rest frame;
- the polar θ_f^* and azimuthal ϕ_f^* angles of the fermion in $W^- \to f\bar{f}'$ measured in the rest frame of its parent W^-;
- the corresponding polar and azimuthal angles of the fermion in the W^+ rest frame.

In the semileptonic $W^+W^- \to qql\nu$ channel the charge of the lepton identifies without ambiguities the W^-. The missing momentum provides information on the direction and energy of the undetected neutrino; kinematic fitting is used to improve the measurement, similarly to what is done for the measurement of the W mass. Since in $W^+W^- \to qql\nu$ the quark and the anti-quark from the hadronic W decay are not identified, there are two ambiguous solutions both entering (with weight 0.5) the angular distributions used for the measurements. Ambiguities are more important in the fully hadronic and fully leptonic channels. In the first case jets are paired using the method described for the W mass measurement (here the closeness to the W mass can also be used); after pairing the charges of the charged particles associated to jets belonging to the individual W's are weighted to form a charge estimator (this is similar to the jet charge method employed for the measurement of the b asymmetry, see Chapter 8). The correct charge can be identified with purities of about 70–80 %. As far as the fully leptonic channel is concerned the constraint that the two $l\nu$ systems should have an invariant mass consistent with the W mass helps in reconstructing the neutrino momenta. The quadratic nature of the constraint, however, yield a two-fold ambiguity: solutions obtained by flipping both neutrinos with

respect to the plane defined by the two leptons are equally valid. Again, both solutions enter the experimental distribution with equal weight. The semileptonic channel is clearly the best suited for TGC analyses, providing the highest sensitivity. All channels are used in the measurements based on the effective lagrangian described in next Subsection, while semileptonic decays only are used to determine the W polarization. Examples of angular distributions in semileptonic WW decays are shown in Fig. 9.12.

In the W rest frame transversely polarized W^- bosons with helicity $\pm$ have angular distributions $(1 \mp cos\theta_f^*)^2$; the sign is reversed for W^+. Longitudinally polarized W bosons feature a $sin^2\theta_f^*$ dependence. The W^- polarization can be measured by fitting the differential distribution

$$\frac{1}{N}\frac{dN}{dcos\theta_f^*} = \rho_{--}\frac{3}{8}(1+cos\theta_f^*)^2 + \rho_{++}\frac{3}{8}(1-cos\theta_f^*)^2 + \rho_{00}\frac{3}{4}sin^2\theta_f^* \quad (9.19)$$

with the ρ_{ii} fraction representing the contributions from the three W helicity states and N is the number of events in each bin. A similar distribution is used for the W^+ and the ρ_{ii} from W bosons of opposite charge can be combined if CP invariance is assumed. In practice Eq. (9.19) can be used only for the leptonic decay, as the quark charge is not reconstructed ρ_{--} and ρ_{++} are summed and $|cos\theta_f^*|$ is used for quarks. The helicity fractions are measured as a function of the W^- scattering angle θ_W and agree with the Standard Model expectations, as can be seen in Fig. 9.13. At LEP2 energies the expected average fraction of longitudinally polarized W bosons is 24 %. The combined experimental result agree, within 2%, with this expectation [128, 129].

The fit can be generalized with the spin density matrix (SDM) formalism. The matrix is defined as

$$\rho_{ij}(s, cos\theta_W) = \frac{F_i F_j^*}{\sum_i |F_i|^2} \quad (9.20)$$

where F_i is the W^- helicity amplitude for helicity i and has to be taken as summed over the initial electron and positron beam helicities. An analogous matrix can be defined for W^+; the elements are the same if CP conservation is assumed and their comparison sets limits on CP violation in TGC's. The spin density matrix is a hermitian tensor with unit trace, the diagonal

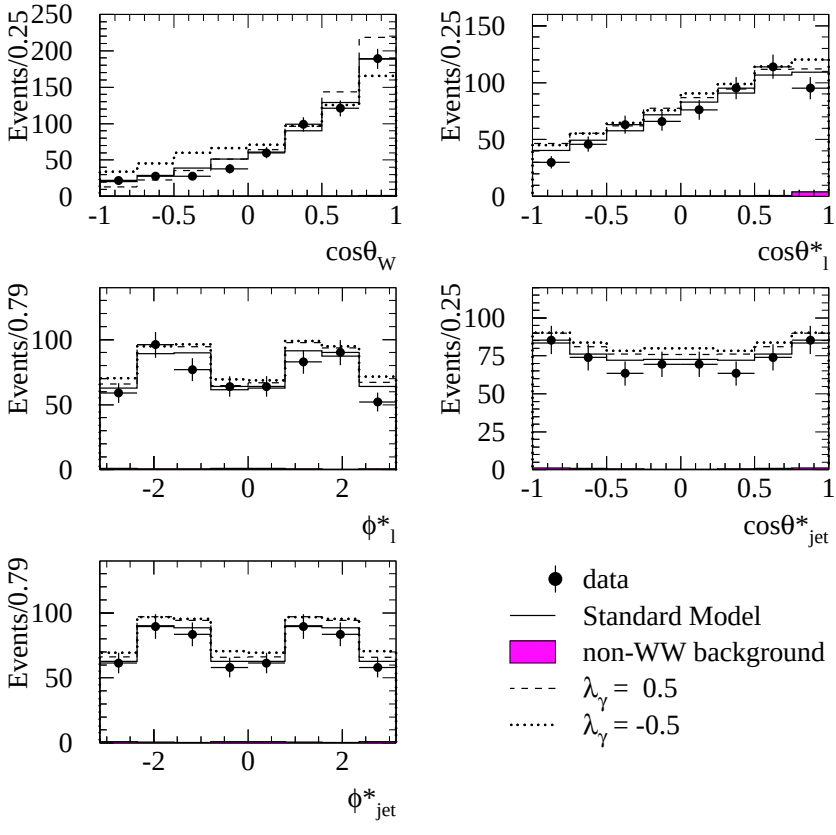

Fig. 9.12 Examples of angular distributions in $e^+e^- \to W^+W^-$ semileptonic events. The first plot represents the cosine of the angle θ_W between the W^- and initial e^- in the W^+W^- rest frame. The cosine of the polar angle, θ_l^*, and of the azimuthal angle, ϕ_l^*, angles of the lepton measured in the rest frame of its parent W are shown in the second and third plots, respectively. The last two plots show the same two angles for the jets in the W hadronically decaying. The solid histograms show the Standard Model simulation, while the two different dashing indicates the expectations for particular values of an anomalous triple gauge couplings, λ_γ. The data are from the Aleph experiment.

components corresponds to the helicity fractions of Eq. (9.19). For a generic polarization vector $\vec{e}$ the SDM allows to compute the probability that the W is in that specific polarization state by taking $\rho_{ij} e_i^* e_j$. The matrix element can be computed by means of projection operators applied to the differential cross section [130].

9.4.2 *The effective TGC lagrangian and the couplings*

The most general form for an effective charged TGC lagrangian consistent with Lorentz invariance involves 14 complex couplings, 7 for the $WW\gamma$ vertex and 7 for the WWZ vertex [131]:

$$\begin{aligned}\mathcal{L} = & ig_1^V(W^\dagger_{\mu\nu}W^\mu V^\nu - W^\dagger_\mu V_\mu W^{\mu\nu}) + i\kappa_V W^\dagger_\mu W_\nu V^{\mu\nu} \\ & + \frac{i\lambda_V}{m_W^2} W^\dagger_{\lambda\mu} W^\mu{}_\nu V^{\nu\lambda} - g_4^V W^\dagger_\mu W_\nu(\partial^\mu V^\nu - \partial^\nu V^\mu) \\ & + g_5^V \epsilon^{\mu\nu\rho\sigma}(W^\dagger_\mu \overleftrightarrow{\partial}_\rho W_\nu)V_\sigma + i\tilde{\kappa}_V W^\dagger_\mu W_\nu \tilde{V}^{\mu\nu} \\ & + \frac{i\tilde{\lambda}_V}{m_W^2} W^\dagger_{\lambda\mu} W^\mu{}_\nu \tilde{V}^{\nu\lambda}\,. \end{aligned} \tag{9.21}$$

Some couplings are C- or P-violating while in the Standard Model C- and P-conservation is predicted in triple gauge couplings. In Eq. (9.21) $V^\mu (= V^{\mu\dagger})$ stands either for the γ or Z field, W^μ for the W^- field, $W_{\mu\nu} = \partial_\mu W_\nu - \partial_\nu W_\mu$, $V_{\mu\nu} = \partial_\mu V_\nu - \partial_\nu V_\mu$, $\tilde{V}_{\mu\nu} = \frac{1}{2}\epsilon_{\mu\nu\rho\sigma}V^{\rho\sigma}$ and $(A \overleftrightarrow{\partial}_\mu B) = A(\partial_\mu B) - (\partial_\mu A)B$.

All couplings have been experimentally tested with the $e^+e^- \to W^+W^-$ sample collected at LEP2. A fit of the total cross section and the angular distributions described in the previous Subsection has been performed to models where only one coupling at the time is allowed to vary, while all the others were set to zero [132]. Bounds on several couplings can also be set from precision measurements at the Z pole [133] . In most analyses C- and P-conservation and electromagnetic gauge invariance is assumed and the 14 couplings are reduced to 5 : g_1^Z, κ_γ, κ_Z, λ_γ, λ_Z. Within the Standard Model $g_1^Z = \kappa_\gamma = \kappa_Z = 1$ and $\lambda_\gamma = \lambda_Z = 0$. The couplings can be related to physical properties of the gauge bosons, for instance the W anomalous magnetic moment (μ_W) and the W anomalous electric quadrupole moment (Q_W) can be written as

$$\mu_W = \frac{e}{2m_W}(1 + \kappa_\gamma + \lambda_\gamma)$$
$$Q_W = -\frac{e}{m_W}(\kappa_\gamma - \lambda_\gamma).$$

The requirement of local $SU(2)_L \times U(1)_Y$ gauge invariance introduces the further constraints

$$\begin{aligned} \Delta\kappa_Z &= -\Delta\kappa_\gamma tan^2\theta_W + \Delta g_1^Z \\ \lambda_\gamma &= \lambda_Z \end{aligned} \tag{9.22}$$

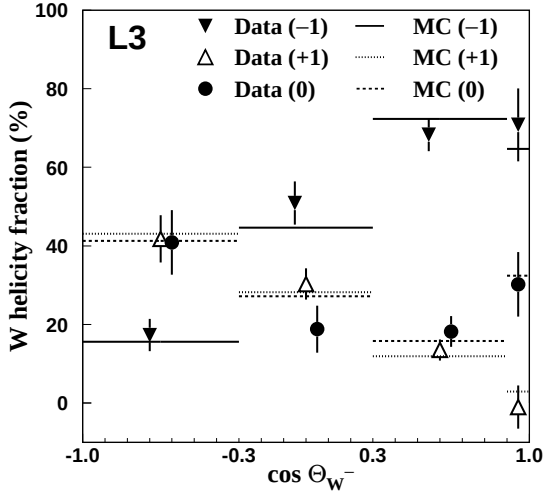

Fig. 9.13 W helicity fractions, $\rho_{--}(-1), \rho_{++}(+1), \rho_{00}(0)$, measured in four different $cos\theta_W$ bins. The Standard Model expectations are indicated.

with Δ indicating the deviation with respect to the Standard Model prediction (θ_W here is the electroweak mixing angle), leaving three independent couplings: $g_1^Z, \kappa_\gamma, \lambda_\gamma$. The three couplings have been measured at LEP using $e^+e^- \to W^+W^-$ (Fig. 9.5) and $e^+e^- \to W^+e\nu$ (Fig. 9.6, second diagram) events. The second process, single W production, is very useful to enhance sensitivity in the measurement of the $WW\gamma$ vertex. For this purpose also the single photon $e^+e^- \to \gamma\nu\bar{\nu}$ is useful. The analyses are based on the measurement of the total cross sections and of angular distributions, described in the previous Subsection for the WW case. The constraints obtained from the LEP experiment's [134] combination are shown in Fig. 9.14.

The three couplings are consistent with the Standard Model expectation, in particular the g_1^Z and κ_γ measurements confirm the presence of triple gauge interactions with the expected strength, with a precision of $\sim 2\%$.

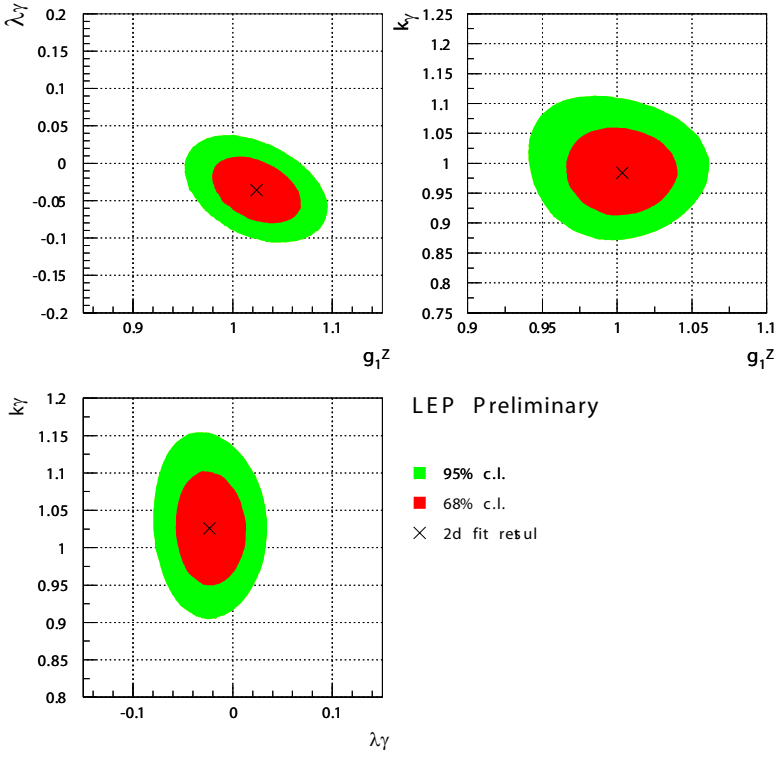

Fig. 9.14 The 68% and 95% confidence level contours allowed by LEP data for the triple gauge couplings $\Delta g_1^Z, \Delta\kappa_\gamma, \lambda_\gamma$. In each of the three plots one coupling is fixed to the Standard Model value, while the others are allowed to vary. (Courtesy of the LEP Electroweak Working Group.)

This page intentionally left blank

Chapter 10

The Top Quark and Its Mass

Many electroweak observables described in this book, as the forward-backward asymmetries at the Z peak or the W mass, are very sensitive to the value of the mass of the top quark. This is because of the non-decoupling property of the pure electroweak radiative corrections: the effect of particle masses much larger than the electroweak scale ($m_t \approx 170$ GeV) instead of vanishing with some power of $\frac{m_Z}{m_X}$ grows with m_X. The contribution of the top quark mass to the Z self-energy, for instance, is proportional to $(\frac{m_t}{m_Z})^2$, to be compared with its contribution to the photon vacuum polarization (pure QED) that is $\approx (\frac{m_Z}{m_t})^2$. Not surprisingly, the top mass is very relevant to draw conclusions from electroweak global fits; on the other hand electroweak measurements can be used to predict rather precisely the value of the top mass. There are reasons to believe that the top mass is a fundamental parameter of the electroweak theory. This is suggested by the closeness to unity of its coupling with the Higgs field (the Yukawa coupling)

$$Y_t = \sqrt{2}\frac{m_t}{v} \tag{10.1}$$

with v, the vacuum expectation value, ≈ 246 GeV.

In this chapter, after reviewing the main properties of the top, the experimental issues related to the measurement of the mass of the most heavy quark are discussed. The results are then compared with the predictions of electroweak fits.

10.1 Top-quark properties

The top quark is the up-like ($I_{3L} = +1/2, Q = 2/3e$) weak isospin partner of the b quark. Many experimentally-measured b-quark properties show

that the b quark is the down-like member of a doublet, requiring the existence of the top. The couplings of the b quark to the Z (Chapter 8) are consistent with this picture, in particular the measurement of R_b would be dramatically different with an isospin-singlet b quark since

$$\frac{\Gamma(Z \to b\bar{b})^{I_3=-1/2}}{\Gamma(Z \to b\bar{b})^{I_3=0}} = \frac{1 - \frac{4}{3}sin^2\theta_W + \frac{8}{9}sin^4\theta_W}{\frac{4}{9}sin^4\theta_W} \approx 30 \tag{10.2}$$

as can be seen from Eq. (1.118). The energy dependence of the b forward-backward asymmetry precisely determine the electric charge of the b as being $Q = -1/3e$. The existence of the top is also required by the cancellation of triangular anomalies [22] that show divergences independent on the fermion mass, but dependent on the couplings. The b quark requires a partner for the cancellation to hold.

The top decays almost exclusively through charged-current weak interaction to a W boson and a b quark. Other charged currents decays are negligible, as can be seen from the following argument. If CKM unitary is assumed, $|V_{tb}|^2 + |V_{cb}|^2 + |V_{ub}|^2 = 1$, one gets $|V_{tb}|$ from the measurements of $|V_{cb}| = (41.6 \pm 0.6) \times 10^{-3}$ and $|V_{ub}| = (4.31 \pm 0.30) \times 10^{-3}$ [13]. The decay fraction to Wb can then be computed from

$$\frac{BR(t \to Wb)}{BR(t \to Wq)} = \frac{|V_{tb}|^2}{|V_{tb}|^2 + |V_{td}|^2 + |V_{ts}|^2} = 0.99825 \pm 0.00005 \tag{10.3}$$

where the denominator has been taken as unity, again from the assumption of unitarity. Flavour changing neutral currents decays as $t \to cZ, c\gamma, cg$ are not expected in the Standard Model at tree level, loop calculations give $BR(t \to cZ, c\gamma, cg) \approx \mathcal{O}(10^{-13})$. Experimental evidence for top FCNC would be a sign of new physics; direct searches gave, until now, negative results [135].

The fact that the top quark should be much heavier than the b was expected before electroweak measurements took place: from the frequency of the $B_d^0\bar{B}_d^0$ oscillations one could predict a top mass larger than 50 GeV [136]. Indeed the oscillation occurs through box diagrams where the top lines play an important role. A large top mass implies a very short lifetime, since the top quark bW partial width is

$$\Gamma(t \to bW) = \frac{G_F}{8\pi\sqrt{(2)}} m_t^3 |V_{tb}|^2 \approx 1.5\,\mathrm{GeV/c^2}. \tag{10.4}$$

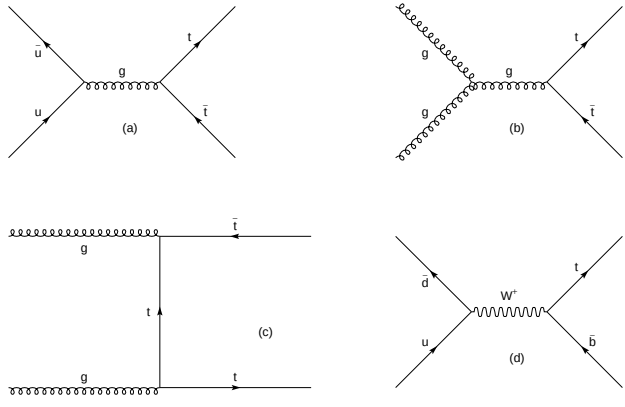

Fig. 10.1 Diagrams contributing to top production at hadron colliders: (a) quark annihilation (b) and (c) gluon-gluon fusion (d) example of single-top production.

about one order of magnitude larger than the typical hadronization scale. It follows that the top behaves as a free quark and decays before top hadrons are formed. In the purely weak $t \to bW$ decay only longitudinal and left-handed W's can be produced. Right-handed W's are suppressed from helicity arguments: since the b mass can be neglected the b is essentially produced as left-handed (because of the V-A structure of charged currents) and the conclusion follows from angular momentum conservation. Since the coupling to longitudinal W's is related to the Yukawa coupling, a measurement of the longitudinal-W decay-fraction in the top rest frame [137]

$$\mathcal{F}(t \to W_0 b) = \frac{m_t^2}{m_t^2 + 2M_W^2} \approx 70\% \tag{10.5}$$

is an important test of the Standard Model.

10.2 Direct measurement of the top mass

The top mass is too heavy for production via $e^+e^- \to t\bar{t}$ at colliders such as LEP or SLC, an e^+e^- centre-of-mass energy in excess of 350 GeV is required. The top was discovered in hadron collisions at the Tevatron in 1995 [36]. At hadron colliders the cross section can be written as a convolution

of the parton density functions (PDF's) for the (anti)protons (Section 9.1) and the cross section for the hard process $q\bar{q}, gg \to t\bar{t}$

$$\sigma(s, m_t^2) = \sum_{a,b} \int_0^1 dx_1 \int_0^1 dx_2 f_{h1}^a(x_1, \mu_f^2) f_{h2}^b(x_2, \mu_f^2) \hat{\sigma}_{ab}(\hat{s}, m_t, \alpha_s(\mu_r^2)) \tag{10.6}$$

where a, b are the possible combinations of partons (quark-antiquark or gluons), $f_{h1}^a(x_1, \mu_f^2)$ and $f_{h2}^b(x_2, \mu_f^2)$ represents the PDF's at factorization scale μ_f^2 and $\hat{\sigma}_{ab}$ is the cross section for the hard subprocess. The latter depends on the top mass, on $\hat{s} = x_1 x_2 s$ and on α_s evaluated at the scale μ_r^2. The scales are relevant for a proper evaluation of the higher order corrections. The hard subprocess cross section is maximal at $\approx 1.5 \times$ threshold $= 3\mathrm{m_t}$; taking for simplicity $x_1 \sim x_2$ one gets $x_{1,2} \sim \frac{525\ \mathrm{GeV}}{\sqrt{s}}$. At Tevatron energies the typical values of $x_{1,2}$ fall in a range where quark PDF's are much larger than gluon PDF's, on the contrary at LHC the gluons dominate. As a consequence the dominant $t\bar{t}$ production mechanism in $p\bar{p}$ interactions at 1.8 TeV (2.0 TeV for Tevatron RUN II) is $q\bar{q}$ annihilation. This process accounts for 90% (85% at RUN II) of the cross section (Fig. 10.1(a)), followed by gluon gluon fusion (Fig. 10.1(b), 10.1(c)) essentially accounting for the rest. At the LHC gluon gluon fusion will be the main production process, about nine times larger than annihilation. Another relevant production mechanism at hadron colliders is single-top production by weak interaction, see for instance Fig. 10.1(d) or the corresponding cross-diagram in the t-channel. The cross section for single-top is only a factor three lower than pair production, but single top events are much more difficult to detect. The $t\bar{t}$ cross section at the Tevatron is shown in Fig. 10.2 as a function of centre-of-mass energy, QCD-based theoretical calculations are in agreement with experimental measurements. The typical value for the cross section at LHC is 800 pb^{-1}, about two order of magnitudes larger.

As in the Standard Model all top decays include a W boson, the classification of $t\bar{t}$ events at hadron colliders has some analogy with the W^+W^- selection at e^+e^- machines, described in Chapter 9. Semileptonic, di-leptonic and fully hadronic decays can be defined according to the decay mode of the W, accounting for 45%, 11% and 44% of the events, respectively. The analogy, however, stops here since $t\bar{t}$ decays must be selected from an overwhelming hadronic background. The total proton-(anti)proton cross section at Tevatron energies is about 80 mb, raising to 100 mb at the LHC. Top identification is further complicated by the presence of low p_t remnants of the proton-(anti)proton interaction, caused by the partons not involved

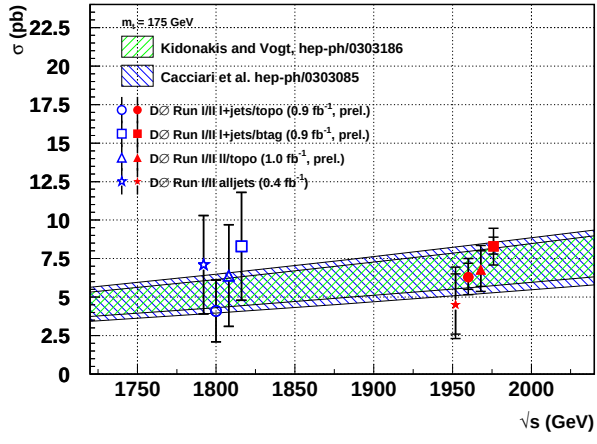

Fig. 10.2 Cross section for $t\bar{t}$ production at the Tevatron Collider, as measured by the D0 experiment. The cross section is measured using various final states; for each final state the total cross section is computed taking into account the expected final-state branching ratio. Dots and squares show the result obtained with two different selections of lepton+jet events (without or with b tagging), triangles are related to the dilepton channel and stars to the fully-hadronic channel. The two bands show the expected cross section, from two different QCD-based calculations. (Courtesy of Elizaveta Shabalina.)

in the hard process (*underlying event*) and by multiple final state interactions. An additional difficulty, especially at high luminosity (LHC), is due to interactions of other protons in the same bunch of beam-particles, superimposed to the same event (*pile up*).

Top events must be selected with stringent criteria, taking advantage of their distinctive signatures. The initial selection is based on the requirement of high p_t decay products, i.e. high energy jets and leptons in the central part of the detector. The central part is normally referred to as the low pseudorapidity region, with the pseudorapidity defined as $\eta = -\ln(\tan\frac{\theta}{2})$, where θ is the angle with respect to the beam line. A typical variable that helps suppressing the QCD background is the scalar sum of the transverse energy of all observed objects, where the transverse energy is $\mathrm{E_t} = \mathrm{E}\,\sin\theta$. Other variables inspired by e^+e^- physics, as the eigenvalues of Fox-Wolframm momenta, sphericity and acoplanarity are used to select spherical events.

A powerful tool to suppress background, and to choose the correct jet

combinations for the mass measurement, is b tagging. Most b tagging methods described in Chapter 7, in particular lifetime tagging and lepton tagging, can be successfully applied at hadron colliders for top selection and mass measurement. As for e^+e^- colliders lifetime tagging, based on impact-parameter measurements and secondary-vertex tagging, is more efficient than lepton tagging based on the detection of semileptonic b decays.

At hadron colliders jets are usually reconstructed with a *cone* algorithm. The energy deposited in a cone of radius $R = \sqrt{\Delta\eta^2 + \Delta\phi^2}$ around a starting direction (roughly defined using initial *seeds*) is summed up, the direction is re-defined after the initial cone clustering and the process is iterated until the algorithm converges. Typical values of R are around 0.5. This method, differently from the one described in Sections 7.1, 9.3 does not necessarily associate all particle in the events to jets.

As already anticipated, three main channels are defined for the mass measurement:

- The lepton-plus-jet channel, where one W is required to decay to an electron or muon and the other hadronically. The event is characterized by four jets, a lepton and missing transverse energy. In this channel b tagging is useful to reduce background and correctly identify the two b-jets.
- The dilepton channel, where both W's are leptonically decaying to electron or muons, and two jets, possibly tagged as b-jets, are detected.
- The fully-hadronic channel, characterized by six-jet events. In this channel b tagging is mandatory, to suppress the large background from QCD events and to reduce the number of three-jet combinations.

Since W decays to taus are not used for the mass measurement (they suffer a larger background and have additional missing neutrinos) the lepton-plus-jet-channel and the dilepton-channel yields are reduced to 30% and 5% of the total, respectively.

The top mass is measured from kinematic properties of top-decay products, the most sensitive being the invariant mass of the three objects belonging to the $W - b$ system. Kinematic fitting techniques, already described for the W mass measurement (Section 9.3), are employed to determine the momentum and direction of neutrinos and to improve the measurement of other decay products. At an hadron collider the four-vector of the initial state is only partially known: the momenta of the initial partons involved in the hard process are undetermined, hence momentum conservation can be

applied only in a plane perpendicular to the beam axis (transverse plane). Five constraints can be imposed:

- The total transverse momentum of the event must be equal to zero. As the final state is $t\bar{t} + X$, all detected objects (i.e. all energy deposits in the calorimeters) must be included in computing the total event transverse momentum. Since the transverse momentum is defined by the two components of the momentum on the transverse plane, these two components are set to zero, yielding two constraints.
- The invariant mass of the two objects assumed to originate from a W decays must equal the W mass. This constraint can be applied to both W bosons, one for each top (anti-top) decay.
- The top and anti-top masses, reconstructed in the same event, are required to be the same. (The top natural width is one order of magnitude smaller than the typical experimental resolution.)

In the semileptonic channel three constraints are used to determine the three-momentum of the unmeasured neutrino. In practice the missing transverse momentum gives the neutrino transverse momentum, while the momentum component along the beam axis is given by constraining the invariant mass of the lepton-neutrino system to the W mass. The latter, however, being a quadratic constraint yields two solutions for the neutrino longitudinal momentum, resulting in a two-fold ambiguity. An additional ambiguity arises from the choice of of the jet to assign to the lepton-neutrino system to form the top candidate. If the two b-jets are identified the additional ambiguity is two-fold, otherwise four possibilities have to be taken into account. Without b identification there are also three possible choices for the di-jet system to assign to the W hadronic decay, resulting in a total of 24 combinations. The reduction in combinatorial background (and in background from non-$t\bar{t}$ events) obtained with b tagging can be appreciated by comparing the invariant mass distributions shown in Fig. 10.3. The top mass can be measured by comparing experimental distributions, similar to the ones shown in the figure, to distributions computed with Monte Carlo simulations with different top-mass hypotheses. The simulations include an appropriate fraction of non-top background. A likelihood function can be computed for each hypothesis; the measured top mass is given by the maximum likelihood and the statistical error is determined by the mass values giving $\Delta(\text{Ln(Likelihood)}) = 0.5$, where Δ indicates the variation with respect to the maximum. The sensitivity of the measurement can be

enhanced by taking into account all kinematical properties of the event in the construction of the likelihood [139].

Fully hadronic $t\bar{t}$ events have the advantage of a larger branching fraction and can use all available constraints; the overwhelming multi-jet QCD background, however, makes these events very difficult to detect. The use of b tagging greatly helps in reducing the QCD background and the number of possible combinations. Even with one b-tagged jet, 30 different jet combinations must be taken into account for the event reconstruction.

Di-leptonic events have the cleanest signature, but a small branching fraction and require the reconstruction of two un-measured neutrinos. These events are underconstrained since the five possible constraints are not enough to determine the six components of the neutrinos momenta. Nevertheless methods have been developed to extract information on the top mass. A widely used technique is based on the assumption of a particular top mass: the event can then be reconstructed, with a eightfold ambiguity due to the two quadratic equations related to the W mass constraints and the two possible lepton-b pairing. Subsequently, the matrix element corresponding to a $t\bar{t}$ event with that particular final state configuration is computed and employed to construct a likelihood function, which is then examined to determine the most probable value of the top mass. Another method [140] relates the top mass to the invariant mass, m^2_{bl} of the b-lepton system. By observing that in the top rest frame, if the W width is neglected, the b quark energy is $\frac{m_t}{2}$, one gets

$$m_t^2 = \langle m_{bl}^2 \rangle + \sqrt{m_W^4 + 4m_W^2 \langle m_{bl}^2 \rangle + \langle m_{bl}^2 \rangle^2}. \tag{10.7}$$

The combination of the results obtained by the CDF and DO experiments in the various channels gives [141]

$$m_t = (170.9 \pm 1.1 \pm 1.5)\ \text{GeV}\,. \tag{10.8}$$

The most important sources of systematic uncertainties are

- the jet energy scale, which is limited by the calibration of the calorimeters,
- the modeling of the signal shape in the invariant mass distributions used for the measurement,
- the modeling of the background.

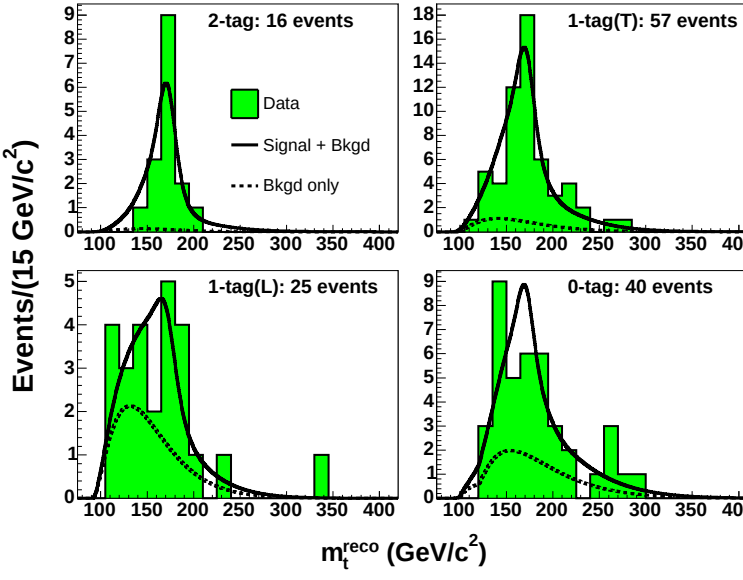

Fig. 10.3 Examples of measured top mass distributions for lepton-multijet events at the Tevatron Collider (Run II) from the CDF experiment [138]. The data sample corresponds to an integrated luminosity of approximately 318 pb^{-1}. The four subsamples are, respectively, (*i*) events with two b-tagged jets, (*ii*) events with only one b-tagged jet, (*iii*) events with only one b-tagged jet and a looser jet transverse energy threshold, (*iv*) events without b-tagged jets and a tighter transverse energy threshold. The expected distributions for signal+background and background only are overlaid using, for the signal, the measured top quark mass.

10.3 Electroweak constraints on the top mass

The electroweak observables described in this book feature radiative corrections that can be parameterised as a function of the top mass, of the logarithm of the Higgs mass, of $\alpha(m_Z^2)$ and α_s. The dependence of the electroweak radiative corrections on the top mass is quadratic at one-loop level. The tree-level W mass, for instance, is modified by the Δr^W term (Eq. (3.312)), whose top mass dependence is essentially given by Eq. (3.288), i.e.

$$\Delta r^{W(top)} \simeq -\frac{c_0^2}{s_0^2}\frac{3G_F m_t^2}{8\sqrt{2}\pi^2}. \tag{10.9}$$

The indirect determination of the top mass from electroweak observables requires a proper treatment of m_H, $\alpha(m_Z^2)$ and α_s. This treatment is trivial

for R_b: as already emphasized in Chapter 4 all other corrections cancel in the $\Gamma_{Z\to b\bar{b}}$ to Γ_{had} ratio leaving solely the quadratic dependence on the top mass given by the $Z \to b\bar{b}$ vertex. From the LEP measurement of R_b one gets

$$m_t = (150 \pm 20)\,\mathrm{GeV/c^2} \tag{10.10}$$

in fair agreement with the direct determination.

The uncertainty of this prediction can be decreased with a global fit of the most relevant electroweak observables measured at LEP and SLC (Z-pole asymmetries, Z-lineshape parameters, W mass). The common χ^2 fit of the measurements to their Standard Model predictions is performed [142] by assuming that both statistical and systematic errors have a Gaussian behaviour. The Standard Model predictions for the various observables are computed using the very high precision measurements of G_F, m_Z and of the fine structure constant, $\alpha(0)$. The correlation of the Z mass uncertainty to some of the observables is taken into account, as well as correlations among observables themselves. The fine structure constant is run to m_Z^2, this is done by using low-energy e^+e^- data to compute the contribution of the vacuum polarization due to hadrons, as described in Subsection 3.2.4. The minimum of the χ^2 is found by recomputing the Standard Model predictions of the observables with different values of the radiative corrections parameters. The fit gives [143]

$$m_t = 178^{+12}_{-9}\,\mathrm{GeV/c^2} \tag{10.11}$$

$$\log_{10}(m_H/\mathrm{GeV}) = 2.14^{+0.43}_{-0.35} \tag{10.12}$$

$$\alpha_s = 0.1190 \pm 0.0028 \tag{10.13}$$

in agreement with the direct measurement of the top mass, given by the combination of the CDF and D0 results described in the previous Section. The direct and indirect determinations of the top mass in various years are compared in Fig. 10.4. The m_t and $\log(m_H/\mathrm{GeV})$ values obtained by the fit are strongly correlated (the correlation coefficient is +0.86). This implies that, by including the direct measurement of the top mass into the global fit, a sizeable reduction of the $\log(m_H/\mathrm{GeV})$ uncertainty is expected.

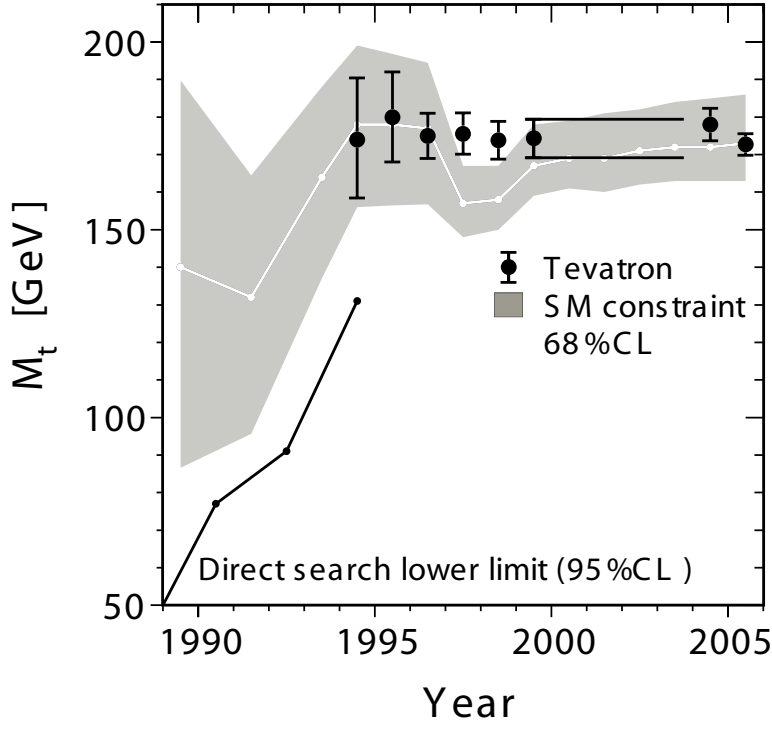

Fig. 10.4 The time evolution of the top mass measured at the Tevatron, compared to the value extrapolated from electroweak radiative corrections, in the same years. The areas represent the 68% CL contours. (Courtesy of the LEP Electroweak Working Group.)

This page intentionally left blank

Chapter 11

The Search for the Higgs Boson and Tests of the Electroweak Interaction

The quest for the Higgs has been one of the main experimental activities of the end-of-XXth-century high-energy physics. At the start of the new millennium the largest experimental projects and the exploration of the high energy frontier are still largely motivated by directly probing the Higgs sector of the theory.

As described in Chapter 1 the requirement of local gauge invariance together with the necessity of giving mass to the W and Z bosons leads, within the Standard Model, to the Higgs mechanism. The electroweak symmetry is broken spontaneously and a new scalar is created, the Higgs boson. The mass of the new scalar is not predicted by the electroweak theory, however, as seen in Subsection 1.5.1, there are reasonable expectations that the scalar should be light, i.e. below about 1 TeV. For higher values the unitarity bounds for the $WW \to WW$ process would be violated, furthermore a perturbative approach would lose its validity.

If the SU(2)×U(1) symmetry is assumed, the precision electroweak measurements described in this book, together with one-loop electroweak calculations (Chapters 3 and 4), can be used to set a more stringent limit on the Higgs mass, as anticipated in Section 10.3. In this Chapter we will see that the global fit to electroweak observables yields

$$m_H < 144\,\mathrm{GeV/c^2}$$

at 95% confidence level. This result indicates a relatively light Higgs boson; nevertheless it should be reminded that the dependence of one-loop electroweak corrections on the Higgs mass is logarithmic, hence a larger mass cannot be ruled out.

The direct search for the Higgs boson is guided by an important property of the implementation of the Higgs mechanism in most theoretical scenarios:

the interactions terms defining the production and decay properties of the Higgs can be predicted. In particular, in the Standard Model, the Higgs coupling to fermions is proportional to the square of the fermion mass (m_f) and the partial decay width is [144]

$$\Gamma(H \to f\bar{f}) = \frac{N_c g^2 m_f^2}{32\pi m_W^2}\beta^3 m_H$$

where N_c is equal to the number of coulors for quarks and is set to 1 for leptons, while β is the center-of-mass velocity of the fermion in the Higgs rest frame. Similarly the widths for the decay to W and Z gauge bosons are [145]

$$\Gamma(H \to W^+W^-) = \frac{g^2 m_H^3}{64\pi m_W^2}\sqrt{1-x_W}(1 - x_W + \frac{3}{4}x_W^2) \tag{11.1}$$

and

$$\Gamma(H \to ZZ) = \frac{g^2 m_H^3}{64\pi m_W^2}\sqrt{1-x_Z}(1 - x_Z + \frac{3}{4}x_Z^2) \tag{11.2}$$

respectively, where $x_V = 4\frac{M_V^2}{m_H^2}$ and $x_V \leq 1$ for allowed decays. The decay of the Higgs boson to photon (or gluon) pairs goes through loops and is suppressed by the α^2 (or α_s^2) factor [9]. In Fig. 11.1 the decay branching fractions versus the Higgs mass are shown for Higgs masses below 200 GeV/c^2. The tendency to decay into the pair of heaviest particles, among the ones kinematically allowed, is clearly seen. In a wide region, between 10 to 130 GeV/c^2, the decay to b quarks pairs is dominating, for higher masses this role is taken by massive gauge bosons pairs. For low masses, below the $b\bar{b}$ production threshold, decays to charm and tau pairs are dominant and, for even lower masses the branching ratios to muon and electron pairs, as well as to low multiplicity hadronic final states and $\gamma\gamma$, become important.

11.1 Search for the Higgs boson before LEP

The mass region below 5 GeV has been widely investigated before 1989 by means of a variety of processes. The interference between possible long-range muon-hadron interactions and pure QED in the X-ray transition of muonic atoms has been used to set limits on Higgs mediated interactions, in the mass region around 1 MeV/c^2 [146]. An Higgs boson with a mass

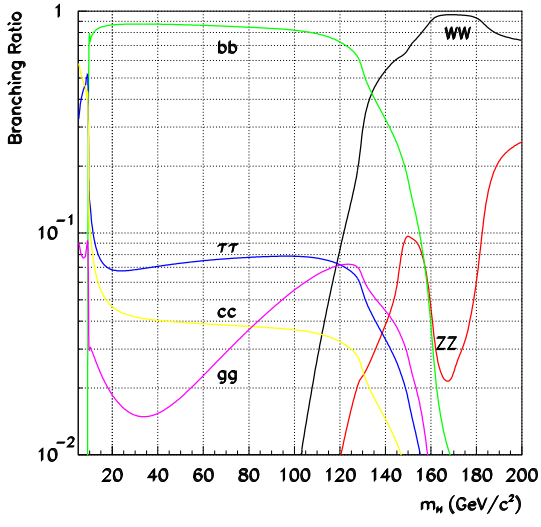

Fig. 11.1 Higgs boson branching ratios as a function of its mass. (Courtesy of Patrick Janot.)

of a few MeV/c^2 was also expected to affect the angular distribution of neutron-nucleon scattering [147]. Indeed a very low mass scalar would contribute with an interaction term similar to Coulomb scattering, normally not present in neutron scattering. Other processes potentially able to produce a very low mass Higgs boson would have been nuclear $0^+ - 0^+$ transitions. The decay of a new spin 0 particle in e^+e^- pairs was searched in $0^+ - 0^+$ nuclear decays and no evidence was found [148]. Particle decays, in particular rare decays of pions [149], kaons [150], B mesons [151], J/ψ and Υ [152] were used to set limits at higher masses . Unfortunately while the Higgs coupling to quarks is predicted by the theory, sizeable uncertainties are affecting meson decays through QCD effects. Therefore, while indicating that the existence of a Higgs boson below 5 GeV was unlikely, the interpretation of the results was not straightforward. The only region that could be unambiguously excluded before LEP was the range 1.2 MeV to 52 MeV thanks to a beam dump experiment [153]. Electrons with an energy of 1.6 GeV were sent to a tungsten target. The Higgs boson was expected to be produced in the interaction of the electron beam with the target nuclei, in a process similar to the bremsstrahlung, called *higgs-strahlung* in

the following. An Higgs boson of low mass is weakly interacting and has a long lifetime, and it can exit a thick target stopping all electromagnetic products. It is possible to detect it in the laboratory thanks to its subsequent decay to an e^+e^- pair. As the electron higgs-strahlung cross section is well known and Higgs production was not detected by the beam dump experiment, the mass range covered by the experiment could be completely excluded.

11.2 Higgs production at LEP

As seen in the previous paragraphs only a very limited mass region could be explored before the advent of LEP and the interpretation of most results was not easy. The scenario changed with LEP because Higgs bosons can be copiously produced by higgs-strahlung from Z vector bosons. The coupling to the Z is large and can be exactly computed: LEP experiments were able to explore the mass range from 0 to 65 GeV/c^2 at LEP1 and extend the search up to 115 GeV/c^2 at LEP2 . The Feynman diagrams responsible for Z higgs-strahlung are shown in Fig. 11.2. At the Z resonance (LEP1) the Higgs can be produced together with an off-shell Z (indicated as Z^* in the figure), with subsequent decays of the Z^* into leptons and quarks (Fig. 11.2(a)). At higher centre-of-mass energies (LEP2) the role of Z and Z^* is exchanged and Higgs bosons can be produced in association with real Z's (Fig. 11.2(b)). In e^+e^- collisions the Higgs bosons can also be produced by WW or ZZ fusion, yielding a final state were the Higgs is produced in association with a pair of neutrinos or electrons, respectively. This process gives only a small contribution at LEP2 centre-of-mass energies, of some relevance at the edge of the kinematic range reached by the higgs-strahlung process.

11.3 Searching the Higgs at LEP1

The branching ratio of the Z to Higgs-fermion-antifermion is shown in Fig. 11.3 as a function of the Higgs mass.
Since 18 million Z decays were collected by the four LEP experiments thousands of Higgs bosons would have been produced at LEP1 for masses lower than 50 GeV/c^2. Dedicated analyses were designed for particular mass ranges. Very low mass (and even mass-less!) Higgs can be investigated by selecting acoplanar lepton pairs originating from the Z^* decay

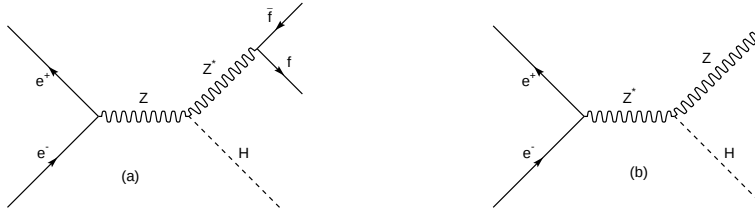

Fig. 11.2 Higgs-strahlung at LEP1 (a) and at LEP2 (b).

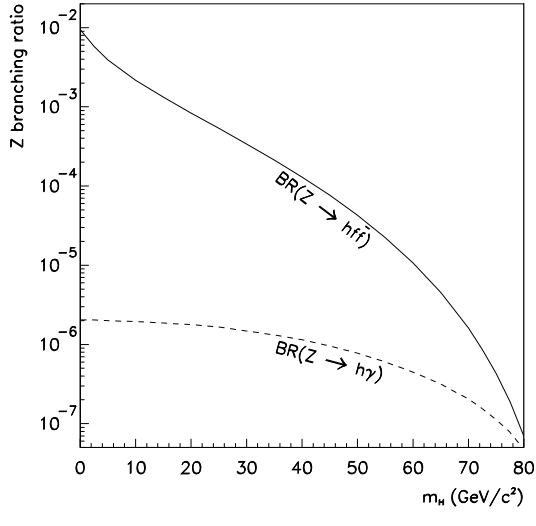

Fig. 11.3 Branching Ratio of $Z \to Hf\bar{f}$ at the Z resonance.

(Fig. 11.4(a)). Indeed for Higgs masses below the e^+e^- threshold ($2m_e$) the Higgs decay width is so small that it would leave an apparatus of the size of a typical LEP experiment before decaying. In this case the decay products of the recoiling Z^* must be detected. Above the e^+e^- threshold the acoplanar lepton selection is still useful to select Higgs candidates: Higgs

decaying to lepton-antilepton accompanied by a Z^* decaying to a neutrino-antineutrino pair would be detected by such a search. To deal with higher masses, where the Higgs can decay to hadron pairs, the search is generalized to acoplanar charged tracks pairs (Fig. 11.4(b)). The selection of low multiplicity mono-jets (Fig. 11.4(c)) is useful to extend the search to Higgs masses up to about 20 GeV/c^2. Thanks to the high rate and the very distinctive signatures, LEP1 searches below 20 GeV/c^2 were easy and it was possible to design analysis cuts aimed at rejecting all background, while keeping an high efficiency for the potential Higgs signal. As can be seen from Fig. 11.1, for Higgs masses above 10 GeV/c^2 most of Higgs decays are to $b\bar{b}$ quark pairs: with increasing Higgs masses their hadronization products gets more and more separated and tend to cluster into a pair of separated jets. Therefore the selection of Higgs candidates for masses above 20 GeV/c^2 was based on the search for two jets recoiling against the Z^* decay products. The relevant topologies are sketched in Fig. 11.5. The higher rate is given by the four jet topology (Fig. 11.5(c)), but at the Z resonance the high background of hadronic Z decays makes this channel much less sensitive than the acoplanar jet channel (Fig. 11.5(a), the Z^* yields two neutrinos and missing energy) and the two-jet and two-lepton channel (Fig. 11.5(b), the Z^* yields two leptons). The latters were used for LEP1 searches: a total of 13 events were detected with an expected background of 20.6 events [155], [156], [157] [158]. The main background was due to in the missing energy channel where b tagging was used and to four-fermion processes in the two-lepton channel. At the end of LEP1 the combined 95% confidence level lower limit on the Higgs boson mass was 65.6 GeV/c^2 and the entire region below this limit could be excluded [159].

Before describing the Higgs searches at LEP2, it is useful to briefly recall the main methods to set Confidence Levels.

11.4 Setting confidence levels

When searches for a new phenomena yield a negative result, the problem arises of setting statistically well defined confidence levels (CL) for exclusion limits. The solution is straightforward for counting experiments with no background as, for example, the Higgs searches at LEP1 for masses below 20 GeV/c^2. In this case the probability of observing 0 events when s events are expected is given by the Poisson distribution as e^{-s}. A signal hypothesis

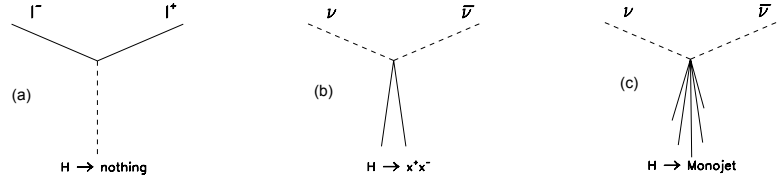

Fig. 11.4 Search of the Higgs boson at LEP1 in the low mass region: main topologies for the final state.

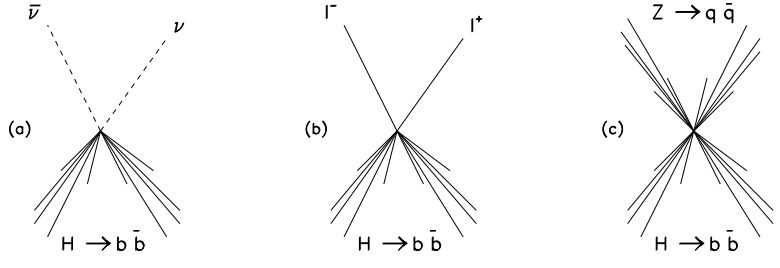

Fig. 11.5 Topologies used in the search of the Higgs boson at high masses at LEP.

is excluded at a certain confidence level CL when

$$1 - e^{-s} \leq CL\,. \tag{11.3}$$

It turns out that for negative searches with no background all regions where more than 3 signal events are expected can be excluded at 95% confidence level.

The problem is slightly more complex when the expected background is different from zero, as in the Higgs searches at LEP1 above 20 GeV/c^2. In this case one can define

$$CL_{s+b} = (\sum_{i=0}^{n}[e^{-(s+b)}\frac{(s+b)^i}{i!}]) \tag{11.4}$$

where s is the number of expected signal events, b the number of expected background events and n the number of events observed by the experiment.

In analogy with Eq. (11.3) one could use $1 - CL_{s+b} \leq CL$ to define the confidence level; this criterion, however, has a drawback since it may happen that the number of observed events is lower than the expected background because of statistical fluctuations, as in the final result of the Higgs searches at LEP1 described in the previous Section. To avoid this problem a new confidence level related to background only is defined as

$$CL_b = (\sum_{i=0}^{n} [e^{-(b)} \frac{(b)^i}{i!}]) \tag{11.5}$$

and the ratio

$$CL_s = \frac{CL_{s+b}}{CL_b} \tag{11.6}$$

is used to set the exclusion limits. A signal hypothesis is therefore excluded at a certain confidence level CL when

$$1 - CL_s \leq CL.$$

It turns out that CL_b is also a useful tool to analyse results where an excess of events is observed. Indeed in this case $1-CL_b$ gives the probability that the observed excess is due to a positive fluctuation of the background and a very low value of this quantity gives evidence of a new phenomenon.

Often the analysis of the experiment requires more than simple counting of events, as in the Higgs searches at LEP2 described in the next Section. A shape term modifies the simple Poisson distribution when not only the information concerning the number of events is used, but other variables related to the properties of the collected events are used [154]. These can be, for example, the invariant mass of the Higgs candidate decay products, or the b tagging probability of the jets originating from the Higgs candidate. The additional information can be taken into account by using the likelihood ratio $Q = \frac{L_{s+b}}{L_b}$, where L_{s+b} is the likelihood for the signal+background hypothesis, while L_b is the likelihood for the background only hypothesis. One use as test statistic

$$Q = \frac{L_{s+b}}{L_b} = \frac{e^{-(s+b)}}{e^{-b}} \prod_{i=0}^{n} \frac{s f_s(\vec{X}_i) + b f_b(\vec{X}_i)}{b f_b(\vec{X}_i)} \tag{11.7}$$

where the functions f_s and f_b are the probability density functions that a signal or background event will be found in a given final state with the

set of properties (invariant masses, b tagging values, etc.) described by the vector of values $\vec{X}_i$. The likelihood ratio is a function of the assumed Higgs mass, which enters in Q through the cross section used to compute s. If the terms f_s and f_b are neglected Eq. (11.7) reduces to the simple ratio of Poisson probabilities to observe n events. The confidence levels can be defined similarly to the simple Poisson-distribution case, the compatibility of the experiment with a given hypothesis can be determined by calculating the probability of obtaining a likelihood ratio smaller than the one observed. In general the computation cannot be performed analytically and Monte Carlo techniques are used to compute CL_s and CL_b from the observed likelihood ratio.

11.5 Higgs searches at LEP2

As already mentioned, in e^+e^- collisions above the Z resonance Higgs production is dominated by the higgs-strahlung process of Fig. 11.2(b). Since a real Z has to be produced in association with the Higgs boson the production rate is sharply falling above the kinematic limit given by $m_H \sim \sqrt{s} - m_Z$, as shown in Fig. 11.6.

Therefore at LEP2 the effort to reach the highest possible energy was particularly important [159], with a record center-of-mass energy of 209 GeV that was exceeding any initial expectation. For Higgs boson masses relevant at LEP2 (Fig. 11.1) the main decay channel is $b\bar{b}$ with a branching ratio of about 74% for a mass of 115 GeV/c^2. It follows that at LEP2 b tagging (Chapter 7) was extremely relevant for Higgs searches and vertex detectors were upgraded in the four LEP experiments to increase the sensitivity of Higgs searches. The decay topologies can be classified in terms of the Higgs and Z decays, as shown in Fig. 11.5:

- Four-jet channel. The Higgs is decaying to $b\bar{b}$ and the Z to a pair of quarks. This is the dominant channel, the expected rate being about 51%. Contrary to the LEP1 case this channel gives the highest sensitivity, when b tagging is used. The main backgrounds are from four-fermion WW and ZZ production, two-fermion $b\bar{b}$ production with emission of two-gluons and two-fermion $q\bar{q}$ production with an emitted gluon splitting into a $b\bar{b}$ pair.
- Missing energy channel. The Z is decaying to a pair of neutrinos. At the kinematic limit this channel has a contributions from WW and ZZ

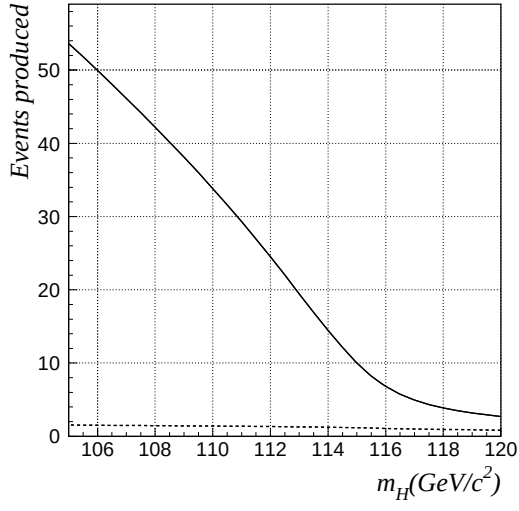

Fig. 11.6 Expected events as a function of the Higgs mass at $\sqrt{s} = 206$ GeV for an integrated luminosity of $\approx 200\ pb^{-1}$. The dashed line shows the contribution of the WW, ZZ fusion processes.

fusion. The expected rate is about 15%. The main backgrounds are ZZ production and the $Z\gamma\gamma$ process when the photons are at low angle and undetected in the apparatus.

- Leptonic channel. The Z is decaying to a pair of electrons or muons. This is in principle a very clean channel, but the rate is rather poor ($\sim 5\%$). The main background is ZZ production.

Another channel used in LEP2 searches was $H \to \tau\bar{\tau}$ (BR $\sim 7\%$). In the tau selection both cases ($H \to b\bar{b}$,$Z \to \tau\bar{\tau}$) and ($Z \to b\bar{b}$,$H \to \tau\bar{\tau}$) were considered, the total expected rate being $\sim 7\%$. An important issue concerns the Higgs mass reconstruction, which was performed in all decay channels. Since in a e^+e^- collider the total center-of-mass energy is known and the total momentum of the event is zero, energy-momentum conservation can be imposed by means of a kinematic fit, improving considerably the experimental resolution on the reconstructed Higgs mass. It has to be stressed that the $e^+e^- \to ZZ$ process represents an irreducible background. For a mass $m_H = m_Z$ the Higgs boson is indistinguishable from the Z on

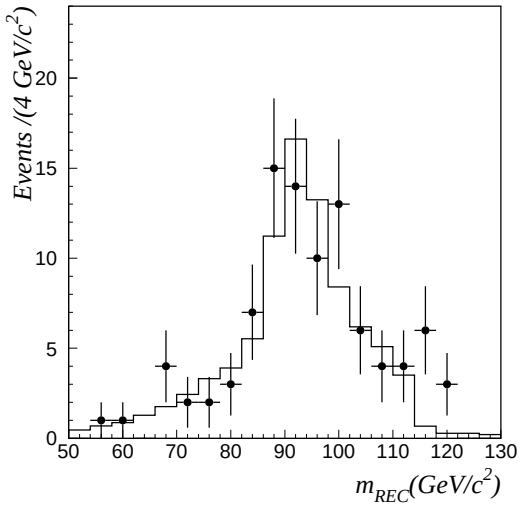

Fig. 11.7 Reconstructed Higgs mass at $\sqrt{(}s) \sim 206$ GeV by the Aleph experiment.

an event-by-event basis and would have shown up at LEP2 by an excess of events on the Z peak which is clearly visible in the mass distribution of reconstructed Higgs candidates (Fig 11.7).

The final results of the four LEP experiments [161], [162], [163], [164], were subject to a statistical analysis, following the concepts described in the previous Section. The combined confidence level CL_s is given in Fig. 11.8, showing that a Higgs boson mass below 114.4 GeV/c^2 is excluded at 95% CL [165]. The expected 95% CL sensitivity, computed from Gedanken experiments was 115.3 GeV/c^2. The excluded region is about 1 GeV lower than expected because of three events in the four jets channel seen by the ALEPH experiment in the region around 115 GeV/c^2.

11.6 The Higgs mass from electroweak fits

Electroweak radiative corrections depends logarithmically on the Higgs mass, as discussed in Chapter 3. In analogy with the indirect determination of the top mass (Section 10.3), the W mass sensitivity is taken here as an example. From Eqs. (3.312), (3.309) and (3.310) one gets

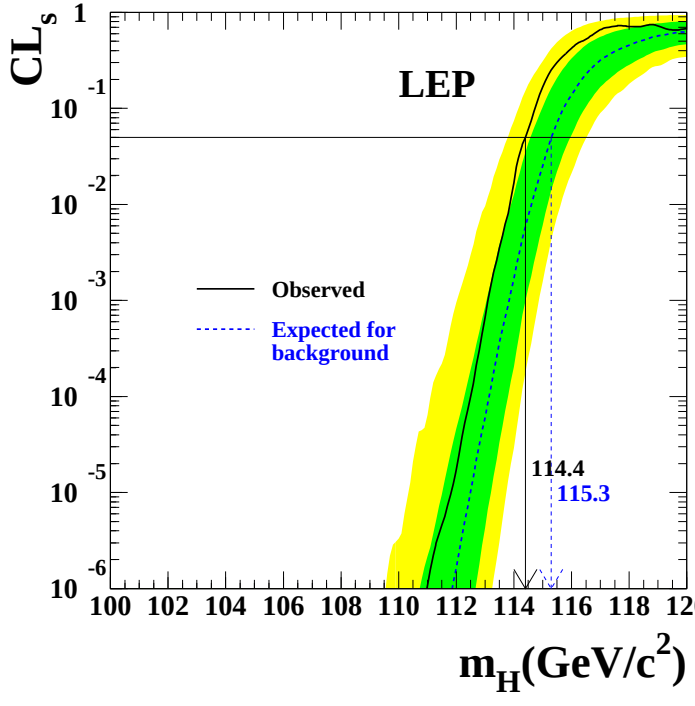

Fig. 11.8 Final signal confidence levels on the Higgs mass from the direct LEP search. (Courtesy of the LEP Higgs Working Group.)

$$\Delta r^{W(Higgs)}\,(large \quad m_H) \simeq \frac{11\,G_F m_W^2}{12\sqrt{2}\pi^2}\ln\frac{m_H}{m_Z} \tag{11.8}$$

where the superscript *Higgs* indicates that only the leading Higgs dependence is shown. The above relation is valid for large Higgs mass only. The general expression can be found in [52]; the dependence of the predicted W mass as a function of the Higgs mass is shown in Fig. 9.11, where the logarithmic behaviour is clearly seen.

Among the observables described in this book the effective electroweak mixing angle, extracted from the LEP-pole asymmetries (Fig. 8.11), shows the largest sensitivity on the Higgs mass. The experimental determination of $\sin^2\theta_{W,eff}$ and of the W mass are compared to the Standard Model prediction in Fig. 11.9. The measurements are consistent with a light Higgs

boson. In the same figure the tree-level prediction (with the running of α included) is shown, providing a strong evidence of the need of genuine electroweak radiative corrections to describe the data, as seen also in Fig. 9.1.

In Section 10.3 it has been shown that from a global fit of Z-pole observables [142] and the precise determination of the W mass the logarithm of the Higgs mass can be constrained to a value corresponding to [143] $\mathrm{m_H} = 137^{+228}_{-76}\ \mathrm{GeV/c^2}$. It has also been observed that the direct determination of the top mass greatly helps in constraining the mass of the Higgs, since the large quadratic term is fixed by the measurement. If the top mass value given in Ref. [141] is used ($m_t = (170.9 \pm 1.8)$ GeV) one gets

$$\mathrm{m_H} = 85^{+37}_{-27}\,\mathrm{GeV/c^2}\ ,$$

corresponding to

$$\mathrm{m_H} < 144\ \mathrm{GeV/c^2}$$

at 95% CL. Figure 11.10 shows the variation of the χ^2 value of this global electroweak fit with respect to the χ^2 value at the minimum, as a function of the Higgs mass. When the limit from the direct search ($\mathrm{m_H} > 114.4\ \mathrm{GeV/c^2}$) is combined with the electroweak global fit in a common likelihood function, the upper bound increases to $\mathrm{m_H} < 182\ \mathrm{GeV/c^2}$. It is instructive to compare the direct measurements of the top and W masses to values computed from the dependence of all other measurements, when their dependence on electroweak radiative corrections are used. As shown in Fig. 11.11 the direct and indirect determinations are consistent, showing a success of the electroweak theory. In both cases a light Higgs boson is favoured.

11.7 Model independent analysis of electroweak data

The bounds on the Higgs boson mass presented in the previous Section were obtained assuming the validity of the Minimal Standard Model. The impressive wealth of precision measurements collected in the past 25 years and described in this book provide a test of the model at one-loop level in perturbation theory. An example of such a test is given in Fig. 11.11 where direct measurements are found to match indirect determinations from radiative corrections. Nevertheless is important to verify to which extent the experimental measurements are consistent with alternative models and to present the data in a model-independent form.

In Chapter 3 and 4 it has been shown that there are four parameters $(\varepsilon_1, \varepsilon_2, \varepsilon_3, \delta_{bV})$ related to the relevant loop corrections contributing beyond tree level to the prediction of the measurements described in this book. The first (ε_1) and the third (ε_3) include the dominant m_t and m_H dependences, the second (ε_2) has a logarithmic dependence on the top mass and the last one $(\delta_{bV}$) is related to the quadratic m_t dependence of the $Z \to b\bar{b}$ vertex correction.

In order to describe the data in a model independent form it is useful to relate the ε variables to measurable observables, sensitive to the dominant contributions. The W mass, the lepton asymmetries (or $\sin^2\theta_{W,eff}$), the Z leptonic width and R_b are natural choices. Relating $\Delta\kappa'$ and $\Delta\rho$ to, respectively, $A^0_{FB}(\ell)$ and Γ_ℓ as

$$\begin{aligned} A^0_{FB}(\ell) \to \sin^2\theta_{W,eff} &= s_0^2(1-\Delta\kappa') \\ \Gamma_\ell \to g_{A_l} &= -\frac{1}{2}(1+\frac{\Delta\rho_l}{2}) \end{aligned} \tag{11.9}$$

one can define [167]

$$\begin{aligned} \varepsilon_1 &= \Delta\rho_l \\ \varepsilon_2 &= c_0^2\Delta\rho_l + \frac{s_0^2}{c_0^2-s_0^2}\Delta r^W - 2s_0^2\Delta\kappa' \\ \varepsilon_3 &= c_0^2\Delta\rho_l + (c_0^2-s_0^2)\Delta\kappa' \end{aligned} \tag{11.10}$$

where Δr^W includes the relation to the W mass. The b couplings can be described by an alternative parameter ε_b that was introduced in Ref. [168] and is related to the b width as follows

$$\begin{aligned} \Gamma_b \to g_{A_b} &= -\frac{1}{2}\left(1+\frac{\Delta\rho_l}{2}\right)(1+\varepsilon_b) \\ \frac{g_{V_b}}{g_{A_b}} &= (1-\frac{4}{3}\sin^2\theta_{W,eff}+\varepsilon_b)/(1+\varepsilon_b). \end{aligned}$$

The connection with the parameters of Chapter 4 reads, essentially

$$\varepsilon_b = \frac{1}{2}\frac{2-\frac{8}{3}s_0^2+\frac{16}{9}s_0^4}{1+\frac{8}{3}s_0^2-\frac{32}{9}s_0^4}\delta_{bV} \approx \frac{1}{2}\delta_{bV}\ ; \tag{11.11}$$

from Eq. (4.39) and $\delta_{bV} = (\varepsilon_{1b} - \varepsilon_1)$ one can derive

$$\varepsilon_b \approx \frac{1}{2}(\varepsilon_{1b} - \varepsilon_1) = Re\left(\Gamma_b^{\mu(Z)}\left(m_Z^2\right), j_b^{\mu(Z)}\right)^{NU}. \tag{11.12}$$

These "experimental" definitions of the ε variables are identical, within the MSM, to the definitions of Chapter 3 and 4. In other models, because of the contributions of yet undiscovered particles, the vacuum polarization terms could be different. The ε_2 and ε_3 variables, in particular, do not have quadratic top mass contributions and have enhanced sensitivity to physics beyond the MSM.

The experimental results presented in this book can be expressed, in terms of the ε variables, as [142]

$$\begin{aligned}
\varepsilon_1 &= (5.54 \pm 1.0) \times 10^{-3} \\
\varepsilon_2 &= (-8.9 \pm 1.2) \times 10^{-3} \\
\varepsilon_3 &= (5.34 \pm 0.94) \times 10^{-3} \\
\varepsilon_b &= (-5.0 \pm 1.6) \times 10^{-3}
\end{aligned}$$

in good agreement with the Standard Model expectations, as shown in Fig. 11.12 for two of them. As expected from previous Section, a light Higgs boson is preferred.

The experimental results can be compared to extensions of the Standard Model. The Minimal Supersymmetric Standard Model (MSSM) [166] assumes the existence of supersymmetric partners of ordinary particles. Supersymmetry transforms bosons in fermions and fermions in bosons. It is a complete and consistent model, providing a framework for unification of gauge interactions. In its minimal version two Higgs field doublets are required, leading to five Higgs bosons (three are neutrals, two are charged ones). The model has a large number of free parameters. The prediction of this model for ε_1 and ε_3 when its parameters are set to yield massive partners of the ordinary fermions (i.e. massive sparticles) is shown in Fig. 11.13. For this set of parameters the model predicts at least one light neutral Higgs boson, and agrees with the experimental data, similarly to the MSM. On the other hand simple versions of technicolor models [169], where the Higgs boson is replaced by colour condensates, lead to large and positive corrections to ε_3, disfavouring the models, as seen in Fig. 11.13. The R_b measurement is also in disagreement with such models, since they imply a large and negative correction to ε_b which is not observed.

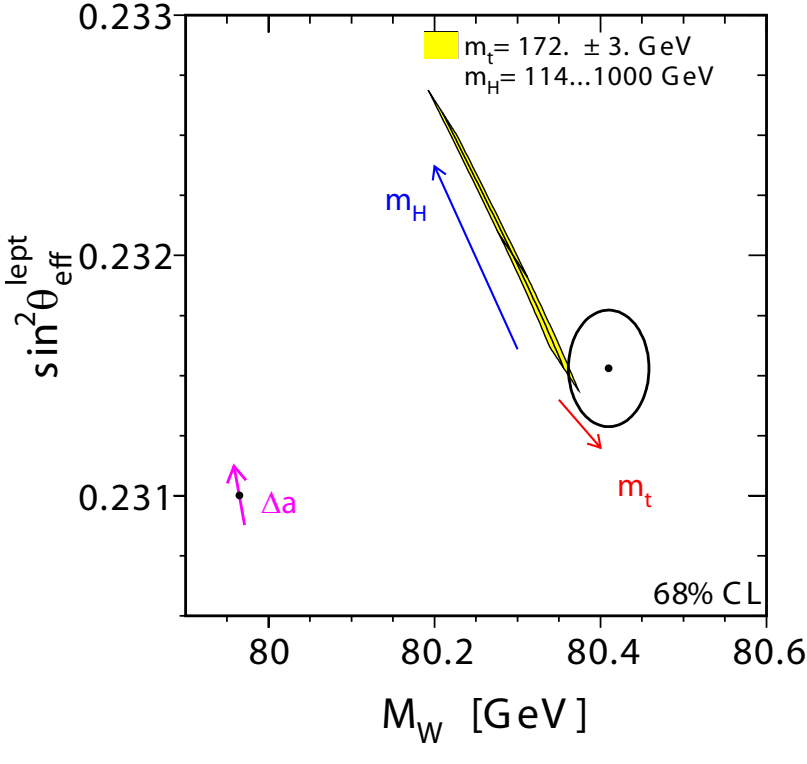

Fig. 11.9 Contours at 68% confidence levels of m_W and $\sin^2\theta_{W,eff}$ compared to the prediction of the MSM. The arrows indicate the Higgs, top and $\Delta\alpha$ dependences (the latter is drawn at the position of the tree-level prediction). (Courtesy of the LEP Electroweak Working Group.)

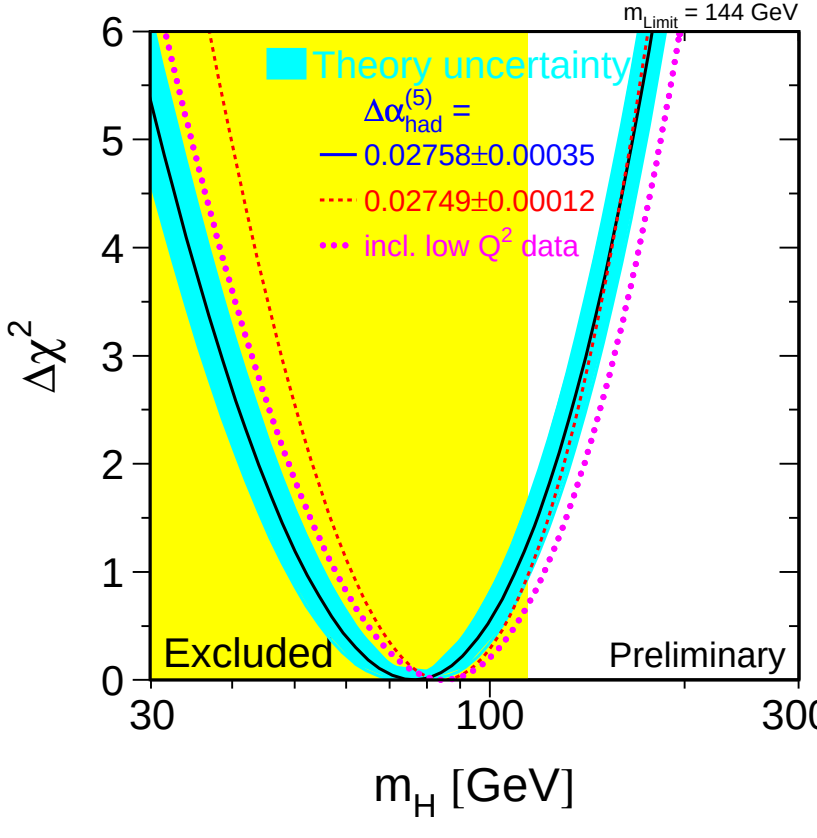

Fig. 11.10 The variation in χ^2 of the fit using all electroweak observables as a function of the Higgs mass. The limit from direct searches is indicated. The uncertainty from two-loop calculations and for different values of the hadron contribution to the fine-structure-constant running is shown. (Courtesy of the LEP Electroweak Working Group.)

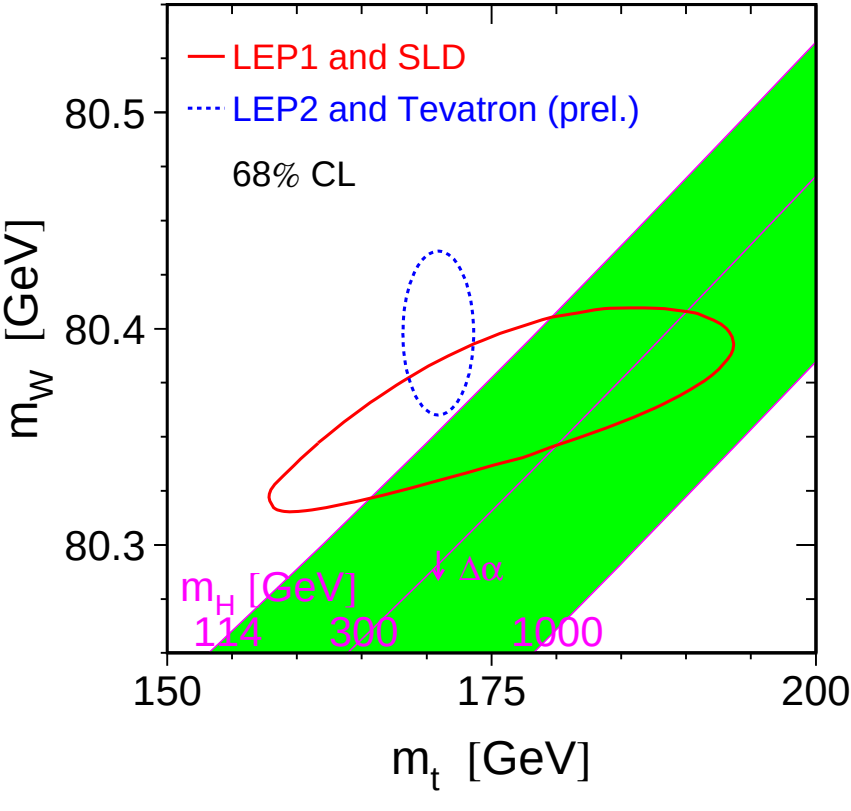

Fig. 11.11 The direct (LEP2, Tevatron) and indirect (LEP1, SLC) determinations of the mass of the W boson (m_W) and of the top quark (m_t). The 68% CL allowed regions are indicated. The band represents the Standard Model expectations for different values of the Higgs boson mass (m_H). (Courtesy of the LEP Electroweak Working Group.)

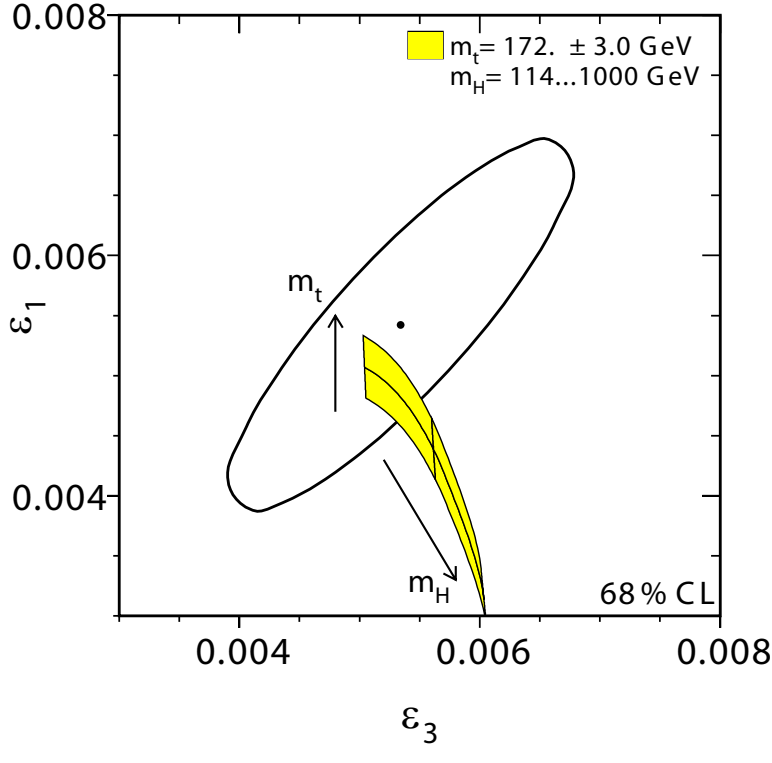

Fig. 11.12 The 68% CL contour for ε_1 and ε_3 compared to the prediction of the MSM. (Courtesy of the LEP Electroweak Working Group.)

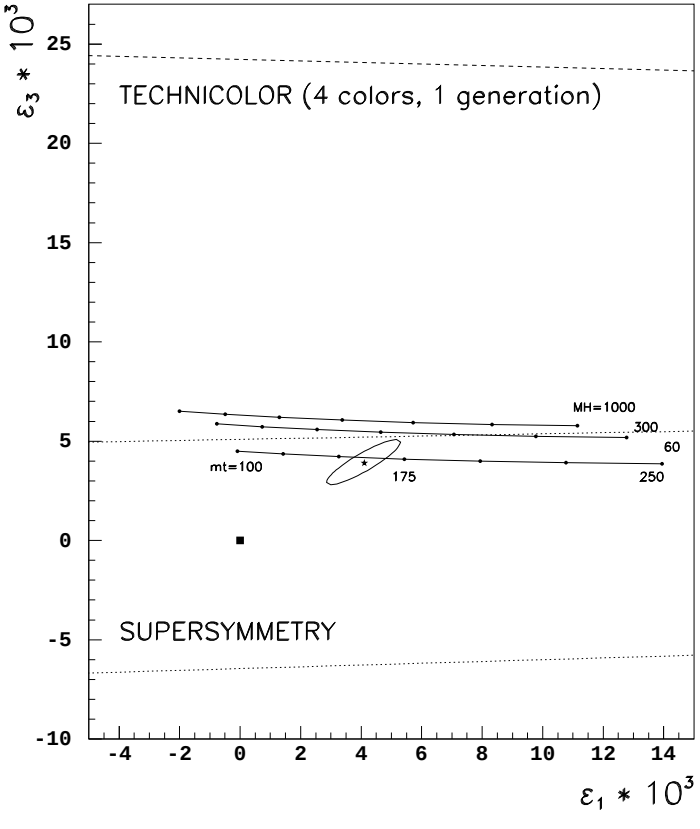

Fig. 11.13 The 39% CL contour for ε_1 and ε_3 compared to the prediction of the Minimal Supersymmetric Standard Model (with massive supersymmetric particles) and to the prediction of a simple technicolor model. (Courtesy of Manel Martinez.)

Chapter 12

Conclusions and Perspectives

The authors of this book have described, for the benefit of the patient readers, some relevant aspects of the physics of the W and Z bosons. It has been shown that a gauge theory of electroweak interactions, also known as the Standard Model of electroweak interactions, describes all experimental features of W and Z physics. The experimental tests of the electroweak theory, ongoing since 30 years, have reached their mature stage, thanks to the precision measurements performed at LEP, SLC and Tevatron. Some of these measurements are of unprecedented precision; as an example it can be recalled that the mass of the Z boson is presently known with the precision of ten part over a million and it is one of the most precisely measured physical observables. As a consequence of this remarkable effort the electroweak theory has been tested at the one-loop level.

At the time of writing this book the most important missing actor, from the experimental point of view, is the Higgs boson. If the Standard Model is assumed, however, its mass is constrained by existing measurements in the region below ≈ 200 GeV/c^2, with good confidence level. Direct searches at LEP have excluded the region below 114 GeV/c^2, and some interesting events have been detected at the edge of LEP sensitivity; if the Higgs boson exists, it is unlikely that will escape detection at the Large Hadron Collider (LHC), whose operations are due to start in summer 2008. The LHC will collide two beams of protons of 7 TeV and is expected to collect an integrated luminosity of 300 fb^{-1} in 5 years. The Higgs boson would be copiously produced by gluon-gluon fusion and detected by its decay to $WW^{(*)}$ or $ZZ^{(*)}$ if its mass is above 130 GeV/c^2. For lower masses Higgs detection will be more tricky, but its decay through the $\gamma\gamma$ channel should be feasible with adequate luminosity and well understood detectors.

Additional insight on the Higgs boson and its properties will be gained

at a future high energy e^+e^- linear collider. The International Linear Collider (ILC), based on the TESLA technology is presently under study. It is expected to reach a centre-of-mass energy of 800 GeV, collecting an integrating luminosity of 500 fb^{-1}. The main production mechanism would be the higgs-strahlung process, allowing to study the mass region below 700 GeV/c^2. At the ILC a precision measurement of the Higgs mass could be performed by direct reconstruction from the decay products, reaching a precision below 100 MeV for a wide mass range.

When the Higgs is discovered, matching its mass with electroweak indirect predictions will be important, and could potentially signal physics beyond the Standard Model, unveiling itself through loop corrections. At present one of the electroweak observables giving the best constraint on the Higgs mass is the electroweak mixing angle. Additional information on this parameter can potentially be gained at the LHC by using Z bosons produced at very high rate through the Drell-Yan mechanism. The electroweak mixing angle could be measured by the forward-backward asymmetry of Z decays to electron and muon pairs. Such a measurement requires the knowledge of the initial quark direction; since at LHC the anti-quark can only come from the sea, the Z are expected to be boosted in the same direction as the incoming quark: therefore the Z boost gives a natural definition of the quark direction. The analysis of this channel requires, however, a careful study of the quark and anti-quark PDF's and, while being potentially promising because of the small statistical error, will be rather challenging from the point of view of the systematic uncertainties. A sizeable step in the knowledge of the electroweak mixing angle will have to wait for a high luminosity run at the Z resonance with the ILC. Indeed with this machine independent polarization of both beams is expected to be available, and A_{LR} can be measured independently of any external measurement of polarization. This would probably shed light on the apparent inconsistency between the determinations of $\sin^2\theta_{W,eff}$ coming from A_{LR} and from the b forward-backward asymmetry.

The most important improvements in constraining the Higgs mass at LHC are likely to come from precise measurements of the W and top masses. The two observables are presently known with an uncertainty of 25 MeV/c^2 and 1.8 GeV/^{2}, respectively, and are giving similar contributions to the Higgs mass constraint coming from the most recent electroweak fit. Improved measurements of these two parameters will come with the final results of Tevatron Run II; the LHC should ultimately reach an uncertainty of 10 MeV/c^2 on the W mass and of about 1 GeV/^{2} on the top mass.

Such a precision requires a detailed understanding of many systematic uncertainties, as in both cases the statistical error will be very low thanks to high cross sections (30 nb for W inclusive production, including the branching ratio for W into electron and muon decays, and 830 pb for $\mathrm{t\bar{t}}$ production). In particular for the W mass the limiting factor is likely to be the knowledge of the lepton energy scale, while a good control of the jet energy scale will be particularly important for the top mass measurement. A further increase of precision is expected at the ILC. The W mass could potentially be measured with a 6 MeV error from a high-statistics WW threshold scan, single W production at high energy could give additional information (the $We\nu$ cross section at 500 GeV is 5 pb). The top mass could be measured with very high precision by means a top-threshold scan at 350 GeV, reaching an experimental precision of the order of one permil.

Lower energy experiments could have an impact to the global electroweak fit through improved determination of the fine structure constant at $q^2 = M_Z^2$. This important ingredient is currently limited by the knowledge of the hadron contribution to the vacuum polarization, which is computed using lower energy e^+e^- data. The error on the extrapolated Higgs mass coming from present data is equivalent to an uncertainty of about 10 MeV on the W mass. It will be an important source of error in electroweak fits when W mass measurements reach a similar uncertainty. A set of measurements of the e^+e^- hadronic cross section from the $\pi\pi$ threshold up to the Υ resonance, resulting in a determination of the e^+e^- cross section at 1% level, would match an error of 1 MeV on the mass of the W boson.

Triple vector-boson couplings have been shown to exist and to be consistent with Standard Model expectations. The $e^+e^- \rightarrow W^+W^-$ and $e^+e^- \rightarrow We\nu$ differential cross sections, measured at LEP, have determined WWZ and $WW\gamma$ couplings with a precision of about 1%. At LHC vector-boson pair production, and in particular $W\gamma$ and WZ events, will allow a completely independent measurement of WWZ and $WW\gamma$ triple gauge couplings, without any hypothesis linking the two sectors. Typical observables will be the $\mathrm{p_t}$ distribution of high energy photon or Z associated with a semileptonic W decay. Good control of the shape of such distributions, and reliable expectations including higher order terms (such as $\mathcal{O}(\alpha_s)$ and $\mathcal{O}(\alpha)$ radiative corrections) will be required. The precision is expected to be better than LEP (in particular for λ_Z and λ_γ) but unlikely to reach the permil accuracy needed to test Standard Model loop contributions. Production of W pairs and of single W at high energy in e^+e^- collisions will be thoroughly tested at future liner colliders. Detailed analyses of integrated

cross sections and of angular distributions, using techniques similar to that employed at LEP, will allow surpassing the 10^{-3} precision for all couplings, challenging theoretical TGC calculations at one loop level.

The Large Hadron Collider will open a new window on electroweak measurements thanks to the large yield of top quarks. Millions of $t\bar{t}$ events are expected to be detected and analysed by ATLAS and CMS, complemented by an equally large amount of single top events, thanks to the large cross section of this electroweak-production channel (about 320 pb) at the LHC. Beyond the measurement of the top mass, these sample will be used to perform detailed studies of top properties. An important example is the measurement of the fraction of longitudinally polarized W bosons in top decays, precisely predicted by the electroweak theory. As longitudinal W bosons are closely related to the mechanism of electroweak symmetry breaking this is an important test of the theory. This test is particularly interesting in single top events produced through W-gluon fusion, since in this case the top is almost completely polarized, allowing precision measurements of the helicity both at production and decay. Let's finally mention that another sector would be open if associated $t\bar{t}H$ production is detected, allowing the direct measurement of the ttH Yukawa coupling. In conclusion the top quark is likely to take soon the witness from W and Z bosons in precision tests of the electroweak theory.

So far, we avoided to discuss the possibility that new physics, beyond the Standard Model maybe soon discovered. In particular we have not mentioned the fact that neutrinos are not massless, which nowadays is commonly accepted [170], and we have only briefly mentioned the existing proposals of Supersymmetric models. In fact, both Tevatron and LHC are notoriously preparing a huge experimental effort aiming to produce, and identify, supersymmetric particles. Although this topic is clearly beyond the purpose of our book, we cannot avoid to mention the fact that one of the main arguments in favour of Supersymmetry came from the failure of the SU(5) prediction for the numerical relationship between the three Standard Model couplings $\alpha_s, \alpha, \sin^2\theta_{W,eff}$ at the Z peak. From the high precision measurements of the three couplings, the SU(5) prediction, based on the attractive idea of grand unification, had to be discarded. A possible way out was the ad hoc introduction of a new set of supersymmetric partners, modifying the renormalization group equation coefficients. Although no experimental evidence of Supersymmetry has been nowadays reached, a widespread hope exists in the physics community that LHC will make this spectacular discovery. Then a new era of precision measurements of

the discovered entities at the ILC would open, with a rôle versus LHC quite similar to that assumed by LEP1 versus UA1, UA2. Whether this fascinating scenario will be reached, is still not known. Perhaps, different fundamental discoveries will be achieved at LHC. In any case the general feeling is that the next decade appears to be, for the history of physics, an exciting one.

Acknowledgments

We would like to thank Duccio Abbaneo for his precious help with the heavy quark sections of this book.

We are grateful to Franco Bedeschi, Alain Blondel, Erik Brubaker, Martin Grünewald, Patrick Janot, Manel Martinez, Salvatore Mele, Gigi Rolandi, André Rougé, Elizaveta Shabalina, Evelyn Thomson, Andrea Venturi and Jorg Wenninger for providing figures and useful information. A special thanks to all members of the LEP Electroweak Working Group.

List of figures from publications

Figure 6.3 is from Z. Phys. C66 (1995) 45; Figs. 6.5, 8.7 are from Eur. Phys. J. C14 (2000) 1; Figs. 6.8, 7.10, 8.5, 10.4 are from Physics Reports 427 (2006) 257; Fig. 7.11 is from Phys. Lett. 401 (1997) 150; Fig. 7.12 is from Eur. Phys. J. 16 (2000) 597; Fig. 7.13 is from Eur. Phys. J. 1 (1998) 439; Fig. 7.14 is from Rev. Mod. Phys. 71 (1999) 575 (see also Phys. Lett. B252 (1990) 140); Figs. 8.3, 8.4 are from Eur. Phys. J. C20 (2001) 401; Fig. 8.8 is from Eur. Phys. J. 24 (2002) 177; Fig. 8.9 is from Phys. Lett. B355 (1994) 99; Fig. 9.4 is from the Prooceedings of the XXXIInd Rencontre de Moriond, Les Arcs, (Editions Frontieres, Paris); Fig. 9.10 is from Eur. Phys. J. C45 (2006) 307; Fig. 9.12 is from Eur. Phys. J. C21 (2001) 423; Fig. 9.13 is from Phys. Lett. B557 (2003) 147; Fig. 10.3 is from Phys. Rev. D73 (2006) 032003; Figs. 11.6, 11.7 are from Phys. Lett. B495 (2000) 1; Fig. 11.8 is from Phys. Lett. B565 (2003) 61; Figs. 6.1, 11.13 are from Rev. Mod. Phys. 71 (1999) 575.

This page intentionally left blank

Bibliography

[1] J. Schwinger, Ann. Phys. **2** (1957) 407;
R.P. Feynman and M. Gell-Mann, Phys. Rev. **109** (1958) 193;
G. Feinberg, Phys. Rev. **110** (1958) 1482;
T.D. Lee and C. N. Yang, Phys. Rev. **119** (1960) 1410.

[2] S.L.Glashow, Nucl. Phys. **22** (1961) 579;
A.Salam, Proc. 8^{th} Nobel Symposium, Aspenaegarden, Almqvist and Wiksell ed., Stockolm (1968) 367;
S. Weinberg, Phys. Rev.Lett. **19** (1967)1264; Phys. Rev. **D5** (1972)1412.

[3] J.D. Bjorken and A.L. Glashow, Phys. Lett. **11** (1964) 255.

[4] S.L.Glashow, J.Iliopoulos, L.Maiani, Phys. Rev. **2** (1970) 1285.

[5] G.'t Hooft, Nucl.Phys. **B33** (1971) 173; Nucl.Phys. **B35** (1971) 167.

[6] B. Desplanques and J. Missimer, Phys. Lett. **B84** (1979) 363;
M. A. Bouchiat and C. Bouchiat, Rep. Prog. Phys. **60** (1997) 1351.

[7] C. Y. Prescott et al., Phys. Lett. **B84** (1979) 524.

[8] J.D. Bjorken and S.D. Drell, "Relativistic Quantum Mechanics", (1965) McGraw-Hill, New York.

[9] L. B. Okun, "Leptons and Quarks", (1982) North Holland Physics Publishing, Amsterdam.

[10] L. Michel, Proc. Phys. Soc. **A63** (1950) 154.

[11] S. E. Derenzo, R. H. Hildebrand and C. Vossler, Phys. Lett. **B28** (1968) 401.

[12] I. Beltrami et al., Phys. Lett. **B194** (1987) 326.

[13] Particle Data Group, J. Phys. **G33** (2006) 1.

[14] T. Kinoshita and A. Sirlin, Phys. Rev. **113** (1959) 1652.

[15] T. van Ritbergen and R. G. Stuart, Phys. Rev. Lett. **82** (1999) 488.

[16] E. Abers and B. Lee, Physics Reports **9** (1973) 1.

[17] H. Georgi and S.L. Glashow, Phys. Rev. Lett. **28** (1972) 1494.

[18] T. Cheng and L. Li, "Gauge theory of elementary particle physics", (1984) Oxford University Press, New York.

[19] V. de Alfaro, S. Furbini, G. Furlan and C. Rossetti, "Currents in Hadron Physics", (1973) North-Holland, Amsterdam.

[20] C.N. Yang and R. Mills, Phys. Rev. **96** (1954) 191.

[21] S.Weinberg, Phys. Rev. **D19** (1979) 1277;
L.Susskind, Phys. Rev. **D20** (1979) 2619.
[22] S. Adler, Phys. Rev. **177** (1969) 2426;
J. S. Bell and R. Jackiw, Nuovo Cimento **60A** (1969) 47.
[23] F.J. Hasert et al., Phys. Lett. **46B** (1973) 138.
[24] C.H. Llewellyn Smith, Nucl. Phys. **B228** (1983) 205.
[25] UA1 Collaboration, Phys. Lett. **B122** (1983) 103.
[26] UA2 Collaboration, Phys. Lett. **B122** (1983) 476.
[27] N. Cabibbo, Phys. Rev. Lett. **10** (1963) 531.
[28] M. Kobayashi and M. Maskawa, Prog. Theor. Phys. **49** (1973) 652.
[29] G. Altarelli, Physics Reports **81** (1981) 1.
[30] M.E. Peskin and D.V. Schroeder, "An introduction to quantum field theory", (1995) Perseus Books Publishing LLC, Cambridge (Massachusetts).
[31] F.M. Renard,"Basics of Electron Positron Collisions", (1981) Editions Frontieres, Dreux.
[32] A.Blondel, B.W. Lynn, F.M. Renard and C. Verzegnassi Nucl. Phys. **B304** (1998) 438.
[33] "Z physics at LEP1", CERN 89-08, eds. G. Altarelli, R. Kleiss and C. Verzegnassi (1989).
[34] L. Maiani and M. Veltman, Nucl. Phys. **B123** (1977) 89.
[35] T. Appelquist and J. Carazzone, Phys. Rev. **D11** (1975) 2856.
[36] CDF Collaboration, Phys. Rev. Lett. 74 (1995) 2626;
D0 Collaboration, Phys. Rev. Lett. 74 (1995) 2632.
[37] M. Veltman, Acta Phys. Pol. **B8** (1977) 475.
[38] A. Sirlin, Phys. Rev. **D22** (1980) 971.
[39] G. Altarelli, R. Barbieri, S. Jadach, Nucl. Phys. **B369** (1992) 3.
[40] L.D. Faddeev and V.N. Popov, Phys. Lett. **B25** (1967) 29.
[41] G.'t Hooft, M. Veltman, Nucl. Phys. **B44** (1972) 189.
[42] G. Passarino, M.J.G. Veltman, Nucl. Phys. **B160** (1979) 151.
[43] G. Degrassi and A. Sirlin, Nucl. Phys. **B383** (1992) 73;
G. Degrassi and A. Sirlin, Phys. Rev. **D46** (1992) 3104.
[44] K.G. Wilson, Phys. Rev. **179** (1969) 1499.
[45] M. Roos and A. Sirlin, Nucl. Phys. **B29** (1971) 296;
A. Sirlin, Rev. Mod. Phys. **50** (1978) 573.
[46] H. Georgi and S.L. Glashow, Phys. Rev. Lett. **32** (1974) 438.
[47] H. Burkhhardt, F. Jegerlehner, G. Penso, C. Verzegnassi, Z. Phys. **C43** (1989) 497.
[48] H. Burkhardt and B. Pietrzyk, Phys.Rev. **D72** (2005) 057501.
[49] H. Burkhardt and B. Pietrzyk, Phys. Lett. **B513** (2001) 46, and references therein.
[50] B. Lynn and C. Verzegnassi, Phys. Rev. **D35** (1987) 3326.
[51] F.M. Renard and C. Verzegnassi, Phys. Rev. **D52** (1995) 1369.
[52] G. Burgers, F. Jegerlener, B. Kniehl and J. H. Kühn, in "Z Physics at LEP1", CERN 89-08 (1989), Vol. 1, page 71.
[53] R. Barbieri, M. Beccaria, P. Ciafaloni, G. Curci, A. Viceré, Nucl. Phys. **B409** (1993) 105.

[54] A. Djouadi and C. Verzegnassi, Phys. Lett. **195** (1987) 265.
[55] Z. Kunszt and P. Nason, in "Z Physics at LEP1", CERN 89-08 (1989), Vol. 1, page 373.
[56] J. Bernabeu, A. Pich and A. Santamaria, Nucl. Phys. **B363** (1991) 326.
[57] A. Blondel, A. Djouadi and C. Verzegnassi, Phys. Lett. **B293** (1992) 253.
[58] Particle Data Group, Phys. Lett. **B204** (1988) 1.
[59] G. Montagna, O. Nicrosini and F. Piccinini, Riv. Nuovo Cimento **21N9**, (1998) 1.
[60] J. Chyla, A.L. Kataev, in "Proceedings of the Working Group on Precision Calculations for the Z resonance", hep-ph/9502383, CERN 95-03 (1995), page 313.
[61] S. van der Meer, Rev. Mod. Phys. **57** (1985) 689.
[62] ALEPH Collaboration, Nucl. Instrum. Methods **A294** (1990) 121;
DELPHI Collaboration, Nucl. Instrum. Methods **A303** (1991) 233;
L3 Collaboration, Nucl. Instrum. Methods **A289** (1990) 35;
OPAL Collaboration, Nucl. Instrum. Methods **A305** (1991) 275;
CDF Collaboration, Nucl. Instrum. Methods **A271** (1988) 387;
D0 Collaboration, Nucl. Instrum. Methods **A565** (2006) 463;
SLD Design Report, SLAC-273 (1984).
[63] K. Kleinknecht, "Detectors for particle radiation", (1998) Cambridge University Press, Cambridge.
[64] J. M. Jauch and F. Rohrlich, Helv. Phys. Acta **27** (1954) 613.
[65] F. Bloch and A. Nordsiek, Phys. Rev. **52** (1937) 54.
[66] D. R. Yennie, S. C. Frautschi and H. Suura, Ann. Phys. **13** (1961) 379.
[67] M. Greco, G. Pancheri, Y. Srivastava, Phys. Lett. **B56** (1975) 367.
[68] G. Bonneau and F. Martin, Nucl. Phys. **B27** 381.
[69] F. A. Berends, G. J. H. Burgers and W. L. Van Neerven Phys. Lett. **B185** (1987) 395.
[70] "Proceedings of the Working Group on Precision Calculations for the Z resonance", CERN 95-03, eds. D. Bardin, W. Hollik and G. Passarino (1995).
[71] S. Jadach and B. F. L. Ward, Phys. Rev. **D38** (1988) 2897.
[72] F. A. Berends et al., in "Z Physics at LEP1", CERN 89-08 (1989), Vol. 1, page 89.
[73] G. Barbiellini, B. Borgia, M. Conversi and R. Santonico, Atti Accad. Naz. Lincei **44** (1968) 233 ;
J. F. Crawford, E. B. Hughes, L. H. O'Neill and R. E. Rand, Nucl. Instrum. Methods **127** (1975) 173.
[74] S. Jadach and B. F. L. Ward, Phys. Lett. **B389** (1996) 129;
M. Cacciari, A. Deandrea, G. Montagna, O. Nicrosini and L. Trentadue, Phys. Lett. **B271** (1991) 431.
[75] J.D. Jackson, "Classical Electrodynamics", (1975) John Wiley and Sons, New York.
[76] A. Sokolov and I. M. Ternov, Sov. Phys. Dokl. **8** (1963) 1203.
[77] The LEP Energy Working Group, The Aleph, Delphi, L3 and Opal Collaborations, Phys. Lett. **B307** (1993) 187.
[78] L. Arnaudon et al., "Accurate Determination of LEP Beam Energy by

Resonant Depolarization", CERN SL/94-71.
[79] T. Hebbeker, M. Martinez, G. Passarino and G. Quast, Phys. Lett. **B331** (1994) 165.
[80] M. Martinez, R. Miquel, L. Rolandi and R. Tenchini, Rev. Mod. Phys. **71** (1999) 575.
[81] ALEPH Collaboration, Eur. Phys. J. **C28** (2003) 1.
[82] ALEPH Collaboration, Eur. Phys. J **C14** (2000) 1;
DELPHI Collaboration, Eur. Phys. J **C16** (2000) 371;
L3 Collaboration, Eur. Phys. J **C16** (2000) 1;
OPAL Collaboration, Eur. Phys. J **C19** (2001) 587.
[83] A. Leike, T. Riemann, J. Rose, Phys. Lett. **B273** (1991) 513;
R. G. Stuart, Phys. Lett. **B272** (1991) 353.
[84] W. Hollik, in "Precision Tests of the Standard Model", edited by P. Langacker (World Scientific, Singapore), (1995) page 37;
W. Hollik,"Electroweak Theory", hep-ph/9602380.
[85] W. Beenakker, F.A. Berends, S.C. Van Der Marck, Nucl. Phys. **B349** (1991) 323.
[86] D. Bardin et al., Z. Phys. **C44** (1989) 493.
D. Bardin et al., ZFITTER v6.10 "A Semi-Analytical Program for Fermion Pair Production in e^+e^- Annihilation", DESY 99-070, hep-ph/9908433 (1999).
[87] G. Montagna et al., Nucl. Phys. **B401** (1993) 3;
G. Montagna et al., Comput. Phys. Commun. **117** 278.
[88] JADE Collaboration, Z. Phys. **C33** (1986) 23.
JADE Collaboration, Phys. Lett. **B213** (1988) 235.
[89] ALEPH Collaboration, Nucl. Instrum. Methods Phys. Res. **A346** (1994) 461.
[90] ALEPH Collaboration, Phys. Lett. **B313** (1993) 535.
[91] OPAL Collaboration, Z. Phys. **C65** (1995) 17.
[92] D.J. Jackson, Nucl. Instrum. Methods **A388** (1997) 247.
[93] ALEPH Collaboration, Phys. Lett. **B434** (1998) 437;
ALEPH Collaboration, Eur. Phys. J. **C16** (2000) 597;
DELPHI Collaboration, Phys. Lett. **B405** (1997) 202;
DELPHI Collaboration, Phys. Lett. **B462** (1999) 425;
L3 Collaboration, Phys. Lett. **B476** (2000) 243;
OPAL Collaboration, Eur. Phys. J. **C13** (2001) 1;
OPAL Collaboration, Eur. Phys. J. **C18** (2001) 447;
SLD Collaboration, Phys. Lett. **B507** (2001) 61.
[94] MarkIII Collaboration, Phys. Rev. Lett. **54** (1985) 1976.
[95] ALEPH Collaboration, Phys. Lett. **B401** (1997) 150;
ALEPH Collaboration, Phys. Lett. **B401** (1997) 163;
DELPHI Collaboration, Eur. Phys. J. **C10** (1999) 415;
L3 Collaboration, Eur. Phys. J. **C13** (2000) 47;
OPAL Collaboration, Eur. Phys. J. **C8** (1999) 217;
SLD Collaboration, Phys. Rev. **D71** (2005) 112004.
[96] ALEPH Collaboration, Eur. Phys. J. **C4** (1998) 557;

ALEPH Collaboration, Eur. Phys. J. **C16** (2000) 597;
DELPHI Collaboration, Eur. Phys. J. **C12** (2000) 225;
OPAL Collaboration, Eur. Phys. J. **C1** (1998) 439;
OPAL Collaboration, Z. Phys. **C72** (1996) 1;
SLD Collaboration, hep-ex/0503005, 2005.

[97] "Polarization at LEP", eds. G. Alexander et al., CERN 88-06 (1988).

[98] N. Phinney, Int. J. Mod. Phys. **A45** (1993) 2;
M. Woods, in "Proceedings of the 12th International Symposium on High Energy Spin Physics" eds. C.W. Jager et al. (World Scientific, Signapore, 1997), page 621.

[99] F. W. Lipps and H. A. Tolhoek, Physica **20** (1954) 85.

[100] B. Schumm, "Electroweak results from SLD", SLAC-PUB-7697.

[101] SLD Collaboration, Phys. Rev. Lett. **84** (2000) 5945.

[102] Y.S. Tsai, Phys. Rev. **D4** (1971) 2821.

[103] M. Davier, L. Duflot, F. Le Diberder, A. Rougé, Phys. Lett. **B306** (1993) 411.

[104] A. Rougé, in "Proceedings of the 1st International Workshop on τ Lepton Physics", Orsay (1990), eds. M. Davier and B. Jean-Marie (Editions Frontieres, Paris), p. 213.

[105] J.H. Khun, E. Mirkes, Z. Phys. **C56** (1992) 661; **C67** (1995) 364 (erratum).

[106] ALEPH Collaboration, Eur. Phys. J **C20** (2001) 401.

[107] DELPHI Collaboration, Eur. Phys. J **C14** (2000) 585.

[108] L3 Collaboration, Phys. Lett. **B429** (1998) 387.

[109] OPAL Collaboration, Eur. Phys. J **C21** (2001) 1.

[110] ALEPH Collaboration, Eur. Phys. J. **C24** (2002) 177;
DELPHI Collaboration, Eur. Phys. J. **C34** (2004) 109;
L3 Collaboration, Phys. Lett. **B448** (1999) 152;
OPAL Collaboration, Phys. Lett. **B577** (2003) 18;
ALEPH Collaboration, Eur. Phys. J. **C22** (2001) 201;
DELPHI Collaboration, Eur. Phys. J. **C40** (2005) 1;
L3 Collaboration, Phys. Lett. **B439** (1998) 225;
OPAL Collaboration, Phys. Lett. **B546** (2002) 29;
ALEPH Collaboration, Phys. Lett. **B434** (1998) 415;
DELPHI Collaboration, Eur. Phys. J. **C10** (1999) 219;
OPAL Collaboration, Z. Phys. **C73** (1997) 379.

[111] SLD Collaboration, Phys. Rev. Lett. **88** 151801 (2002);
SLD Collaboration, Phys. Rev. Lett. **90** 141804 (2003).

[112] ALEPH, DELPHI, L3, OPAL Collaborations, Nucl. Instr. Meth. **A378** (1996) 101.

[113] G. Altarelli and B. Lampe, Nucl. Phys. **B391** (1993) 3;
V. Ravidran and W. L. van Neerven, Phys. Lett. **B445** (1998) 214;
S. Catani and M. Seymour, JHEP **9907** (1999) 023.

[114] D. Abbaneo et al., Eur. Phys. J **C4** (1998) 185.

[115] DELPHI Collaboration, Eur. Phys. J. **C14** (2000) 613;
SLD Collaboration, Phys. Rev. Lett. **85** (2000) 5059.

[116] OPAL Collaboration, Z. Phys. **C76** (1997) 387.

[117] CDF and D0 Collaborations, Phys. Rev. **D70** (2004) 092008.
[118] C. Hays, "Les Rencontres de Physique de la Vallee d'Aoste", La Thuile, March 4-10 (2007), Italy;
O. Stelzer-Chilton, "Les Rencontres de Moriond", La Thuile, March 11-18 (2007), Italy.
CDF Collaboration, CDF Note 8665 (2007).
[119] "Physics at LEP2", eds. G. Altarelli, T. Sjöstrand and F. Zwirner, CERN 96-01 (1996), Vol. 1, page 79.
[120] W. Beenakker and A. Denner, Int. J. Mod. Phys. **A9** (1994) 4837.
[121] L3 Collaboration, Phys. Lett. **B602** (2004) 157;
OPAL Collaboration, Eur. Phys. J. **C31** (2003) 307.
[122] ALEPH Collaboration, Eur. Phys. J. **C49** (2007) 411;
DELPHI Collaboration, Eur. Phys. J. **C45** (2006) 589;
L3 Collaboration, Eur. Phys. J. **C47** (2006) 1;
OPAL Collaboration, Eur. Phys. J. **C33** (2004) 173.
[123] S. Jadach et al., Phys. Rev. **D61** 113010 (2000);
A. Denner et al., Phys. Lett. **B475** 127 (2000).
[124] ALEPH Collaboration, Eur. Phys. J. **C38** (2004) 147;
DELPHI Collaboration, Eur. Phys. J. **C34** (2004) 127;
L3 Collaboration, Phys. Lett. **B600** (2004) 22;
OPAL Collaboration, Contribution to 2001 Summer Conferences, OPAL Physics Note PN469.
[125] R. Assman et al., LEP Energy Working Group, Eur. Phys. J. **C39** (2005) 253.
[126] G. Gustafson, U. Petterson, P. Zerwas, Phys. Lett. **B209** (1988) 90;
T. Sjöstrand and V. Khoze, Z. Phys. **C62** (1994) 281;
T. Sjöstrand and V. Khoze, Phys. Rev. Lett. **72** (1994) 28.
[127] ALEPH Collaboration, Eur. Phys. J. **C47** (2006) 309;
DELPHI Collaboration, Contributed Paper for ICHEP 2006 (Moscow), DELPHI 2006-011 CONF 757;
L3 Collaboration, Eur. Phys. J. **C45** (2006) 569;
OPAL Collaboration, Eur. Phys. J. **C45** (2006) 307.
[128] L3 Collaboration, Phys. Lett. **B557** (2003) 147.
[129] OPAL Collaboration, Phys. Lett. **B585** (2004) 223.
[130] G. Gounaris, J. Layssac, G. Moultaka and F.M. Renard, Int. J. Mod. Phys. **A8** (1993) 3285.
[131] K. Hagiwara, R.D.Peccei, D. Zeppenfeld and K. Hikasa, Nucl. Phys. **B282** (1987) 253.
[132] ALEPH Collaboration, Eur. Phys. J. **C21** (2001) 423.
[133] A. De Rujula, M.B. Gavela, P. Hernandez, E. Masso, Nucl. Phys. **B384** (1992) 3.
J. Ellison, J. Wudka, Ann. Rev. Nucl. Part. Sci. **48** (1998) 33.
[134] ALEPH Collaboration, Phys. Lett. **B614** (2005) 7;
DELPHI Collaboration, Contributed Paper to EPS 2003 (Aachen) , DELPHI 2003-051 CONF 672;
L3 Collaboration, Phys. Lett. **B586** (2004) 151;

OPAL Collaboration, Eur. Phys. J. **C33** (2004) 463.
[135] ALEPH Collaboration, Phys. Lett. **B543** (2002) 173;
CDF Collaboration, Phys. Rev. Lett. **80** (1998) 2525;
OPAL Collaboration, Phys. Lett. **B521** (2001) 181.
[136] ARGUS Collaboration, Phys. Lett. **B192** (1987) 245.
[137] R. Peccei and X. Zhang, Nucl. Phys. **B337** (1990) 269.
[138] CDF Collaboration, Phys. Rev. **D73** (2006) 032003.
[139] Kondo K. J. Phys. Soc. Jpn. **57** (1988) 4126;
Kondo K. J. Phys. Soc. Jpn. **60** (1991) 836.
[140] Dalitz RH and Goldstein GR, Proc. R. Soc. Lond. **A445** (1999) 2803.
[141] The Tevatron Electroweak Working Group for the CDF and D0 Collaborations, hep-ex/0703034.
[142] The ALEPH, DELPHI, L3, OPAL, SLD Collaborations, the LEP Electroweak Working Group, the SLD Electroweak and Heavy Flavour Groups, Physics Reports **427** (2006) 257.
[143] The ALEPH, DELPHI, L3, OPAL, SLD Collaborations, the LEP Electroweak Working Group, "A Combination of Preliminary Electroweak Measurements and Constraints on the Standard Model", (2006) CERN-PH-EP/2006-042, hep-ex/0612034.
[144] S. Weinberg, Phys. Rev. Lett. **36** (1976) 294.
[145] B.W. Lee, C. Quigg and G.B. Thacker, Phys. Rev. Lett. **38** (1977) 883.
[146] I. Beltrami et al., Nucl. Phys. **A451** (1986) 679.
[147] R. Barbieri and T.E.O. Ericson, Phys. Lett. **B57** (1975) 270.
[148] S. J. Freedman et al., Phys. Rev. Lett. **52** (1984) 240.
[149] S. Egli et al., Phys. Lett. **B222** (1989) 533.
[150] G. D. Barr et al., Phys. Lett. **B235** (1990) 356.
[151] M. S. Alam et al., Phys. Rev. **D40** (1989) 712.
[152] J. Lee-Franzini et al., in "Proceedings of the XXIVth Int. Conf. on High Energy Physics", Munich (1988), eds. R. Kotthaus and J.H. Kuhn (Springer-Verlag, Berlin), page 1432.
[153] M. Davier and H. Nguyen Ngoc, Phys. Lett. **B150** (1989) 150.
[154] P. Janot and F. Le Diberder, Nucl. Instr. and Meth. **A411** (1998) 449 and references therein.
[155] ALEPH Collaboration, Phys. Lett. **B384** (1996) 427.
[156] DELPHI Collaboration, Nucl. Phys. **B421** (1994) 3.
[157] OPAL Collaboration, Z. Phys. **C73** (1997) 189.
[158] L3 Collaboration, Phys. Lett. **B385** (1996) 454.
[159] P. Janot, Nucl. Phys. **B38** (Proc. Suppl.) (1995) 264.
[160] P. Janot and M. Kado, C.R. Physique **3** (2002) 1193.
[161] ALEPH Collaboration, Phys. Lett. **B495** (2000) 1;
ALEPH Collaboration, Phys. Lett. **B526** (2002) 191
[162] DELPHI Collaboration, Eur. Phys. J. **C32** (2004) 145.
[163] L3 Collaboration, Phys. Lett. **B517** (2001) 319.
[164] OPAL Collaboration, Eur. Phys. J. **C26** (2003) 479.
[165] ALEPH, DELPHI, L3 and OPAL Collaborations, The LEP Working Group for Higgs Boson Searches, Phys. Lett. **B565** (2003) 61.

[166] H.P. Nilles, Physics Reports **110** (1984) 1;
H.E. Haber and G.L. Kane, Physics Reports **117** 75;
R. Barbieri, Riv. Nuovo Cimento **11** 1.
[167] G. Altarelli, R. Barbieri and F. Caravaglios, Int. J. Mod. Phys. **A13** (1998) 1031.
[168] G. Altarelli, R. Barbieri and F. Caravaglios, Nucl. Phys. **B405** (1993) 3.
[169] J. Ellis, G.L. Fogli and E. Lisi, Phys. Lett. **B343** 282.
[170] SuperKamiokande Collaboration, Phys. Rev. Lett. **81** (1998) 1562;
The Sudbury Neutrino Observatory, Phys. Rev. Lett. **87** (2001) 071301;
Kamland Collaboration, Phys. Rev. Lett. **90** (2003) 021802.

Index